

CO<sub>2</sub> SEQUESTRATION:  
CAPACITY, SECURITY, & ENHANCED GAS RECOVERY  
IN CENTRAL NEW YORK STATE

NYSERDA Agreement # 10501

Task 6, Part A (Tasks 6.1, 6.2, and 6.3)

Final Report, February 2, 2012

Final Revised Report, January 7, 2013

Contractor

Research Foundation of SUNY, on behalf of the University at Buffalo

Project Director and Editor: Dr. Robert Jacobi,  
University at Buffalo  
Geology Department, 411 Cooke Hall  
Buffalo, New York 14260  
(716) 645-4294  
Email:rdjacobi@buffalo.edu

Co-Project Director: Dr. Terry Jordan  
Department of Earth & Atmospheric Sciences  
Snee Hall  
Cornell University  
Ithaca, New York 14853-1504

Co-Project Director: Rick Frappa  
AMEC Geomatrix  
90B John Muir Drive, Suite 104  
Amherst, NY 14228

Co-Principal Investigators  
Dr. Matt Becker (UB), Dr. Larry Brown (Cornell), Dr. Bea Csatho (UB),  
Dr. Lou Derry (Cornell), Jason Phipps Morgan (Cornell)

Primary Funding from:  
New York State Energy Research and Development Authority  
Additional Sponsors:  
AES, Anschutz, Fortuna, Norse Energy

Submitted to:  
Dr. John Martin and Amanda Stevens, NYSERDA Project Managers  
NYS Energy Research and Development Authority  
17 Columbia Circle  
Albany, NY 12203-6399

## NOTICE

This report was prepared by Dr. Robert Jacobi, Dr. Terry Jordan, Rick Frappa, Dr. Matt Becker, Dr. Larry Brown, Dr. Bea Csatho, Dr. Lou Derry, and Jason Phipps Morgan in the course of performing work contracted for and sponsored by the New York State Energy Research and Development Authority and AES, Anschutz, Fortuna, and Norse Energy (hereafter the “Sponsors”). The opinions expressed in this report do not necessarily reflect those of the Sponsors or the State of New York, and reference to any specific product, service, process, or method does not constitute an implied or expressed recommendation or endorsement of it. Further, the Sponsors and the State of New York, and the contractor make no warranties or representations, expressed or implied, as to the fitness for particular purpose or merchantability of any product, apparatus, or service, or the usefulness, completeness, or accuracy of any processes, methods, or other information contained, described, disclosed, or referred to in this report. The Sponsors, the State of New York, and the contractor make no representation that the use of any product, apparatus, process, method, or other information will not infringe privately owned rights and will assume no liability for any loss, injury, or damage resulting from, or occurring in connection with, the use of information contained, described, disclosed, or referred to in this report.

## **ABSTRACT**

All the significant published data related to lineaments and structures in the project area were compiled, georeferenced in the ArcView GIS environment, and digitized. The structural data were utilized to predict fracture trends and the presence (or absence) of faults in the vicinity of the AES power plants in central New York State, as well as in the project area. The data base of structural information can be used as both an exclusionary function (for faults) and potentially as a tool to assist in the planning process for optimum injection of CO<sub>2</sub> along fractures.

All five AES power plants are close to bands of lineaments identified in satellite imagery that have been interpreted as faults. ENE-striking, steeply dipping, reactivated Iapetan-opening fault systems pass near the western three power plants, Hickling, Greenidge and Cayuga. E-trending lineaments and associated faults occur near the Greenidge, Cayuga Westover and Jennison power plants. All AES power plants in the project area also are close to northerly-trending lineament bands, and the Jennison and Westover also have strong NE lineament bundles. High structural level salt-cored anticlines that commonly involve thrust ramps off the Silurian salt decollements occur near the Westover and Cayuga power plants. Since these anticlines are restricted to units above the Silurian evaporate seal, and all the CO<sub>2</sub> sequestration targets are below the Silurian evaporate seal, these anticlines are not a significant factor in the considerations a CO<sub>2</sub> sequestration site. However, many salt-cored anticlines do correspond with deeper structures.

The orientation of the predominant fracture sets at the power plant sites can be estimated from the general fracture orientations of sets I, II, and III across New York State. Additionally, it is probable that closely-spaced fracture sets (sub) parallel to faults are localized along the faults in most of the sedimentary units except possibly the Utica and deeper carbonates. All these sets can be represented by long, relatively planar fractures.

## **KEY WORDS**

CO<sub>2</sub> sequestration, lineaments, faults, fractures, Appalachian Basin

## TABLE OF CONTENTS

### TASK 6: FAULTS AND FRACTURES IN THE FOCUS AREAS

SUBTASK 6.1 COLLECTION OF HISTORICAL DATA,

SUBTASK 6.2 MAPS FOR THE FOCUS AREAS OF LINEAMENTS ALONG  
PROMINENT AEROMAGNETIC ANOMALIES

SUBTASK 6.3: ESTIMATES OF FAULT AND FRACTURE CHARACTER NEAR  
THE AES POWER PLANTS BASED ON SUBTASKS 6.1 AND 6.2 (HISTORICAL  
AND AEROMAGNETIC DATA)

|  | Page     |
|--|----------|
| <u>Introduction</u>                          | 6.1-3-1  |
| <u>Methodology</u>                           | 6.1-3-2  |
| <u>Previous Studies.</u>                     | 6.1-3-2  |
| <u>Limited Field Studies.</u>                | 6.1-3-3  |
| <u>Lineaments of Aeromagnetic Gradients.</u> | 6.1-3-3  |
| <u>Data Sets</u>                             | 6.1-3-4  |
| <u>Results</u>                               | 6.1-3-6  |
| <u>Overview.</u>                             | 6.1-3-6  |
| <u>Hickling Power Plant.</u>                 | 6.1-3-9  |
| <u>Lineaments and Faults.</u>                | 6.1-3-9  |
| <u>Fractures.</u>                            | 6.1-3-10 |
| <u>Greenidge Power Plant.</u>                | 6.1-3-11 |
| <u>Lineaments and Faults.</u>                | 6.1-3-11 |
| <u>Fractures.</u>                            | 6.1-3-12 |
| <u>Cayuga Power Plant.</u>                   | 6.1-3-13 |
| <u>Lineaments and Faults.</u>                | 6.1-3-13 |
| <u>Fractures.</u>                            | 6.1-3-14 |
| <u>Westover Power Plant.</u>                 | 6.1-3-16 |
| <u>Lineaments and Faults.</u>                | 6.1-3-16 |
| <u>Fractures.</u>                            | 6.1-3-17 |
| <u>Jennison Power Plant.</u>                 | 6.1-3-17 |
| <u>Lineaments and Faults.</u>                | 6.1-3-17 |
| <u>Fractures.</u>                            | 6.1-3-18 |
| <u>Aeromagnetic Anomalies.</u>               | 6.1-3-19 |
| <u>Conclusions</u>                           | 6.1-3-20 |
| <u>Selected References</u>                   | 6.1/5-21 |



## LIST OF GRAPHICAL MATERIALS

|   |        |
|---|--------|
| Figure 6.1-1. Onondaga Outcrop (Engelder & Geiser, 1979)  | 6.1-27 |
| Figure 6.1-2. West Falls Group Outcrop (Engelder & Oertel, 1989)  | 6.1-28 |
| Figure 6.1-3a. Lineaments identified on a LandSat image (EarthSat, 1997)  | 6.1-29 |
| Figure 6.1-3b. Lineaments identified on a LandSat image (EarthSat, 1997), project   | 6.1-30 |
| Figure 6.1-4a. Lineaments identified by Isachsen and McKendree (1977)   | 6.1-31 |
| Figure 6.1-4b. Lineaments identified by Isachsen and McKendree (1977), project area view  | 6.1-32 |
| Figure 6.1-5a. Combined lineaments from EarthSat (1997) and Isachsen and<br>McKendree (1977)  | 6.1-33 |
| Figure 6.1-5b. Combined lineaments from EarthSat (1997) and Isachsen and<br>McKendree (1977), project area view.  | 6.1-34 |
| Figure 6.1-6a. Selected major fault systems (Jacobi, 2002)  | 6.1-35 |
| Figure 6.1-6b. Selected major fault systems (Jacobi, 2002), project area view.  | 6.1-36 |
| Figure 6.1-6c. Selected major fault zones (Jacobi, 2002), project area view.  | 6.1-37 |
| Figure 6.1-7a. Anticlines (Wedel, 1932)   | 6.1-38 |
| Figure 6.1-7b. Faults from Bradley et al. (1941)  | 6.1-39 |
| Figure 6.1-7c. Faults from Murphy (1981)  | 6.1-40 |
| Figure 6.1-8. Set I fractures measured in outcrop (Engelder & Geiser, 1980)   | 6.1-41 |
| Figure 6.1-9. Set I fractures in project area (Engelder & Geiser, 1980)   | 6.1-42 |
| Figure 6.1-10. Trajectories of Set I fractures (Faculty and Students of Cornell<br>University, 1959)  | 6.1-43 |
| Figure 6.1-11. Set II fractures measured in outcrop (Engelder & Geiser, 1980)   | 6.1-44 |
| Figure 6.1-12. Set II fractures measured in outcrop inside of the project area<br>(Engelder & Geiser, 1980)   | 6.1-45 |
| Figure 6.1-13. Set I & II fractures measured in outcrop inside of the project area<br>(Engelder & Geiser, 1980)   | 6.1-46 |
| Figure 6.1-14. Set II fracture trajectories based on Set II fractures measured in outcrop<br>(Engelder & Geiser, 1979)  | 6.1-47 |
| Figure 6.1-15. Set II trajectories based on Set II fracture measurements in the project area<br>(Engelder & Geiser, 1980)   | 6.1-48 |
| Figure 6.1-16. Set II trajectories compiled with Set I and II joints (Engelder & Geiser, 1980)  | 6.1-49 |
| Figure 6.1-17. Trajectories of fractures called Set II (Faculty and Students of Cornell<br>University, 1959), but are most likely Set III in the nomenclature of Engelder and<br>Geiser (1980). | 6.1-50 |
| Figure 6.1-18. Trajectories of fractures called Set III (Faculty and Students of Cornell  |        |

|  |        |
|--|--------|
| University,1959), but are most likely Set II in the nomenclature of Engelder and Geiser (1980).  | 6.1-51 |
| Figure 6.1-19. Sites of twist hackles (red and blue dots).   | 6.1-52 |
| Figure 6.1-20. Parent joints, Set I (Younes & Engelder, 1999)  | 6.1-53 |
| Figure 6.1-21. Clockwise fringe cracks on the parent joint of Set I in the western section of the project area (Younes & Engelder, 1999)                     | 6.1-54 |
| Figure 6.1-22. Counterclockwise fringe cracks on the parent joint of Set I in the eastern section of the project area (Younes & Engelder, 1999)              | 6.1-55 |
| Figure 6.1-23. Parent joint Set I of fringe crack kinks (Younes & Engelder, 1999)  | 6.1-56 |
| Figure 6.1-24. Fringe crack kinks on the parent joint of Set I with green dots showing the location of the data (Younes & Engelder, 1999)                    | 6.1-57 |
| Figure 6.1-25. Parent joint of Set II (Younes & Engelder, 1999)  | 6.1-58 |
| Figure 6.1-26. Fringe cracks on parent joints of Set II (Younes & Engelder, 1999)  | 6.1-59 |
| Figure 6.1-27. Unoriented crinoid locations (Engelder & Oertel, 1989)  | 6.1-60 |
| Figure 6.1-28. Deformed crinoid locations (Engelder & Oertel, 1989)  | 6.1-51 |
| Figure 6.1-29. Strike of the long axes of crinoids (Engelder & Oertel, 1989)   | 6.1-62 |
| Figure 6.1-30. Strike of the normal to compression inferred crinoid long axes (Engelder & Oertel, 1989)  | 6.1-63 |
| Figure 6.1-31. Field Sites on Seneca and Cayuga lakes (Lugert et al, 2001, Cruz, 2005, Jacobi, 2007)   | 6.1-64 |
| Figure 6.1-32. Field Sites with NW striking fractures with a fracture frequency of 0-2 fractures/m (Lugert et al, 2001, Cruz, 2005, Jacobi, 2007)            | 6.1-65 |
| Figure 6.1-33. Field Sites with NW striking fractures with a fracture frequency of 2-4 fractures/m (Lugert et al, 2001, Cruz, 2005, Jacobi, 2007)            | 6.1-66 |
| Figure 6.1-34. Field Sites with NW striking fractures with a fracture frequency of greater than 4 fractures/m (Lugert et al, 2001, Cruz, 2005, Jacobi, 2007) | 6.1-67 |
| Figure 6.1-35. Field Sites with NS striking fractures with a fracture frequency of 0-2 fractures/m (Lugert et al, 2001, Cruz, 2005, Jacobi, 2007)            | 6.1-68 |
| Figure 6.1-36. Field Sites with NS striking fractures with a fracture frequency of 2-4 fractures/m (Lugert et al, 2001, Cruz, 2005, Jacobi, 2007)            | 6.1-69 |
| Figure 6.1-37. Field Sites with NS striking fractures with a fracture frequency of greater than 4 fractures/m (Lugert et al, 2001, Cruz, 2005, Jacobi, 2007) | 6.1-70 |
| Figure 6.1-38. Field Sites with NNW striking fractures with a fracture frequency of 0-2 fractures/m (Lugert et al, 2001, Cruz, 2005, Jacobi, 2007)           | 6.1-71 |
| Figure 6.1-39. Field Sites with NNW striking fractures with a fracture frequency of 2-4 fractures/m (Lugert et al, 2001, Cruz, 2005, Jacobi, 2007)           | 6.1-72 |

|   |        |
|---|--------|
| Figure 6.1-40. Field Sites with NNW striking fractures with a fracture frequency of greater than 4 fractures/m (Lugert et al, 2001, Cruz, 2005, Jacobi, 2007) | 6.1-73 |
| Figure 6.1-41. Field Sites with NNE striking fractures with a fracture frequency of 0-2 fractures/m (Lugert et al, 2001, Cruz, 2005, Jacobi, 2007)            | 6.1-74 |
| Figure 6.1-42. Field Sites with NNE striking fractures with a fracture frequency of 2-4 fractures/m (Lugert et al, 2001, Cruz, 2005, Jacobi, 2007)            | 6.1-75 |
| Figure 6.1-43. Field Sites with NNE striking fractures with a fracture frequency of greater than 4 fractures/m (Lugert et al, 2001, Cruz, 2005, Jacobi, 2007) | 6.1-76 |
| Figure 6.1-44. Field Sites with ENE striking fractures with a fracture frequency of 0-2 fractures/m (Lugert et al, 2001, Cruz, 2005, Jacobi, 2007)            | 6.1-77 |
| Figure 6.1-45. Field Sites with ENE striking fractures with a fracture frequency of 2-4 fractures/m (Lugert et al, 2001, Cruz, 2005, Jacobi, 2007)            | 6.1-78 |
| Figure 6.1-46. Field Sites with ENE striking fractures with a fracture frequency of greater than 4 fractures/m (Lugert et al, 2001, Cruz, 2005, Jacobi, 2007) | 6.1-79 |
| Figure 6.1-47. Field Sites with EW striking fractures with a fracture frequency of 0-2 fractures/m (Lugert et al, 2001, Cruz, 2005, Jacobi, 2007)             | 6.1-80 |
| Figure 6.1-48. Field Sites with EW striking fractures with a fracture frequency of 2-4 fractures/m (Lugert et al, 2001, Cruz, 2005, Jacobi, 2007)             | 6.1-81 |
| Figure 6.1-49. Field Sites with EW striking fractures with a fracture frequency of greater than 4 fractures/m (Lugert et al, 2001, Cruz, 2005, Jacobi, 2007)  | 6.1-82 |
| Figure 6.1-50. Field Sites with WNW striking fractures with a fracture frequency of 0-2 fractures/m (Lugert et al, 2001, Cruz, 2005, Jacobi, 2007)            | 6.1-83 |
| Figure 6.1-51. Field Sites with WNW striking fractures with a fracture frequency of 2-4 fractures/m (Lugert et al, 2001, Cruz, 2005, Jacobi, 2007)            | 6.1-84 |
| Figure 6.1-52. Field Sites with WNW striking fractures with a fracture frequency of greater than 4 fractures/m (Lugert et al, 2001, Cruz, 2005, Jacobi, 2007) | 6.1-85 |
| Figure 6.1-53. Field Sites with NE striking fractures with a fracture frequency of 0-2 fractures/m (Lugert et al, 2001, Cruz, 2005, Jacobi, 2007)             | 6.1-86 |
| Figure 6.1-54. Field Sites with NE striking fractures with a fracture frequency of greater than 4 fractures/m (Lugert et al, 2001, Cruz, 2005, Jacobi, 2007)  | 6.1-87 |
| Figure 6.1-55. Fracture orientation and intensity (Sheldon, 1912)   | 6.1-88 |
| Figure 6.1-56: Lineaments and field sites displaying ENE striking fractures with a fracture frequency of less than 2 fractures/m.                             | 6.1-89 |
| Figure 6.1-57. Lineaments and field sites displaying ENE striking fractures with a fracture frequency of 2 to 4 fractures/m.                                  | 6.1-90 |
| Figure 6.1-58. Lineaments and field sites displaying ENE striking fractures with a fracture   |        |

|  |         |
|--|---------|
| frequency of greater than 4 fractures/m.   | 6.1-91  |
| Figure 6.1-59. Lineaments and field sites displaying EW-striking fractures with a fracture frequency of less than 2 fractures/m.     | 6.1-92  |
| Figure 6.1-60. Lineaments and field sites displaying EW-striking fractures with a fracture frequency of 2 to 4 fractures/m.          | 6.1-93  |
| Figure 6.1-61. Lineaments and field sites displaying EW-striking fractures with a fracture frequency of greater than 4 fractures/m.  | 6.1-94  |
| Figure 6.1-62. Lineaments and field sites displaying NE-striking fractures with a fracture frequency of less than 2 fractures/m.     | 6.1-95  |
| Figure 6.1-63. Lineaments and field sites displaying NE-striking fractures with a fracture frequency of greater than 4 fractures/m.  | 6.1-96  |
| Figure 6.1-64. Lineaments and field sites displaying NNE-striking fractures with a fracture frequency of less than 2 fractures/m.    | 6.1-97  |
| Figure 6.1-65. Lineaments and field sites displaying NNE-striking fractures with a fracture frequency of 2 to 4 fractures/m.         | 6.1-98  |
| Figure 6.1-66. Lineaments and field sites displaying NNE-striking fractures with a fracture frequency of greater than 4 fractures/m. | 6.1-99  |
| Figure 6.1-67. Lineaments and field sites displaying NNW-striking fractures with a fracture frequency of less than 2 fractures/m.    | 6.1-100 |
| Figure 6.1-68. Lineaments and field sites displaying NNW-striking fractures with a fracture frequency of 2 to 4 fractures/m.         | 6.1-101 |
| Figure 6.1-69. Lineaments and field sites displaying NNW-striking fractures with a fracture frequency of greater than 4 fractures/m. | 6.1-102 |
| Figure 6.1-70. Lineaments and field sites displaying NS-striking fractures with a fracture frequency of less than 2 fractures/m.     | 6.1-103 |
| Figure 6.1-71. Lineaments and field sites displaying NS-striking fractures with a fracture frequency of 2 to 4 fractures/m.          | 6.1-104 |
| Figure 6.1-72. Lineaments and field sites displaying NS-striking fractures with a fracture frequency of greater than 4 fractures/m.  | 6.1-105 |
| Figure 6.1-73. Lineaments and field sites displaying NW-striking fractures with a fracture frequency of less than 2 fractures/m.     | 6.1-106 |
| Figure 6.1-74. Lineaments and field sites displaying NW-striking fractures with a fracture frequency of 2 to 4 fractures/m.          | 6.1-107 |
| Figure 6.1-75. Lineaments and field sites displaying NW-striking fractures with a fracture frequency of greater than 4 fractures/m.  | 6.1-108 |
| Figure 6.1-76. Lineaments and field sites displaying WNW-striking fractures with a fracture  |         |

|  |         |
|--|---------|
| frequency of less than 2 fractures/m.  | 6.1-109 |
| Figure 6.1-77. Lineaments and field sites displaying WNW-striking fractures with a fracture frequency of 2 to 4 fractures/m.         | 6.1-110 |
| Figure 6.1-78. Lineaments and field sites displaying WNW-striking fractures with a fracture frequency of greater than 4 fractures/m. | 6.1-111 |
| Figure 6.1-79. Lineaments and field sites displaying ENE-striking fractures with a fracture frequency of less than 2 fractures/m.    | 6.1-112 |
| Figure 6.1-80. Lineaments and field sites displaying ENE-striking fractures with a fracture frequency of 2 to 4 fractures/m.         | 6.1-113 |
| Figure 6.1-81. Lineaments and field sites displaying ENE-striking fractures with a fracture frequency of greater than 4 fractures/m. | 6.1-114 |
| Figure 6.1-82. Lineaments and field sites displaying EW-striking fractures with a fracture frequency of less than 2 fractures/m.     | 6.1-115 |
| Figure 6.1-83. Lineaments and field sites displaying EW-striking fractures with a fracture frequency of 2 to 4 fractures/m.          | 6.1-116 |
| Figure 6.1-84. Lineaments and field sites displaying EW-striking fractures with a fracture frequency of greater than 4 fractures/m.  | 6.1-117 |
| Figure 6.1-85. Lineaments and field sites displaying NE-striking fractures with a fracture frequency of less than 2 fractures/m.     | 6.1-118 |
| Figure 6.1-86. Lineaments and field sites displaying NE-striking fractures with a fracture frequency of greater than 4 fractures/m.  | 6.1-119 |
| Figure 6.1-87. Lineaments and field sites displaying NNE-striking fractures with a fracture frequency of less than 2 fractures/m.    | 6.1-120 |
| Figure 6.1-88. Lineaments and field sites displaying NNE-striking fractures with a fracture frequency of greater than 4 fractures/m. | 6.1-121 |
| Figure 6.1-89. Lineaments and field sites displaying NNW-striking fractures with a fracture frequency of less than 2 fractures/m.    | 6.1-122 |
| Figure 6.1-90. Lineaments and field sites displaying NNW-striking fractures with a fracture frequency of 2 to 4 fractures/m.         | 6.1-123 |
| Figure 6.1-91. Lineaments and field sites displaying NNW-striking fractures with a fracture frequency of greater than 4 fractures/m. | 6.1-124 |
| Figure 6.1-92. Lineaments and field sites displaying NS-striking fractures with a fracture frequency of less than 2 fractures/m.     | 6.1-125 |
| Figure 6.1-93. Lineaments and field sites displaying NS-striking fractures with a fracture frequency of 2 to 4 fractures/m.          | 6.1-126 |
| Figure 6.1-94. Lineaments and field sites displaying NS-striking fractures with a fracture   |         |

|   |         |
|---|---------|
| frequency of greater than 4 fractures/m.  | 6.1-127 |
| Figure 6.1-95. Lineaments and field sites displaying NW-striking fractures with a fracture frequency of less than 2 fractures/m.  | 6.1-128 |
| Figure 6.1-96. Lineaments and field sites displaying NW-striking fractures with a fracture frequency of 2 to 4 fractures/m.   | 6.1-129 |
| Figure 6.1-97. Lineaments and field sites displaying NW-striking fractures with a fracture frequency of greater than 4 fractures/m.                                       | 6.1-130 |
| Figure 6.1-98. Lineaments and field sites displaying WNW-striking fractures with a fracture frequency of less than 2 fractures/m.   | 6.1-131 |
| Figure 6.1-99. Lineaments and field sites displaying NW-striking fractures with a fracture frequency of 2 to 4 fractures/m.   | 6.1-132 |
| Figure 6.1-100. Cayuga Field Sites (see Figures 108-113 for enlarged view)  | 6.1-133 |
| Figure 6.1-101. Cayuga field sites from the 2007 DOE report (black) and summer 2009 field work (red) inside the Region of Interest (ROI) defined for statistical analyses | 6.1-134 |
| Figure 6.1-102. Northern Cayuga field sites with modified rose diagrams   | 6.1-135 |
| Figure 6.1-103. Southern Cayuga field sites with modified rose diagrams   | 6.1-136 |
| Figure 6.1-104. Southernmost Cayuga field site with modified rose diagram   | 6.1-137 |
| Figure 6.1-105. Cayuga field sites exhibiting ENE trending fractures with a frequency of less than 2 fractures/m.   | 6.1-138 |
| Figure 6.1-106. Cayuga field sites exhibiting ENE trending fractures with a frequency greater than 4 fractures/m.   | 6.1-139 |
| Figure 6.1-107. Cayuga field sites exhibiting EW-striking fractures with a frequency of 2 to 4 fractures/m.   | 6.1-140 |
| Figure 6.1-108. Cayuga field sites exhibiting EW-striking fractures with a frequency of greater than 4 fractures/m.   | 6.1-141 |
| Figure 6.1-109. Cayuga field sites exhibiting NE-striking fractures with a frequency of less than 2 fractures/m.  | 6.1-142 |
| Figure 6.1-110. Cayuga field sites exhibiting NNE-striking fractures with a frequency of less than 2 fractures/m.   | 6.1-143 |
| Figure 6.1-111. Cayuga field sites exhibiting NNE-striking fractures with a frequency of greater than 4 fractures/m.  | 6.1-144 |
| Figure 6.1-112. Cayuga field sites exhibiting NNW-striking fractures with a frequency of less than 2 fractures/m.   | 6.1-145 |
| Figure 6.1-113. Cayuga field sites exhibiting NNW-striking fractures with a frequency of 2 to 4 fractures/m.  | 6.1-146 |
| Figure 6.1-114. Cayuga field sites exhibiting NNW-striking fractures with a frequency of  |         |

|  |         |
|--|---------|
| greater than 4 fractures/m.  | 6.1-147 |
| Figure 6.1-115. Cayuga field sites exhibiting NS-striking fractures with a frequency of less than 2 fractures/m.   | 6.1-148 |
| Figure 6.1-116. Cayuga field sites exhibiting NW-striking fractures with a frequency of less than 2 fractures/m.   | 6.1-149 |
| Figure 6.1-117. Cayuga field sites exhibiting NW-striking fractures with a frequency of greater than 4 fractures/m.  | 6.1-150 |
| Figure 6.1-118. Buffers surrounding ENE trending lineaments in the ROI on Cayuga Lake.   | 6.1-151 |
| Figure 6.1-119. Buffers surrounding EW trending lineaments in the ROI on Cayuga Lake.  | 6.1-153 |
| Figure 6.1-120. Graphical representation of the statistical Weights of Evidence  | 6.1-153 |
| Figure 6.1-121. Reduced to pole (RTP) total magnetic intensity   | 6.1-154 |
| Figure 6.1-122. Horizontal gradient of RTP aeromagnetics   | 6.1-155 |
| Figure 6.1-123. Vertical gradient of RTP aeromagnetics   | 6.1-156 |
| Figure 6.1-124. Second derivative of RTP aeromagnetics   | 6.1-157 |
| Figure 6.1-125. Linear feature analysis of RTP aeromagnetics   | 6.1-158 |
| Figure 6.1-126. Interpretation of gradients in the aeromagnetic field  | 6.1-159 |
| Figure 6.1-127. Eastern part of the project area (“Chenango AOI”): Jennison Power Plant with lineaments (EarthSat,97) and field sites from McGuire et al (2006), Terech et al (2005) and Jacobi (2007b). | 6.1-160 |
| Figure 6.1-128. North-central Chenango field sites exhibiting ENE-striking fractures with a frequency of less than 2 fractures/m.  | 6.1-161 |
| Figure 6.1-129. North-central Chenango field sites exhibiting ENE-striking fractures with a frequency of 2 to 4 fractures/m.   | 6.1-162 |
| Figure 6.1-130. North-central Chenango field sites exhibiting ENE-striking fractures with a frequency of greater than 4 fracture/m.  | 6.1-163 |
| Figure 6.1-131. North-central Chenango field sites exhibiting EW-striking fractures with a frequency of less than 2 fractures/m.   | 6.1-164 |
| Figure 6.1-132. North-central Chenango field sites exhibiting EW-striking fractures with a frequency of 2 to 4 fractures/m.  | 6.1-165 |
| Figure 6.1-133. North-central Chenango field sites exhibiting EW-striking fractures with a frequency of greater than 4 fractures/m.  | 6.1-166 |
| Figure 6.1-134. North-central Chenango field sites exhibiting NE-striking fractures with a frequency of less than 2 fractures/m.   | 6.1-167 |
| Figure 6.1-135. North-central Chenango field sites exhibiting NE-striking fractures with a frequency of 2 to 4 fractures/m.  | 6.1-168 |
| Figure 6.1-136. North-central Chenango field sites exhibiting NE-striking fractures with a   |         |

|   |         |
|---|---------|
| frequency of greater than 4 fractures/m.  | 6.1-169 |
| Figure 6.1-137. North-central Chenango field sites exhibiting NNE-striking fractures with a frequency of less than 2 fractures/m.   | 6.1-170 |
| Figure 6.1-138. North-central Chenango field sites exhibiting NNE-striking fractures with a frequency of 2 to 4 fractures/m.  | 6.1-171 |
| Figure 6.1-139. North-central Chenango field sites exhibiting NNE-striking fractures with a frequency of greater than 4 fractures/m.  | 6.1-172 |
| Figure 6.1-140. North-central Chenango field sites exhibiting NNW-striking fractures with a frequency of less than 2 fractures/m.   | 6.1-173 |
| Figure 6.1-141. North-central Chenango field sites exhibiting NNW-striking fractures with a frequency of 2 to 4 fractures/m.  | 6.1-174 |
| Figure 6.1-142. North-central Chenango field sites exhibiting NNW-striking fractures with a frequency of greater than 4 fractures/m.  | 6.1-175 |
| Figure 6.1-143. North-central Chenango field sites exhibiting NS-striking fractures with a frequency of less than 2 fractures/m.  | 6.1-176 |
| Figure 6.1-144. North-central Chenango field sites exhibiting NS-striking fractures with a frequency of 2 to 4 fractures/m.   | 6.1-177 |
| Figure 6.1-145. North-central Chenango field sites exhibiting NS-striking fractures with a frequency of greater than 4 fractures/m.   | 6.1-178 |
| Figure 6.1-146. North-central Chenango field sites exhibiting NW-striking fractures with a frequency of less than 2 fractures/m.  | 6.1-179 |
| Figure 6.1-147. North-central Chenango field sites exhibiting NW-striking fractures with a frequency of 2 to 4 fractures /m.  | 6.1-180 |
| Figure 6.1-148. North-central Chenango field sites exhibiting NW-striking fractures with a frequency of greater than 4 fractures /m.  | 6.1-181 |
| Figure 6.1-149. North-central Chenango field sites exhibiting WNW-striking fractures with a frequency of less than 2 fractures/m.   | 6.1-182 |
| Figure 6.1-150. North-central Chenango field sites exhibiting WNW-striking fractures with a frequency of 2 to 4 fractures/m.  | 6.1-183 |
| Figure 6.1-151. North-central Chenango field sites exhibiting WNW-striking fractures with a frequency of greater than 4 fractures/m.  | 6.1-184 |
| Figure 6.1-152. North-central Chenango field sites showing rose diagrams of fracture intensification domains  | 6.1-185 |
| Figure 6.1.-153. North-central Chenango field sites showing associated rose diagrams of fracture intensification domains on top of a shaded DEM with ellipses highlighting prominent fracture orientations that are consonant with the topographic lineaments | 6.1-186 |



|   |         |
|---|---------|
| Figure 6.1-154. Southwestern Chenango field sites exhibiting ENE-striking fractures with a frequency of less than 2 fractures/m.    | 6.1-187 |
| Figure 6.1-155. Southwestern Chenango field sites exhibiting ENE-striking fractures with a frequency of 2 to 4 fractures/m.         | 6.1-188 |
| Figure 6.1-156. Southwestern Chenango field sites exhibiting ENE-striking fractures with a frequency of greater than 4 fractures/m. | 6.1-189 |
| Figure 6.1-157. Southwestern Chenango field sites exhibiting EW-striking fractures with a frequency of less than 2 fractures/m.     | 6.1-190 |
| Figure 6.1-158. Southwestern Chenango field sites exhibiting EW-striking fractures with a frequency of 2 to 4 fractures/m.          | 6.1-191 |
| Figure 6.1-159. Southwestern Chenango field sites exhibiting EW-striking fractures with a frequency of greater than 4 fractures/m.  | 6.1-192 |
| Figure 6.1-160. Southwestern Chenango field sites exhibiting NE-striking fractures with a frequency of less than 2 fractures/m.     | 6.1-193 |
| Figure 6.1-161. Southwestern Chenango field sites exhibiting NE-striking fractures with a frequency of 2 to 4 fractures/m.          | 6.1-194 |
| Figure 6.1-162. Southwestern Chenango field sites exhibiting NNE-striking fractures with a frequency of less than 2 fractures/m.    | 6.1-195 |
| Figure 6.1-163. Southwestern Chenango field sites exhibiting NNE-striking fractures with a frequency of 2 to 4 fractures/m.         | 6.1-196 |
| Figure 6.1-164. Southwestern Chenango field sites exhibiting NNE-striking fractures with a frequency of greater than 4 fractures/m. | 6.1-197 |
| Figure 6.1-165. Southwestern Chenango field sites exhibiting NNW-striking fractures with a frequency of less than 2 fractures/m.    | 6.1-198 |
| Figure 6.1-166. Southwestern Chenango field sites exhibiting NNW-striking fractures with a frequency of 2 to 4 fractures/m.         | 6.1-199 |
| Figure 6.1-167. Southwestern Chenango field sites exhibiting NNW-striking fractures with a frequency of greater than 4 fractures/m. | 6.1-200 |
| Figure 6.1-168. Southwestern Chenango field sites exhibiting NS-striking fractures with a frequency of less than 2 fractures/m.     | 6.1-201 |
| Figure 6.1-169. Southwestern Chenango field sites exhibiting NS-striking fractures with a frequency of 2 to 4 fractures/m.          | 6.1-202 |
| Figure 6.1-170. Southwestern Chenango field sites exhibiting NS-striking fractures with a frequency of greater than 4 fractures/m.  | 6.1-203 |
| Figure 6.1-171. Southwestern Chenango field sites exhibiting NW-striking fractures with a frequency of less than 2 fractures/m.     | 6.1-204 |

|   |         |
|---|---------|
| Figure 6.1-172. Southwestern Chenango field sites exhibiting NW-striking fractures with a frequency of 2 to 4 fractures/m.  | 6.1-205 |
| Figure 6.1-173. Southwestern Chenango field sites exhibiting NW-striking fractures with a frequency of greater than 4 fractures/m.  | 6.1-206 |
| Figure 6.1-174. Southwestern Chenango field sites exhibiting WNW-striking fractures with a frequency of less than 2 fractures/m.  | 6.1-207 |
| Figure 6.1-175. Southwestern Chenango field sites exhibiting WNW-striking fractures with a frequency of 2 to 4 fractures/m.   | 6.1-208 |
| Figure 6.1-176. Southwestern Chenango field sites exhibiting WNW-striking fractures with a frequency of greater than 4 fractures/m.   | 6.1-209 |
| Figure 6.1-177. Southwestern Chenango field sites showing associated rose diagrams of fracture intensification domains on top of a shaded DEM   | 6.1-210 |
| Figure 6.1-178. Southwestern Chenango field sites showing associated rose diagrams of fracture intensification domains on top of a shaded DEM with ellipses highlighting prominent topographic lineaments that are consonant with FID orientation | 6.1-211 |
| Figure 6.1-179. Index map for Figure 6.1-180.   | 6.1-212 |
| Figure 6.1-180. Lineaments from Pyron et al. (2003)   | 6.1-213 |
| Figure 6.1-181. Joint rose diagrams from Engelder and Oertel (1985)   | 6.1-214 |
| Figure 6.1-182. Rose diagrams of joints from Parker (1942)  | 6.1-215 |
| Figure 6.2-1. Smoothed residual aeromagnetics.  | 6.1-216 |
| Figure 6.2-2. Smoothed residual aeromagnetics with lineaments (thick black lines) drawn along the trends of significant linear aeromagnetic gradients.  | 6.1-217 |
| Figure 6.2-3. Smoothed residual aeromagnetics with EarthSat (1997) lineaments.  | 6.1-218 |

## LIST OF TABLES

|   |         |
|---|---------|
| TABLE 6.1-1 Hickling Power Plant Lineaments and Faults  | 6.1-219 |
| TABLE 6.1-2 Hickling Power Plant Fracture Trends        | 6.1-220 |
| TABLE 6.1-3 Greenidge Power Plant Lineaments and Faults | 6.1-221 |
| TABLE 6.1-4 Greenidge Power Plant Fracture Trends       | 6.1-222 |
| TABLE 6.1-5 Cayuga Power Plant Lineaments and Faults    | 6.1-223 |
| TABLE 6.1-6 Cayuga Power Plant Fracture Trends          | 6.1-224 |
| TABLE 6.1-7 Westover Power Plant Lineaments and Faults  | 6.1-225 |
| TABLE 6.1-8 Westover Power Plant Fracture Trends        | 6.1-226 |
| TABLE 6.1-9 Jennison Power Plant Lineaments and Faults  | 6.1-227 |
| TABLE 6.1-10 Jennison Power Plant Fracture Trends       | 6.1-228 |

## SUMMARY

The objective of research Task 6.1 was to compile all the significant published data related to lineaments and structures in the project area, as well as to collect new fracture data in selected areas. The structural data were to be utilized in predicting 1) fracture trends and 2) the presence (or absence) of fault systems and the trends of these fault systems in the immediate vicinity of the AES power plants in central New York State. The areas surrounding the power plants are potentially the first choice for sequestration of CO<sub>2</sub> from the power plants. The data base of structural information can be used as both an exclusionary function (for faults) and potentially as a tool to assist in the planning process for optimum injection of CO<sub>2</sub> along fractures. The objective of research Task 6.2 was to identify lineaments in aeromagnetic data in the project area. Steep, linear (in map view) aeromagnetic gradients may indicate locations of faults in the basement. All data are presented in the form of maps that are digital and georeferenced in the Arc View GIS environment. The objective of Subtask 6.3 was to use the compiled database of structural information from Subtasks 6.1 and 6.2 to determine the possibility and character of faults and fractures near the AES power plants. These considerations can be used as both an exclusionary factor (for faults) near the targeted power plants and as a tool to assist in predicting fracture character (spacing and trends) near the power plants as part of the planning process for optimum injection of CO<sub>2</sub>.

All five AES power plants are close to bands of lineaments identified in satellite imagery by EarthSat (1997) and Isachsen and McKendree (1977); these lineaments were interpreted as faults by Jacobi (2002). The western three power plants, Hickling, Greenidge and Cayuga, all are in close proximity to ENE-trending lineaments. In the regions of the Hickling and Cayuga power plants, proprietary 3D seismic reflection data confirm earlier integrated studies (surface fractures, soil gas, 2D seismic reflection data and aeromagnetics; Jacobi, 2007) that proposed these lineament trends are representative of ENE-striking steeply dipping, reactivated Iapetan-opening fault systems. All the ENE-striking fault systems were active during Iapetan opening time (and therefore affect basement), but they experienced variable amounts of motion in the following orogenies (e.g., Jacobi 2010). Some of these fault systems extend to the (near) surface, and the fracture systems associated with the faults do reach the surface. Many of the Iapetan-opening faults were reactivated with relatively large throws during the Taconic Orogeny. In the Hickling power plant region, the ENE-striking fault systems have relatively close spacings (across the ENE strike), on the order of 1.5-2.5 km. The length between major along-strike variations in the faults (e.g., cross fault trends) has a range between 1.5 km and 10 km.

The Greenidge, Cayuga Westover and Jennison power plants are close to E-trending lineaments and lineament bundles. In the region of the Cayuga power plant, proprietary 3D seismic shows that these faults also sustained their greatest motion in Taconic times. Jennison and Westover also have strong NE lineament bundles which are interpreted as fault systems. All AES power plants in the project area also are

close to northerly-trending lineament bands. For example, the Greenidge power plant is located east of NNE-lineaments that are coincident with significant aeromagnetic anomalies, suggesting NNE-striking faults and associated fractures that extend from basement to (near) surface. These fault systems are believed to be related to intra-Grenvillian sutures (terrane boundaries) that have been episodically reactivated (e.g., Jacobi, 2002).

High structural level salt-cored anticlines that commonly involve thrust ramps off the Silurian salt decollements occur near the Westover and Cayuga power plants. Since these anticlines are restricted to units above the Silurian evaporate seal, and all the CO<sub>2</sub> sequestration targets are below the Silurian evaporate seal, these anticlines are not a significant factor in the considerations a CO<sub>2</sub> sequestration site. However, 3D seismic surveys in eastern NYS (Jacobi, 2011; Jacobi et al. 2011) confirmed earlier suppositions based on 2D seismic reflection data (e.g., Scanlin and Engelder, 2003; Jacobi, 2010) and on the coincidence of the folds with aeromagnetic anomalies (Jacobi, 2002, 2003a,b, 2004, 2005, 2010) that steeply-dipping faults systems extending from the basement do appear to control the fabric of the anticlines, i.e., the trend and general location of the anticlines do seem to correspond with deeper structures.

The orientation of the predominant fracture sets at the power plant sites can be estimated from the general fracture orientations of sets I, II, and III across New York State. In general Set I fractures trend NW at the Hickling and Greenidge power plants, NNW/N at the Cayuga power plant, N/NNE at the Westover plant and NNE at the Jennison power plant. Set II fractures are generally orthogonal to Set I fractures. Set III fractures generally trend ENE. Additionally, it is probable that closely-spaced fracture sets (sub) parallel to faults are localized along the faults in most of the sedimentary units except possibly the Utica and deeper carbonates. All these sets can be represented by long, relatively planar fractures.

The fracture frequency of these fracture sets the surface in Upper Devonian interbedded shales and siltstones is generally on the order of (less than) 1 fracture/m for Set I, < 4 fractures/m for Set II, and variable spacing for Set III. The spacing of the fractures related to faults (FIDs) could vary from about 4 to as many as 20 fractures/m near the surface. The spacing of the fracture sets is not known at depth.

## **TASK 6: FAULTS AND FRACTURES IN THE FOCUS AREAS, PART A**

### **SUBTASK 6.1 COLLECTION OF HISTORICAL DATA,**

### **SUBTASK 6.2 FOCUS AREA MAPS OF LINEAMENTS ALONG PROMINENT**

### **AEROMAGNETIC ANOMALIES,**

### **SUBTASK 6.3: ESTIMATES OF FAULT AND FRACTURE CHARACTER NEAR THE AES**

### **POWER PLANTS BASED ON SUBTASKS 6.1 AND 6.2 (HISTORICAL AND**

### **AEROMAGNETIC DATA)**

**Robert Jacobi and Jodi Fisher, University at Buffalo**

#### **Introduction**

Task 6, Part A integrates Subtasks 6.1, 6.2 and 6.3 (structure, lineaments from aeromagnetic gradients, and implications for CO<sub>2</sub> storage), whereas Task 6, Part B integrates Subtasks 6.4, 6.5, 6.6, and 6.7 (lineaments from remotely sensed data, lineaments from topography, and implications for CO<sub>2</sub> storage). The objective of Subtask 6.1 was to compile significant published data related to structures in the areas of interest, as well as collect new fracture data (Figures 6.1-1 to 6.1-120, Figures 6.1-127 to 6.1-182) in selected areas in order to be able to predict:

- 1) Fracture trends
- 2) Presence of fault systems and the trends of these fault systems

Additionally, published lineaments along steep aeromagnetic gradients in part of the project area were also compiled in this section (Figures 6.1-121 to 6.1-126).

The objective of Subtask 6.2 was to identify lineaments along aeromagnetic anomalies in the entire project area (Figures 6.2-1 to 6.2-3). The steep aeromagnetic gradients may indicate fault locations. The locations of the aeromagnetic lineaments were compared to the EarthSat (1997) lineaments in order to ascertain which LandSat lineaments (EarthSat, 1997) represented structural features that extend into the Precambrian basement, since aeromagnetic anomalies larger than about 50 nT in central NYS generally arise from magnetic contrasts (induced and remnant) in the basement (Jacobi, 2007a). The aeromagnetic lineaments thus function as a type of “groundtruth” for the LandSat lineaments.

Subtask 6.3 is the “Results” section of Task 6, Part A. The “Results” section uses the compiled database of structural information from Subtasks 6.1 and 6.2 to determine the possibility and character of faults and fractures near the AES power plants. These considerations can be used as both an exclusionary factor (for faults) near the targeted power plants and as a tool to assist in predicting fracture character (spacing and trends) near the power plants as part of the planning process for optimum injection of CO<sub>2</sub>.

The data maps in Subtasks 6.1 and 6.2 are digital and georeferenced in a GIS environment. The GIS program used for georeferencing and for display is ArcView. All digitization of data and construction of

figures in Subtasks 6.1 and 6.2 was accomplished by Fisher; Jacobi calculated the data in the tables and wrote the report (except for the methodology section, on which they both collaborated). Field work was performed by Fisher and Jacobi.

### **Methodology**

**Previous Studies (Subtask 6.1).** A comprehensive suite of structural maps of the five focus areas in the project area of New York State was synthesized through the compilation of previous studies in the region. The data compilation included lineaments, faults and fractures. In order to organize the large amount of previous research, a database of publications and unpublished theses was constructed in Microsoft Excel. Some of the prior research was already in a digital, georeferenced format, such as certain data in the Seneca Lake area (e.g., Drechsel et al., 2004; Cruz et al. 2005; Cruz, 2005). For the non-georeferenced, non-digital data sources, Ms. Fisher digitized the germane material in Arc GIS version 9. This digitization was accomplished by first georeferencing a scanned image of the published figure or georeferencing a PDF the published. The relevant features of the figure were then digitized. The digitized images were converted into layers in Arc GIS version 9 and then were used in the creation of a series of figures displayed in this report.

An issue with georeferencing images in Arc GIS is the number of control (georeference) points used during the georeferencing (warping) process. Although in early versions of Arc INFO, only a few points (3) could be handled optimally by the program, in recent versions of Arc GIS, warping with relatively numerous points is possible, and optimal. Another issue is possible distortions in the original figures due to drafting problems or unknown/faulty map projections. It is therefore better to georeference maps that cover small areas (on the order of a single county) so that these possible errors are not promulgated and amplified across large distances. Most layers were therefore originally digitized for each county and then joined.

Unpublished theses from the University of Buffalo provided an important data source for fracture maps. Map layers displaying the orientation and frequency of fractures at outcrops were created from Excel tables that were imported into Arc GIS. The tables were constructed from the data in the theses or in some cases existing thesis tables were reworked. The tables included information such as the latitude and longitude of each site, the fracture sets observed in outcrop, the strike and dip of the fractures, the actual spacing of the fractures<sup>1</sup>, and master and abutting relationships with other fracture sets, and the rock type (black shale sites were separated from the other sites). The fracture frequency and standard deviation of the fracture frequency were calculated for each site. These data and calculations were imported into Arc GIS and a database file was created. The sites were then displayed as points on the base map with an attribute table showing all of the frequency and orientation data. The frequency of each fracture set (based on the fracture

---

<sup>1</sup>or the apparent spacing along a scanline between fractures of the same set; these apparent spacings must be corrected to true spacings.

orientations at each site) was then queried. The selected features from the query were then exported into their own layer and added the synthesized map.

**Limited Field Studies (Subtask 6.1).** Limited field studies of fractures were conducted in the region of the AES Cayuga power plant since a decision was made by the members of the research team (including the AES representatives) that the AES Cayuga power plant would be the probable focus of any further research (Phase II), based primarily on early data concerning the capability to sequester CO<sub>2</sub> in sands. The fracture data were collected at various sites near the power plant using the abbreviated method (e.g., Jacobi and Zhao, 1996; Jacobi, 2007). Data included latitude and longitude of each site from a GPS unit, the fracture sets observed in outcrop, the strike and dip of the fractures for each set, the actual spacing of the fractures for each set, the master and abutting relationships with other fracture sets and sedimentary rock units, the observed length and height of the fractures, and the rock type and unit thickness.

The fracture frequency and abutting relationships of the fracture sets at each site are shown in modified rose diagrams (e.g., Jacobi, 2007). The modified rose diagrams display the fracture frequency of the various observed fracture sets in the upper half of modified rose diagrams and present the order of fracture development (based on abutting relationships) in the lower half of the rose diagrams. Modified rose diagrams were created in Adobe Illustrator. The modified rose diagrams were added to the base geography maps at their proper field location.

In order to determine statistically the degree of coincidence among the fracture measured in outcrop and the various lineament data sets in the AES Cayuga power plant region, a weights of evidence statistical analysis was conducted (for more details, see Jacobi, 2007). The lineament sets included those from Landsat images (EarthSat, 1997), ASTER images (this report) and DEM images (this report). This analysis entails creating areal buffers around the lineaments and around the outcrops. The area of buffer overlaps among lineaments of a certain orientation and sites with fractures of the same orientation is then calculated and compared to the total area. These operations are conducted for each orientation set of fractures and lineaments. The resulting number (contrast index) yields a relative measure of the coincidence of lineaments with outcrop fractures with the same orientation; i.e., the contrast index value provides a measure of the relative strength of the groundtruthing of the lineaments.

**Lineaments of Aeromagnetic Gradients (Subtask 6.2).** In the project area Jacobi picked the location of lineaments along the steepest portion of significant aeromagnetic gradients that are linear in map view; the source was a generalized aeromagnetic anomaly map from Jacobi (2002) (Figures 6.2-1 to 6.2-3). The aeromagnetic lineaments should be viewed as general locations and trends. The lineaments along anomalies greater than about 50 nT most likely represent Grenvillian lithofacies contacts that commonly are faults. The aeromagnetic lineaments (Figure 6.2-2) were picked by Jacobi first, without reference to



EarthSat (1997) or other lineaments or fault maps, in order to preserve an unbiased view of the aeromagnetics. Then the EarthSat (1997) lineaments were inspected with respect to the aeromagnetic lineaments and gradients, and the EarthSat (1997) lineaments that were collinear and near the aeromagnetic gradients were highlighted by Jacobi (in white on Figure 6.2-3). Fisher accomplished the digitization of the lineaments in Arc GIS.

### **Data Sets (Subtasks 6.1 and 6.2)**

Published data sets that can aid in identifying the location and trends of fault systems in the project area, and more specifically, in the vicinity of the power plants include:

- 1) Lineaments from remotely sensed images, such as those from
  - a) EarthSat (1997, Figures 6.1-3, 6.1-5), and
  - b) Isachsen and McKendree (1977, Figures 6.1-4, 6.1-5),
  - c) Pyron et al. (2003, Figure 6.1-180)
- 2) Lineaments along prominent aeromagnetic gradients
  - a) Jacobi (2007) aeromagnetic lineaments based on high resolution aeromagnetic data in the Keuka-Seneca-Cayuga lakes area (Figure 6.1-121 to 6.1-126)
- 3) Selected published major fault systems including those
  - a) proposed by Jacobi (2002, Figure 6.1-6), based on integrated geophysical and geological data sets),
  - b) miscellaneous local faults observed in outcrops (e.g., Sheldon, 1912, Figure 6.1-55).
  - c) high-structural level folds that were first mapped by Wedel (1932, Figure 6.1-7a), confirmed in the Seneca Lake region by Bradley et al. (1941, Figure 6.1-7b), and modified by Jacobi (2007) in the Seneca and Cayuga lakes region. The folds are related to thrust ramps off decollement in the Silurian salt section. The location and trend of the folds is partly controlled by deeper high angle fault systems in western NYS (e.g., Jacobi et al., 2003; 2004 a, b; 2005; 2006; 2007) and western Pennsylvania (Scanlin and Engelder, 2003). These deep faults are believed to be Iapetan-opening faults that were reactivated several times during later orogenies (e.g., Jacobi et al., 2003; 2004 a, b; 2005; 2006; 2007).

Published data sets that can aid in characterizing the fracture fabric in the project area and more specifically in the vicinity of the power plants are sourced primarily from two groups of investigators: the fracture study group headed by Engelder (e.g., Engelder and Geiser, 1980), and the University at Buffalo Rock Fracture Group (UBRFG) guided by Jacobi (e.g., Jacobi et al., 2003). Both the Engelder group and the Jacobi group have produced detailed data sets in the Seneca/Cayuga region, but only the Jacobi group has examined the structure in parts of the eastern focus area (e.g., Jacobi, 2007). Miscellaneous studies include the early fracture study in the southern reaches of Cayuga Lake (Sheldon, 1912), the Cornell faculty and students along the eastern side of Cayuga Lake (Cornell faculty and students, 1959), and the fractures analyzed for

this project at outcrops near the Cayuga power plant (Figures 6.1-100 to 6.1-117). All studies reveal the trend of fracture systems, but only the UBRFG studies routinely document 11 characteristics of the fractures, including the fracture spacing of each set and the abutting relationships.

The data sources for Set I (“cross-strike” or J2) fractures include:

- a) Engelder & Geiser (1980) in central NYS (Figures 6.1-9, 6.1-13, and 6.1-16)
- b) Faculty and Students of Cornell University (1959) in the Cayuga Lake area (Figure 6.1-10)
- c) Younes & Engelder (1999) in the project area (Figures 6.1-20, 6.1-23)
- d) Lugert et al (2001), Cruz (2005) and Jacobi (2007) between Seneca and Cayuga lakes (Figures 6.1-35 to 6.1-40)
- e) Sheldon (1912) along the shores of Cayuga Lake (Figure 6.1-55)
- f) Wehn et al. (2002) and Jacobi et al. (2002, 2003) on the western shore of Cayuga Lake (Figures 6.1-67 to 6.1-72 and a more detailed view in Figures 6.1-89 to 6.1-94)
- g) Fracture data collected for this project near the Cayuga power plant on the east side of Cayuga Lake (Figures 6.1-102 to 6.1-104, 6.1-112 and 6.1-115)
- h) Terech et al (2005 and Jacobi (2007) in the northern part of the eastern region of the project area (Figures 6.1-137 to 6.1-139)
- i) McGuire et al. (2006) and Jacobi (2007) in the eastern project region (Figures 6.1-162 to 6.1-164)
- j) Engelder and Oertel (1985, Figure 6.1-181)
- k) Parker (1942, Figure 6.1-182)

The data sources for Set II (“strike or fold parallel”) fractures include:

- a) Engelder & Geiser (1980) in central NYS (Figures 6.1-11 to 6.1-16)
- b) Faculty and Students of Cornell University (1959) in the Cayuga Lake area (Figure 6.1-18)
- c) Younes & Engelder (1999) in the project area (Figure 6.1-25)
- d) Lugert et al (2001), Cruz (2005) and Jacobi (2007) between Seneca and Cayuga lakes (Figures 6.1-47 to 6.1-49)
- e) Wehn et al. (2002) and Jacobi et al. (2002, 2003) on the western shore of Cayuga Lake (Figures 6.1-59 to 6.1-61 and a more detailed view in Figures 6.1-82 to 6.1-84)
- f) Fracture data collected for this project near the Cayuga power plant on the east side of Cayuga Lake (Figures 6.1-101 to 6.1-104, and 6.1-107 to 6.1-108)
- g) Terech et al (2005 and Jacobi (2007) in the eastern part of the project area (Figures 6.1-149 to 6.1-151)
- h) McGuire et al. (2006) and Jacobi (2007) in the eastern project region (Figures 6.1-174 to 6.1-176)
- i) Engelder and Oertel (1985, Figure 6.1-181)
- j) Parker (1942, Figure 6.1-182)

The data sources for other strain markers consistent with Set II fractures (long axes of crinoids) include

- a) Engelder & Oertel (1989, Figures 6.1-29, 6.1-30)

The data sources for Set III (“J1”) fractures include:

- a) Faculty and Students of Cornell University (1959) in the Cayuga Lake area (Figure 6.1-17)
- b) Younes & Engelder (1999) in the project area (Figure 6.1-25)
- c) Lugert et al (2001), Cruz (2005) and Jacobi (2007) between Seneca and Cayuga lakes (Figures 6.1-44 to 6.1-46)
- d) Sheldon (1912) along the shores of Cayuga Lake Figure (6.1-55)
- e) Wehn et al. (2002) and Jacobi et al. (2002, 2003) on the western shore of Cayuga Lake (Figures 6.1-56 to 6.1-58 and a more detailed view in Figures 6.1-79 to 6.1-81)
- f) Fracture data collected for this project near the Cayuga power plant on the east side of Cayuga Lake (Figures 6.1-105 and 6.1-106)
- g) A limited number of Set III (J1) fractures in the northern part of the eastern project region by Terech et al (2005) and Jacobi (2007) (Figures 6.1-128 to 6.1-130)
- h) A limited number of Set III (J1) fractures in the eastern project region by McGuire et al. (2006) and Jacobi (2007) (Figures 6.1-154 to 6.1-156)
- k) Engelder and Oertel (1985, Figure 6.1-181)
- l) Parker (1942, Figure 6.1-182)

### **Results (Subtask 6.3)**

**Overview.** Inspection of figures that compare the location of the AES power plants to EarthSat (1997) lineaments (Figures 6.1-3 and 6.1-5) and Isachsen and McKendree (1977) lineaments (Figures 6.1-4 and 6.1-5) to the proposed major fault systems from Jacobi (2002) (Figure 6.1-6) reveals that all five AES power plants are close to bands of lineaments that were interpreted as faults by Jacobi (2002). All but the Westover AES power plant near Binghamton are in close proximity to proposed reactivated high angle Iapetan-opening faults (e.g., Jacobi et al., 2004a; Jacobi 2010) that have an east-northeasterly trend in the project area (Figure 6.1-6). These faults are generally steeply dipping fault systems that affect basement. All were active during Iapetan opening time, but they experienced variable amounts of motion in the following orogenies (e.g., Jacobi 2010). Depending upon their fault motion history, some of these fault systems extend to the (near) surface, and the fracture systems associated with the faults do reach the surface, as evidenced by the coincident lineaments. The Iapetan-opening faults that were reactivated during the Taconic Orogeny were pathways for fluid migration that resulted in the Trenton/Black River gas reservoirs in the southern tier of NYS (e.g., Jacobi et al., 2004a, b) near the Hickling power station and possibly near the Cayuga power plant. In the Hickling power plant region, these faults have relatively close spacings (across the ENE strike), on the order of 1.5-2.5 km (unpublished proprietary data). The length between major along-strike variations in the faults (e.g., cross fault trends) has a range between 1.5 km and 10 km (unpublished proprietary data). Based on the fault systems exposed at the surface (e.g., Jacobi 2002, 2007), it is probable that a closely-spaced fracture set parallel to the faults is localized along the faults in

most units except possibly the Utica and deeper carbonates. The spacing of the fractures parallel to the faults could vary from about 4 to as many as 20 fractures/m.

All AES power plants in the project area also are close to northerly-trending lineament bands (Figures 6.1-3 to 6.1-5). For example lineaments trending approximately parallel to the east shore of Cayuga Lake and the west shore of Seneca Lake pass near the Cayuga and Greenidge power plants, respectively. Both these trends have been interpreted as fault systems (Jacobi, 2002, 2007, and references therein). These fault systems are believed to be intra-Grenvillian sutures (terrane boundaries) that have been episodically reactivated (e.g., Jacobi, 2002).

High structural level salt-cored anticlines that commonly involve thrust ramps off the Silurian salt decollements occur near the Westover and Cayuga power plants (Figure 6.1-7a). Since these anticlines are restricted to units above the Silurian evaporate seal, and all the CO<sub>2</sub> sequestration targets are below the Silurian evaporate seal, these anticlines are not a significant factor in the considerations a CO<sub>2</sub> sequestration site. However, 3D seismic surveys in eastern NYS (Jacobi, 2011; Jacobi et al. 2011) confirmed earlier suppositions based on 2D seismic reflection data (e.g., Scanlin and Engelder, 2003; Jacobi, 2010) and the coincidence of the folds with aeromagnetic anomalies (Jacobi, 2002, 2003a,b, 2004, 2005, 2010) that steeply-dipping faults systems extending from the basement do appear to control the fabric of the anticlines, i.e., the trend and general location of the anticlines do seem to correspond with deeper structures. Jacobi et al (2007) suggested that the reactivated faulting and associated fracturing halo above the fault weakened the structural members above the salt sufficiently to localize thrust ramps off the salt decollement. Additionally, it is a traditional view that actual offsets on relatively steeply dipping faults can provide a “nick-point” that will control the location of a ramp (and thus an anticline). This scenario suggests that although the anticline itself is not a concern, it may be a “smoking gun” that indicates structure below the salt.

The regional orientation of the predominant fracture sets (sets I, II, and III) can be estimated from the fracture orientations displayed in Figures 6.1-8 to 6.1-25. These expected fracture trends are collated in Tables 6.1-1 to 6.1-10. It should be noted that while in general Set I fractures trend from NNW to NNE, Set II fractures strike from ENE to WNW, and Set III fractures we assume trend ENE. All these sets can be represented by long, relatively planar fractures. The spacing of these fracture sets is not known at depth, but at the surface in Upper Devonian interbedded shales and siltstones the spacing is generally on the order of less than 1 fracture/m for Set I, 1 fracture/m for Set II, and variable spacing for Set III. The strike of fractures at local sites may vary from the regional view, although sets I and II appear to be locally slightly more stable than Set III (e.g., Jacobi, 2011d; Jacobi et al., 2009, 2010). In addition to sets I, II and III, local zones of fracture intensification (FIDs, e.g., Jacobi and Fountain, 1996) related to faults can locally affect sites. These FIDs are seldom very wide (usually <40m), but they can disrupt the expected fracture patterns.

Knowledge of the fault locations and strikes can assist in predicting the possibility of FIDs in the same areas as the faults.

Estimates concerning the extent to which the fracture spacing varies with depth are poorly constrained by published reports for New York State. Hickman et al. (1985) found that near-vertical fractures were present down the entire 1540 m well through Lower Paleozoic units at Auburn, NY (north of the project area). In this well the observed spacing of all fractures intersecting the hole varied more among units, rather than down hole. Higher fracture frequencies were observed in much of the Queenston, Trenton, lower Black River Group, Theresa, and the Precambrian marble near the contact with the Paleozoic. In contrast, almost no fractures crossed the well bore in the Lorraine/Utica, a ~ 90 m section in the upper part of the Queenston, the Medina Group, and the Clinton Group. Significantly, the fracture frequency of open fractures remains, overall, rather constant to the Precambrian basement marbles. The lack of fractures in the Lorraine/Utica at depths between ~880 m and 1050 m is consistent with a detailed structure study of a 360 m core in the Utica/Lorraine section in eastern NYS (Hanson et al., 2010, 2011, Jacobi, 2011e). No natural, steeply dipping, macroscopic (visible to the eye), open fractures were observed in the entire core (although many vein-filled fractures were evident). The lack of fractures was typical not only of the Utica black shale, but also the overlying “Lorraine” dark gray shale that is interbedded with thin turbidites/storm beds. Proprietary information in eastern New York also suggests that even faults may be tight in the some shaly units of the Clinton Group. This tight nature is in contrast to fractures (both steeply dipping and horizontal) observed down hole in the Vernon Shale of the Salina Group.

Outside of NYS, several studies show that fractures can be found to considerable depth. For example, Laubach (2003) found open fractures at -5910 ft (1800 m) in the Weber Sandstone in the Rangley Field in Colorado, and identified open fractures as deep as -7828 ft (~2400 m) in the Wolfcamp Sandstone in west Texas. In the review of natural fracture distribution with depth in crystalline rocks Seeburger and Zoback (1982) indicated that in two wells drilled to -1200 m in granodiorites in South Carolina, fractures did not show any significant reduction in number with depth. Even horizontal fractures were observed in both wells at about 1000 m depth.

Thus, it appears that fractures in shales are sealed/annealed at some depth, but some fractures in coarser-grained material can remain partly open, even in presently compressional conditions, perhaps because of natural proppants, partial vein-filling (cement) bridging the fracture, or slight mis-alignment of micro decorations on the fractures surface that prop the fracture open when the fracture enters a compressive regime after development in an extensional regime.

Estimates concerning the down-section stability of the fracture strikes are also poorly constrained by published reports for New York State. Hickman et al. (1985) found that the fracture strikes did not deviate

significantly in the Paleozoic section from -400 to -1550 m, except for fractures in the Queenston. This deviation in the Queenston could be misleading, and merely a function of the small number of fracture observations made down hole in a complicated fracture network. Conversely, the variance could also indicate a different fracture history for this unit, either in time or space. For example, an undetected fault could be close to the Queenston section of the well, resulting in a local stress deviation at the time of fracture development. In homogenous crystalline rocks in a region with fairly uniform stress gradients, Seeburger and Zoback (1982) showed that fractures did not show any significant strike variations with depth. Additionally, proprietary data from wells in eastern NYS did not indicate significant variance in fracture strike downsection in areas where local high structural level features (salt cored anticline) did not occur. 3D seismic in eastern and central NYS shows that, except for the high structural level features), most of the faults dip steeply and the fault systems extend for kms. Possible FIDs associated with the faults at the surface, therefore, should remain with the same strike at depth. Local areas where transfer zones are located between tails of fault segments may have complicated fractures patterns that may not be uniform downsection.

In conclusion, as a first estimate (“best guess”), the local fracture and fault patterns observed or predicted at the surface near a power plant can be used as an indicator of the patterns at depth, recognizing the caveat that it is possible that the surface patterns may not characterize the patterns at certain depths or areas.

#### **Specific Location: Hickling Power Plant.**

**Lineaments and Faults.** This power plant is located near Corning, NY (e.g., Figure 6.1-1). Strongly developed, long lineaments were identified in the Landsat data by EarthSat (1997) that pass close to the power plant (Table 6.1-1). Within 8 km of the plant site, four lineaments trending ENE (N54<sup>0</sup>E to N80<sup>0</sup>E) range from 0 to 5.3 km away from the plant site. These lineaments most likely represent the arcuate (in map view) Iapetan-opening fault set (e.g., Jacobi, 2010). Five related lineaments are the NE/NNE-trending lineaments (N32<sup>0</sup>E to N47<sup>0</sup>E) that range from 2.2 to 7.6 km away from the plant site. Two NW-trending lineaments (312<sup>0</sup> to 326<sup>0</sup>) occur within 7 km of the site, as does one N-trending lineament. Earlier lineament identification by Isachsen and McKendree (1977) also found seven NE/ENE trending lineaments within 8 km of the plant site (Table 6.1-1). Some of these lineaments are coincident with those of EarthSat (1997). High structural level ENE-striking faults were identified by Isachsen and McKendree (1977) and Murphy (1981) about 3 to 11 km away from the site. Similar ENE-striking faults in the region (4 to 17 km from the site) were proposed by Jacobi (e.g., Jacobi, 2002, 2007a). Finally, Wedel (1932) mapped high structural level, salt-cored folds in the region, the closest about 3.5 km away from the plant site.

Where seismic reflection data lies beneath the ENE/NE lineaments, reactivated Iapetan-opening faults are imaged in (e.g., Jacobi, 2007a; 2010). Individual faults in these fault system have different reactivation histories. Some ceased activity after the Taconic orogeny, whereas others ceased activity during the Salinic. Still others appear to have been reactivated even more recently, in the Acadian and Alleghanian orogenies, and some near the Mohawk Valley remain active. That these lineaments are observed at the surface suggests that fracture sets associated with the faults extend to the top of bedrock. As discussed above, the high structural level salt cored folds are above the targeted stratigraphic levels, but these folds and associated faults are commonly indicators of deeper structures. Thus, all indicators are that this site has a number of reactivated Iapetan-opening faults in close proximity

The ENE-striking faults have relatively close spacings (across the ENE strike), on the order of 1.5-2.5 km (unpublished proprietary data). The length between major along-strike variations in the faults (e.g., cross fault trends) has a range between 1.5 km and 10 km (unpublished proprietary data). Based on ENE-striking fault systems exposed at the surface (e.g., Jacobi 2002, 2007a), it is probable that a closely-spaced fracture set parallel to the faults is localized along the faults in most units except possibly the Utica and deeper carbonates. The spacing of the fractures parallel to the faults could vary from about 4 to as many as 20 fractures/m.

**Fractures.** As detailed in table 6.1-2, the cross-strike (Set I, J2) fractures in the region of the AES Hickling power plant trend about  $326^{\circ}$ , and the along-strike (set II) fractures strike between  $64^{\circ}$  and  $82^{\circ}$ . Set III (J1) fractures are difficult to distinguish from Set II fractures in this region, since Set III (J1) fractures have been proposed to strike consistently ENE across the state, especially in black shales (e.g., Engelder and Geiser, 1980; Lash et al., 2004; Engelder et al., 2009). However, against that regional background of ENE-striking J1 fractures, it is not uncommon to find Set III fractures with variable trends, and non-existent in some areas, even in black shales (e.g., Jacobi and Smith, 2000; Jacobi et al., 2010; 2011b; Jacobi, 2011c). It is thus not possible to predict with certainty what the orientation of J1 will be at the site, but a best guess is ENE. Fracture intensification domains (FIDs, Jacobi and Fountain, 1996) associated with the fault zones may add local additional fracture systems, especially the ENE-striking fault systems. Fracture spacing has not been published in this region for surface bedrock, but elsewhere the fracture spacings are generally about 1 or 2 fractures/m or less, except for FIDs where the fracture frequency can increase to more than 20 fractures/m, and

generally are above 4 fractures/m, and in black shales, where the ENE J1 set can have high fracture frequencies as well.

### **Specific Location: Greenidge Power Plant.**

**Lineaments and Faults.** This power plant is located near the western shore of Seneca Lake, about midway along the length of the lake (e.g., Figure 6.1-1). Strongly developed, long lineaments were identified in the Landsat data by EarthSat (1997) that pass close to the power plant (Table 6.1-3). Predominant trends include ENE, NNE and EW/WNW. Within 8 km of the plant site, nine lineaments trending ENE (N64<sup>0</sup>E to N74<sup>0</sup>E) are disposed in two bundles; these ENE-trending lineaments are from 2.7 to 7.1 km away from the plant site. These lineaments most likely represent the arcuate (in map view) Iapetan-opening fault set (e.g., Jacobi, 2010). A large number of EW trending lineaments (274<sup>0</sup> to 287<sup>0</sup>) also occur within 7 km of the site. These lineaments may represent another fault trend that was active during Iapetan opening times, and was certainly active during the Taconic (e.g., Jacobi, 2007a, 2010). Their trend is consistent with high-structural level salt-cored folds that are mapped to the south, and may therefore also represent small, unmapped faults/folds associated with times of salt deformation. Five NNE trending lineaments (33<sup>0</sup> and 38<sup>0</sup>) are located within 7 km of the site. These lineaments are associated with prominent aeromagnetic gradients that indicate these lineaments represent fault systems that are basement-rooted, and part of the Keuka Lake fault system (e.g., Jacobi, 2007a). One NW-trending lineament (322<sup>0</sup>) is passes through the power plant site, and two NNW-trending lineaments (348<sup>0</sup> and 352<sup>0</sup>) are located within 7 km of the site. Two northerly-trending lineaments also are located farther from the site than the lineaments discussed above (8-13 km). Earlier lineament identification by Isachsen and McKendree (1977) also found one ENE-trending lineament within 7 km of the plant site, one EW-trending lineament within 2.5 km, and two northerly trending lineaments 4 and 10 km away from the site. Some of these lineaments are coincident with those of EarthSat (1997).

Jacobi's (2002) proposed fault systems generally replicate the trends found in the EarthSat (1997) and Isachsen and McKendree (1977) data: ENE, NNE, and EW/WNW (Table 6.1.3). These proposed fault systems pass the site within about 8 km. The proposed EW-striking fault closest to the site (at 2 km) is the same fault system as that proposed by Bradley et al. (1941) and Murphy (1981). Bradley et al. (1941) and Murphy (1961) proposed another E-striking fault farther from the site (5.3 and 5.8 km respectively) that is probably the same fault system, and which is in the same general location as the E-trending EarthSat (1997) lineaments #14 and 15 and Isachsen and



McKendree (1977) lineament #2. The proposed faults based on steep aeromagnetic gradients (Jacobi, 2007) trend NNE and ENE, and the ENE-trending lineament is approximately coincident with an ENE-trending EarthSat (1997) lineament (#19) that is part of a bundle of ENE-trending lineaments. Finally, Wedel (1932) mapped high structural level, salt-cored folds in the region to the south of the power plant site, the closest about 8 km away.

No seismic reflection data has been examined in the close vicinity of the Greenidge power plant. However, where seismic reflection data does exist beneath the ENE/NE lineaments, reactivated Iapetan-opening faults are imaged in (e.g., Jacobi, 2007; 2010). As discussed above individual faults in these fault system have different reactivation histories. Some ceased activity after the Taconic orogeny, whereas others ceased activity during the Salinic. Still others appear to have been reactivated even more recently, in the Acadian and Alleghanian orogenies, and some near the Mohawk Valley remain active. That these lineaments are observed at the surface suggests that fracture sets associated with the faults extend to the top of bedrock. The high structural level salt cored folds are above the targeted stratigraphic levels, but these folds and associated faults are commonly indicators of deeper structures. Thus, all indicators are that this site has a number of reactivated Iapetan-opening faults in close proximity. The tightly spaced nature of the EarthSat (1997) ENE-trending lineaments in the lineament bundles suggests that these fault systems are closely spaced, similar to that found to the south near the Hickling power plant (see discussion above)

**Fractures.** As detailed in Table 6.1-4, no fractures were measured close to the AES Greenidge power plant site; rather the outcrops are from 6 to 16 km away from the power plant. The cross-strike (Set I, J2) fractures in the region of the Greenidge power plant trend between  $318^{\circ}$  to  $336^{\circ}$  (with a second N-striking set) and the along-strike (set II) fractures strike between  $80^{\circ}$  and  $274^{\circ}$ . Fractures with more ENE strikes ( $54^{\circ}$ ,  $72^{\circ}$ , and  $74^{\circ}$ ; Engelder and Geiser, 1980 and Younes and Engelder, 1999) that are nominally Set II fractures in Engelder and Geiser (1980) could also be set III (J1) fractures. Set III (J1) fractures are difficult to distinguish from Set II fractures in this region, since Set III (J1) fractures have been proposed to strike consistently ENE across the state, especially in black shales (e.g., Engelder and Geiser, 1980; Lash et al., 2004; Engelder et al., 2009). However, against that regional background of ENE-striking J1 fractures, it is not uncommon to find Set III fractures with variable trends, and non-existent in some areas, even in black shales (e.g., Jacobi and Smith, 2000; Jacobi et al., 2010; 2011b; Jacobi,

2011c). It is thus not possible to predict with certainty what the orientation of Set II and Set III J1 will be at the site, but a best guess is nearly EW and ENE, respectively.

Fracture intensification domains (FIDs, Jacobi and Fountain, 1996) associated with the fault zones may add local additional fracture systems, especially the ENE-striking fault systems. Fracture spacing have been calculated for outcrops about 6 to 7 km SSE of the power plant in this region for surface bedrock (Lugert et al, 2001, Cruz, 2005, Jacobi, 2007, see Table 6.1-4 and Figures 6.1-35 to 6.1-40 and Figures 6.1-45 to 6.1-49). It is evident from these figures that Sets I, II and III display fracture frequencies of < 4 fractures/m at most outcrops, with more outcrops at < 2 fractures/m. The exceptions are FIDs where the fracture frequency can increase to more than 20 fractures/m, and generally is above 4 fractures/m, and in black shales where the ENE J1 set can have high fracture frequencies as well.

#### **Specific Location: Cayuga Power Plant.**

**Lineaments and Faults.** This power plant is located near the eastern shore of Cayuga Lake, about 20 km north of Ithaca (e.g., Figure 6.1-1). Strongly developed, long lineaments were identified in the Landsat data by EarthSat (1997) that pass close to the power plant (Table 6.1-5). The predominant trend is ENE-trending lineament bundles; other trends include a NS-trending lineament bundle, NW-and E- trending lineaments. Within 12 km of the plant site, eight lineaments trending ENE ( $60^{\circ}$  to  $72^{\circ}$ ) are disposed in two bundles; these ENE-trending lineaments are from 1.4 to 11.6 km away from the plant site. These lineaments most likely represent the arcuate (in map view) Iapetan-opening fault set (e.g., Jacobi, 2010).

An EW trending lineament ( $276^{\circ}$ ) also occurs within 1 km of the site. These lineaments may represent another fault trend that was active during Iapetan opening times, and was certainly active during the Taconic (e.g., Jacobi, 2007, 2010). Their trend is also consistent with high-structural level salt-cored folds that are mapped to the south, and may therefore also represent small, unmapped faults/folds associated with times of salt deformation. One NW-trending lineament bundle (with lineaments trending  $320^{\circ}$  and  $326^{\circ}$ ) passes about 10 km east of the power plant site, and a northerly-trending lineament bundle is located farther from the site than the lineaments discussed above (8-13 km). The northerly-trending lineaments probably represent faults like the Clarendon-Linden Fault System, which is an intra-Grenvillian suture fault system that was reactivated during all subsequent orogenies for which we have a rock record (e.g., Jacobi and Fountain, 1996, 2002). Earlier lineament identification by Isachsen and McKendree

(1977) also found one ENE-trending lineament within 7 km of the plant site and one northerly trending lineament about 10 km away from the site (Table 6.1-5). Both of these lineaments are coincident with those of EarthSat (1997).

NE-trending steep aeromagnetic gradients (with trends between  $50^{\circ}$  and  $54^{\circ}$ , Jacobi, 2007, Table 6.1.-5) intersect the Cayuga lakeshore area in the vicinity of the ENE-trending EarthSat (1997) lineaments. A NW-trending aeromagnetic lineament occurs along the lake shore at the power plant site (Jacobi, 2007, Table 6.1.-5).

Jacobi's (2002) proposed fault systems generally replicate the trends found in the EarthSat (1997) and Isachsen and McKendree (1977) data: ENE, EW, and NS/NNW (Table 6.1.5). The proposed ENE and EW-striking fault systems pass the site within about 2 km, and the NS fault is located about 8 km to the west. Murphy's (1981) well-log-based northerly-striking fault at Ithaca (southeast of the power plant), is on strike with the N-trending EarthSat (1997) lineament bundle and Jacobi's (2002) proposed faults located to the north (and about 8 km east of the power plant). Finally, Wedel (1932) mapped high structural level, salt-cored folds in the region to the south of the power plant site, the closest about 7 km away.

Proprietary seismic reflection data in the close vicinity of the power plant indicated that both the ENE and the EW lineaments do reflect the general fabric of predominant faults, and that these faults were active in the Taconic. These faults probably are reactivated Iapetan-opening faults. As discussed above individual faults in these fault systems have different reactivation histories. The northerly-striking fault at Ithaca proposed by Murphy (1981) is based on well log analyses and thus confirms the along-strike proposed faults east of the power plant based on lineaments. The high structural level salt cored folds are above the targeted stratigraphic levels, but these folds and associated faults are commonly indicators of deeper structures. Thus, all indicators are that this site has a number of fault systems in close proximity to the power plant. The tightly spaced nature of the EarthSat (1997) ENE-trending lineaments in the lineament bundles suggests that the faults in the fault systems are closely spaced, similar to that found to the south near the Hickling power plant (see discussion above).

**Fractures.** As detailed in Table 6.1-6, no fractures were measured by Engelder and Geiser (1980) close to the AES Cayuga power plant site; rather their outcrops are from 5 to 11 km away from the power plant. Engelder and Geiser's (1980) cross-strike (Set I, J2) fractures in the region of the Cayuga power plant strike between  $336^{\circ}$  and  $340^{\circ}$  (with a second N-striking set) and the along-strike (set II) fractures strike between  $70^{\circ}$  and  $274^{\circ}$ ,

with a concentration at about  $84^{\circ}$ . Detailed fracture analyses along Seneca and Cayuga lakes (Lugert et al, 2001, Cruz, 2005, Jacobi, 2007) determined that Set II generally trends about EW to  $80^{\circ}$  in this region, and that the Set III (J1) fractures definitely have a more ENE strike at about  $60^{\circ}$ - $70^{\circ}$ . Thus, fractures with more ENE strikes ( $70^{\circ}$ ) that are nominally Set II fractures in Engelder and Geiser (1980) could also be set III (J1) fractures. Set III (J1) fractures are difficult to distinguish from Set II fractures in this region, since the ENE ( $60^{\circ}$ - $70^{\circ}$ ?) strike of Set III (J1) fractures is close to the  $80^{\circ}$ - $90^{\circ}$  strike of Set II fractures. Additionally, it is not uncommon to find Set III fractures with variable trends, and non-existent in some areas, even in black shales (e.g., Jacobi and Smith, 2000; Jacobi et al., 2010; 2011b; Jacobi, 2011c). It is thus not possible to predict with certainty what fracture orientations will occur at the site with respect to Set II and Set III, but a best guess is nearly EW and ENE, respectively.

Detailed fracture data collected for this project in close proximity to the power plant (Figures 6.1-102 to 6.1-104) show that the Set I fractures strike NNW/NW with generally low fracture frequencies, except for a few FIDs. ENE-striking fractures with low fracture frequencies are typical (Figures 6.1-102 and especially 6.1-103), but near the power plant E-striking fractures are observed in some outcrops (Figure 6.1-102). The E-striking fractures may be Set II and related to the folds in the area, whereas the ENE-striking fractures may be Set III, but as discussed above, these designations in this area where the Set II and II are nearly parallel are difficult to assign. North-striking fractures are also observed (Figures 6.1-103 and 6.1-104), and are located in an area with N-trending lineaments in figure 6.1-104.

Fracture intensification domains (FIDs, Jacobi and Fountain, 1996) associated with the fault zones may add local additional fracture systems, especially the ENE-striking fault systems and NNW-trending lineaments. Fracture spacing have been calculated for outcrops about 6 to 7 km SSE of the power plant in this region for surface bedrock (Lugert et al, 2001, Cruz, 2005, Jacobi, 2007, see Table 6.1-6 and Figures 6.1-35 to 6.1-40 and Figures 6.1-45 to 6.1-49). It is evident from these figures that Sets I, II and III display fracture frequencies of  $< 4$  fractures/m at most outcrops, with more outcrops at  $< 2$  fractures/m. The exceptions are FIDs where the fracture frequency can increase to more than 20 fractures/m, and generally is above 4 fractures/m, and in black shales where the ENE J1 set can have high fracture frequencies as well. In the data collected for this project (Figures 6.1-102 to 6.1-104), FIDs are observed in NNW/NW-, NNE/N-striking fracture sets.

### **Specific Location: Westover Power Plant.**

**Lineaments and Faults.** This power plant is located about 5 km west of Binghamton (e.g., Figure 6.1-1). Strongly developed, long lineaments were identified in the Landsat data by EarthSat (1997) in close proximity to the power plant (Table 6.1-7). The most prominent trend is a bundle of six NE-trending ( $36^{\circ}$  to  $50^{\circ}$ ) lineaments that passes within 0.2 km of the power plant site (Figure 6.1-3b). Another bundle of up to six NE-trending lineaments lies about 2 km NW of the power plant. A very long NW-trending lineament passes directly through the site. The NW-trending lineaments do not form bundles, but do have a fairly regular spacing in the region of about 0.5 to 2 km apart. More widely separated N/NNW-trending lineaments also occur, including one discontinuous northerly trending lineament that passes within 0.5 km of the site. Other trends include two bundles of EW/WNW-trending lineaments about 2 km north and south of the power plant. Earlier lineament identification by Isachsen and McKendree (1977) also found one E/ENE-trending discontinuous lineament within 0.3 km of the plant site (Table 6.1-7), as well as NNW, NW, and NE-trending lineaments. A few of the Isachsen and McKendree (1977) lineaments are coincident with those of EarthSat (1997, Figure 6.1-5b, and Table 6.1-7). Jacobi's (2002) proposed fault systems generally replicate the trends found in the EarthSat (1997) and Isachsen and McKendree (1977) data: NE, NW, and farther away, EW (Table 6.1.7).

The NE and NW trends are consistent with the lineament study performed for this report (final report sections 6.2, 6.3, 6.6). The density and length of these lineaments suggests that they represent fault systems. Although no proprietary seismic reflection data was available for inspection in the vicinity of the power plant, 2D and 3D seismic reflection data of significant areal extent in the adjacent county to the NNE (Chenango County, where the Jennison plant is located) do indicate that NE/NNE and NW/WNW faults are common in this region (e.g., Jacobi, 2010, 2011a, b, d). These fault systems generally show Iapetan opening throw followed by reactivated in every orogeny, including Taconic, Salinic and younger (e.g., Jacobi, 2010, 2011a, b, d). Only several of the WNW/NW faults show no throw in Iapetan-opening times (although they were certainly active after that). The Isachsen and McKendree (1977) E/ENE-trending discontinuous lineament that passes within 0.3 km of the plant site is coincident with the fold axes of a salt-cored fold, as mapped by Wedel (1932, Figure 6.1-7a). The high structural level salt cored folds are above the targeted stratigraphic levels, but these folds and associated faults are commonly indicators of deeper structures. Thus, all indicators are that this site has a number of fault systems in close proximity to the power plant. The tightly spaced

nature of the EarthSat (1997) NE-trending lineaments in the lineament bundles suggests that the faults in the fault systems are closely spaced.

**Fractures.** As detailed in Table 6.1-8, no fractures were measured by Engelder and Geiser (1980) close to the AES Westover power plant site; rather their outcrops are from 6 to 8 km away from the power plant. Engelder and Geiser's (1980) and Younes and Engelder's (1999) cross-strike (Set I, J2) fractures in the region of the Westover power plant strike between  $350^{\circ}$  to  $354^{\circ}$  with a second N-striking set at  $2^{\circ}$  to  $7^{\circ}$ . The along-strike (set II) fractures strike between  $274^{\circ}$  and  $288^{\circ}$ . Set III (J1) fractures strike at  $71^{\circ}$ , based on parent joints reported in Younes and Engelder's (1999) about 16 km from the power plant (Table 6.1-8). Thus, in this region, Set II fractures can be differentiated from set III fractures, based on their different orientations ( $\sim 280^{\circ}$  vs.  $\sim 70^{\circ}$ ). It remains probable, however, that Set III fractures may exhibit variable trends, and be non-existent in some areas, even in black shales (e.g., Jacobi and Smith, 2000; Jacobi et al., 2010; 2011b; Jacobi, 2011c).

No outcrop fracture studies with spacing data have been carried out in the vicinity of the power plant. Based on other areas, however, Sets I, II and III (in units other than black shale units) probably display fracture frequencies of  $< 4$  fractures/m at most outcrops, with more outcrops at  $< 2$  fractures/m. The exceptions are FIDs where the fracture frequency can increase to more than 20 fractures/m, and generally is above 4 fractures/m, and in black shales where the ENE J1 set can have high fracture frequencies as well. Fracture intensification domains (FIDs, Jacobi and Fountain, 1996) associated with the fault zones may add local additional fracture systems, especially the EW and NE-striking fault systems.

#### **Specific Location: Jennison Power Plant.**

**Lineaments and Faults.** This power plant is located immediately south of Bainbridge, Chenango County (e.g., Figure 6.1-1). Strongly developed, long lineaments were identified in the Landsat data by EarthSat (1997) in close proximity to the power plant (Table 6.1-9). The most prominent trend is a bundle of four approximately E-trending ( $86^{\circ}$  to  $283^{\circ}$ ) lineaments east of the power plant that are on strike with a similar bundle west of the plant (Figure 6.1-3b). The power plant lies between the two bundles. Another prominent set of lineaments trends NE. Individual NE-trending lineate pass within 0.4 km of the site, but a 1.2 km wide bundle of 6 NE trending lineaments lies about 1.5 km from the power plant. Long NNW- and NNE-trending lineaments also pass near the site. An isolated WNW-trending lineament also lies within 0.3 km of the site. Earlier lineament identification by Isachsen and McKendree (1977) also found the same WNW-trending lineament

as well as a few NE, NNE, NNW, and EW-trending lineaments. The EW and NE-trending lineaments are approximately coincident with EarthSat (1997) lineaments (Figure 6.1-5 and Table 6.1-9). Jacobi's (2002) proposed fault systems generally replicate the trends found in the EarthSat (1997) and Isachsen and McKendree (1977) data: EW, NE, NNW, and farther away, NNW (Table 6.1.7, Figure 6.1-6).

The density and length of the NE- and EW-trending lineaments suggests that they represent fault systems. The NE-trending lineaments are consistent with the lineament study performed for this report (final report section 6.2, 6.3, 6.6). Although no proprietary seismic reflection data was available for inspection in the immediate vicinity of the power plant, 2D and 3D seismic reflection data of significant areal extent exists in Chenango County, where the Jennison plant is located. These seismic data indicate that NE/NNE-striking faults are common in this region (e.g., Jacobi, 2010, 2011a, b, d). These fault systems generally show Iapetan-opening throw followed by reactivation in every orogeny, including Taconic, Salinic and younger (e.g., Jacobi, 2010, 2011a, b, d). The approximately E-trending lineament bundle at the power plant represents faults with an unknown structural history. The high structural level salt-cored folds probably occur south of the power plant. All indicators are that this site has a number of fault systems in close proximity to the power plant. The tightly spaced nature of the EarthSat (1997) NE- and E- trending lineaments in the lineament bundles suggests that the faults in the fault systems are closely spaced.

**Fractures.** As detailed in Table 6.1-10, no fractures were measured by Engelder and Geiser (1980) close to the AES Jennison power plant site; rather their outcrops are from 23 to 29 km west-southwest of the power plant. Engelder and Geiser's (1980) and Younes and Engelder's (1999) cross-strike (Set I, J2) fractures in the region of the Jennison power plant strike between  $350^{\circ}$  to  $2^{\circ}$  with a second N-striking set at  $14^{\circ}$  to  $21^{\circ}$ . Detailed field work about 35 to 45 km WNW and NNW of the power plant (Figure 6.1-127 and Table 6.1-10) revealed that Set I fractures have a mode between  $20^{\circ}$ - $30^{\circ}$ , and the range is about  $5^{\circ}$  to  $35^{\circ}$  (McGuire et al., 2006; Terech et al., 2005 Jacobi, 2007b) Engelder and Geiser's (1980) along-strike (set II) fractures strike between  $274^{\circ}$  and  $288^{\circ}$ . The detailed field work WNW and NNW of the power plant (Figure 6.1-127 and Table 6.1-10) revealed that Set II fractures have a mode between  $285^{\circ}$ - $295^{\circ}$ , and the range is about  $280^{\circ}$  to  $315^{\circ}$  (McGuire et al., 2006; Terech et al., 2005 Jacobi, 2007b). Set III (J1) fractures strike at  $71^{\circ}$ , based on parent joints reported in Younes and Engelder (1999) about 16 km from the power plant (Table 6.1-8). In this region, Set II fractures can be differentiated from Set III fractures, based on their different orientations ( $\sim 280^{\circ}$  vs.  $\sim 70^{\circ}$ ). It remains probable, however, that Set III fractures may exhibit variable trends, and be non-existent in some areas, even in black shales (e.g., Jacobi and Smith, 2000; Jacobi et al., 2010; 2011b; Jacobi, 2011c).

No outcrop fracture studies with spacing data have been carried out in the vicinity of the power plant. Based on extensive studies about 35-45 km to the west and northwest, however, Sets I, II and III (in units other than black shale units) probably display fracture frequencies of < 4 fractures/m at most outcrops, with more outcrops at < 2 fractures/m. The exceptions are FIDs where the fracture frequency can increase to more than 20 fractures/m, and generally is above 4 fractures/m, and in black shales where the ENE J1 set can have high fracture frequencies as well. Fracture intensification domains (FIDs, Jacobi and Fountain, 1996) associated with the fault zones may add local additional fracture systems, as exhibited in the regions 35-45 km west and northwest of the plant (see, for example, Figures 6.1-152, 6.1-153, 6.1-177, and 6.1-178).

**Aeromagnetic Anomalies.** Figure 6.2-2 displays in the project area lineaments along regional steep aeromagnetic gradients that are linear in map view. In the eastern part of the area, NE/ENE and NW/NNW aeromagnetic lineaments are prominent. Rarer trends are EW and NS. In the central and western area, NNE/NE and NW/NNW aeromagnetic lineaments are prominent, but northerly and easterly trending lineaments are also observed. These trends are accentuated after the EarthSat (1997) lineaments are added that are consistent with the aeromagnetic lineaments (Figure 6.2-3). The coincidence of the EarthSat (1997) lineaments with the aeromagnetic lineaments indicates that basement fault systems marked by the aeromagnetic lineaments extend up to the surface or near-surface as at least fractures, if not faults.

Hickling, Greenidge and Cayuga power plants are all located on aeromagnetic lineaments. This coincidence suggests that these power plants are located above fault systems in the Precambrian basement. At both the Hickling and the Greenidge power plants, EarthSat (1997) lineaments are (nearly) coincident with the aeromagnetic lineaments (Figure 6.2-3); such a relationship suggests that the faults in the basement marked by the aeromagnetic lineaments extend up to the surface or near-surface as at least fractures, if not faults. The trend of these faults at Hickling is NE and at Greenidge is NNE. The NNW-trending aeromagnetic anomaly at the Cayuga power plant is not found in the EarthSat (1997) lineaments, but the lake shore does trend collinearly with the anomaly, and NNW-striking FIDs fractures were observed near the Cayuga power plant (Figures 6.1-102 and 6.1-103). The aeromagnetic anomalies in the Cayuga and Greenidge power plants were also observed in more detailed high resolution aeromagnetic data (Jacobi 2007a, Figures 6.1-121 to 6.1-126). The Westover power plant is not located directly on an aeromagnetic lineament; rather, it is located on an aeromagnetic high (Figure 6.2-2). This ENE-trending high does have ENE-trending aeromagnetic lineaments along its flanks, and a few EarthSat (1997) lineaments have similar trends and locations. A significant ENE-trending EarthSat (1997) lineament along the crest of the aeromagnetic high is nearly on strike with the power plant (Figure 6.2-3). The Jennison power plant is located in an area with the least prominent aeromagnetic gradients of the five power plants. The E-trending EarthSat (1997) lineaments at the power plant (discussed above) may be related to a possible regional EW gradient that extends across the county that passes through the power plant site.



### **Conclusions (Subtask 6.3)**

All five AES power plants are close to bands of lineaments identified in satellite imagery that were interpreted as faults. The western three power plants, Hickling, Greenidge and Cayuga, all are in close proximity to ENE-trending lineaments. In the regions of the Hickling and Cayuga power plants, proprietary 3D seismic reflection data confirm earlier integrated studies that proposed these lineament trends are representative of ENE-striking steeply dipping, reactivated Iapetan-opening fault systems. Many of the Iapetan-opening faults were reactivated with relatively large throws during the Taconic Orogeny. In the Hickling power plant region, the ENE-striking fault systems have relatively close spacings (across the ENE strike), on the order of 1.5-2.5 km. The length between major along-strike variations in the faults (e.g., cross fault trends) has a range between 1.5 km and 10 km.

The Greenidge, Cayuga Westover and Jennison power plants are close to E-trending lineaments and lineament bundles. In the region of the Cayuga power plant, proprietary 3D seismic shows that these faults also sustained their greatest motion in Taconic times. Jennison and Westover also have strong NE lineament bundles which are interpreted as fault systems. All AES power plants in the project area also are close to northerly-trending lineament bands. For example, the Greenidge power plant is located east of NNE-lineaments that are coincident with significant aeromagnetic anomalies, suggesting NNE-striking faults and associated fractures that extend from basement to (near) surface. These fault systems are believed to be related to intra-Grenvillian sutures (terrane boundaries) that have been episodically reactivated (e.g., Jacobi, 2002).

High structural level salt-cored anticlines that commonly involve thrust ramps off the Silurian salt decollements occur near the Westover and Cayuga power plants. Since these anticlines are restricted to units above the Silurian evaporate seal, and all the CO<sub>2</sub> sequestration targets are below the Silurian evaporate seal, these anticlines are not a significant factor in the considerations a CO<sub>2</sub> sequestration site. However, some of the salt-cored anticlines have been shown to correspond with deeper structures.

The orientation of the predominant fracture sets at the power plant sites can be estimated from the general fracture orientations of sets I, II, and III across New York State. In general Set I fractures trend NW at the Hickling and Greenidge power plants, NNW/N at the Cayuga power plant, N/NNE at the Westover plant and NNE at the Jennison power plant. Set II fractures are generally orthogonal to Set I fractures. Set III fractures generally trend ENE. Additionally, it is probable that closely-spaced fracture sets (sub) parallel to faults are localized along the faults in most of the sedimentary units except possibly the Utica and deeper carbonates. All these sets can be represented by long, relatively planar fractures.

The fracture frequency of these fracture sets the surface in Upper Devonian interbedded shales and siltstones is generally on the order of (less than) 1 fracture/m for Set I, < 4 fractures/m for Set II, and variable spacing for Set III. The spacing of the fractures related to faults (FIDs) could vary from about 4 to as many as 20 fractures/m near the surface. The spacing of the fracture sets is not known at depth.

### **Selected References**

- Bahat, Dov & Engelder, Terry, 1984, Surface morphology on cross-fold joints of the Appalachian Plateau, New York and Pennsylvania: *Tectonophysics*, v. 104, p. 299-313
- Bradley, W. H., Pepper, J. F. and Richardson, G. B., 1941, Geologic structure and occurrence of gas in part of southwestern New York: United States Geological Survey, Bulletin 899, 93 pp.
- Cornell Faculty & Students, 1959, Guide Book Geology of the Cayuga Lake Basin, NYSGA, 31st annual meeting
- Cruz, C., 2005, Satellite image, enhancement, lineaments identification and quantitative comparison with fracture data, central New York State: Thesis
- Cruz, Cheri, Jacobi, Robert D., Everett, John R., and Staskowski, Ronald J., 2005, ASTER and Landsat lineaments in central NYS: Image processing and groundtruthing for fractures: Geological Society of America, Abstracts with Programs, Geological Society of America, Abstracts with Programs, v. 37, n. 1, p. 5
- Drechsel, Cheri A., Jacobi, Robert D., Everett, John R., and Staskowski, Ronald J., 2004, ASTER lineaments, faults, and reservoirs in the Appalachian Basin of New York State: Geological Society of America, Abstracts with Programs, v. 36, n. 2, p. 146.
- Engelder, T., 1982, Reply to Scheidegger's discussion of "Is There a Relationship Between Regional Joints and Contemporary Stress Within the Lithosphere of North America": *Tectonics*, v 1, n. 5 p. 465-470
- Engelder, Terry, 1984, Loading paths to joint propagation during a tectonic cycle: an example from the Appalachian Plateau, U.S.A.: *Journal of Structural Geology*, vl. 7, n. 3/4, p. 459-476
- Engelder, T., 1990, Smoluchowski's Dilemma Revisited: A Note on the Fluid Pressure History of the Central Appalachian Fold-Thrust Belt: p. 140-147
- Engelder, T. & Geiser, P., 1979, The relationship between pencil cleavage and lateral shortening within the Devonian section of the Appalachian Plateau, New York: *Geology*, v .7, p. 460-464
- Engelder, T. & Geiser, P., 1980, On the Use of Regional Joint Sets as Trajectories of Paleostress Fields During the Development of the Appalachian Plateau, New York: *Journal of Geophysical Research*, v. 85, n. 311, p. 6319-6341
- Engelder, T. & Geiser, P., 1984, Near-Surface in Situ Stress IV. Residual Stress in the Tully Limestone Appalachian Plateau, New York: *Journal of Geophysical Research*, v. 89, n. 311, p. 9365-9370
- Engelder, T. and Oertel, G., 1985, The correlation between under-compaction and tectonic jointing within the Devonian Catskill Delta, *Geology*, v. 13, p. 863-866.

- Engelder, T., Geiser, P., & Bahat, Dov., 1987, Exposures of the Hudson Valley Fold-Thrust Belt, west of Catskill, New York: GSA Centennial Field Guide--Northeastern Section, pp 123
- Engelder, T., Haith, B. & Younes, A., 2001, Horizontal slip along Alleghanian joints of the Appalachian plateau: evidence showing that mild penetrative strain does little to change the pristine appearance of early joints: *Tectonophysics*, v. 336, p. 31-41
- Engelder, T. & Whitaker, Amy E., 2006, The Fractography of joints: Natural analogs for failure in glasses and ceramics: Finger Lakes district field trip, p. 1-21
- Engelder, T., Lash, G.G., and Uzcategui, R., 2009, Joint sets that enhance production from Middle and Upper Devonian gas shales of the Appalachian Basin: *American Association of Petroleum Geologists Bulletin* v. 93, p. 857-889.
- Evans, M. A., 1994, Joints and decollement zones in Middle Devonian shales: evidence for multiple deformation events in central Appalachian Plateau: *GSA Bulletin*, v. 106, p. 447-460
- Fisher, Jodi., Jacobi, Robert., Martin, John., 2010, Compilation of structural features in the northern Appalachian Basin of New York State to assist in site evaluation and CO<sub>2</sub> sequestration: *Geol. Soc. . Am. Abstracts with Programs*, v. 42, n. 1, p. 121
- Geiser, P. & Engelder, T., 1983, The distribution of layer parallel shortening fabrics in the Appalachian foreland of New York and Pennsylvania: Evidence for two non-coaxial phases of the Alleghanian Orogeny: *GSA Memoir* 158, pp 161-175
- Gross, M., Engelder, T., & Poulson, S., 1992, Veins in the Lockport dolostone: Evidence of an Acadian fluid circulation system: *Geology*, v. 20, p. 971-974
- Hanson, Stacey L., Jacobi, Robert D., and Mitchell, Charles E., 2010, Structure and Geochemistry of a Cambro-Ordovician 360m Core from Saratoga Springs Region, New York State: Implications for Tectonics, Gas Exploration, and CO<sub>2</sub> Sequestration: Eastern Section AAPG, 2010 Annual meeting (Kalamazoo, MI)  
[http://www.searchanddiscovery.com/abstracts/pdf/2010/eastern/abstracts/ndx\\_hanson.pdf](http://www.searchanddiscovery.com/abstracts/pdf/2010/eastern/abstracts/ndx_hanson.pdf)  
 accessed 9/20/2011
- Hanson, Stacey, Jacobi, Robert D., and Mitchell, Charles, E., 2011, Structure and Vein Isotopes of a Cambro-Ordovician 360m Core From the Saratoga Springs Region, New York State: Implications For Tectonics and Utica Gas Exploration: *Geol. Soc. Am. Abstracts with Programs*,  
[http://gsa.confex.com/gsa/2011NE/finalprogram/abstract\\_185523.htm](http://gsa.confex.com/gsa/2011NE/finalprogram/abstract_185523.htm), accessed 9/15/2011
- Hickman, Stephen H, Healy, John H., Zoback, Mark D., 1985, In situ stress, natural fracture distribution, and borehole elongation in the Auburn geothermal well, Auburn, New York: *Journal of Geophysical Research*, v. 90, n. B7, p. 5497-5512.
- Isachsen & Mckendree, 1977, Preliminary brittle structure map of New York, New York State Museum and Science Services, Map and Chart Series no.31

- Jacobi, Robert D., 2002, Basement faults and seismicity in the Appalachian Basin of New York State, *in* Neotectonics and Seismicity in the Eastern Great Lakes Basin, R. H. Fakundiny, R. D. Jacobi, and C. F. M. Lewis (eds.): Tectonophysics, v. 353, p. 75-113.
- Jacobi, Robert D., 2007a, Final Technical Report (May 31, 2000-May 15, 2007): Innovative Methodology for Detection of Fracture-Controlled Sweet Spots in the Northern Appalachian Basin: Department of Energy/NETL, Morgantown, WV, 453 pp.
- Jacobi, Robert D., 2007b, Natural gas exploration in Chenango County, New York State: Economic development of stacked reservoirs: NYSERDA (Albany NY) Final report, 62 pp, 94 figures, and 30 tables.
- Jacobi, Robert, 2010, Geophysical and geological evidence for arcuate Iapetan opening rift faults in the Pennsylvania Salient and New York recess: implications for the ragged Laurentian margin: NYSERDA (Albany NY) Final Report, 42 pp.
- Jacobi, Robert, 2011a, Faults in the Appalachian Basin of New York State: AAPG Geosciences Technology Workshop, Success in the Marcellus and Utica Shales: Case Studies and New Developments: Baltimore MD, p. 3.
- Jacobi, Robert D., 2011b, Faults in the Appalachian Basin of NYS: Geol. Soc. Am. Abstracts with Programs, [http://gsa.confex.com/gsa/2011NE/finalprogram/abstract\\_185588.htm](http://gsa.confex.com/gsa/2011NE/finalprogram/abstract_185588.htm), accessed 9/15/2011
- Jacobi, Robert, 2011c, Post-depositional fault effects in black shales of the Appalachian Basin of New York State: fracture/fault heterogeneity and thermal maturity: AAPG Geosciences Technology Workshop, Success in the Marcellus and Utica Shales: Case Studies and New Developments: Baltimore MD, p. 3.
- Jacobi, Robert D., 2011d, Integration of remotely-sensed and geophysical data with ground-truth structure: evidence for fault systems in part of Cayuga County: NYSERDA (Albany NY) Final report, 88 pp.
- Jacobi, Robert D., 2011e, Fracture and geochemical characteristics of Fluid flow in Cambro-Ordovician Units, New York State: NYSERDA (Albany NY) Final report, 64 pp
- Jacobi, Robert and Fountain, John, 1996, Determination of the Seismic Potential of the Clarendon-Linden Fault System in Allegany County, Final Report: Presented 6/10/96 to NYSERDA, 2106 pp. & 31 oversized maps.
- Jacobi, Robert D. and Fountain, John C, 2002, The character and reactivation history of the of the southern extension of the seismically active Clarendon-Linden Fault System, western New York State, *in* Neotectonics and Seismicity in the Eastern Great Lakes Basin, R. H. Fakundiny, R. D. Jacobi, and C. F. M. Lewis (eds.): Tectonophysics, v. 353, p.215-262.
- Jacobi, Robert, and Smith, Gerald, 2000, Part I, Core and cutting analyses, surface structure, faults and lineaments, and stratigraphic cross-sections based on previous investigations, *in*: Geologic Investigation of the Gas Potential in the Otsego County Region, Eastern New York State, Final

- Phase One Report to Millennium Natural Resources Development, L.L.C., (Robert Jacobi, Ed.):  
Final Report: presented to NYSERDA (Albany NY) on 9/8/00, 85 p.
- Jacobi, R.D., Fountain, J., Lugert, C., Nelson, T., Smith, G., Mroz, T., and Martin, J., 2003a, Identifying Trenton/Black River targets in the northern Appalachian Basin (NYS): Demonstration of integrated exploration tools: American Assoc. Petrol. Geol. Annual Meeting program, v. 12, p. A44
- Jacobi, Robert D., Fountain, John, Lugert, Courtney, Nelson, Travis, Smith, Gerald, and Industrial Associates, 2003b, Characteristics of Trenton/Black River structures in the Finger Lakes: Progress Report: Silver Jubilee Anniversary Symposium (Dr. Gerald Friedman, organizer), Northeastern Science Foundation (Troy NY): p. 23-24.
- Jacobi, Robert D., Loewenstein, Stuart, Smith, Gerald, Fountain, John, Lugert, Courtney, and Martin, John, 2004a, Iapetan Opening/Rome Trough-Related Faults and Their Reactivation History in New York State: AAPG Eastern Section Meeting Abstracts,  
<http://www.searchanddiscovery.com/documents/abstracts/2004eastern/jacobi02.htm>  
Accessed January 3, 2005.
- Jacobi, Robert D., Loewenstein, Stuart, Smith, Gerald, Fountain, John, and Nelson, Travis, 2004b, Faults and hydrocarbon resources in the Appalachian Basin of New York State: Geological Society of America, Abstracts with Programs, v. 36, n. 2, p.146.
- Jacobi, Robert D., Loewenstein, Stuart, Smith, Gerald, Fountain, John, Lugert, Courtney, Mroz, Tom, and Martin, John, 2004c, Fault Systems and the Trenton/Black River Play in New York State: AAPG Eastern Section Meeting Abstracts,  
<http://www.searchanddiscovery.com/documents/abstracts/2004eastern/jacobi01.htm>  
Accessed February 10, 2005.
- Jacobi, R. D., Loewenstein, S., and Smith, G. 2005: Seismic Data Bearing on Iapetan Opening/Rome Trough-Related Faults, Their Reactivation History and Effect on Deposition in the Appalachian basin of New York State: AAPG National Meeting Abstracts,  
[http://www.searchanddiscovery.com/documents/abstracts/2005annual\\_calgary/abstracts/jacobi.htm](http://www.searchanddiscovery.com/documents/abstracts/2005annual_calgary/abstracts/jacobi.htm)  
Accessed May 4, 2006
- Jacobi, Robert D. Loewenstein, Stuart, and Smith, Gerald, 2006, Seismic Evidence for Iapetan Fault Control of the Arcuate Map Pattern of the Pennsylvania Salient: Geological Society of America, Abstracts with Programs, v. 41, n. 2, p. 84.
- Jacobi, Robert D., Loewenstein, Stuart, Smith, Gerald, Martin, John, and Mroz, Thomas, 2007, The Pennsylvania salient: seismic and other evidence for an Iapetan arcuate rift influence on the arcuate map pattern: Geological Society of America 2007 national convention.  
[http://gsa.confex.com/gsa/2007AM/finalprogram/abstract\\_130259.htm](http://gsa.confex.com/gsa/2007AM/finalprogram/abstract_130259.htm)  
Accessed May 22, 2008

- Jacobi, Robert, Agle, Paul, Fisher, Jodi, Loewenstein, Stu, Smith, Gerald J., 2009, Structural anomalies in black shales of the Northern Appalachian Basin in New York State: AAPG National Convention, Denver CO:  
[http://aapg09.mapyourshow.com/2\\_1/sessions/session.cfm?ScheduledSessionID=1499&CFID=16152370&CFTOKEN=3b543333e4ce88c0-36743E0A-BC23-81A0-83A1E92588CB683E](http://aapg09.mapyourshow.com/2_1/sessions/session.cfm?ScheduledSessionID=1499&CFID=16152370&CFTOKEN=3b543333e4ce88c0-36743E0A-BC23-81A0-83A1E92588CB683E)  
 (accessed 4/24/10).
- Jacobi, Robert D., Leaver, Al, Loewenstein, Stu, Fisher, Jodi, and Smith, Gerald, 2010, Structural Anomalies in Black Shales of the Northern Appalachian Basin of New York State: Eastern Section AAPG, 2010 Annual meeting (Kalamazoo, MI)  
[http://www.searchanddiscovery.com/abstracts/pdf/2010/eastern/abstracts/ndx\\_jacobi.pdf](http://www.searchanddiscovery.com/abstracts/pdf/2010/eastern/abstracts/ndx_jacobi.pdf) accessed 9/20/2011
- Jacobi, Robert D., Cruz, Cheri, Leaver, Al, and Fisher, Jodi, 2011a, Seismic Signatures of Faults in the Appalachian Basin of NYS, and the Effect of These Faults on Devonian Black Shales: An Update: Eastern Section AAPG, 2011 Annual meeting (Washington, DC)  
[http://www.searchanddiscovery.com/abstracts/pdf/2011/eastern/abstracts/ndx\\_jacobi.pdf](http://www.searchanddiscovery.com/abstracts/pdf/2011/eastern/abstracts/ndx_jacobi.pdf)  
 Accessed 9/29/2011
- Lash, Gary G., Loewy, S. & Engelder, T., 2004, Preferential jointing of Upper Devonian black shale, Appalachian Plateau, USA: evidence supporting hydrocarbon generation as a joint-driving mechanism: Geological Society, London, Special Publications, v. 231, p. 129-151
- Laubach, Stephen E., 2003, Practical approaches to identifying sealed and open fractures: AAPG Bulletin, v. 87, n. 4, p. 561–579
- McGuire, Kelly M., Jacobi, Robert D., Terech, Nicholas, and Agle, Paul, 2006, Integration of Fracture Patterns and Lineaments for Fault Mapping in Southwestern Chenango County, New York: AAPG Eastern Section Meeting Abstracts (Buffalo, NY),  
<http://www.searchanddiscovery.com/documents/2006/06091eastern/abstracts/mcguire.htm> Accessed January 29, 2007
- Oertel, G., Engelder, T., & Evans, K., 1989, A comparison of the strain of crinoid columnals with that of their enclosing silty and shaley matrix on the Appalachian Plateau: Journal of Structural Geology, v.11, n. 8, p. 975-993
- Overbey & Rough, 1968, Surface studies predict orientation of induced formation fractures: Producers monthly, v. 32, n. 6, p. 16-19
- Parker, J. , 1942, Regional systematic jointing in slightly deformed sedimentary rocks: GSA Bulletin, v. 53, p. 381-408
- Pyron, A., Viellenave, J.H. & Fontana, J., 2003, New York Devonian black shale: A Barnett-like play in waiting: Oil and Gas Journal, Jan. 13th, p. 36-42
- Scanlin, M.A., and Engelder, T., 2003, The basement versus the no-basement hypothesis for folding within the Appalachian Plateau detachment sheet: Am. Journal of Science, v. 303, p. 519-563

- Seeburger, Donald A. and Zoback, Mark D., 1982, The Distribution of Natural Fractures and Joints at Depth in Crystalline Rock : USGS Staff -- Published Research, Paper 454, 19 pp.  
<http://digitalcommons.unl.edu/usgsstaffpub/454>, accessed 1/22/12
- Sheldon, P., 1912, Some observations and experiments on joint plans: *Journal of Geology*, Vol. 20, p. 53-70
- Younes, A. & Engelder, T., 1999, Fringe cracks: Key structures for the interpretation of the progressive Alleghanian deformation of the Appalachian Plateau: *GSA Bulletin*, v. 111, n. 2, p. 219-239



**Remote Sensing Laboratory**  
 Dept. of Geology, SUNY at Buffalo



**University at Buffalo**  
 The State University of New York

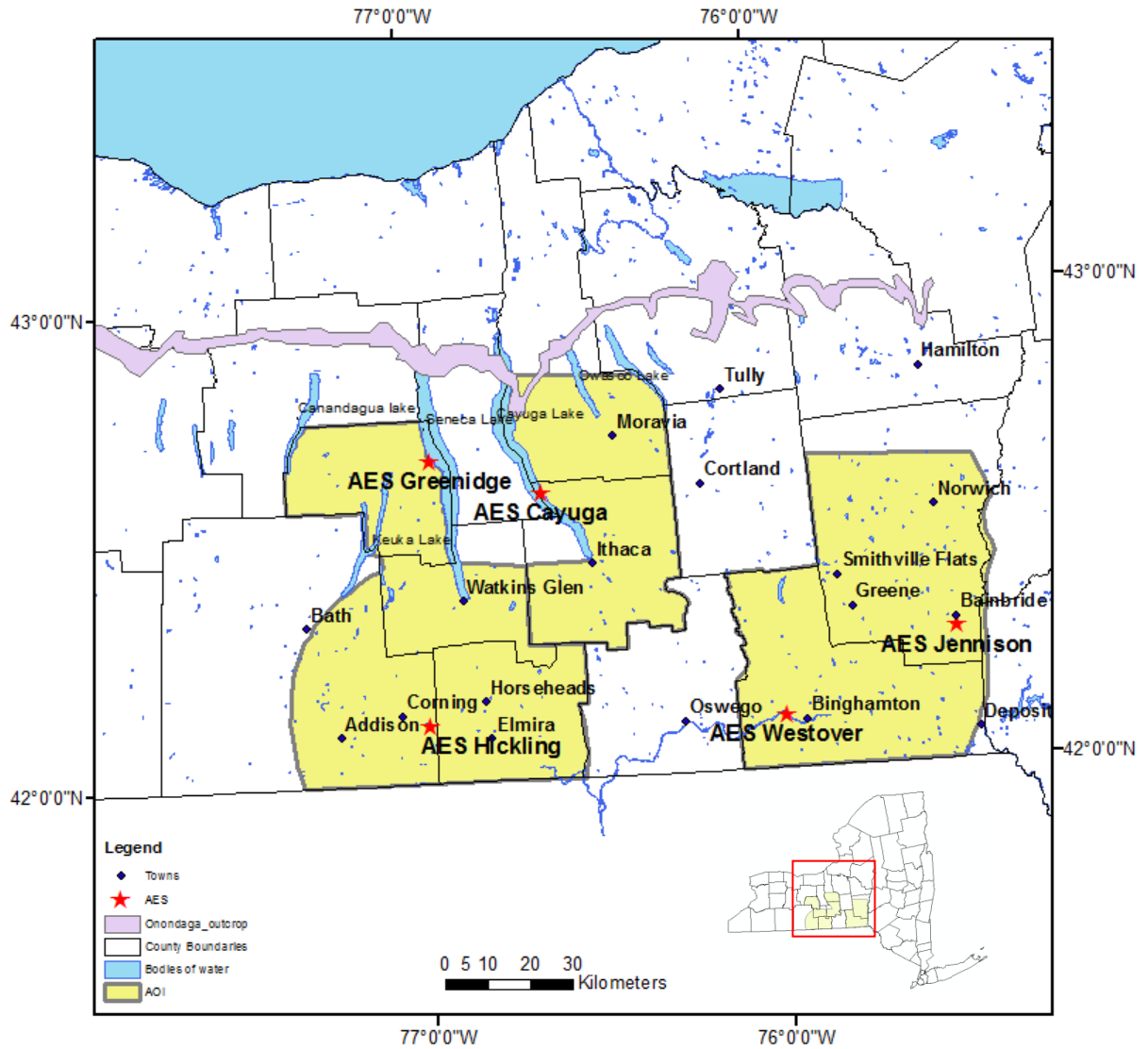


Figure 6.1-1: Onondaga Outcrop (Engelder & Geiser, 1979)





**Remote Sensing Laboratory**  
 Dept. of Geology, SUNY at Buffalo



**University at Buffalo**  
 The State University of New York

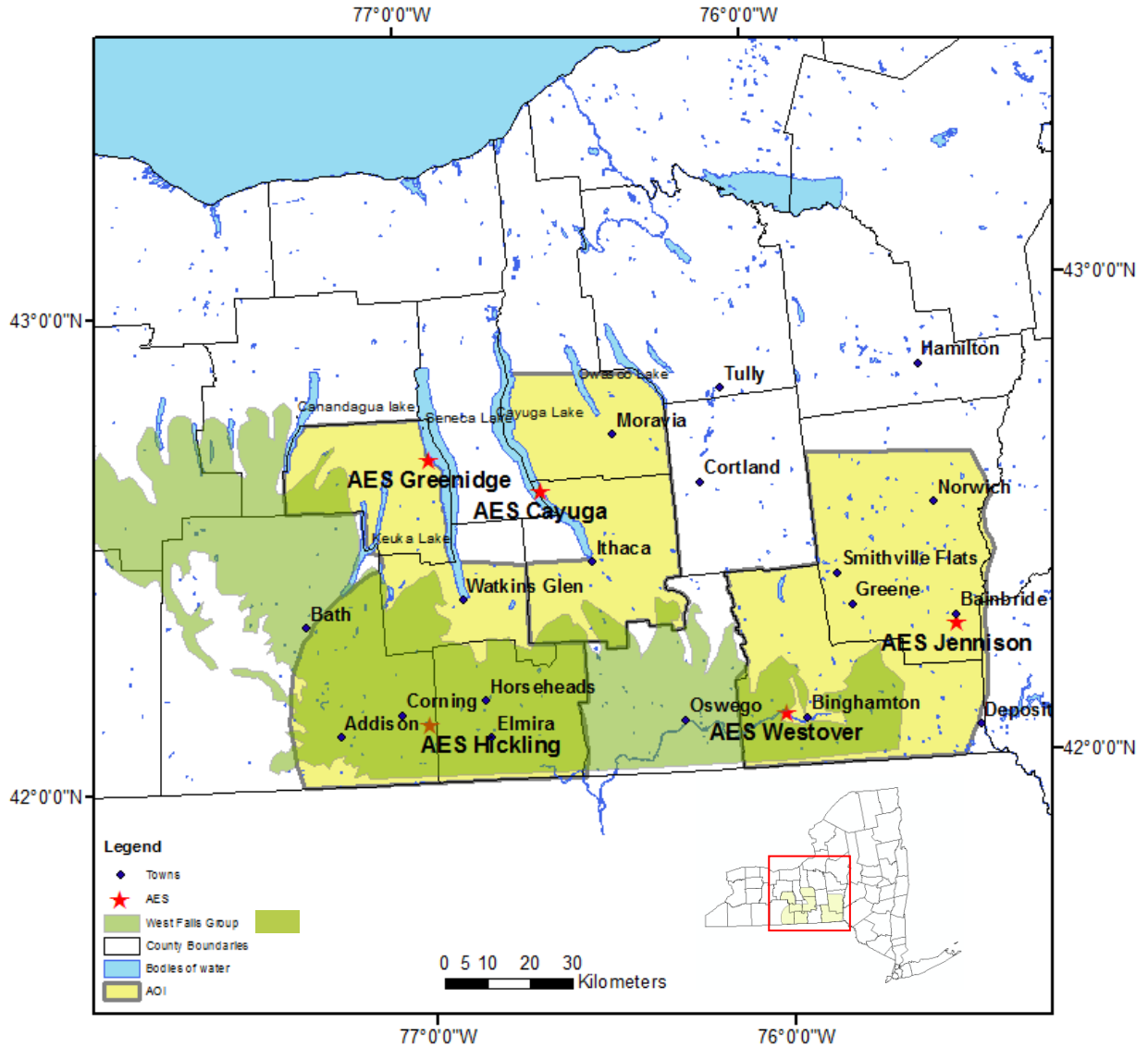


Figure 6.1-2: West Falls Group Outcrop (Engelder & Oertel, 1989)



Remote Sensing Laboratory  
Dept. of Geology, SUNY at Buffalo



University at Buffalo  
The State University of New York

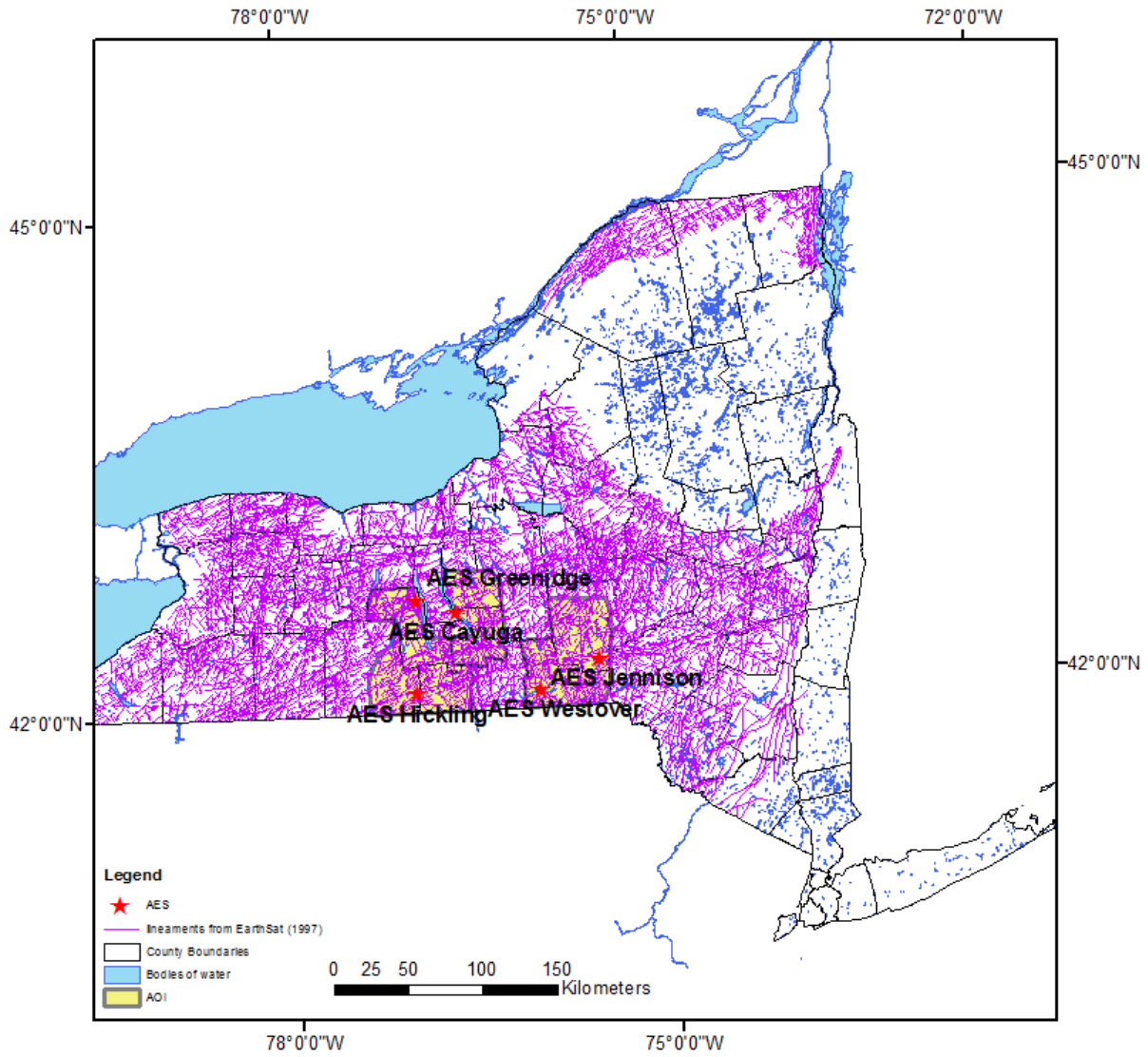


Figure 6.1-3a: Lineaments identified on a LandSat image (EarthSat, 1997)



**Remote Sensing Laboratory**  
 Dept. of Geology, SUNY at Buffalo



**University at Buffalo**  
 The State University of New York

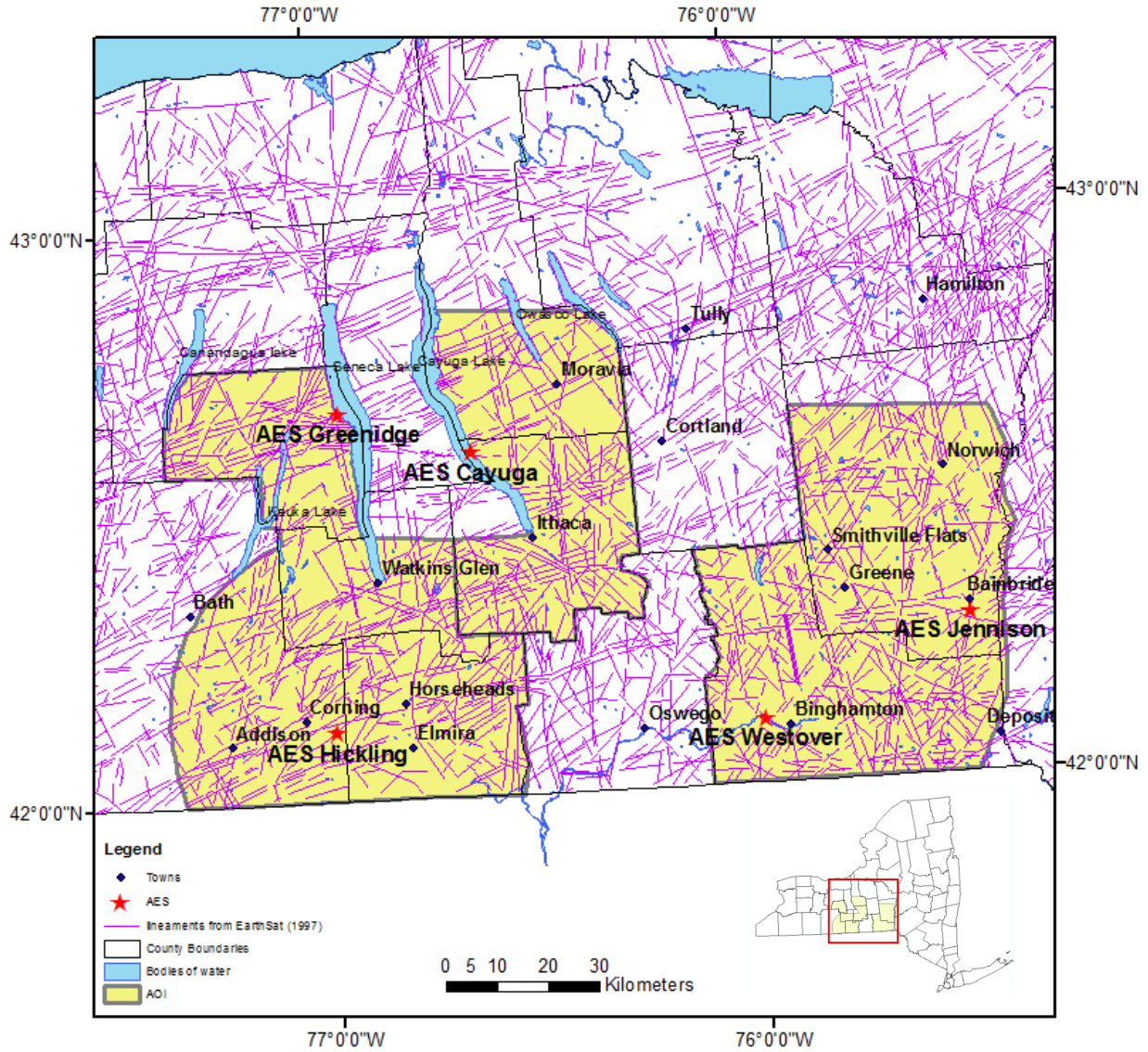


Figure 6.1-3b: Lineaments identified on a LandSat image (EarthSat, 1997), project area view.



Remote Sensing Laboratory  
Dept. of Geology, SUNY at Buffalo



University at Buffalo  
The State University of New York

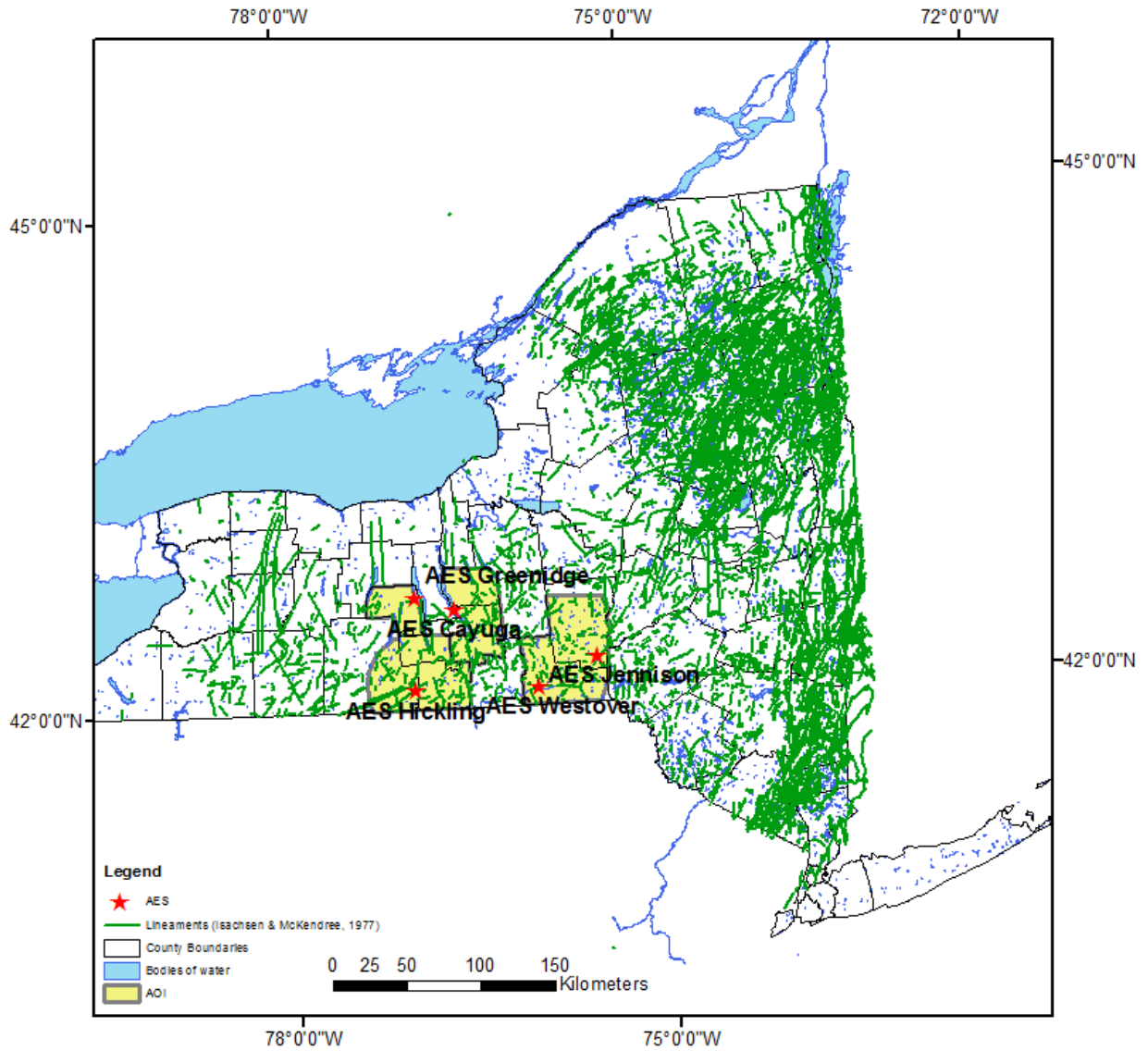


Figure 6.1-4a: Lineaments identified by Isachsen and McKendree (1977)



Remote Sensing Laboratory  
Dept. of Geology, SUNY at Buffalo



University at Buffalo  
The State University of New York

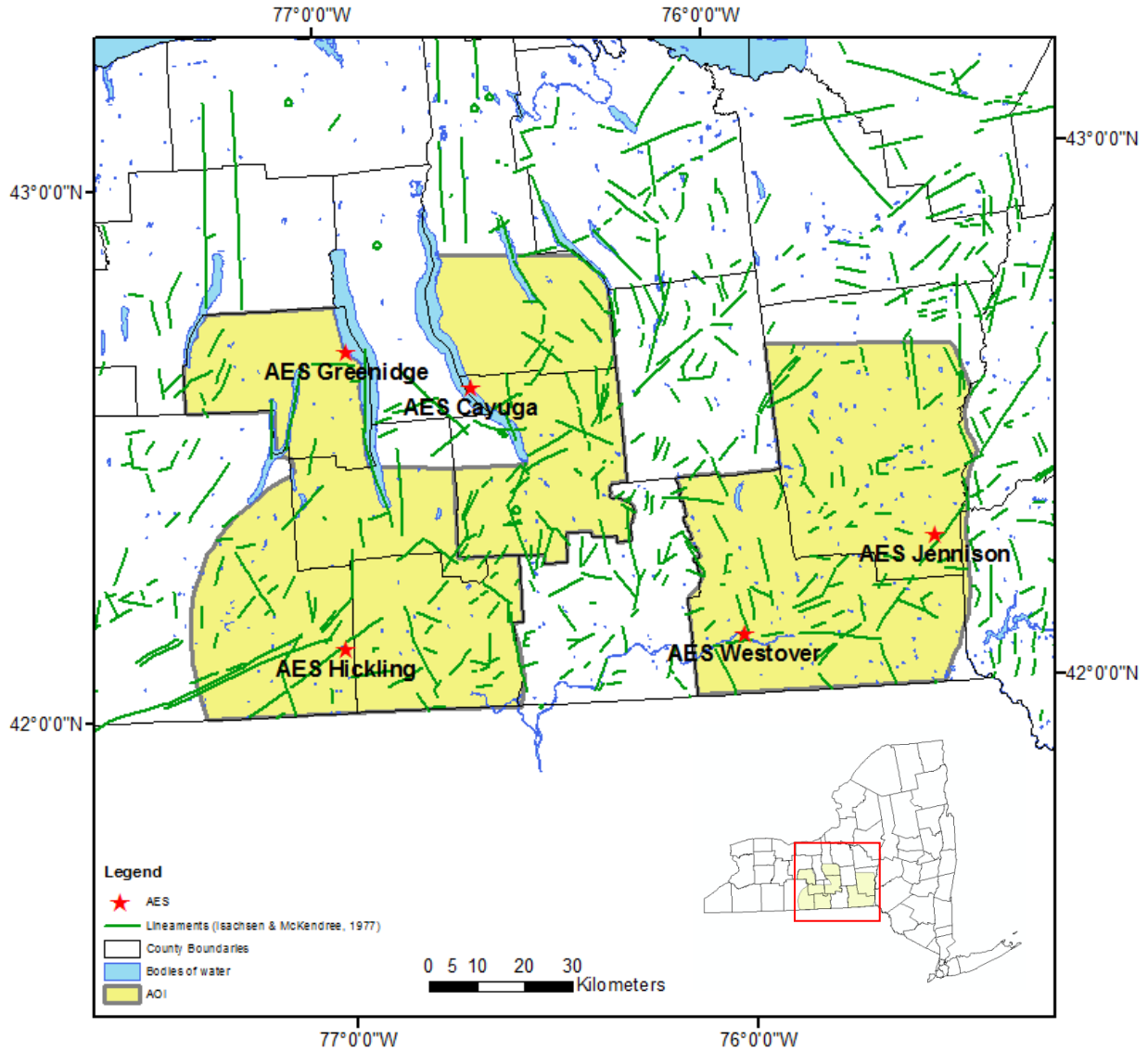


Figure 6.1-4b: Lineaments identified by Isachsen and McKendree (1977), project area view.



Remote Sensing Laboratory  
Dept. of Geology, SUNY at Buffalo



University at Buffalo  
The State University of New York

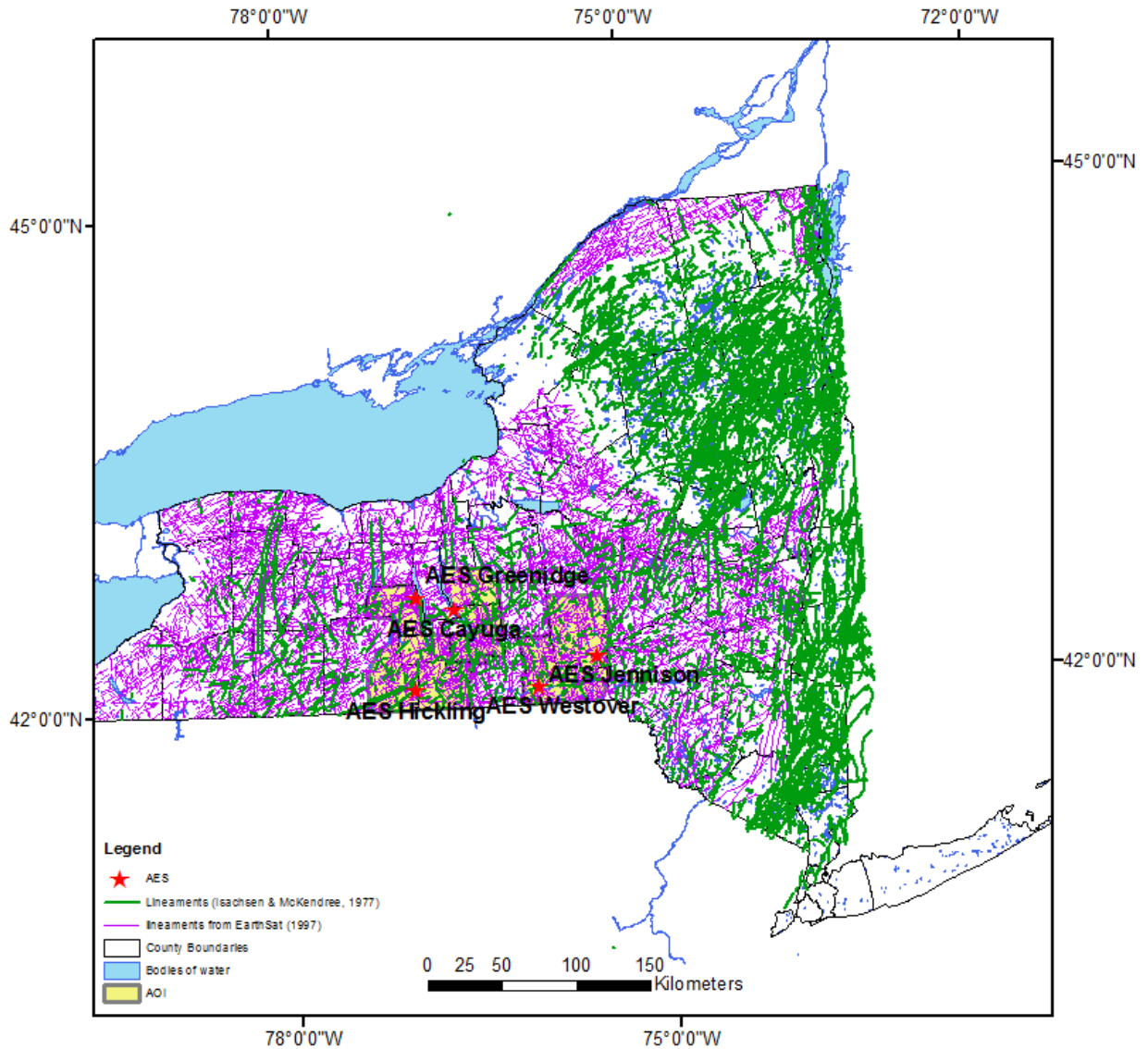


Figure 6.1-5a: Combined lineaments from EarthSat (1997) and Isachsen and McKendree (1977)





**Remote Sensing Laboratory**  
*Dept. of Geology, SUNY at Buffalo*



**University at Buffalo**  
*The State University of New York*

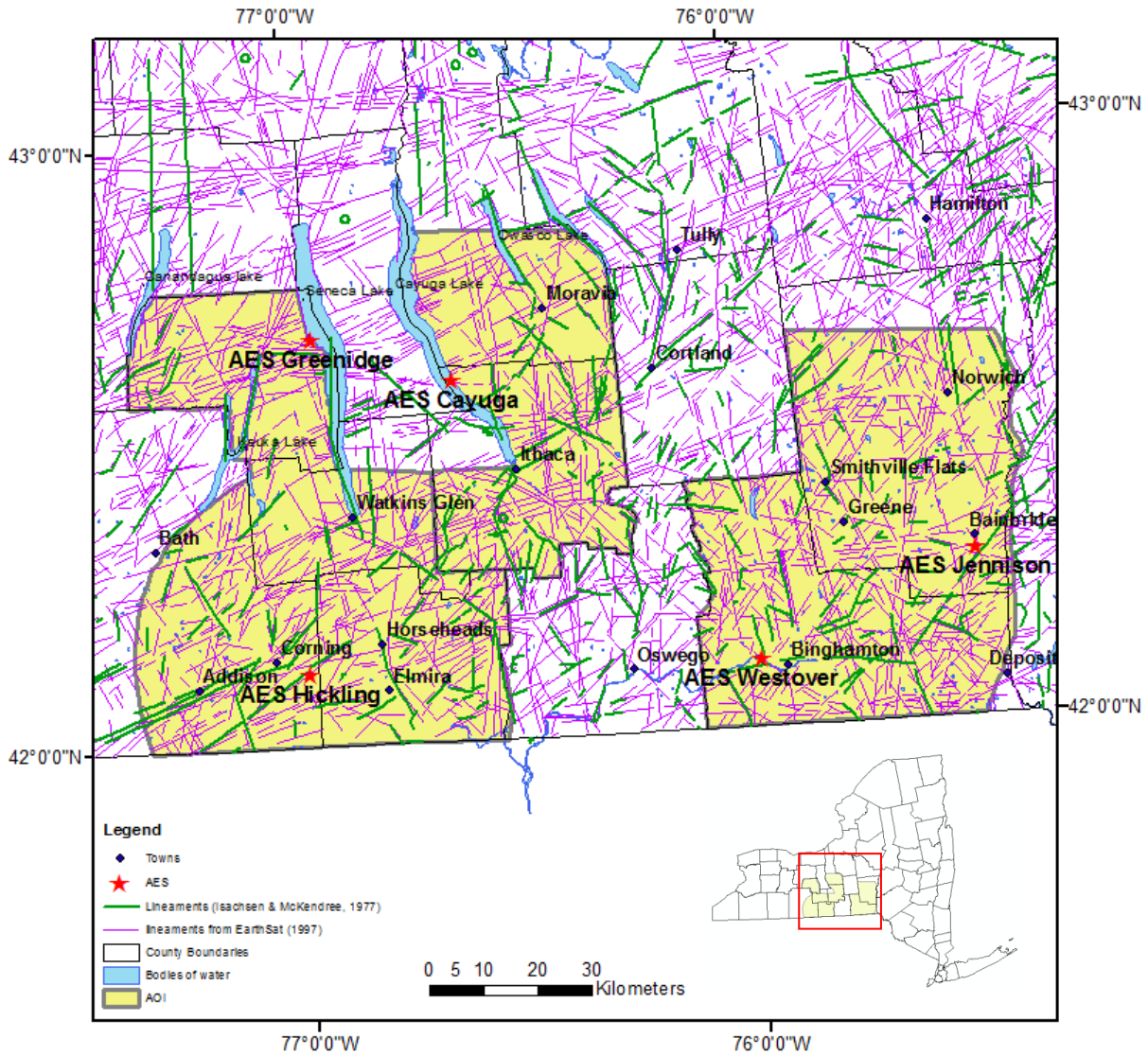


Figure 6.1-5b: Combined lineaments from EarthSat (1997) and Isachsen and Mckendree (1977), project area view.



Remote Sensing Laboratory  
Dept. of Geology, SUNY at Buffalo



University at Buffalo  
The State University of New York

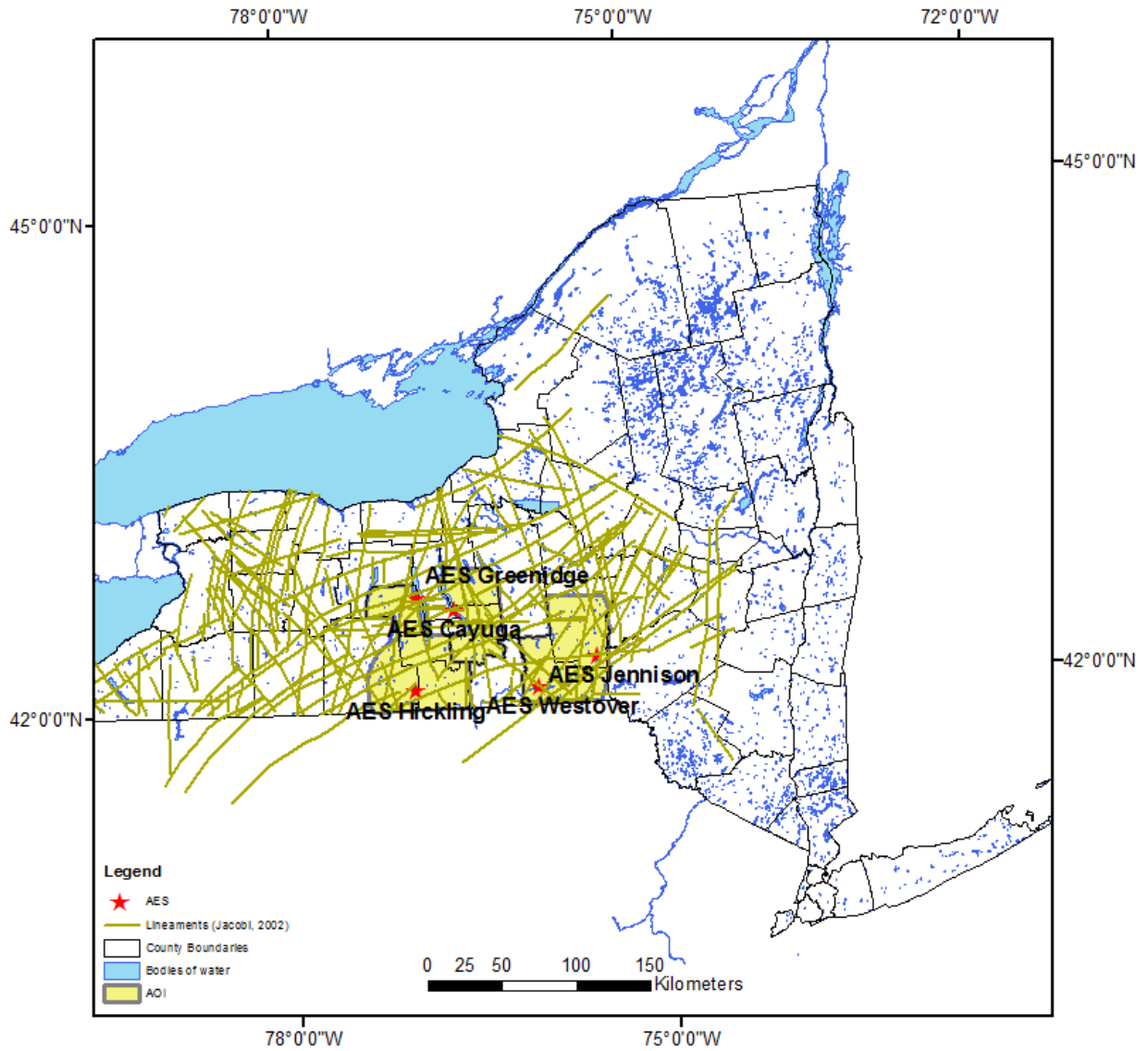


Figure 6.1-6a: Selected major fault systems (Jacobi, 2002)





Remote Sensing Laboratory  
Dept. of Geology, SUNY at Buffalo



University at Buffalo  
The State University of New York

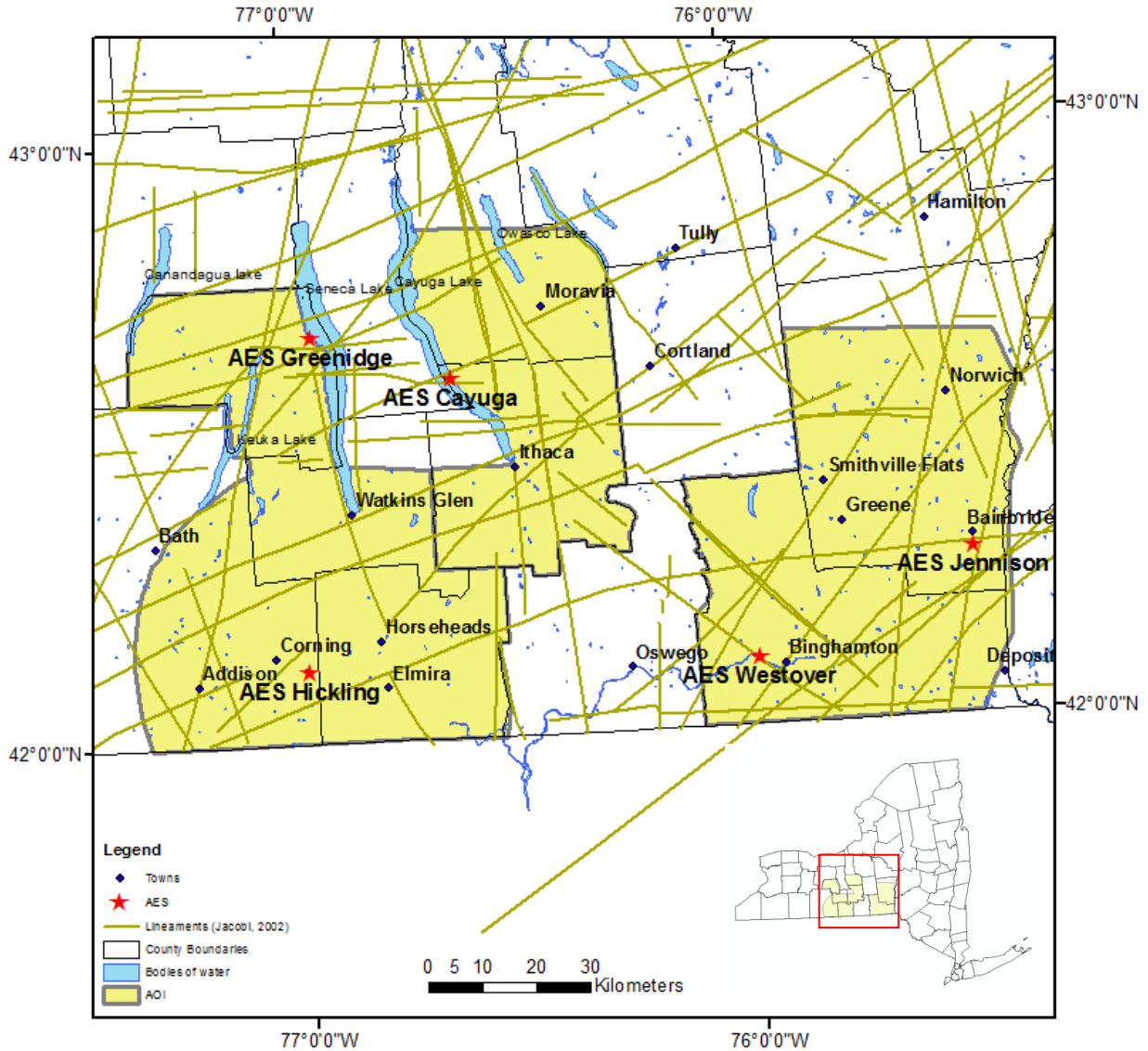


Figure 6.1-6b: Selected major fault systems (Jacobi, 2002), project area view.



Remote Sensing Laboratory  
Dept. of Geology, SUNY at Buffalo



University at Buffalo  
The State University of New York

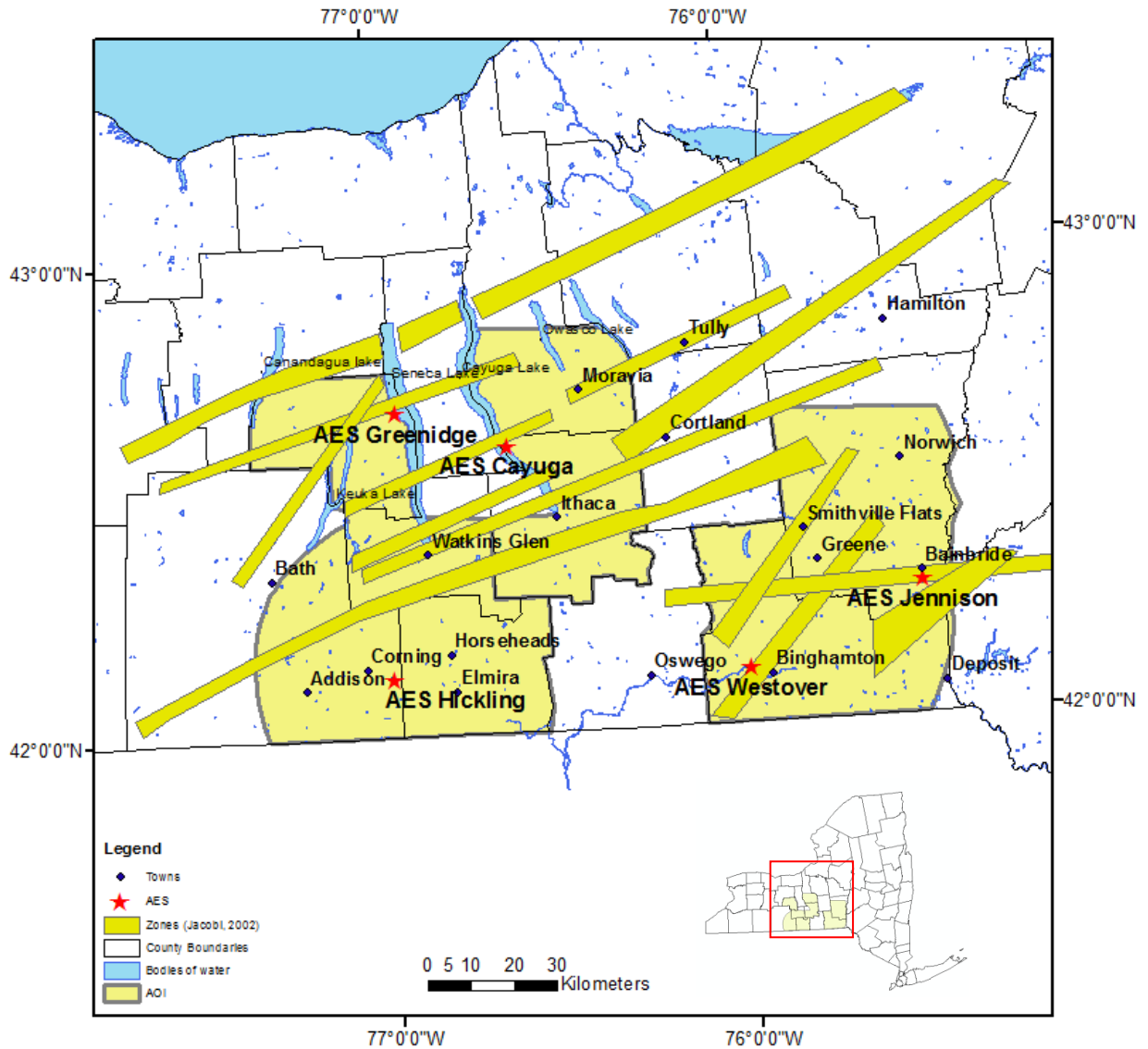


Figure 6.1-6c: Selected major fault zones (Jacobi, 2002), project area view.



**Remote Sensing Laboratory**  
 Dept. of Geology, SUNY at Buffalo



**University at Buffalo**  
 The State University of New York

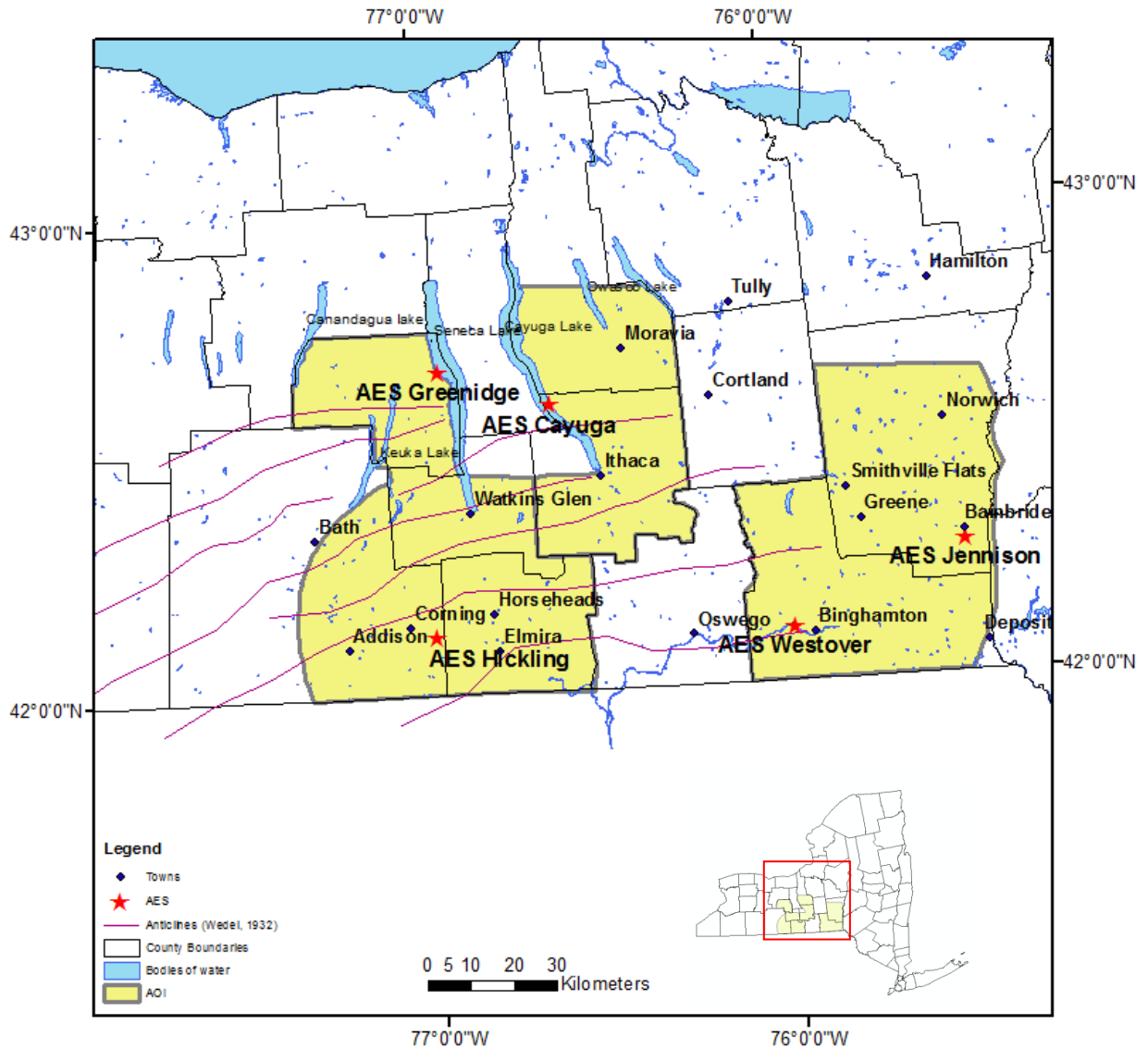


Figure 6.1-7a: Anticlines (Wedel, 1932)



Remote Sensing Laboratory  
Dept. of Geology, SUNY at Buffalo



University at Buffalo  
The State University of New York



Figure 6.1-7b: Faults from Bradley et al. (1941)



Remote Sensing Laboratory  
Dept. of Geology, SUNY at Buffalo



University at Buffalo  
The State University of New York

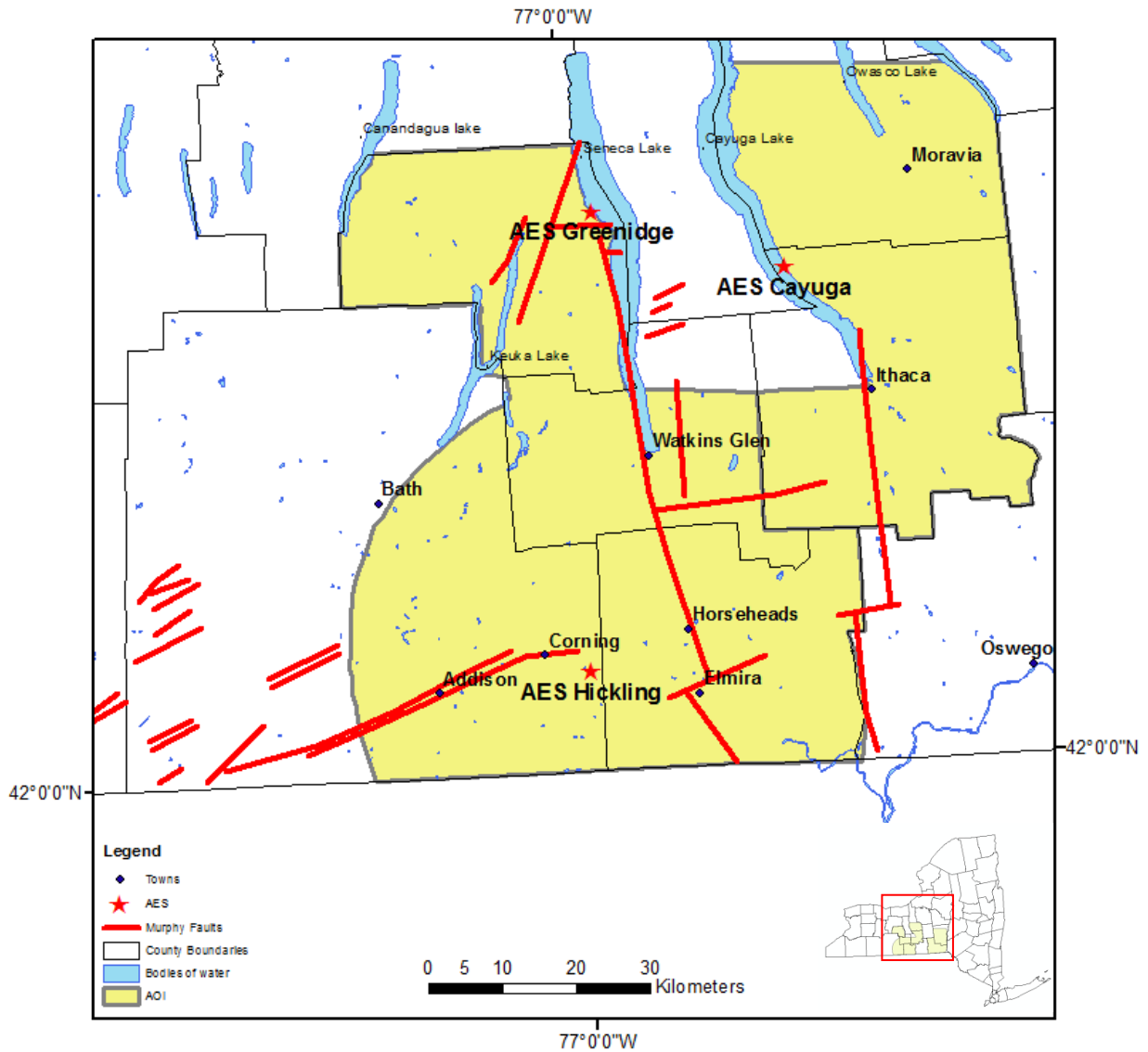


Figure 6.1-7c: Faults from Murphy (1981)



Remote Sensing Laboratory  
Dept. of Geology, SUNY at Buffalo



University at Buffalo  
The State University of New York

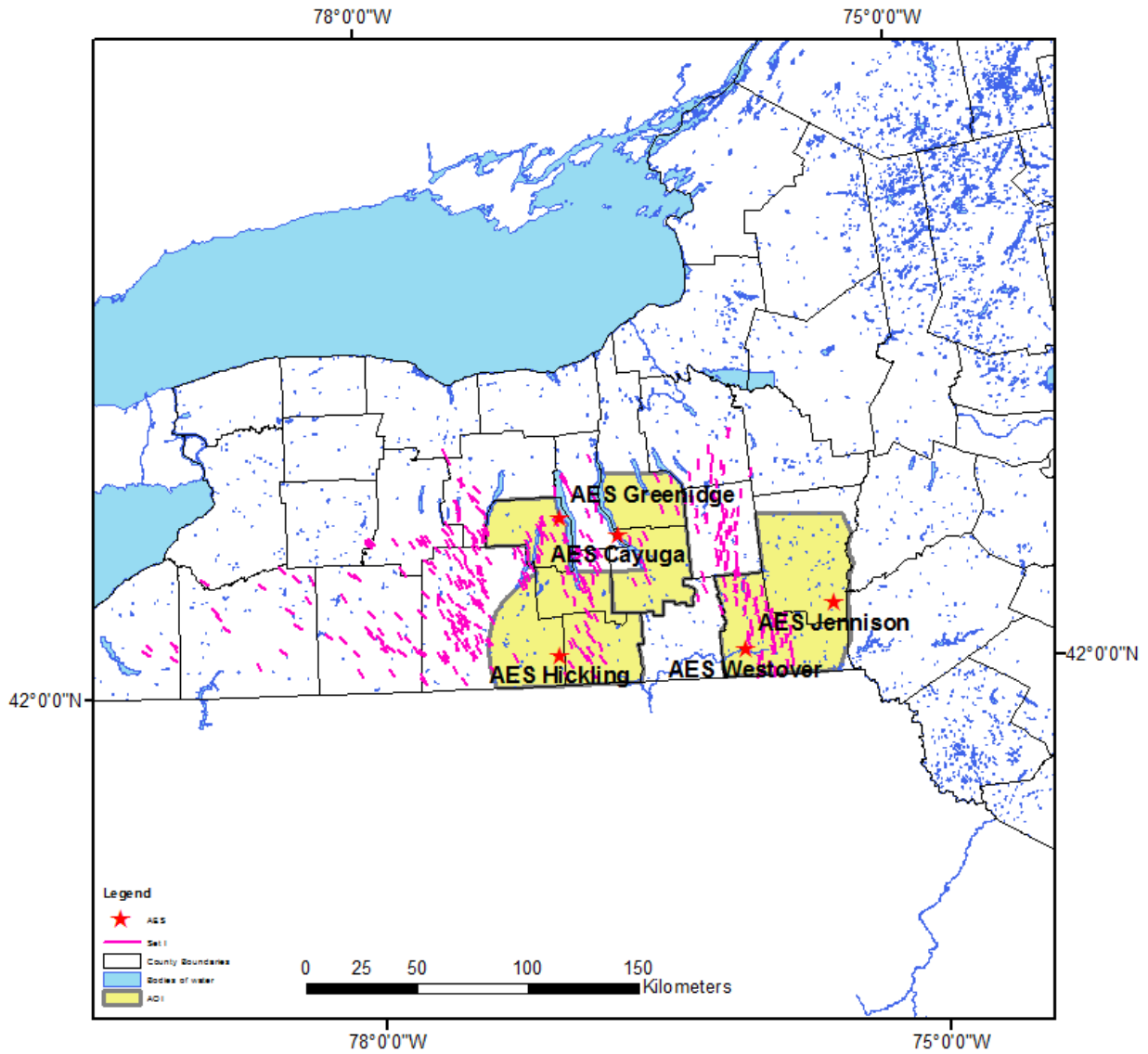


Figure 6.1-8: Set I fractures measured in outcrop (Engelder & Geiser, 1980)



Remote Sensing Laboratory  
Dept. of Geology, SUNY at Buffalo



University at Buffalo  
The State University of New York

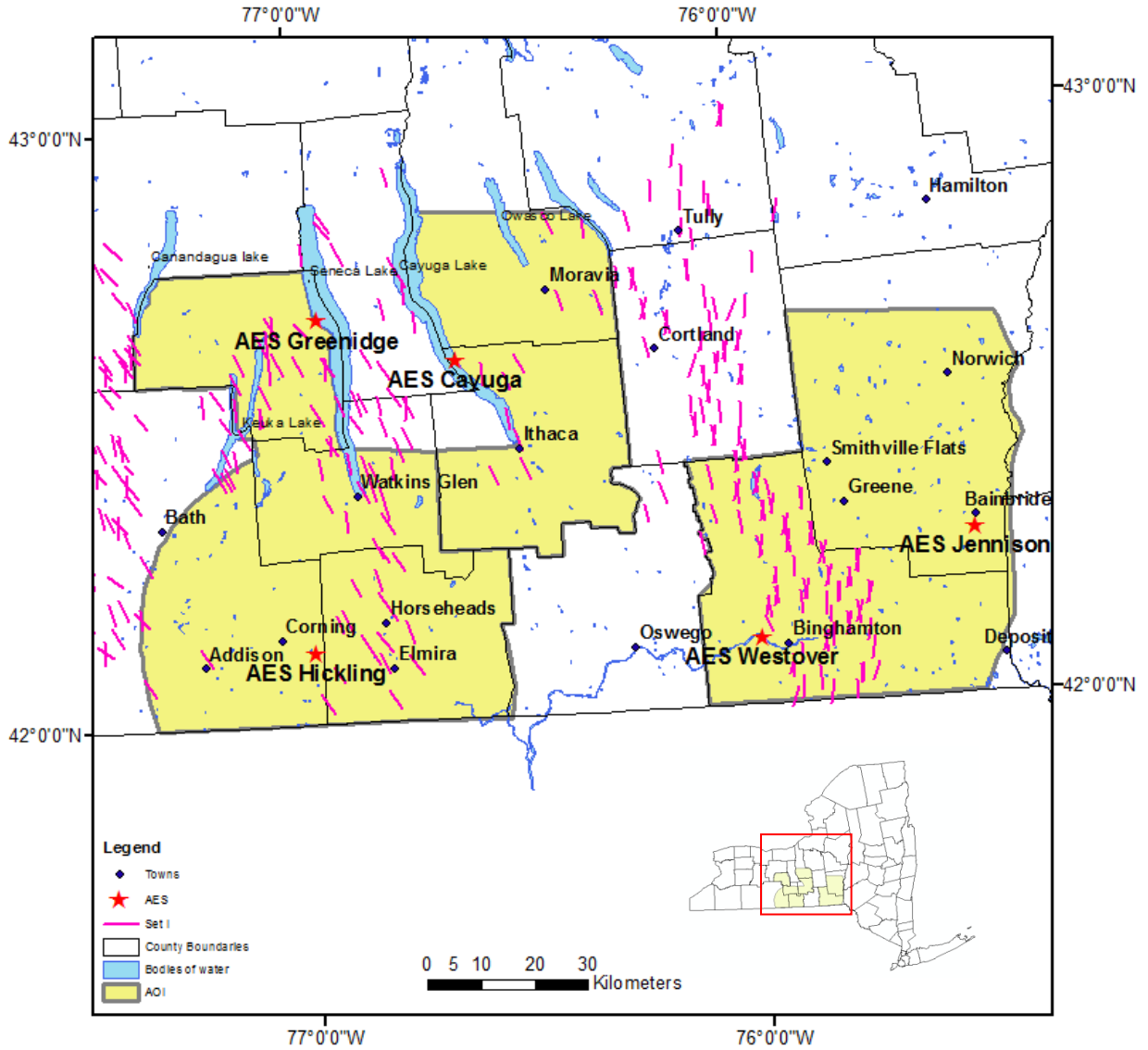


Figure 6.1-9: Set I fractures in project area (Engelder & Geiser, 1980)



**Remote Sensing Laboratory**  
 Dept. of Geology, SUNY at Buffalo



**University at Buffalo**  
 The State University of New York



Figure 6.1-10: Trajectories of Set I fractures (Faculty and Students of Cornell University, 1959)





Remote Sensing Laboratory  
Dept. of Geology, SUNY at Buffalo



University at Buffalo  
The State University of New York

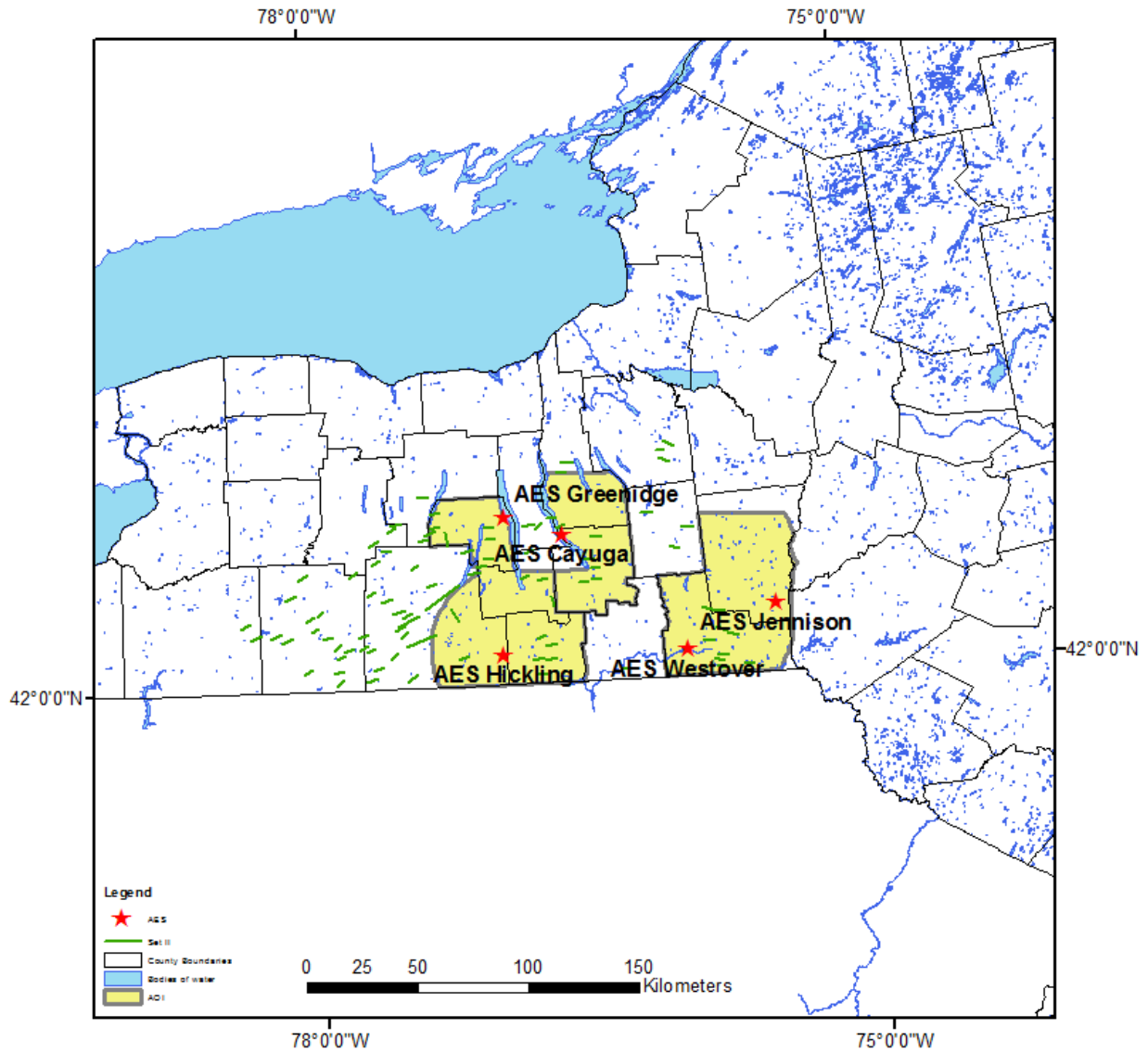


Figure 6.1-11: Set II fractures measured in outcrop (Engelder & Geiser, 1980)



Remote Sensing Laboratory  
Dept. of Geology, SUNY at Buffalo



University at Buffalo  
The State University of New York

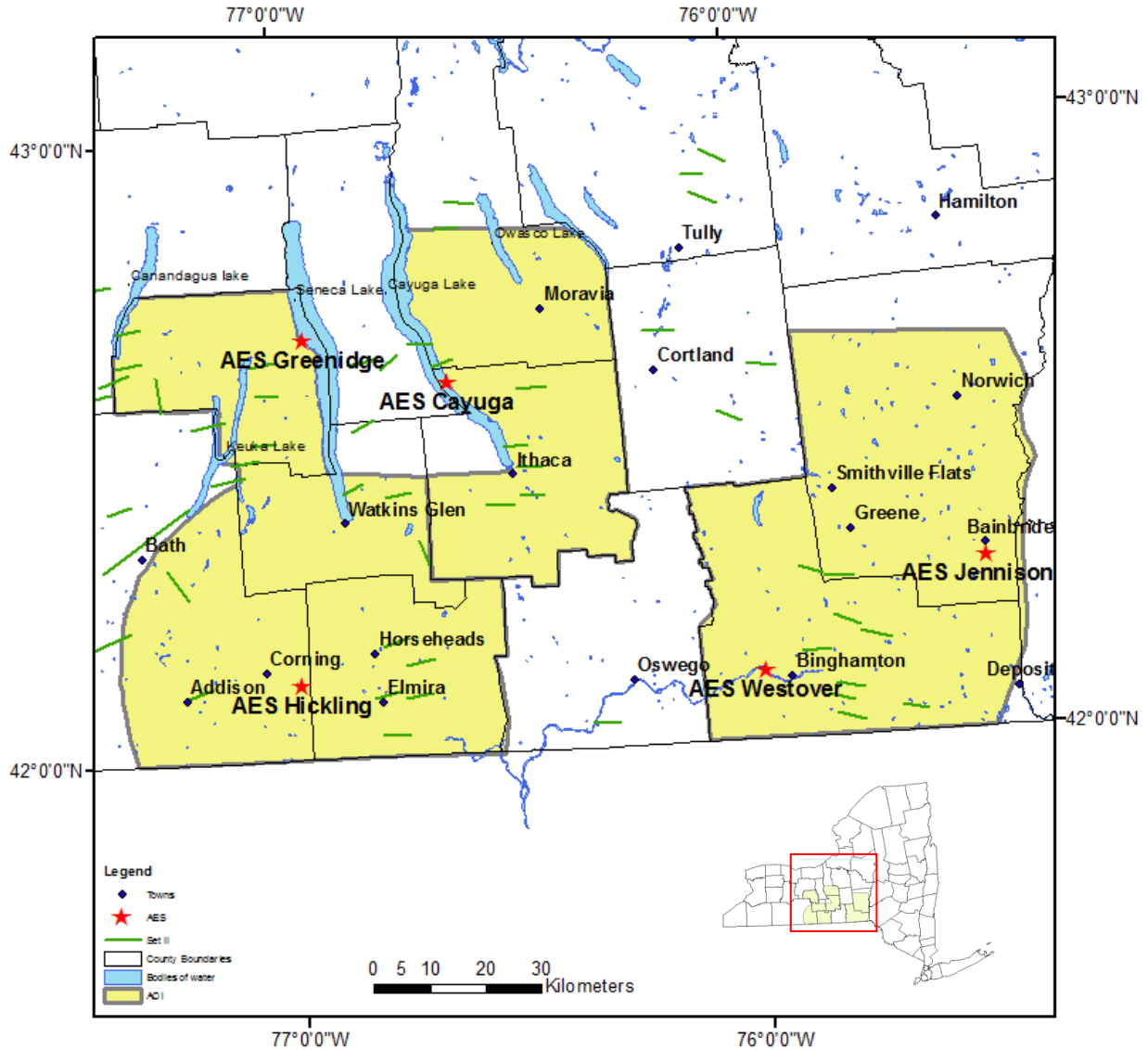


Figure 6.1-12: Set II fractures measured in outcrop inside of the project area (Engelder & Geiser, 1980)



Remote Sensing Laboratory  
Dept. of Geology, SUNY at Buffalo



University at Buffalo  
The State University of New York

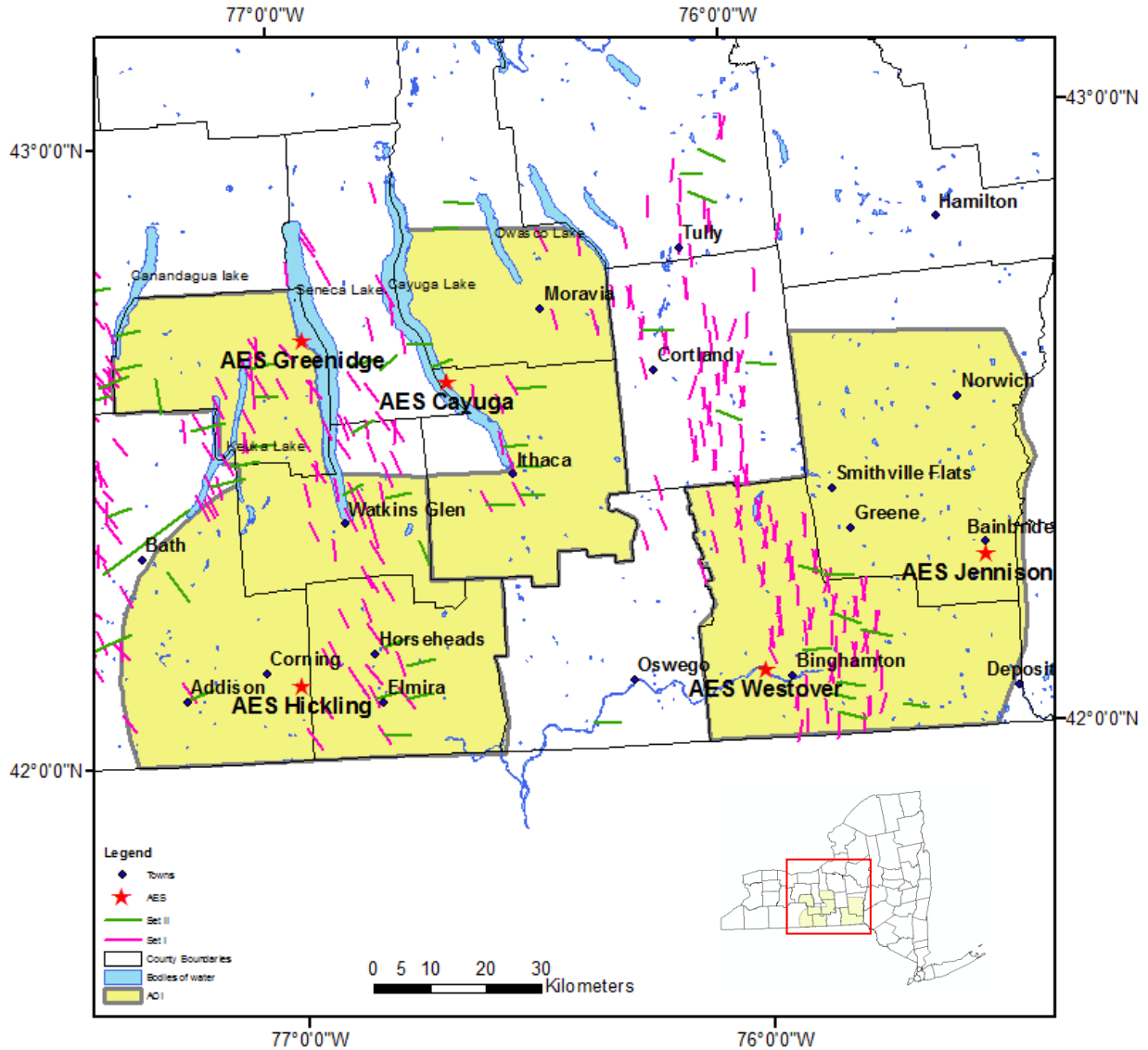


Figure 6.1-13: Set I & II fractures measured in outcrop in the project area (Engelder & Geiser, 1980)



Remote Sensing Laboratory  
Dept. of Geology, SUNY at Buffalo



University at Buffalo  
The State University of New York

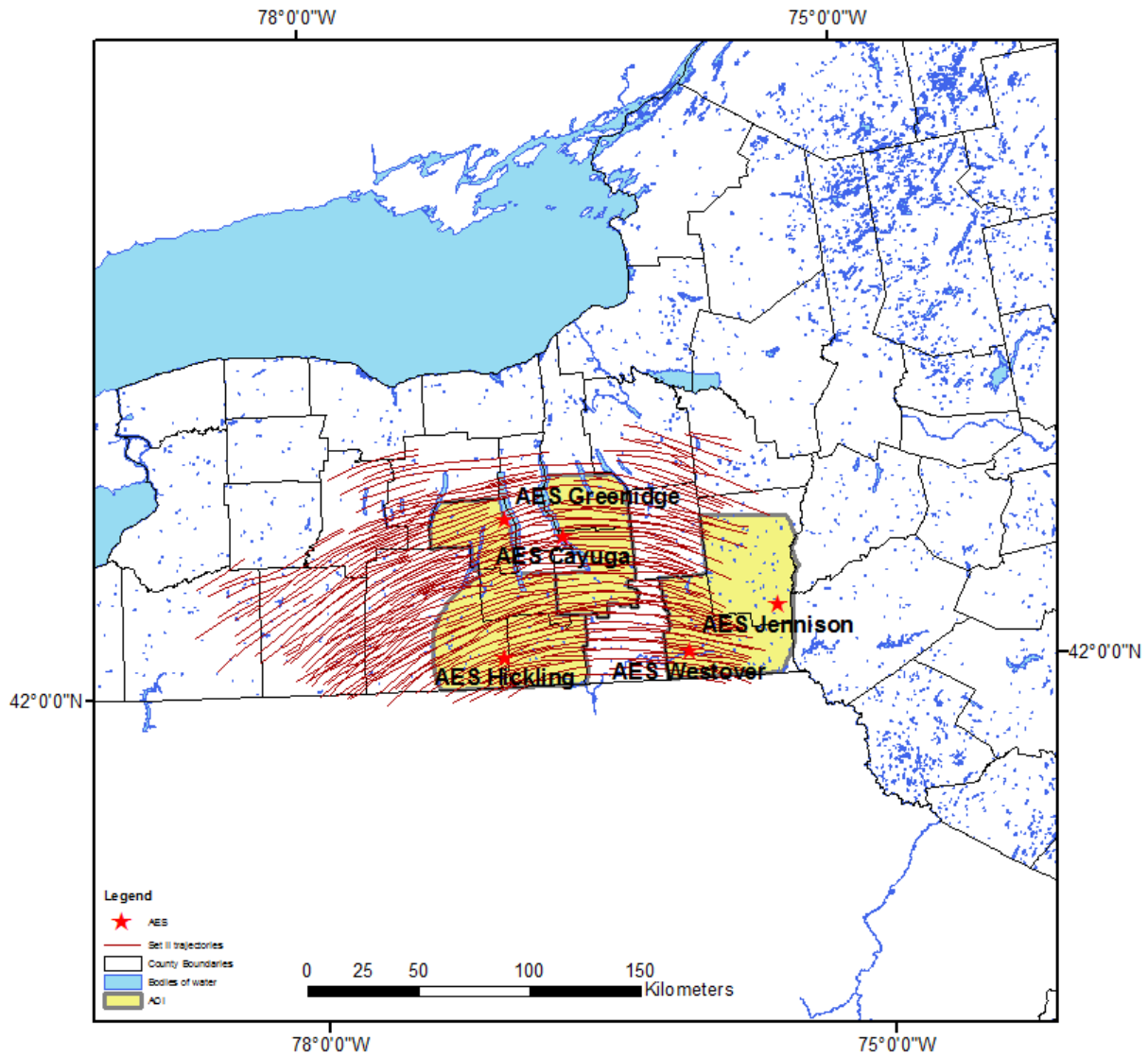


Figure 6.1-14: Set II fracture trajectories based on Set II fractures measured in outcrop (Engelder & Geiser, 1979)



**Remote Sensing Laboratory**  
Dept. of Geology, SUNY at Buffalo



**University at Buffalo**  
The State University of New York

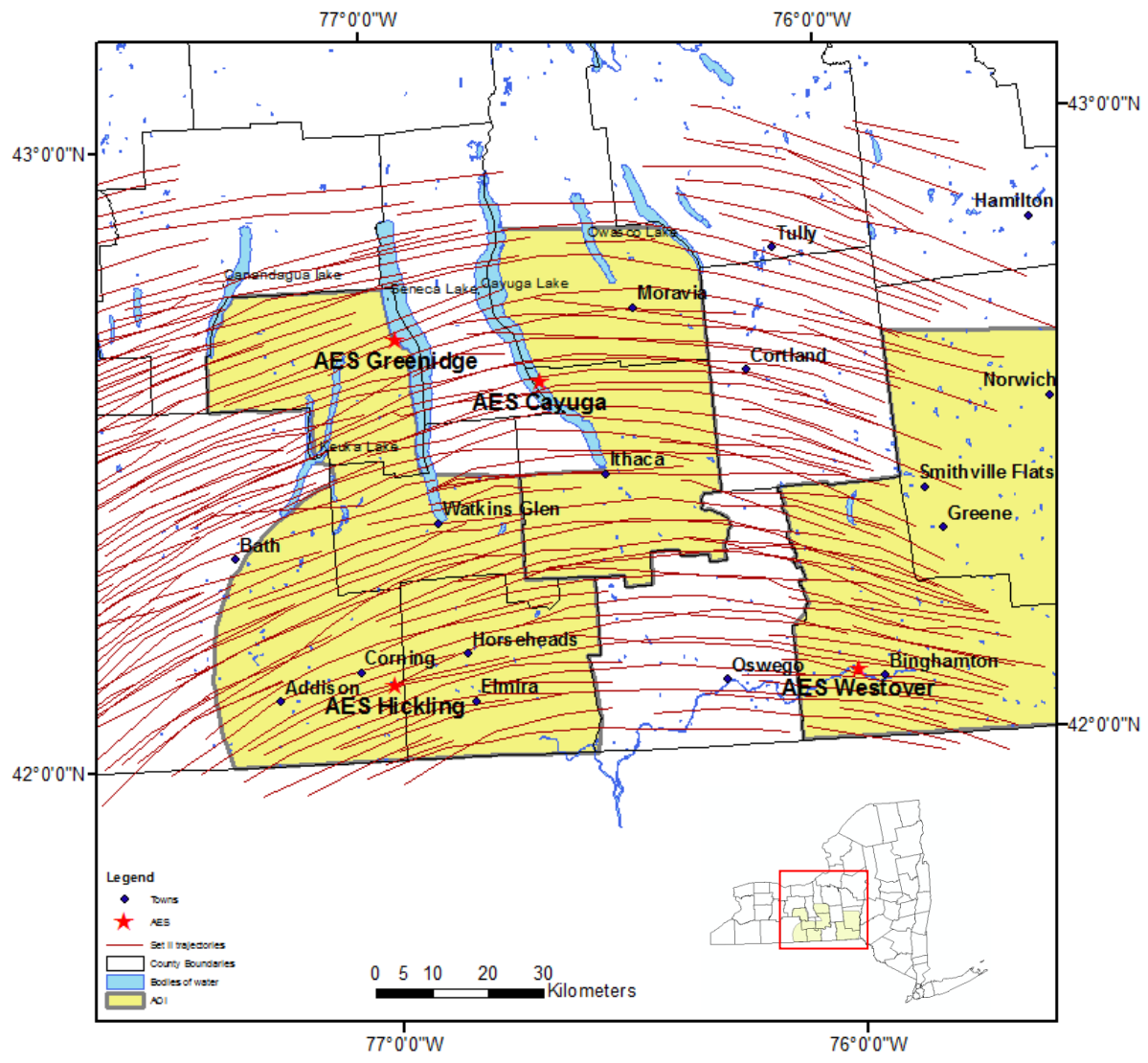


Figure 6.1-15: Set II trajectories based on Set II fracture measurements in the project area (Engelder & Geiser, 1980)



Remote Sensing Laboratory  
Dept. of Geology, SUNY at Buffalo



University at Buffalo  
The State University of New York

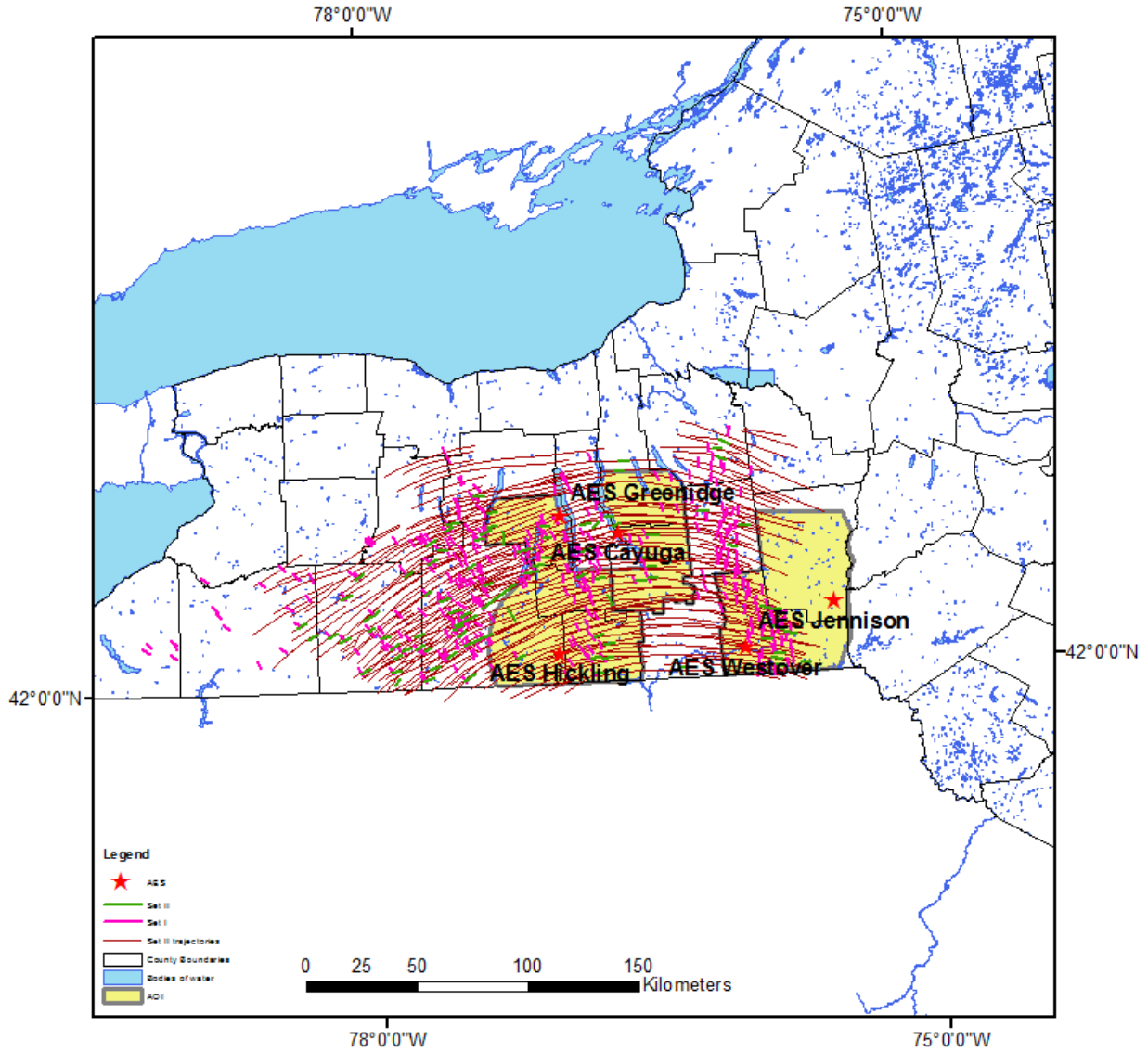


Figure 6.1-16: Set II trajectories compiled with Set I and II joints (Engelder & Geiser, 1980)



Remote Sensing Laboratory  
Dept. of Geology, SUNY at Buffalo



University at Buffalo  
The State University of New York

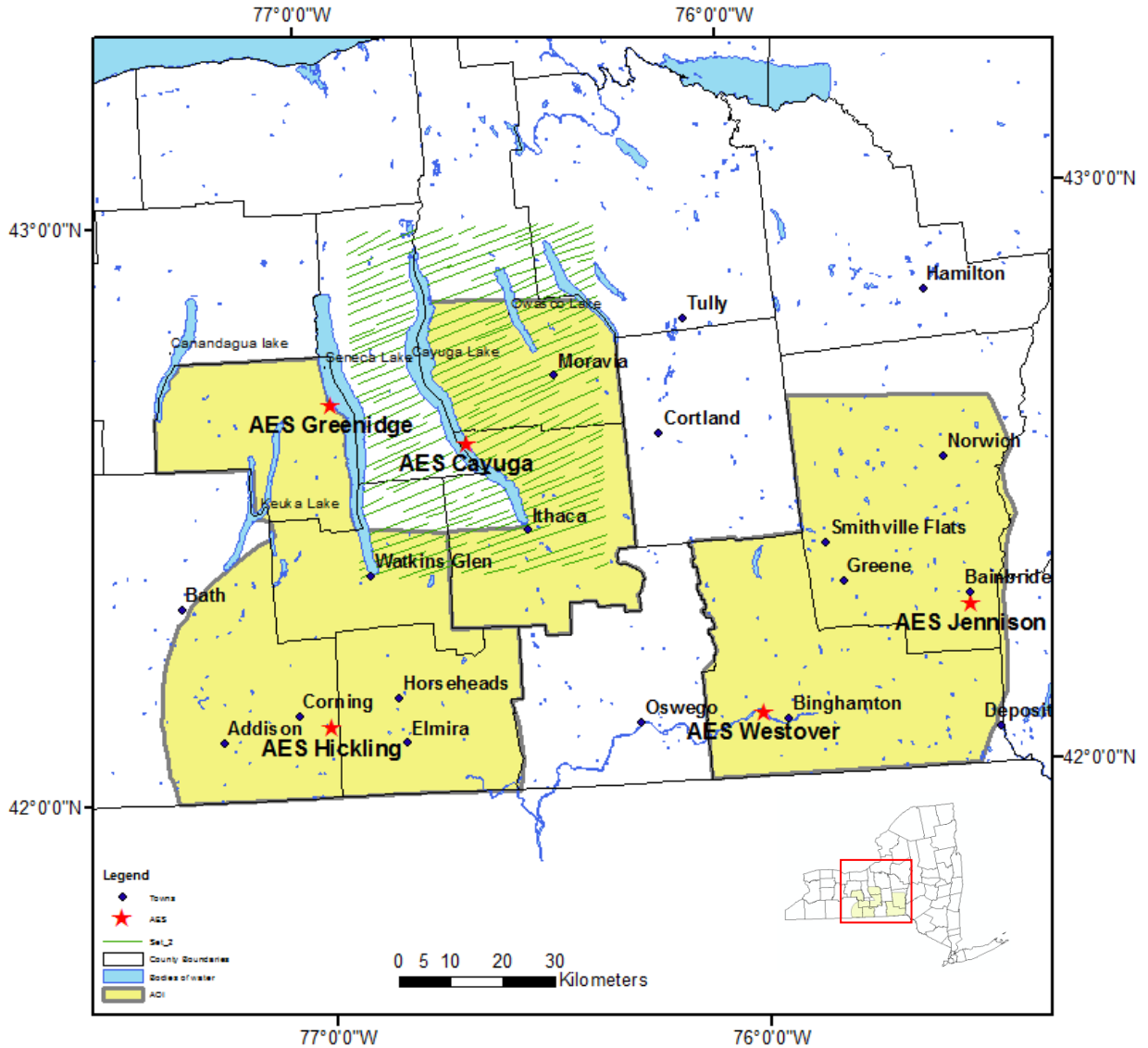


Figure 6.1-17: Trajectories of fractures called Set II (Faculty and Students of Cornell University, 1959), but are most likely Set III in the nomenclature of Engelder and Geiser (1980).



Remote Sensing Laboratory  
Dept. of Geology, SUNY at Buffalo



University at Buffalo  
The State University of New York

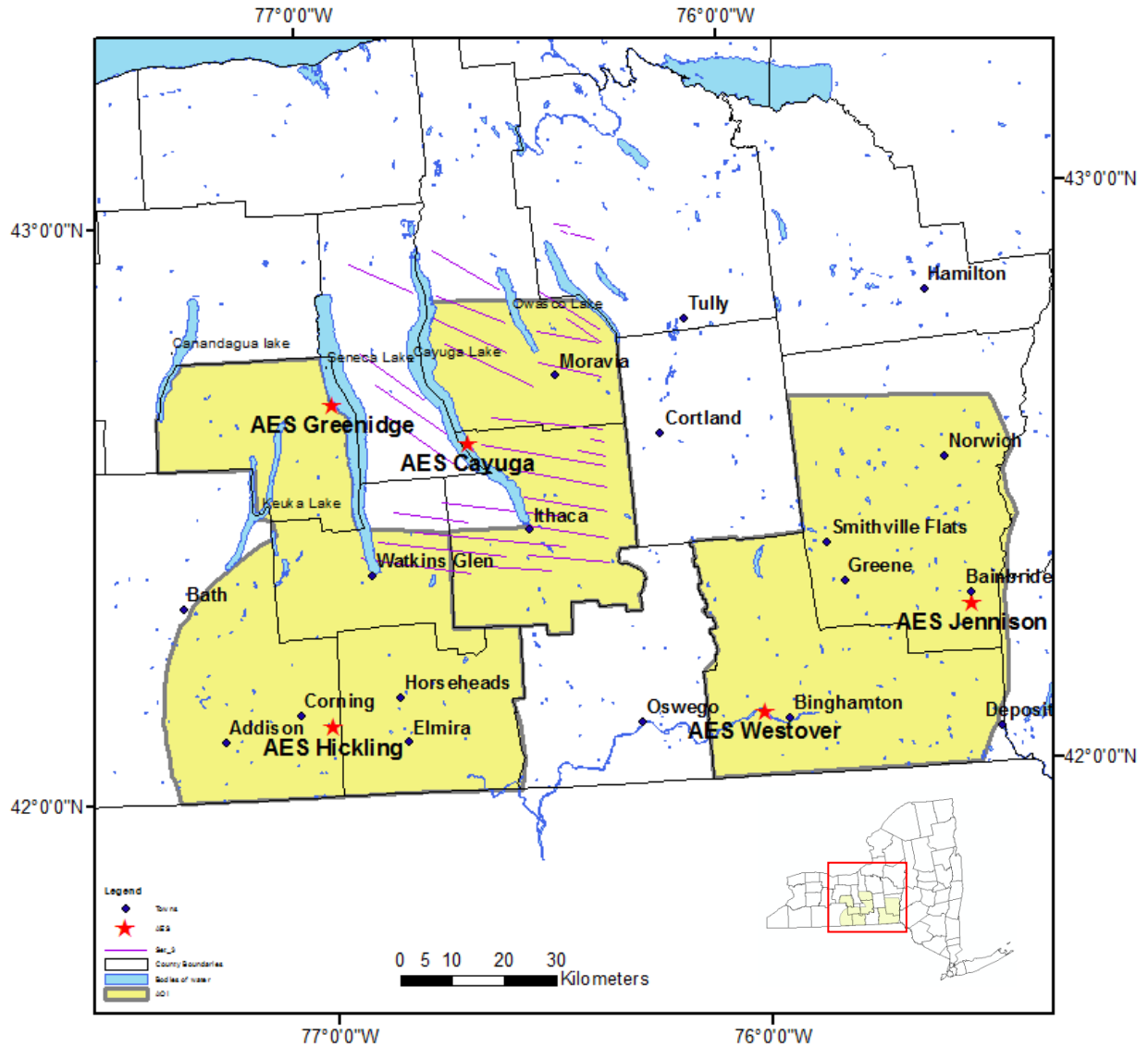


Figure 6.1-18: Trajectories of fractures called Set III (Faculty and Students of Cornell University, 1959), but are most likely Set II in the nomenclature of Engelder and Geiser (1980).





Remote Sensing Laboratory  
Dept. of Geology, SUNY at Buffalo



University at Buffalo  
The State University of New York

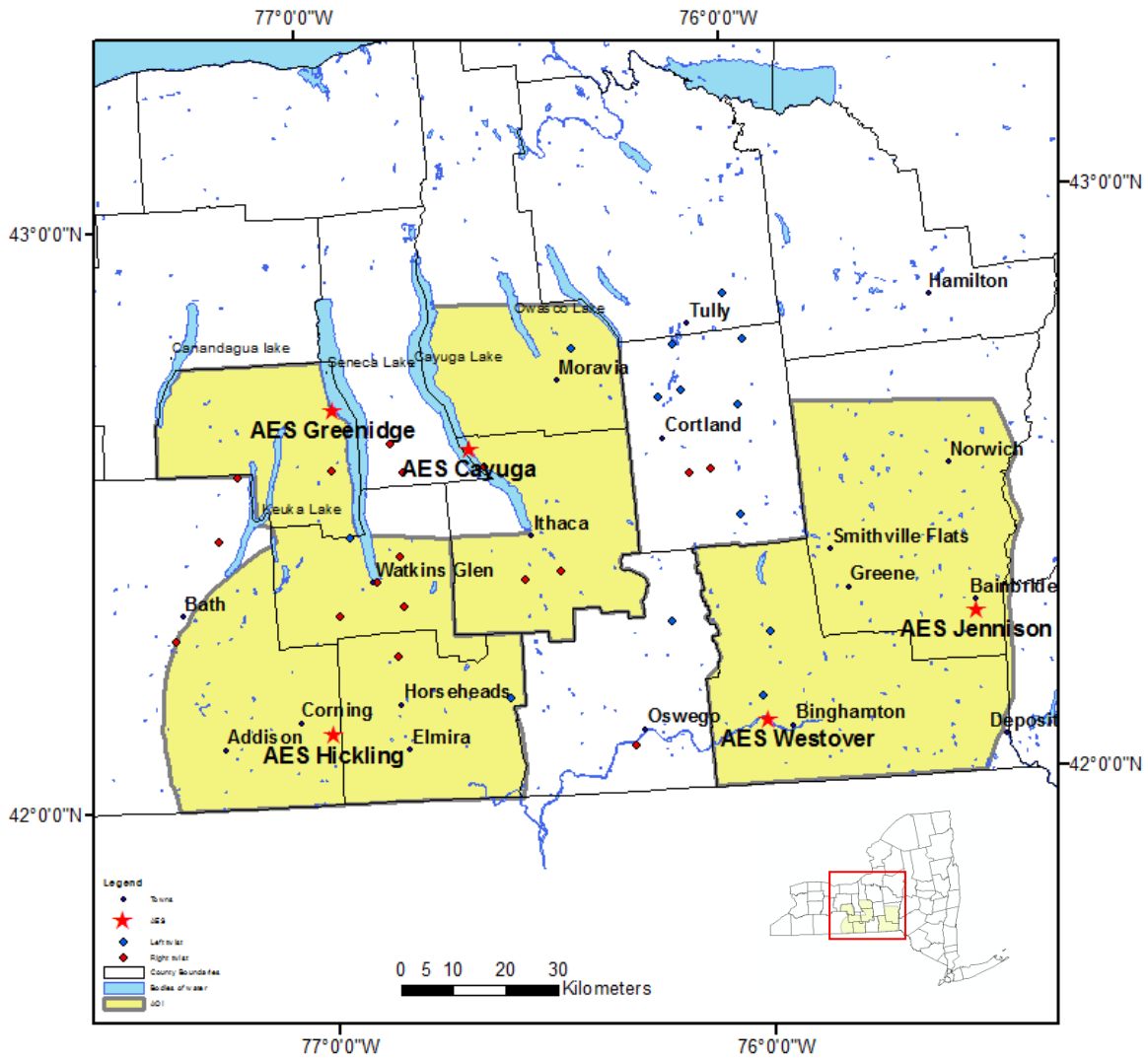


Figure 6.1-19: Sites of twist hackles (red and blue dots). The red dots are gradual twist hackles twisting clockwise (right) and blue dots show gradual twist hackles twisting counterclockwise (left) (Younes & Engelder, 1999)



Remote Sensing Laboratory  
Dept. of Geology, SUNY at Buffalo



University at Buffalo  
The State University of New York

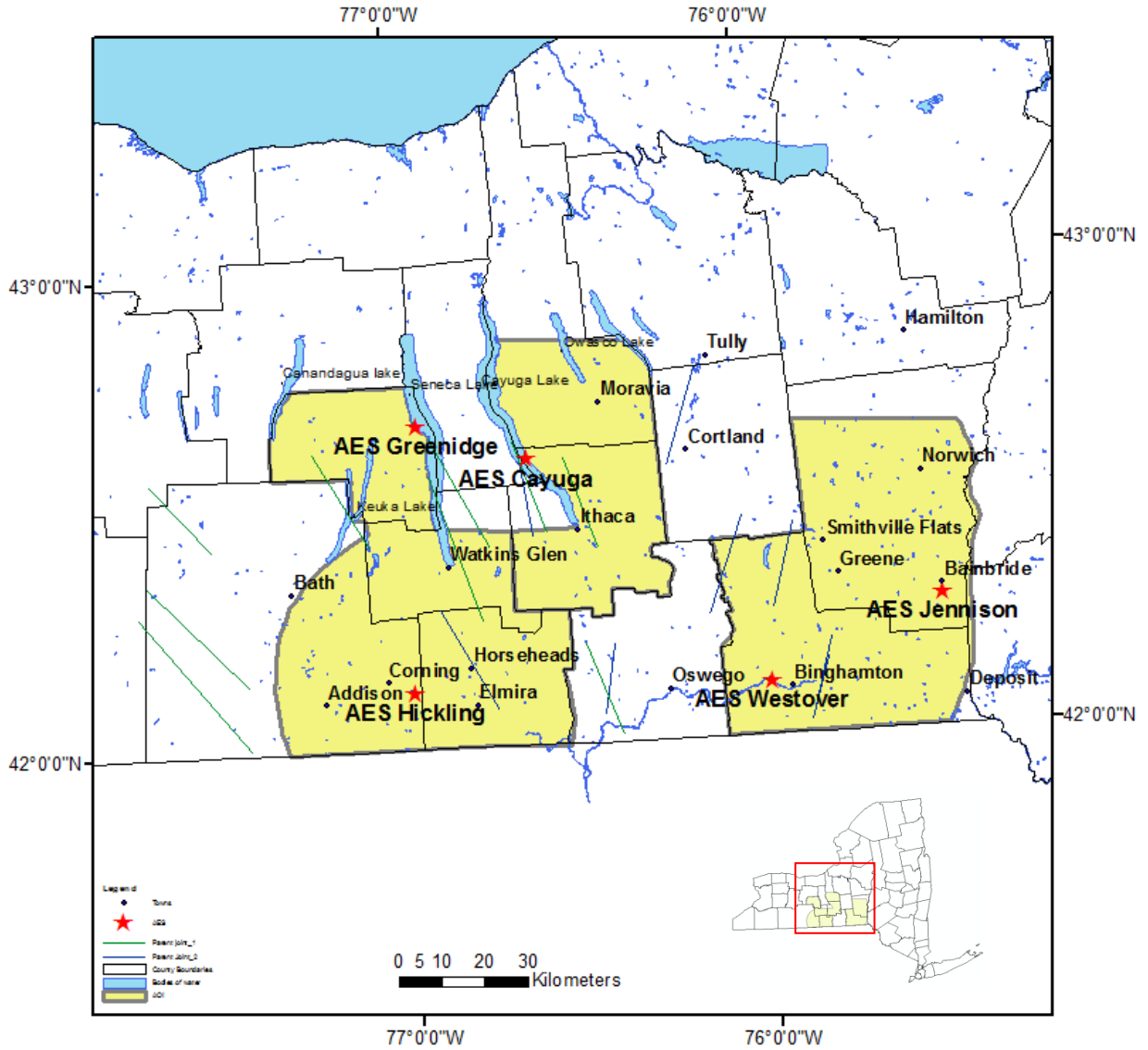


Figure 6.1-20: Parent joints, Set I (Younes & Engelder, 1999)



Remote Sensing Laboratory  
Dept. of Geology, SUNY at Buffalo



University at Buffalo  
The State University of New York

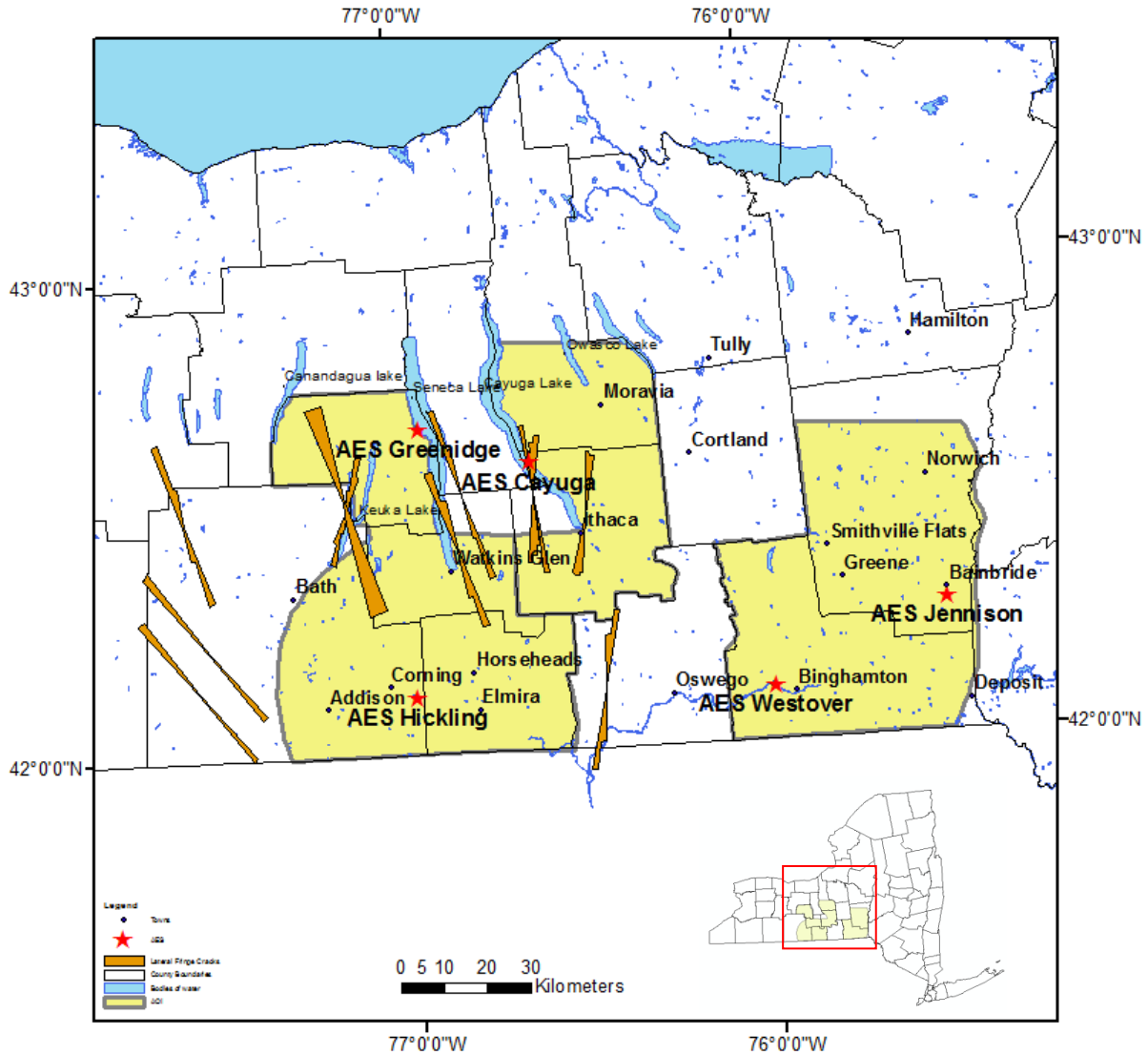


Figure 6.1-21: Clockwise fringe cracks on the parent joint of Set I in the western section of the project area (Younes & Engelder, 1999)



Remote Sensing Laboratory  
Dept. of Geology, SUNY at Buffalo



University at Buffalo  
The State University of New York

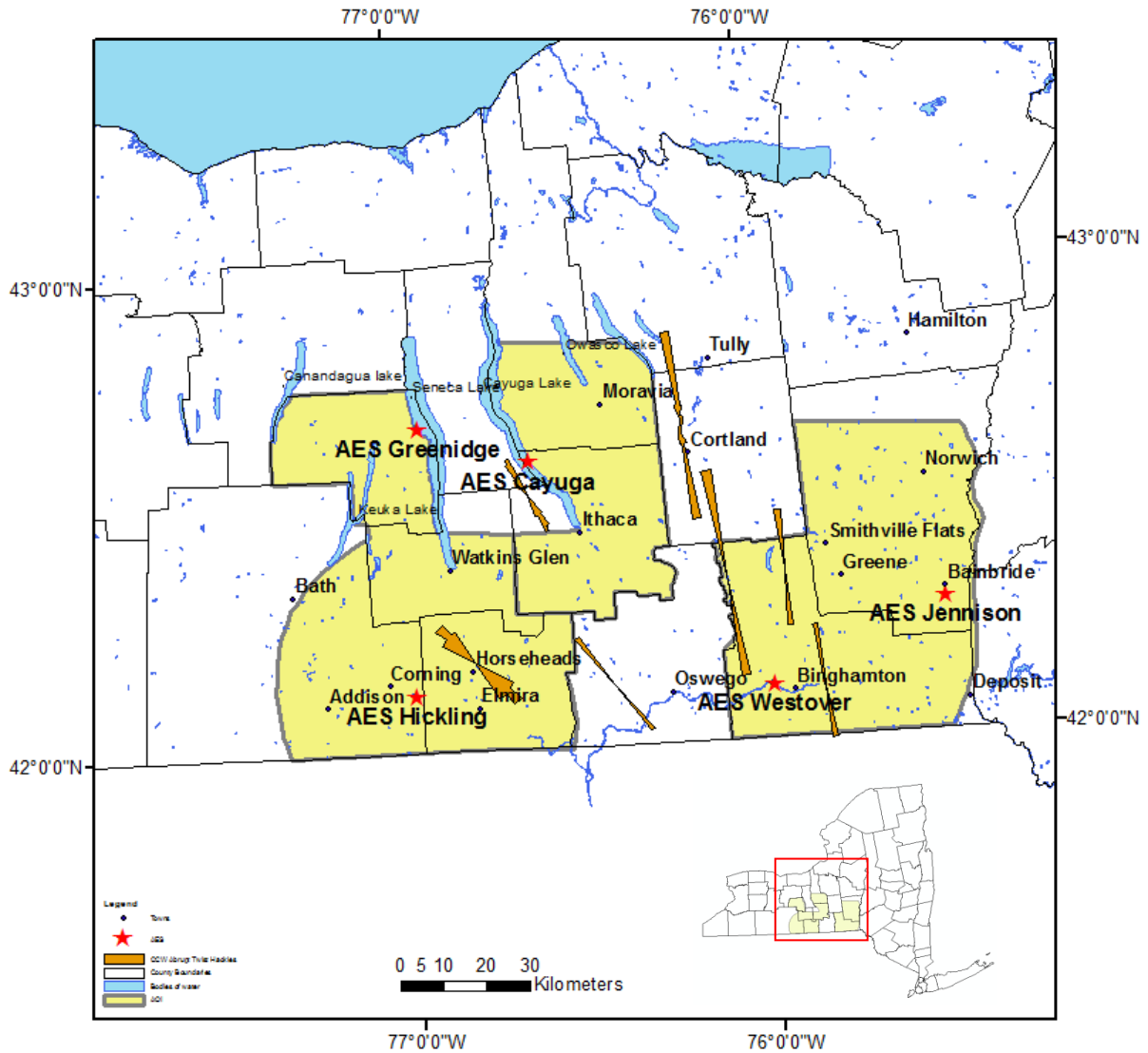


Figure 6.1-22: Counterclockwise fringe cracks on the parent joint of Set I in the eastern section of the project area (Younes & Engelder, 1999)



Remote Sensing Laboratory  
Dept. of Geology, SUNY at Buffalo



University at Buffalo  
The State University of New York

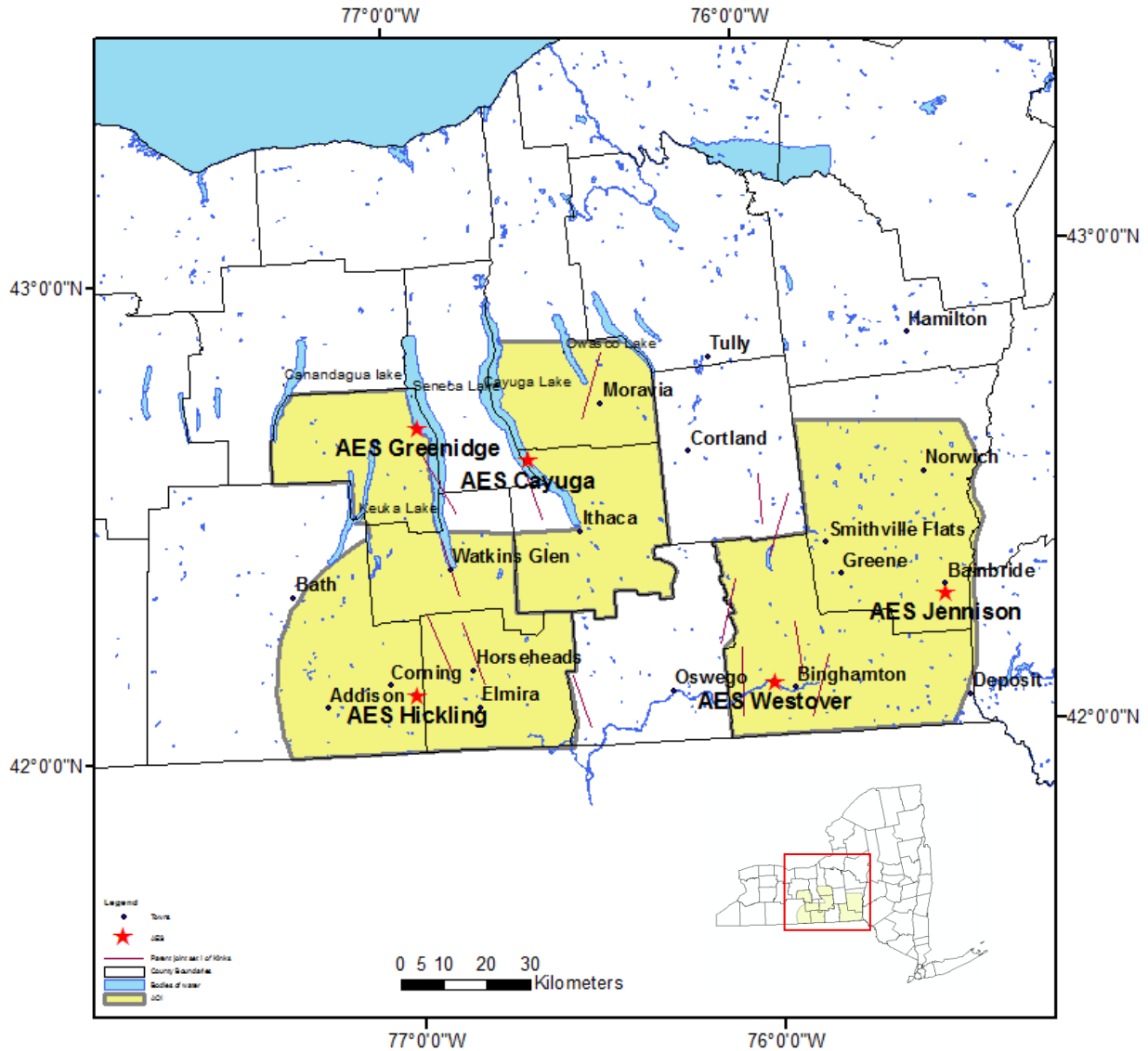


Figure 6.1-23: Parent joint Set I of fringe crack kinks (Younes & Engelder, 1999)



Remote Sensing Laboratory  
Dept. of Geology, SUNY at Buffalo



University at Buffalo  
The State University of New York

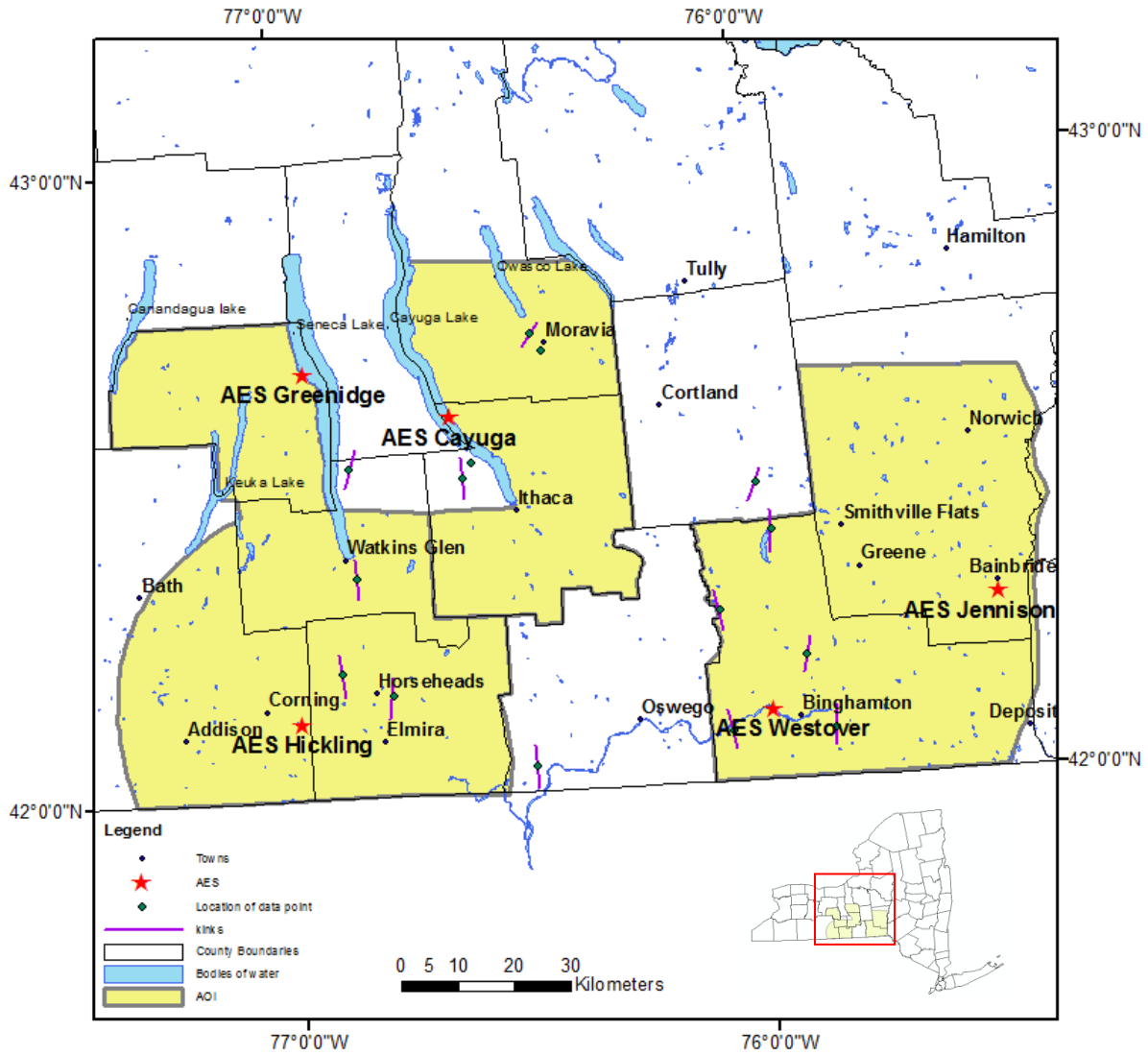


Figure 6.1-24: Fringe crack kinks on the parent joint of Set I with green dots showing the location of the data (Younes & Engelder, 1999)



Remote Sensing Laboratory  
Dept. of Geology, SUNY at Buffalo



University at Buffalo  
The State University of New York

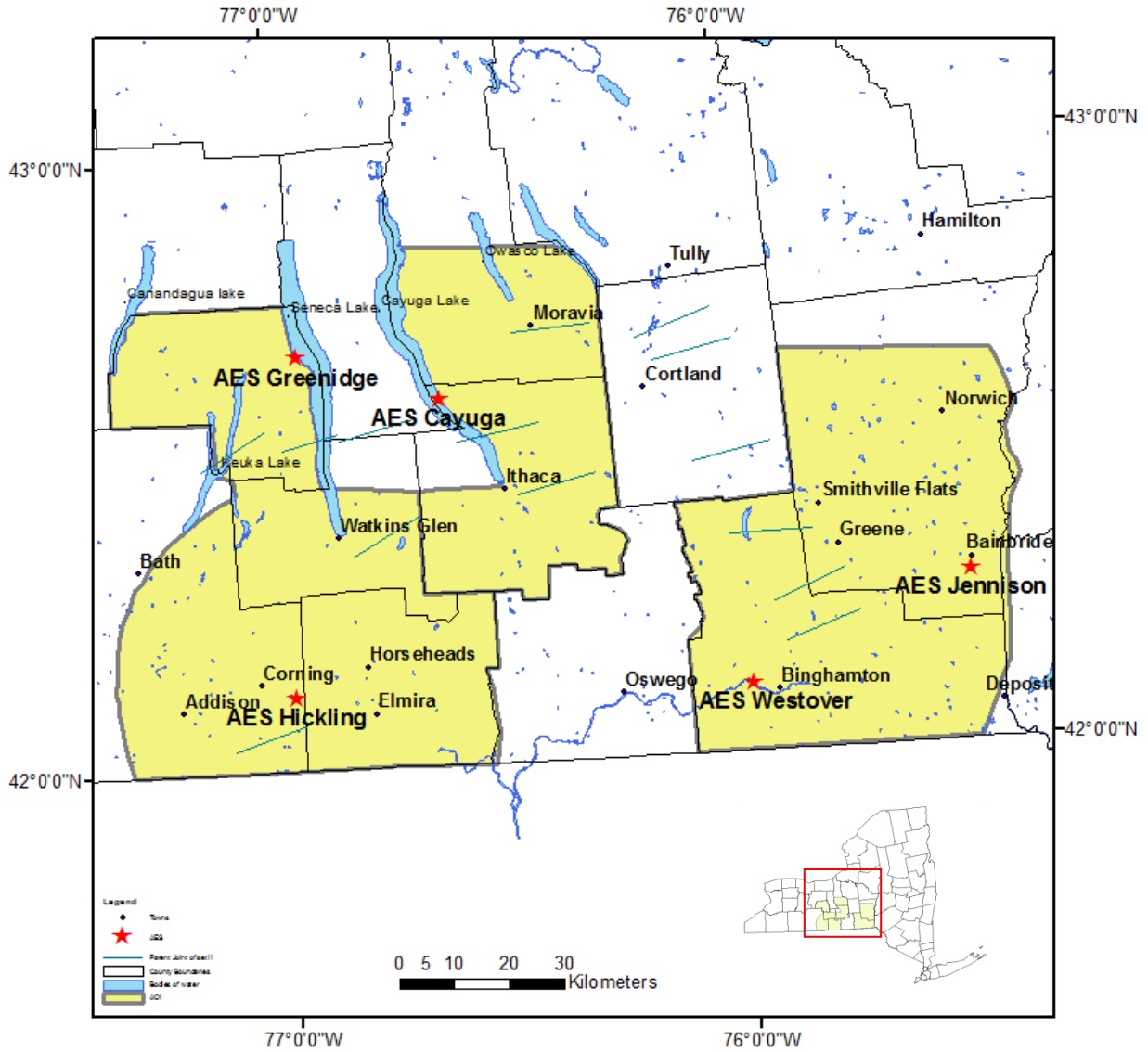


Figure 6.1-25: Parent joint of Set II (and probable Set III in the east) (Younes & Engelder, 1999)



Remote Sensing Laboratory  
Dept. of Geology, SUNY at Buffalo



University at Buffalo  
The State University of New York

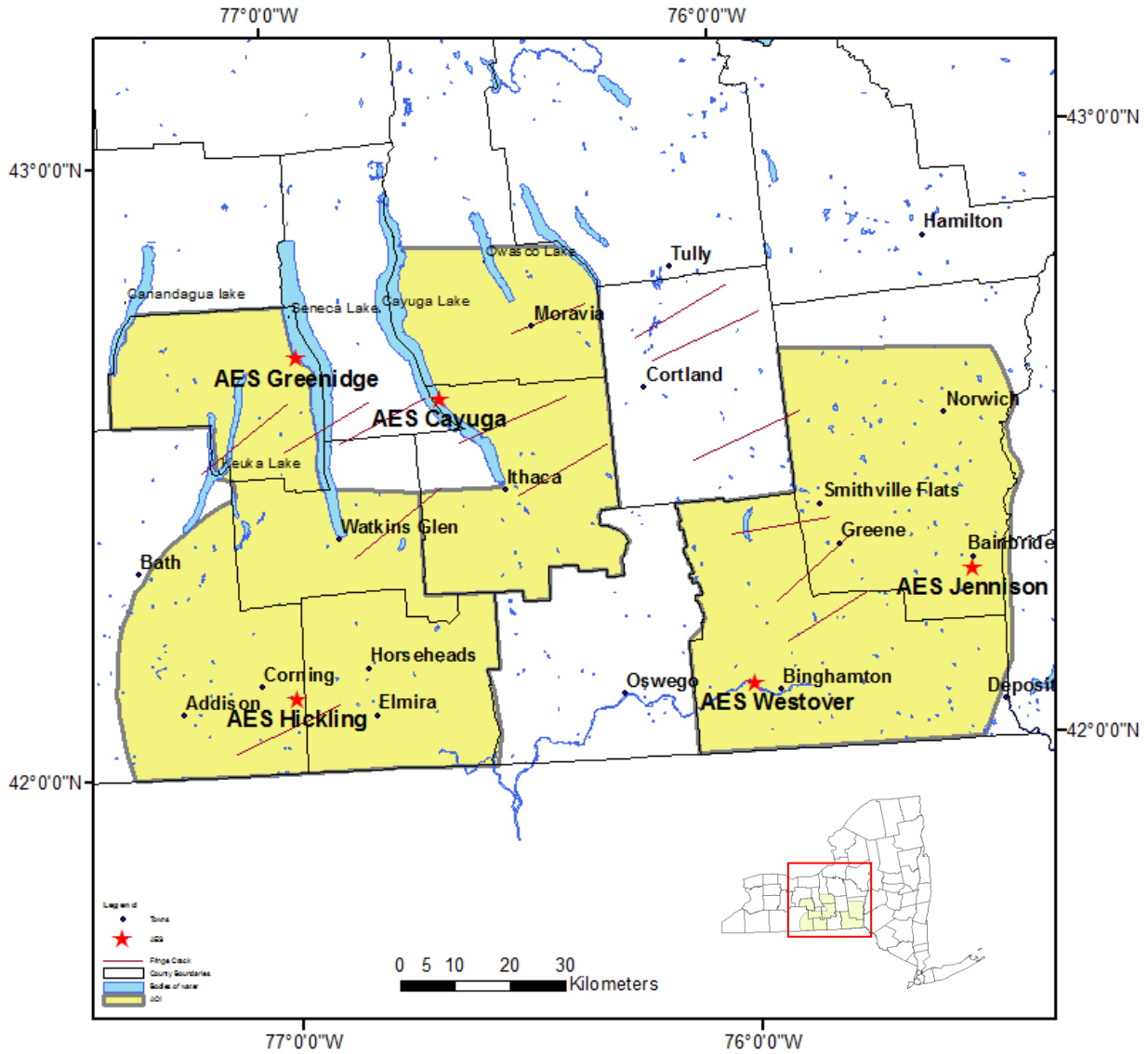


Figure 6.1-26: Fringe cracks on parent joints of Set II (and probable Set III in the east) (Younes & Engelder, 1999)





**Remote Sensing Laboratory**  
 Dept. of Geology, SUNY at Buffalo



**University at Buffalo**  
 The State University of New York

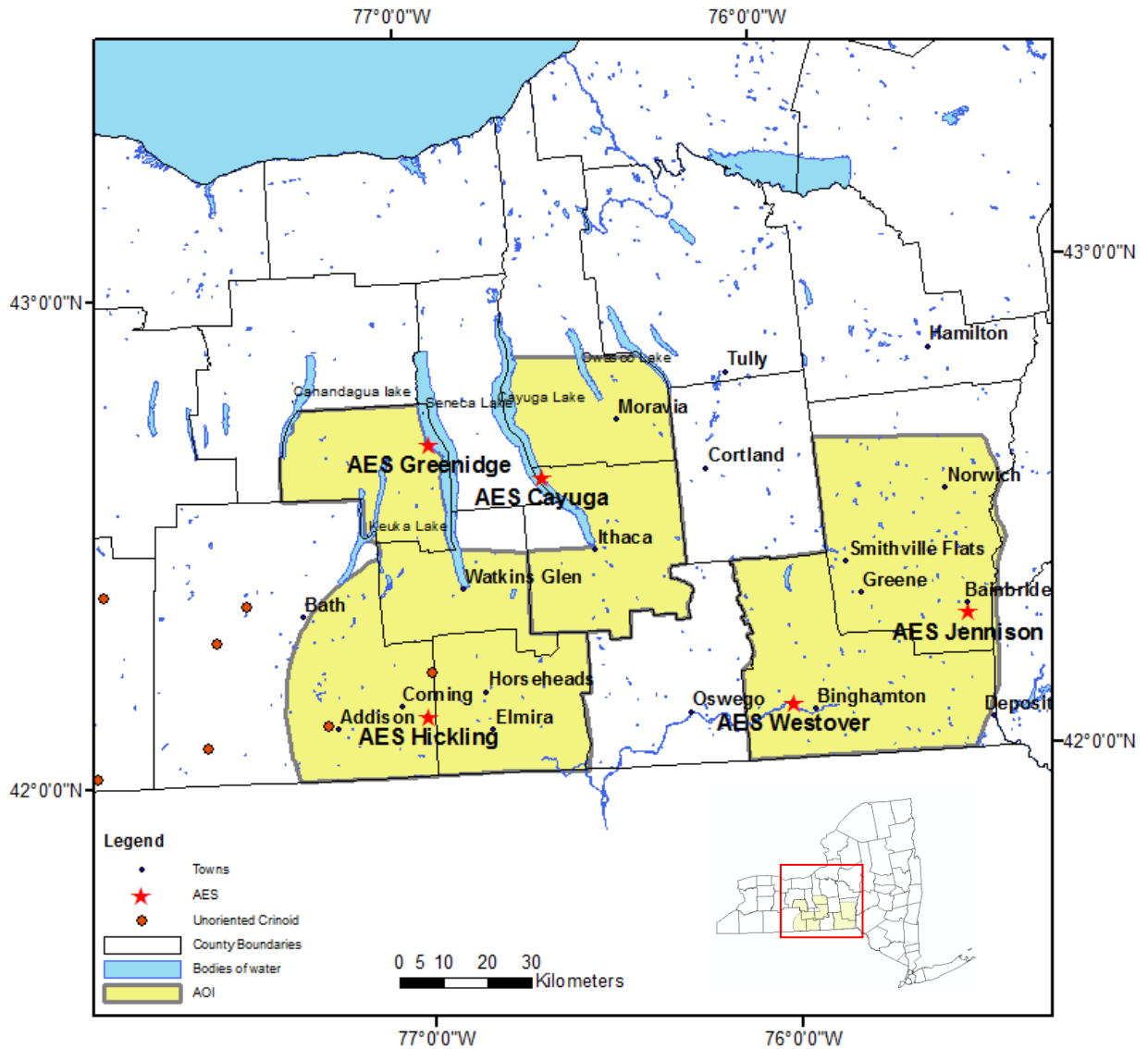


Figure 6.1-27: Unoriented crinoid locations (Engelder & Oertel, 1989)



Remote Sensing Laboratory  
Dept. of Geology, SUNY at Buffalo



University at Buffalo  
The State University of New York

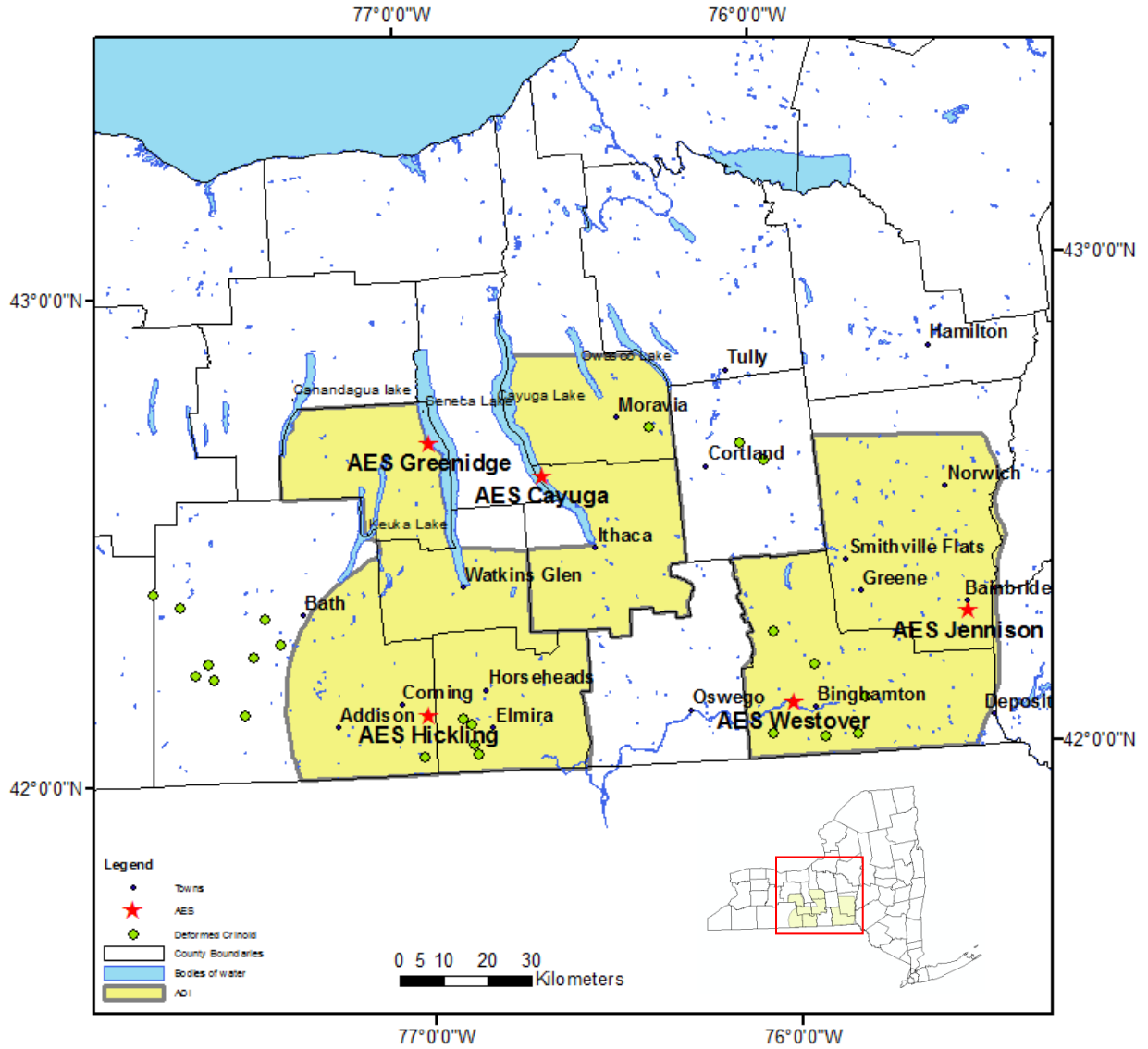


Figure 6.1-28: Deformed crinoid locations (Engelder & Oertel, 1989)



Remote Sensing Laboratory  
Dept. of Geology, SUNY at Buffalo



University at Buffalo  
The State University of New York

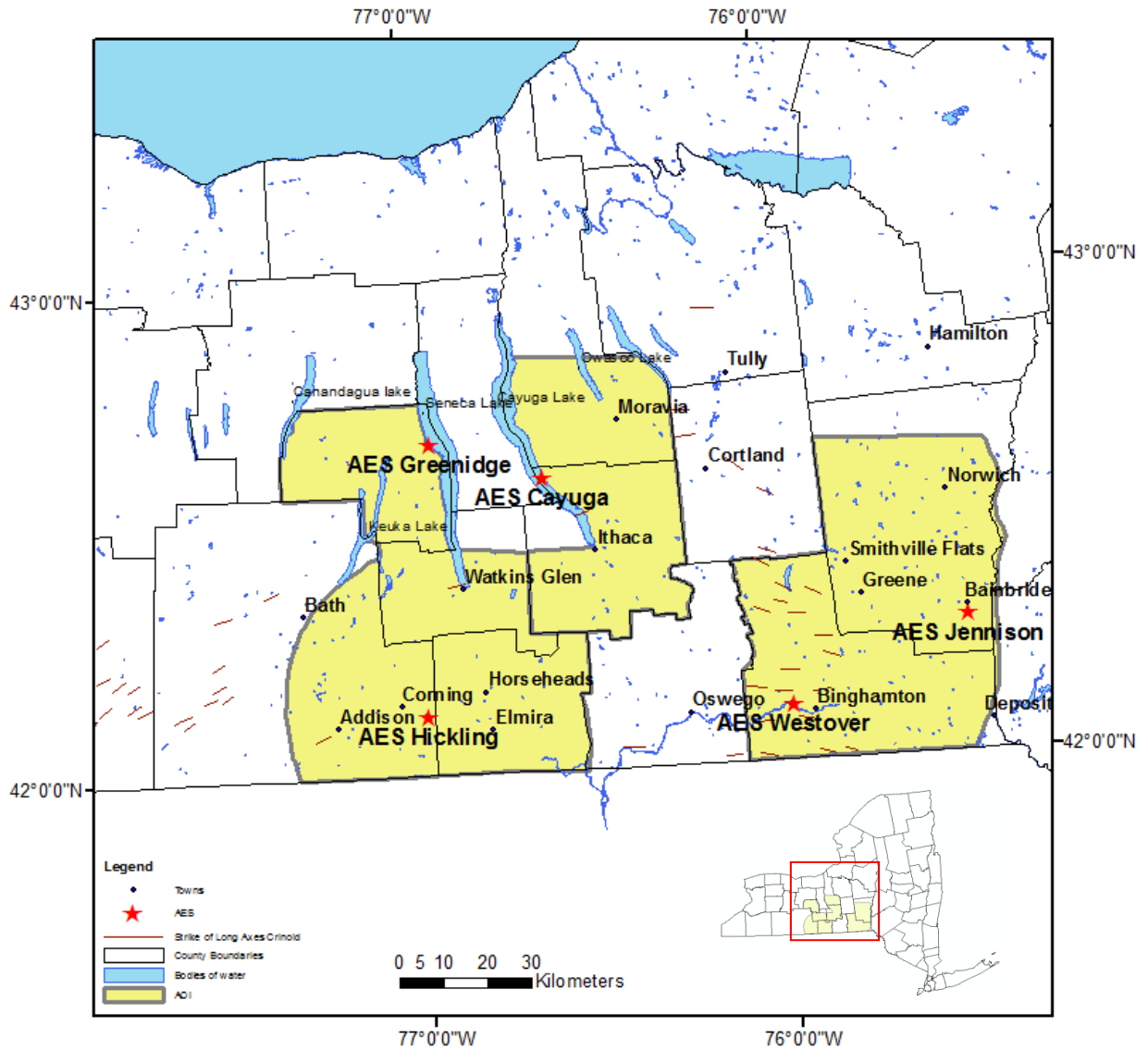


Figure 6.1-29: Strike of the long axes of crinoids (Engelder & Oertel, 1989)



Remote Sensing Laboratory  
Dept. of Geology, SUNY at Buffalo



University at Buffalo  
The State University of New York

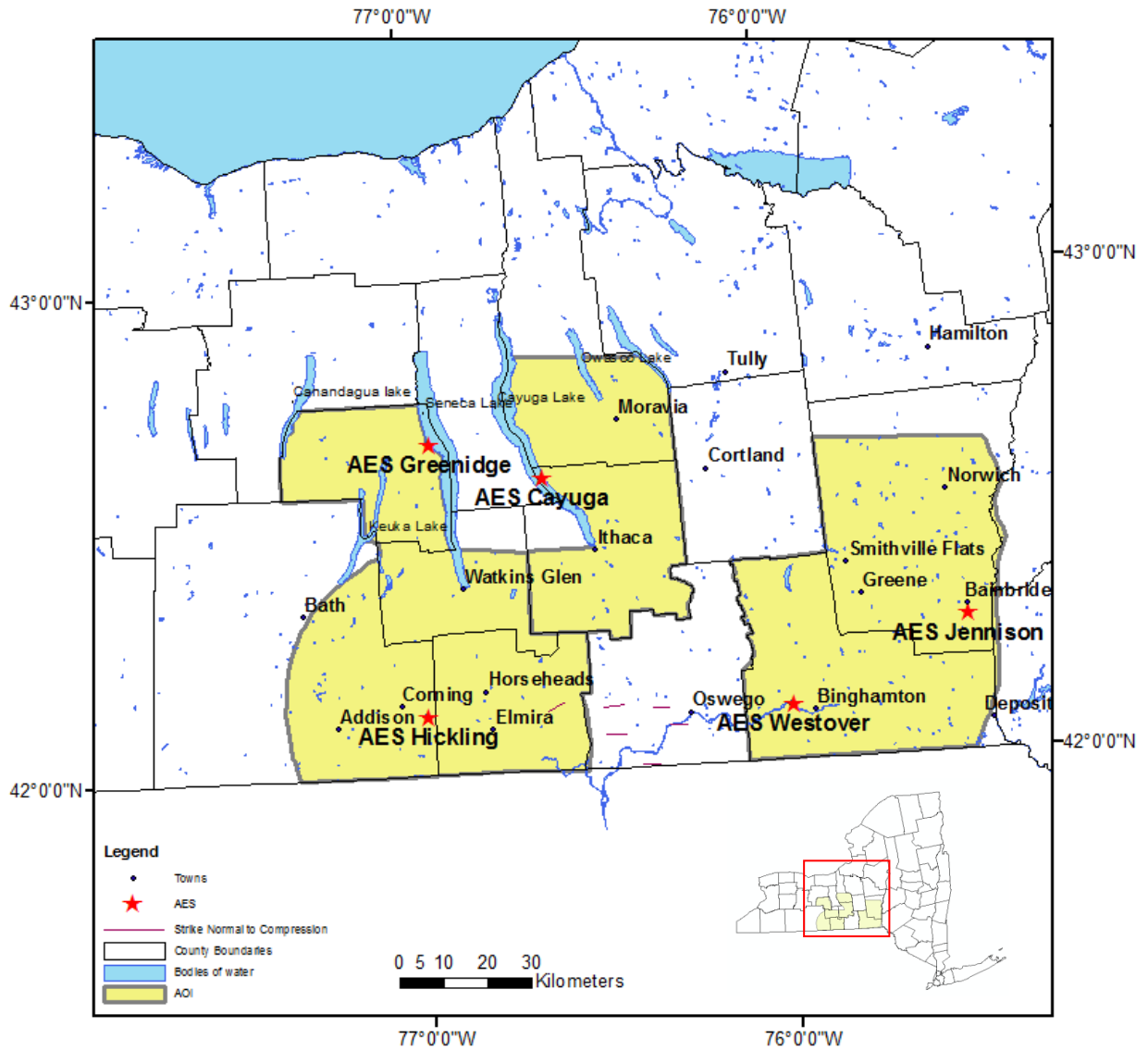


Figure 6.1-30: Strike of the normal to compression inferred crinoid long axes (Engelder & Oertel, 1989)



Remote Sensing Laboratory  
Dept. of Geology, SUNY at Buffalo



University at Buffalo  
The State University of New York

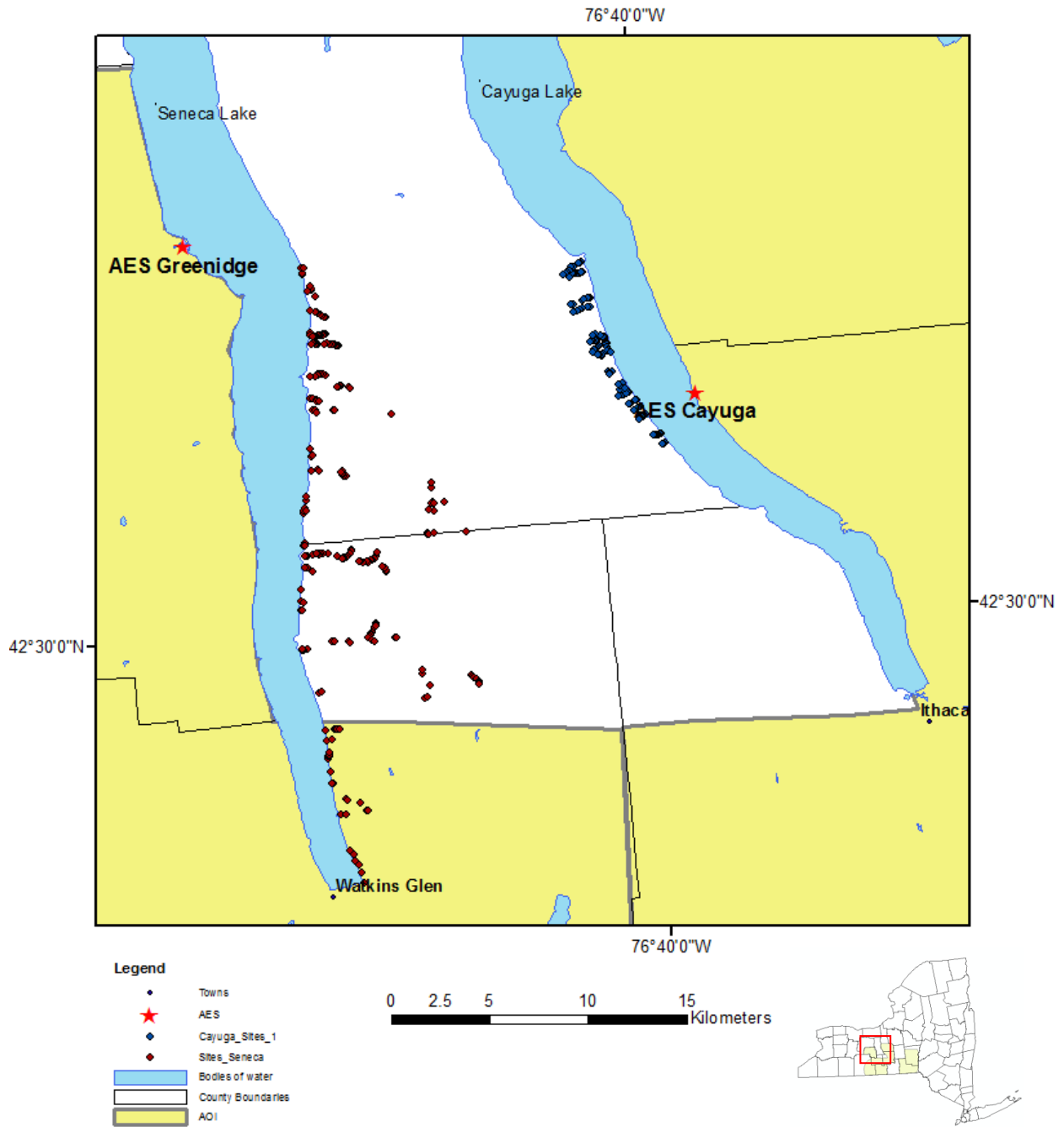


Figure 6.1-31: Field sites on Seneca and Cayuga lakes (Lugert et al, 2001, Cruz, 2005, Jacobi, 2007)



**Remote Sensing Laboratory**  
 Dept. of Geology, SUNY at Buffalo



**University at Buffalo**  
 The State University of New York

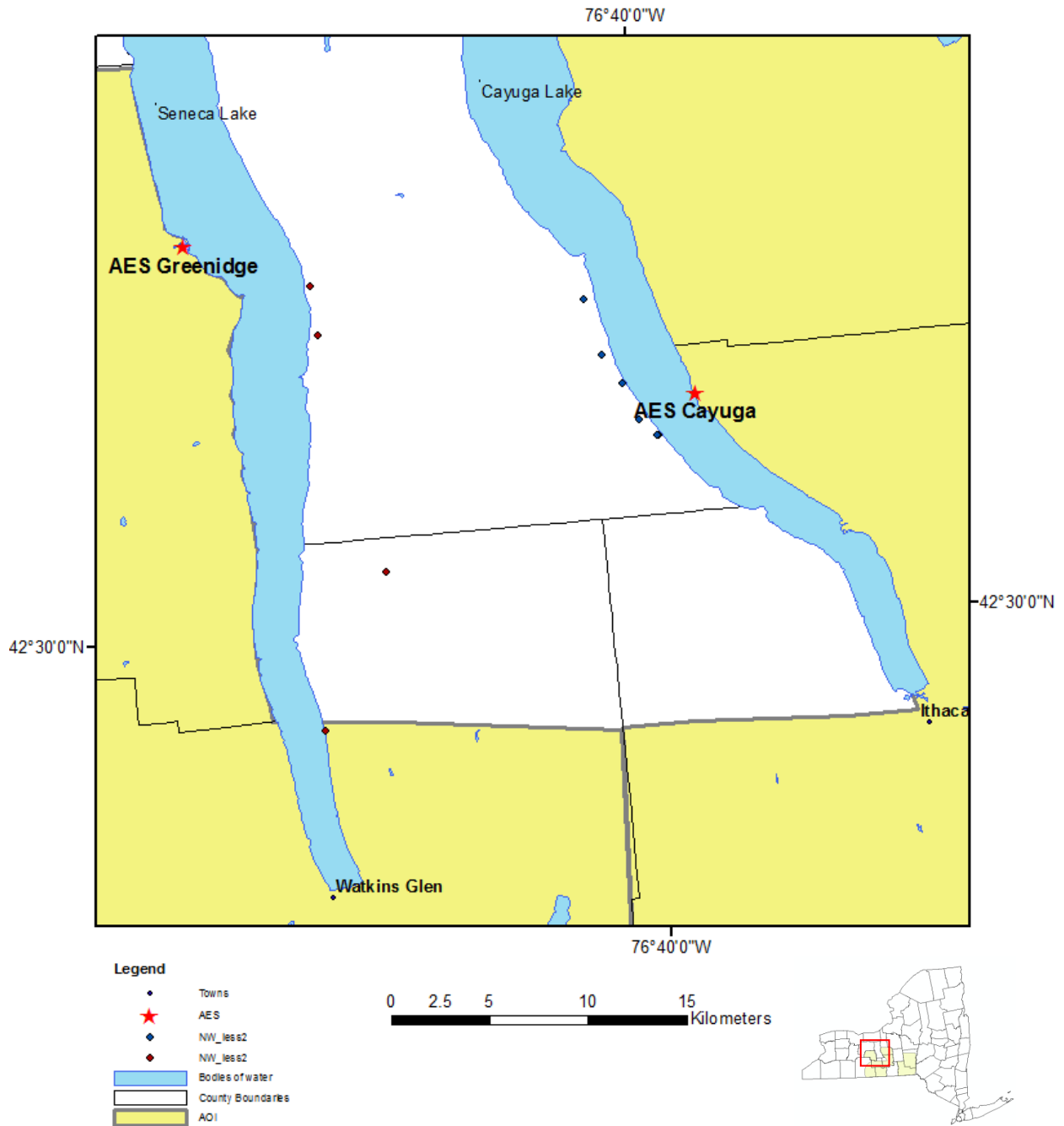


Figure 6.1-32: Field sites with NW striking fractures with a fracture frequency of 0-2 fractures/m (Lugert et al, 2001, Cruz, 2005, Jacobi, 2007)



**Remote Sensing Laboratory**  
*Dept. of Geology, SUNY at Buffalo*



**University at Buffalo**  
*The State University of New York*

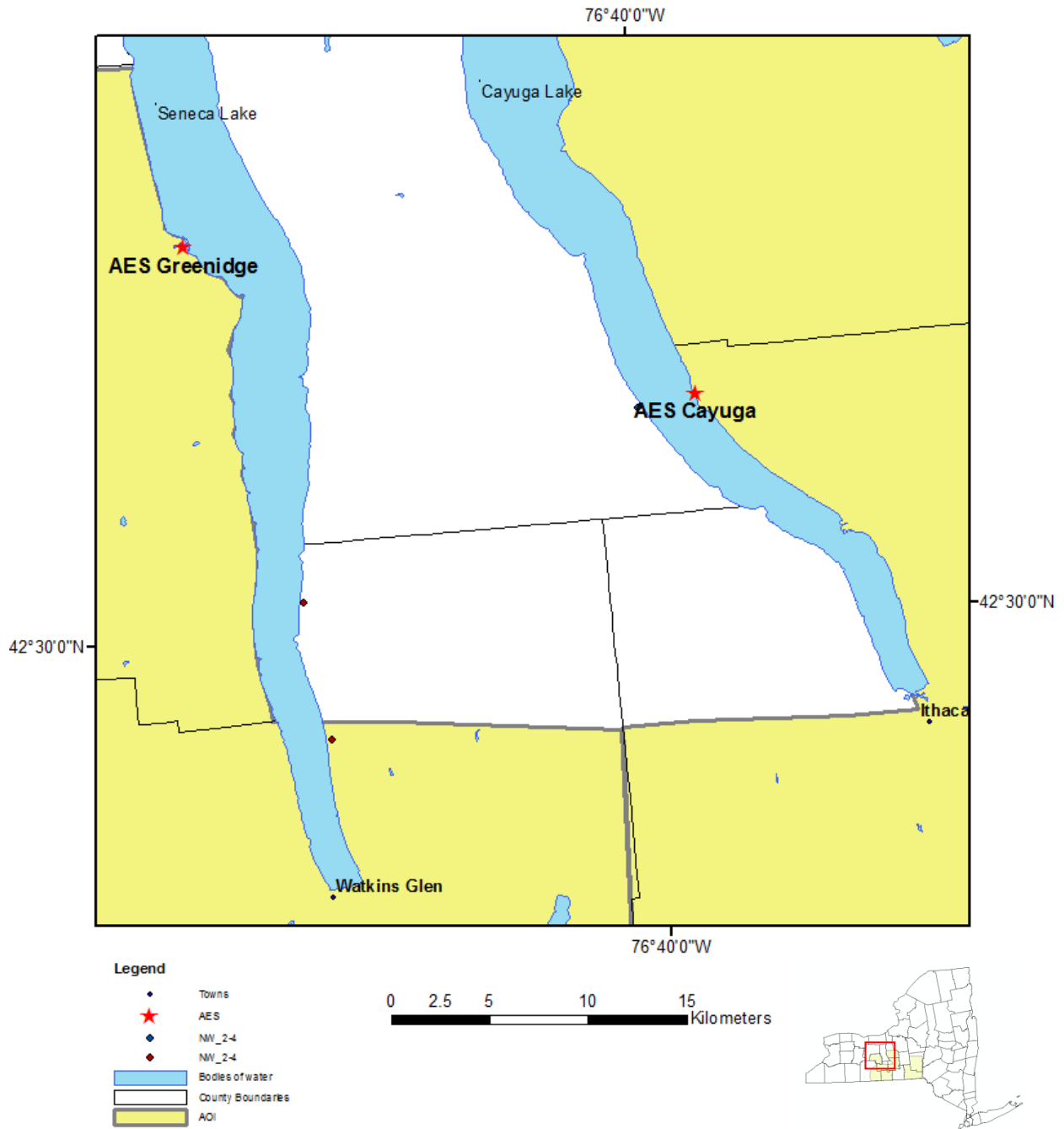


Figure 6.1-33: Field sites with NW striking fractures with a fracture frequency of 2-4 fractures/m (Lugert et al, 2001, Cruz, 2005, Jacobi, 2007)



Remote Sensing Laboratory  
Dept. of Geology, SUNY at Buffalo



University at Buffalo  
The State University of New York

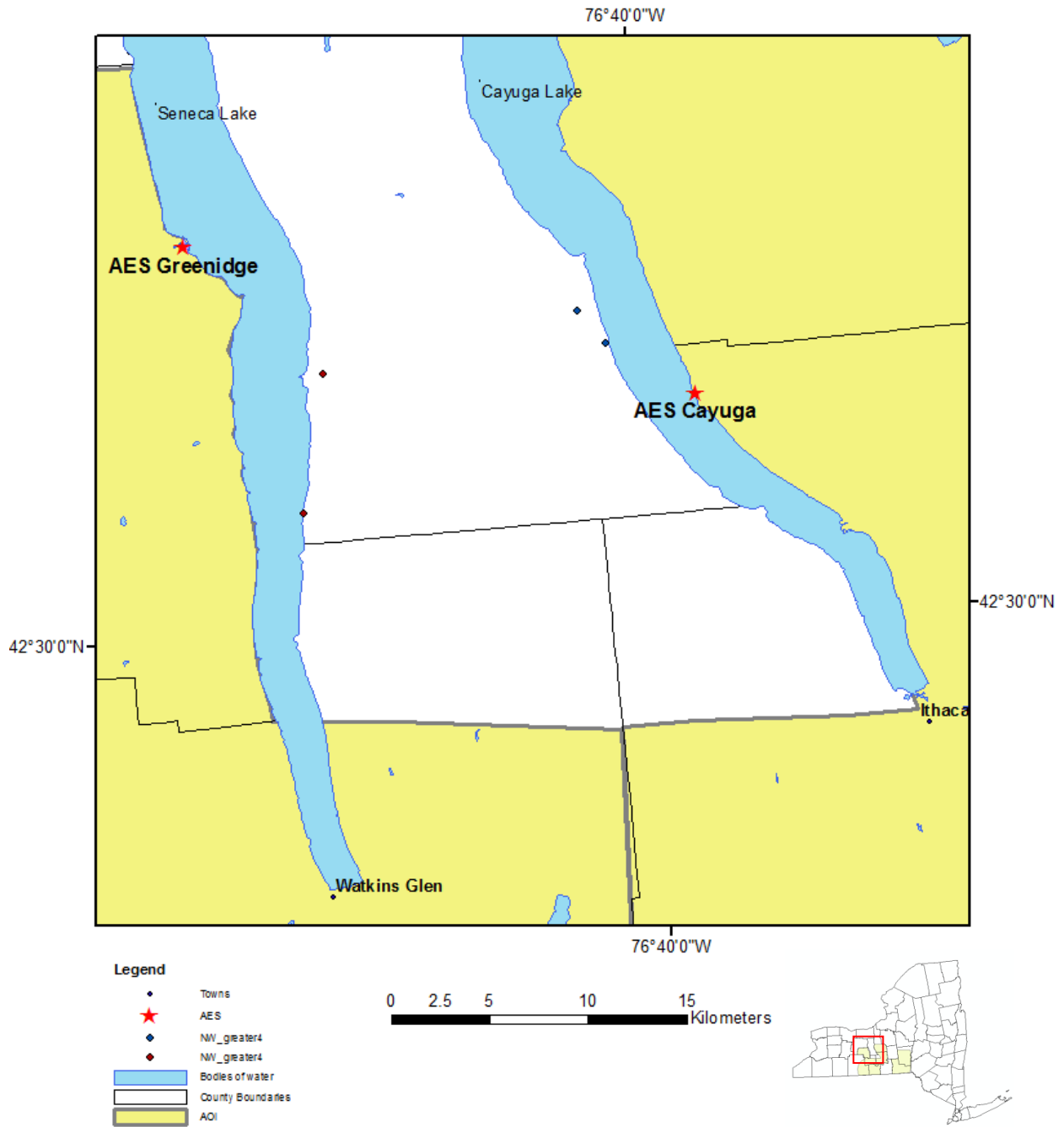


Figure 6.1-34: Field sites with NW striking fractures with a fracture frequency of greater than 4 fractures/m (Lugert et al, 2001, Cruz, 2005, Jacobi, 2007)





**Remote Sensing Laboratory**  
 Dept. of Geology, SUNY at Buffalo



**University at Buffalo**  
 The State University of New York

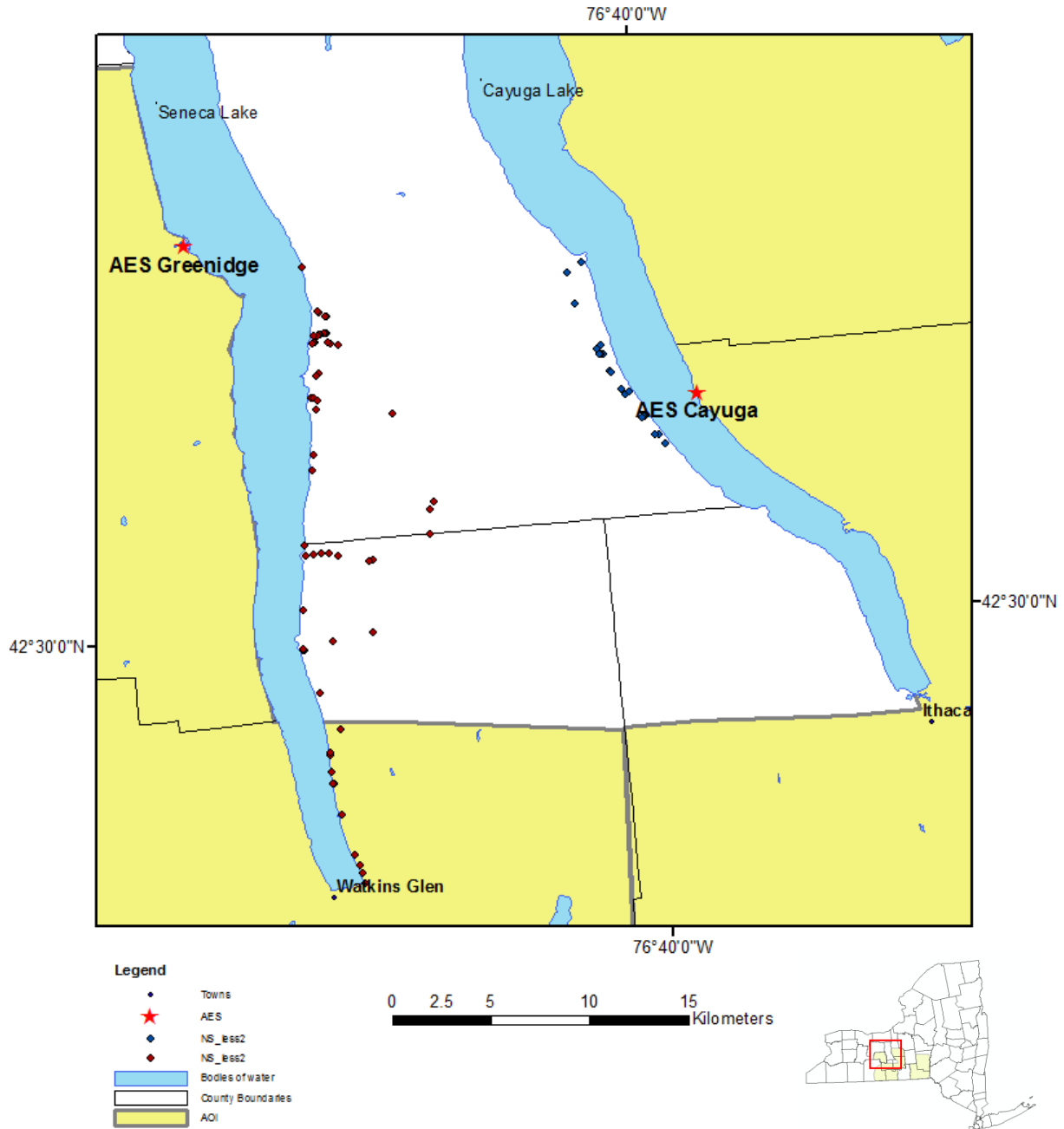


Figure 6.1-35: Field sites with NS striking fractures with a fracture frequency of 0-2 fractures/m (Lugert et al, 2001, Cruz, 2005, Jacobi, 2007)



Remote Sensing Laboratory  
Dept. of Geology, SUNY at Buffalo



University at Buffalo  
The State University of New York

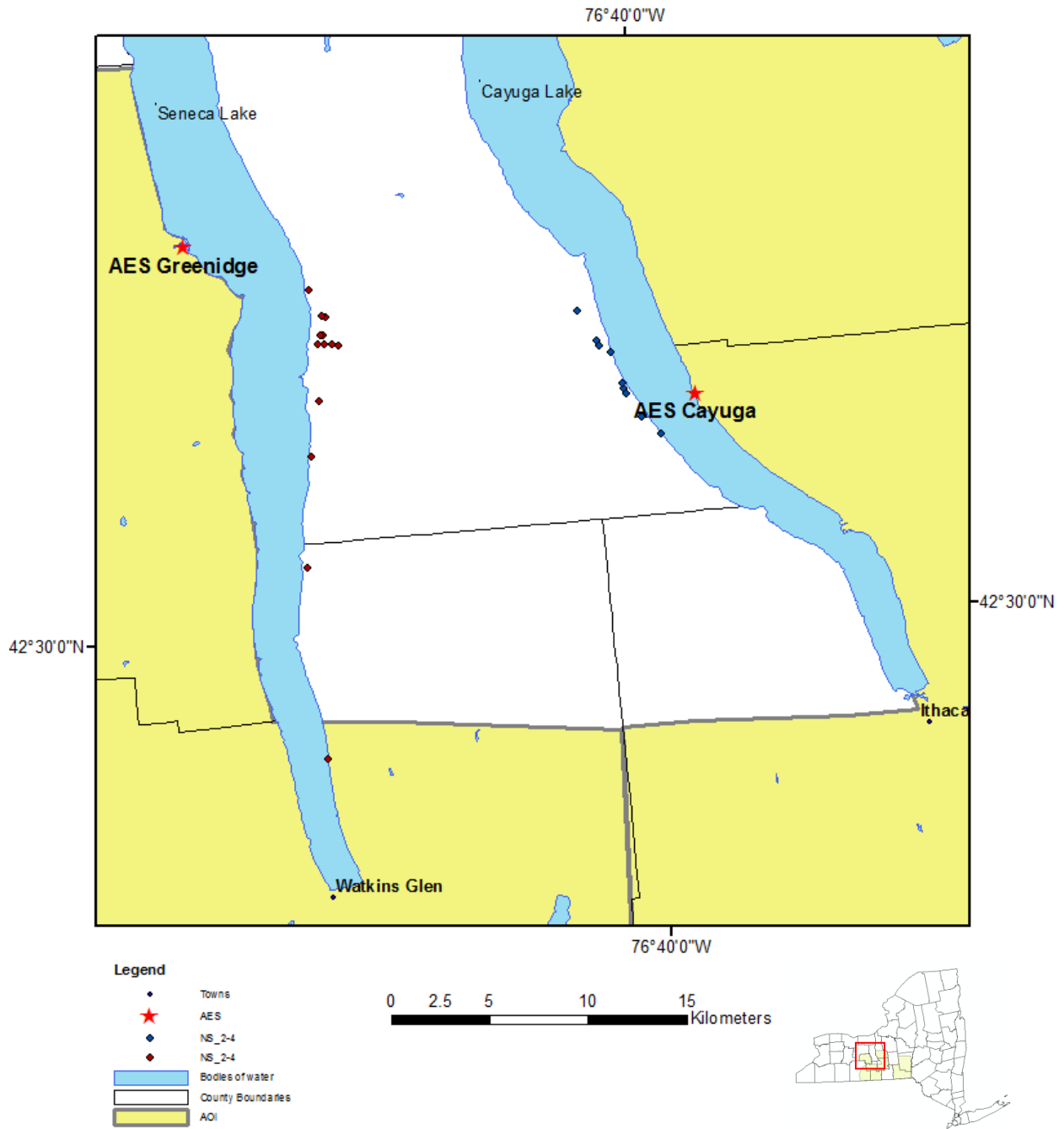


Figure 6.1-36: Field sites with NS striking fractures with a fracture frequency of 2-4 fractures/m (Lugert et al, 2001, Cruz, 2005, Jacobi, 2007)



Remote Sensing Laboratory  
Dept. of Geology, SUNY at Buffalo



University at Buffalo  
The State University of New York

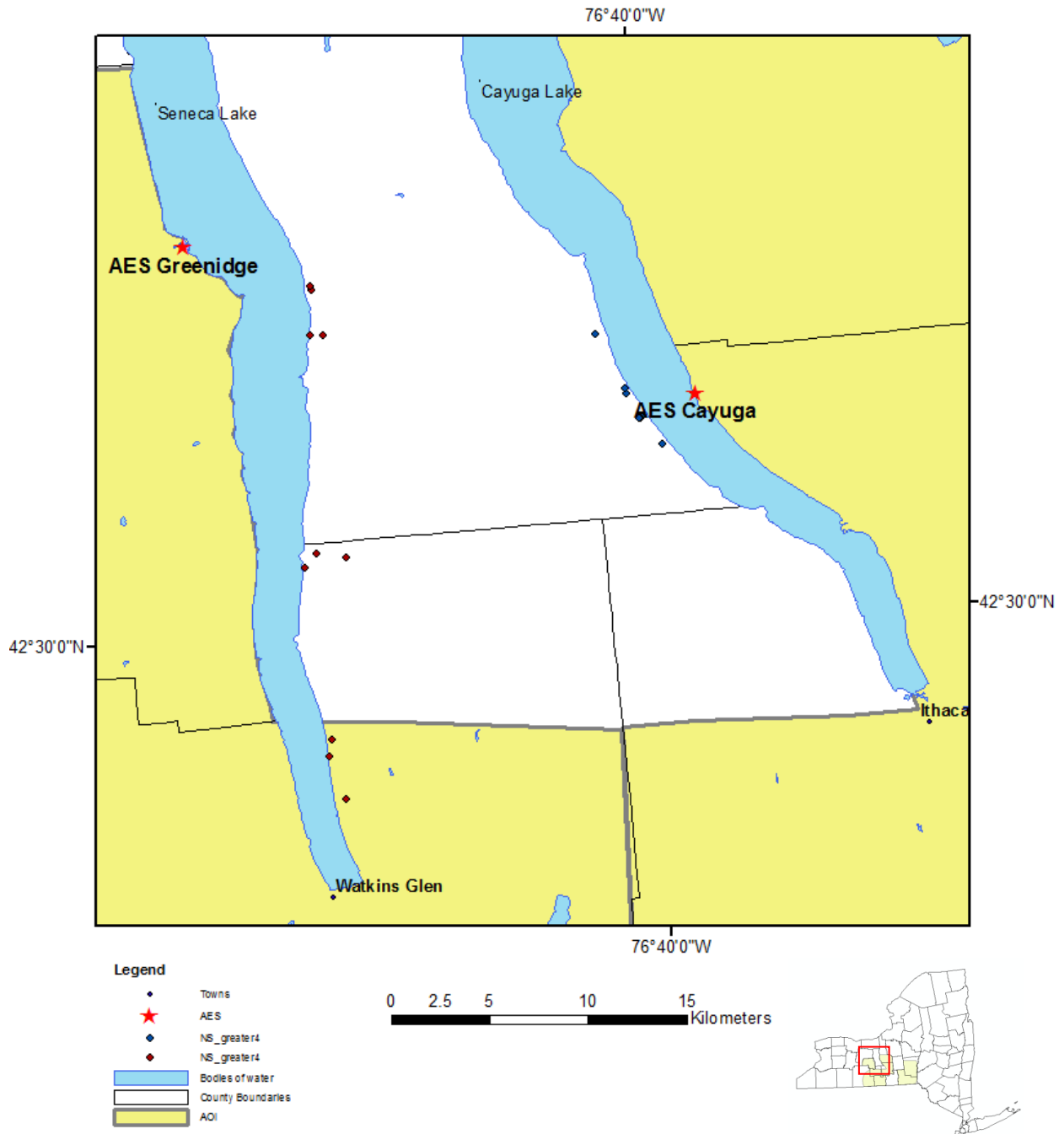


Figure 6.1-37: Field sites with NS striking fractures with a fracture frequency of greater than 4 fractures/m (Lugert et al, 2001, Cruz, 2005, Jacobi, 2007)



**Remote Sensing Laboratory**  
 Dept. of Geology, SUNY at Buffalo



**University at Buffalo**  
 The State University of New York

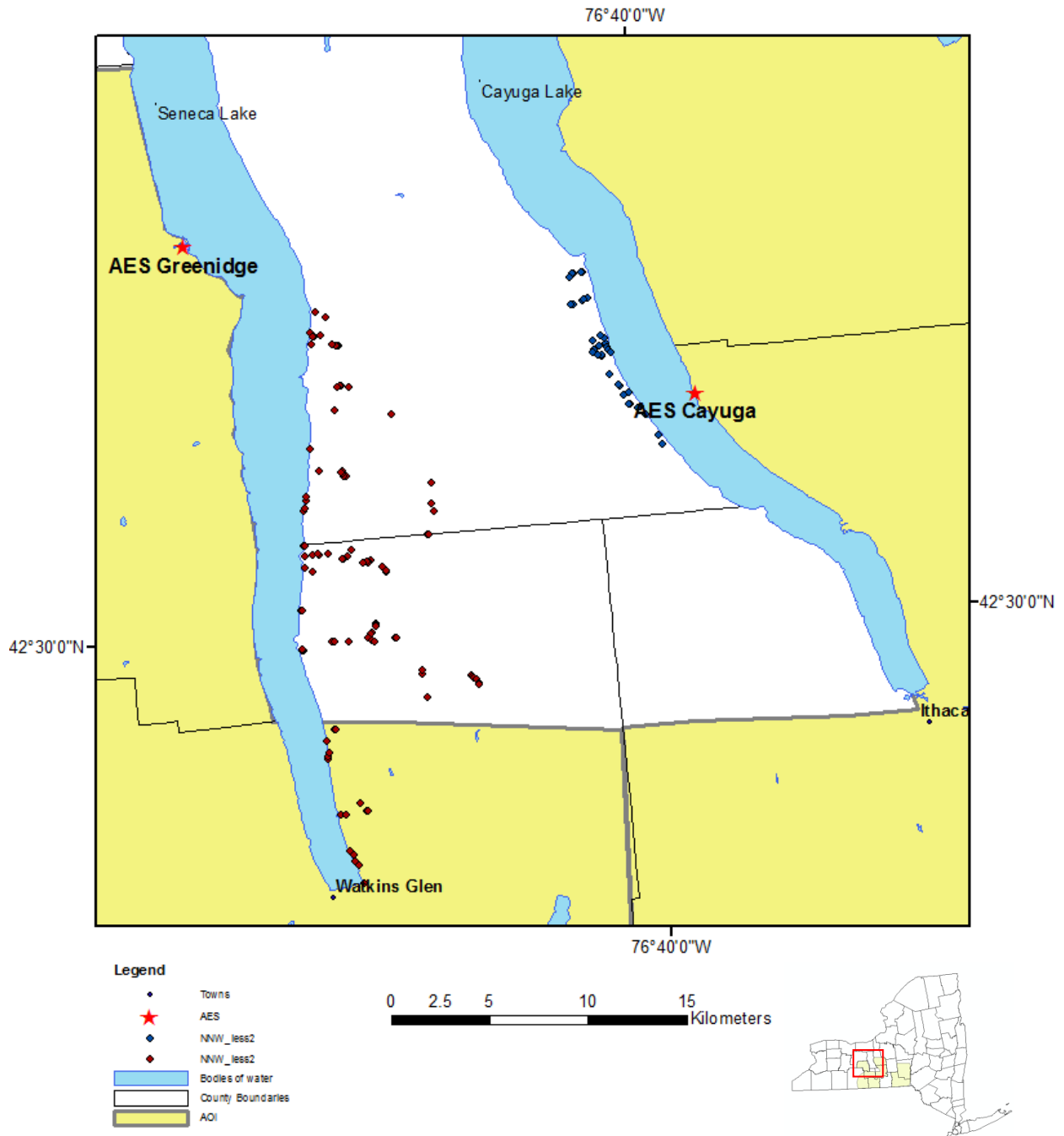


Figure 6.1-38: Field sites with NNW striking fractures with a fracture frequency of 0-2 fractures/m (Lugert et al, 2001, Cruz, 2005, Jacobi, 2007)



Remote Sensing Laboratory  
Dept. of Geology, SUNY at Buffalo



University at Buffalo  
The State University of New York

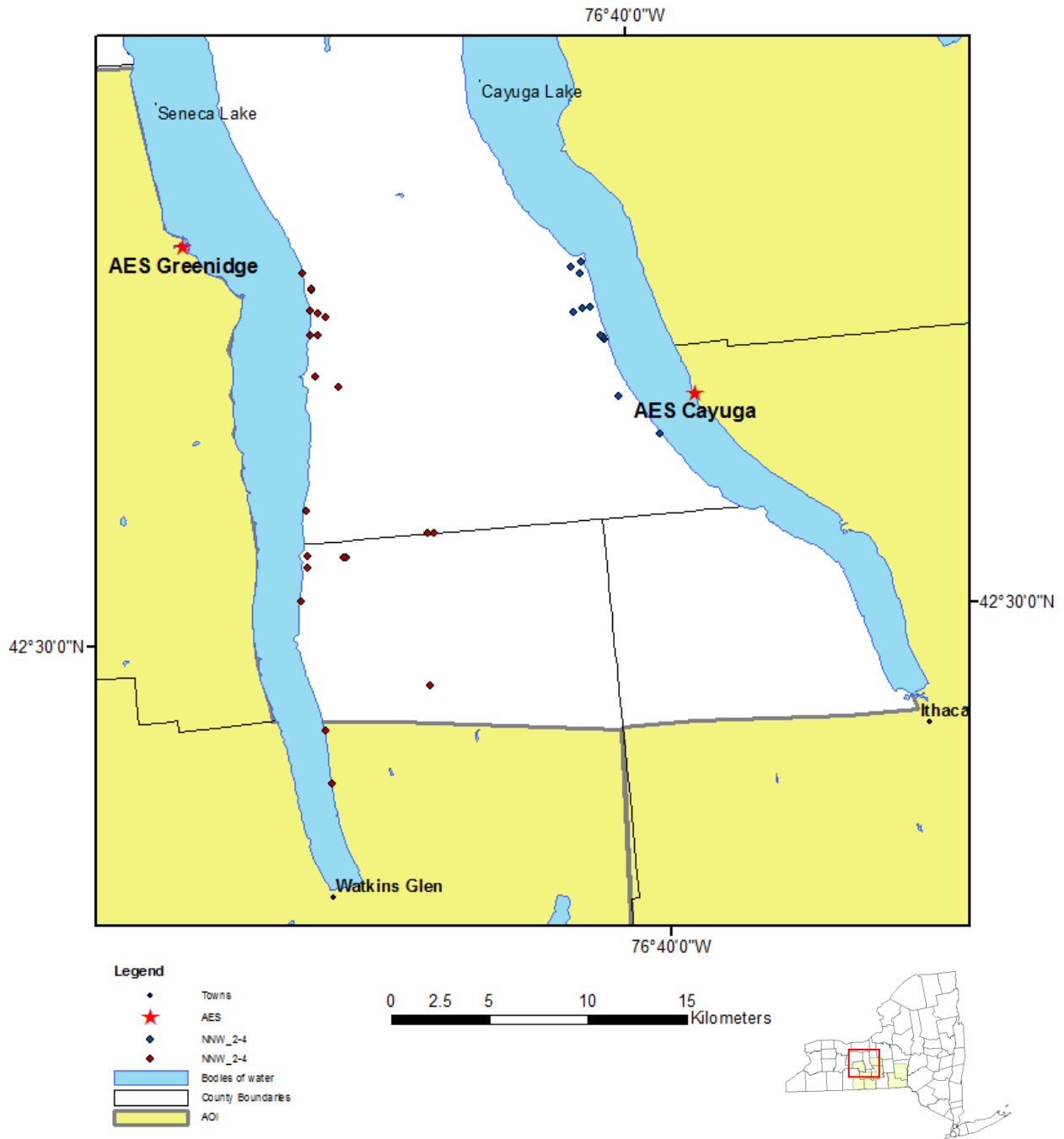


Figure 6.1-39: Field sites with NNW striking fractures with a fracture frequency of 2-4 fractures/m (Lugert et al, 2001, Cruz, 2005, Jacobi, 2007)



Remote Sensing Laboratory  
Dept. of Geology, SUNY at Buffalo



University at Buffalo  
The State University of New York

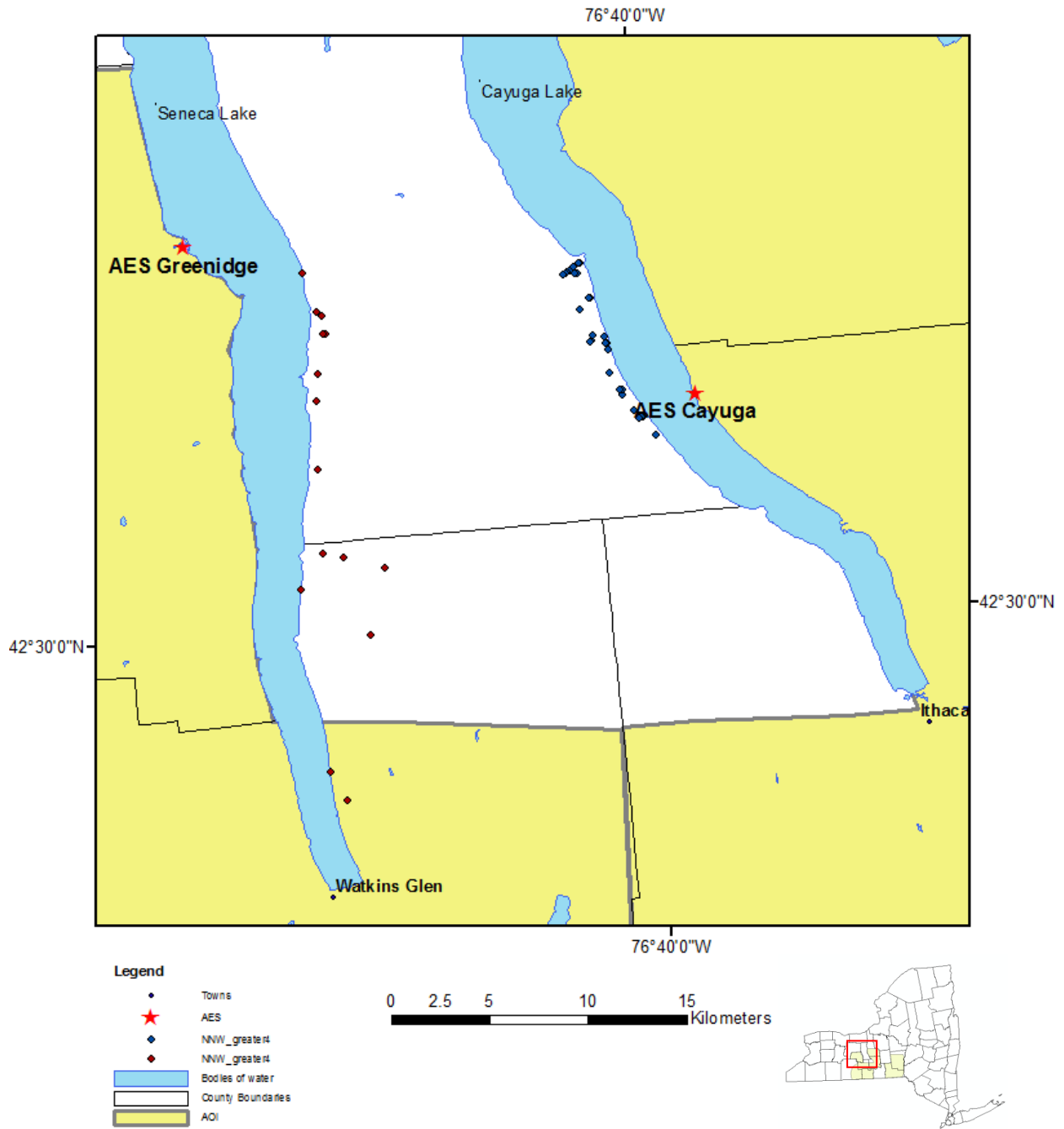


Figure 6.1-40: Field sites with NNW striking fractures with a fracture frequency of greater than 4 fractures/m (Lugert et al, 2001, Cruz, 2005, Jacobi, 2007)



**Remote Sensing Laboratory**  
*Dept. of Geology, SUNY at Buffalo*



**University at Buffalo**  
*The State University of New York*

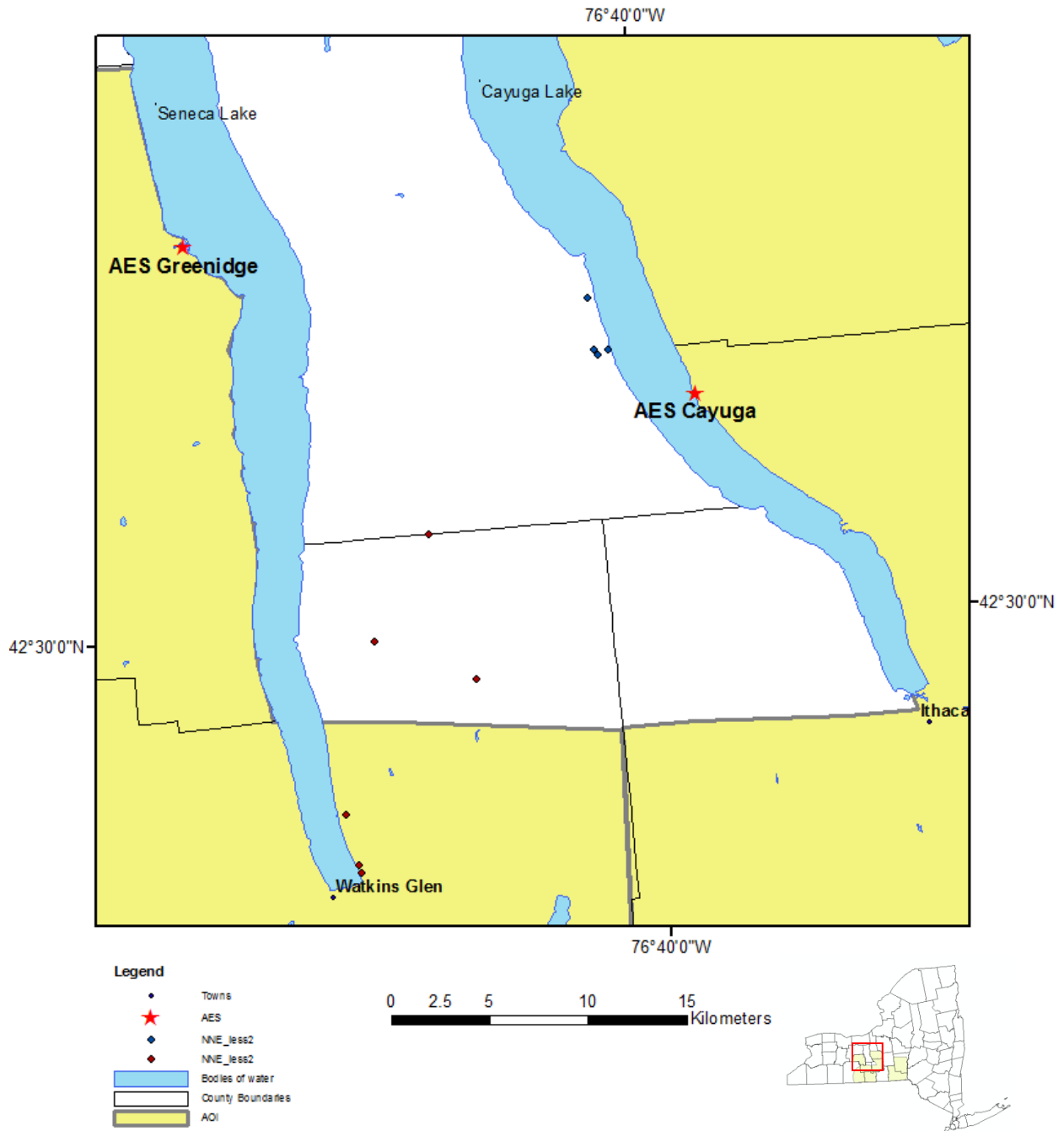


Figure 6.1-41: Field sites with NNE striking fractures with a fracture frequency of 0-2 fractures/m (Lugert et al, 2001, Cruz, 2005, Jacobi, 2007)



**Remote Sensing Laboratory**  
*Dept. of Geology, SUNY at Buffalo*



**University at Buffalo**  
*The State University of New York*

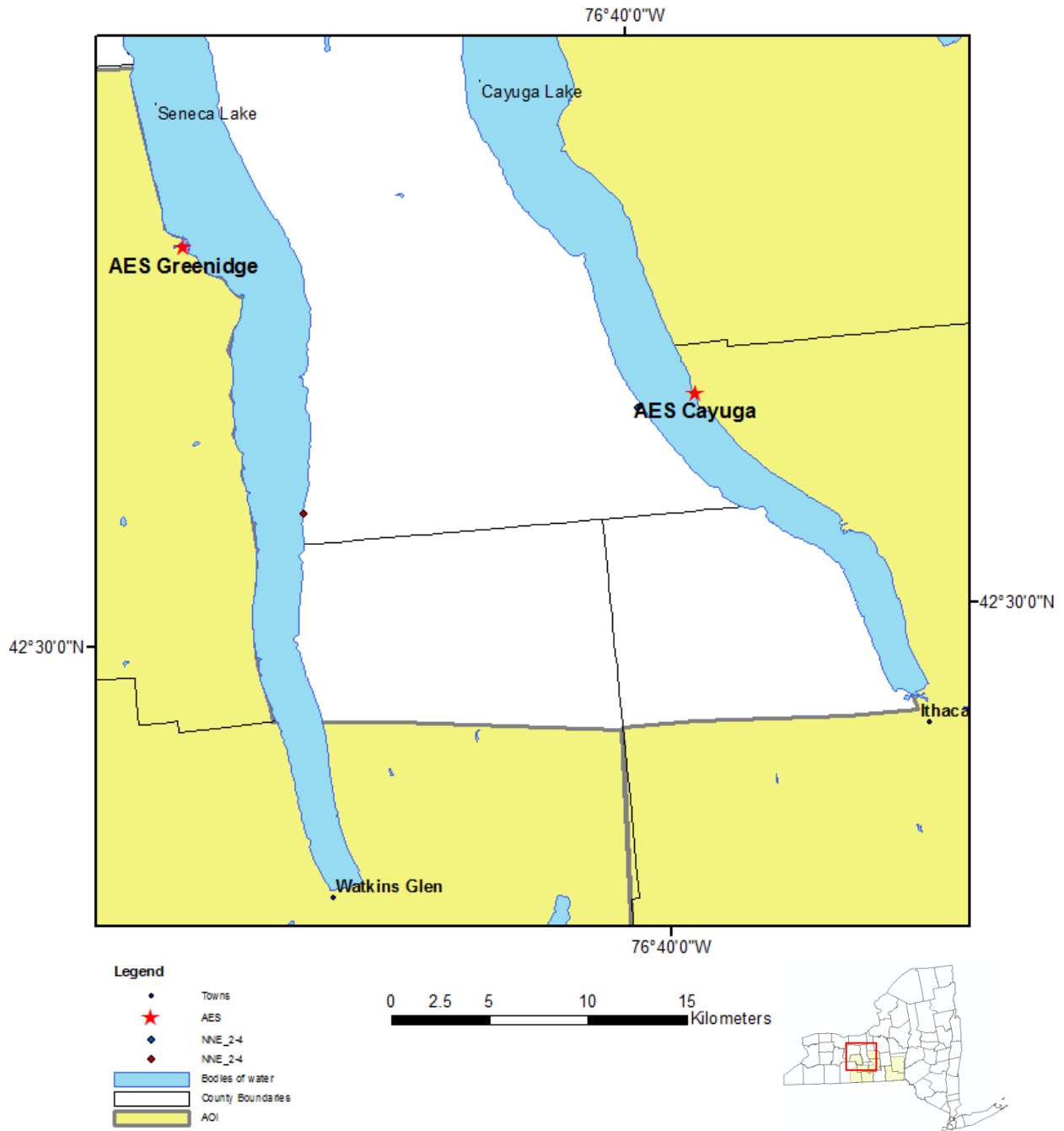


Figure 6.1-42: Field sites with NNE striking fractures with a fracture frequency of 2-4 fractures/m (Lugert et al, 2001, Cruz, 2005, Jacobi, 2007)





Remote Sensing Laboratory  
Dept. of Geology, SUNY at Buffalo



University at Buffalo  
The State University of New York

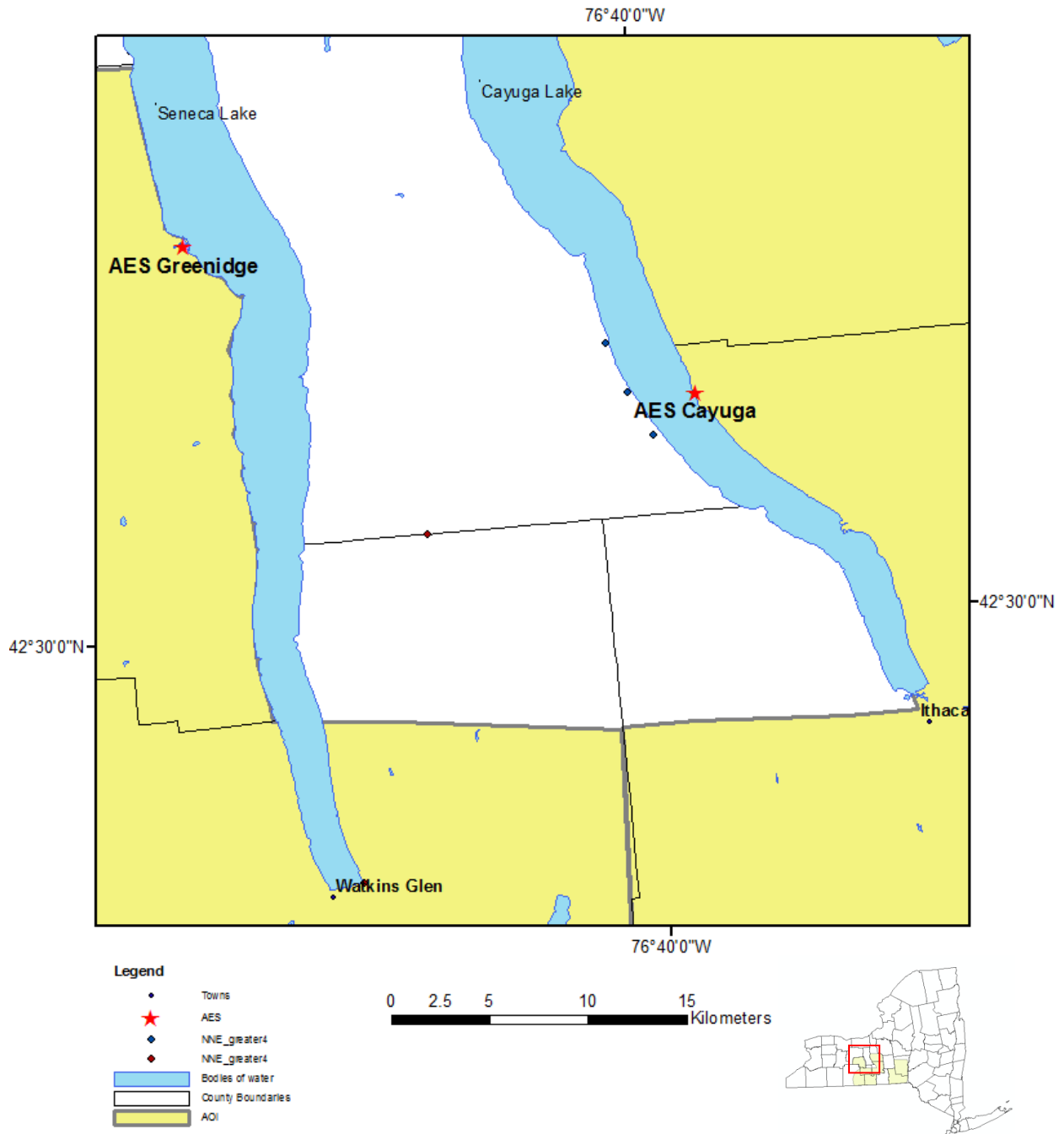


Figure 6.1-43: Field sites with NNE striking fractures with a fracture frequency of greater than 4 fractures/m (Lugert et al, 2001, Cruz, 2005, Jacobi, 2007)



Remote Sensing Laboratory  
Dept. of Geology, SUNY at Buffalo



University at Buffalo  
The State University of New York

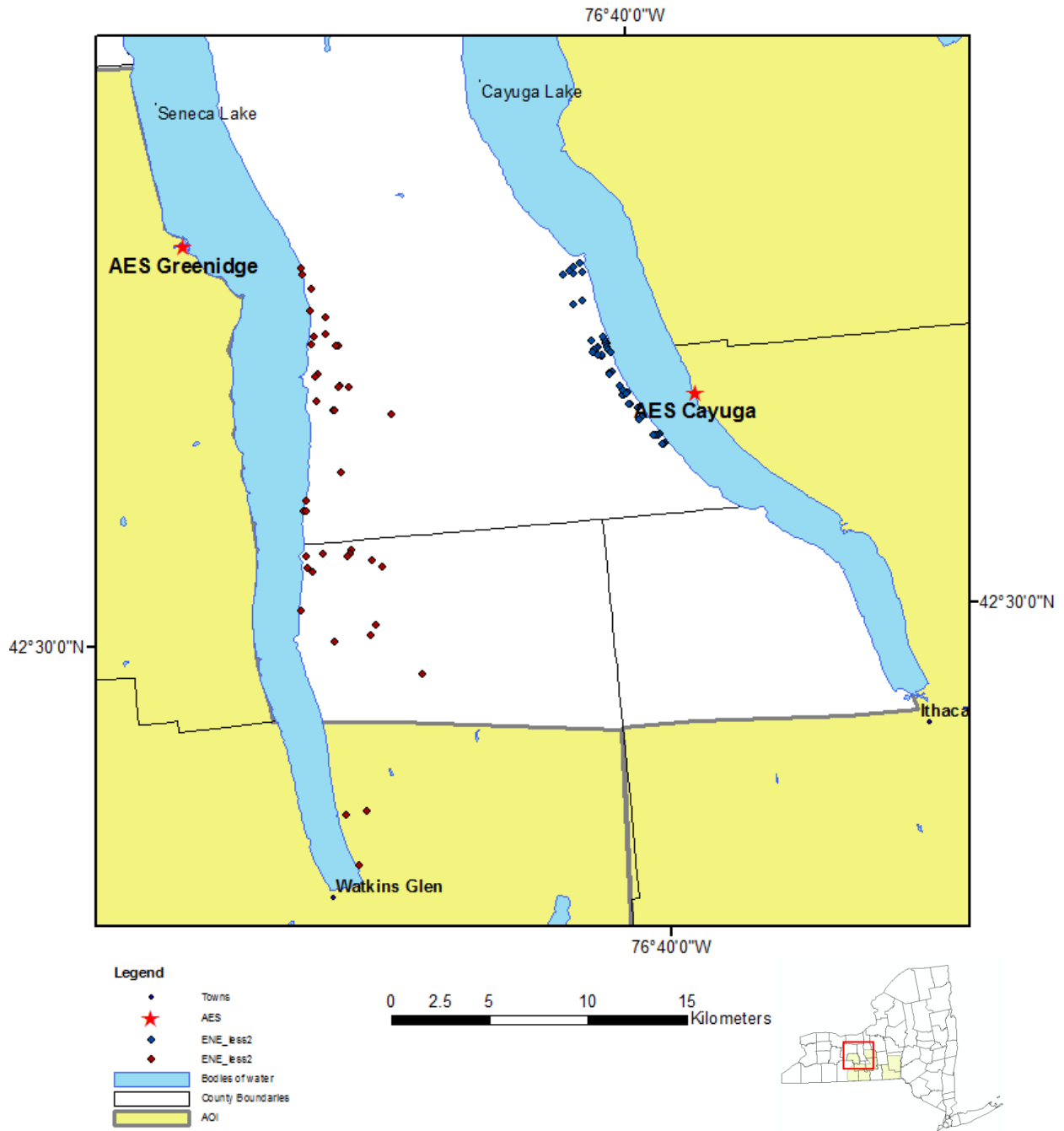


Figure 6.1-44: Field sites with ENE striking fractures with a fracture frequency of 0-2 fractures/m (Lugert et al, 2001, Cruz, 2005, Jacobi, 2007)



**Remote Sensing Laboratory**  
*Dept. of Geology, SUNY at Buffalo*



**University at Buffalo**  
*The State University of New York*

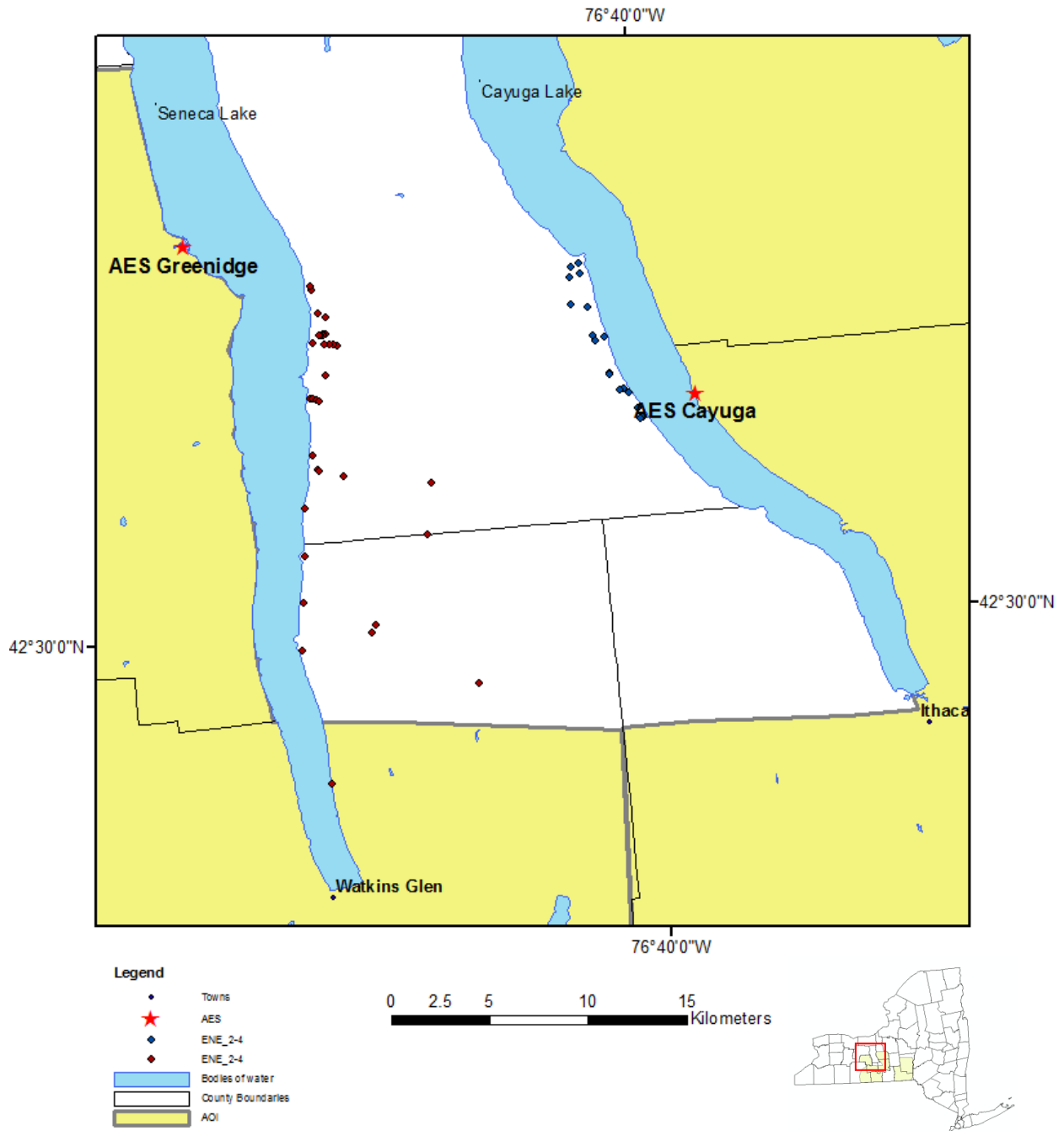


Figure 6.1-45: Field sites with ENE striking fractures with a fracture frequency of 2-4 fractures/m (Lugert et al, 2001, Cruz, 2005, Jacobi, 2007)



**Remote Sensing Laboratory**  
*Dept. of Geology, SUNY at Buffalo*



**University at Buffalo**  
*The State University of New York*

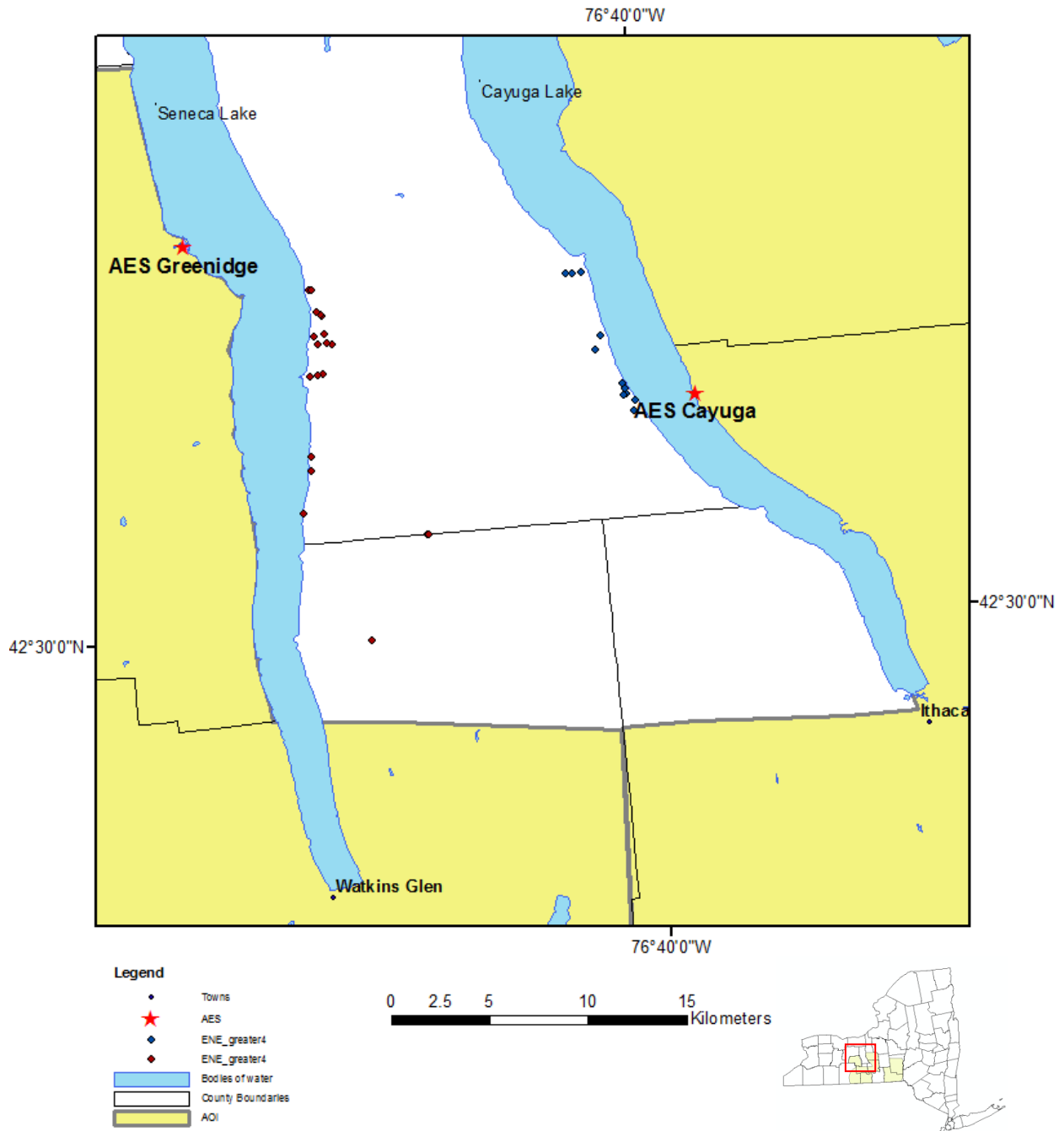


Figure 6.1-46: Field sites with ENE striking fractures with a fracture frequency of greater than 4 fractures/m (Lugert et al, 2001, Cruz, 2005, Jacobi, 2007)



**Remote Sensing Laboratory**  
*Dept. of Geology, SUNY at Buffalo*



**University at Buffalo**  
*The State University of New York*

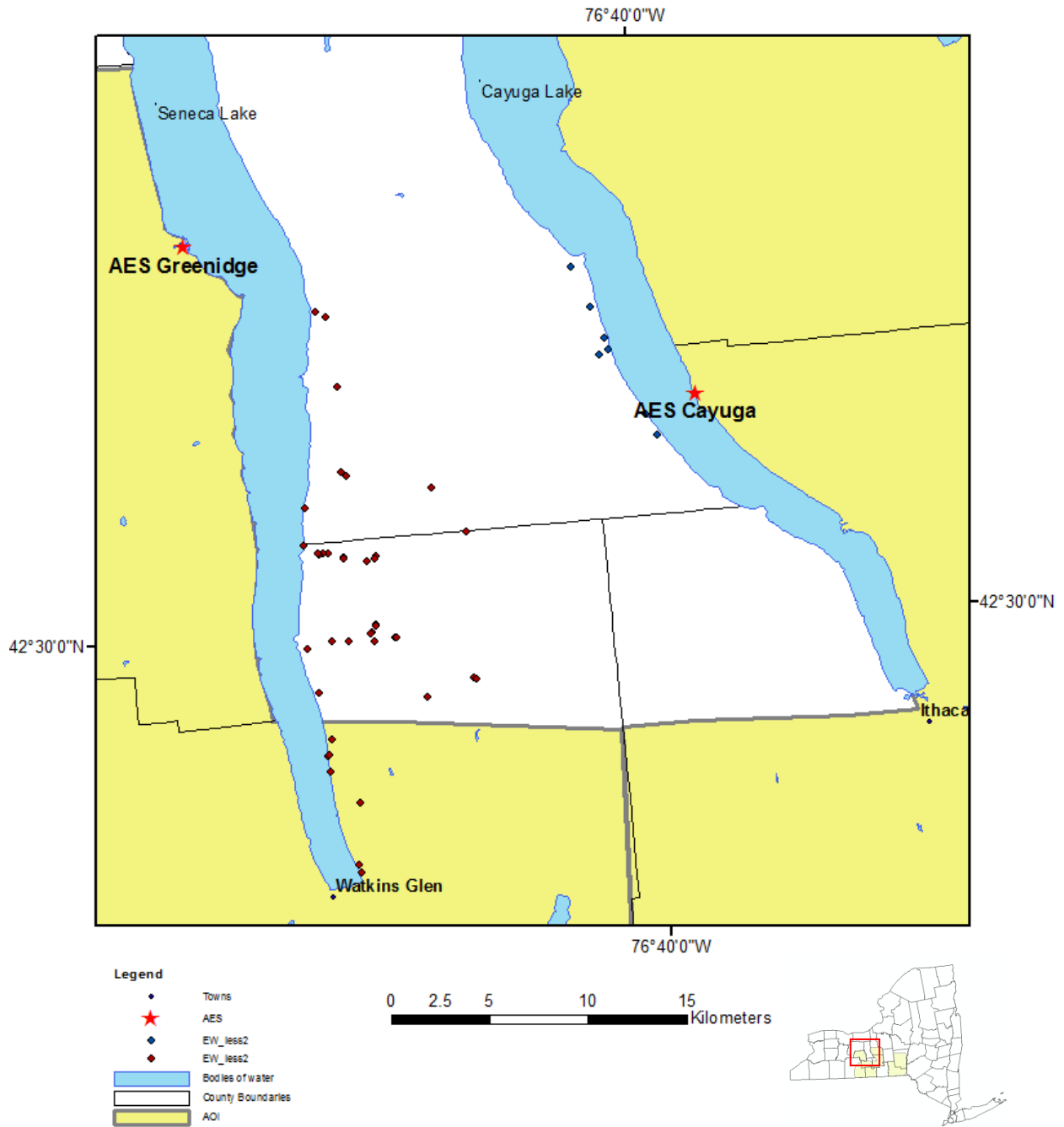


Figure 6.1-47: Field sites with EW striking fractures with a fracture frequency of 0-2 fractures/m (Lugert et al, 2001, Cruz, 2005, Jacobi, 2007)



**Remote Sensing Laboratory**  
 Dept. of Geology, SUNY at Buffalo



**University at Buffalo**  
 The State University of New York

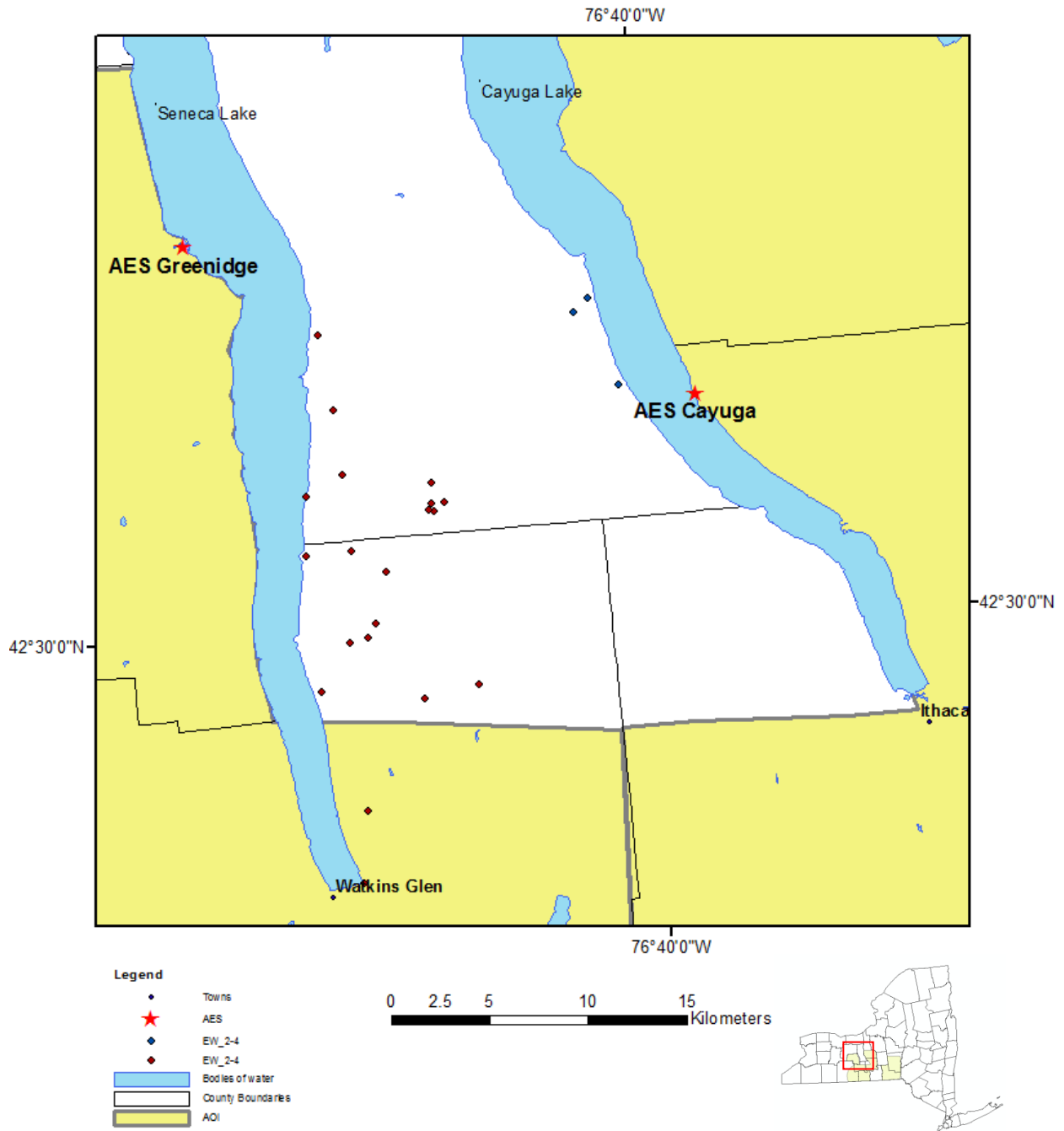


Figure 6.1-48: Field sites with EW striking fractures with a fracture frequency of 2-4 fractures/m (Lugert et al, 2001, Cruz, 2005, Jacobi, 2007)



Remote Sensing Laboratory  
Dept. of Geology, SUNY at Buffalo



University at Buffalo  
The State University of New York

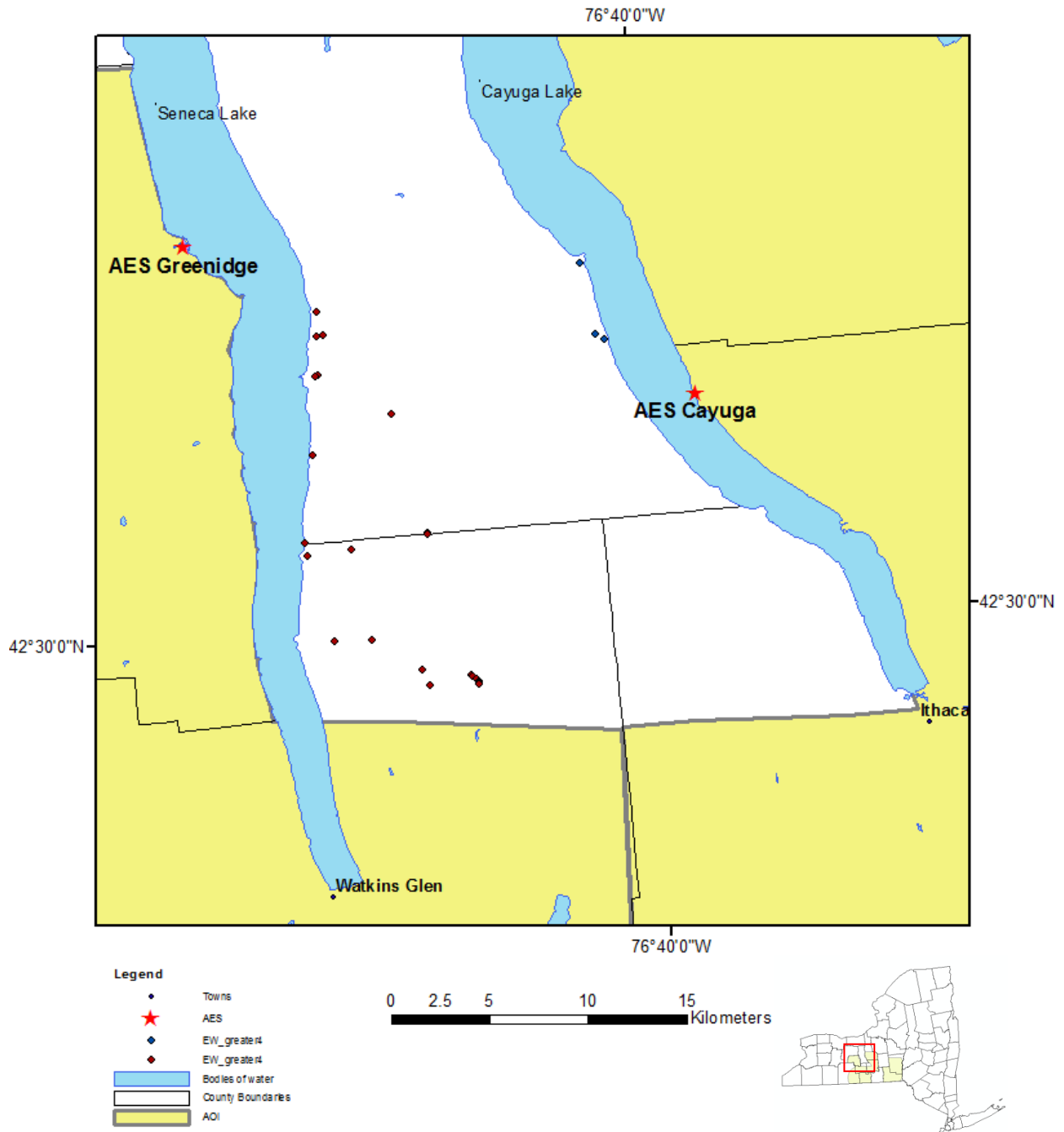


Figure 6.1-49: Field sites with EW striking fractures with a fracture frequency of greater than 4 fractures/m (Lugert et al, 2001, Cruz, 2005, Jacobi, 2007)



**Remote Sensing Laboratory**  
*Dept. of Geology, SUNY at Buffalo*



**University at Buffalo**  
*The State University of New York*

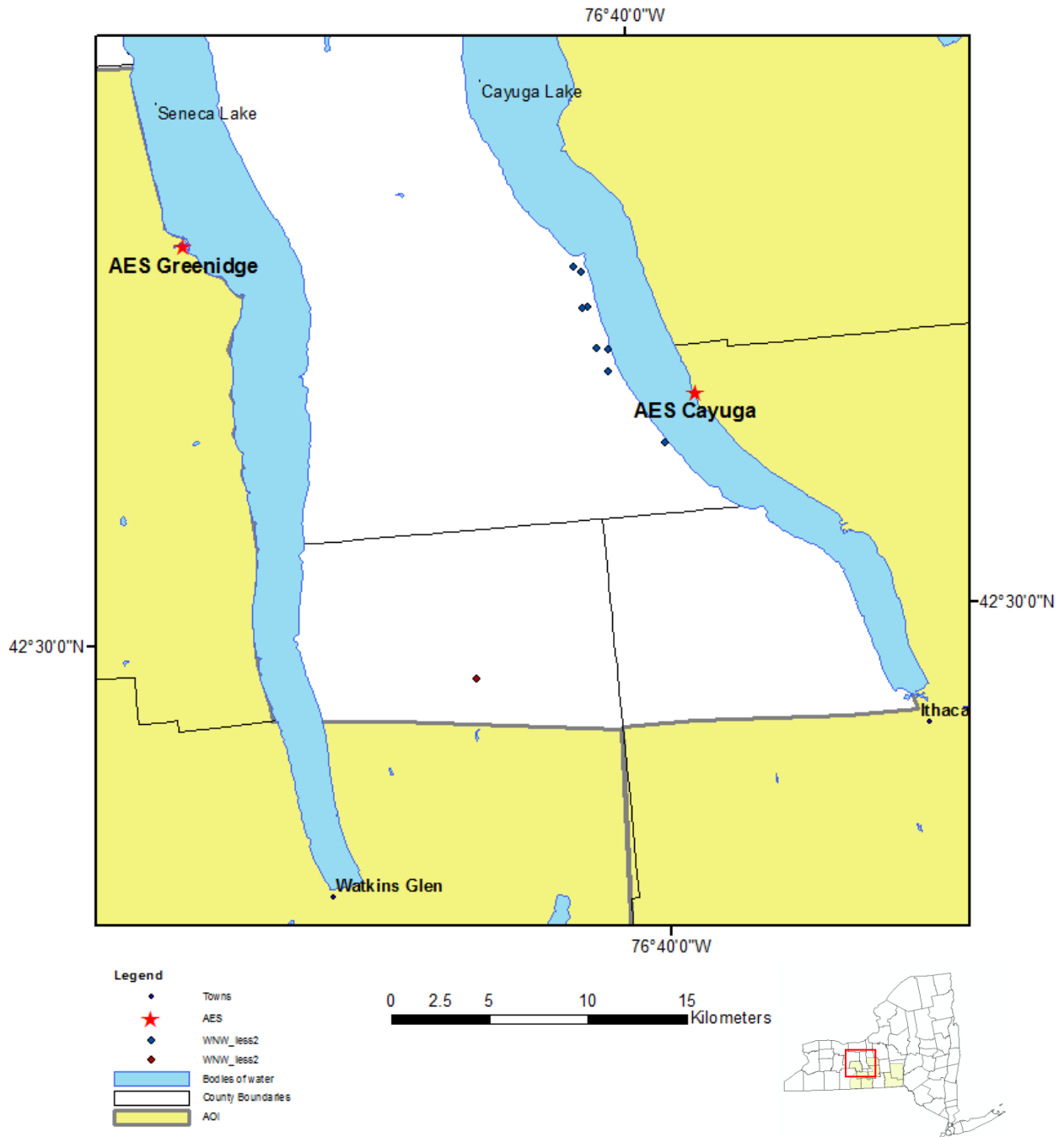


Figure 6.1-50: Field sites with WNW striking fractures with a fracture frequency of 0-2 fractures/m (Lugert et al, 2001, Cruz, 2005, Jacobi, 2007)





**Remote Sensing Laboratory**  
*Dept. of Geology, SUNY at Buffalo*



**University at Buffalo**  
*The State University of New York*

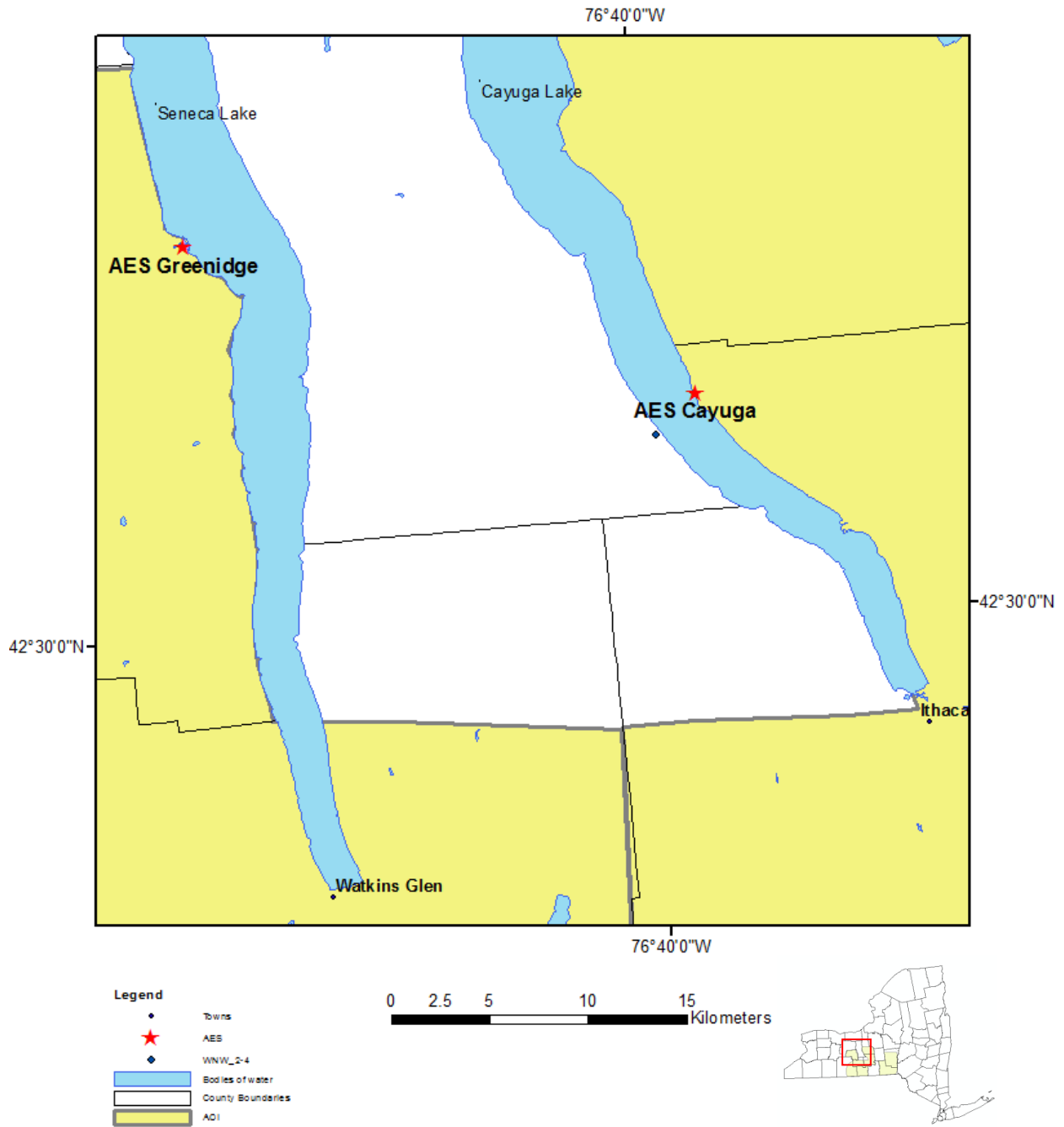


Figure 6.1-51: Field sites with WNW striking fractures with a fracture frequency of 2-4 fractures/m (Lugert et al, 2001, Cruz, 2005, Jacobi, 2007)



**Remote Sensing Laboratory**  
 Dept. of Geology, SUNY at Buffalo



**University at Buffalo**  
 The State University of New York

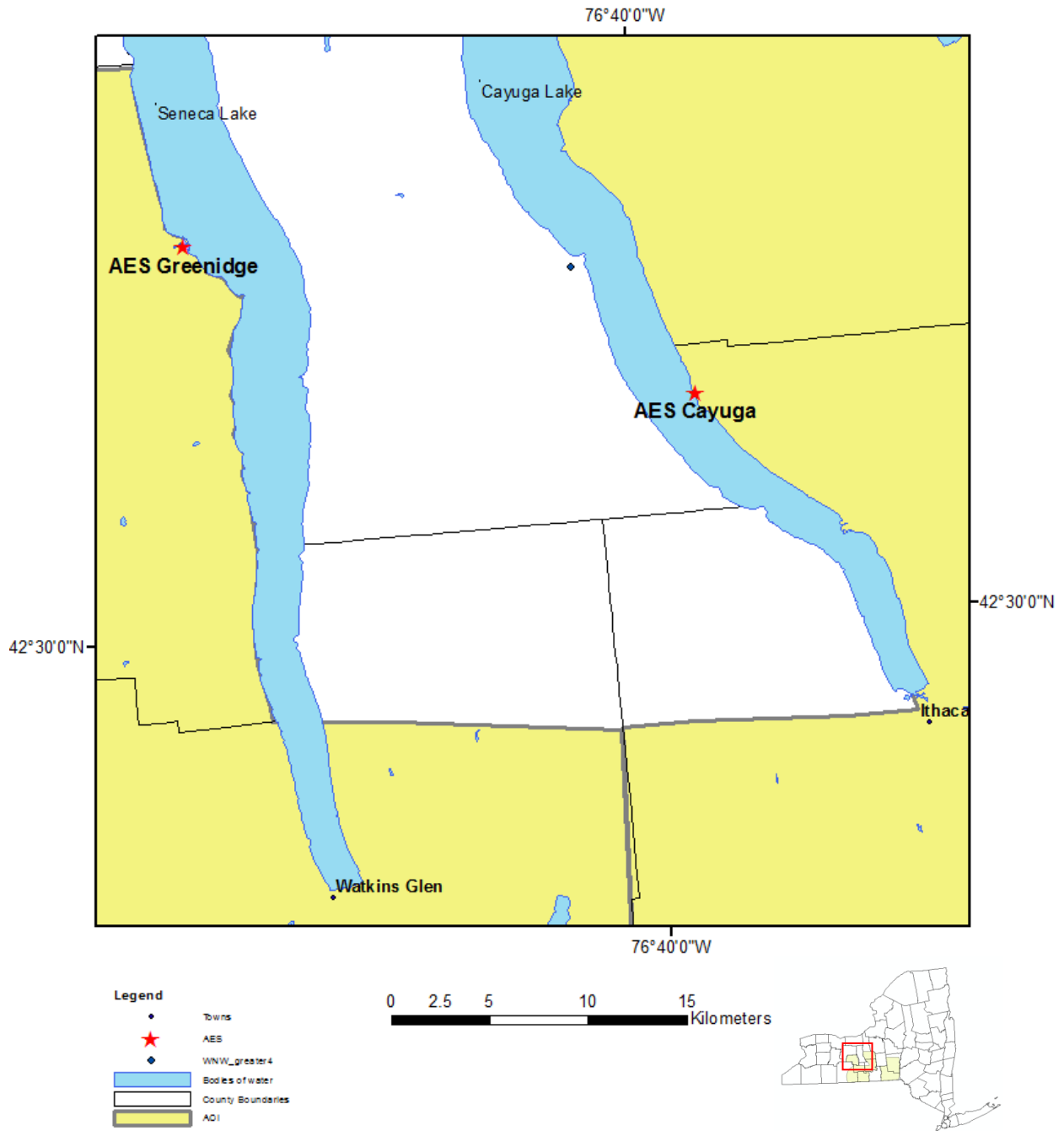


Figure 6.1-52: Field sites with WNW striking fractures with a fracture frequency of greater than 4 fractures/m (Lugert et al, 2001, Cruz, 2005, Jacobi, 2007)



**Remote Sensing Laboratory**  
 Dept. of Geology, SUNY at Buffalo



**University at Buffalo**  
 The State University of New York

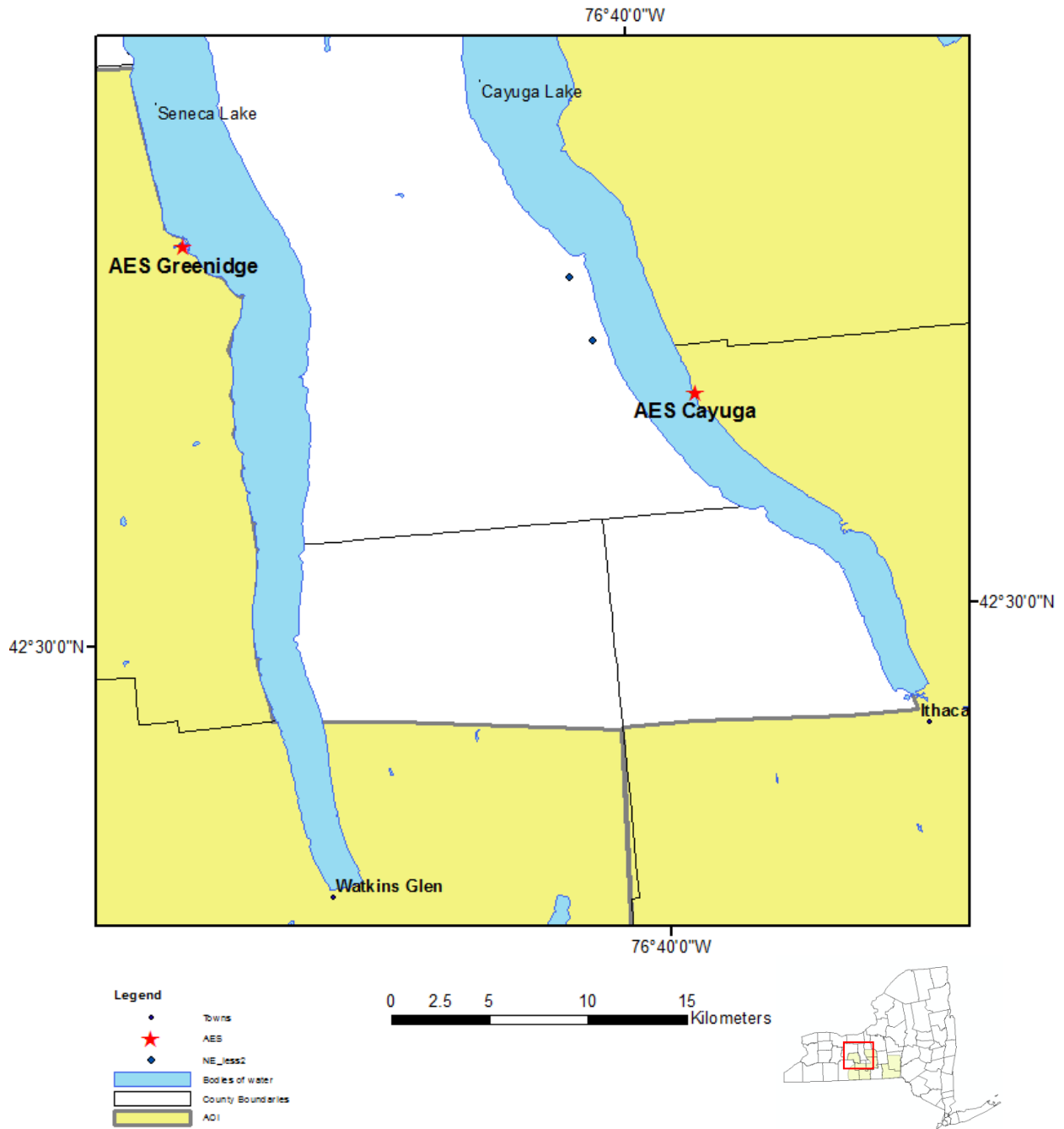


Figure 6.1-53: Field sites with NE striking fractures with a fracture frequency of 0-2 fractures/m (Lugert et al, 2001, Cruz, 2005, Jacobi, 2007)



**Remote Sensing Laboratory**  
*Dept. of Geology, SUNY at Buffalo*



**University at Buffalo**  
*The State University of New York*

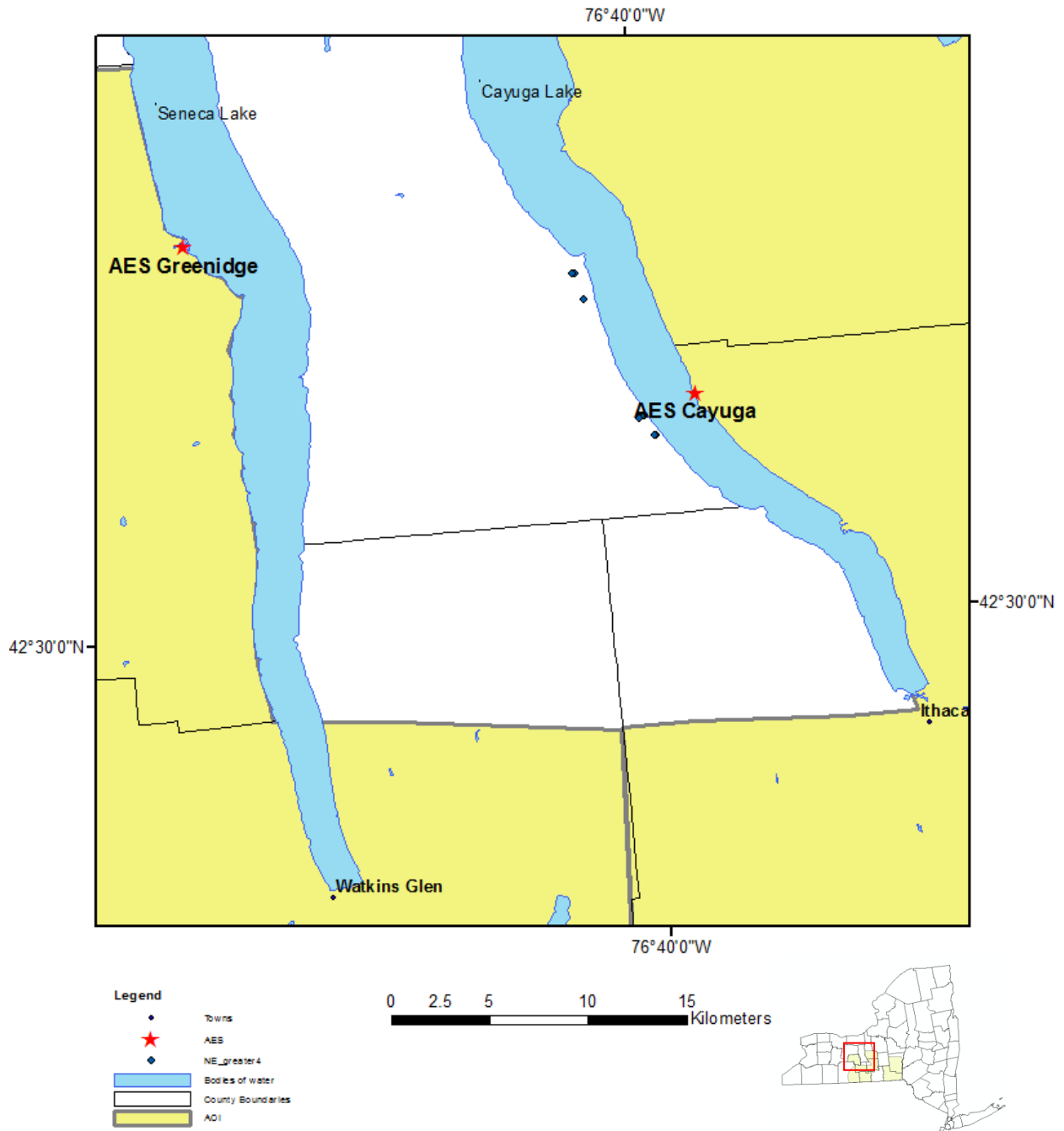


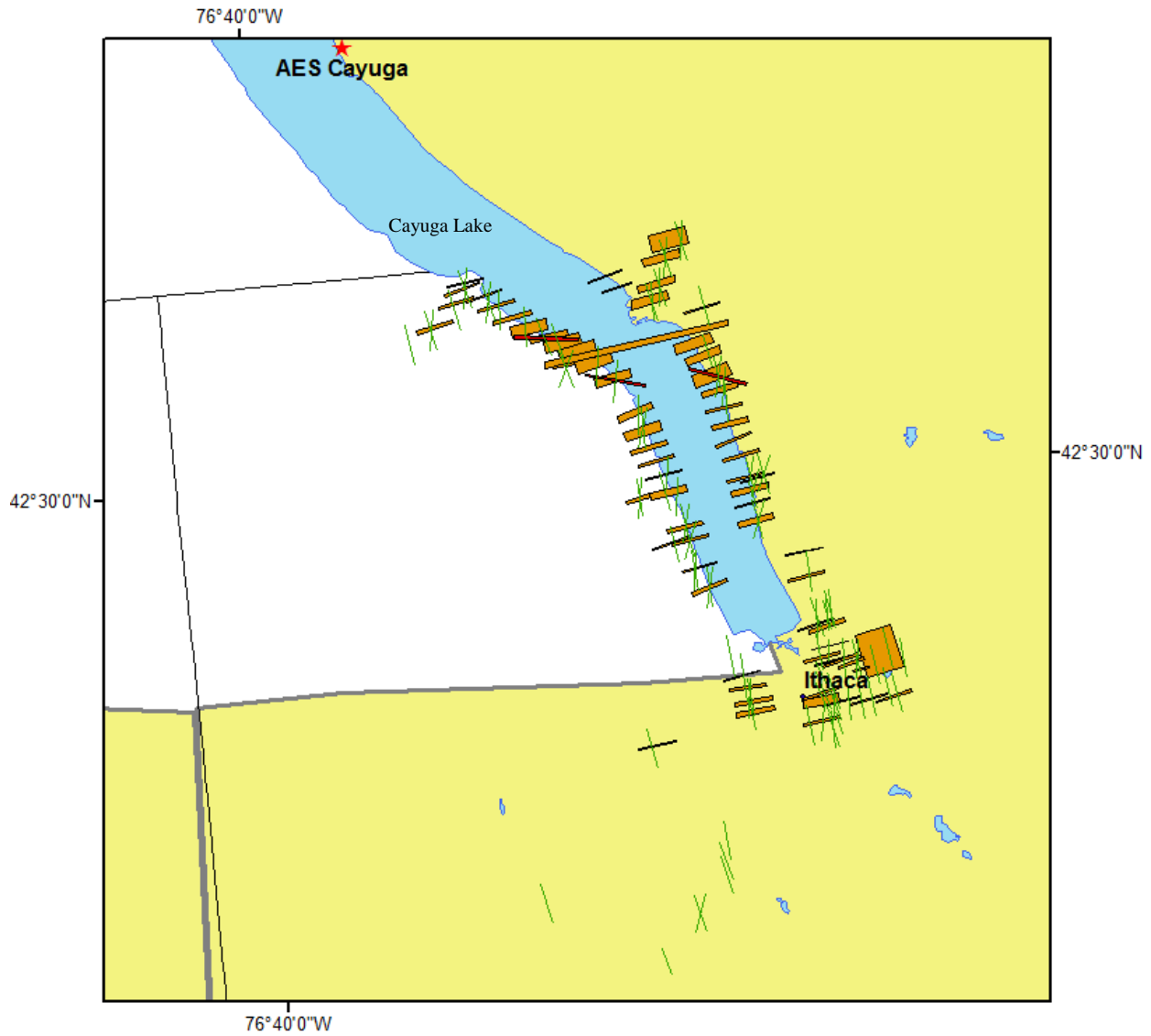
Figure 6.1-54: Field sites with NE striking fractures with a fracture frequency of greater than 4 fractures/m (Lugert et al, 2001, Cruz, 2005, Jacobi, 2007)



**Remote Sensing Laboratory**  
 Dept. of Geology, SUNY at Buffalo



**University at Buffalo**  
 The State University of New York



**Legend**

- ★ AES
- Average\_strike\_of\_dip\_joints
- Strike\_faults
- Average\_strike\_of\_strike\_joints
- AOI

0 0.5 1 2 3 Kilometers

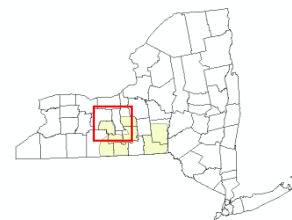


Figure 6.1-55: Fracture orientation and intensity (Sheldon, 1912)



**Remote Sensing Laboratory**  
 Dept. of Geology, SUNY at Buffalo



**University at Buffalo**  
 The State University of New York

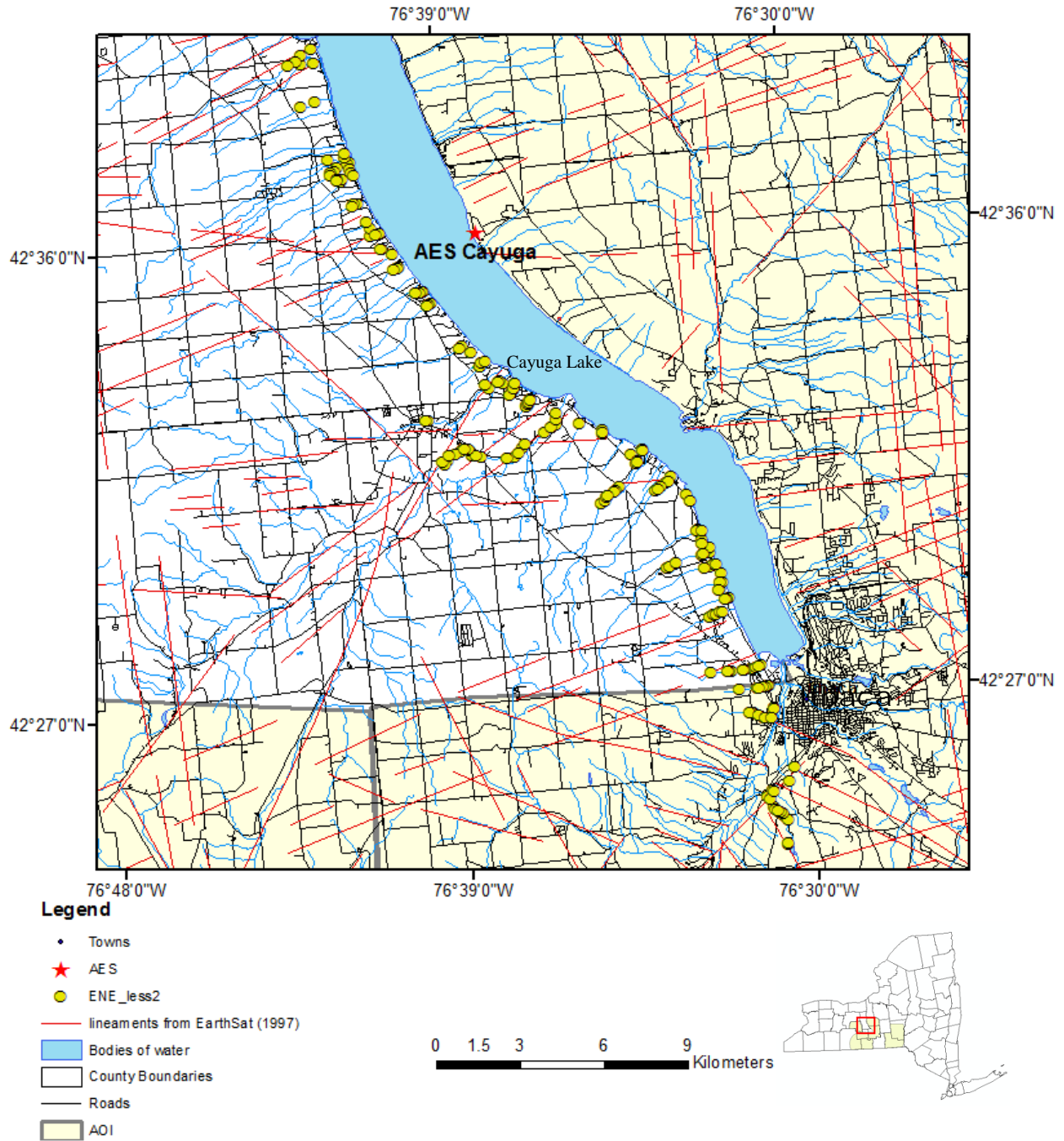


Figure 6.1-56: Lineaments and field sites displaying ENE striking fractures with a fracture frequency of less than 2 fractures/m. Fracture data from Wehn et al. (2002), Jacobi et al. (2002, 2003).



**Remote Sensing Laboratory**  
Dept. of Geology, SUNY at Buffalo



**University at Buffalo**  
The State University of New York

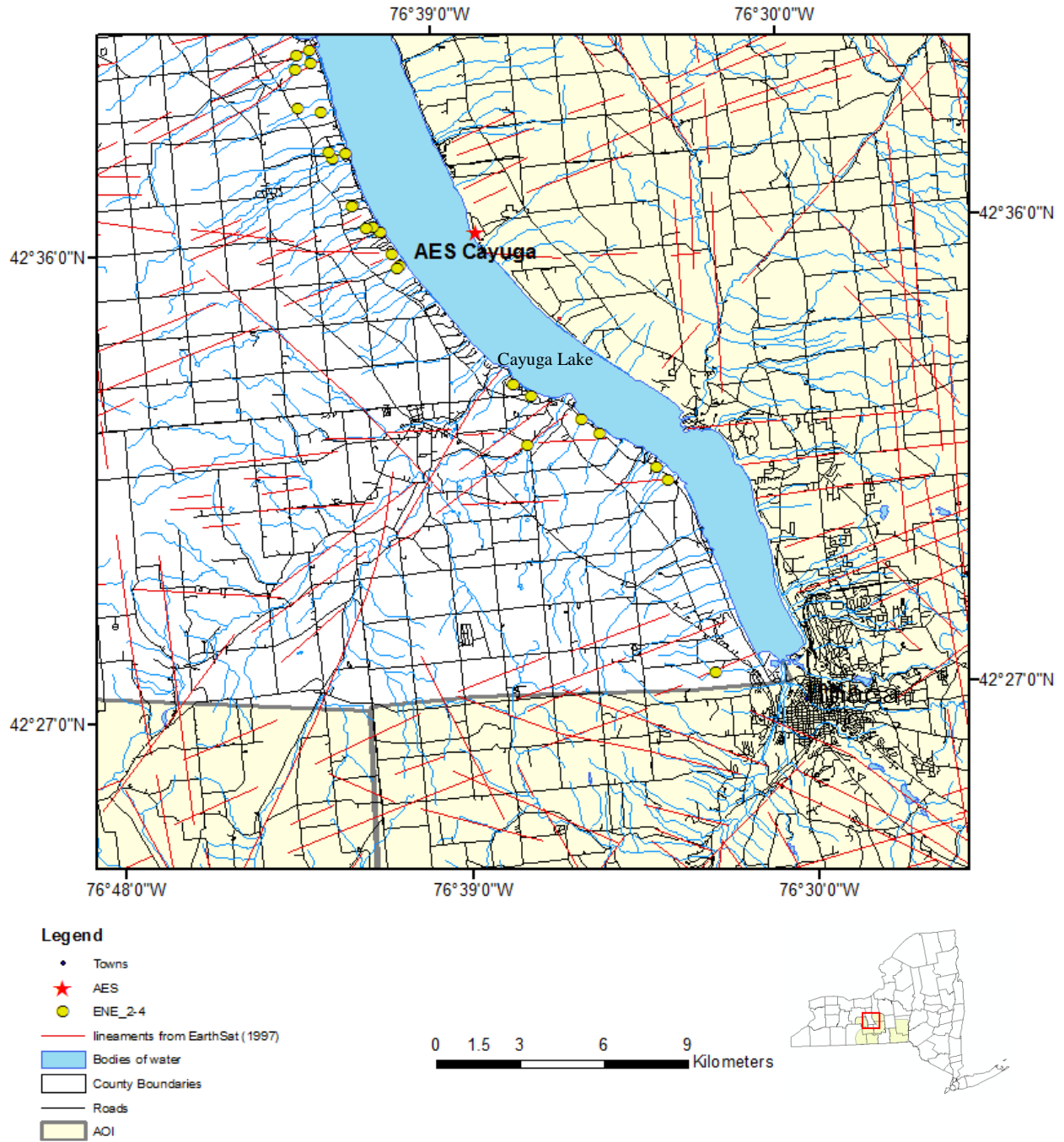


Figure 6.1-57: Lineaments and field sites displaying ENE striking fractures with a fracture frequency of 2 to 4 fractures/m. Fracture data from Wehn et al. (2002), Jacobi et al. (2002, 2003).



**Remote Sensing Laboratory**  
Dept. of Geology, SUNY at Buffalo



**University at Buffalo**  
The State University of New York

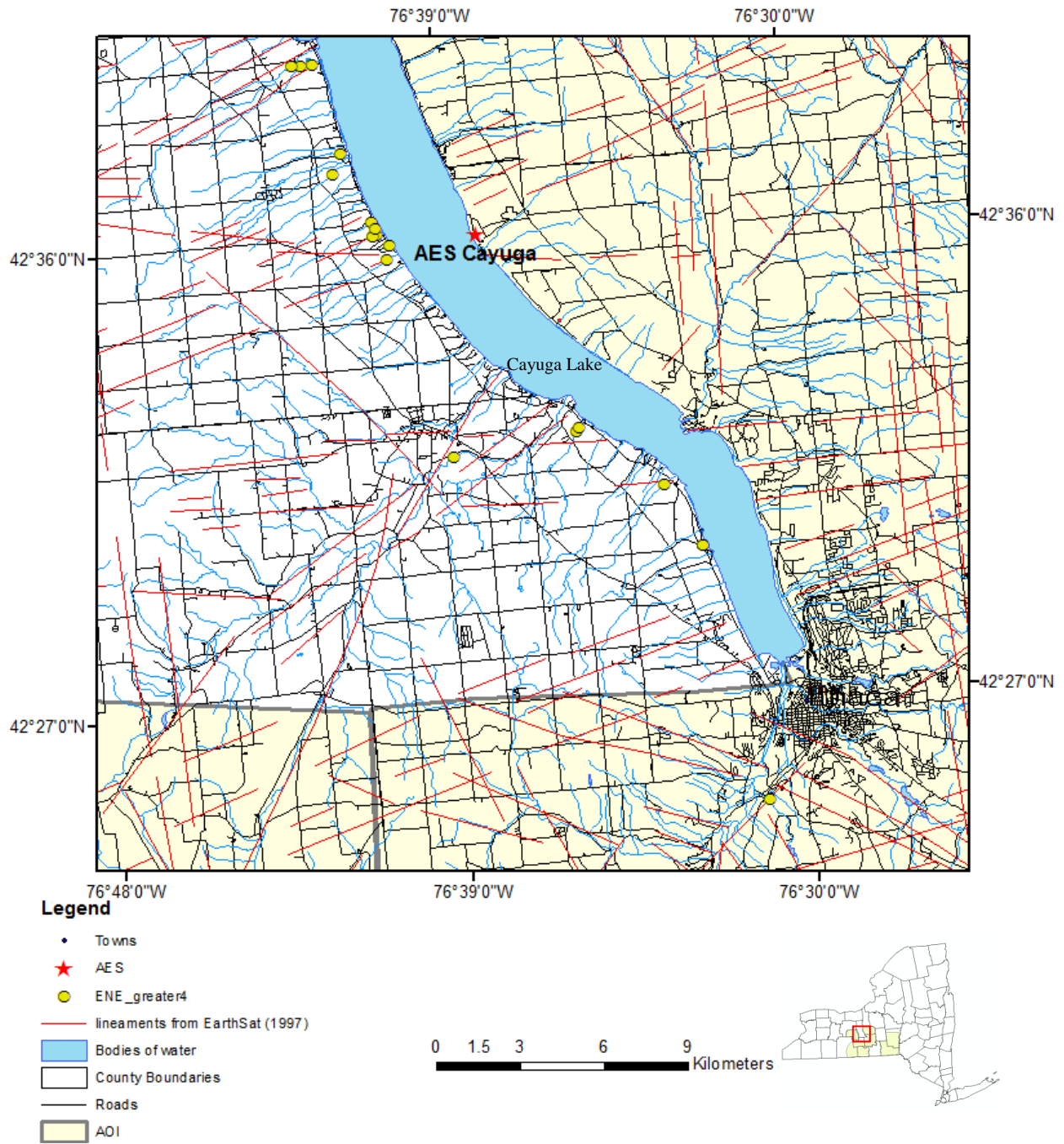


Figure 6.1-58: Lineaments and field sites displaying ENE striking fractures with a fracture frequency of greater than 4 fractures/m. Fracture data from Wehn et al. (2002), Jacobi et al. (2002, 2003).





**Remote Sensing Laboratory**  
Dept. of Geology, SUNY at Buffalo



**University at Buffalo**  
The State University of New York

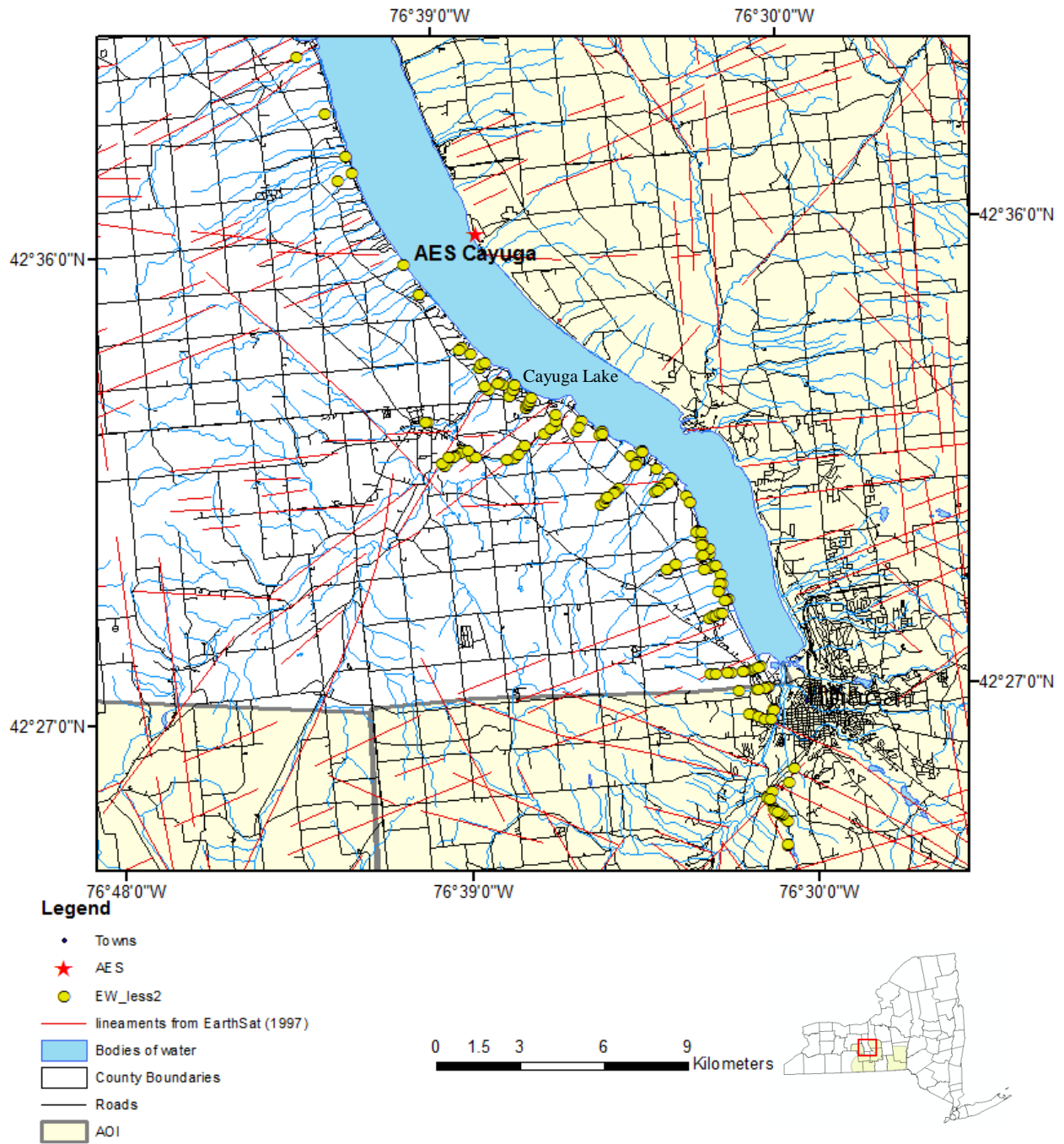


Figure 6.1-59: Lineaments and field sites displaying EW-striking fractures with a fracture frequency of less than 2 fractures/m. Fracture data from Wehn et al. (2002), Jacobi et al. (2002, 2003).



**Remote Sensing Laboratory**  
Dept. of Geology, SUNY at Buffalo



**University at Buffalo**  
The State University of New York

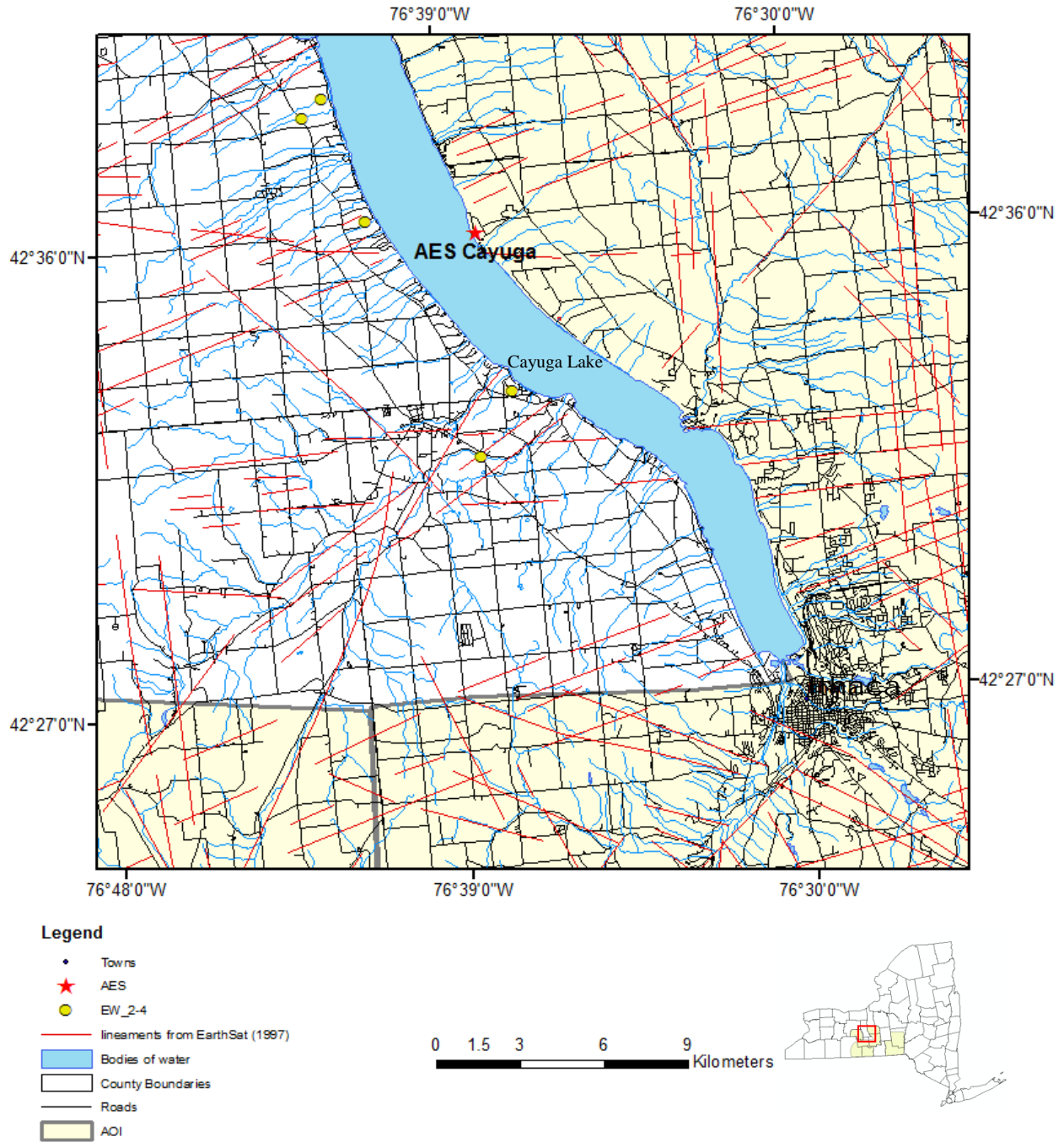


Figure 6.1-60: Lineaments and field sites displaying EW-striking fractures with a fracture frequency of 2 to 4 fractures/m. Fracture data from Wehn et al. (2002), Jacobi et al. (2002, 2003).



**Remote Sensing Laboratory**  
 Dept. of Geology, SUNY at Buffalo



**University at Buffalo**  
 The State University of New York

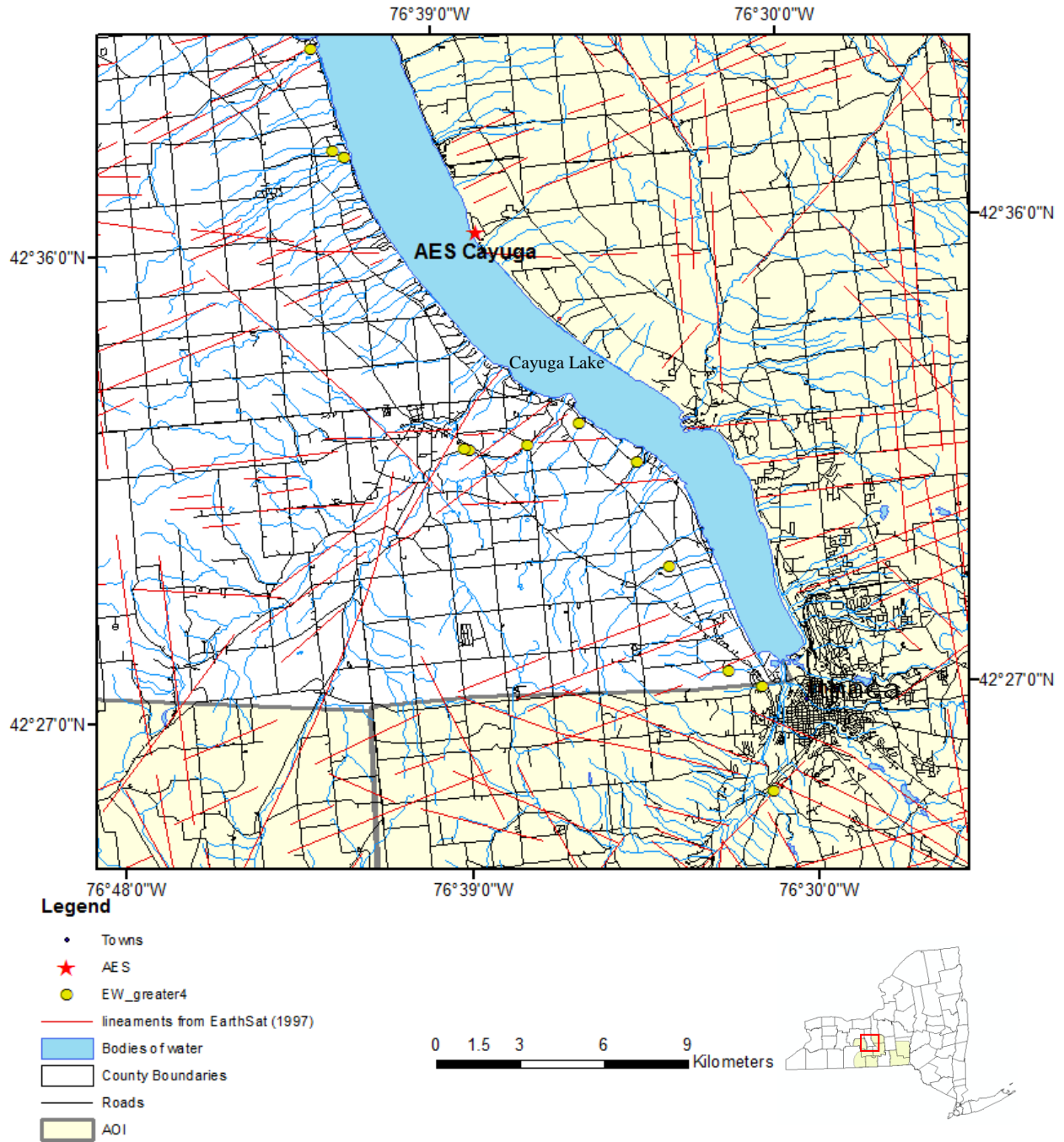


Figure 6.1-61: Lineaments and field sites displaying EW-striking fractures with a fracture frequency of greater than 4 fractures/m. Fracture data from Wehn et al. (2002), Jacobi et al. (2002, 2003).



**Remote Sensing Laboratory**  
Dept. of Geology, SUNY at Buffalo



**University at Buffalo**  
The State University of New York

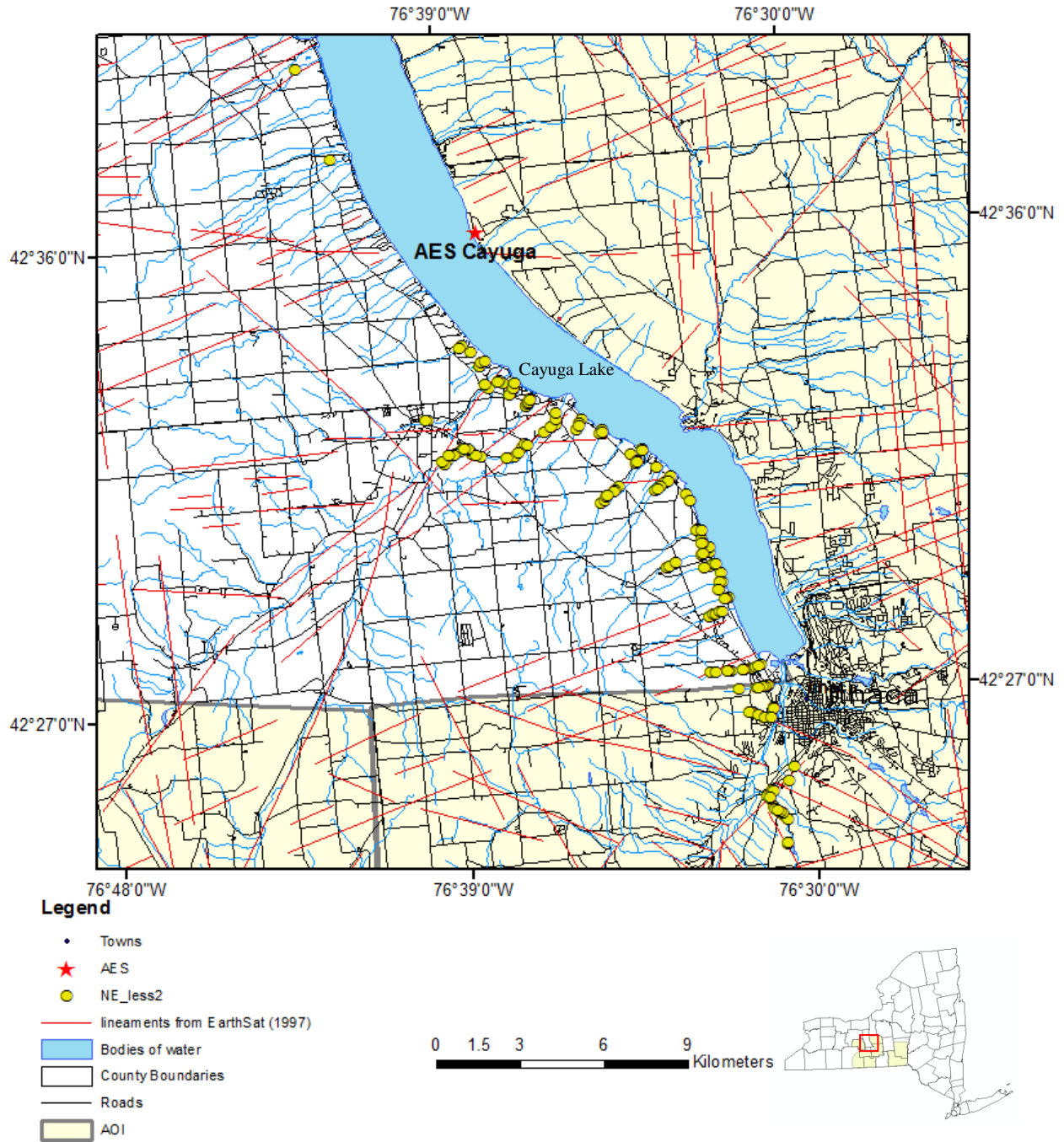


Figure 6.1-62. Lineaments and field sites displaying NE-striking fractures with a fracture frequency of less than 2 fractures/m. Fracture data from Wehn et al. (2002), Jacobi et al. (2002, 2003).





**Remote Sensing Laboratory**  
Dept. of Geology, SUNY at Buffalo



**University at Buffalo**  
The State University of New York

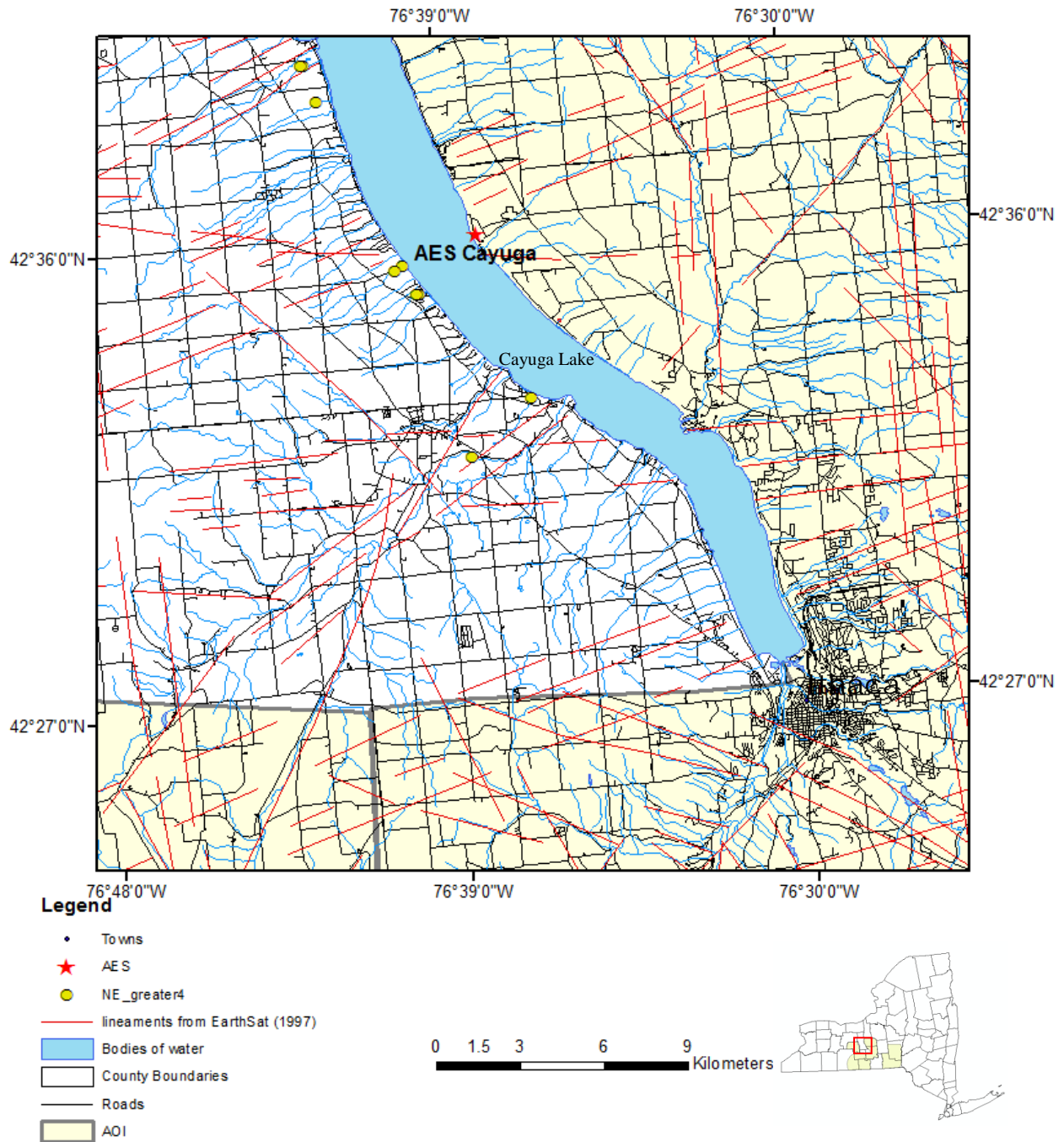


Figure 6.1-63. Lineaments and field sites displaying NE-striking fractures with a fracture frequency of greater than 4 fractures/m. Fracture data from Wehn et al. (2002), Jacobi et al. (2002, 2003).



**Remote Sensing Laboratory**  
Dept. of Geology, SUNY at Buffalo



**University at Buffalo**  
The State University of New York

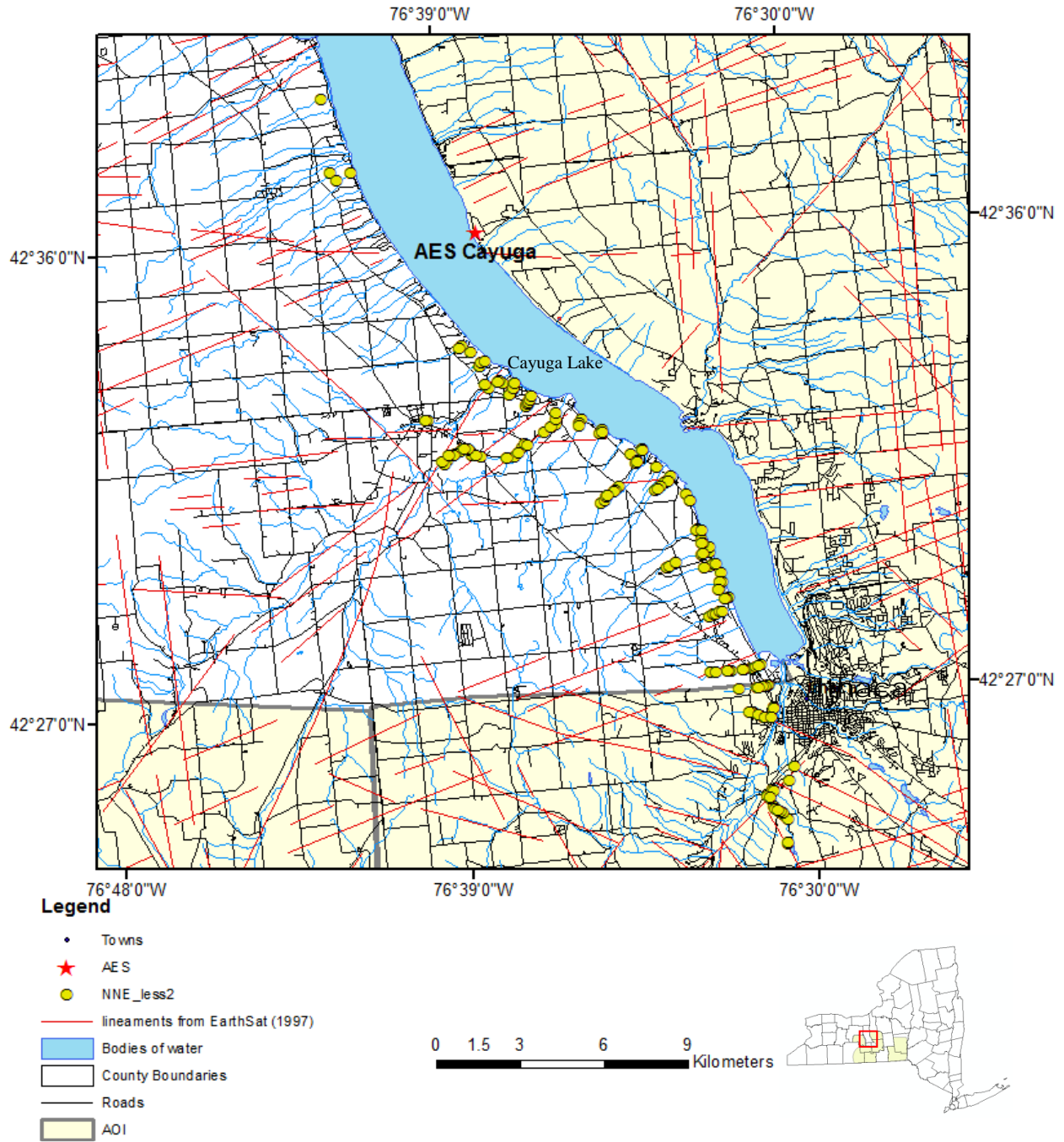


Figure 6.1-64. Lineaments and field sites displaying NNE-striking fractures with a fracture frequency of less than 2 fractures/m. Fracture data from Wehn et al. (2002), Jacobi et al. (2002, 2003).



**Remote Sensing Laboratory**  
Dept. of Geology, SUNY at Buffalo



**University at Buffalo**  
The State University of New York

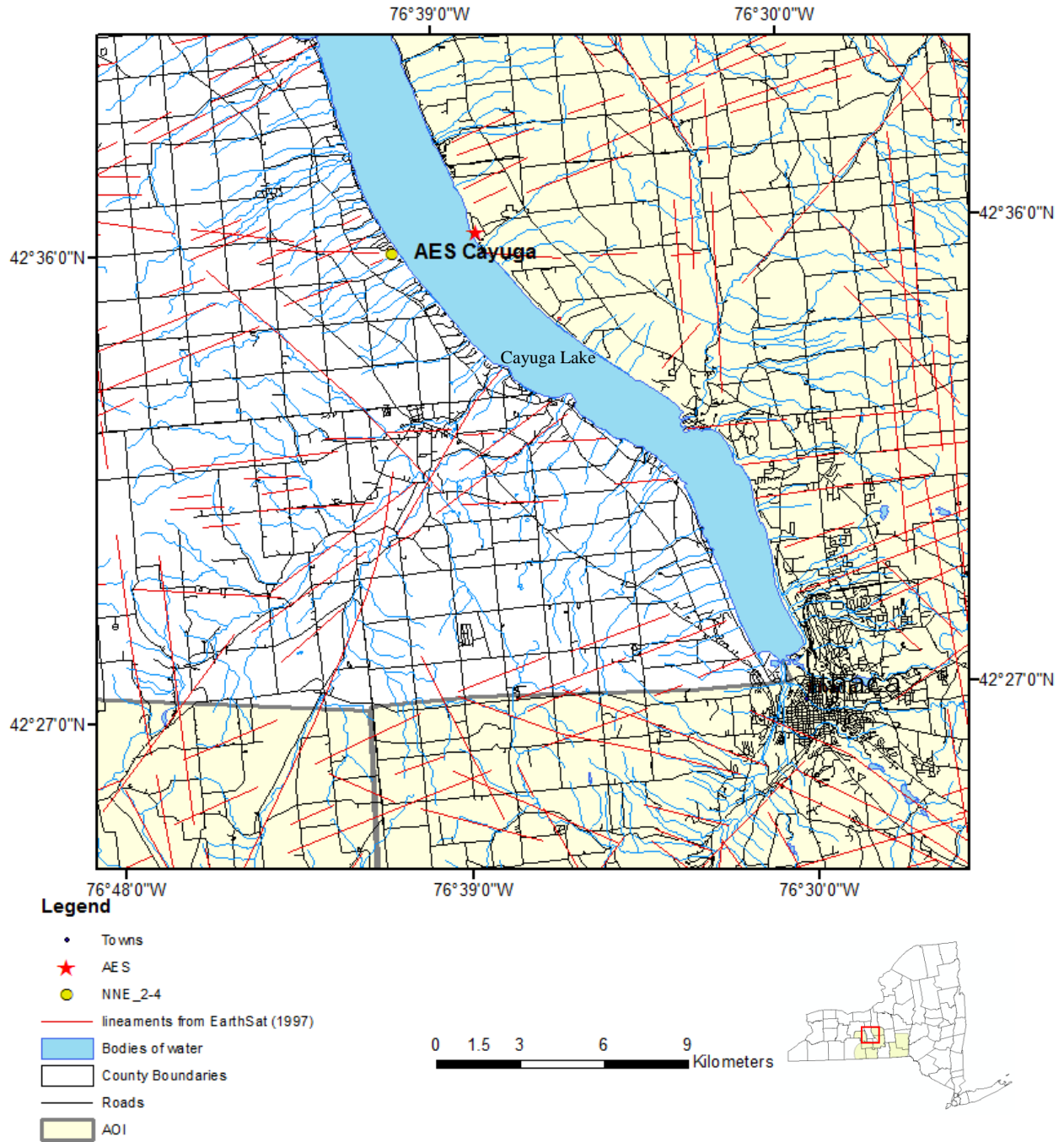


Figure 6.1-65. Lineaments and field sites displaying NNE-striking fractures with a fracture frequency of 2 to 4 fractures/m. Fracture data from Wehn et al. (2002), Jacobi et al. (2002, 2003).



**Remote Sensing Laboratory**  
Dept. of Geology, SUNY at Buffalo



**University at Buffalo**  
The State University of New York

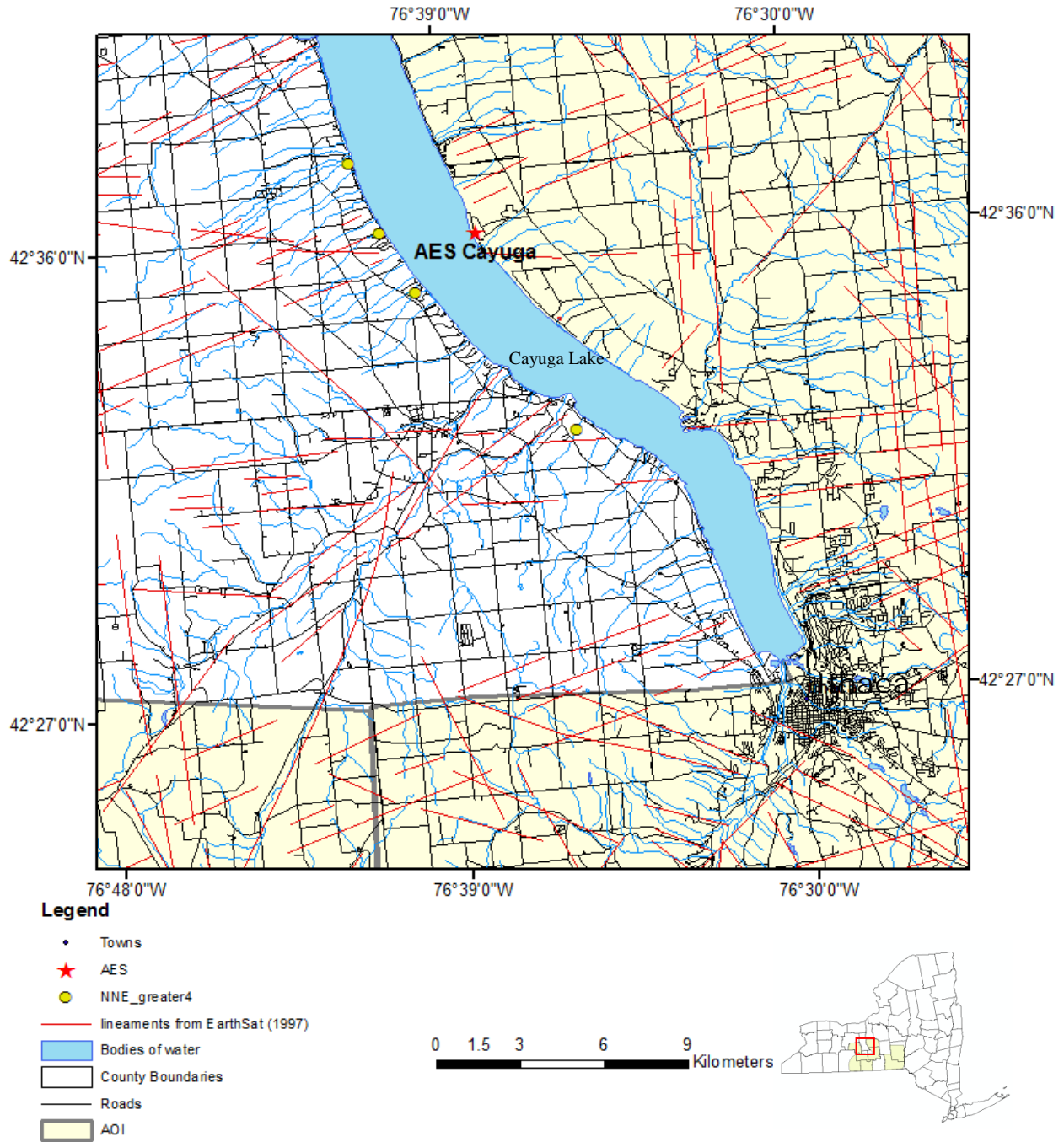


Figure 6.1-66. Lineaments and field sites displaying NNE-striking fractures with a fracture frequency of greater than 4 fractures/m. Fracture data from Wehn et al. (2002), Jacobi et al. (2002, 2003).





**Remote Sensing Laboratory**  
Dept. of Geology, SUNY at Buffalo



**University at Buffalo**  
The State University of New York

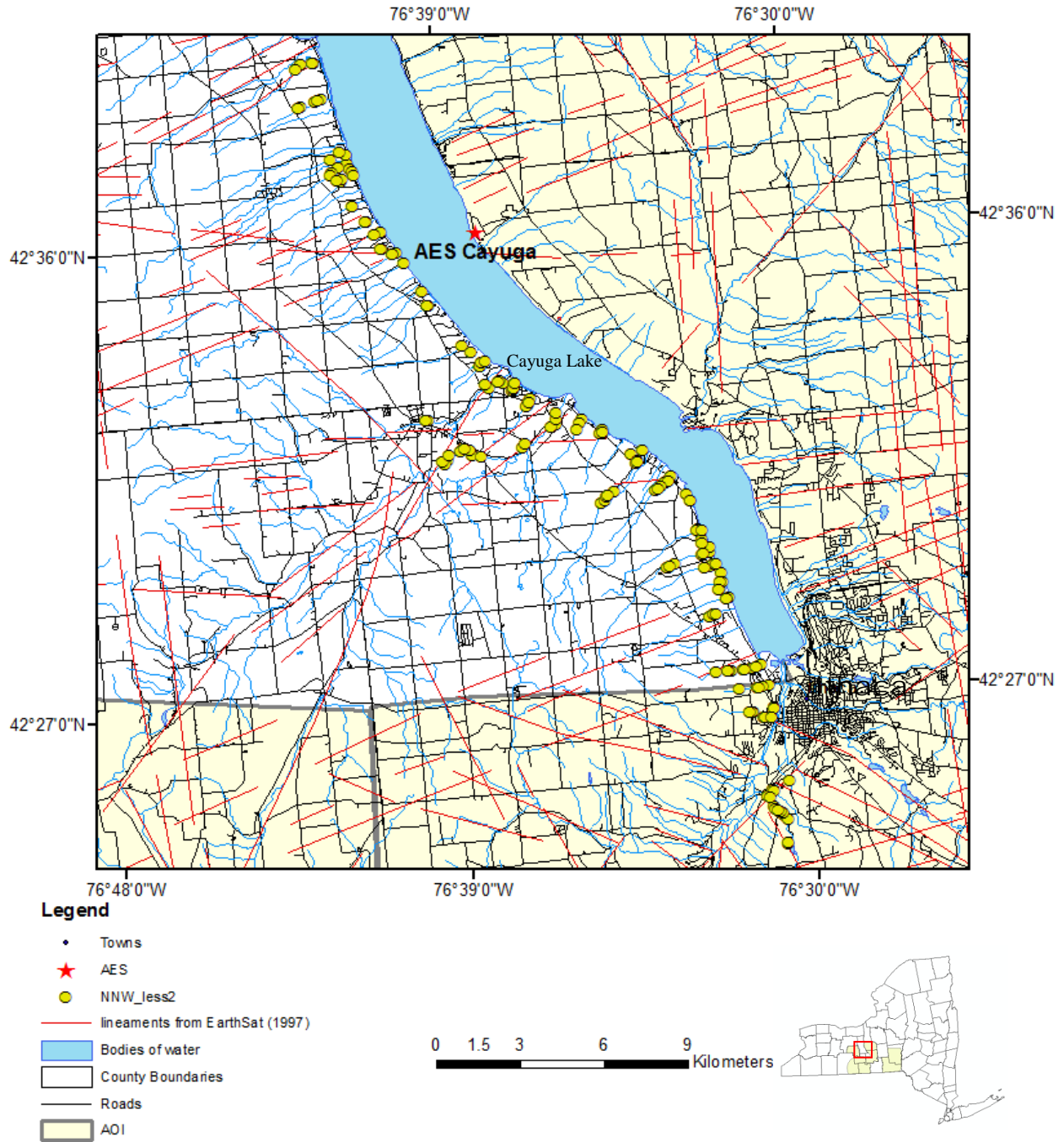


Figure 6.1-67. Lineaments and field sites displaying NNW-striking fractures with a fracture frequency of less than 2 fractures/m. Fracture data from Wehn et al. (2002), Jacobi et al. (2002, 2003).



**Remote Sensing Laboratory**  
Dept. of Geology, SUNY at Buffalo



**University at Buffalo**  
The State University of New York

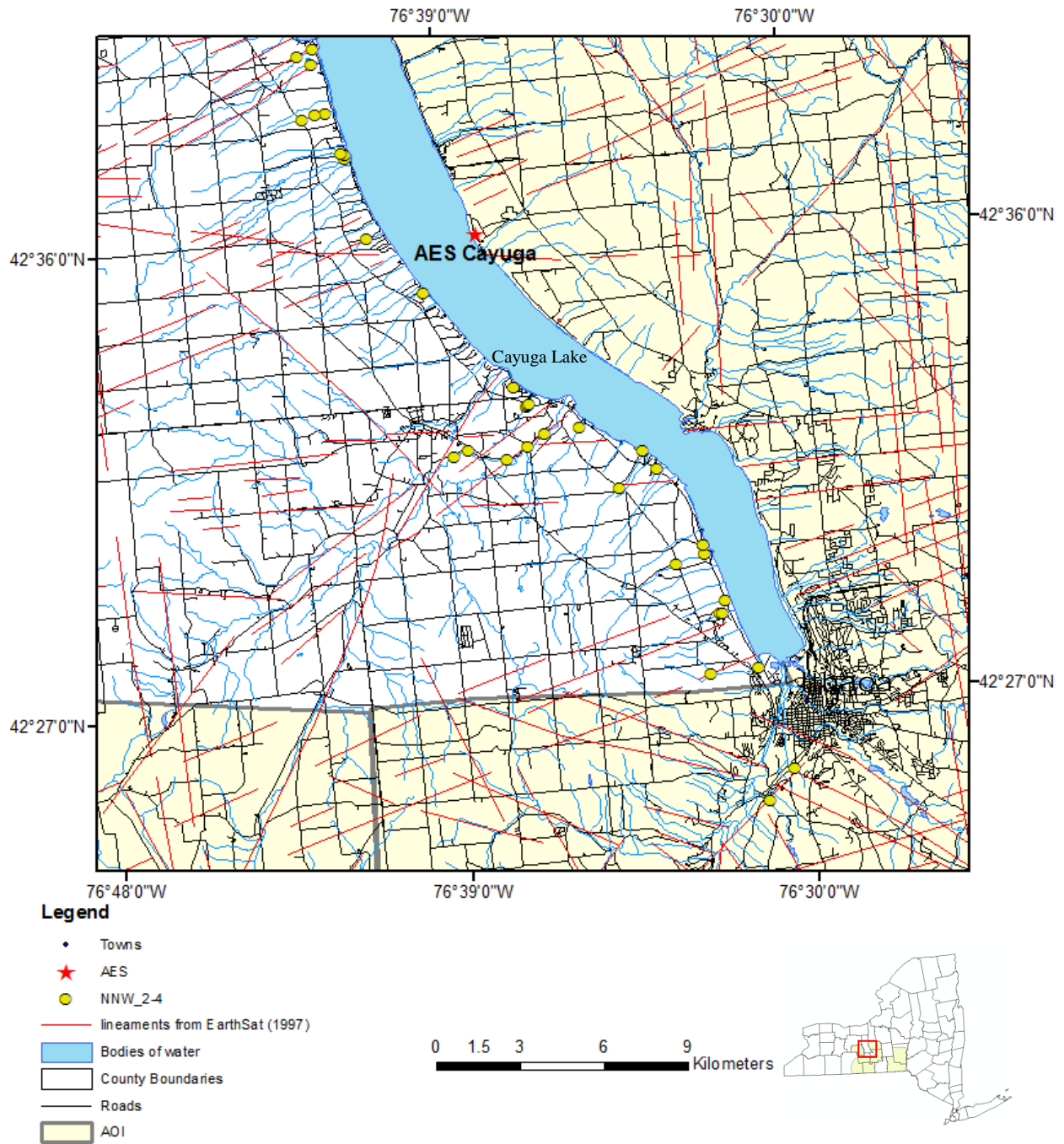


Figure 6.1-68: Lineaments and field sites displaying NNW-striking fractures with a fracture frequency of 2 to 4 fractures/m. Fracture data from Wehn et al. (2002), Jacobi et al. (2002, 2003).



**Remote Sensing Laboratory**  
 Dept. of Geology, SUNY at Buffalo



**University at Buffalo**  
 The State University of New York

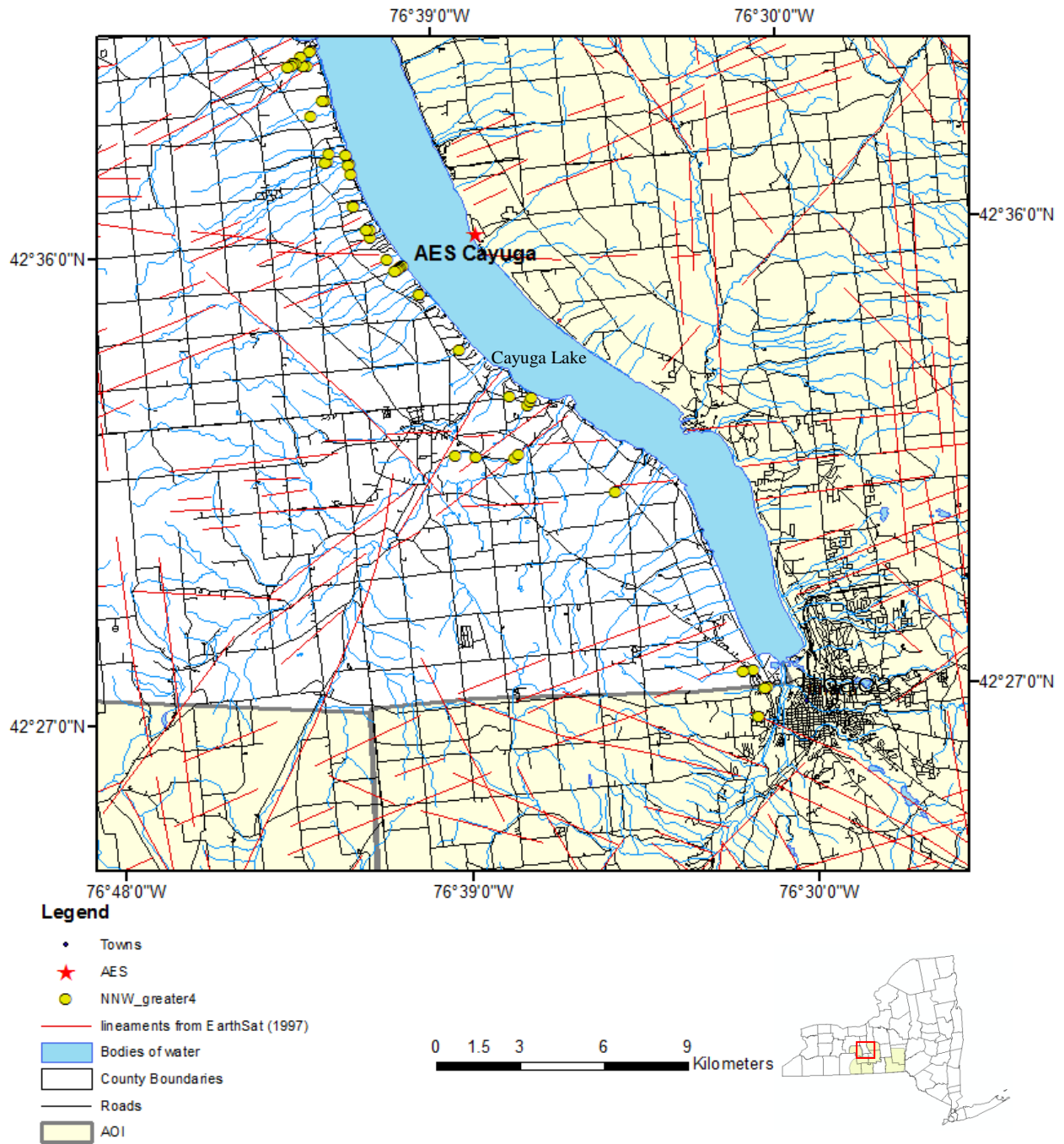


Figure 6.1-69: Lineaments and field sites displaying NNW-striking fractures with a fracture frequency of greater than 4 fractures/m. Fracture data from Wehn et al. (2002), Jacobi et al. (2002, 2003).



**Remote Sensing Laboratory**  
Dept. of Geology, SUNY at Buffalo



**University at Buffalo**  
The State University of New York

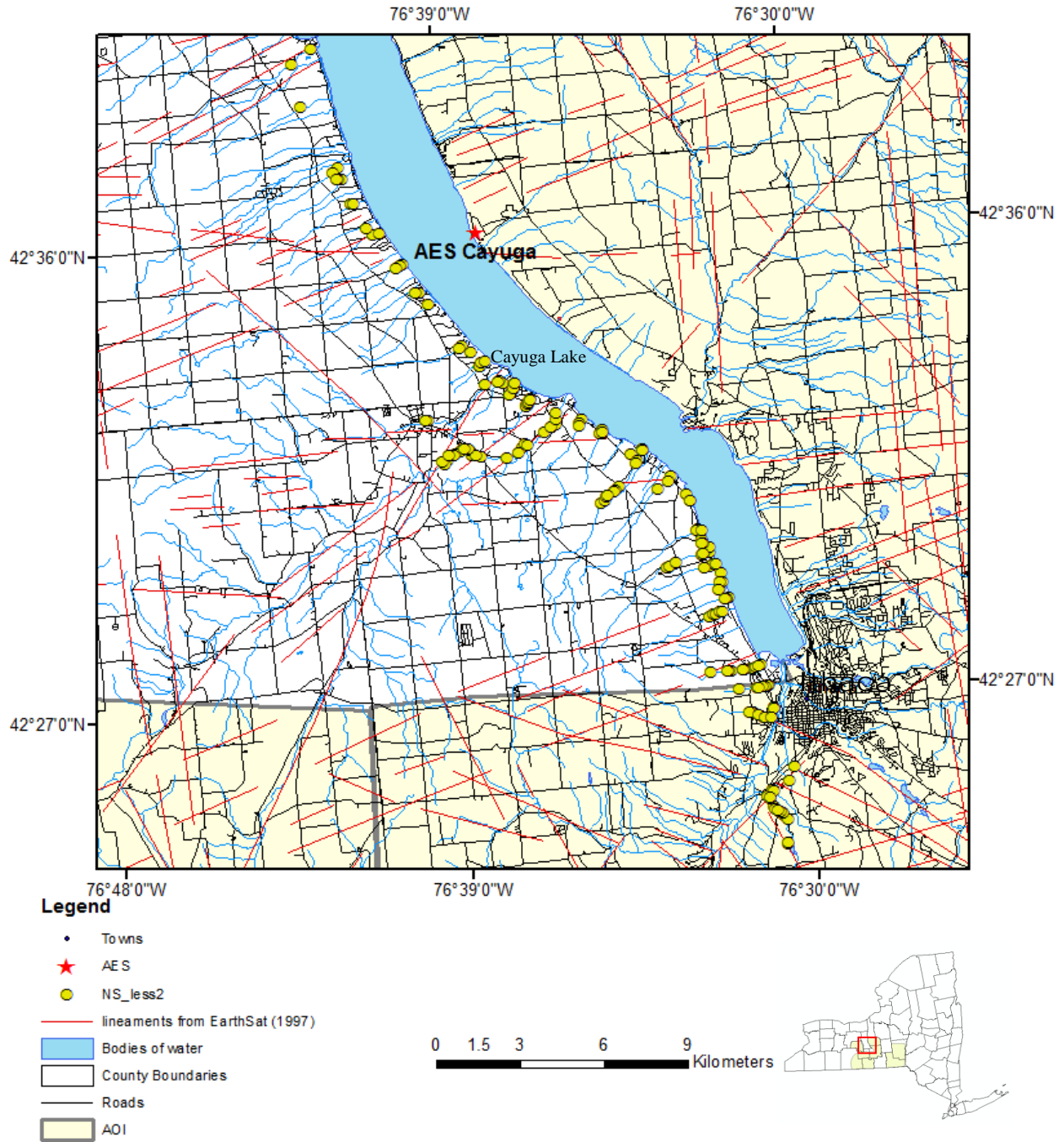


Figure 6.1-70: Lineaments and field sites displaying NS-striking fractures with a fracture frequency of less than 2 fractures/m. Fracture data from Wehn et al. (2002), Jacobi et al. (2002, 2003).





**Remote Sensing Laboratory**  
Dept. of Geology, SUNY at Buffalo



**University at Buffalo**  
The State University of New York

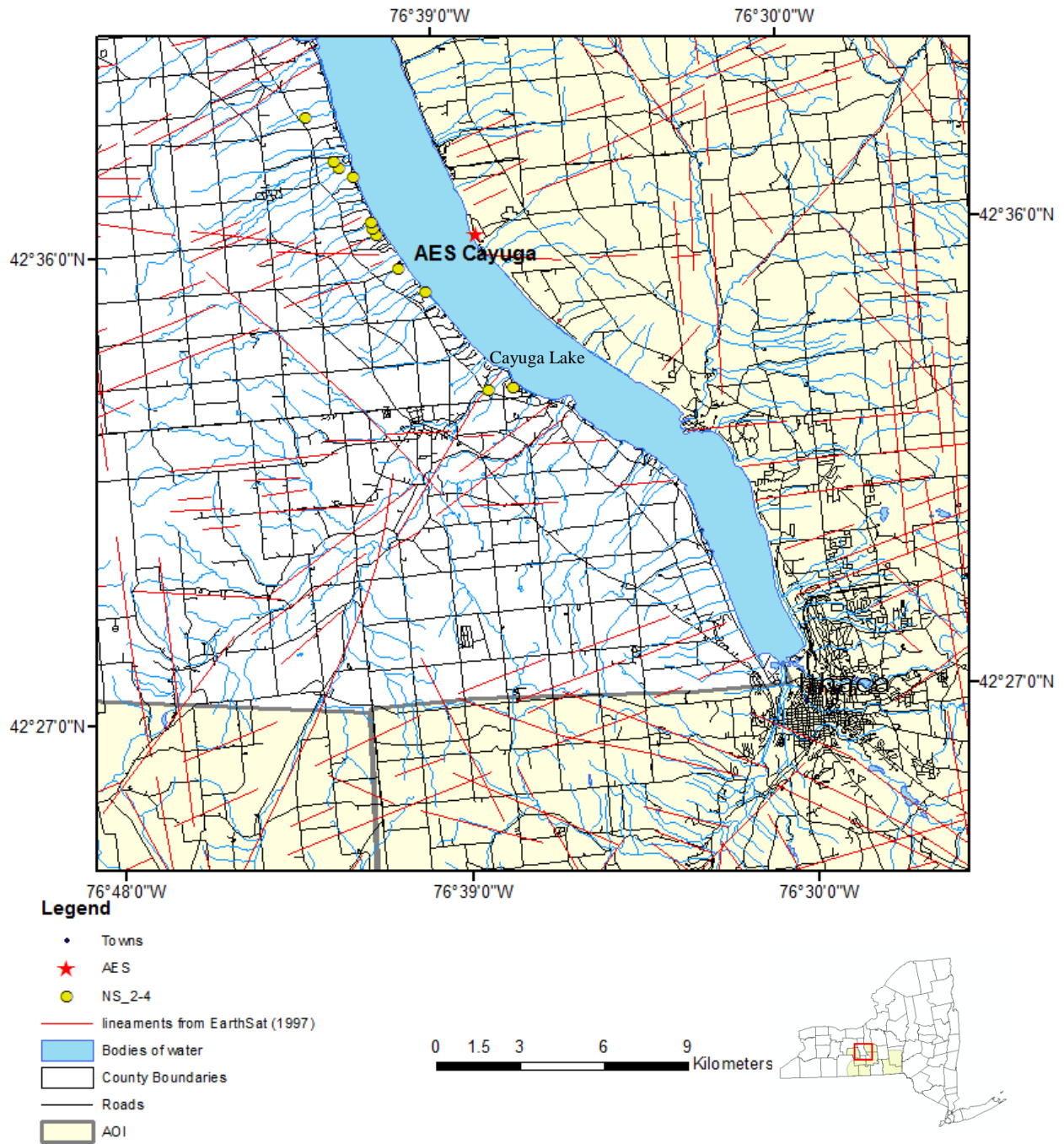


Figure 6.1-71: Lineaments and field sites displaying NS-striking fractures with a fracture frequency of 2 to 4 fractures/m. Fracture data from Wehn et al. (2002), Jacobi et al. (2002, 2003).



**Remote Sensing Laboratory**  
Dept. of Geology, SUNY at Buffalo



**University at Buffalo**  
The State University of New York

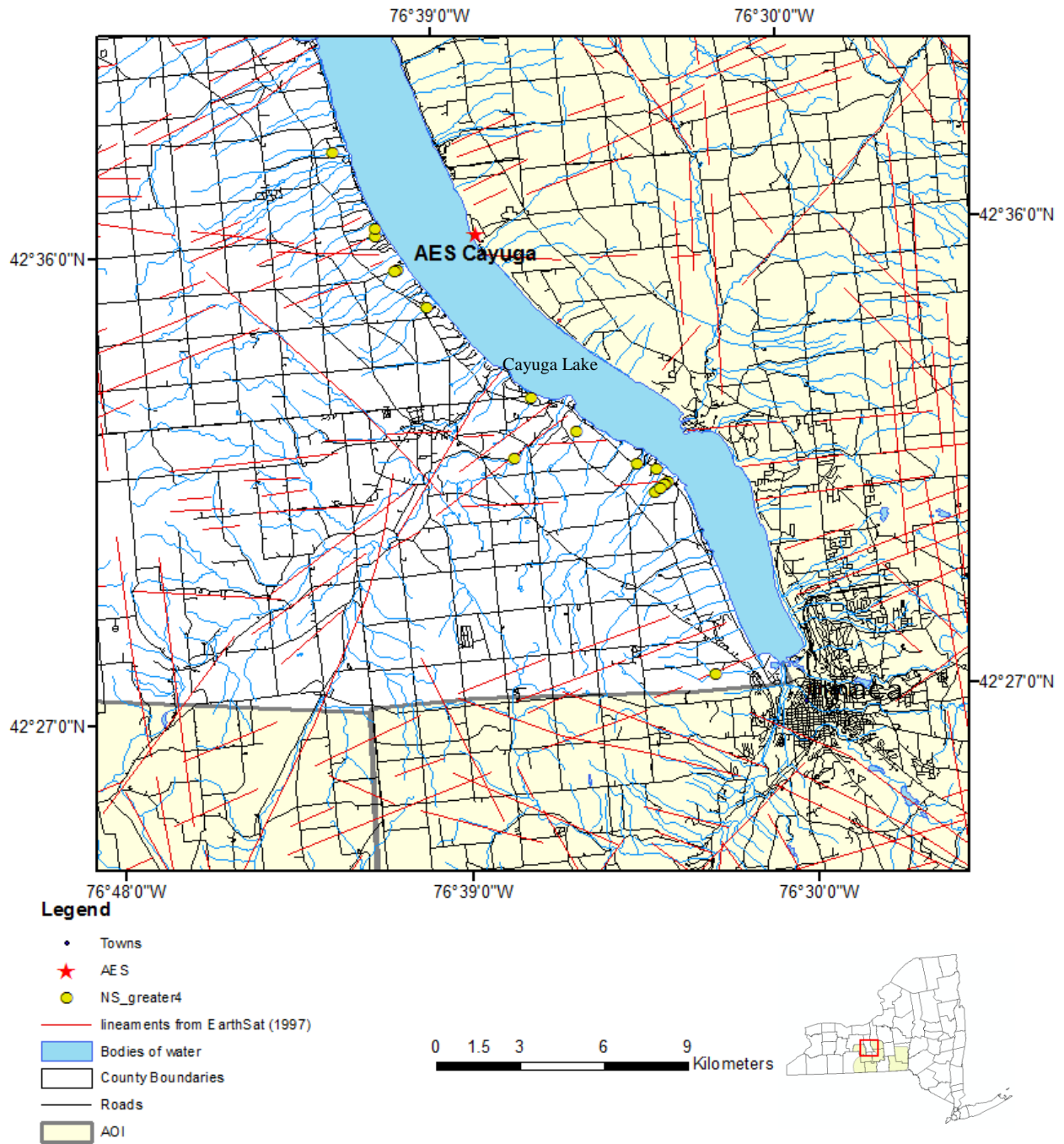


Figure 6.1-72: Lineaments and field sites displaying NS-striking fractures with a fracture frequency of greater than 4 fractures/m. Fracture data from Wehn et al. (2002), Jacobi et al. (2002, 2003).



**Remote Sensing Laboratory**  
Dept. of Geology, SUNY at Buffalo



**University at Buffalo**  
The State University of New York

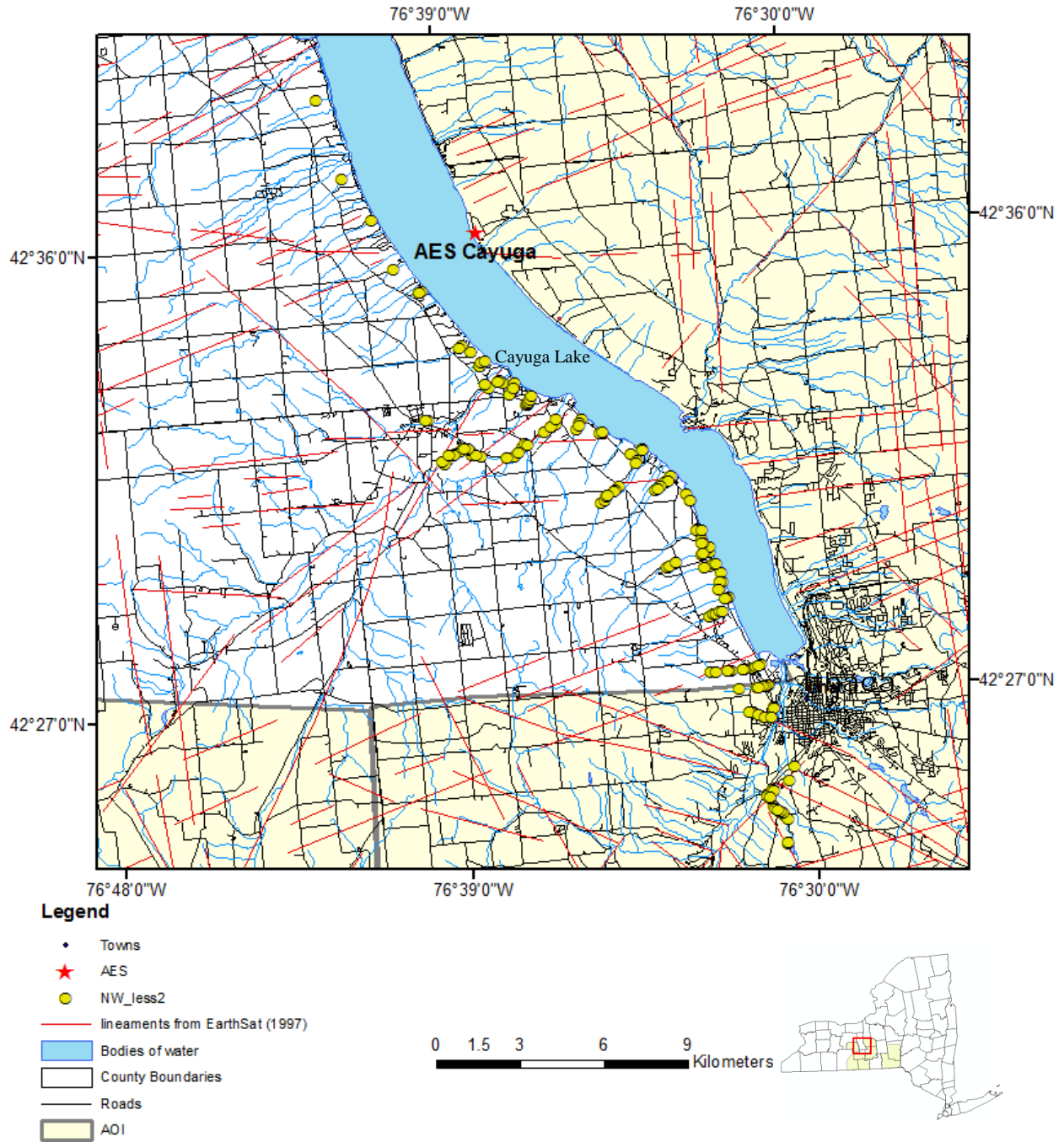


Figure 6.1-73: Lineaments and field sites displaying NW-striking fractures with a fracture frequency of less than 2 fractures/m. Fracture data from Wehn et al. (2002), Jacobi et al. (2002, 2003).



**Remote Sensing Laboratory**  
Dept. of Geology, SUNY at Buffalo



**University at Buffalo**  
The State University of New York

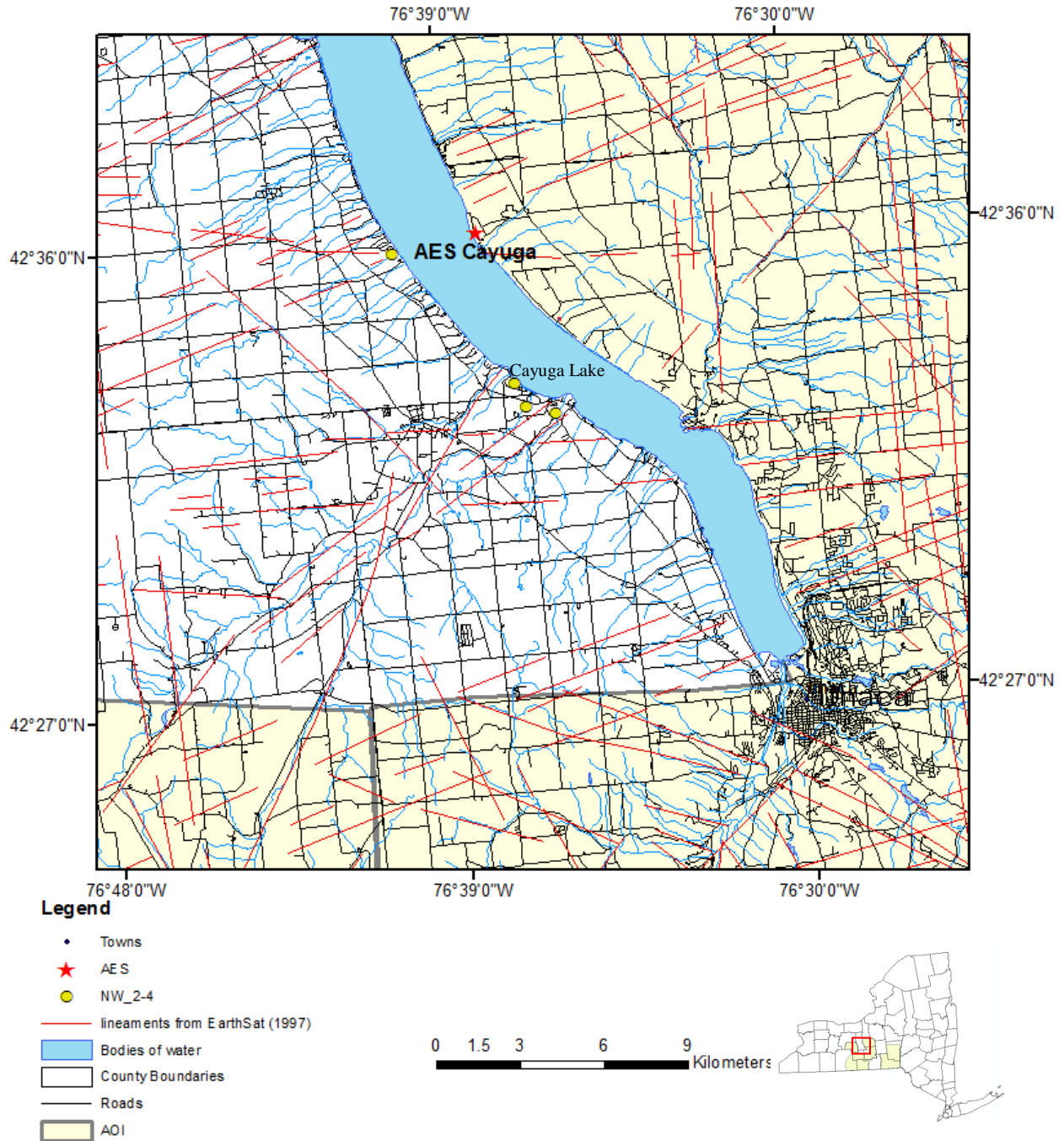


Figure 6.1-74: Lineaments and field sites displaying NW-striking fractures with a fracture frequency of 2 to 4 fractures/m. Fracture data from Wehn et al. (2002), Jacobi et al. (2002, 2003).





**Remote Sensing Laboratory**  
Dept. of Geology, SUNY at Buffalo



**University at Buffalo**  
The State University of New York

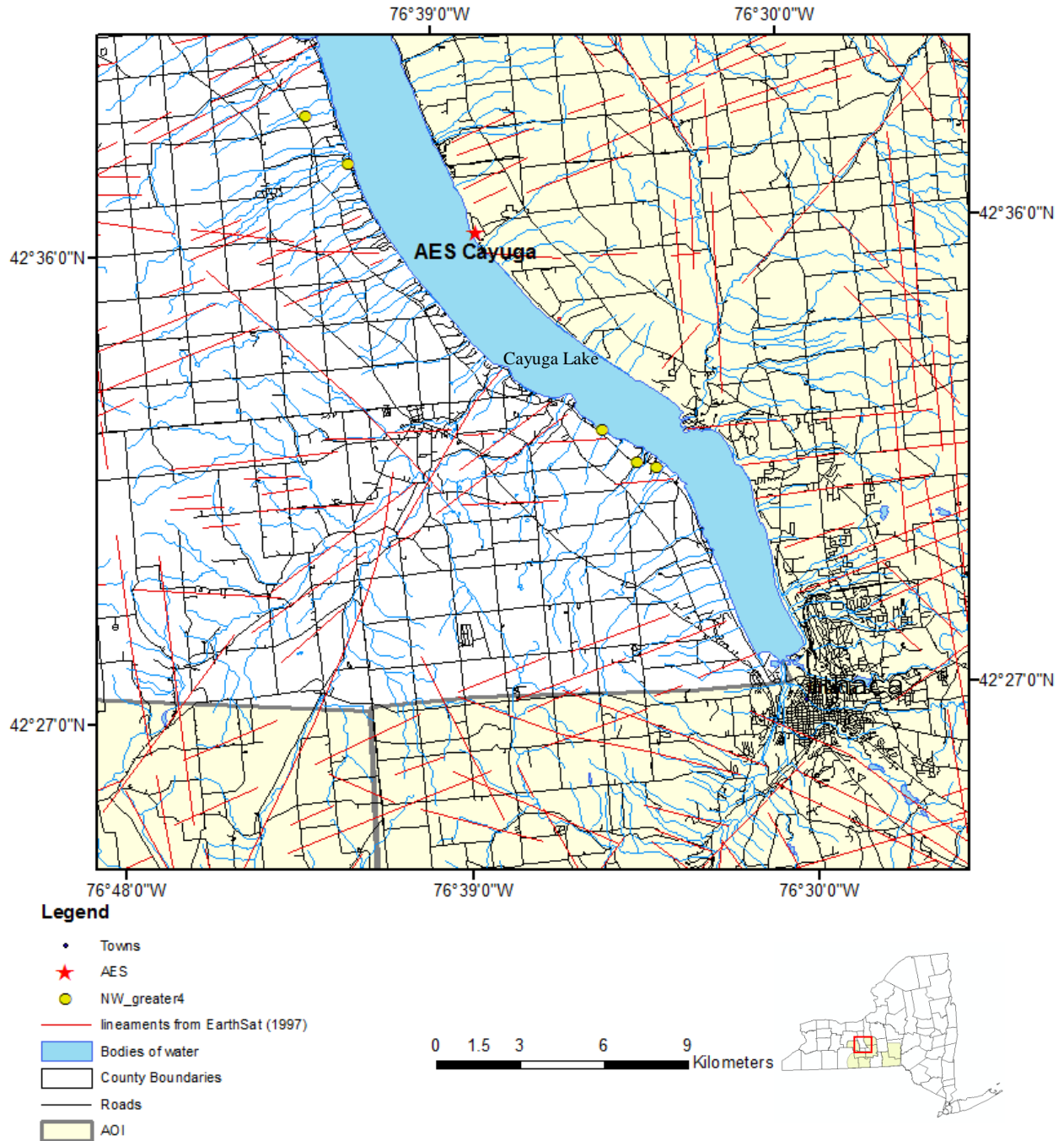


Figure 6.1-75: Lineaments and field sites displaying NW-striking fractures with a fracture frequency of greater than 4 fractures/m. Fracture data from Wehn et al. (2002), Jacobi et al. (2002, 2003).



**Remote Sensing Laboratory**  
Dept. of Geology, SUNY at Buffalo



**University at Buffalo**  
The State University of New York

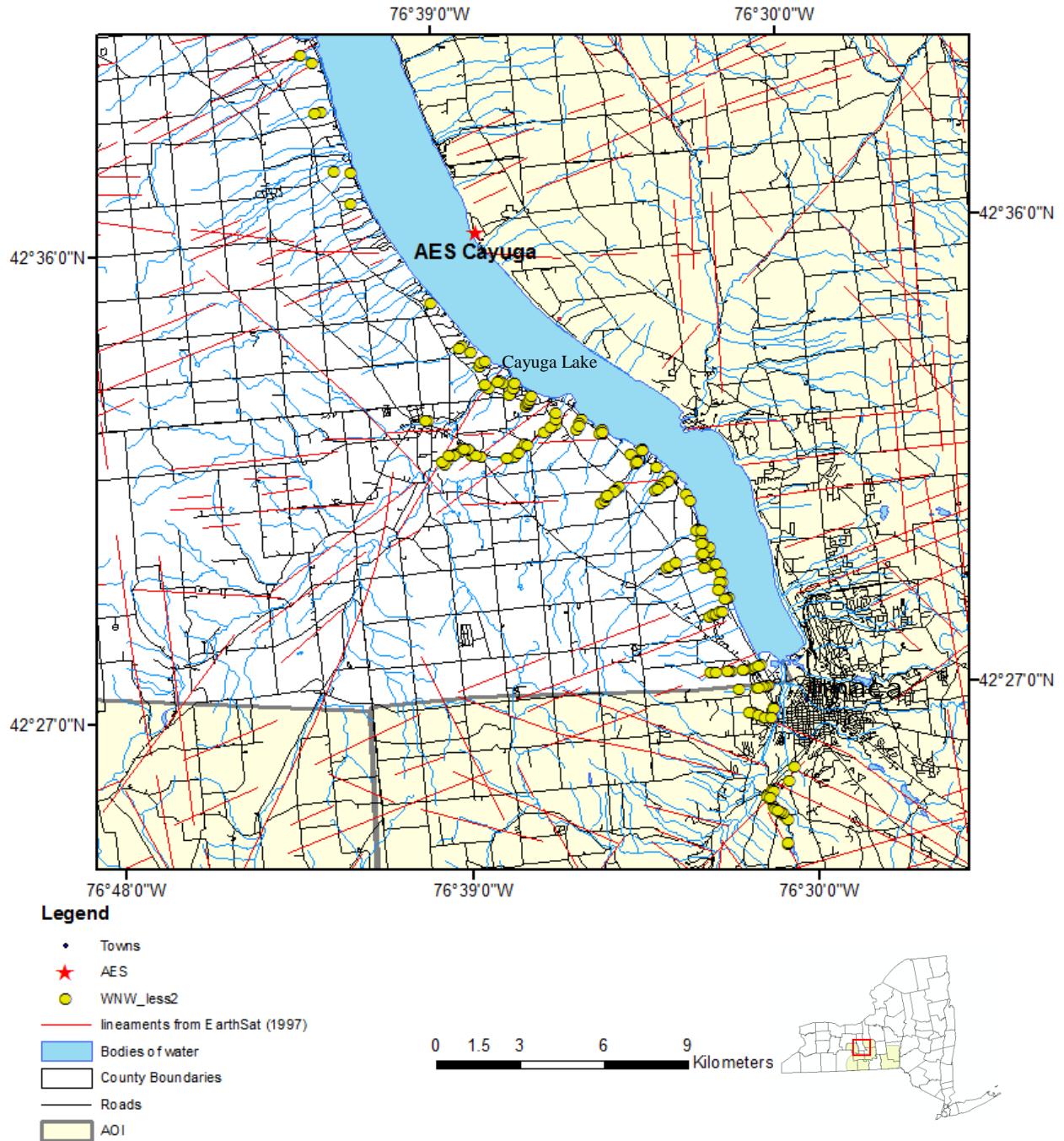


Figure 6.1-76: Lineaments and field sites displaying WNW-striking fractures with a fracture frequency of less than 2 fractures/m. Fracture data from Wehn et al. (2002), Jacobi et al. (2002, 2003).



**Remote Sensing Laboratory**  
Dept. of Geology, SUNY at Buffalo



**University at Buffalo**  
The State University of New York

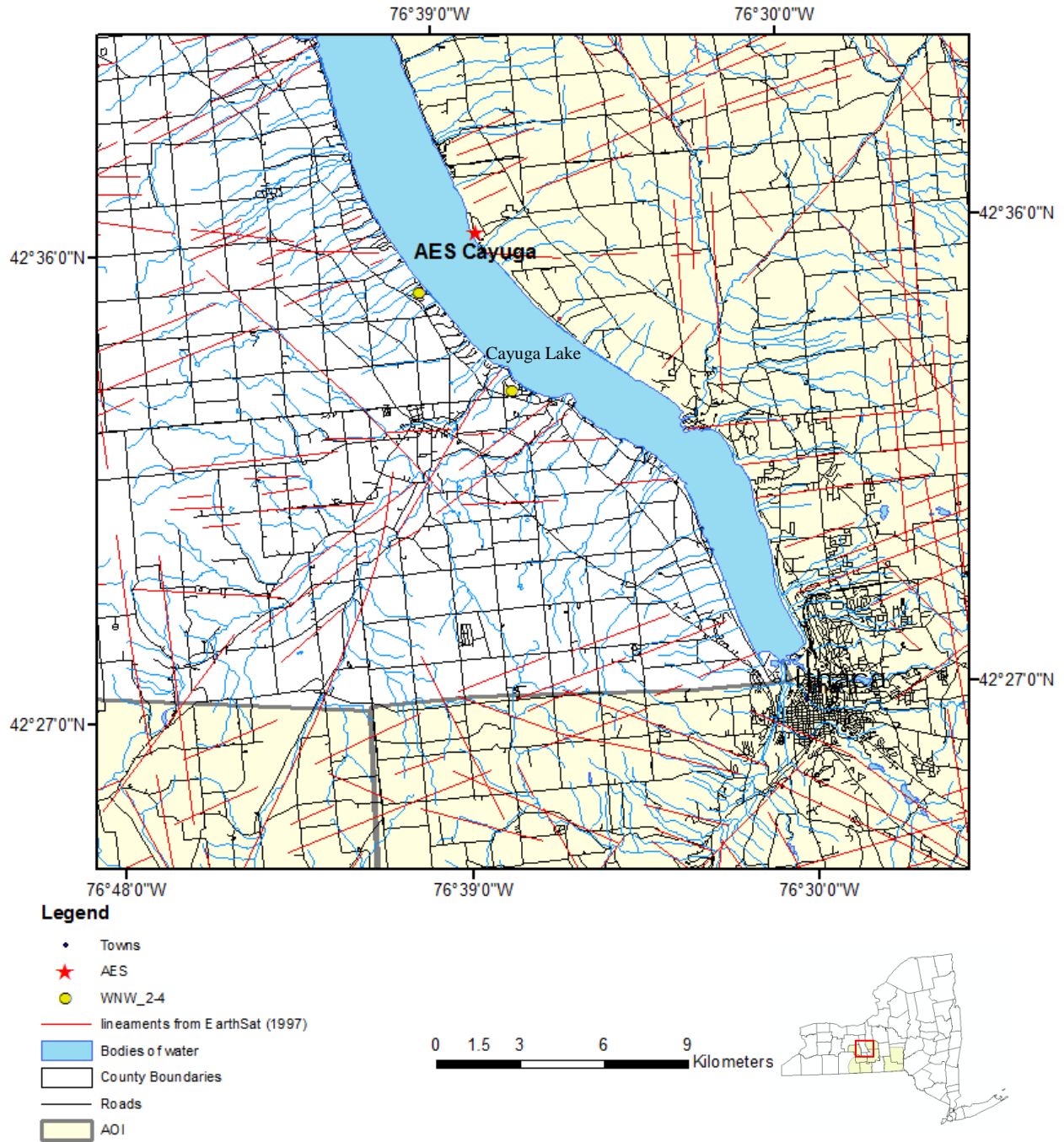


Figure 6.1-77: Lineaments and field sites displaying WNW-striking fractures with a fracture frequency of 2 to 4 fractures/m. Fracture data from Wehn et al. (2002), Jacobi et al. (2002, 2003).



**Remote Sensing Laboratory**  
Dept. of Geology, SUNY at Buffalo



**University at Buffalo**  
The State University of New York

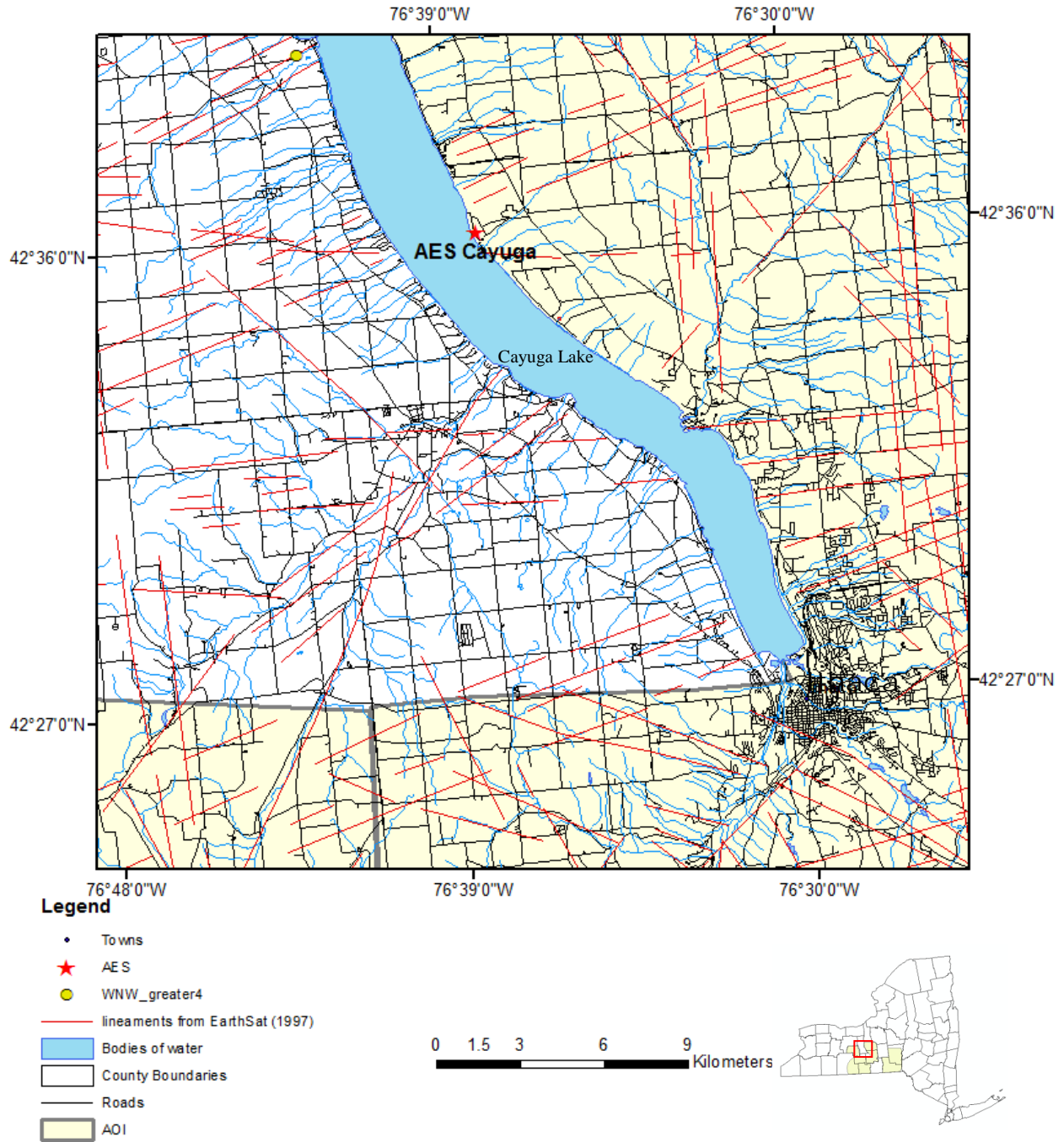


Figure 6.1-78: Lineaments and field sites displaying WNW-striking fractures with a fracture frequency of greater than 4 fractures/m. Fracture data from Wehn et al. (2002), Jacobi et al. (2002, 2003).





**Remote Sensing Laboratory**  
 Dept. of Geology, SUNY at Buffalo



**University at Buffalo**  
 The State University of New York

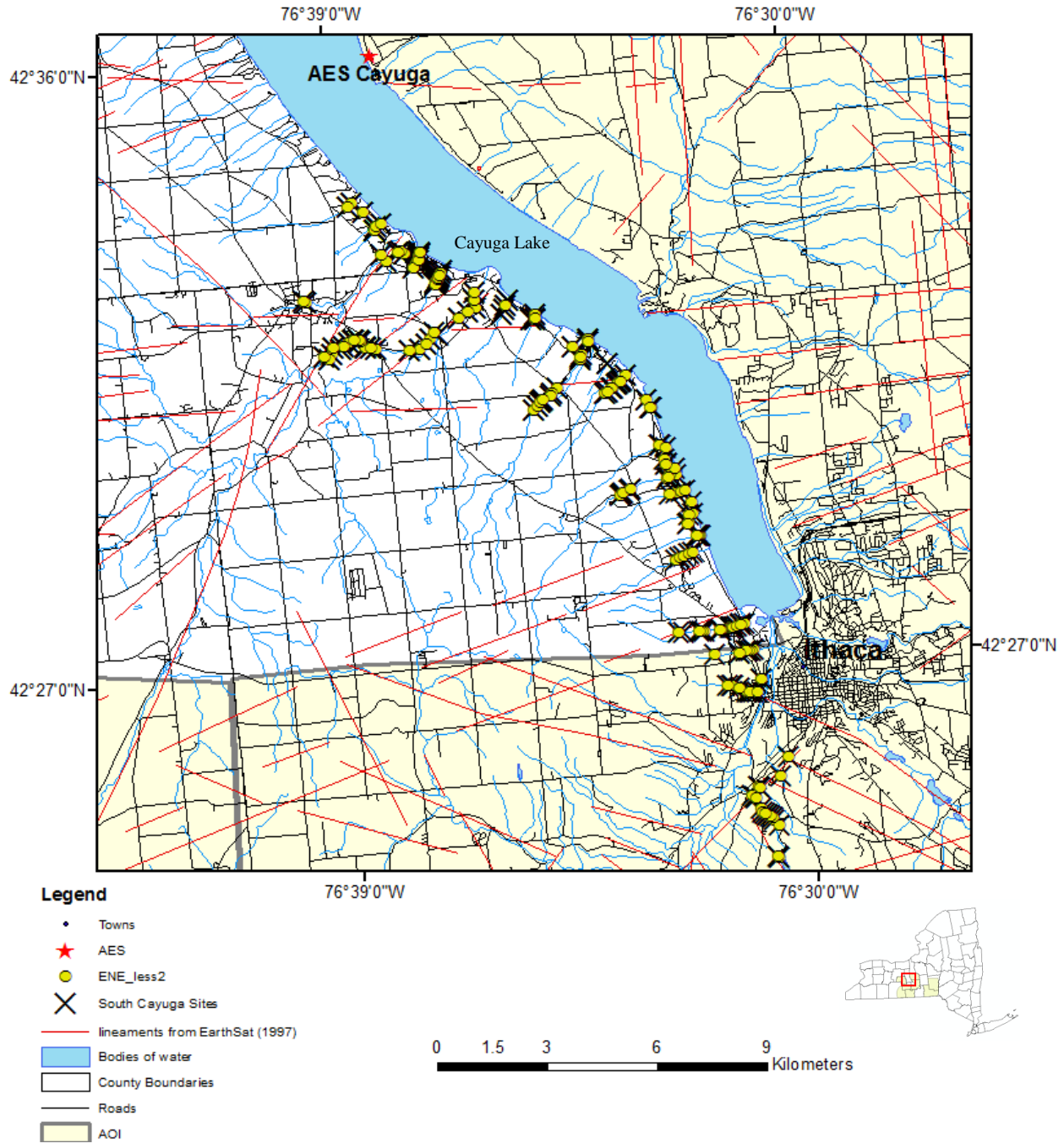


Figure 6.1-79: Lineaments and field sites displaying ENE-striking fractures with a fracture frequency of less than 2 fractures/m. Fracture data from Wehn et al. (2002), Jacobi et al. (2002, 2003).



**Remote Sensing Laboratory**  
 Dept. of Geology, SUNY at Buffalo



**University at Buffalo**  
 The State University of New York

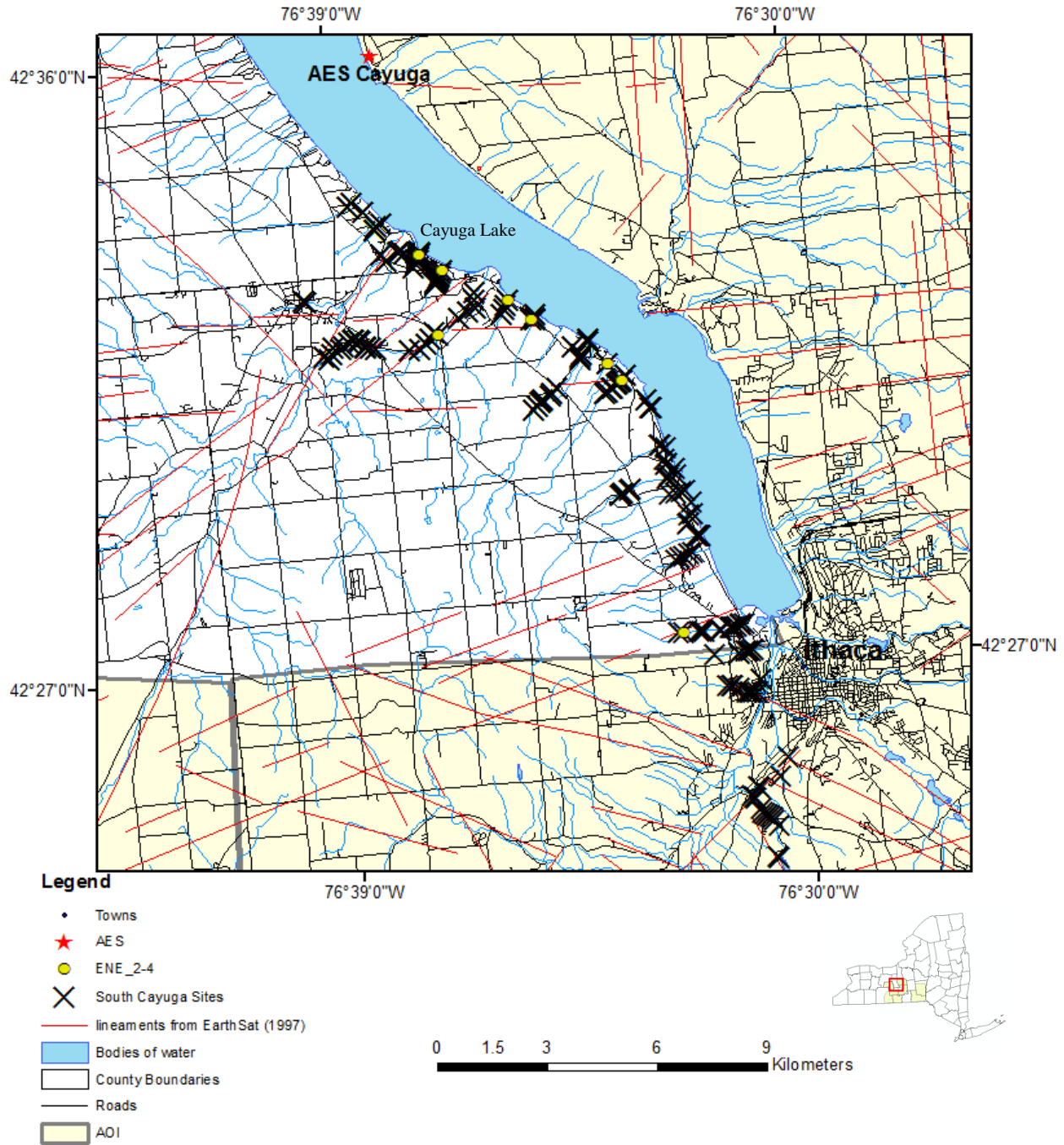


Figure 6.1-80: Lineaments and field sites displaying ENE-striking fractures with a fracture frequency of 2 to 4 fractures/m. Fracture data from Wehn et al. (2002), Jacobi et al. (2002, 2003).



**Remote Sensing Laboratory**  
 Dept. of Geology, SUNY at Buffalo



**University at Buffalo**  
 The State University of New York

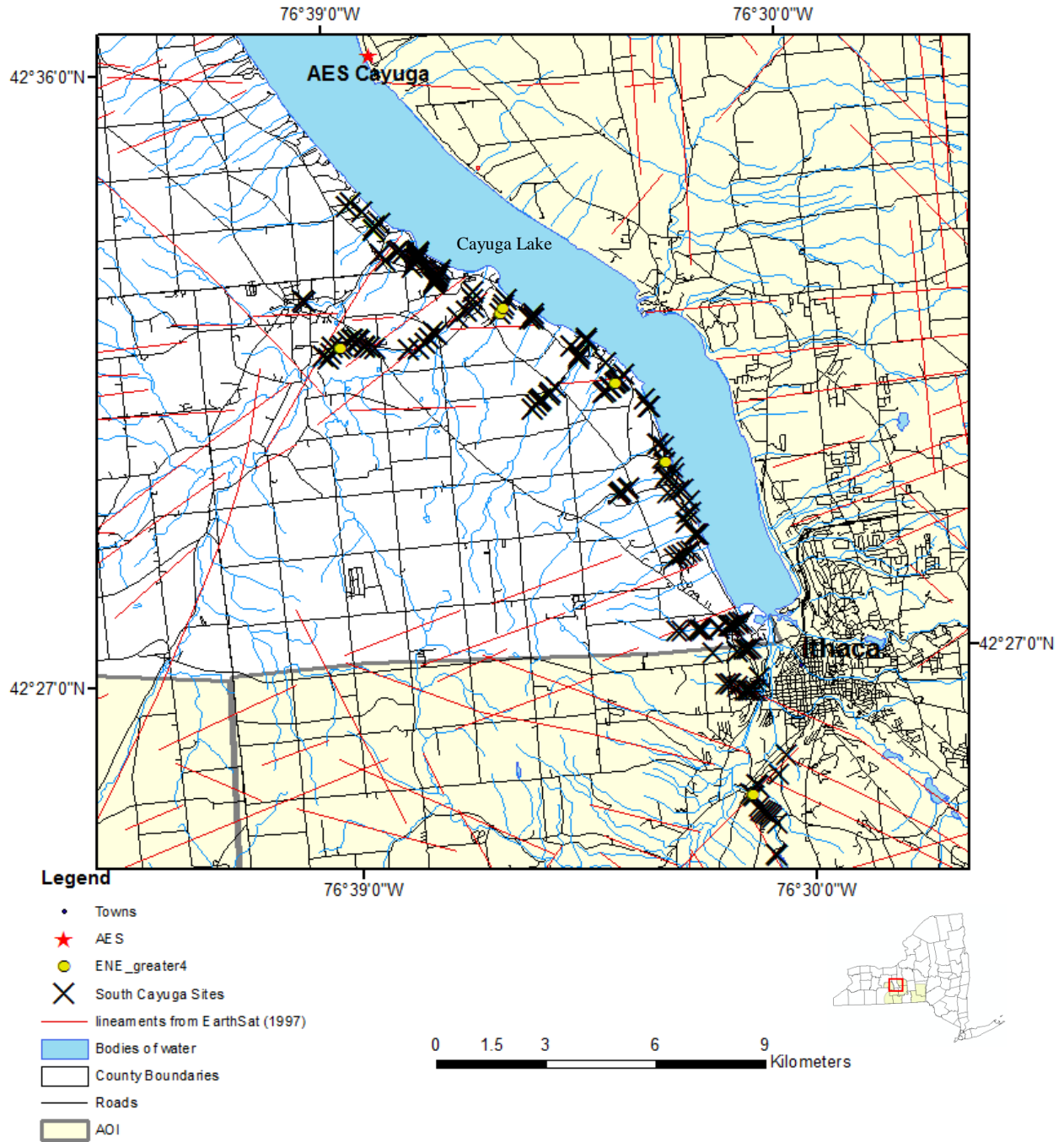


Figure 6.1-81: Lineaments and field sites displaying ENE-striking fractures with a fracture frequency of greater than 4 fractures/m. Fracture data from Wehn et al. (2002), Jacobi et al. (2002, 2003).



**Remote Sensing Laboratory**  
 Dept. of Geology, SUNY at Buffalo



**University at Buffalo**  
 The State University of New York

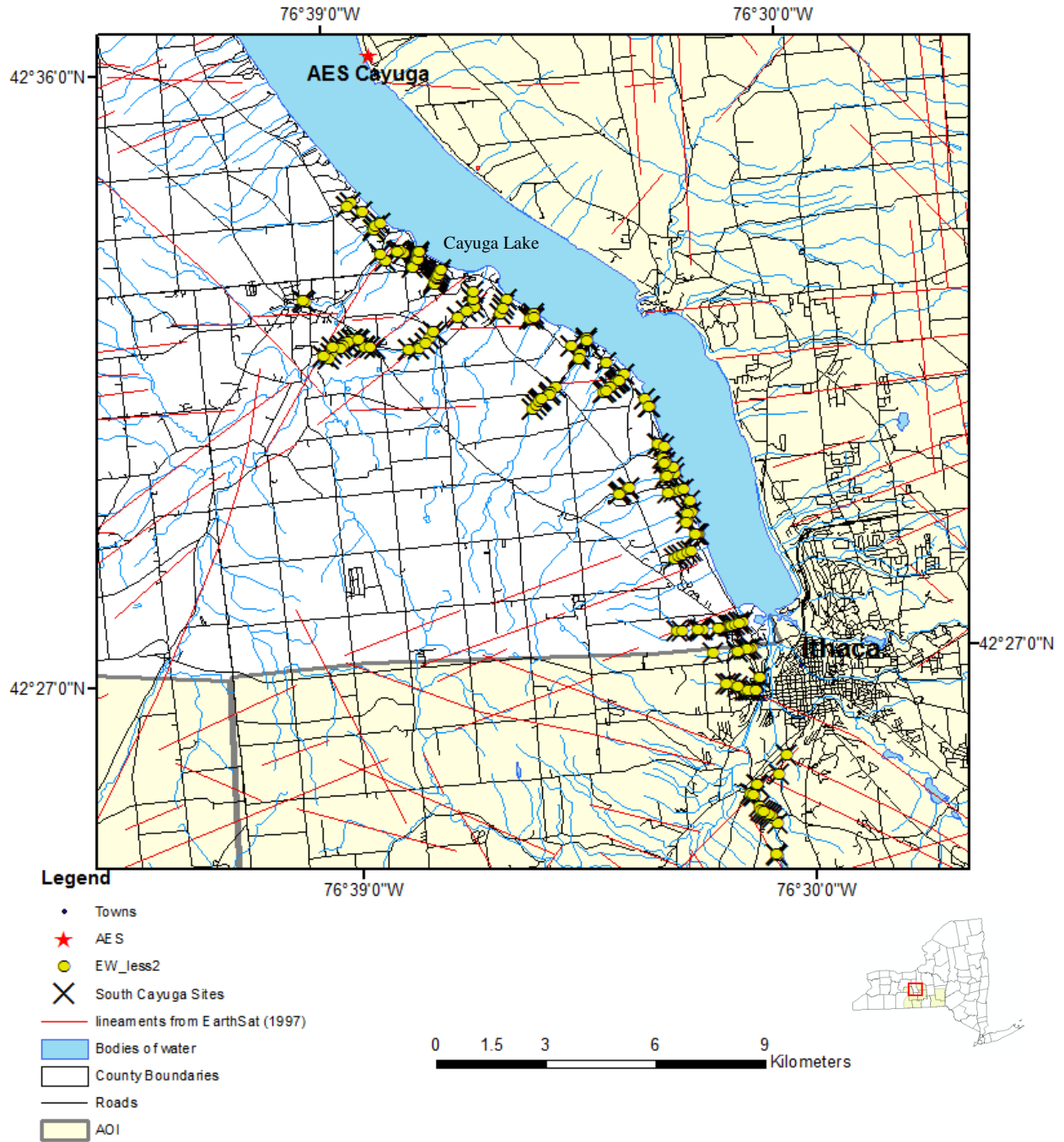


Figure 6.1-82: Lineaments and field sites displaying EW-striking fractures with a fracture frequency of less than 2 fractures/m. Fracture data from Wehn et al. (2002), Jacobi et al. (2002, 2003).





**Remote Sensing Laboratory**  
Dept. of Geology, SUNY at Buffalo



**University at Buffalo**  
The State University of New York

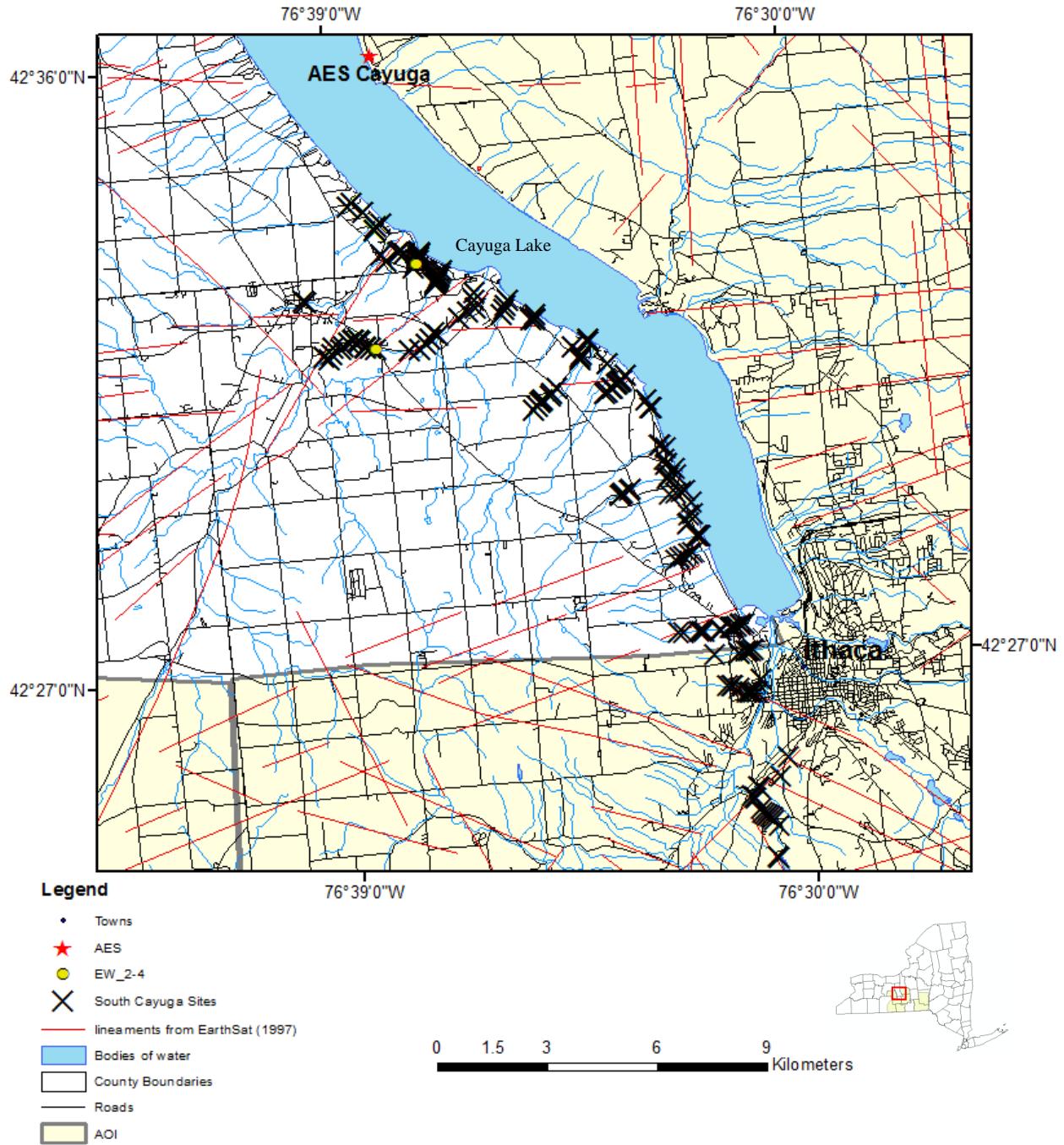


Figure 6.1-83: Lineaments and field sites displaying EW-striking fractures with a fracture frequency of 2 to 4 fractures/m. Fracture data from Wehn et al. (2002), Jacobi et al. (2002, 2003).



**Remote Sensing Laboratory**  
 Dept. of Geology, SUNY at Buffalo



**University at Buffalo**  
 The State University of New York

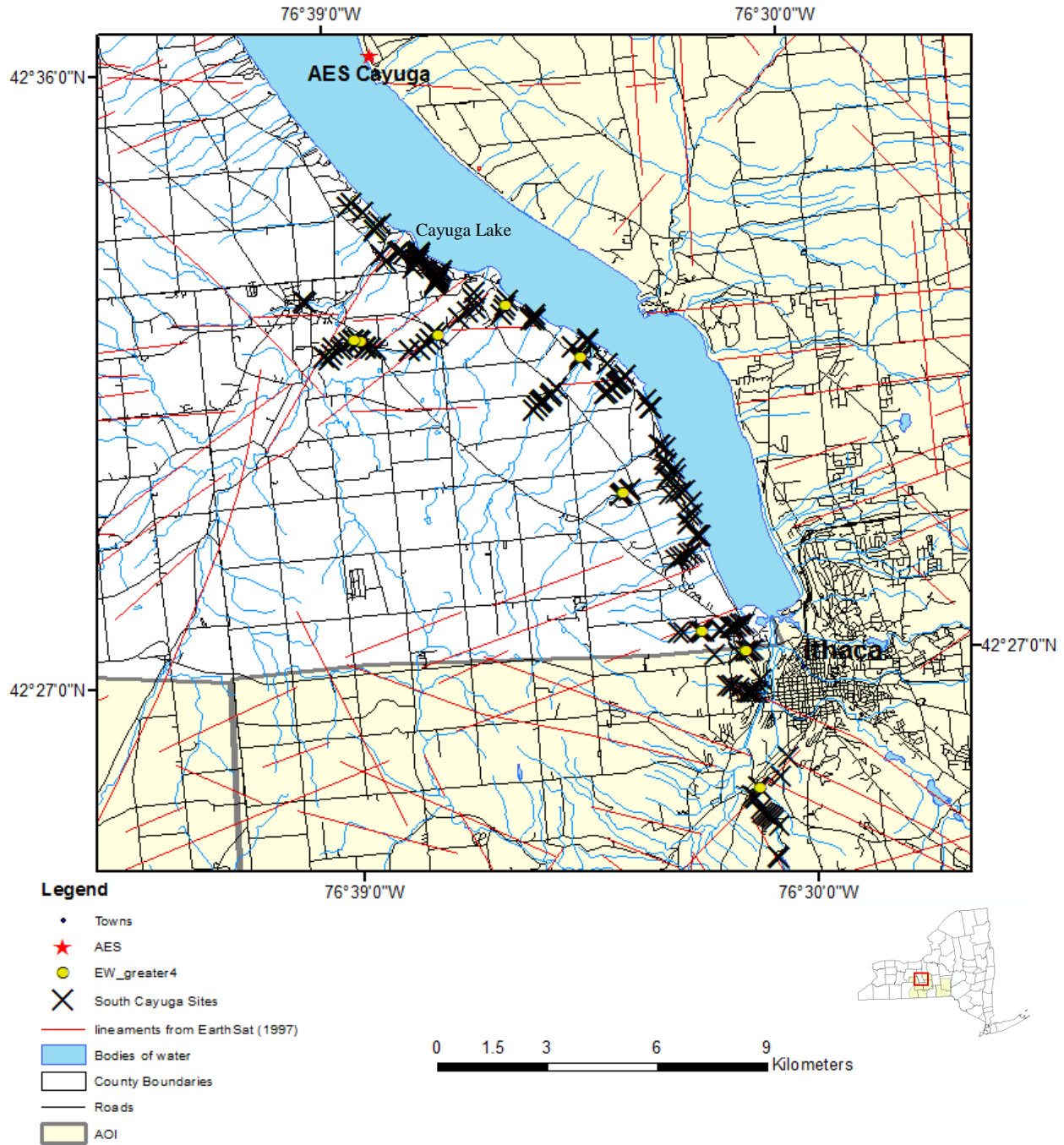


Figure 6.1-84: Lineaments and field sites displaying EW-striking fractures with a fracture frequency of greater than 4 fractures/m. Fracture data from Wehn et al. (2002), Jacobi et al. (2002, 2003).



**Remote Sensing Laboratory**  
 Dept. of Geology, SUNY at Buffalo



**University at Buffalo**  
 The State University of New York

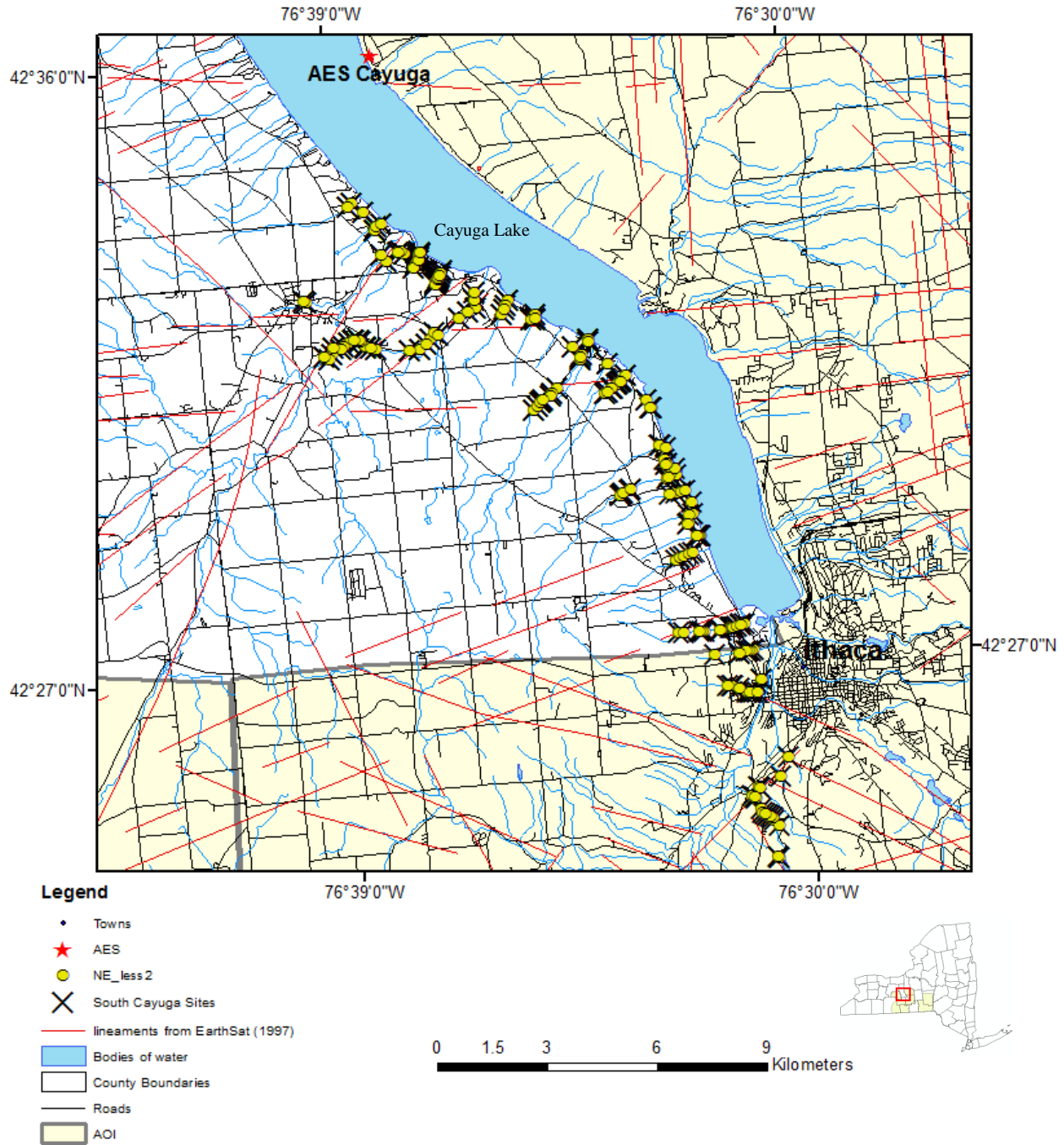


Figure 6.1-85: Lineaments and field sites displaying NE-striking fractures with a fracture frequency of less than 2 fractures/m. Fracture data from Wehn et al. (2002), Jacobi et al. (2002, 2003).



**Remote Sensing Laboratory**  
 Dept. of Geology, SUNY at Buffalo



**University at Buffalo**  
 The State University of New York

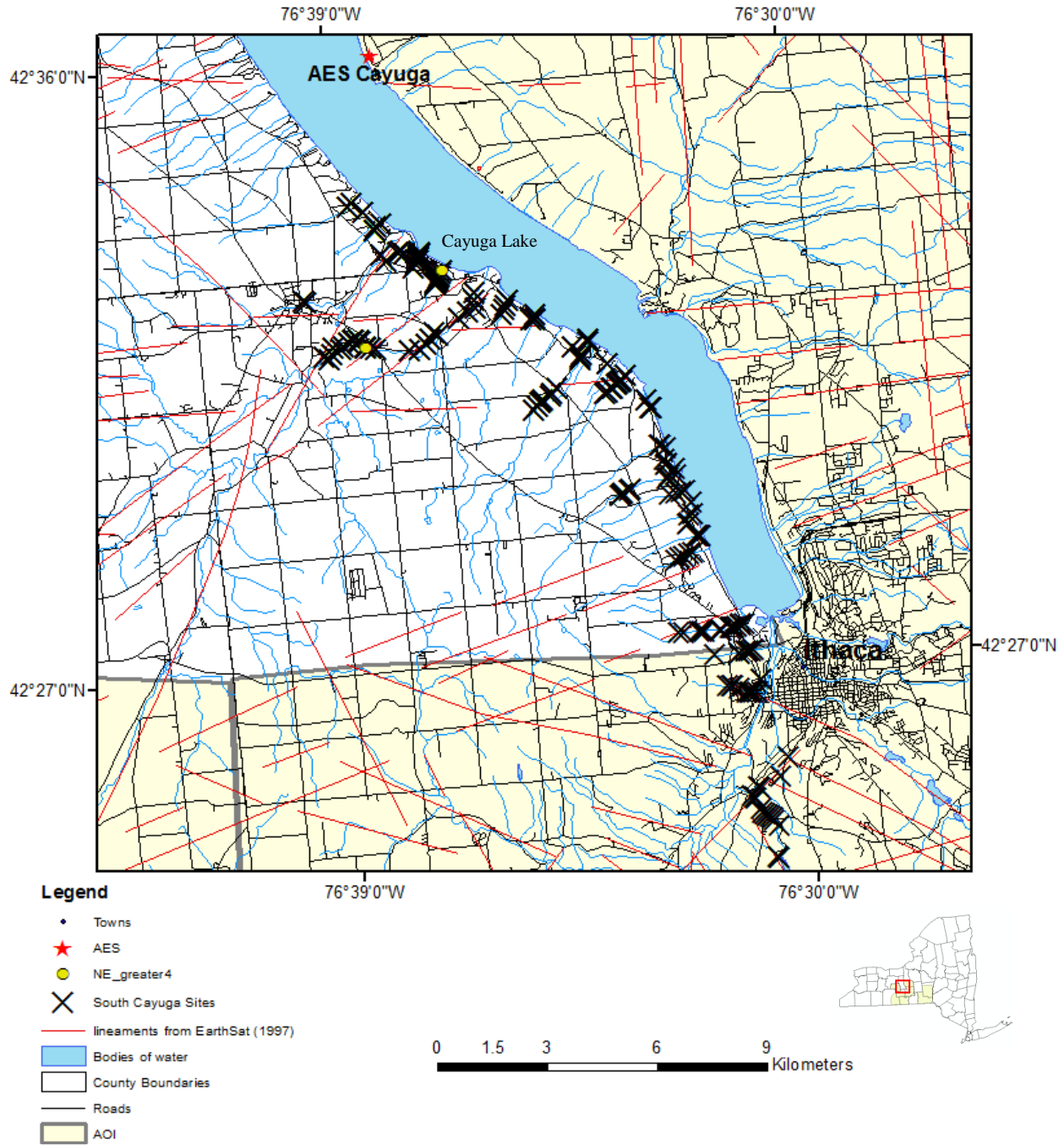


Figure 6.1-86. Lineaments and field sites displaying NE-striking fractures with a fracture frequency of greater than 4 fractures/m. Fracture data from Wehn et al. (2002), Jacobi et al. (2002, 2003).





**Remote Sensing Laboratory**  
 Dept. of Geology, SUNY at Buffalo



**University at Buffalo**  
 The State University of New York

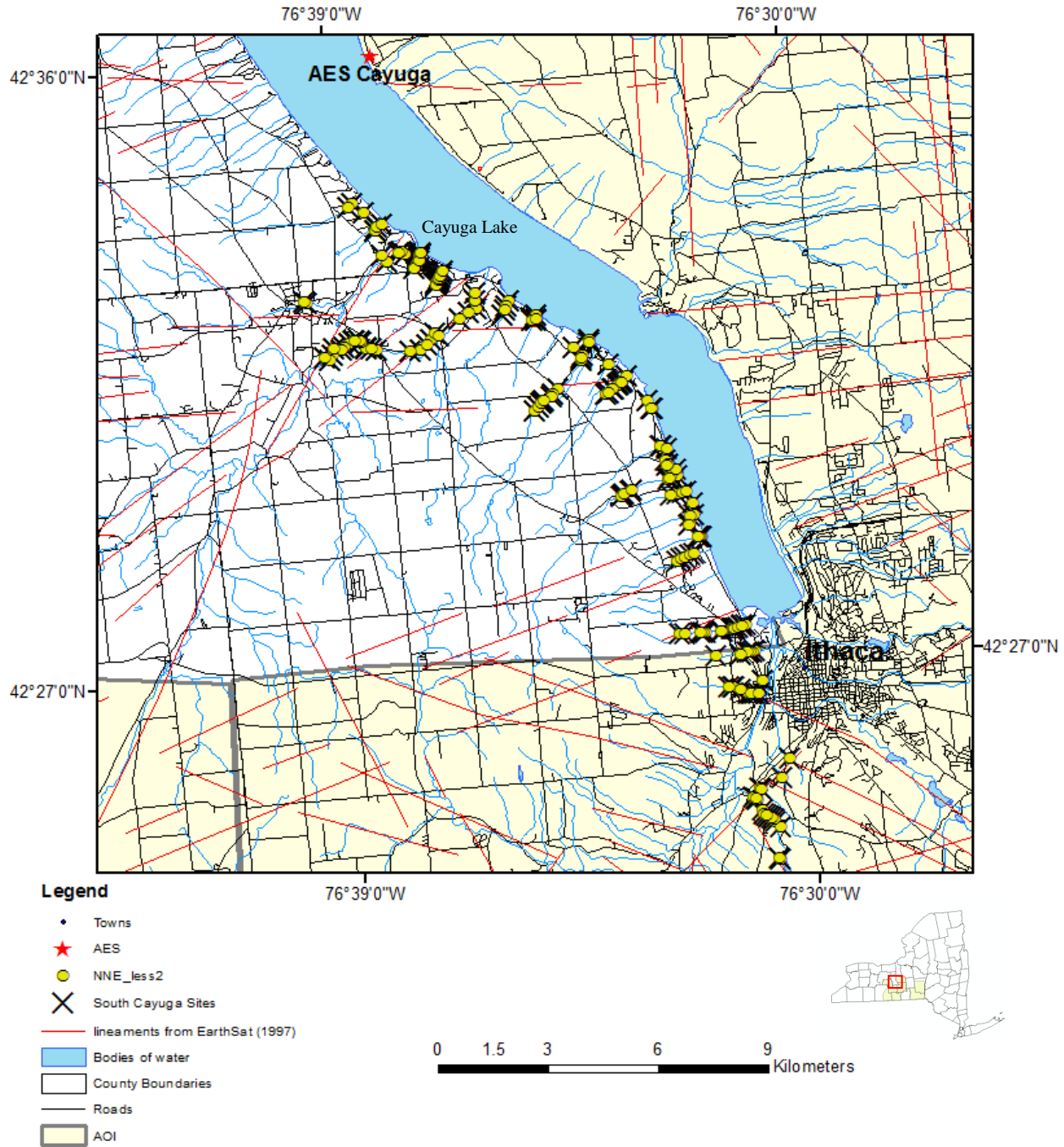


Figure 6.1-87: Lineaments and field sites displaying NNE-striking fractures with a fracture frequency of less than 2 fractures/m. Fracture data from Wehn et al. (2002), Jacobi et al. (2002, 2003).



**Remote Sensing Laboratory**  
 Dept. of Geology, SUNY at Buffalo



**University at Buffalo**  
 The State University of New York

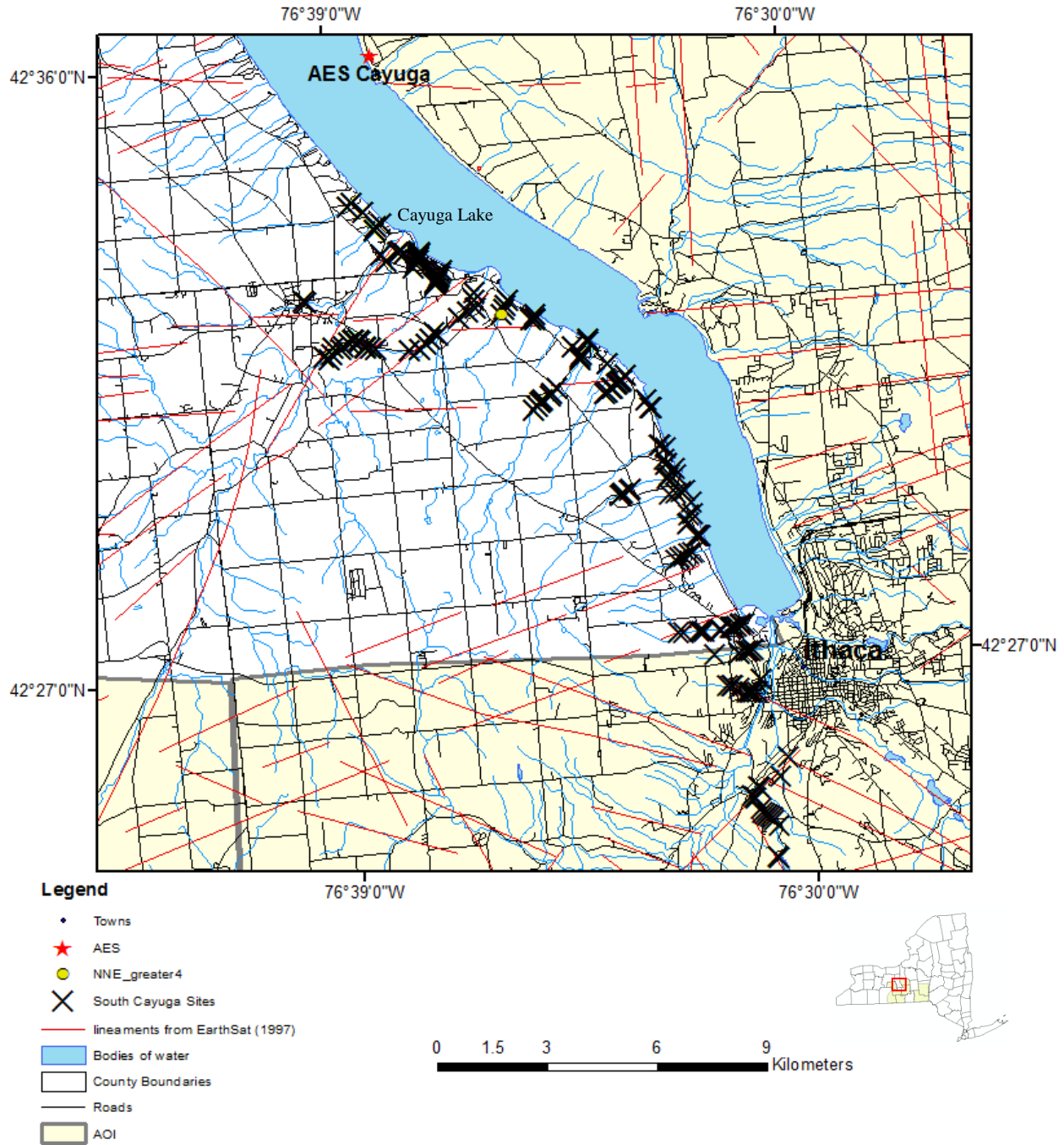


Figure 6.1-88: Lineaments and field sites displaying NNE-striking fractures with a fracture frequency of greater than 4 fractures/m. Fracture data from Wehn et al. (2002), Jacobi et al. (2002, 2003).



**Remote Sensing Laboratory**  
 Dept. of Geology, SUNY at Buffalo



**University at Buffalo**  
 The State University of New York

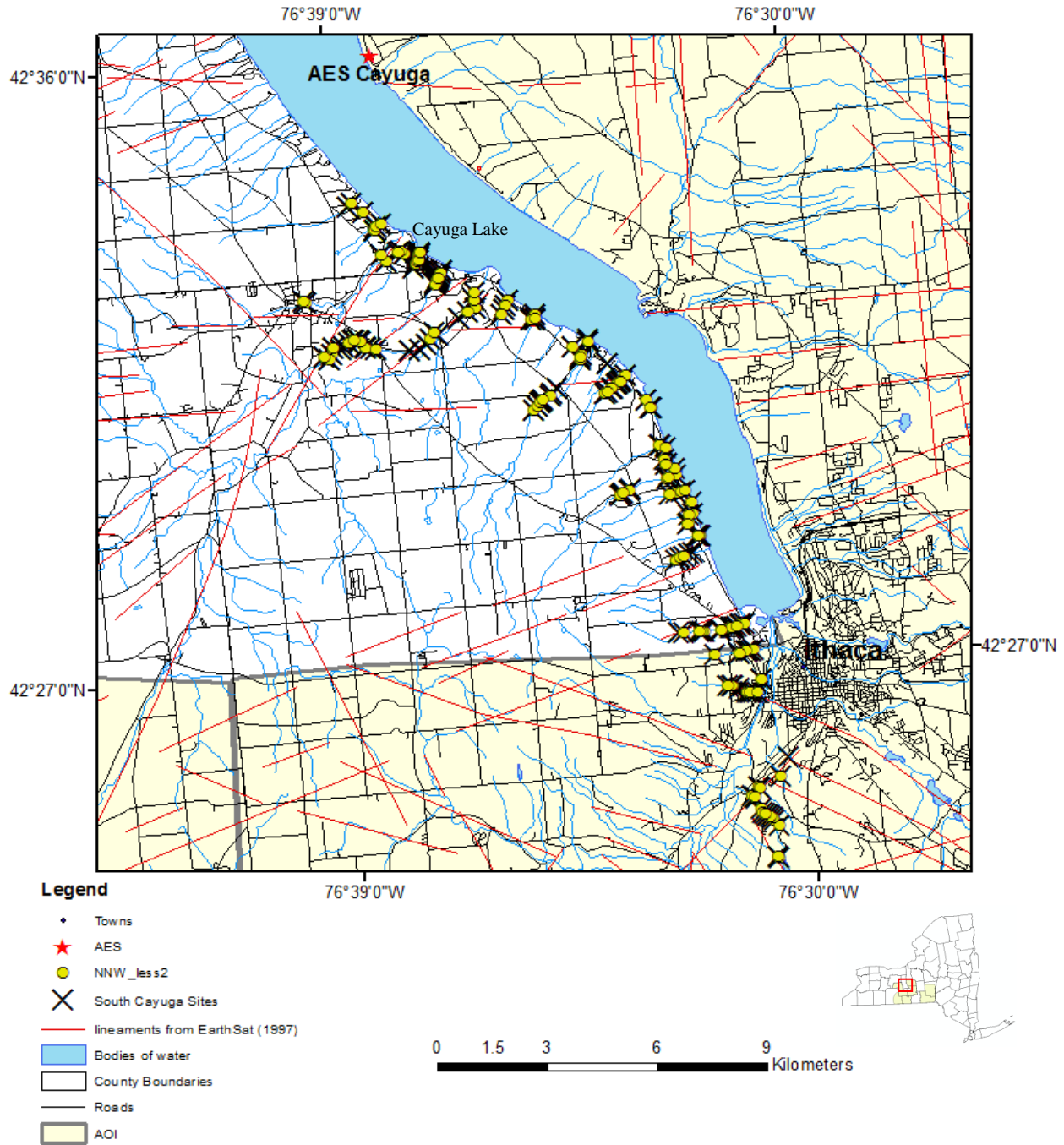


Figure 6.1-89: Lineaments and field sites displaying NNW-striking fractures with a fracture frequency of less than 2 fractures/m. Fracture data from Wehn et al. (2002), Jacobi et al. (2002, 2003).



**Remote Sensing Laboratory**  
 Dept. of Geology, SUNY at Buffalo



**University at Buffalo**  
 The State University of New York

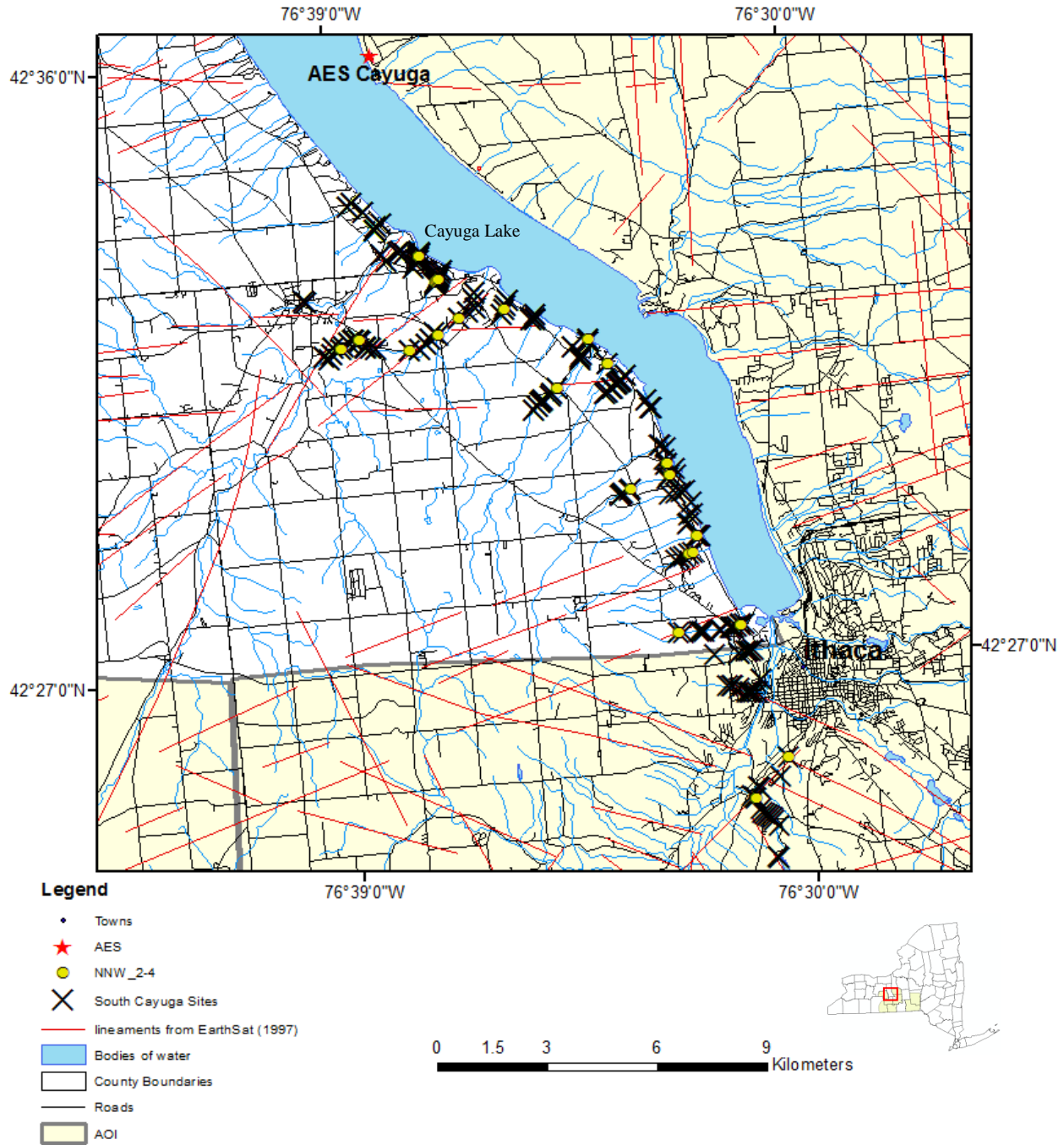


Figure 6.1-90: Lineaments and field sites displaying NNW-striking fractures with a fracture frequency of 2 to 4 fractures/m. Fracture data from Wehn et al. (2002), Jacobi et al. (2002, 2003).





**Remote Sensing Laboratory**  
 Dept. of Geology, SUNY at Buffalo



**University at Buffalo**  
 The State University of New York

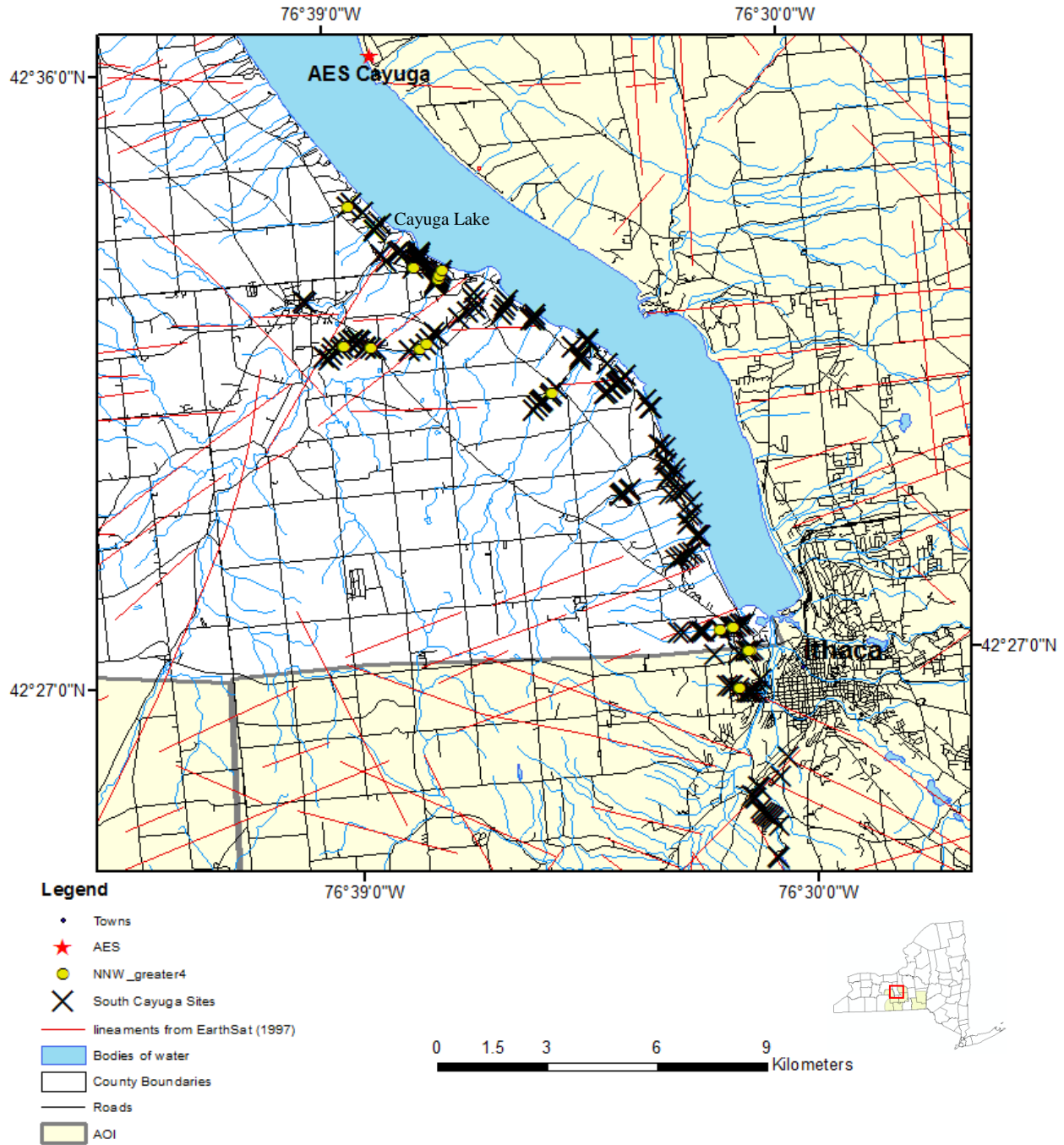


Figure 6.1-91: Lineaments and field sites displaying NNW-striking fractures with a fracture frequency of greater than 4 fractures/m. Fracture data from Wehn et al. (2002), Jacobi et al. (2002, 2003).



**Remote Sensing Laboratory**  
 Dept. of Geology, SUNY at Buffalo



**University at Buffalo**  
 The State University of New York

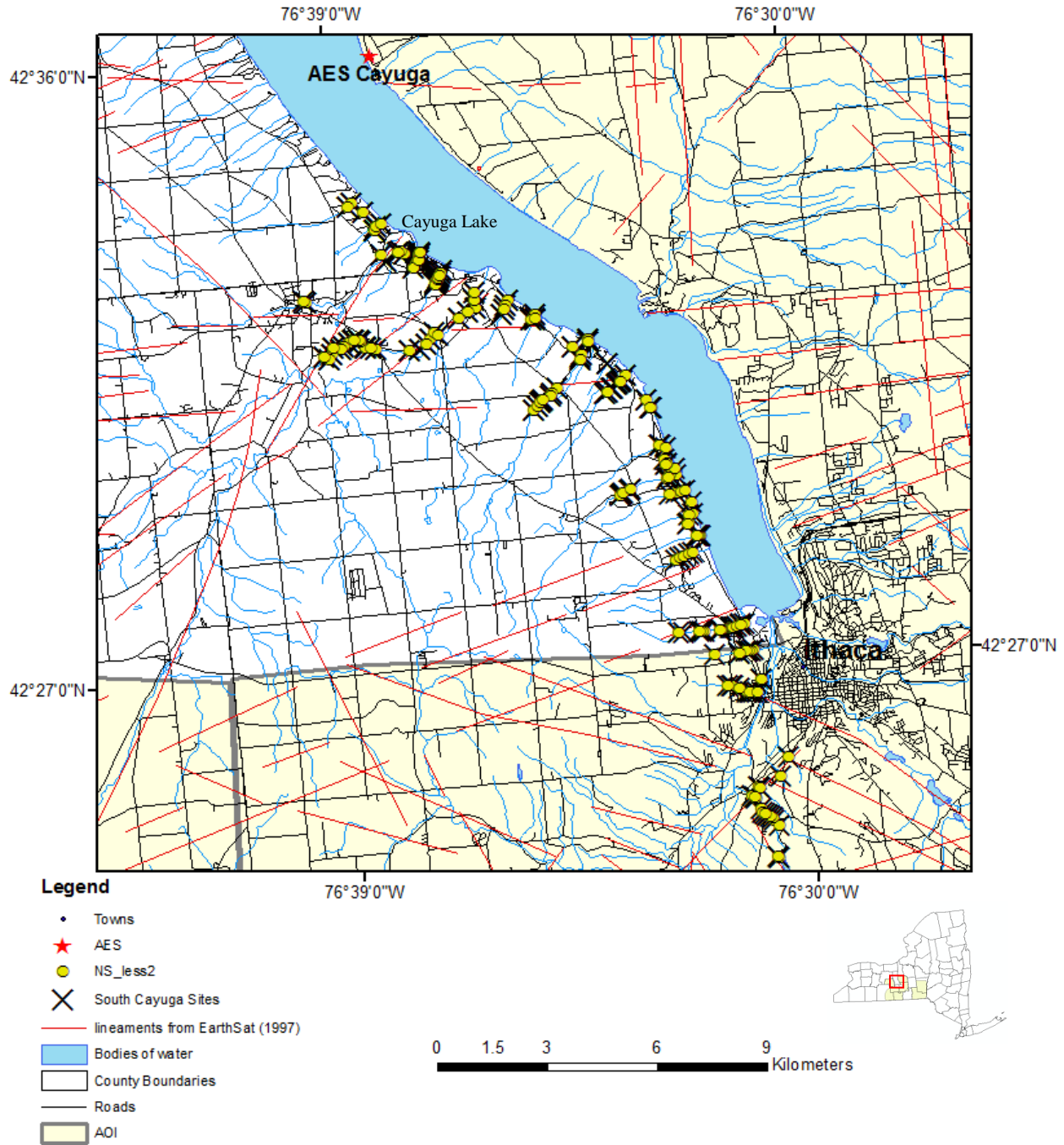


Figure 6.1-92: Lineaments and field sites displaying NS-striking fractures with a fracture frequency of less than 2 fractures/m. Fracture data from Wehn et al. (2002), Jacobi et al. (2002, 2003).



**Remote Sensing Laboratory**  
 Dept. of Geology, SUNY at Buffalo



**University at Buffalo**  
 The State University of New York

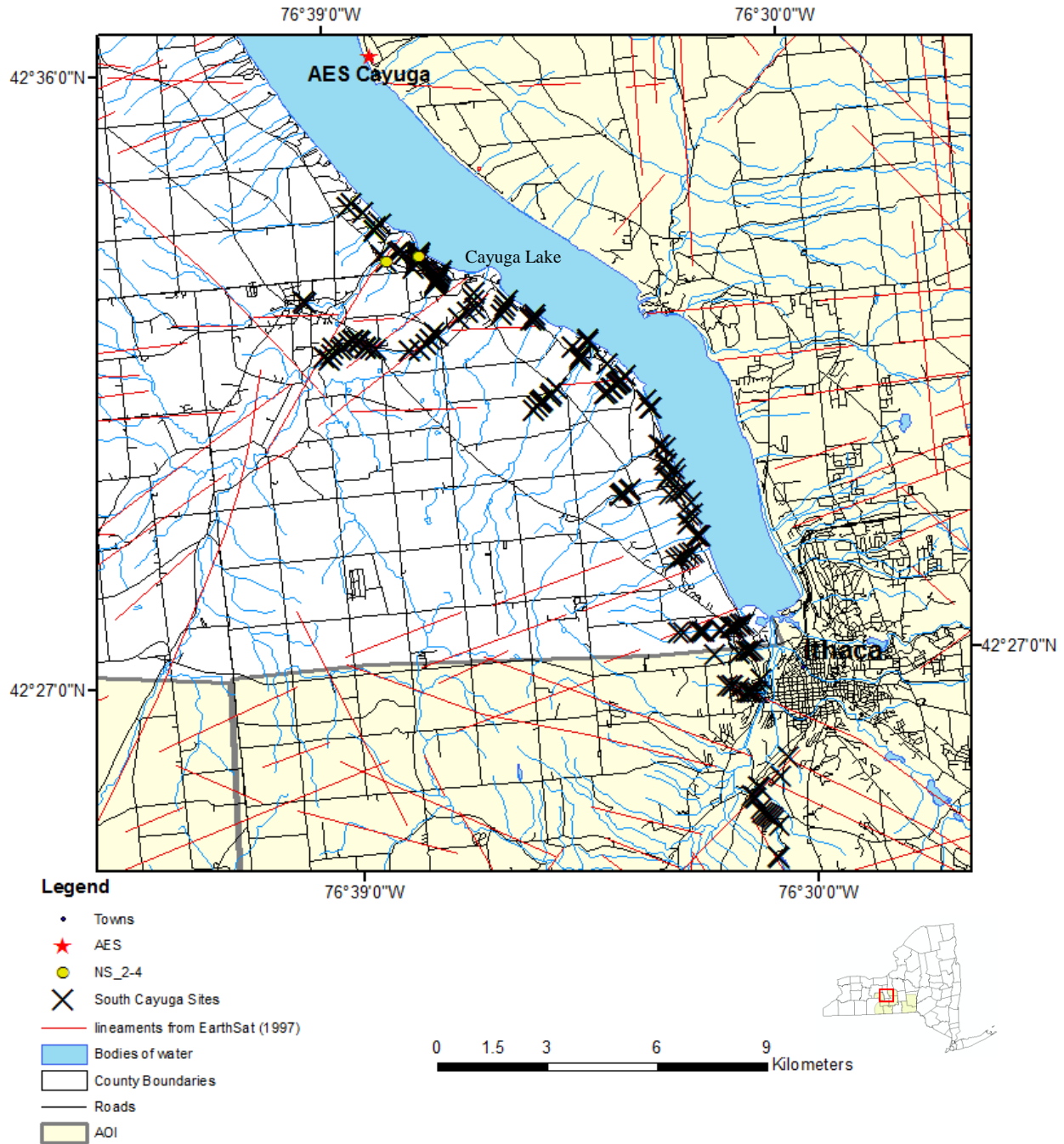


Figure 6.1-93: Lineaments and field sites displaying NS-striking fractures with a fracture frequency of 2 to 4 fractures/m. Fracture data from Wehn et al. (2002), Jacobi et al. (2002, 2003).



**Remote Sensing Laboratory**  
Dept. of Geology, SUNY at Buffalo



**University at Buffalo**  
The State University of New York

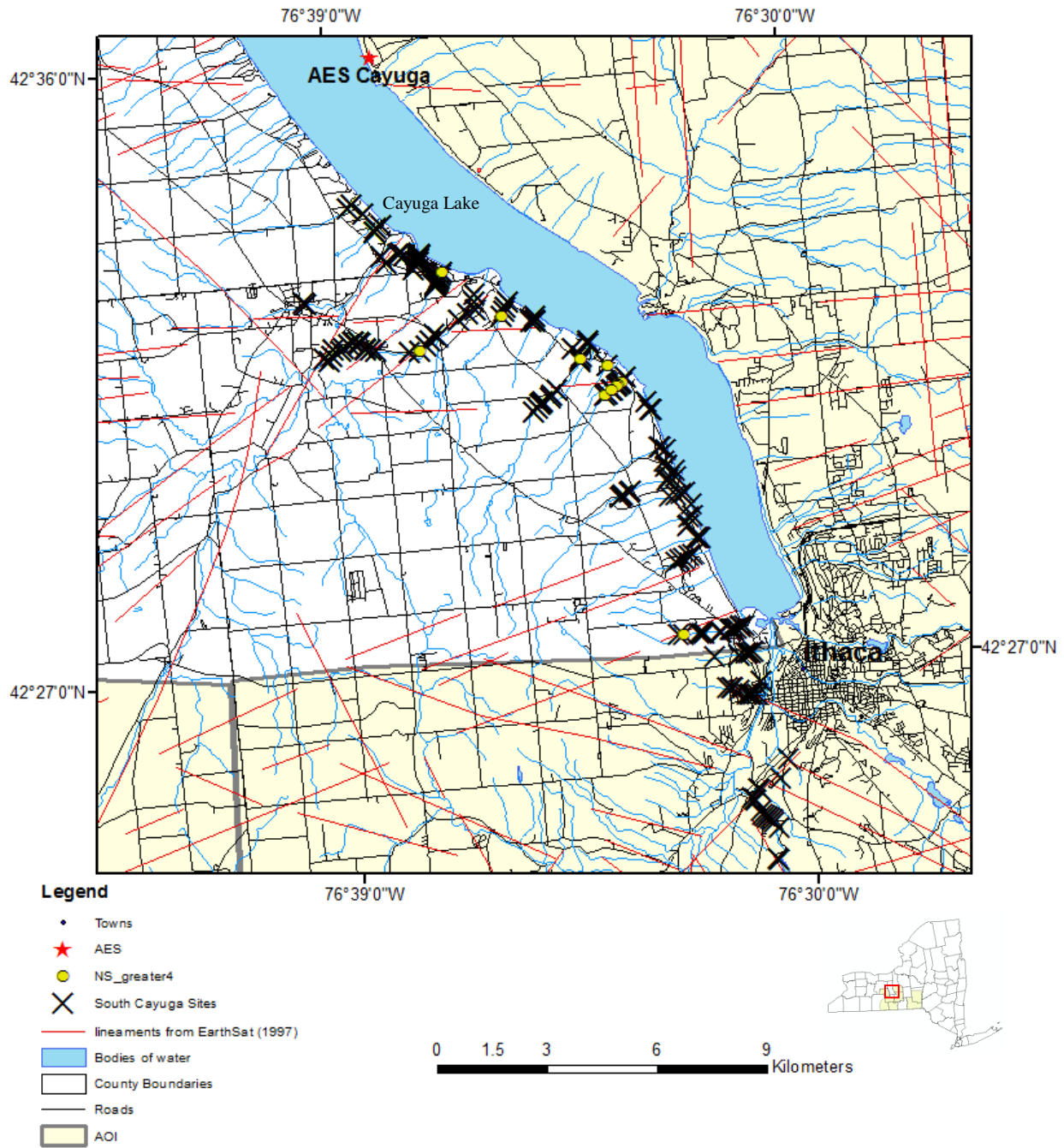


Figure 6.1-94: Lineaments and field sites displaying NS-striking fractures with a fracture frequency of greater than 4 fractures/m. Fracture data from Wehn et al. (2002), Jacobi et al. (2002, 2003).





**Remote Sensing Laboratory**  
 Dept. of Geology, SUNY at Buffalo



**University at Buffalo**  
 The State University of New York

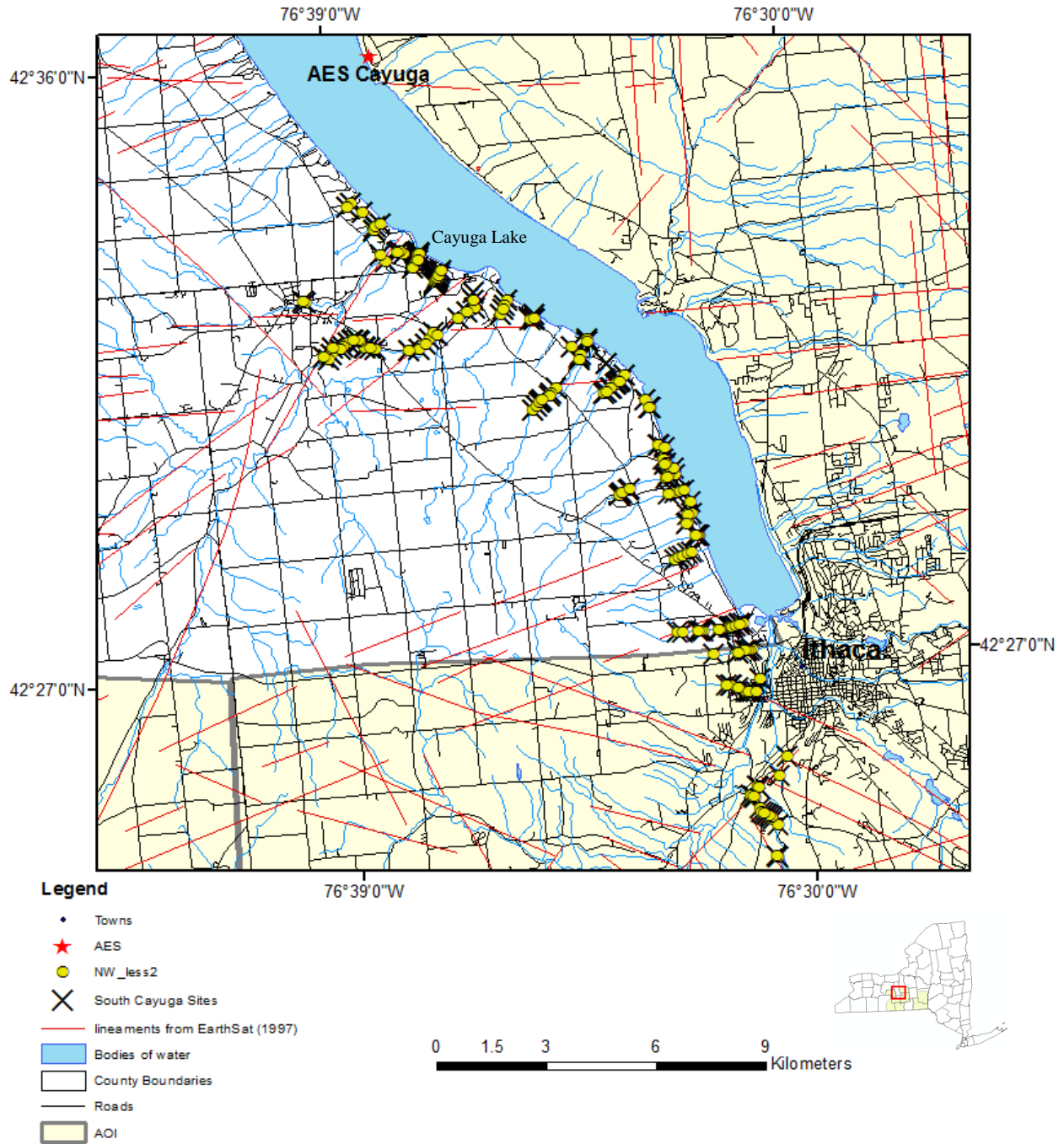


Figure 6.1-95: Lineaments and field sites displaying NW-striking fractures with a fracture frequency of less than 2 fractures/m. Fracture data from Wehn et al. (2002), Jacobi et al. (2002, 2003).



**Remote Sensing Laboratory**  
Dept. of Geology, SUNY at Buffalo



**University at Buffalo**  
The State University of New York

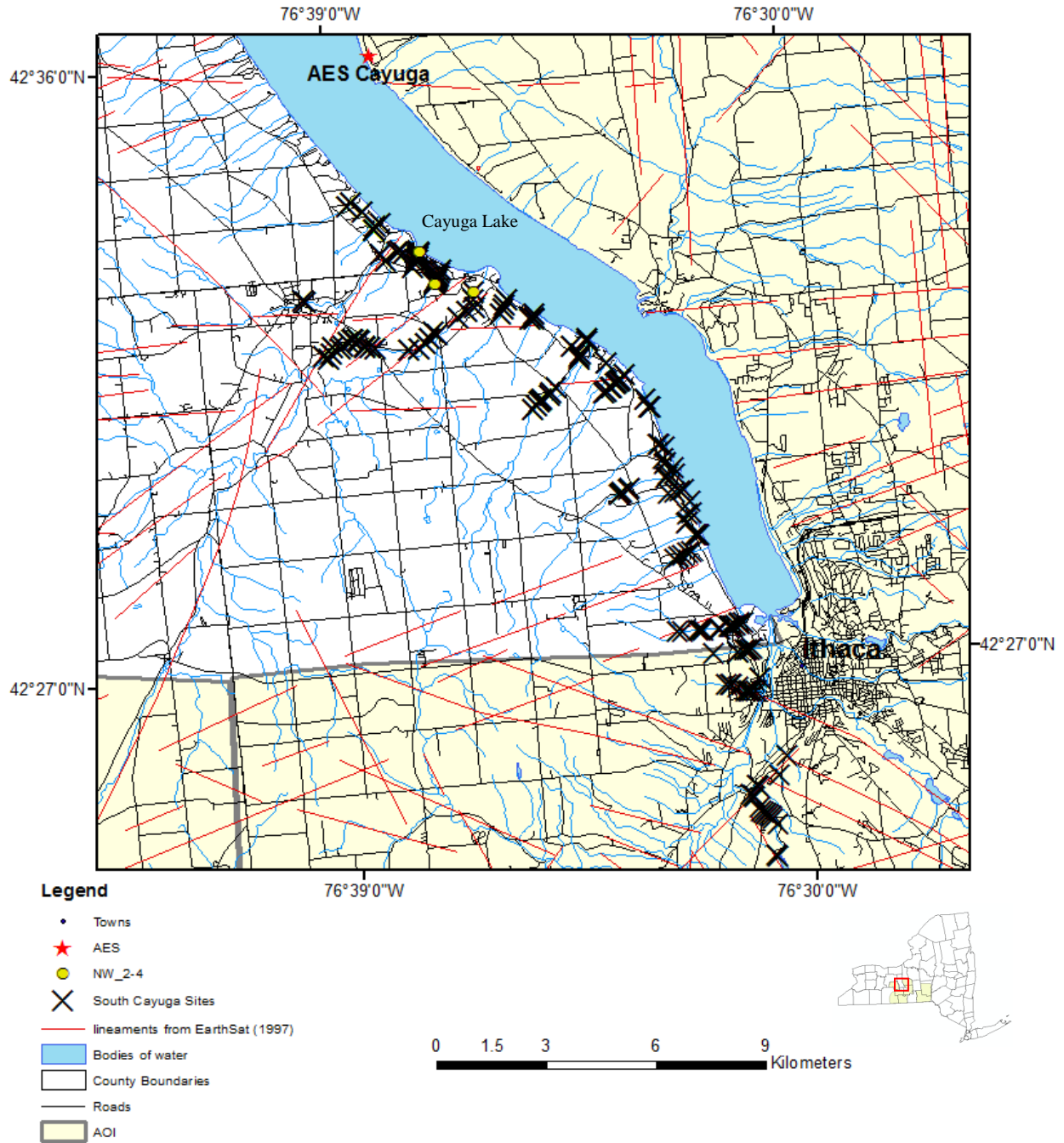


Figure 6.1-96: Lineaments and field sites displaying NW-striking fractures with a fracture frequency of 2 to 4 fractures/m. Fracture data from Wehn et al. (2002), Jacobi et al. (2002, 2003).



**Remote Sensing Laboratory**  
 Dept. of Geology, SUNY at Buffalo



**University at Buffalo**  
 The State University of New York

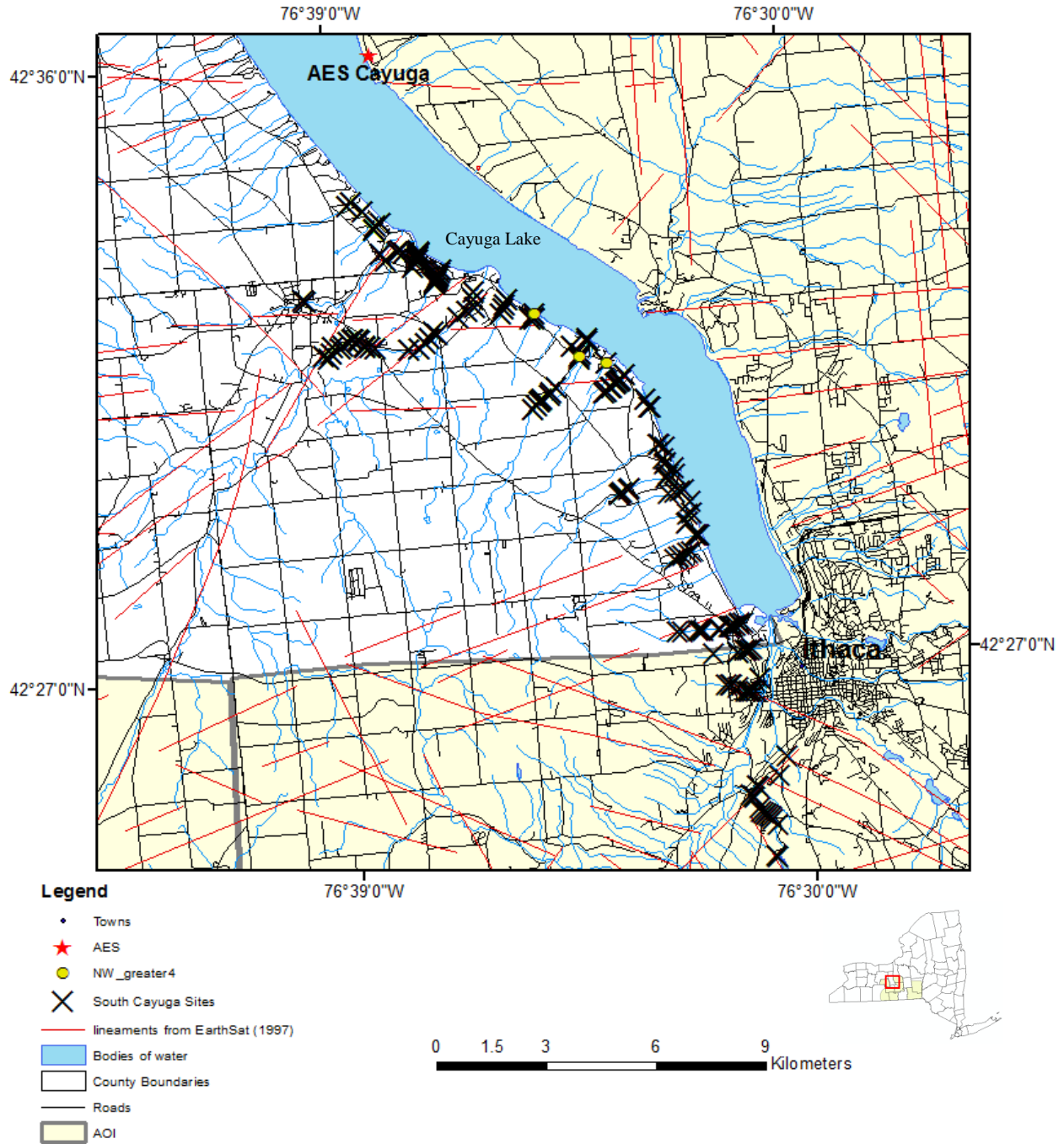


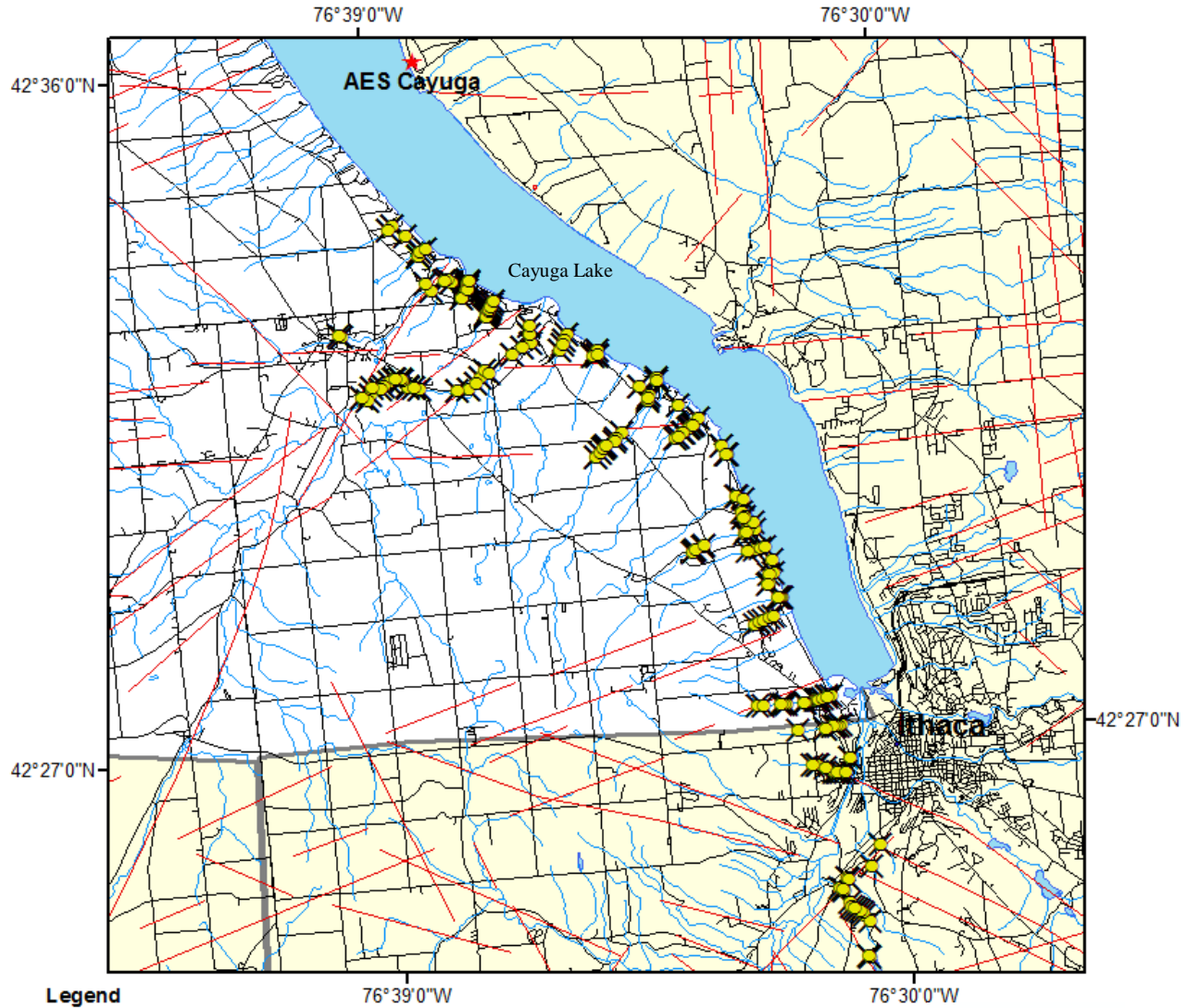
Figure 6.1-97: Lineaments and field sites displaying NW-striking fractures with a fracture frequency of greater than 4 fractures/m. Fracture data from Wehn et al. (2002), Jacobi et al. (2002, 2003).



**Remote Sensing Laboratory**  
Dept. of Geology, SUNY at Buffalo



**University at Buffalo**  
The State University of New York



- Legend**
- Towns
  - ★ AES
  - WNW\_less2
  - ✕ South Cayuga Sites
  - lineaments from EarthSat (1997)
  - Bodies of water
  - County Boundaries
  - Roads
  - AOI

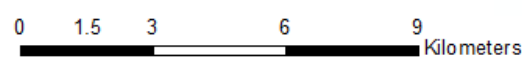


Figure 6.1-98: Lineaments and field sites displaying WNW-striking fractures with a fracture frequency of less than 2 fractures/m. Fracture data from Wehn et al. (2002), Jacobi et al. (2002, 2003).





**Remote Sensing Laboratory**  
 Dept. of Geology, SUNY at Buffalo



**University at Buffalo**  
 The State University of New York

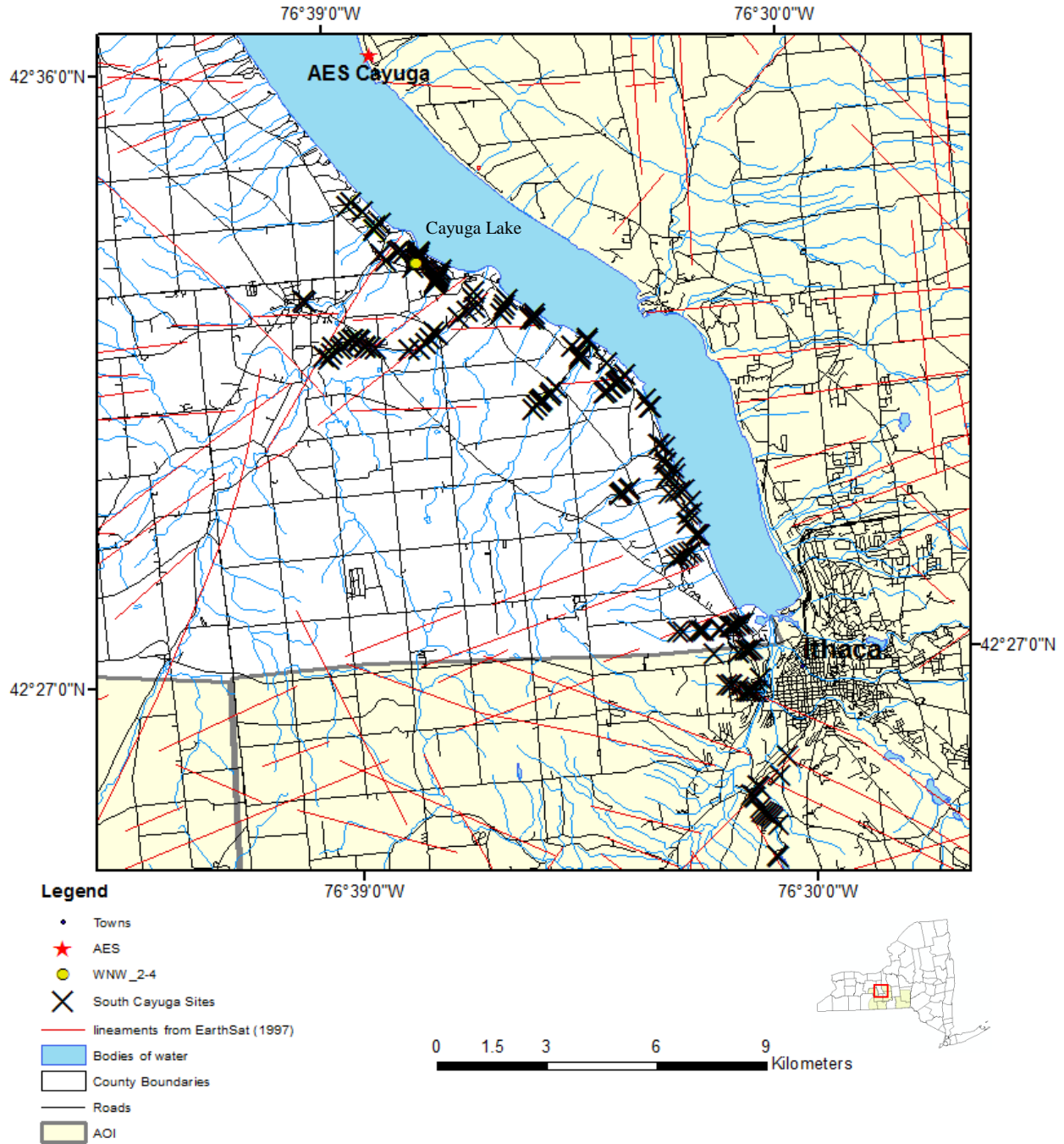


Figure 6.1-99: Lineaments and field sites displaying NW-striking fractures with a fracture frequency of 2 to 4 fractures/m. Fracture data from Wehn et al. (2002), Jacobi et al. (2002, 2003).



**Remote Sensing Laboratory**  
 Dept. of Geology, SUNY at Buffalo



**University at Buffalo**  
 The State University of New York

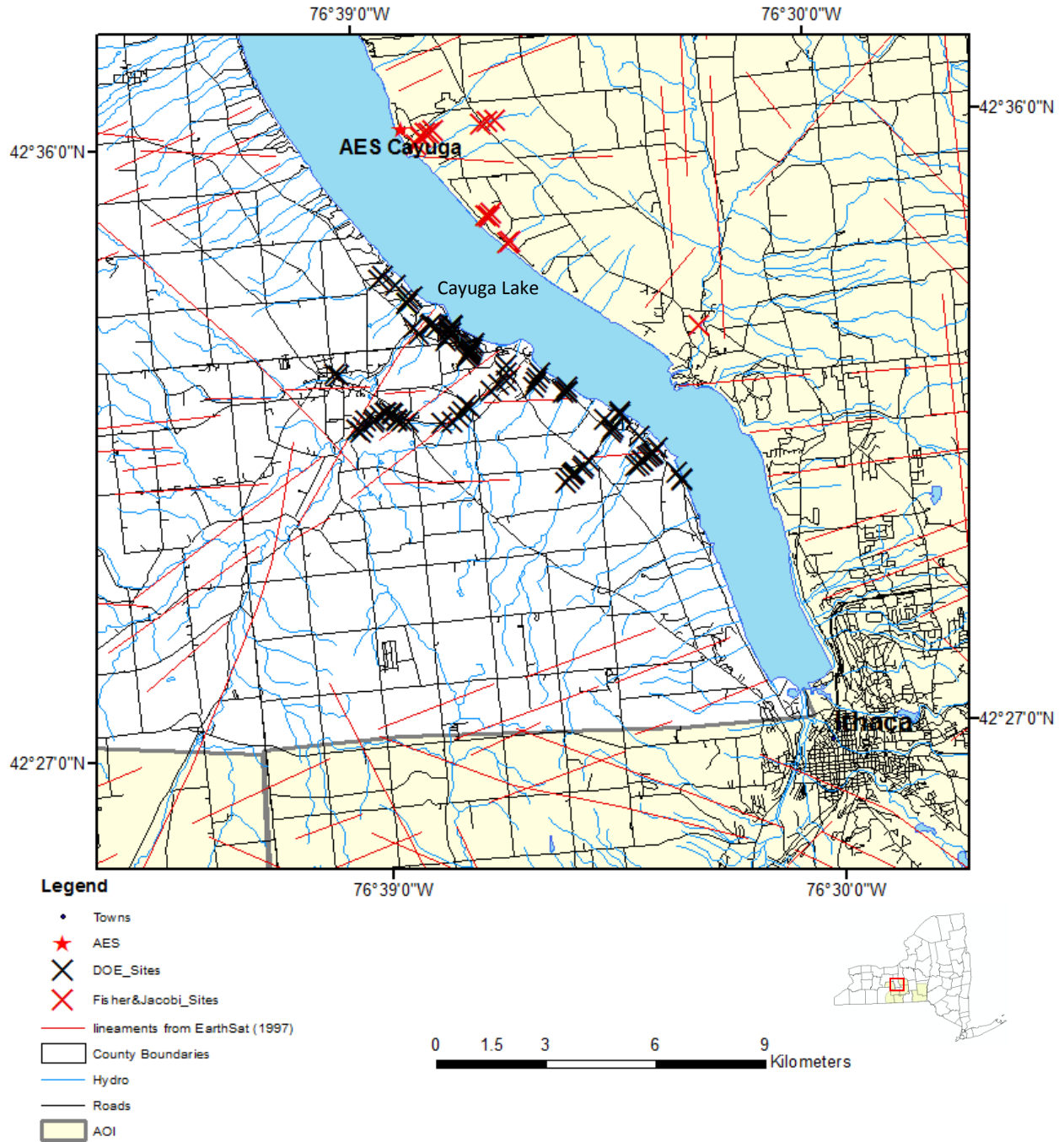


Figure 6.1-100: Cayuga Field Sites (see Figures 108-113 for enlarged view)



Remote Sensing Laboratory  
Dept. of Geology, SUNY at Buffalo



University at Buffalo  
The State University of New York

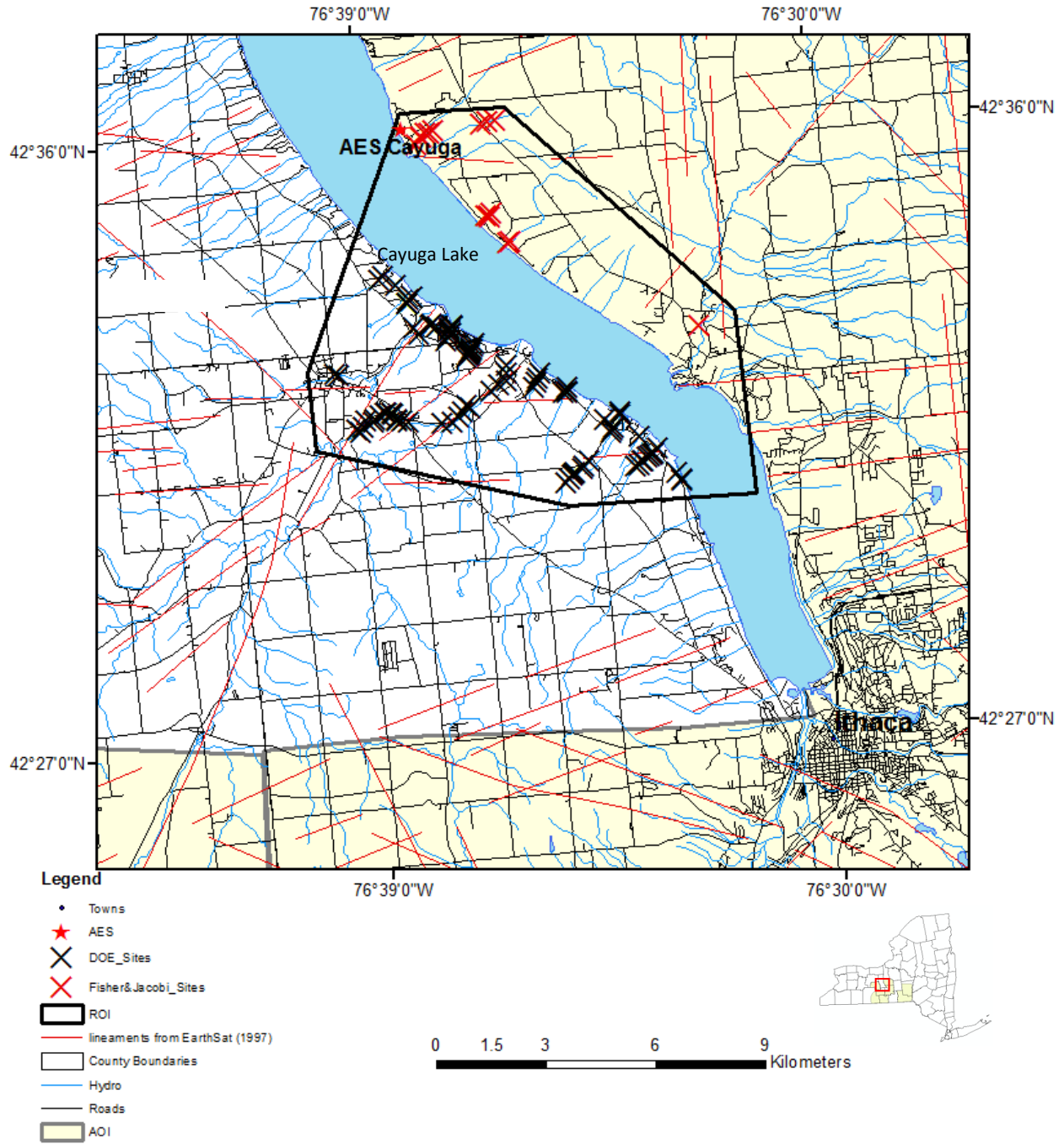


Figure 6.1-101: Cayuga field sites from the 2007 DOE report (black) and summer 2009 field work (red) inside the Region of Interest (ROI) defined for statistical analyses.



**Remote Sensing Laboratory**  
 Dept. of Geology, SUNY at Buffalo



**University at Buffalo**  
 The State University of New York

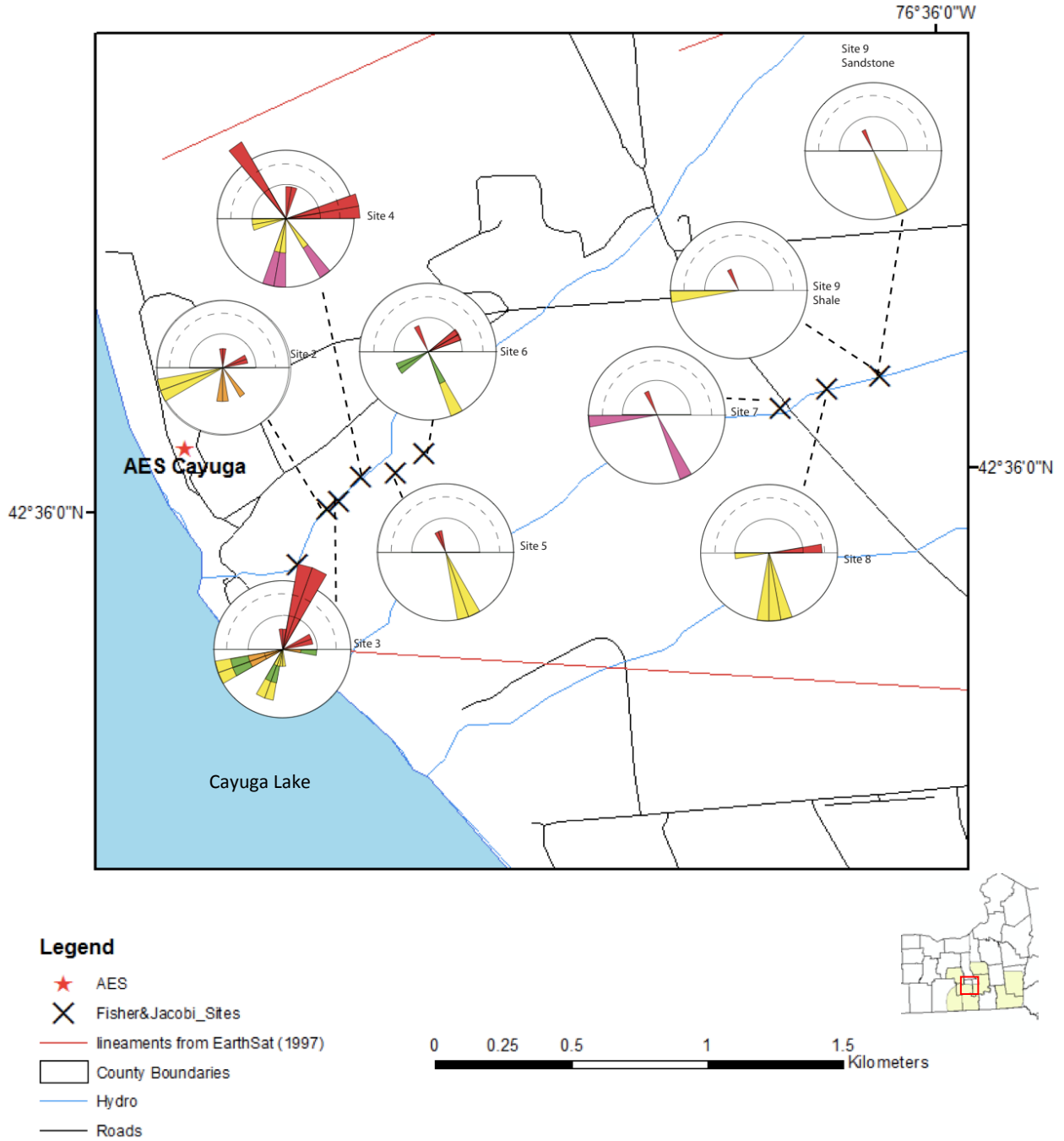


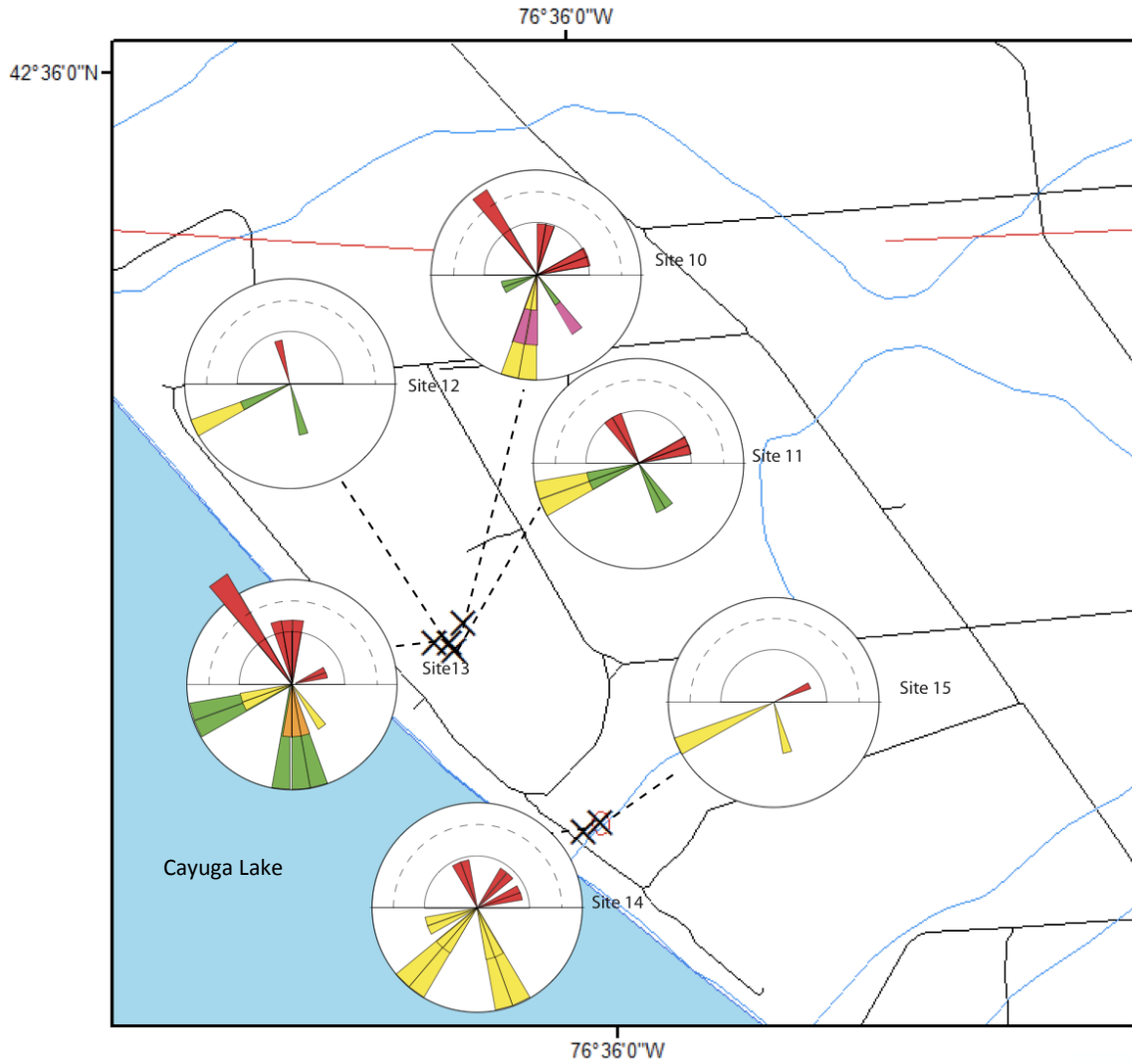
Figure 6.1-102: Northern Cayuga field sites with modified rose diagrams (see Jacobi, 2007a for explanation of modified rose diagrams)



Remote Sensing Laboratory,  
Dept. of Geology, SUNY at Buffalo



University at Buffalo  
The State University of New York



**Legend**

- ★ AES
- ✕ Fisher&Jacobi\_Sites
- lineaments from EarthSat (1997)
- County Boundaries
- Hydro
- Roads

0 0.25 0.5 1 1.5 Kilometers

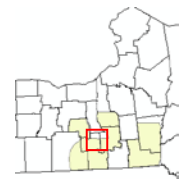


Figure 6.1-103: Southern Cayuga field sites with modified rose diagrams (see Jacobi, 2007a, for explanation of modified rose diagrams)



**Remote Sensing Laboratory**  
*Dept. of Geology, SUNY at Buffalo*



**University at Buffalo**  
*The State University of New York*

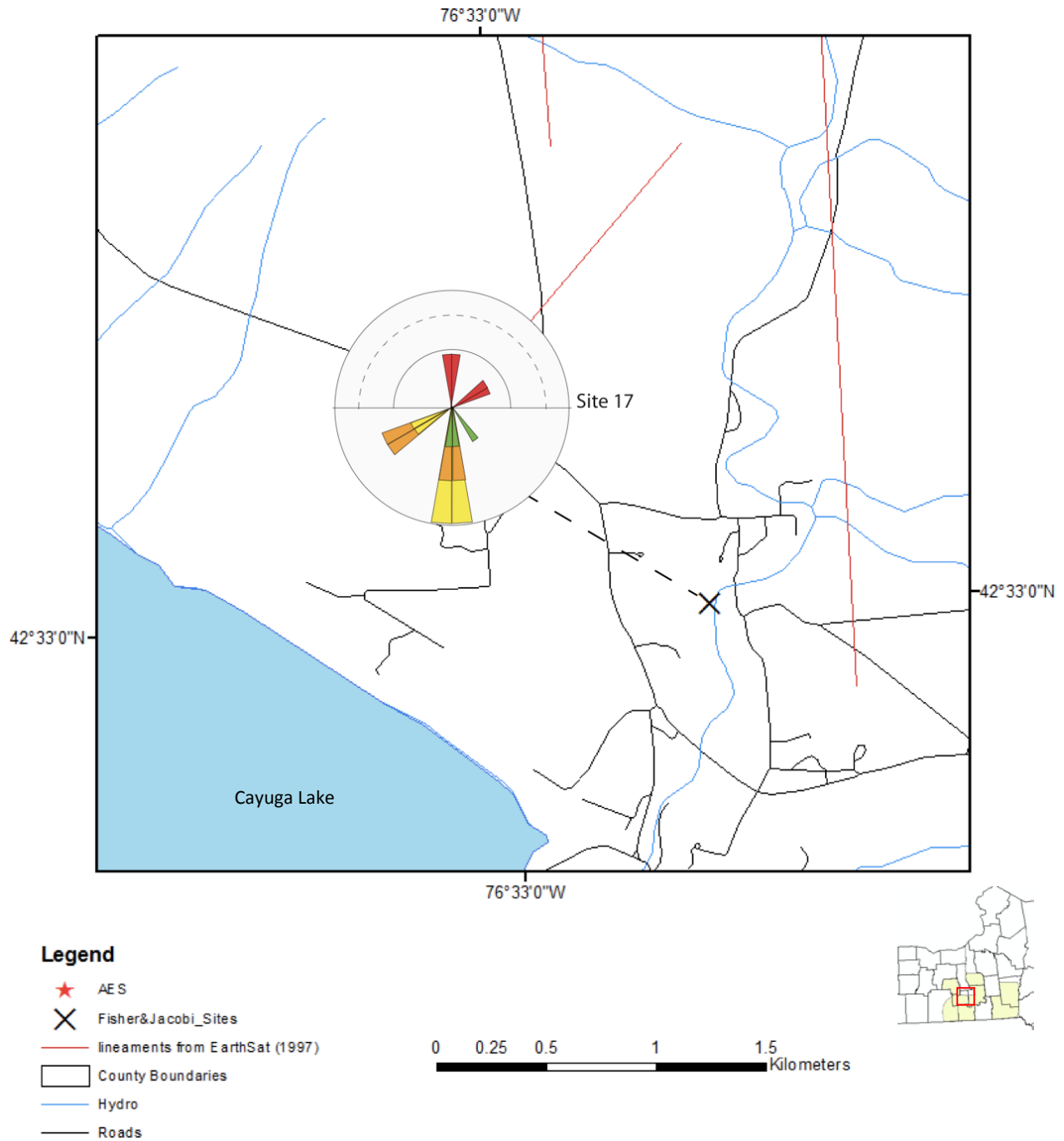


Figure 6.1-104: Southernmost Cayuga field site with modified rose diagram (see Jacobi, 2007a, for explanation of rose diagrams)





**Remote Sensing Laboratory**  
 Dept. of Geology, SUNY at Buffalo



**University at Buffalo**  
 The State University of New York

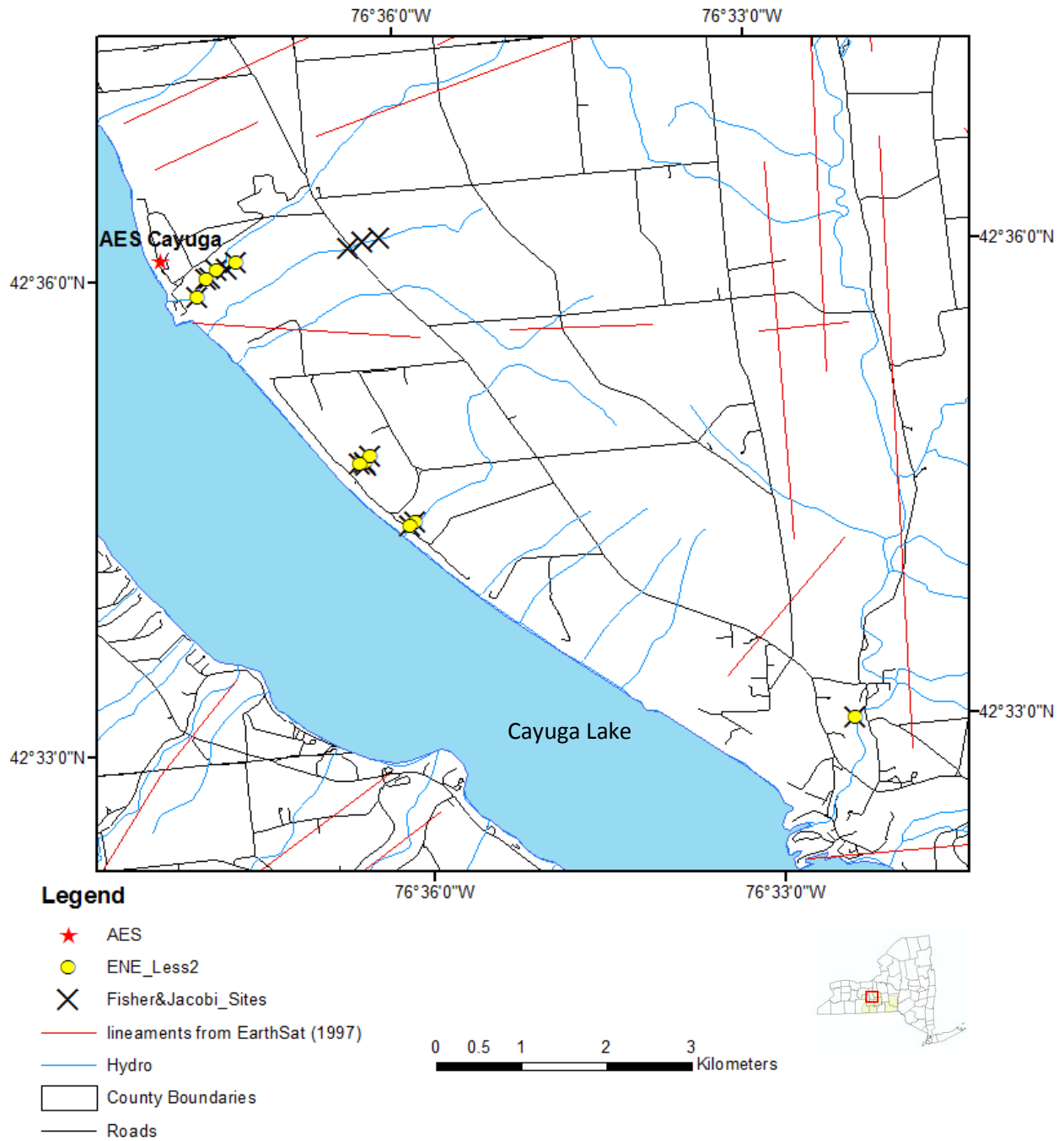


Figure 6.1-105: Cayuga field sites exhibiting ENE trending fractures with a frequency of less than 2 fractures/m.



**Remote Sensing Laboratory**  
 Dept. of Geology, SUNY at Buffalo



**University at Buffalo**  
 The State University of New York

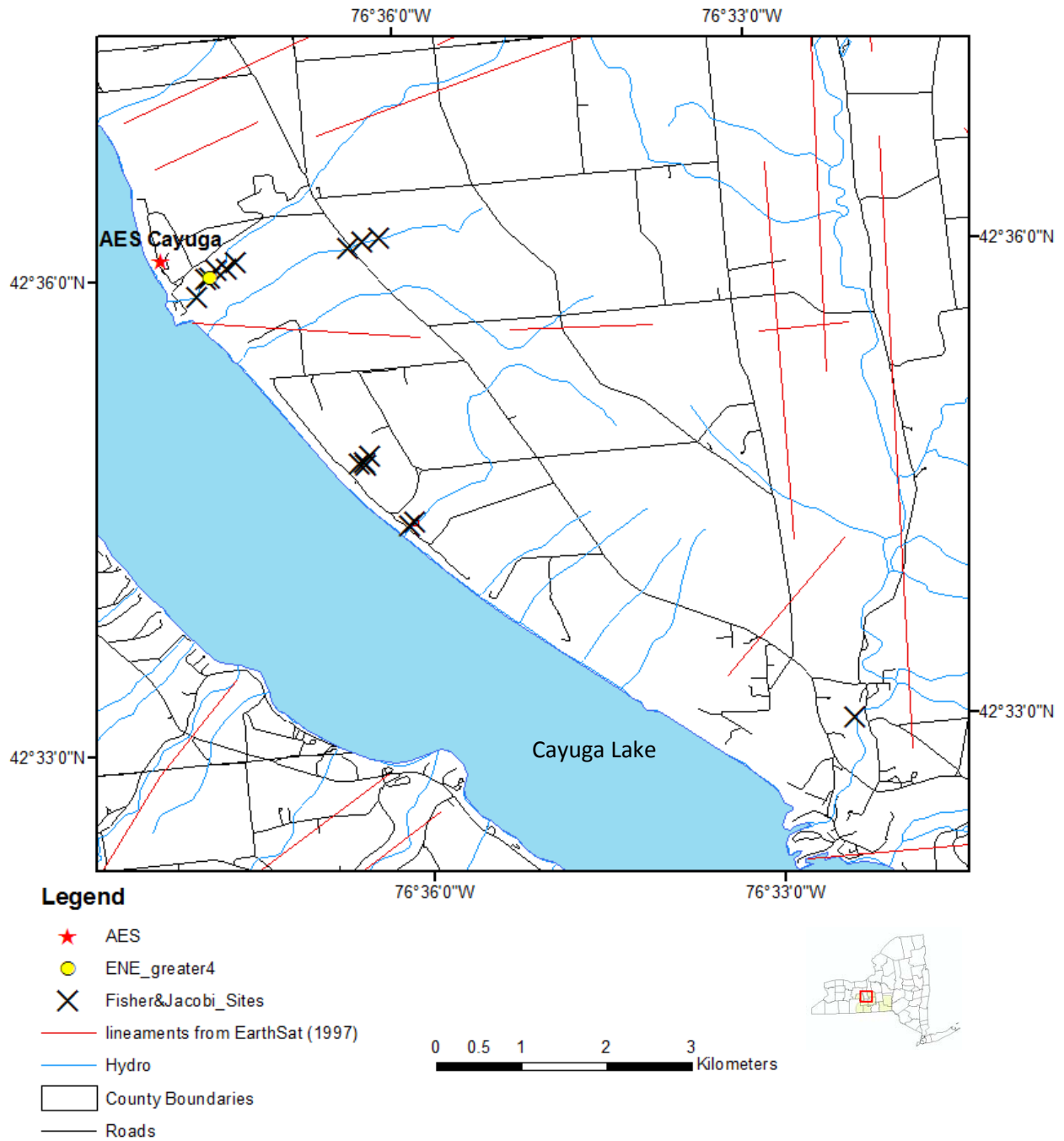


Figure 6.1-106: Cayuga field sites exhibiting ENE trending fractures with a frequency greater than 4 fractures/m.





**Remote Sensing Laboratory**  
 Dept. of Geology, SUNY at Buffalo



**University at Buffalo**  
 The State University of New York

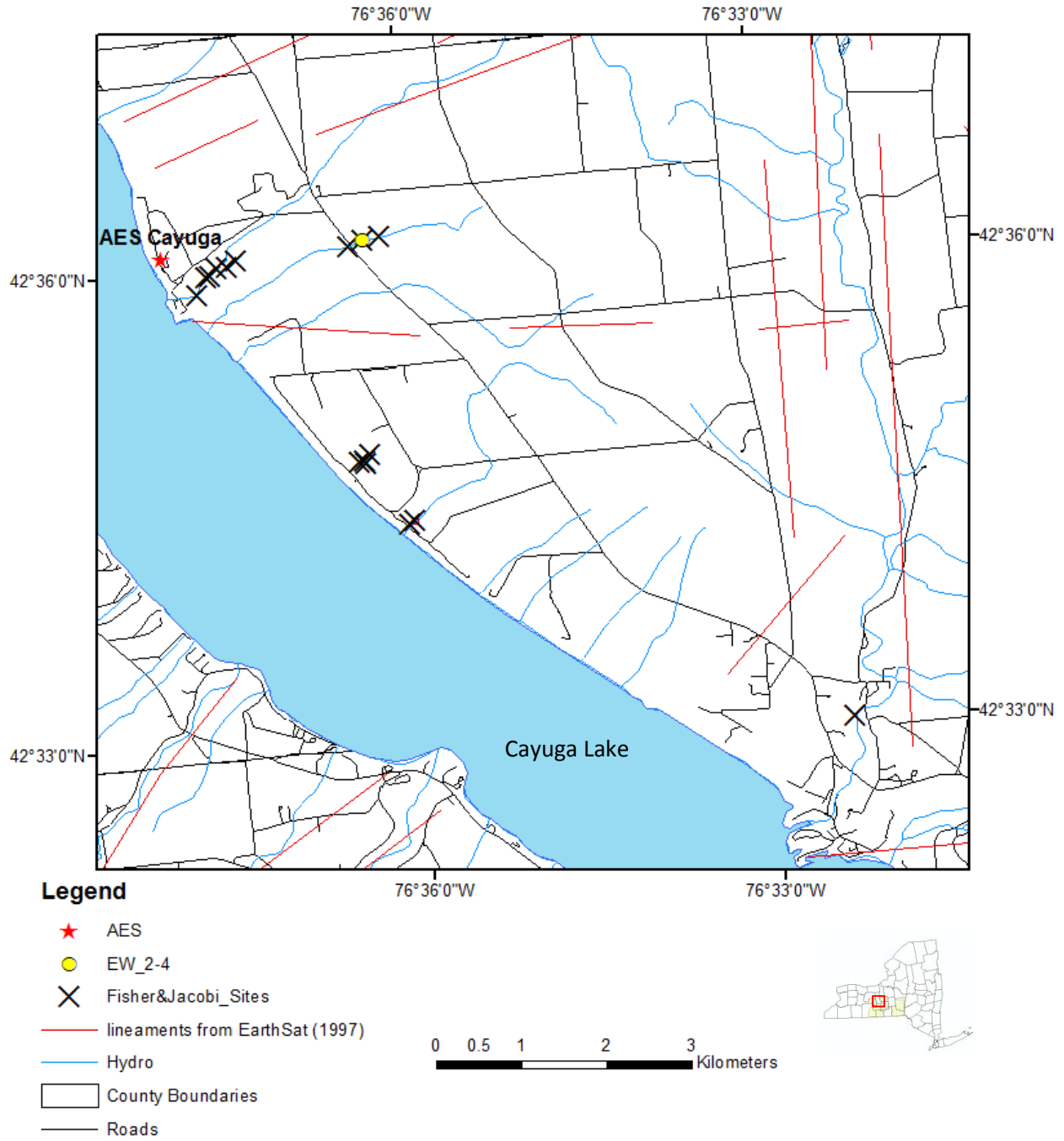


Figure 6.1-107: Cayuga field sites exhibiting EW-striking fractures with a frequency of 2 to 4 fractures/m.



**Remote Sensing Laboratory**  
 Dept. of Geology, SUNY at Buffalo



**University at Buffalo**  
 The State University of New York

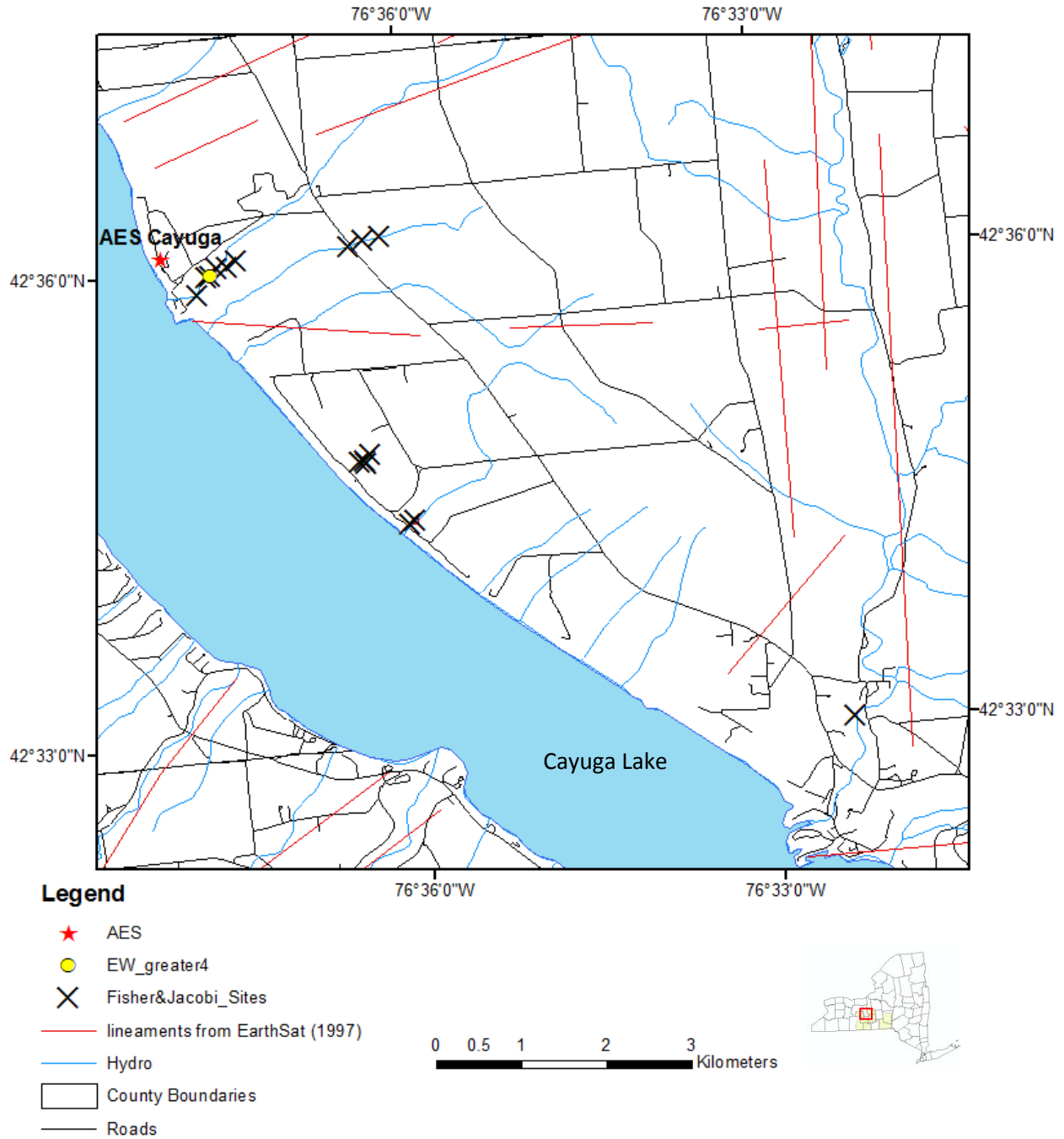


Figure 6.1-108: Cayuga field sites exhibiting EW-striking fractures with a frequency of greater than 4 fractures/m.



**Remote Sensing Laboratory**  
 Dept. of Geology, SUNY at Buffalo



**University at Buffalo**  
 The State University of New York

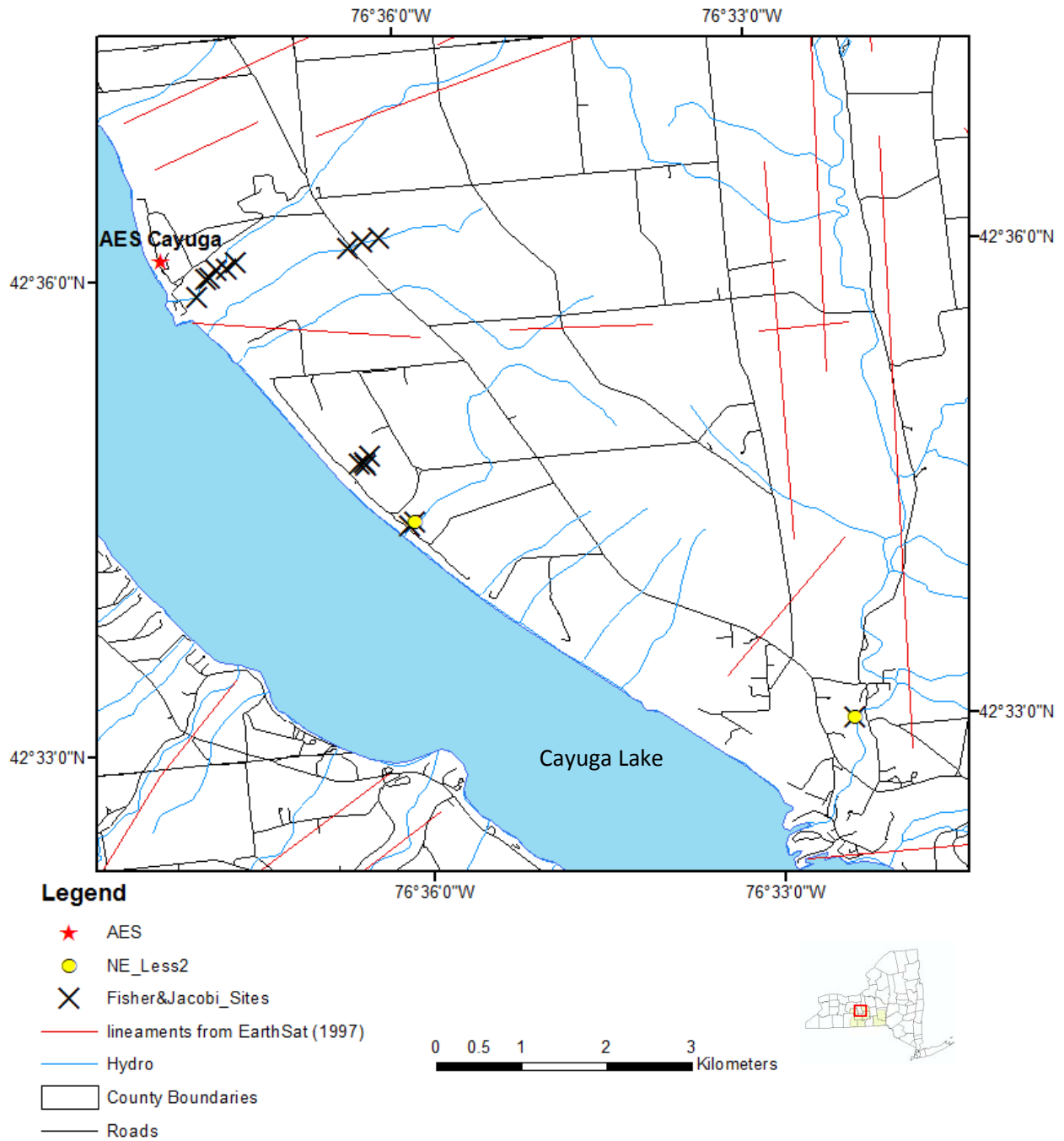


Figure 6.1-109: Cayuga field sites exhibiting NE-striking fractures with a frequency of less than 2 fractures/m.



**Remote Sensing Laboratory**  
 Dept. of Geology, SUNY at Buffalo



**University at Buffalo**  
 The State University of New York

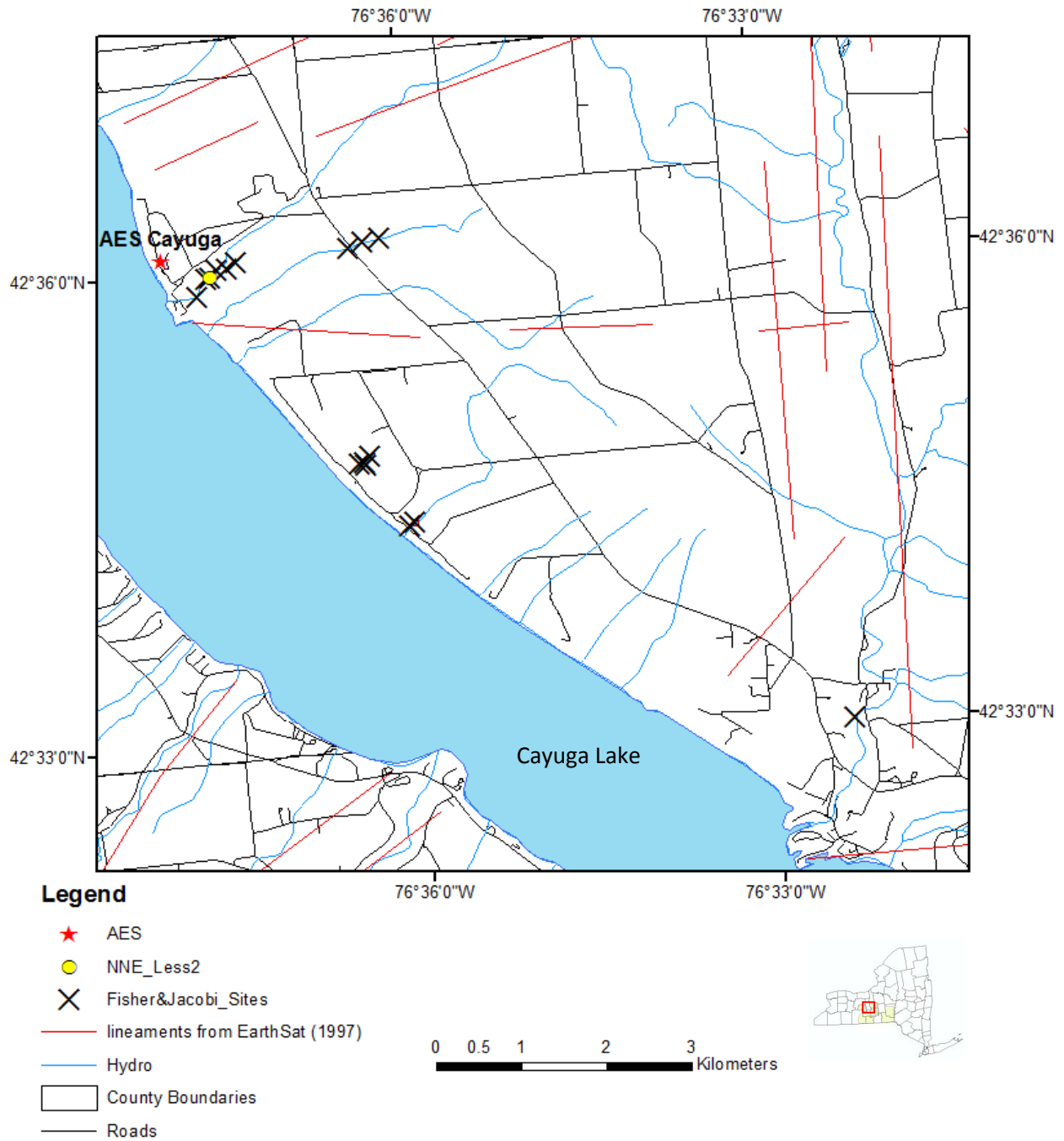


Figure 6.1-110: Chenango field sites exhibiting NNE-striking fractures with a frequency of less than 2 fractures/m.



**Remote Sensing Laboratory**  
 Dept. of Geology, SUNY at Buffalo



**University at Buffalo**  
 The State University of New York

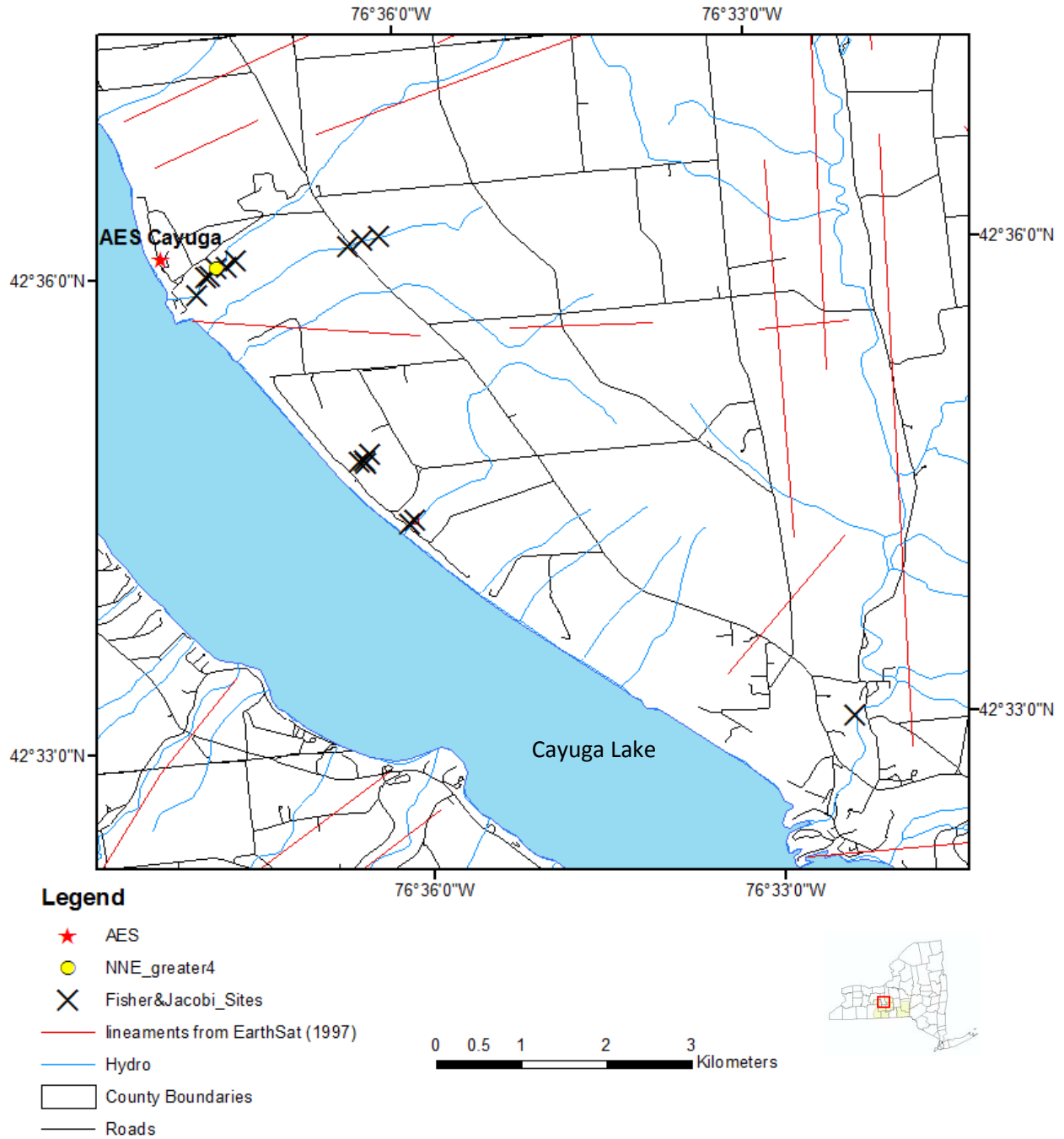


Figure 6.1-111: Chenango field sites exhibiting NNE-striking fractures with a frequency of greater than 4 fractures/m.



**Remote Sensing Laboratory**  
 Dept. of Geology, SUNY at Buffalo



**University at Buffalo**  
 The State University of New York

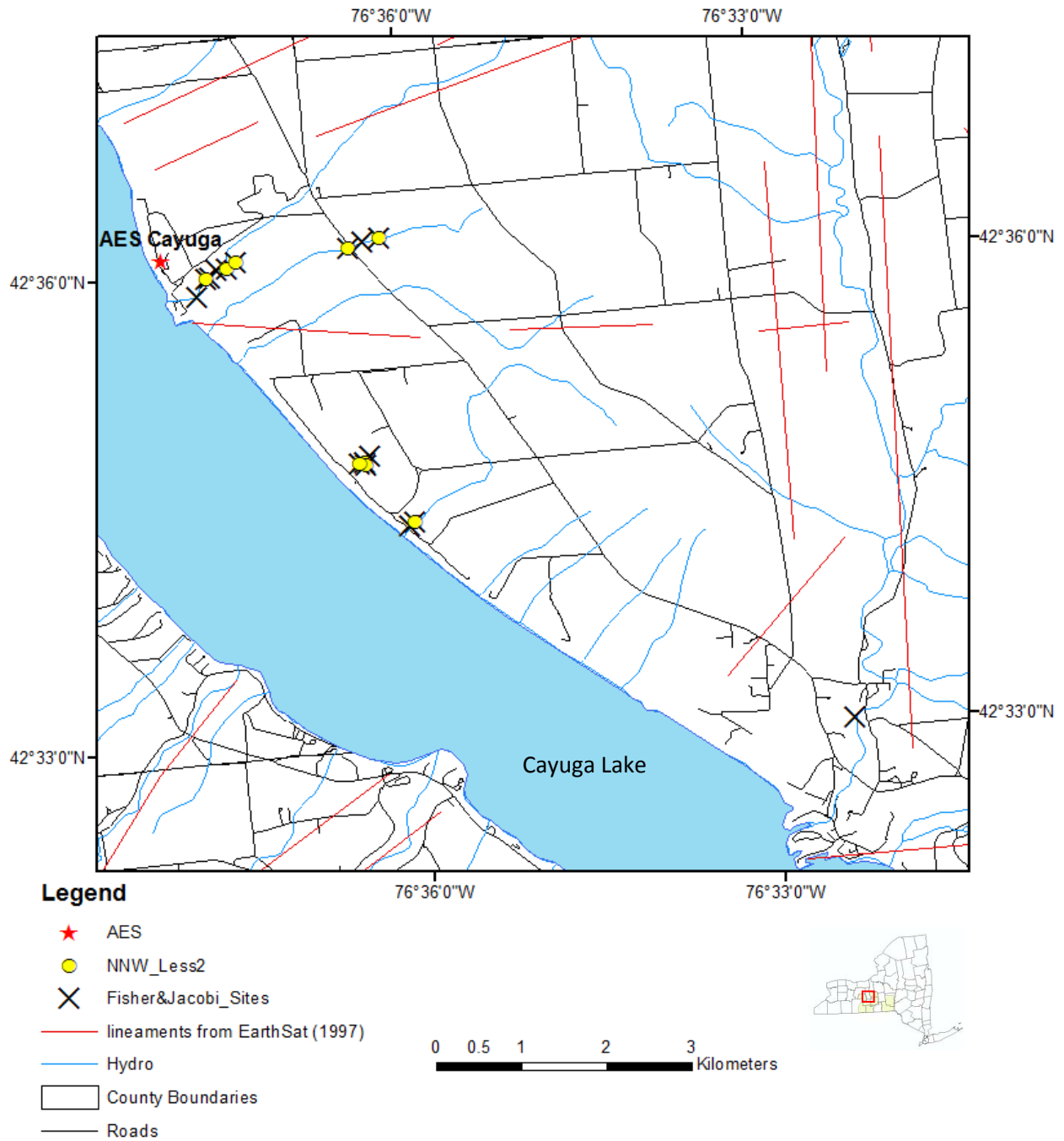


Figure 6.1-112: Chenango field sites exhibiting NNW-striking fractures with a frequency of less than 2 fractures/m.



**Remote Sensing Laboratory**  
 Dept. of Geology, SUNY at Buffalo



**University at Buffalo**  
 The State University of New York

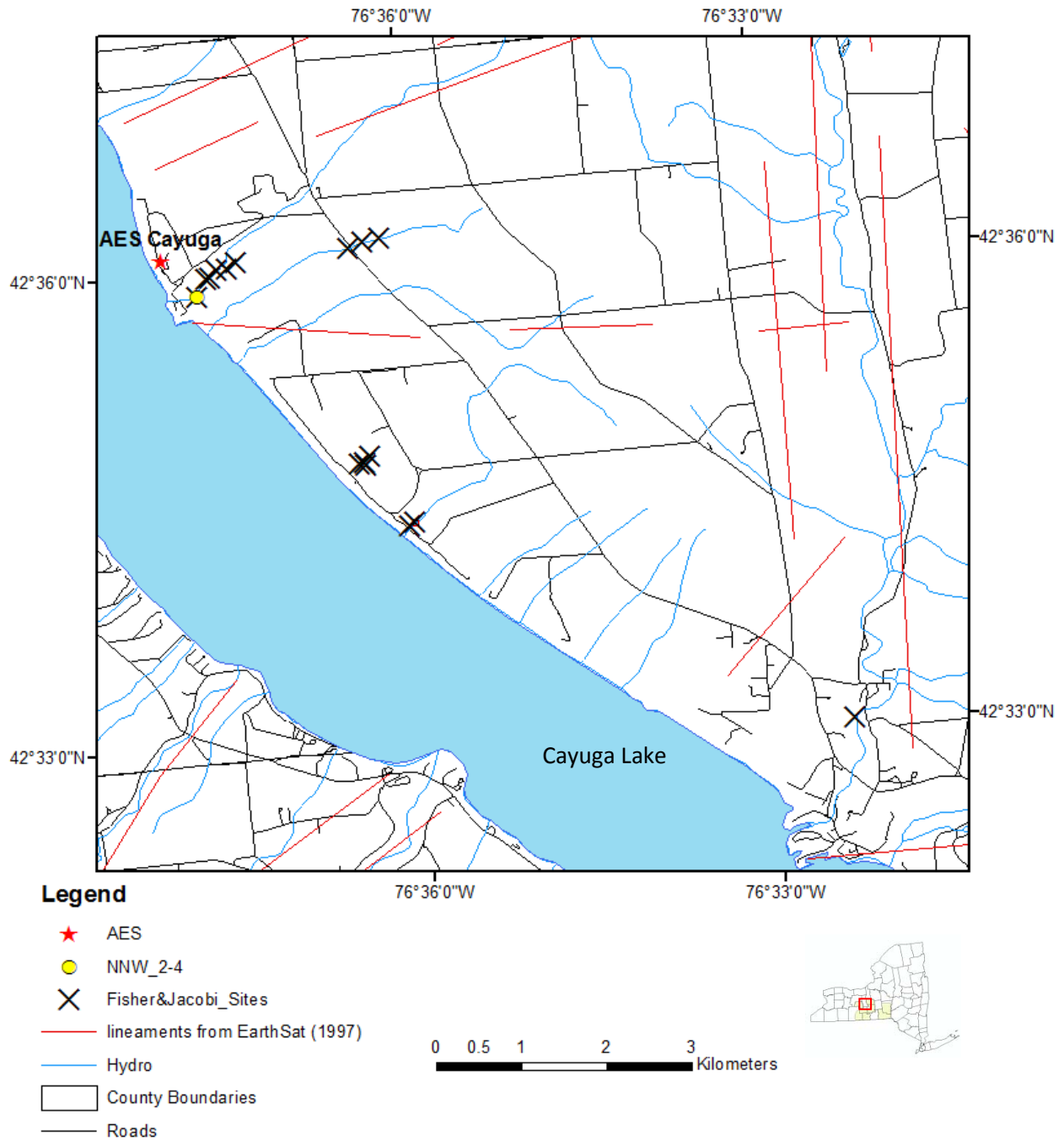


Figure 6.1-113: Chenango field sites exhibiting NNW-striking fractures with a frequency of 2 to 4 fractures/m.



**Remote Sensing Laboratory**  
 Dept. of Geology, SUNY at Buffalo



**University at Buffalo**  
 The State University of New York

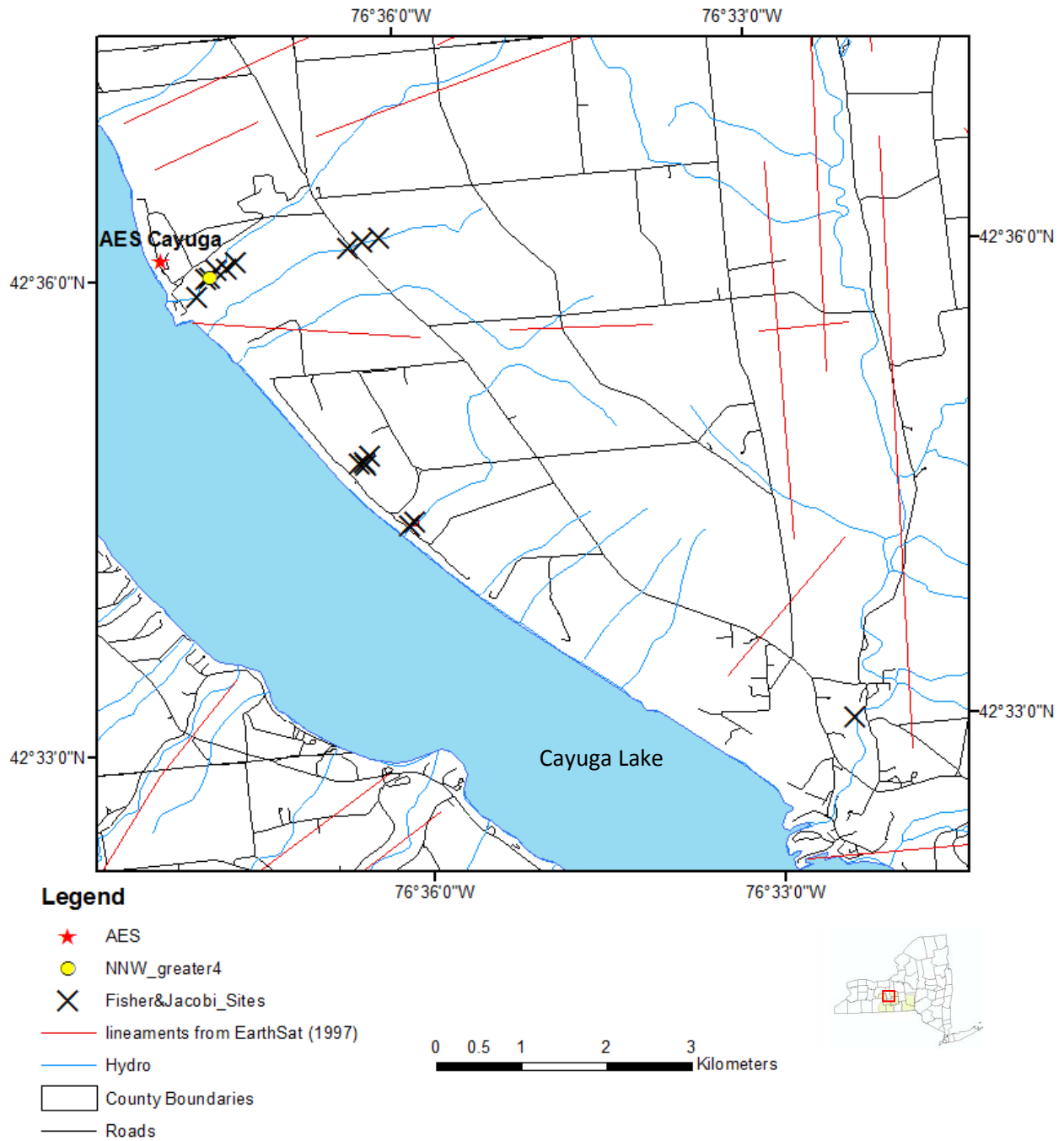


Figure 6.1-114: Chenango field sites exhibiting NNW-striking fractures with a frequency of greater than 4 fractures/m.





**Remote Sensing Laboratory**  
 Dept. of Geology, SUNY at Buffalo



**University at Buffalo**  
 The State University of New York

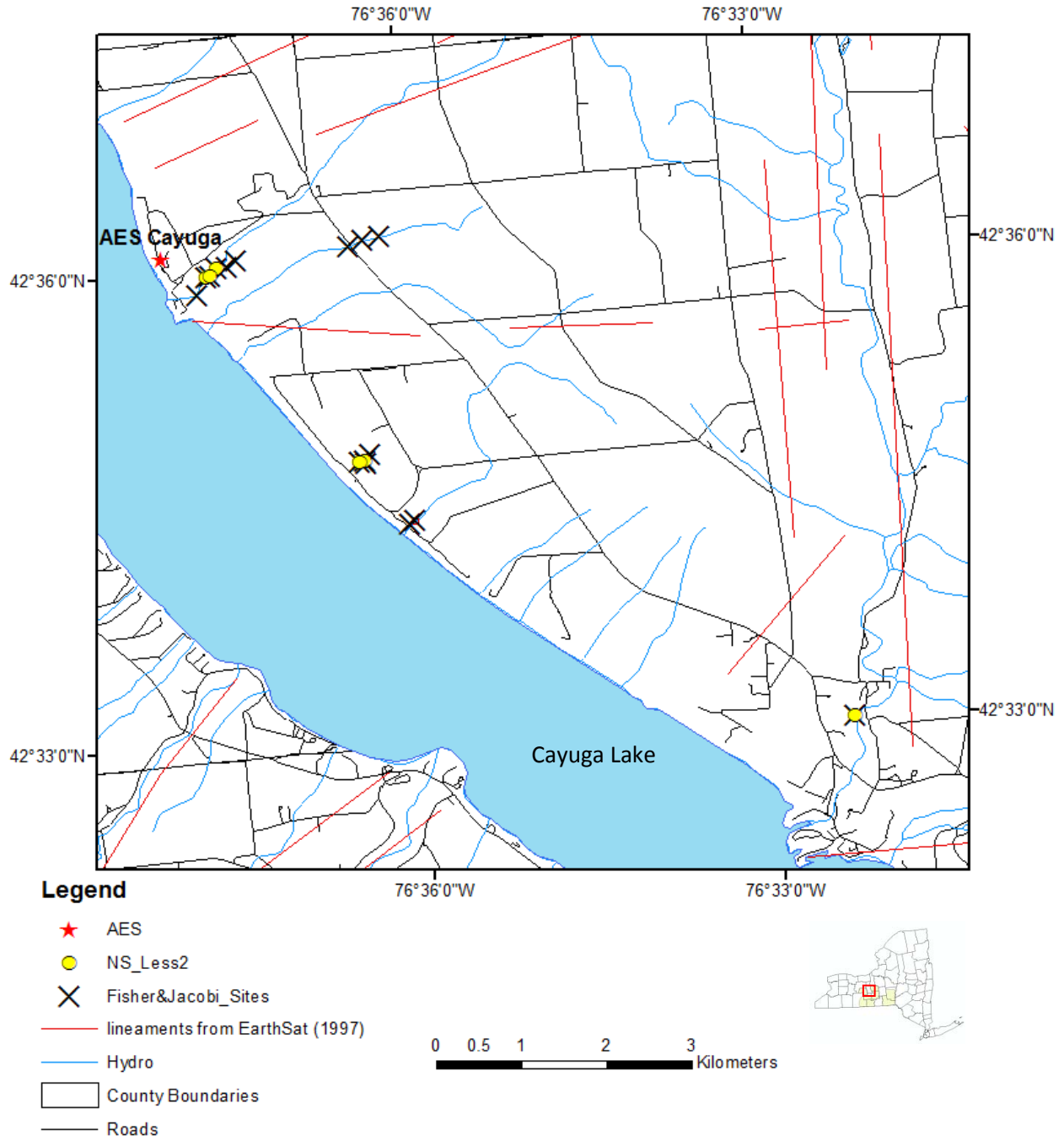


Figure 6.1-115: Chenango field sites exhibiting NS-striking fractures with a frequency of less than 2 fractures/m.



**Remote Sensing Laboratory**  
 Dept. of Geology, SUNY at Buffalo



**University at Buffalo**  
 The State University of New York

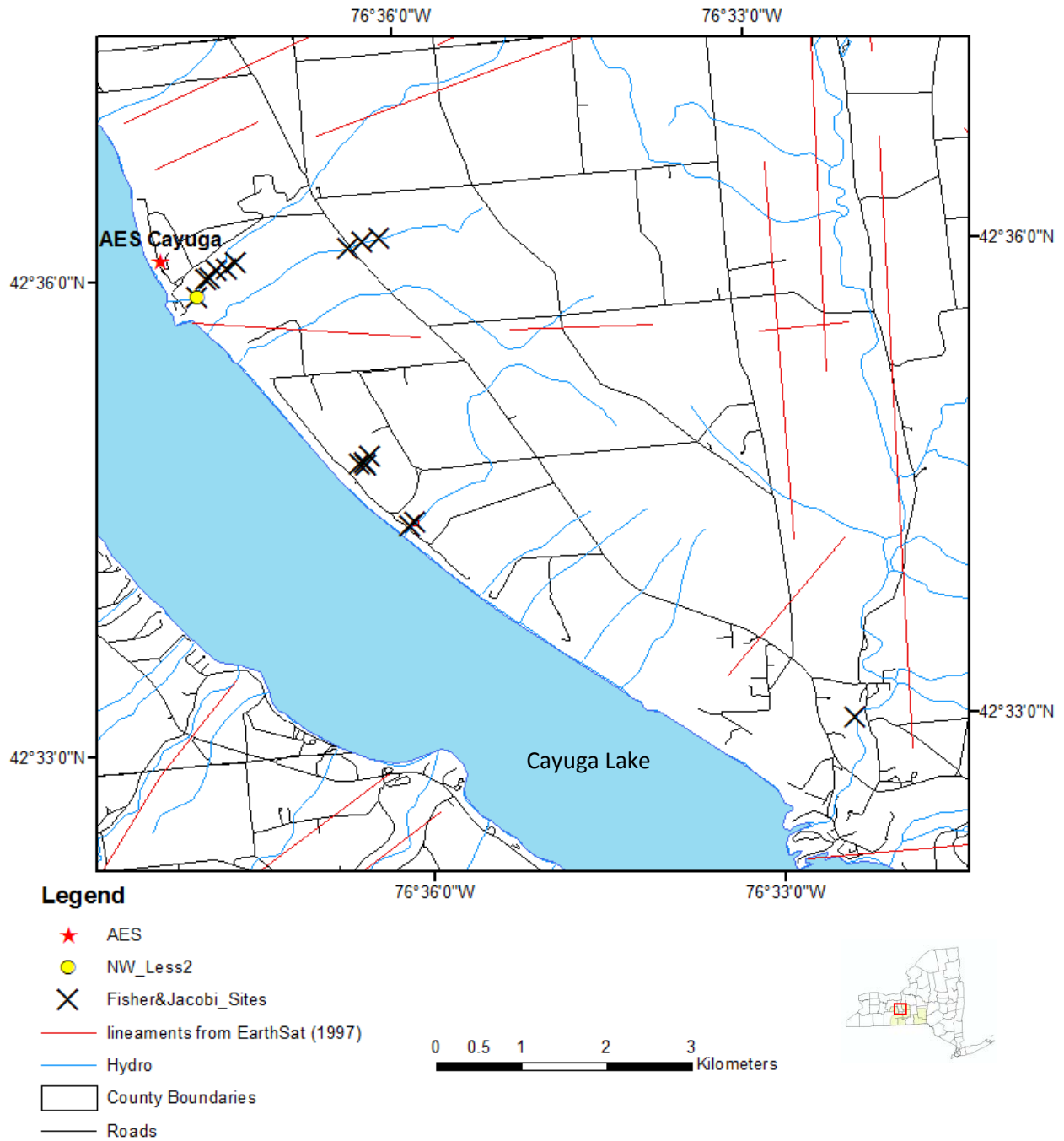


Figure 6.1-116: Chenango field sites exhibiting NW-striking fractures with a frequency of less than 2 fractures/m.



**Remote Sensing Laboratory**  
 Dept. of Geology, SUNY at Buffalo



**University at Buffalo**  
 The State University of New York

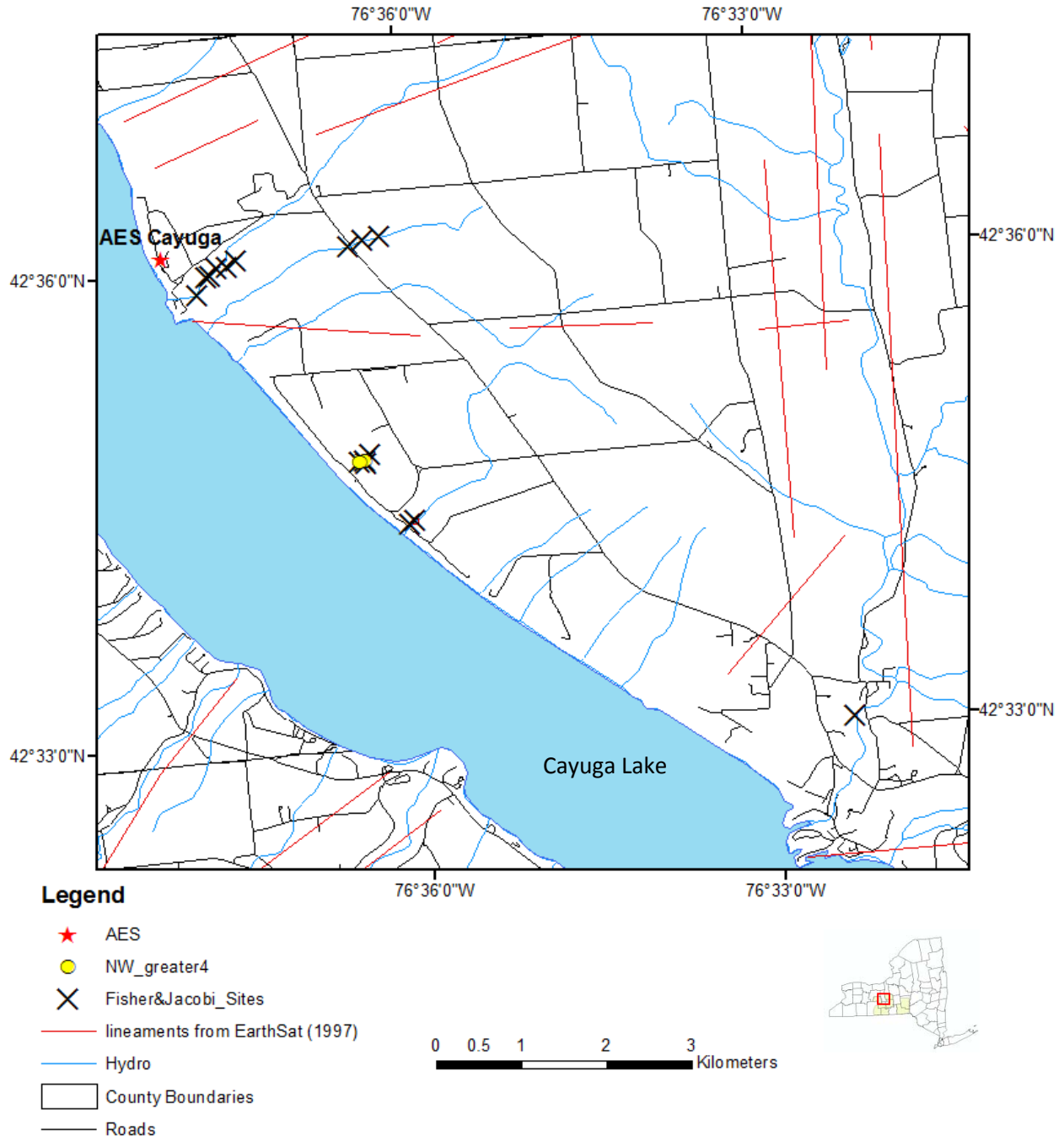


Figure 6.1-117: Cayuga field sites exhibiting NW-striking fractures with a frequency of greater than 4 fractures/m.



**Remote Sensing Laboratory**  
Dept. of Geology, SUNY at Buffalo



**University at Buffalo**  
The State University of New York

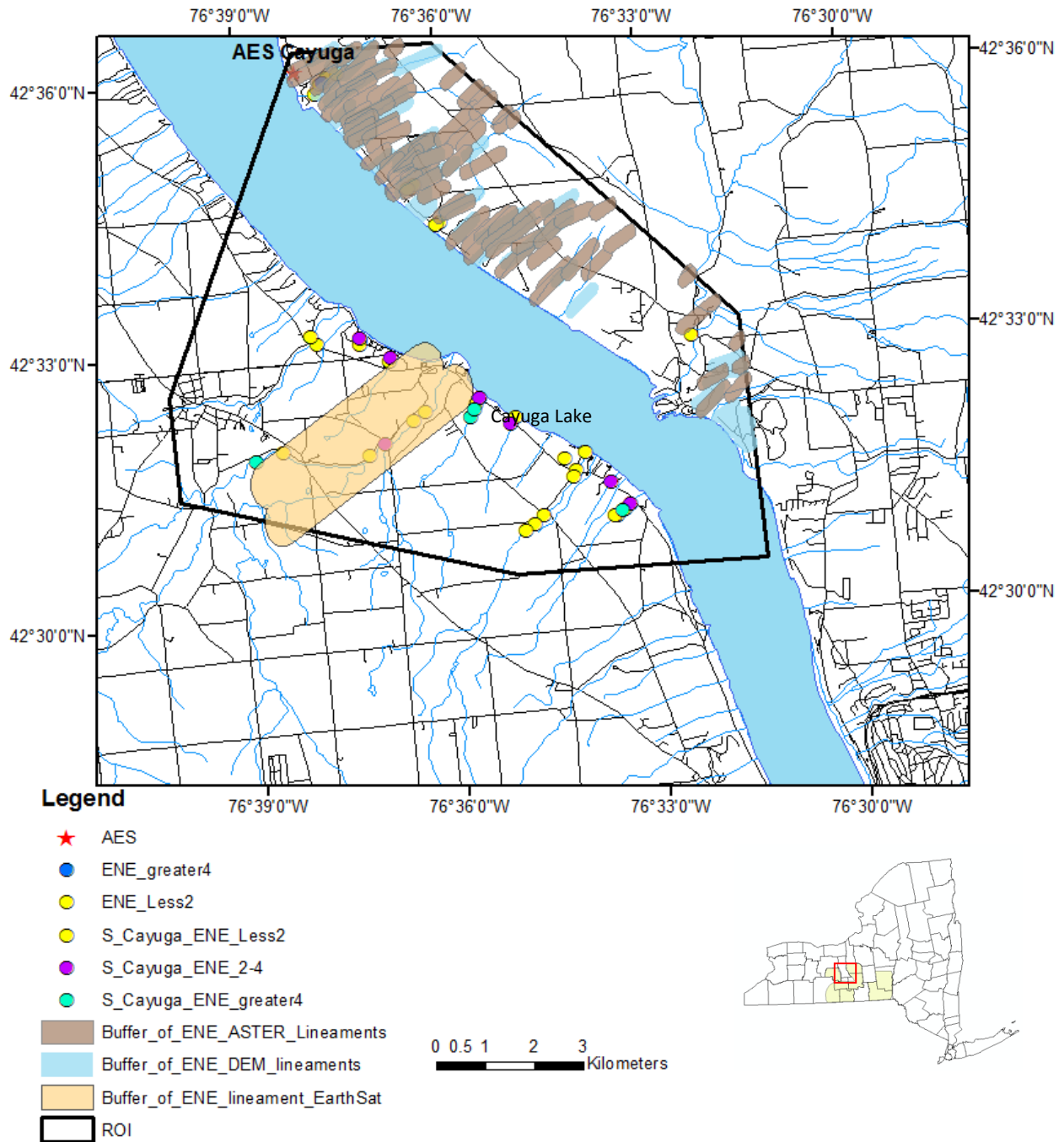


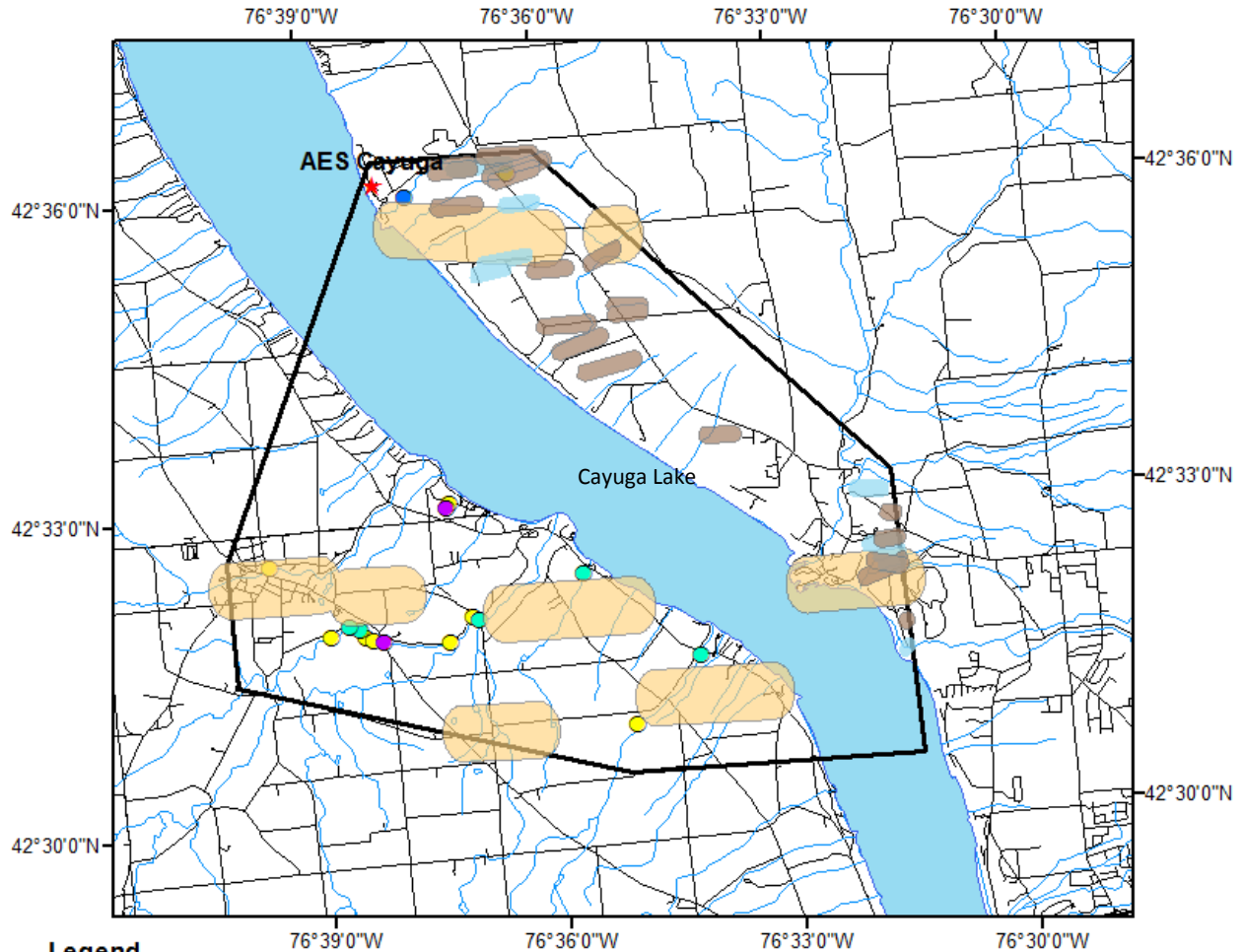
Figure 6.1-118: Buffers surrounding ENE trending lineaments in the ROI on Cayuga Lake. Yellow buffer is 2.5 km for EarthSat (1997) ENE lineaments, 50 m for ASTER and DEM ENE lineaments and 50 ft (16 m) for the field sites.



**Remote Sensing Laboratory**  
Dept. of Geology, SUNY at Buffalo



**University at Buffalo**  
The State University of New York



**Legend**

- ★ AES
- EW\_greater4
- EW\_2-4
- S\_Cayuga\_EW\_Less2
- S\_Cayuga\_EW\_2-4
- S\_Cayuga\_EW\_greater4
- Buffer\_of\_EW\_ASTER\_Lineaments
- Buffer\_of\_EW\_DEM\_lineaments
- Buffer\_of\_EW\_lineaments\_EarthSat
- ROI



Figure 6.1-119: Buffers surrounding EW trending lineaments in the ROI on Cayuga Lake. Yellow buffer is 2.5 km for EarthSat (1997) ENE lineaments, 50 m for ASTER and DEM ENE lineaments and 50 ft (16 m) for the field sites.

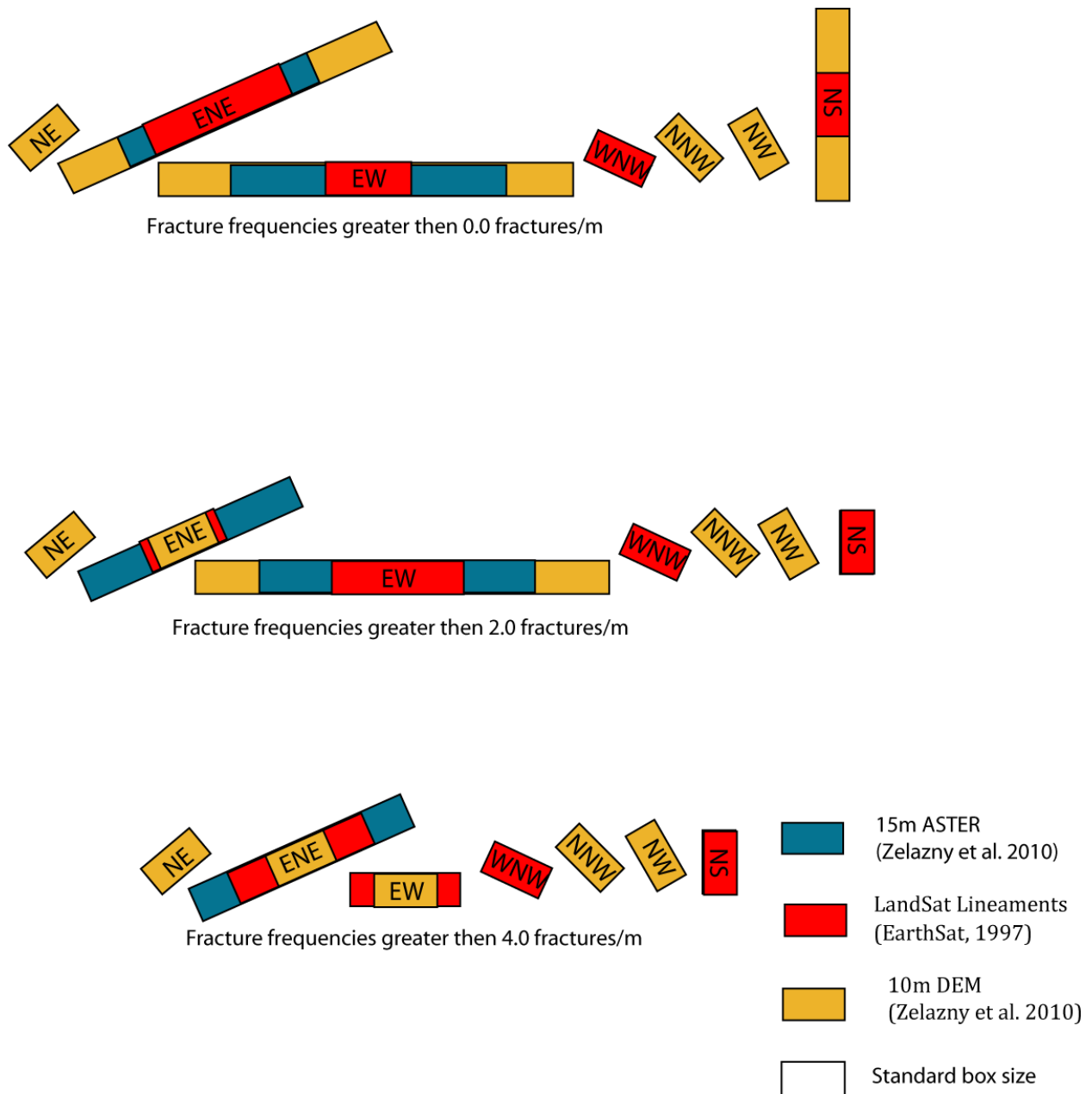


Figure 6.1-120: Graphical representation of the statistical Weights of Evidence results that test lineaments from ASTER, DEM and EarthSat (1997) against fracture frequencies for field sites on Cayuga Lake (WNW-trending lineaments were only observed in the lineaments from EarthSat, 1997). The length of the bar for each orientation indicates the relative contrast index (longer bar implies better coincidence between lineaments and fractures)

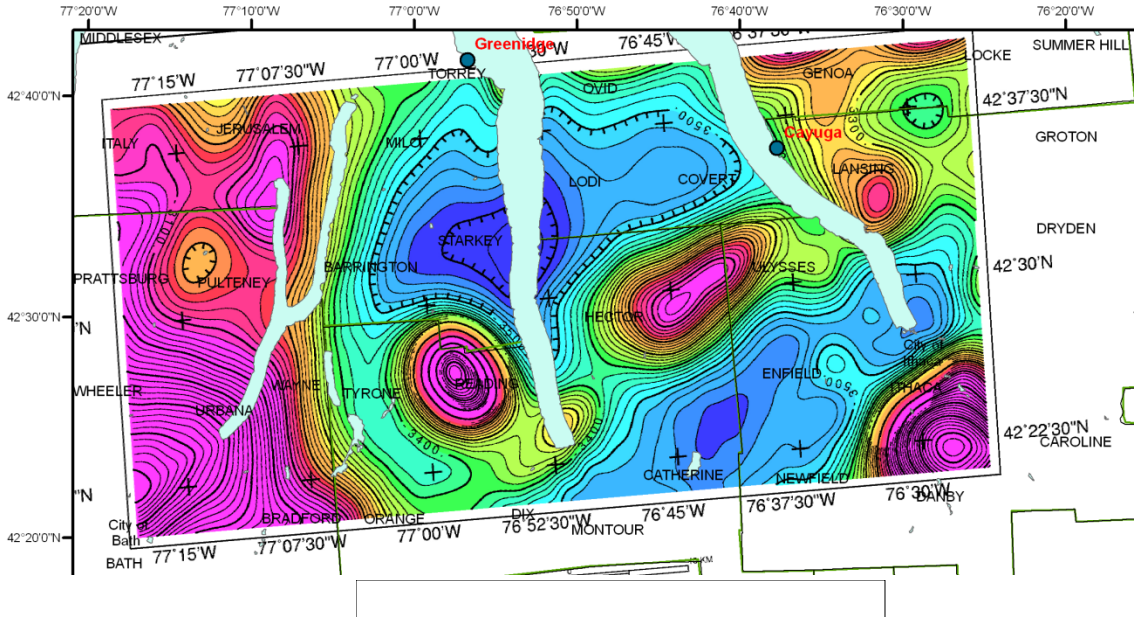


Figure 6.1-121: Reduced to pole (RTP) total magnetic intensity (Figure 3.7-2 in DOE Final Report, Jacobi, 2007a)



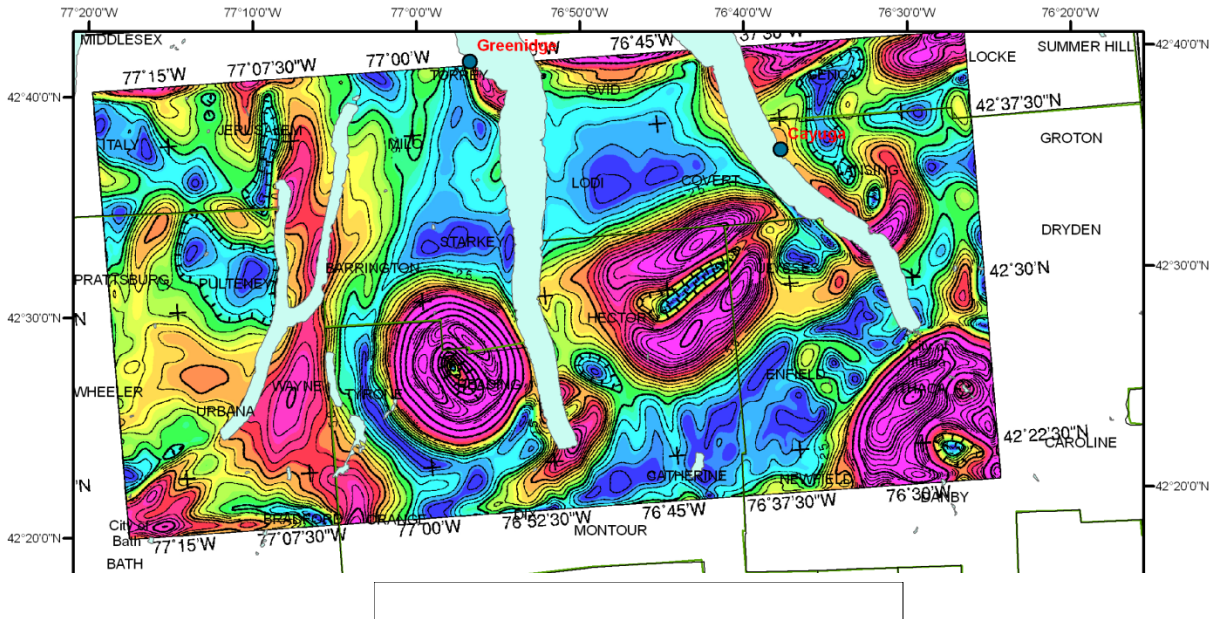


Figure 6.1-122: Horizontal gradient of RTP aeromagnetics (Figure 3.7-3 in DOE Final Report, Jacobi, 2007a)



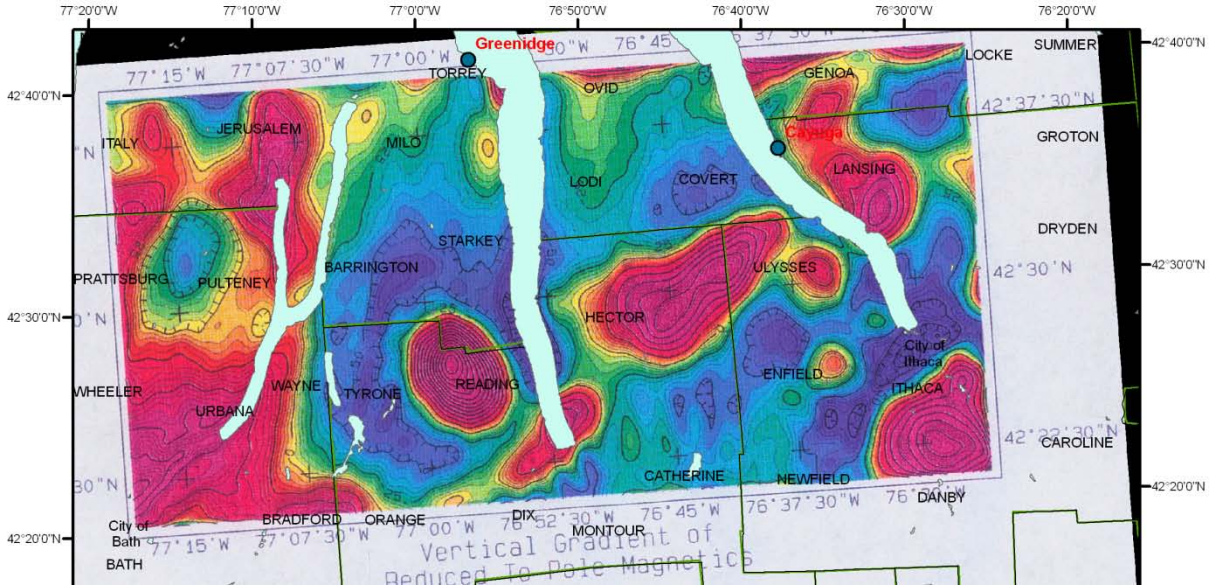


Figure 6.1-123: Vertical gradient of RTP aeromagnetic (Figure 3.7-4 in DOE Final Report, Jacobi, 2007a)

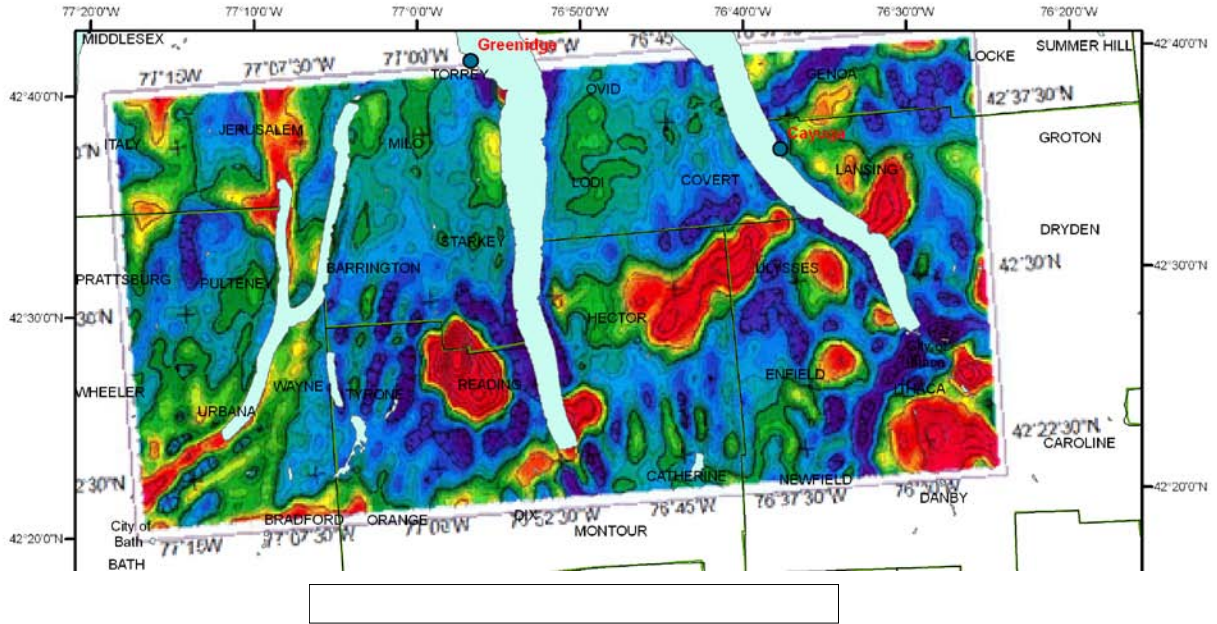
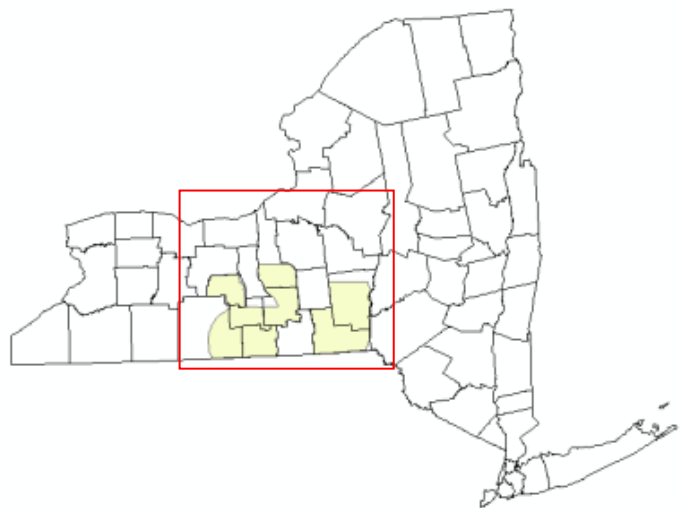


Figure 6.1-124: Second derivative of RTP aeromagnetic (Figure 3.7-5 in DOE Final Report, Jacobi, 2007a)



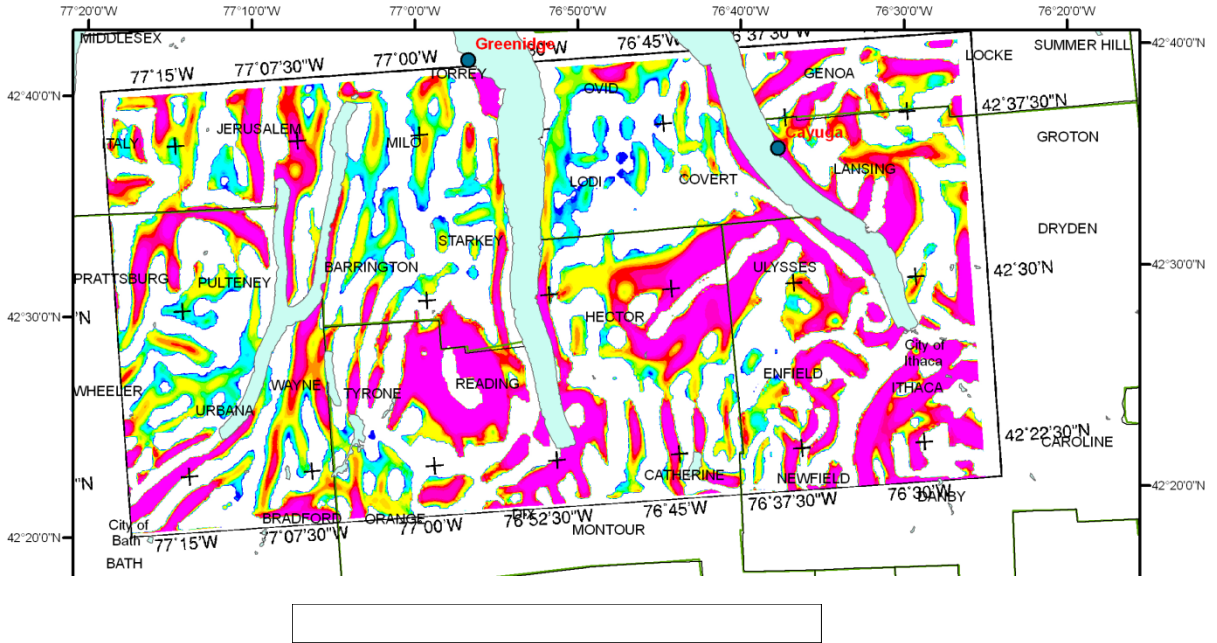


Figure 6.1-125: Linear feature analysis of RTP aeromagnetic (Figure 3.7-6a in DOE Final Report, Jacobi, 2007a)

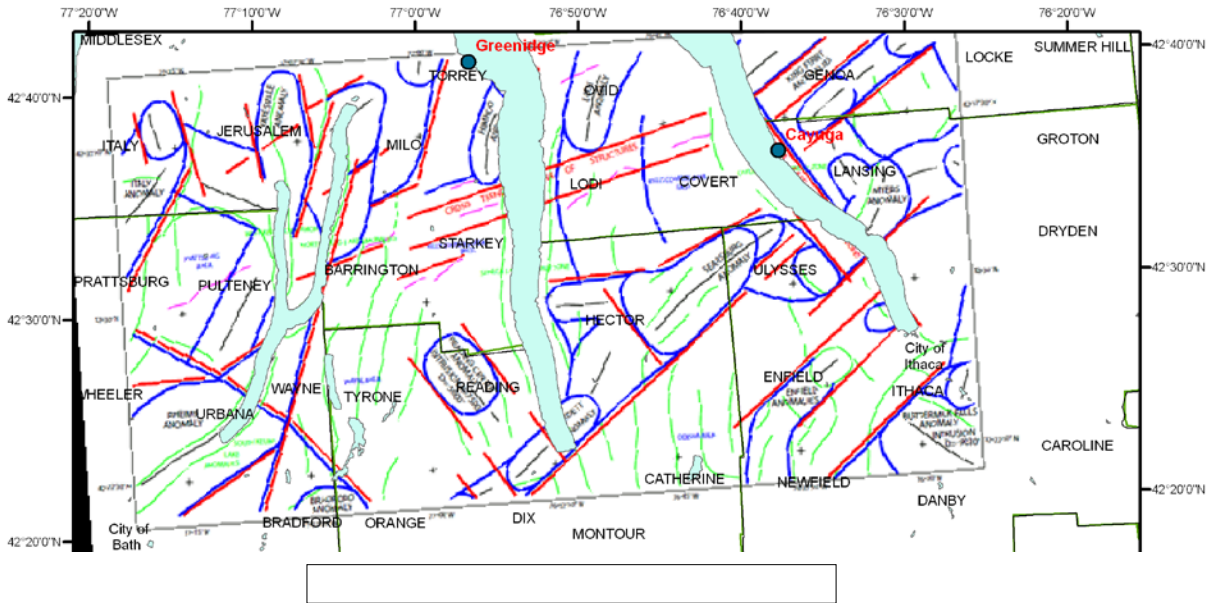


Figure 6.1-126: Interpretation of gradients in the aeromagnetic field (Figure 3.7-7 in DOE Final Report, Jacobi, 2007a)





**Remote Sensing Laboratory**  
Dept. of Geology, SUNY at Buffalo



**University at Buffalo**  
The State University of New York

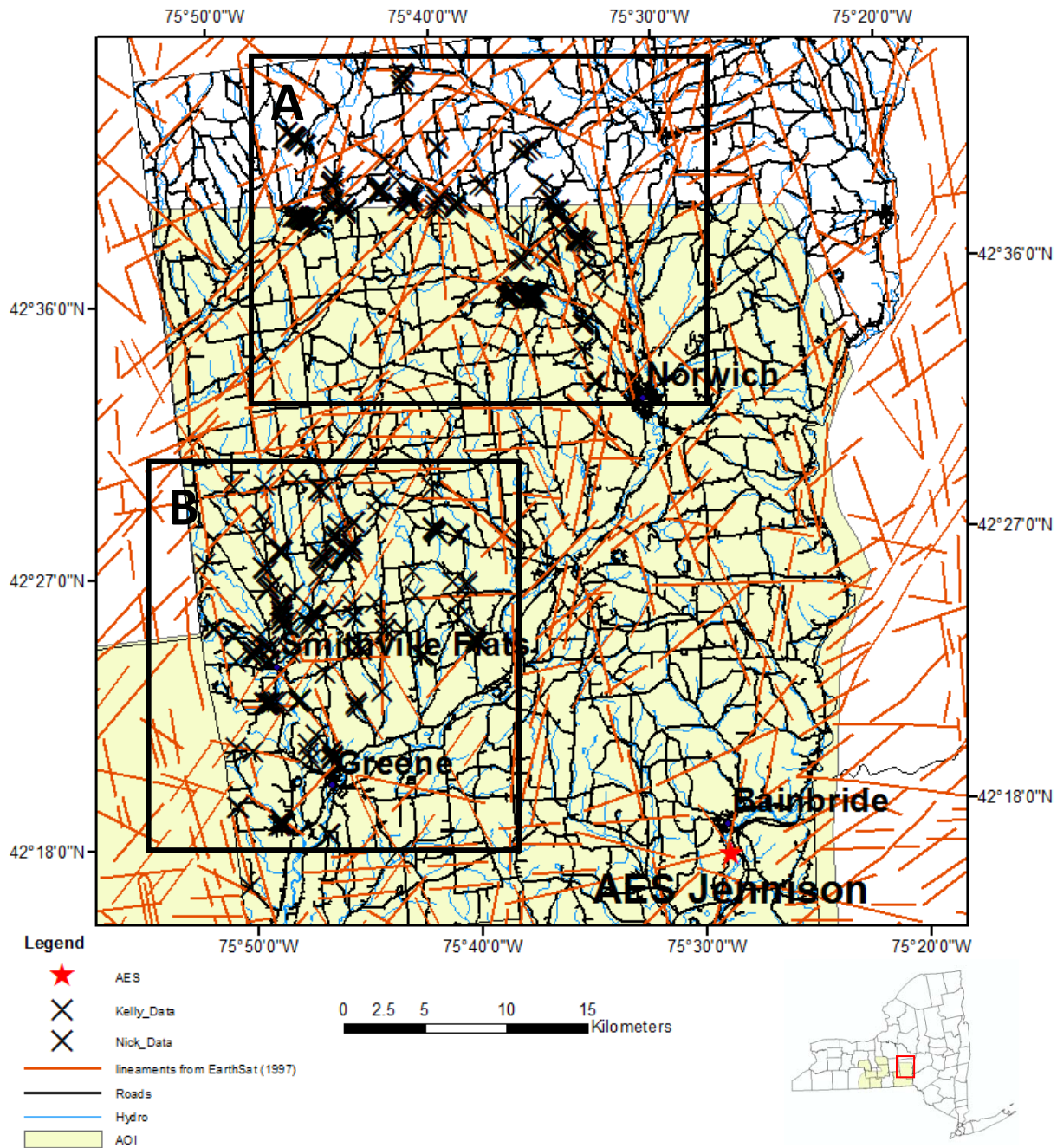


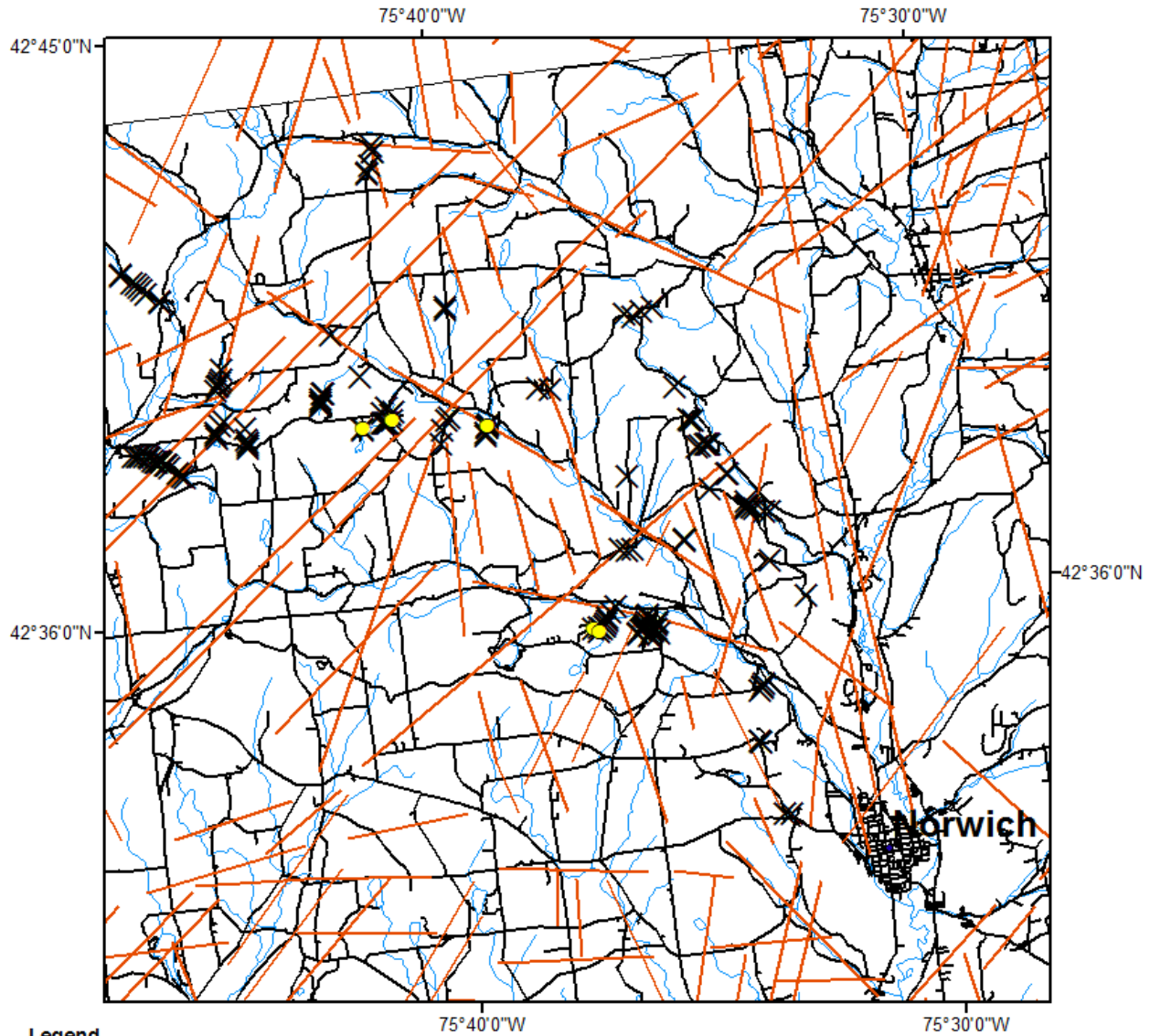
Figure 6.1-127: Eastern part of the project area (“Chenango AOl”): Jennison Power Plant with lineaments (EarthSat,1997) and field sites from McGuire et al (2006), Terech et al (2005) and Jacobi (2007b). Box A shows locations of Figures 128-152. Box B shows locations of Figures 155-177









Remote Sensing Laboratory  
Dept. of Geology, SUNY at Buffalo



University at Buffalo  
The State University of New York



**Legend**

-  AES
-  Nick\_ENE\_Less2
-  Nick\_Data
-  lineaments from EarthSat (1997)
-  Roads
-  Hydro

0 1.5 3 6 9 Kilometers

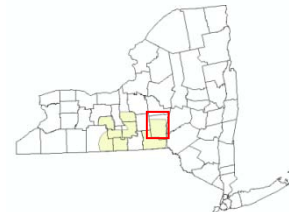


Figure 6.1-128: North-central Chenango field sites exhibiting ENE-striking fractures with a frequency of less than 2 fractures/m. (Terech et al, 2005 and Jacobi, 2007b)



**Remote Sensing Laboratory**  
Dept. of Geology, SUNY at Buffalo



**University at Buffalo**  
The State University of New York

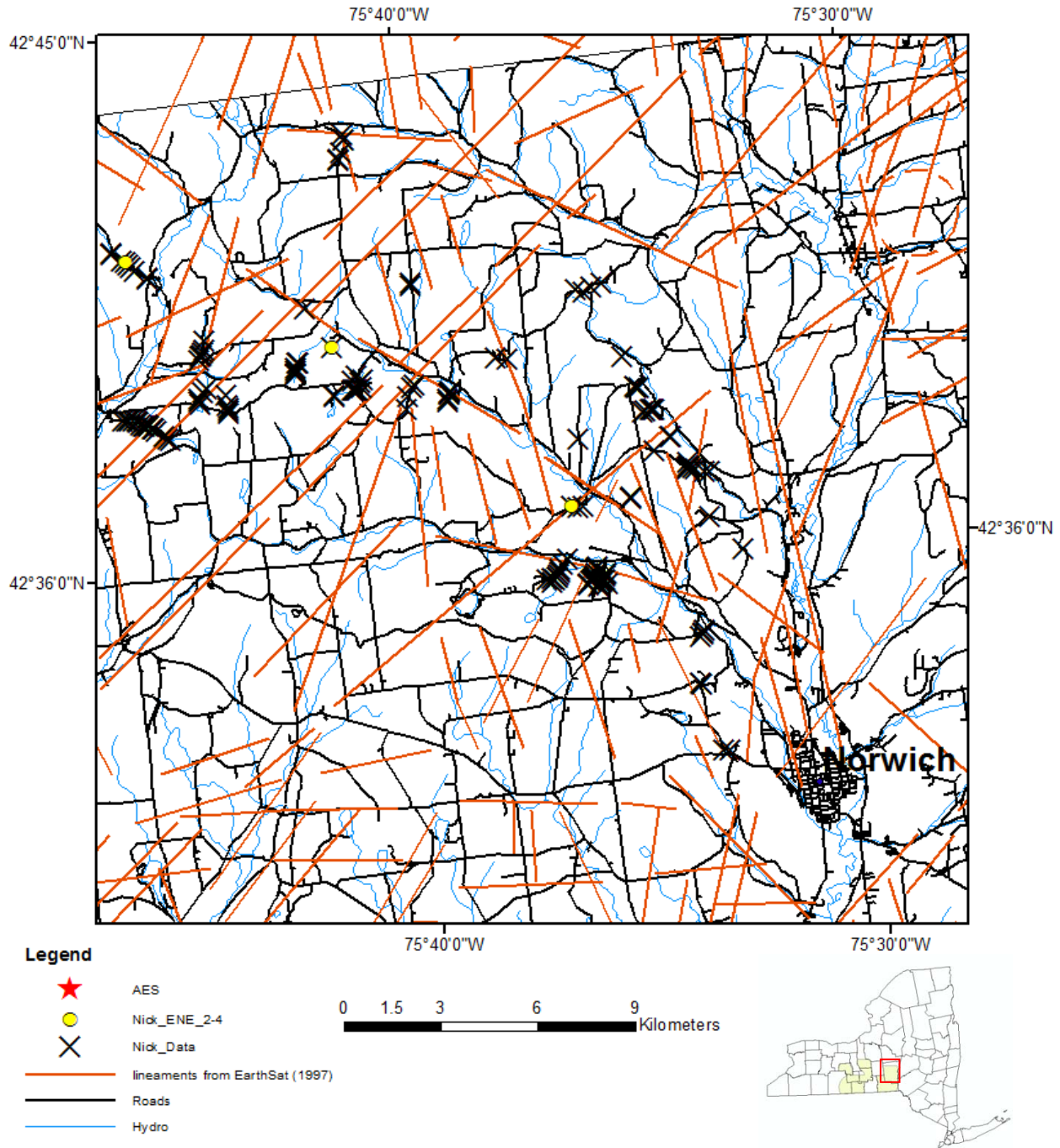


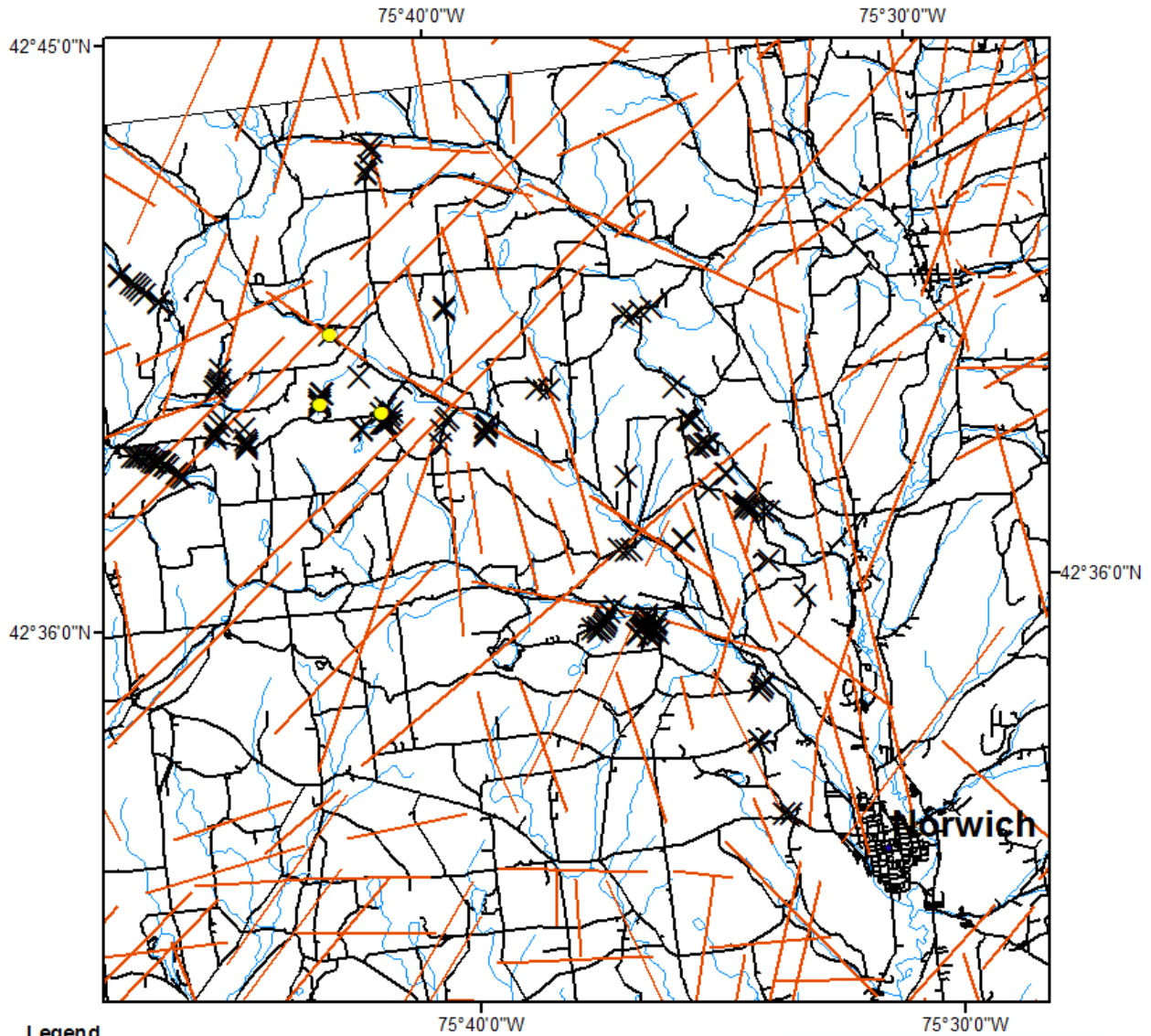
Figure 6.1-129: North-central Chenango field sites exhibiting ENE-striking fractures with a frequency of 2 to 4 fractures/m. (Terech et al, 2005 and Jacobi, 2007b)



**Remote Sensing Laboratory**  
Dept. of Geology, SUNY at Buffalo



**University at Buffalo**  
The State University of New York



**Legend**

- AES
- Nick\_ENE\_greater4
- Nick\_Data
- lineaments from EarthSat (1997)
- Roads
- Hydro

0 1.5 3 6 9 Kilometers

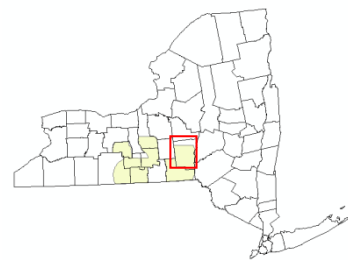


Figure 6.1-130. North-central Chenango field sites exhibiting ENE-striking fractures with a frequency of greater than 4 fracture/m. (Terech et al, 2005 and Jacobi, 2007b) Lineaments from EarthSat (1997).

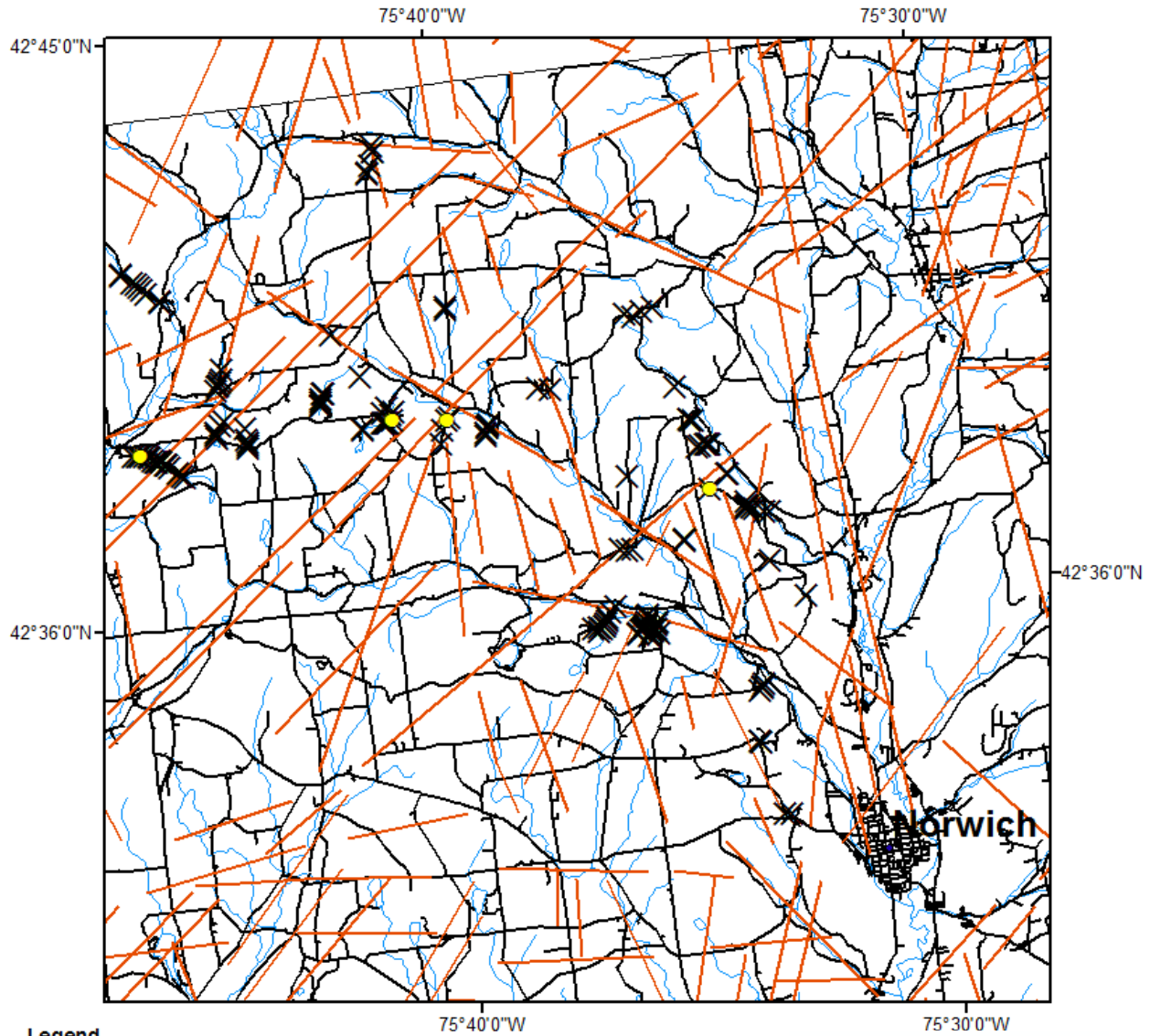










**Remote Sensing Laboratory**  
Dept. of Geology, SUNY at Buffalo



**University at Buffalo**  
The State University of New York



**Legend**

-  AES
-  Nick\_EW\_Less 2
-  Nick\_Data
-  lineaments from EarthSat (1997)
-  Roads
-  Hydro

0 1.5 3 6 9 Kilometers

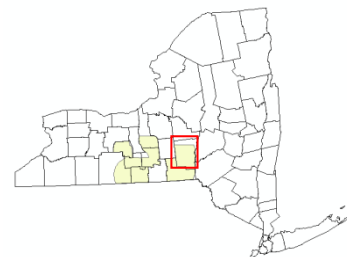


Figure 6.1-131. North-central Chenango field sites exhibiting EW-striking fractures with a frequency of less than 2 fractures/m. (Terech et al, 2005 and Jacobi, 2007b) Lineaments from EarthSat (1997).



**Remote Sensing Laboratory**  
Dept. of Geology, SUNY at Buffalo



**University at Buffalo**  
The State University of New York

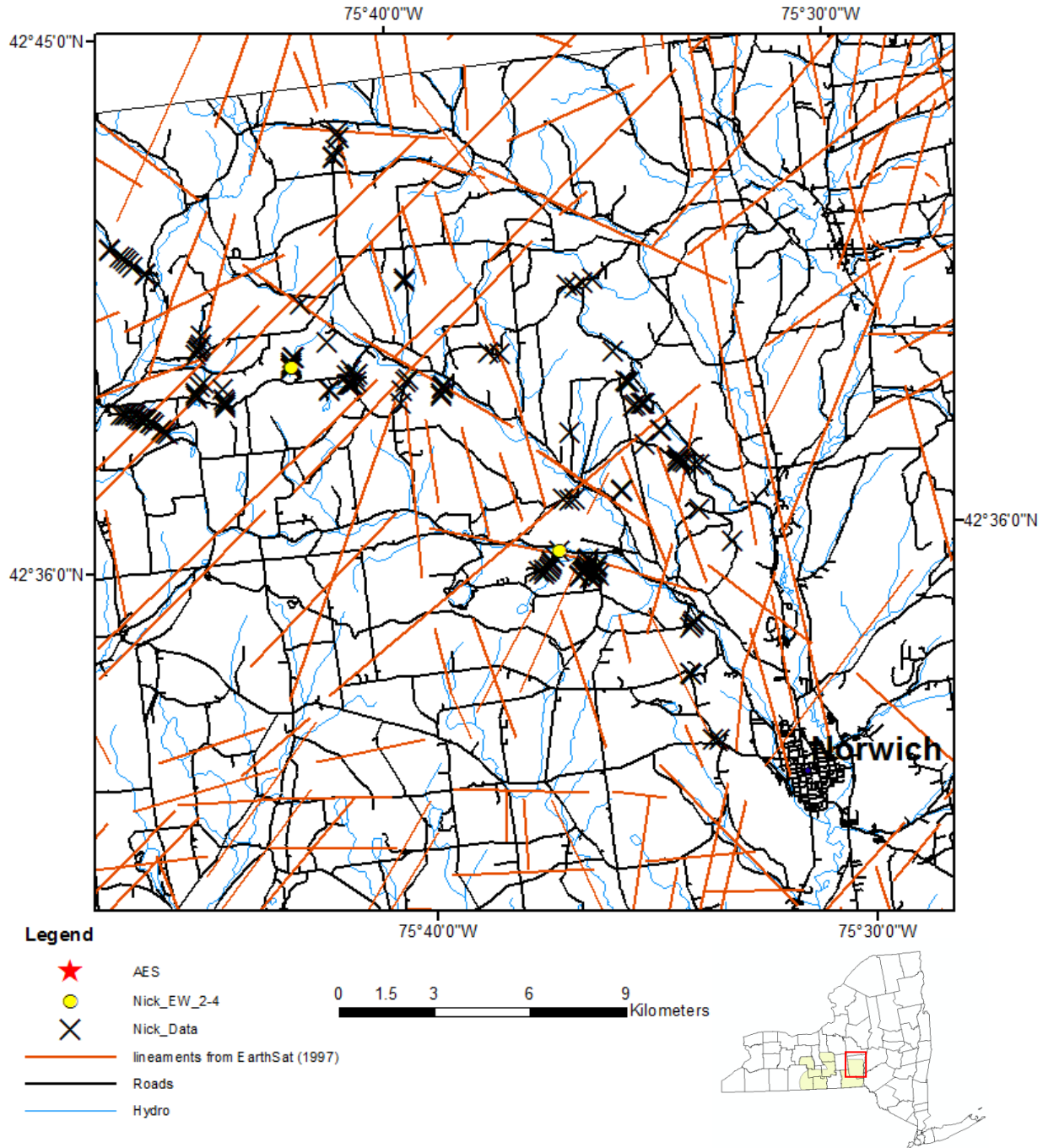


Figure 6.1-132. North-central Chenango field sites exhibiting EW-striking fractures with a frequency of 2 to 4 fractures/m. (Terech et al, 2005 and Jacobi, 2007b) Lineaments from EarthSat (1997).



**Remote Sensing Laboratory**  
 Dept. of Geology, SUNY at Buffalo



**University at Buffalo**  
 The State University of New York

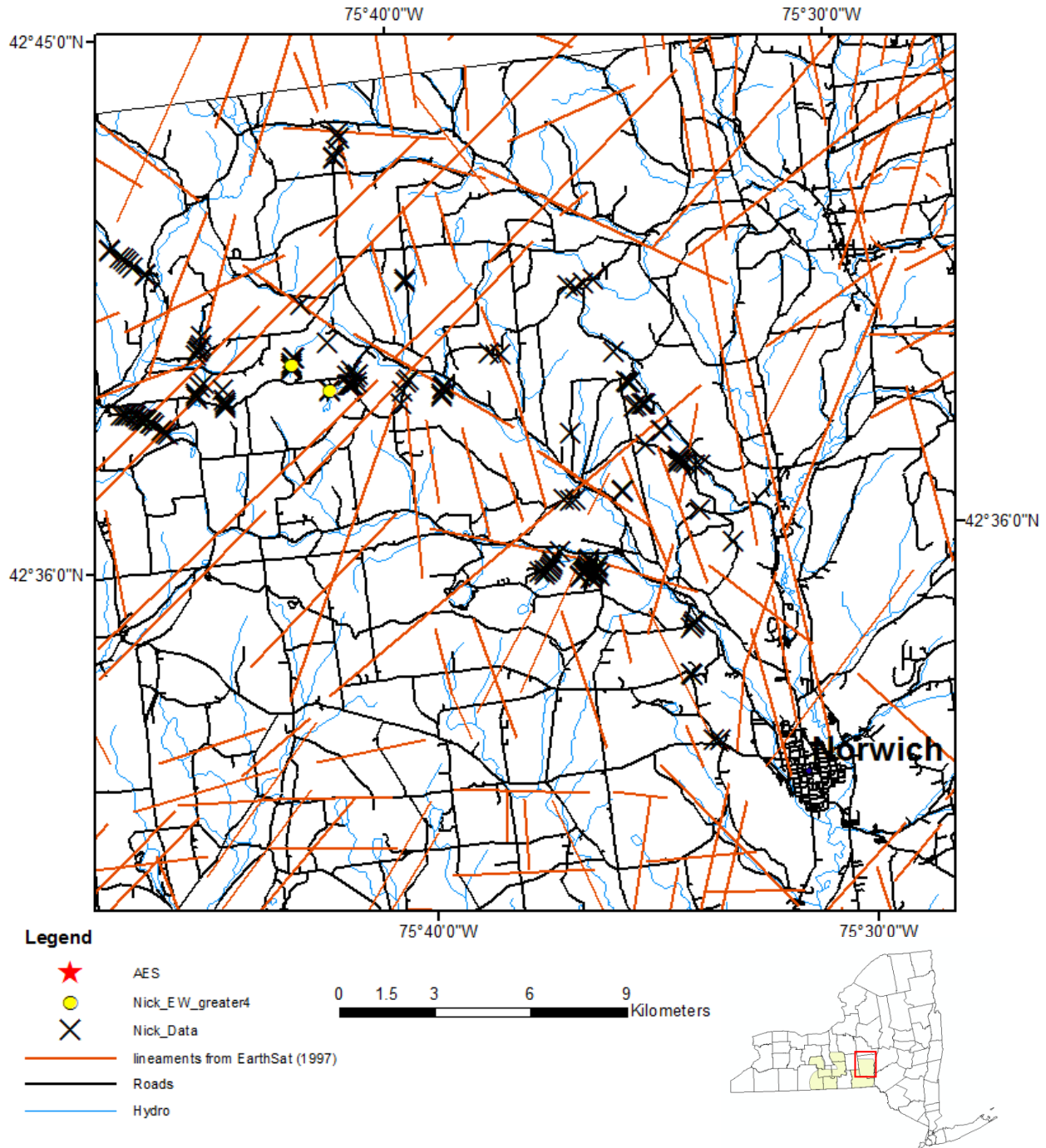


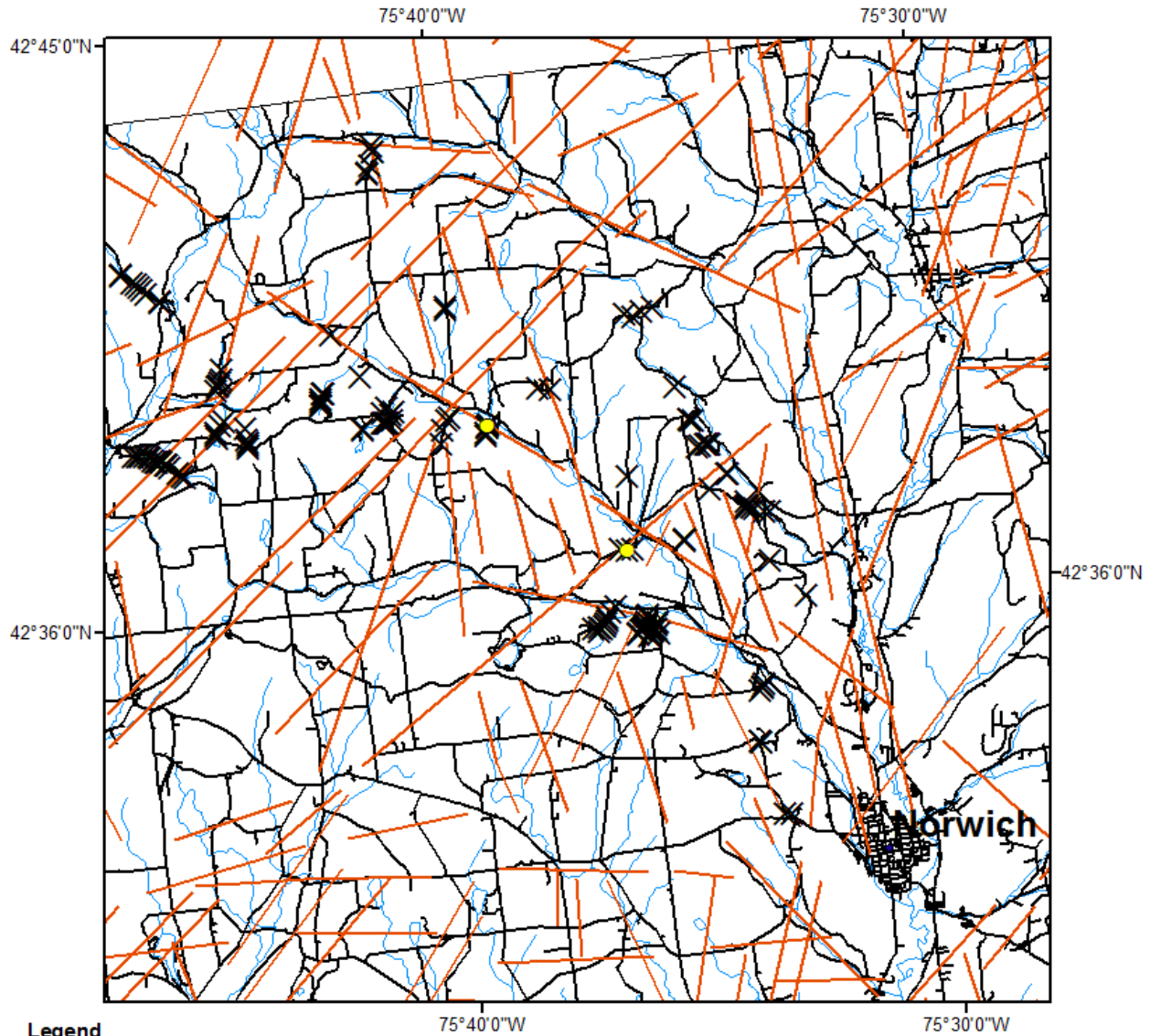
Figure 6.1-133. North-central Chenango field sites exhibiting EW-striking fractures with a frequency of greater than 4 fractures/m. (Terech et al, 2005 and Jacobi, 2007b) Lineaments from EarthSat (1997).









**Remote Sensing Laboratory**  
Dept. of Geology, SUNY at Buffalo



**University at Buffalo**  
The State University of New York



**Legend**

-  AES
-  Nick\_NE\_Less2
-  Nick\_Data
-  lineaments from EarthSat (1997)
-  Roads
-  Hydro

0 1.5 3 6 9 Kilometers

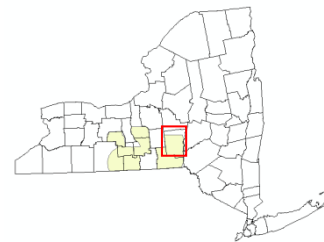


Figure 6.1-134. North-central Chenango field sites exhibiting NE-striking fractures with a frequency of less than 2 fractures/m. (Terech et al, 2005 and Jacobi, 2007b) Lineaments from EarthSat (1997).





**Remote Sensing Laboratory**  
Dept. of Geology, SUNY at Buffalo



**University at Buffalo**  
The State University of New York

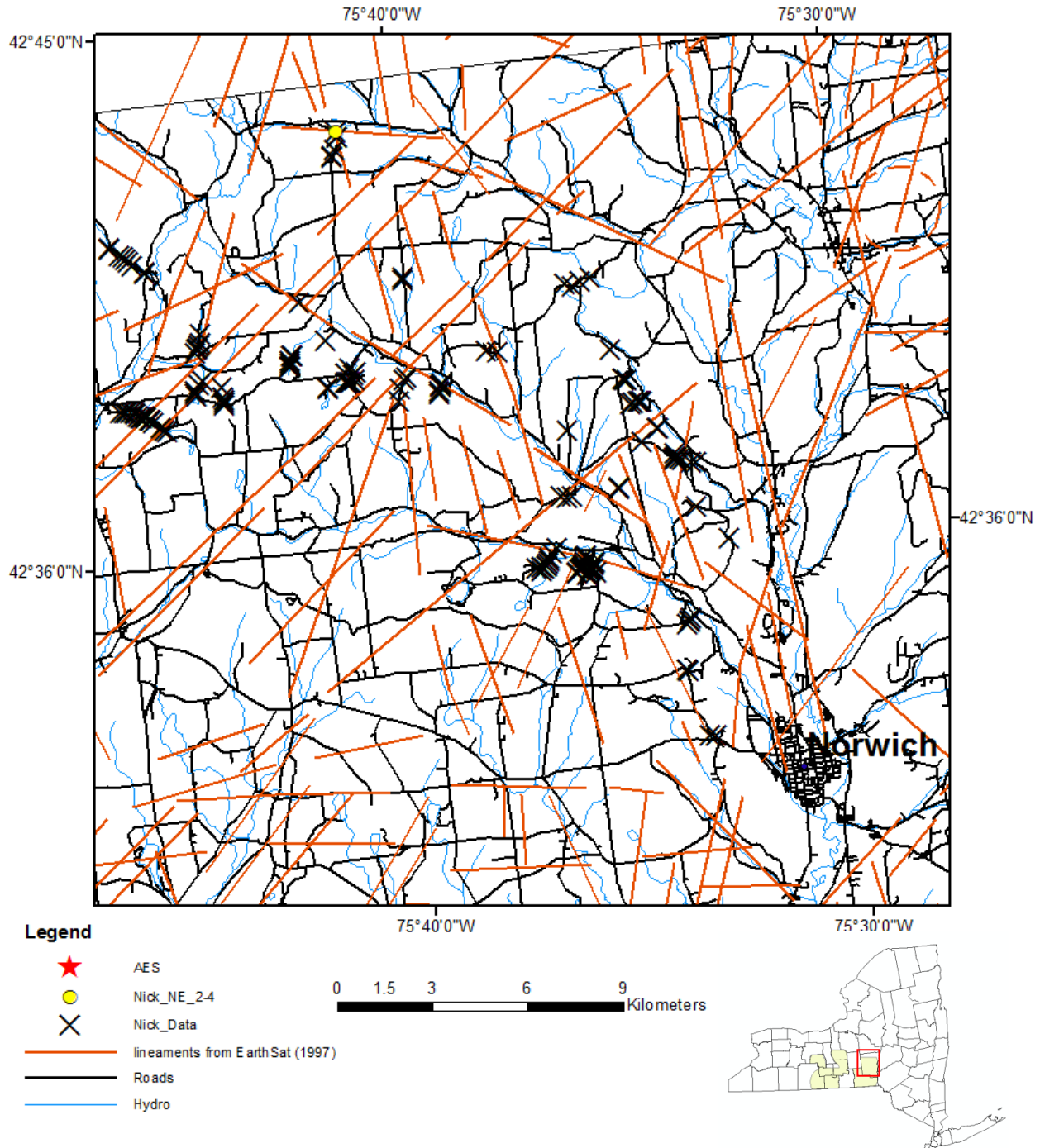


Figure 6.1-135. North-central Chenango field sites exhibiting NE-striking fractures with a frequency of 2 to 4 fractures/m. (Terech et al, 2005 and Jacobi, 2007b) Lineaments from EarthSat (1997).



**Remote Sensing Laboratory**  
Dept. of Geology, SUNY at Buffalo



**University at Buffalo**  
The State University of New York

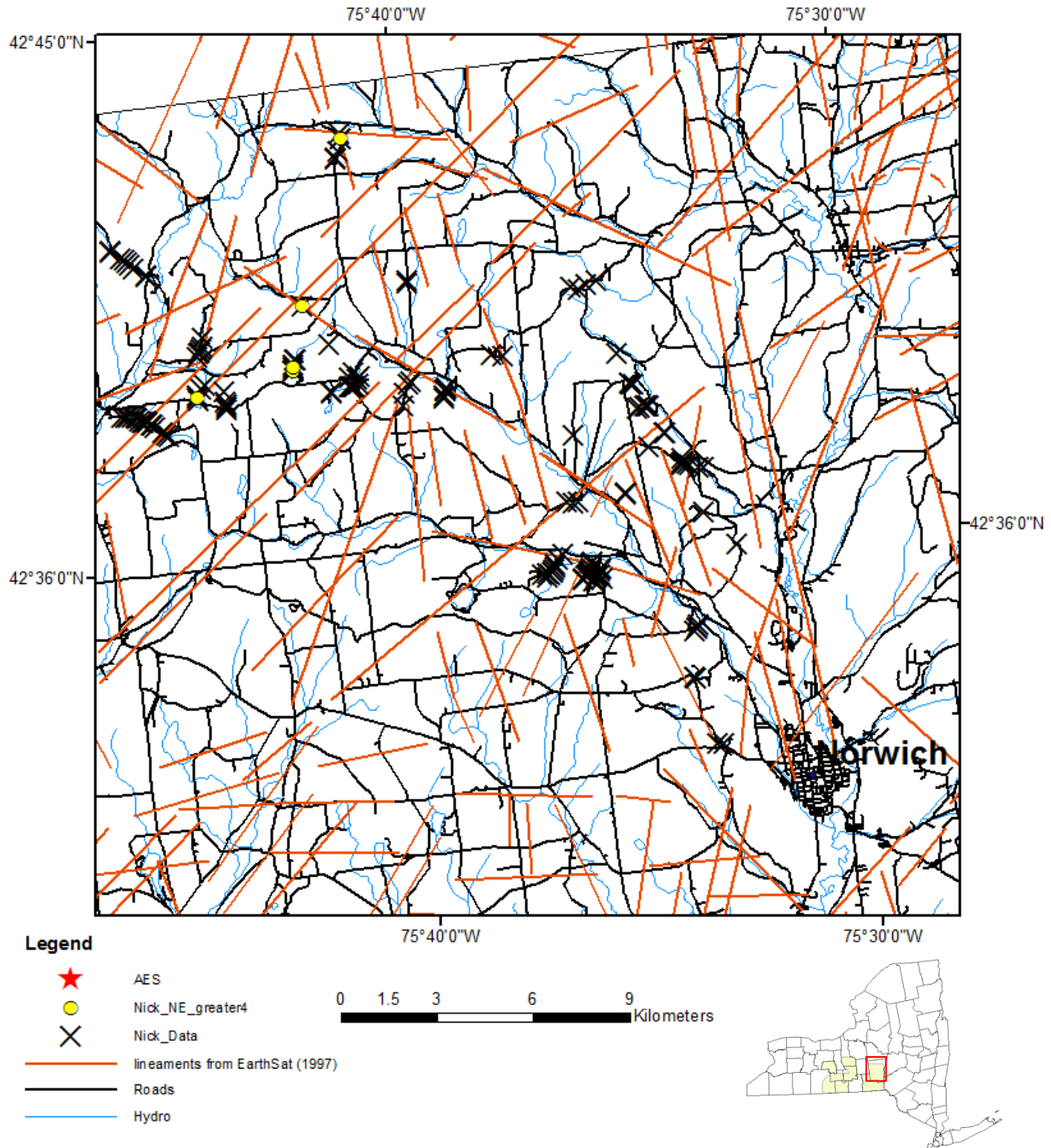


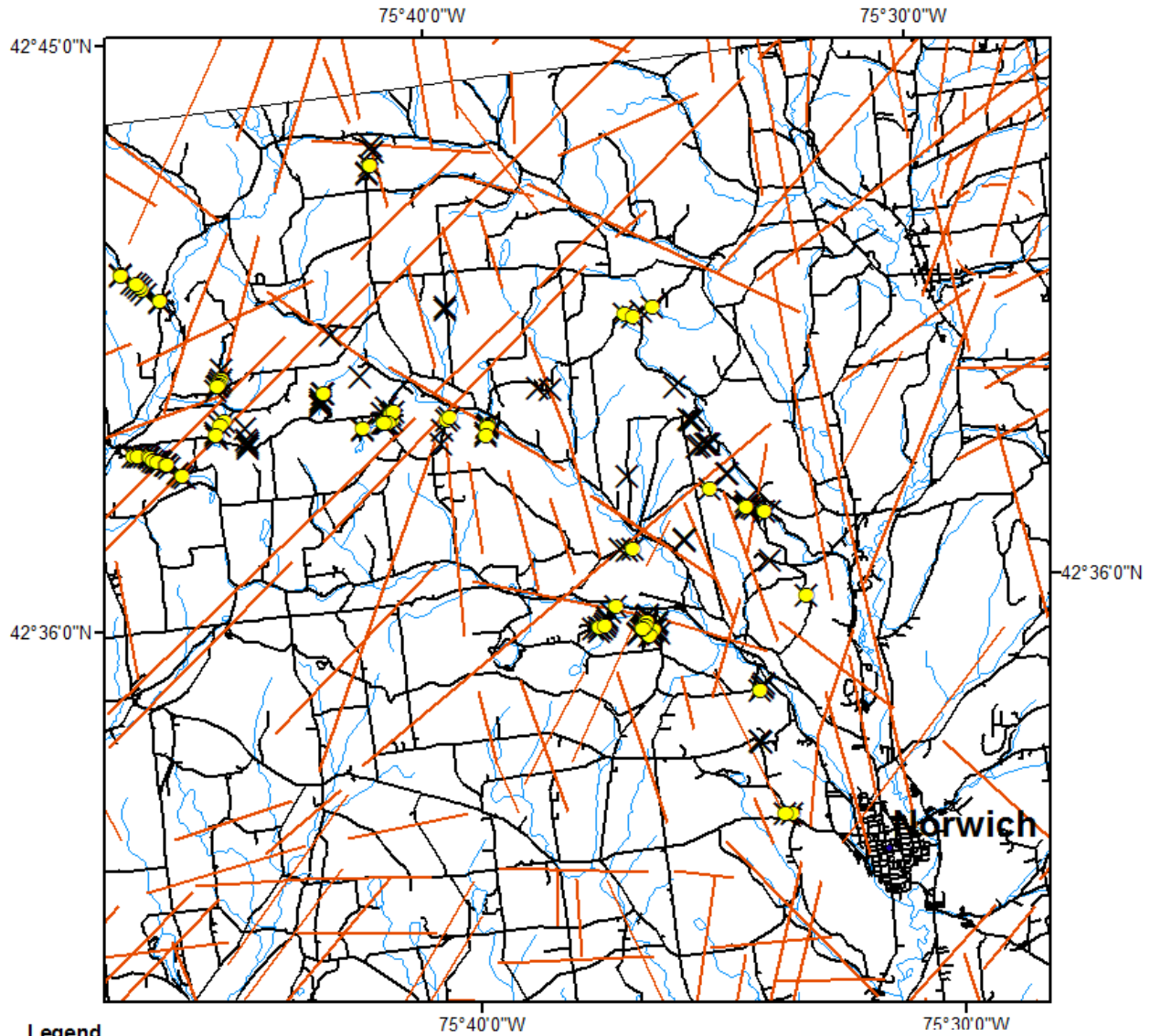
Figure 6.1-136.: North-central Chenango field sites exhibiting NE-striking fractures with a frequency of greater than 4 fractures/m. (Terech et al, 2005 and Jacobi, 2007b) Lineaments from EarthSat (1997).









**Remote Sensing Laboratory**  
Dept. of Geology, SUNY at Buffalo



**University at Buffalo**  
The State University of New York



**Legend**

-  AES
-  Nick\_NNE\_Less2
-  Nick\_Data
-  lineaments from EarthSat (1997)
-  Roads
-  Hydro

0 1.5 3 6 9 Kilometers

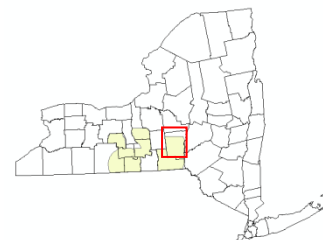


Figure 6.1-137. North-central Chenango field sites exhibiting NNE-striking fractures with a frequency of less than 2 fractures/m. (Terech et al, 2005 and Jacobi, 2007b) Lineaments from EarthSat (1997).





**Remote Sensing Laboratory**  
 Dept. of Geology, SUNY at Buffalo



**University at Buffalo**  
 The State University of New York

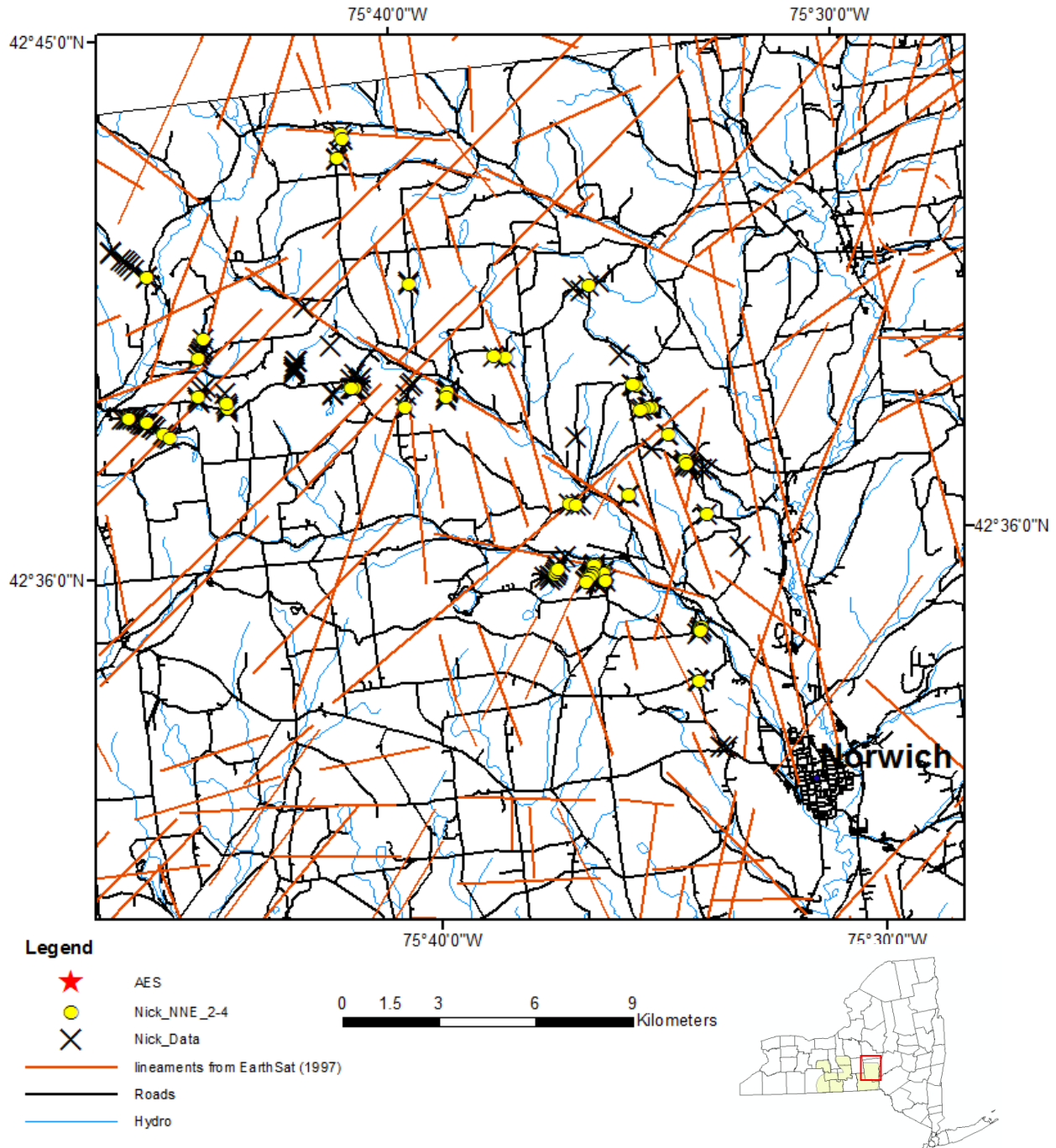


Figure 6.1-138. North-central Chenango field sites exhibiting NNE-striking fractures with a frequency of 2 to 4 fractures/m. (Terech et al, 2005 and Jacobi, 2007b) Lineaments from EarthSat (1997).



**Remote Sensing Laboratory**  
Dept. of Geology, SUNY at Buffalo



**University at Buffalo**  
The State University of New York

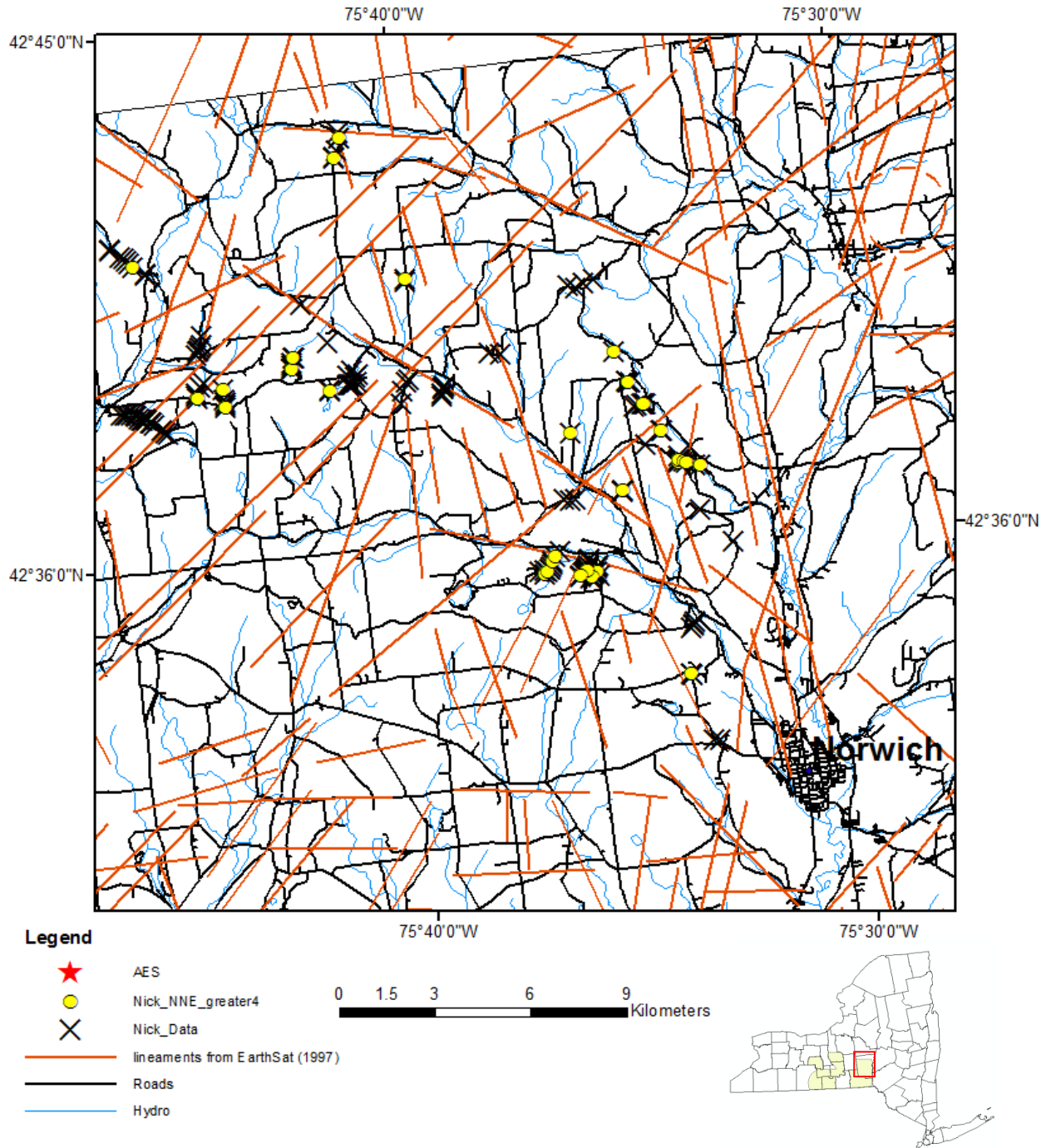


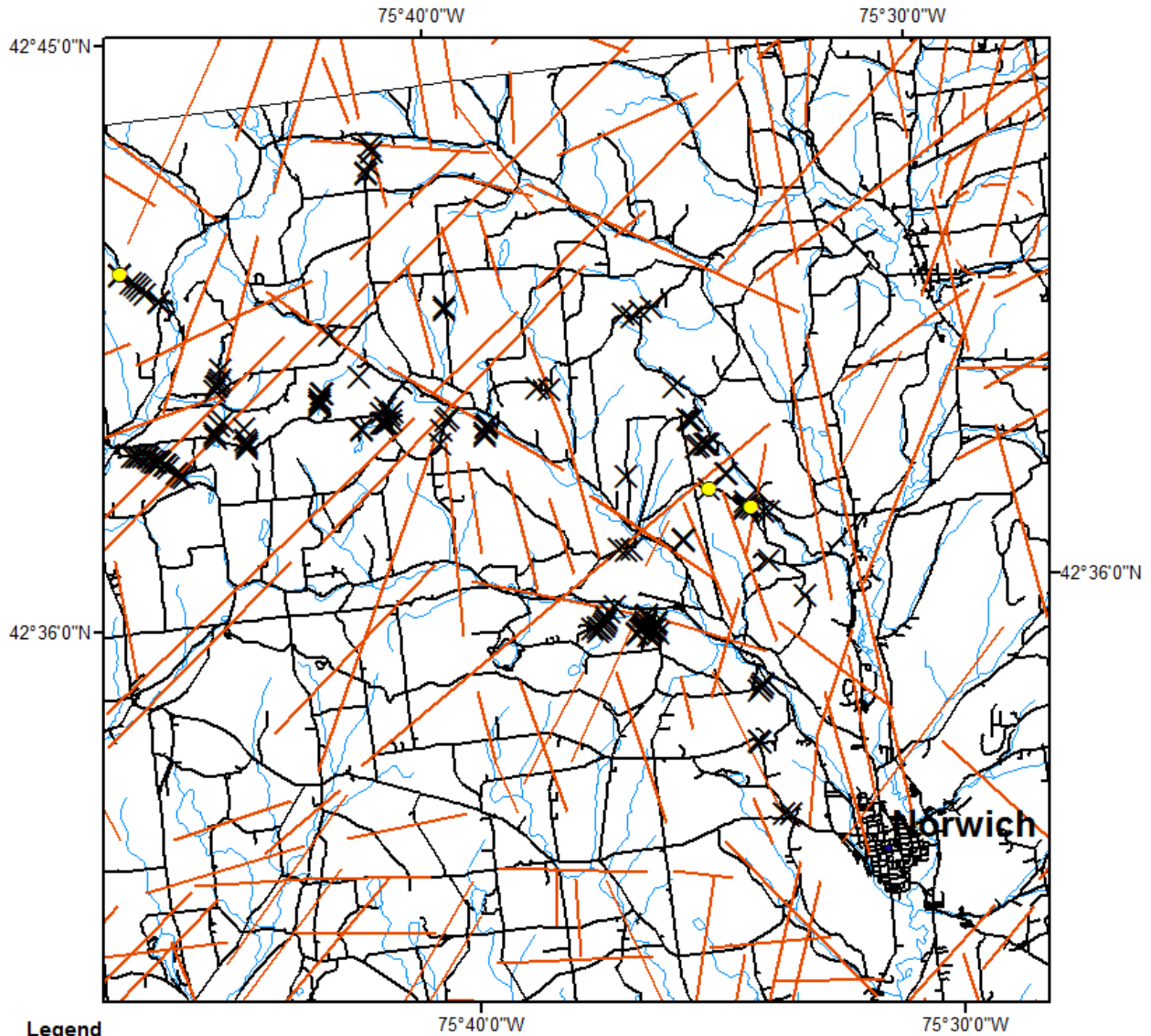
Figure 6.1-139. North-central Chenango field sites exhibiting NNE-striking fractures with a frequency of greater than 4 fractures/m. (Terech et al, 2005 and Jacobi, 2007b) Lineaments from EarthSat (1997).



**Remote Sensing Laboratory**  
Dept. of Geology, SUNY at Buffalo



**University at Buffalo**  
The State University of New York



**Legend**

- ★ AES
- Nick\_NNW\_Less2
- ✕ Nick\_Data
- lineaments from EarthSat (1997)
- Roads
- Hydro

0 1.5 3 6 9 Kilometers

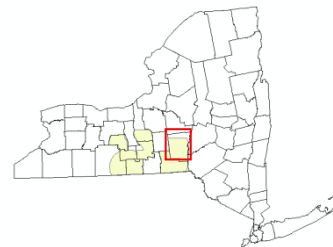


Figure 6.1-140. North-central Chenango field sites exhibiting NNW-striking fractures with a frequency of less than 2 fractures/m. (Terech et al, 2005 and Jacobi, 2007b) Lineaments from EarthSat (1997).



**Remote Sensing Laboratory**  
Dept. of Geology, SUNY at Buffalo



**University at Buffalo**  
The State University of New York

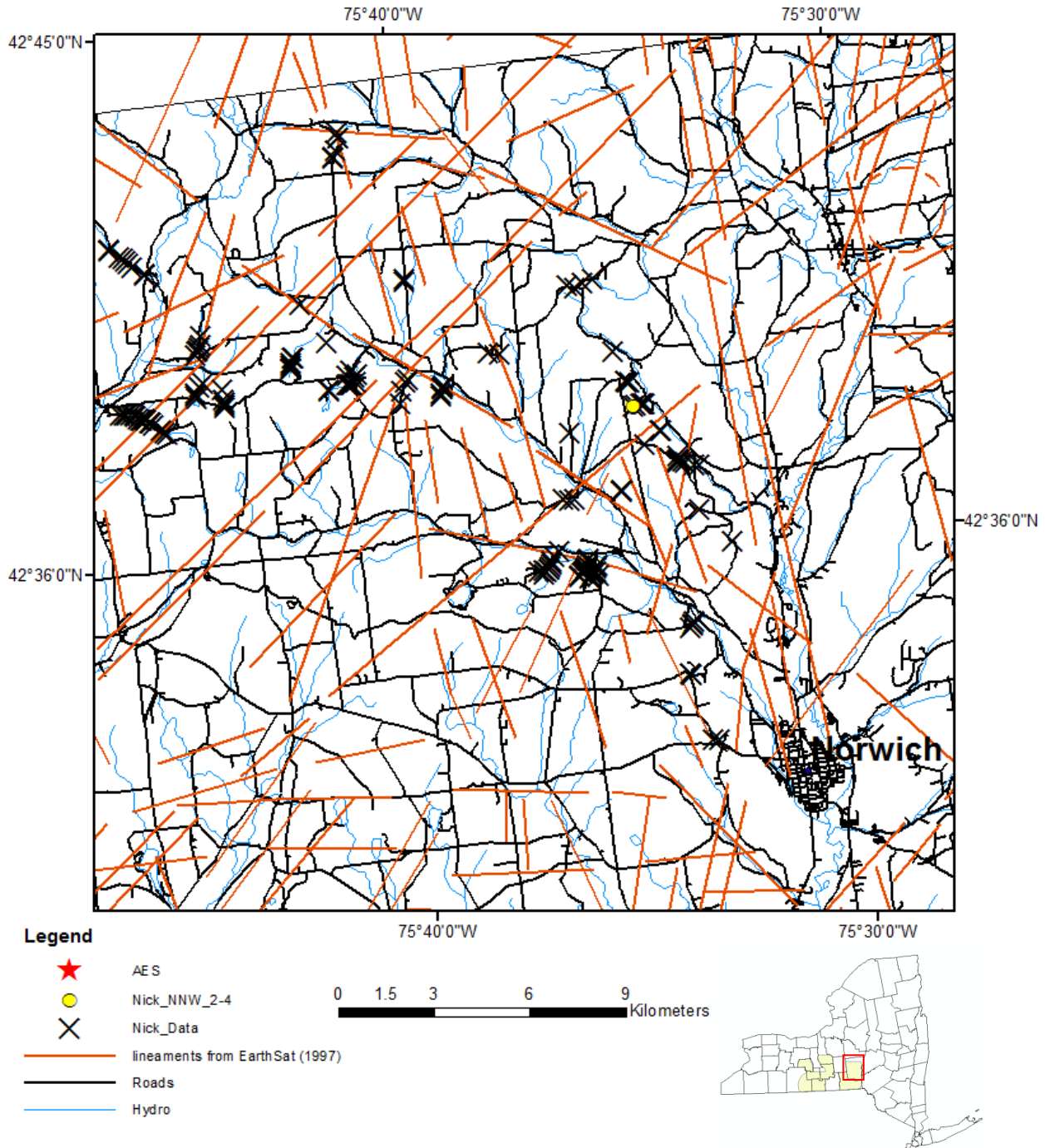


Figure 6.1-141. North-central Chenango field sites exhibiting NNW-striking fractures with a frequency of 2 to 4 fractures/m. (Terech et al, 2005 and Jacobi, 2007b) Lineaments from EarthSat (1997).

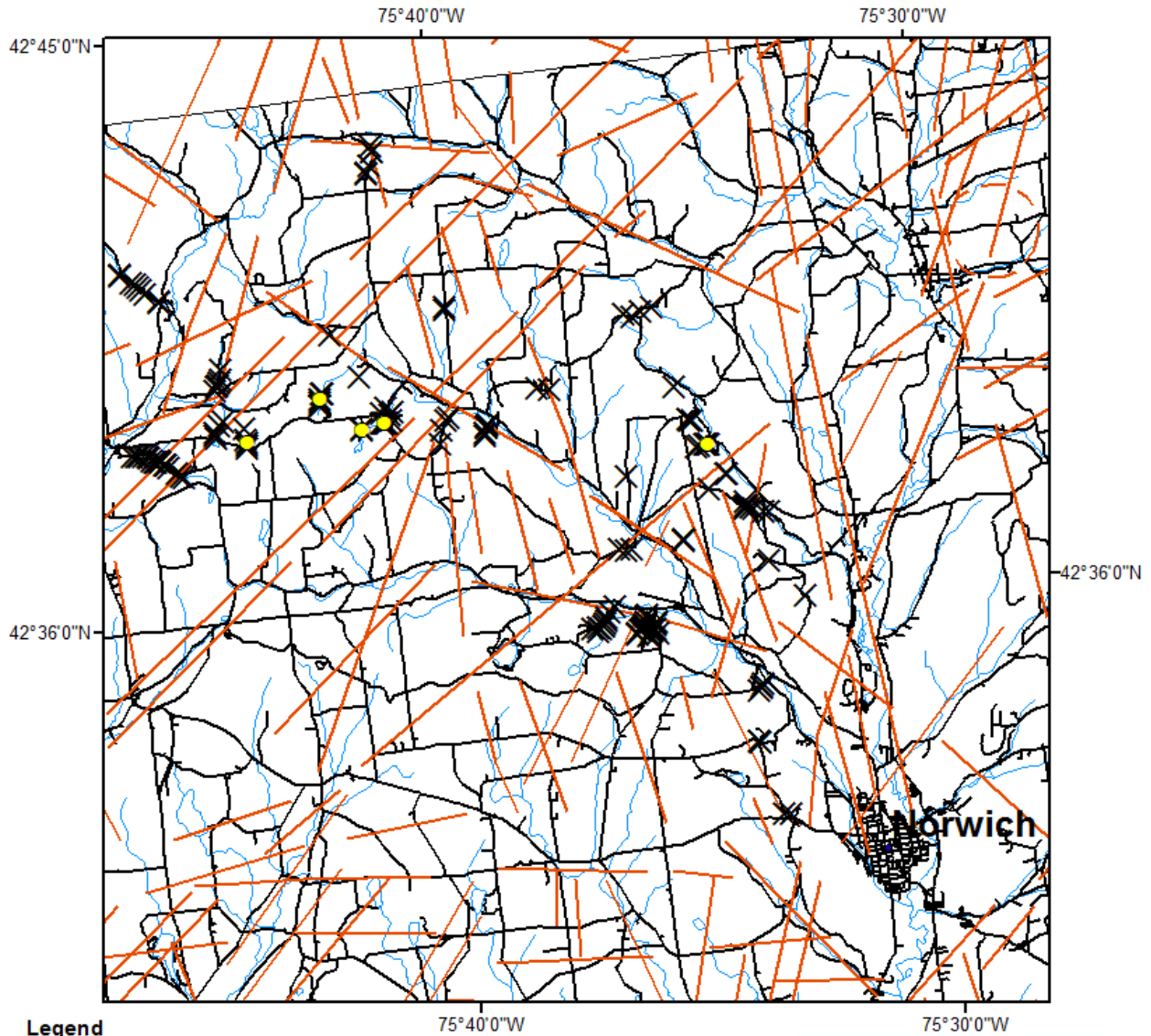




**Remote Sensing Laboratory**  
Dept. of Geology, SUNY at Buffalo



**University at Buffalo**  
The State University of New York



**Legend**

- AES
- Nick\_NNW\_greater4
- Nick\_Data
- lineaments from EarthSat (1997)
- Roads
- Hydro

0 1.5 3 6 9 Kilometers



Figure 6.1-142. North-central Chenango field sites exhibiting NNW-striking fractures with a frequency of greater than 4 fractures/m. (Terech et al, 2005 and Jacobi, 2007b) Lineaments from EarthSat (1997).



**Remote Sensing Laboratory**  
Dept. of Geology, SUNY at Buffalo



**University at Buffalo**  
The State University of New York

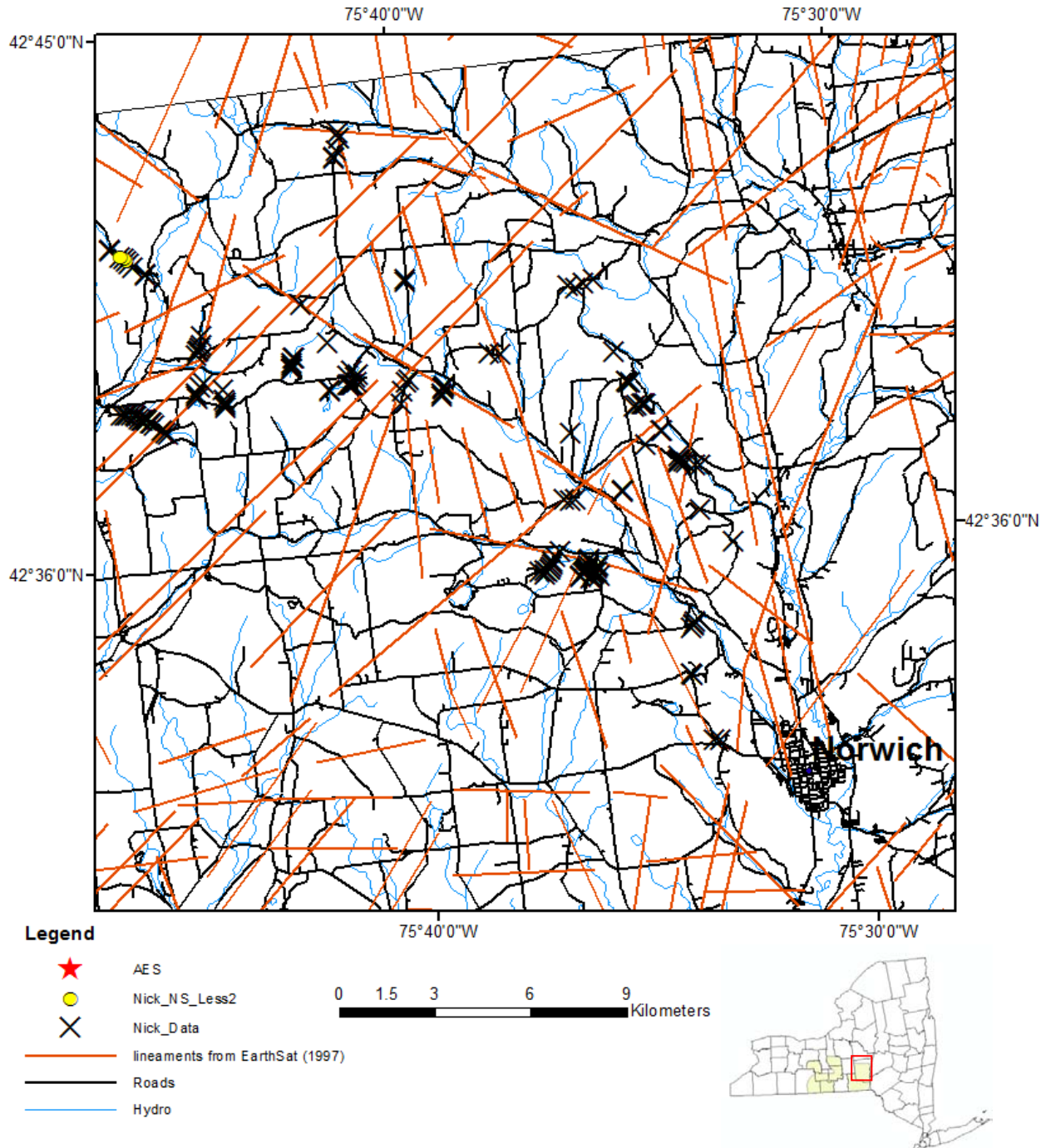


Figure 6.1-143. North-central Chenango field sites exhibiting NS-striking fractures with a frequency of less than 2 fractures/m. (Terech et al, 2005 and Jacobi, 2007b) Lineaments from EarthSat (1997).



**Remote Sensing Laboratory**  
Dept. of Geology, SUNY at Buffalo



**University at Buffalo**  
The State University of New York

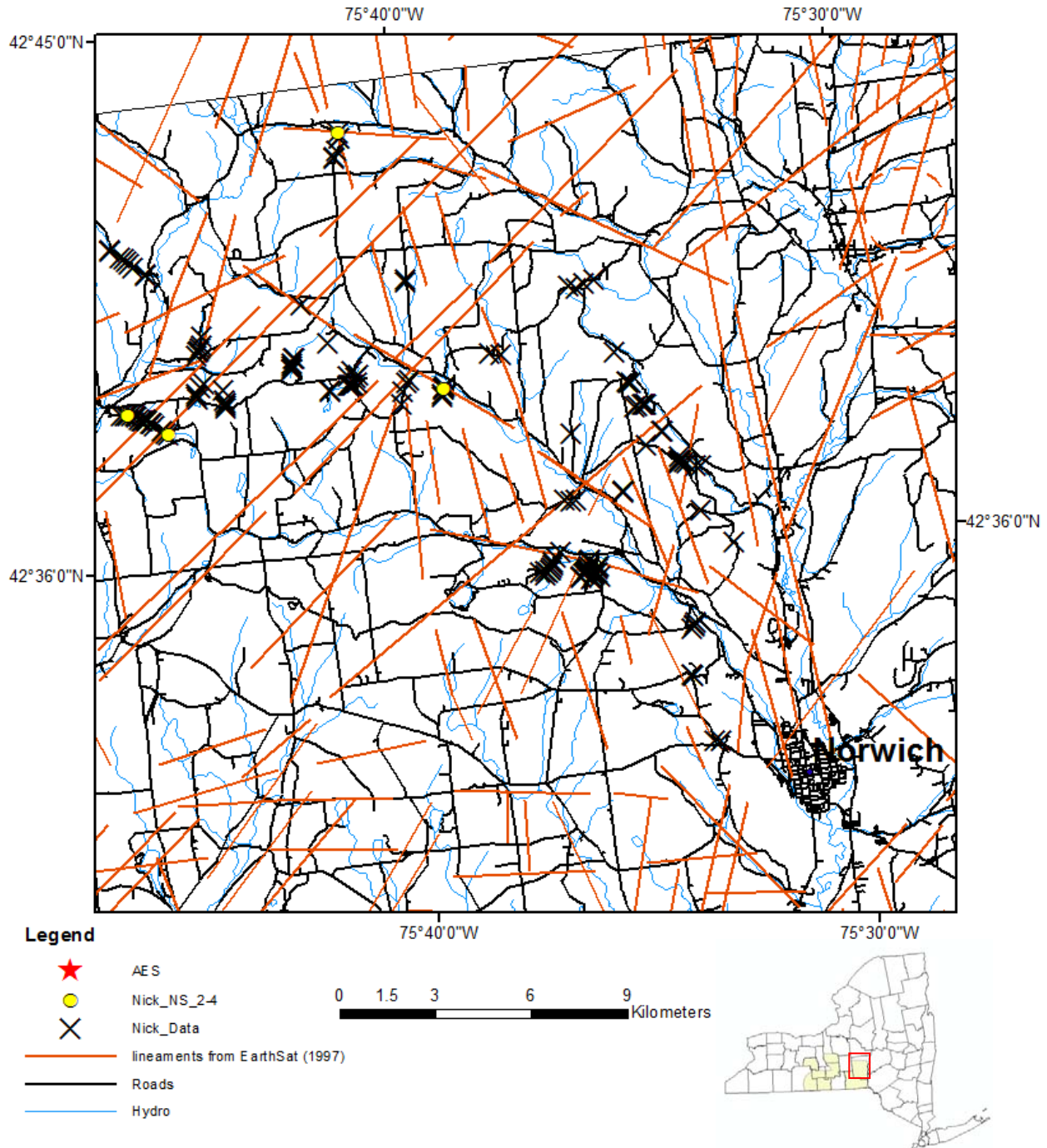


Figure 6.1-144. North-central Chenango field sites exhibiting NS-striking fractures with a frequency of 2 to 4 fractures/m. (Terech et al, 2005 and Jacobi, 2007b) Lineaments from EarthSat (1997).





**Remote Sensing Laboratory**  
Dept. of Geology, SUNY at Buffalo



**University at Buffalo**  
The State University of New York

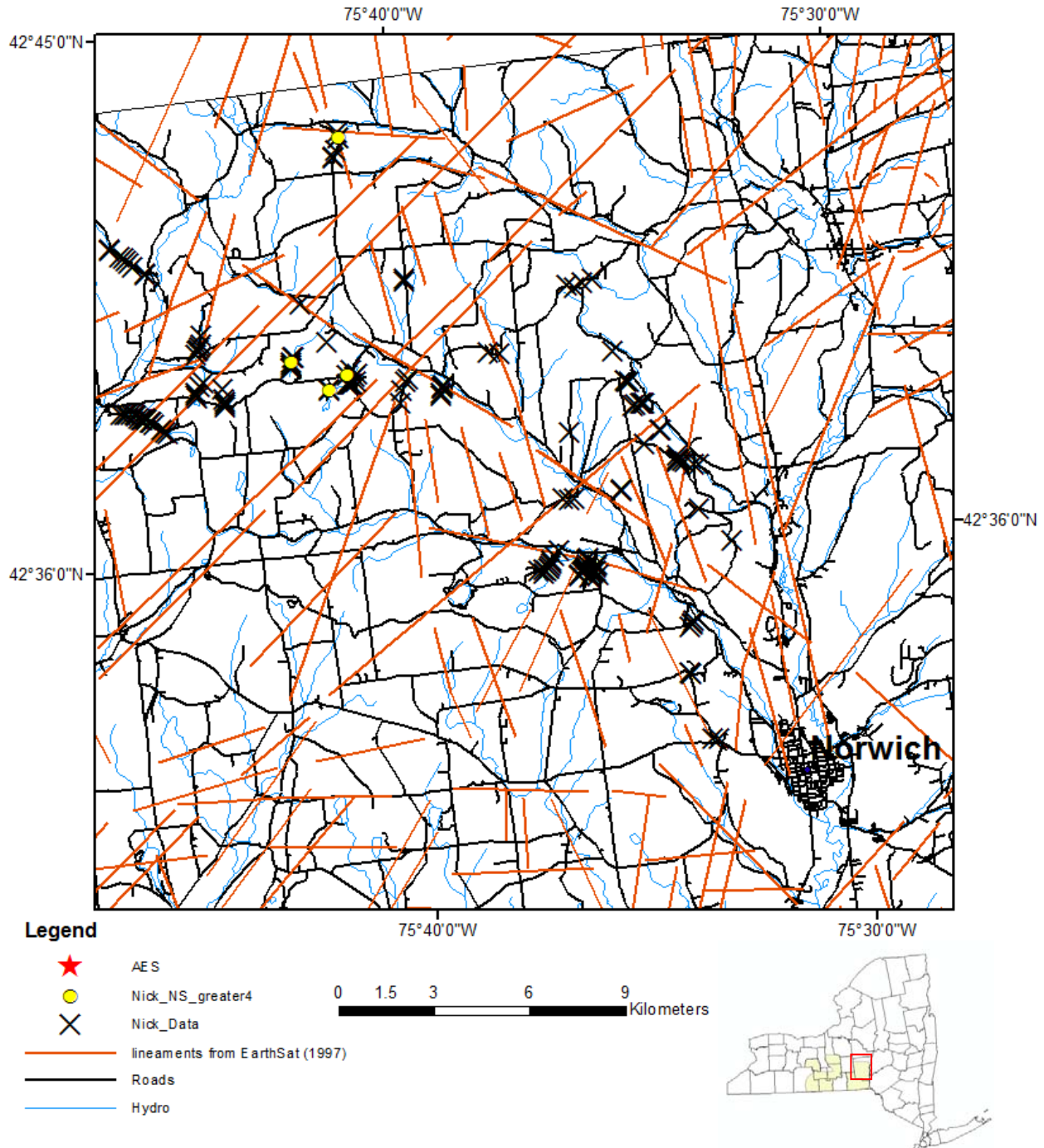


Figure 6.1-145. North-central Chenango field sites exhibiting NS-striking fractures with a frequency of greater than 4 fractures/m. (Terech et al, 2005 and Jacobi, 2007b) Lineaments from EarthSat (1997).



**Remote Sensing Laboratory**  
Dept. of Geology, SUNY at Buffalo



**University at Buffalo**  
The State University of New York

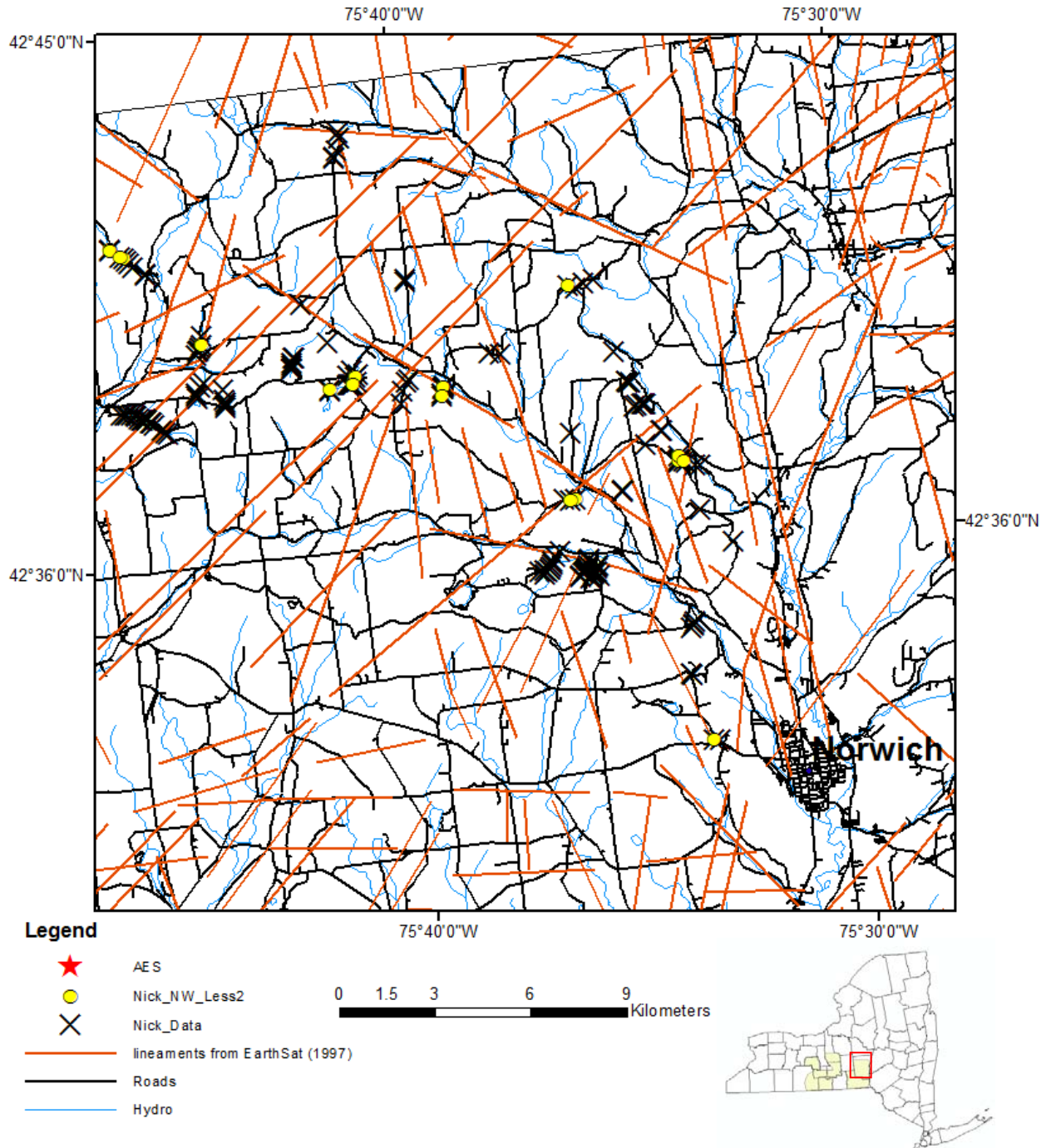


Figure 6.1-146. North-central Chenango field sites exhibiting NW-striking fractures with a frequency of less than 2 fractures/m. (Terech et al, 2005 and Jacobi, 2007b) Lineaments from EarthSat (1997).



**Remote Sensing Laboratory**  
Dept. of Geology, SUNY at Buffalo



**University at Buffalo**  
The State University of New York

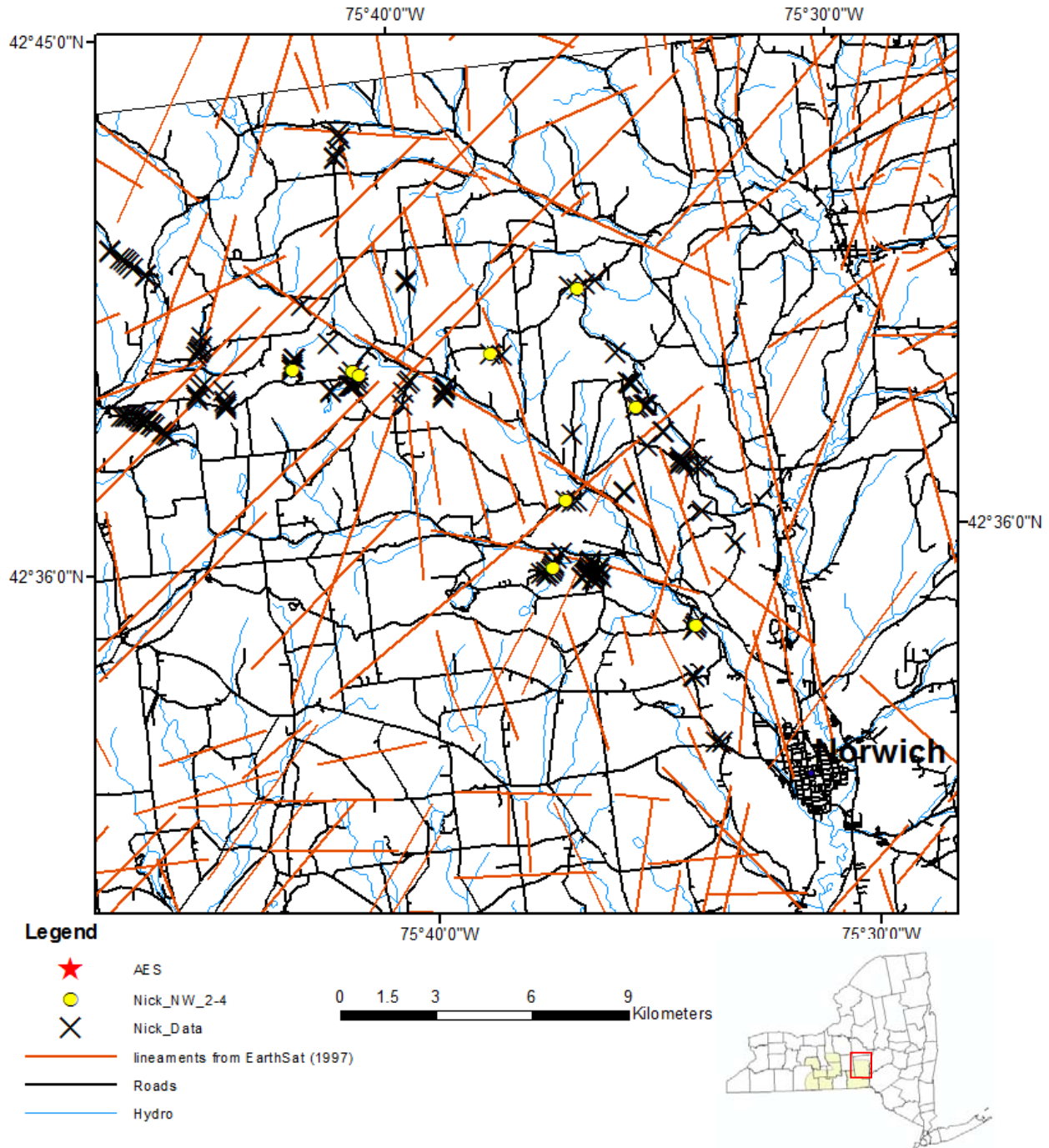


Figure 6.1-147. North-central Chenango field sites exhibiting NW-striking fractures with a frequency of 2 to 4 fractures /m. (Terech et al, 2005 and Jacobi, 2007b) Lineaments from EarthSat (1997).



**Remote Sensing Laboratory**  
Dept. of Geology, SUNY at Buffalo



**University at Buffalo**  
The State University of New York

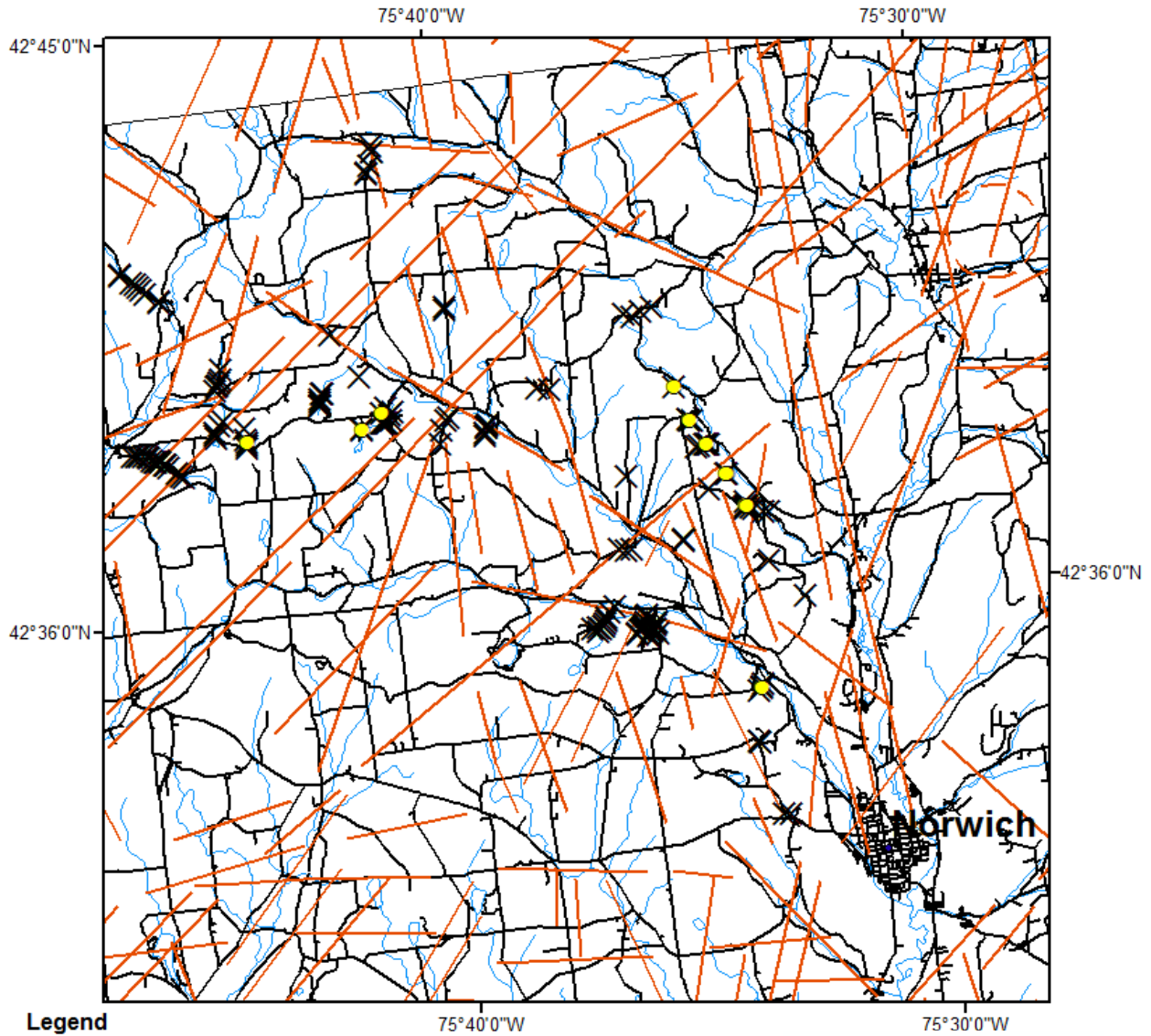


Figure 6.1-148. North-central Chenango field sites exhibiting NW-striking fractures with a frequency of greater than 4 fractures /m. (Terech et al, 2005 and Jacobi, 2007b) Lineaments from EarthSat (1997).





**Remote Sensing Laboratory**  
Dept. of Geology, SUNY at Buffalo



**University at Buffalo**  
The State University of New York

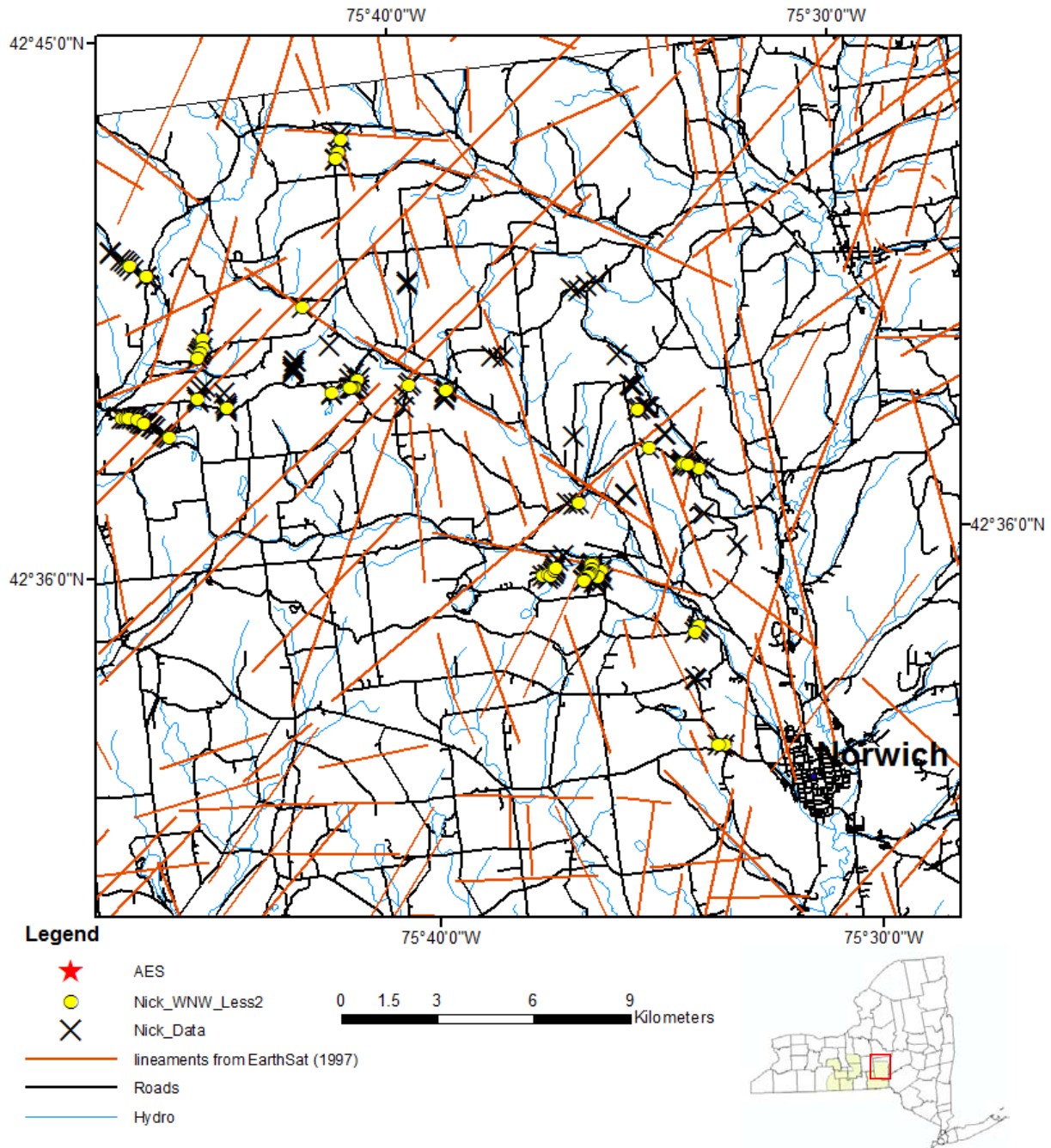


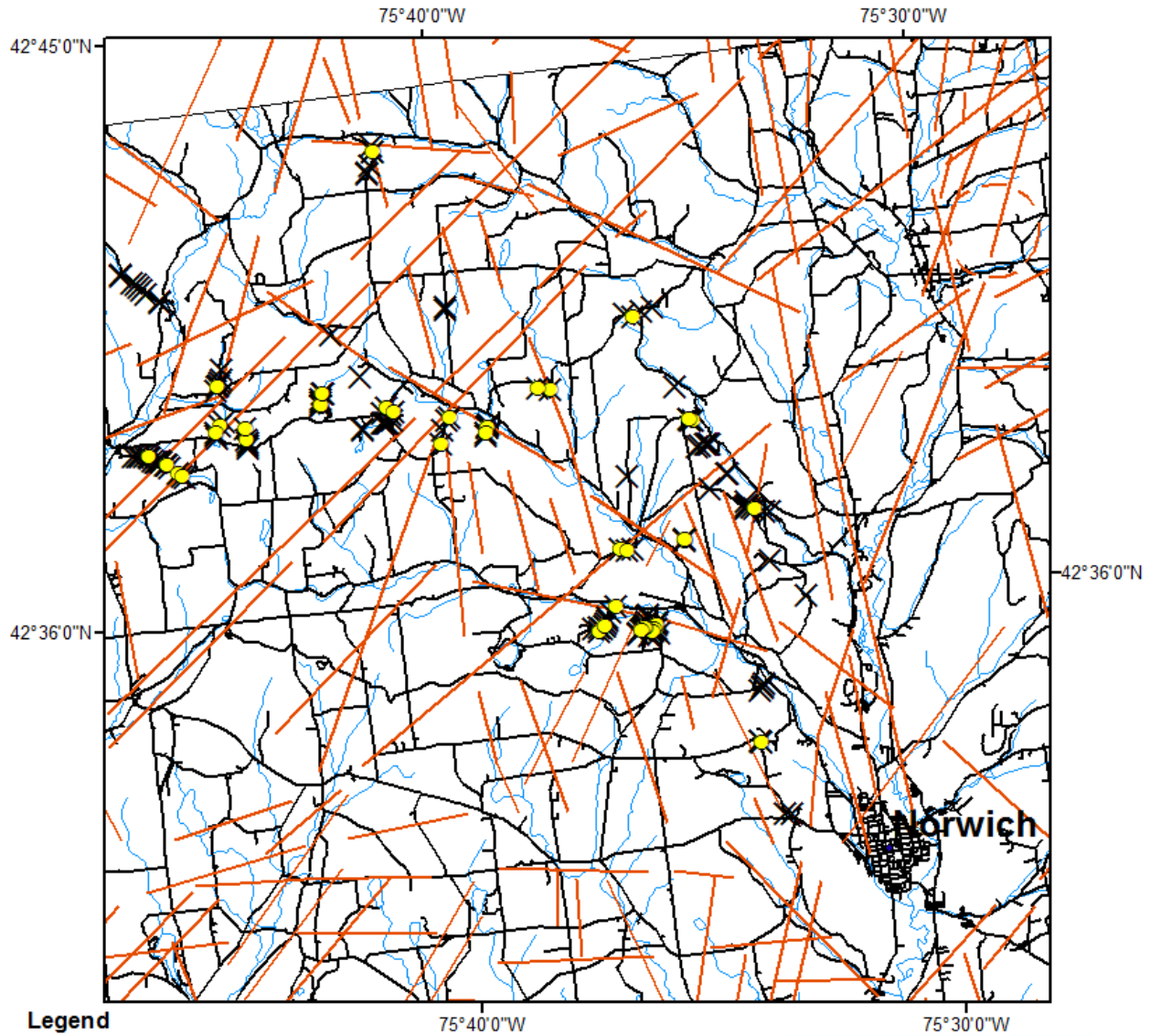
Figure 6.1-149. North-central Chenango field sites exhibiting WNW-striking fractures with a frequency of less than 2 fractures/m. (Terech et al, 2005 and Jacobi, 2007b) Lineaments from EarthSat (1997).



**Remote Sensing Laboratory**  
Dept. of Geology, SUNY at Buffalo



**University at Buffalo**  
The State University of New York



**Legend**

- ★ AES
- Nick\_WNW\_2-4
- ✕ Nick\_Data
- lineaments from EarthSat (1997)
- Roads
- Hydro

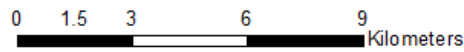


Figure 6.1-150. North-central Chenango field sites exhibiting WNW-striking fractures with a frequency of 2 to 4 fractures/m. (Terech et al, 2005 and Jacobi, 2007b) Lineaments from EarthSat (1997).



**Remote Sensing Laboratory**  
Dept. of Geology, SUNY at Buffalo



**University at Buffalo**  
The State University of New York

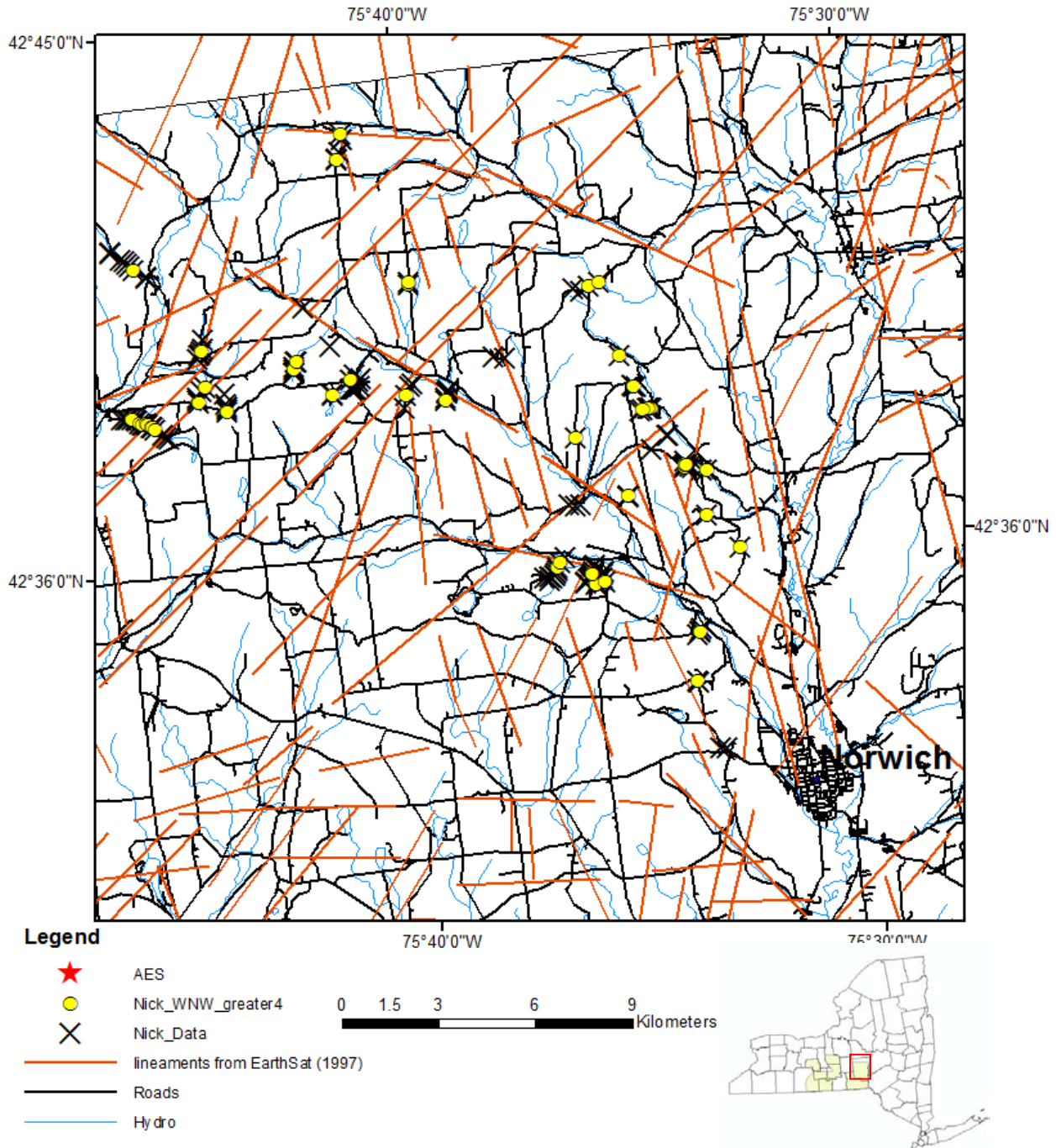


Figure 6.1-151. North-central Chenango field sites exhibiting WNW-striking fractures with a frequency of greater than 4 fractures/m. (Terech et al, 2005 and Jacobi, 2007b) Lineaments from EarthSat (1997).



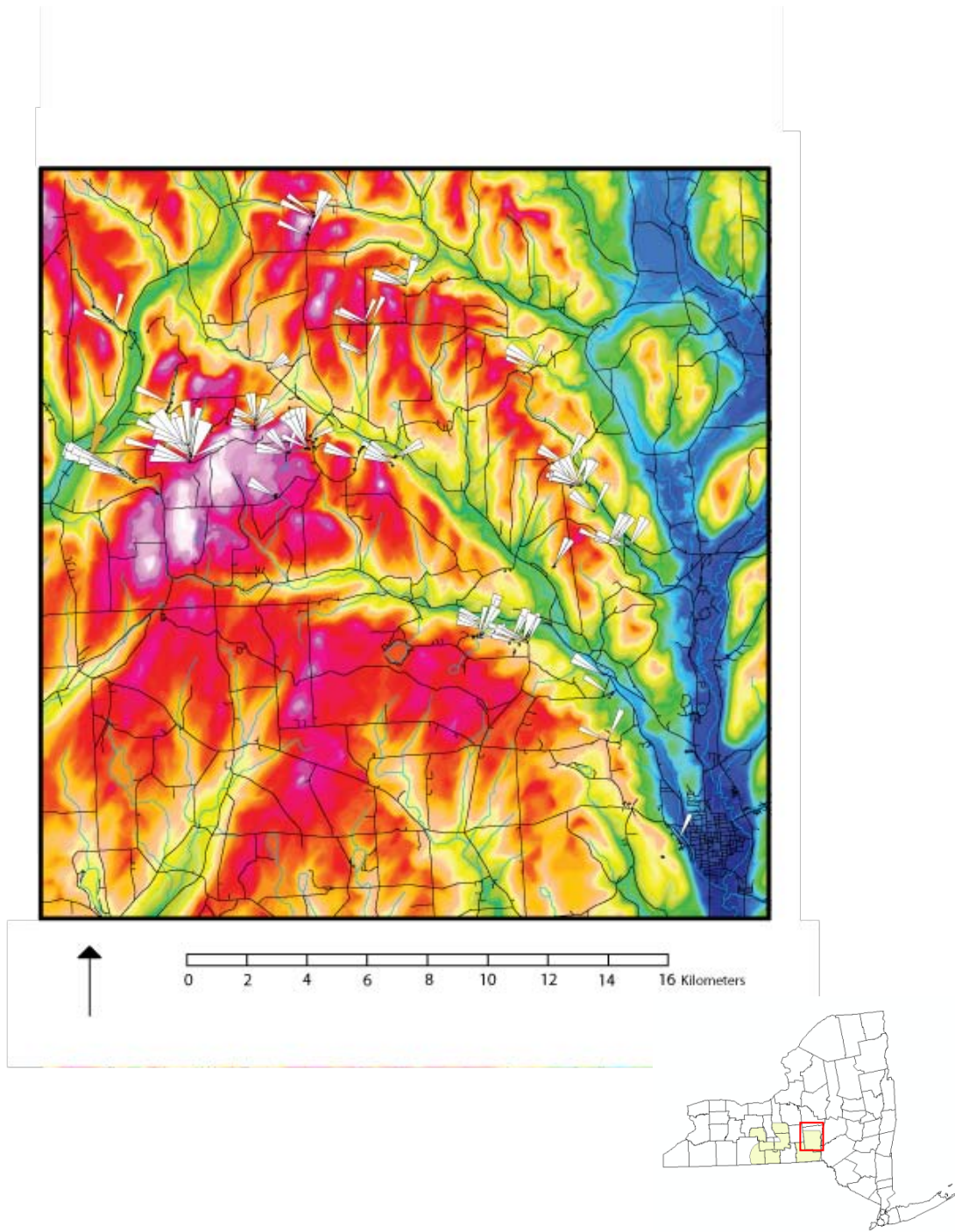


Figure 6.1-152. North-central Chenango field sites showing rose diagrams of fracture intensification domains (Jacobi, 2007b).

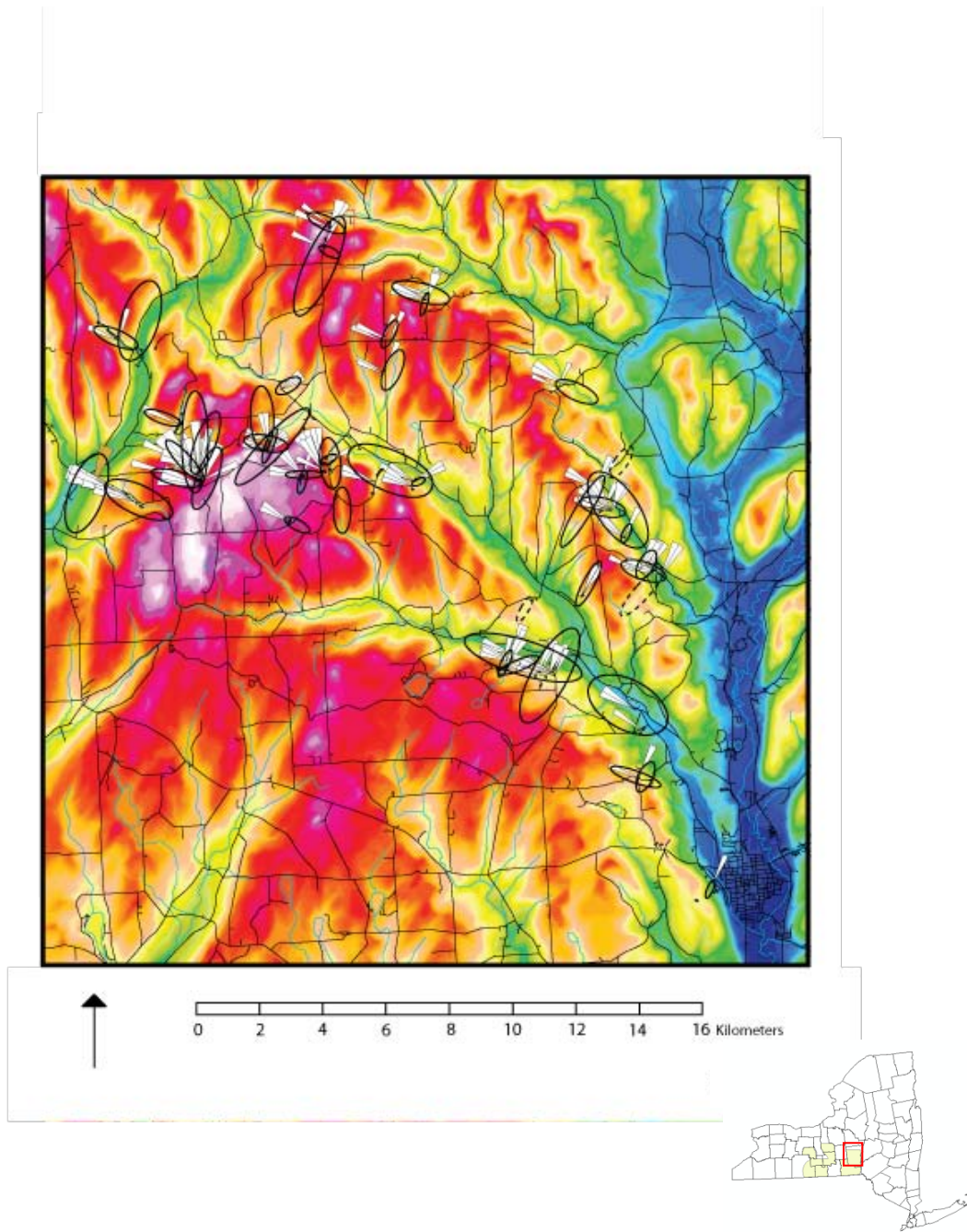


Figure 6.1.-153. North-central Chenango field sites showing associated rose diagrams of fracture intensification domains on top of a shaded DEM with ellipses highlighting prominent fracture orientations that are consonant with the topographic lineaments (Jacobi, 2007b).



**Remote Sensing Laboratory**  
Dept. of Geology, SUNY at Buffalo



**University at Buffalo**  
The State University of New York

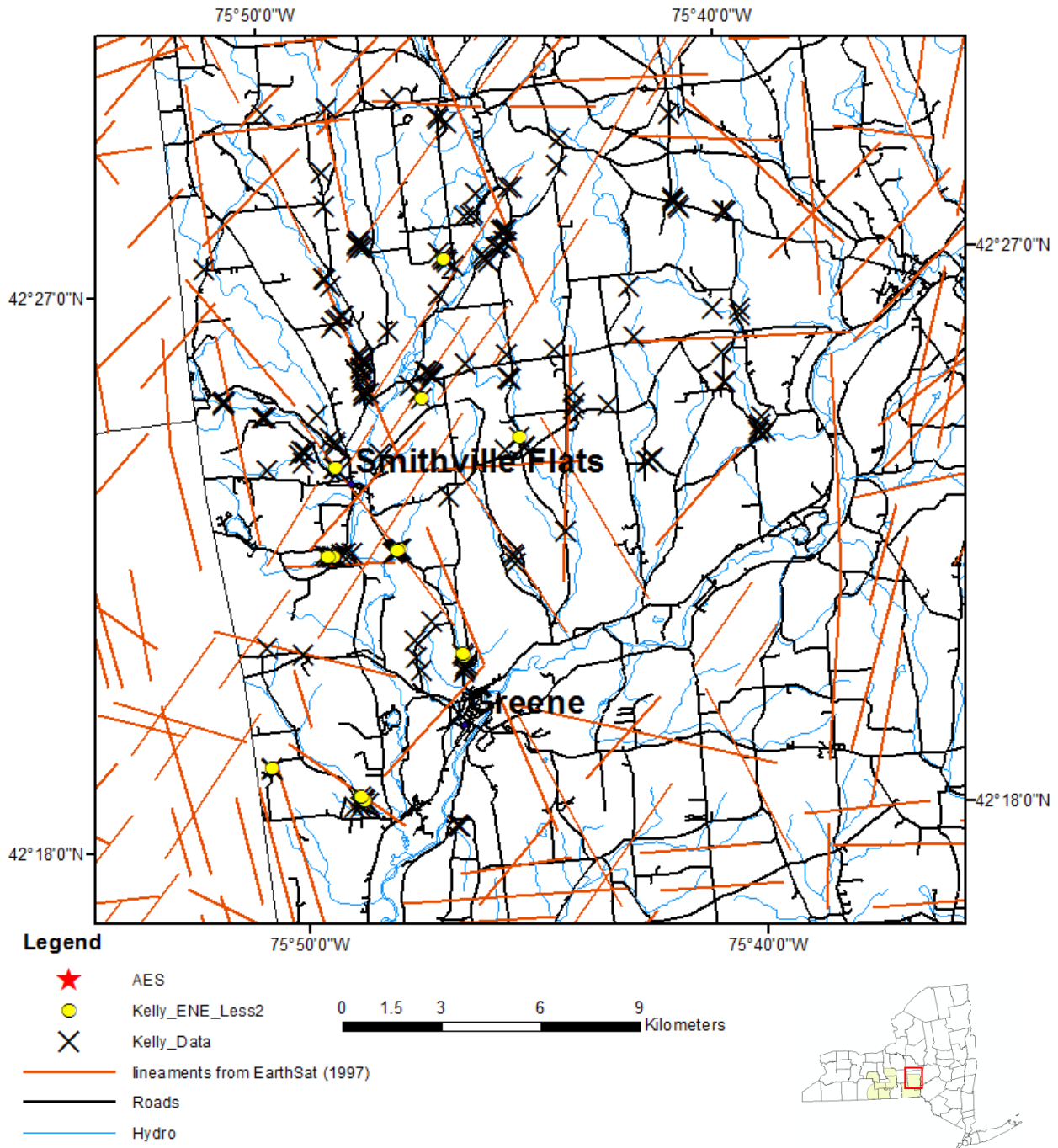


Figure 6.1-154. Southwestern Chenango field sites exhibiting ENE-striking fractures with a frequency of less than 2 fractures/m. (McGuire, 2006 and Jacobi, 2007b) Lineaments from EarthSat (1997).





**Remote Sensing Laboratory**  
Dept. of Geology, SUNY at Buffalo



**University at Buffalo**  
The State University of New York

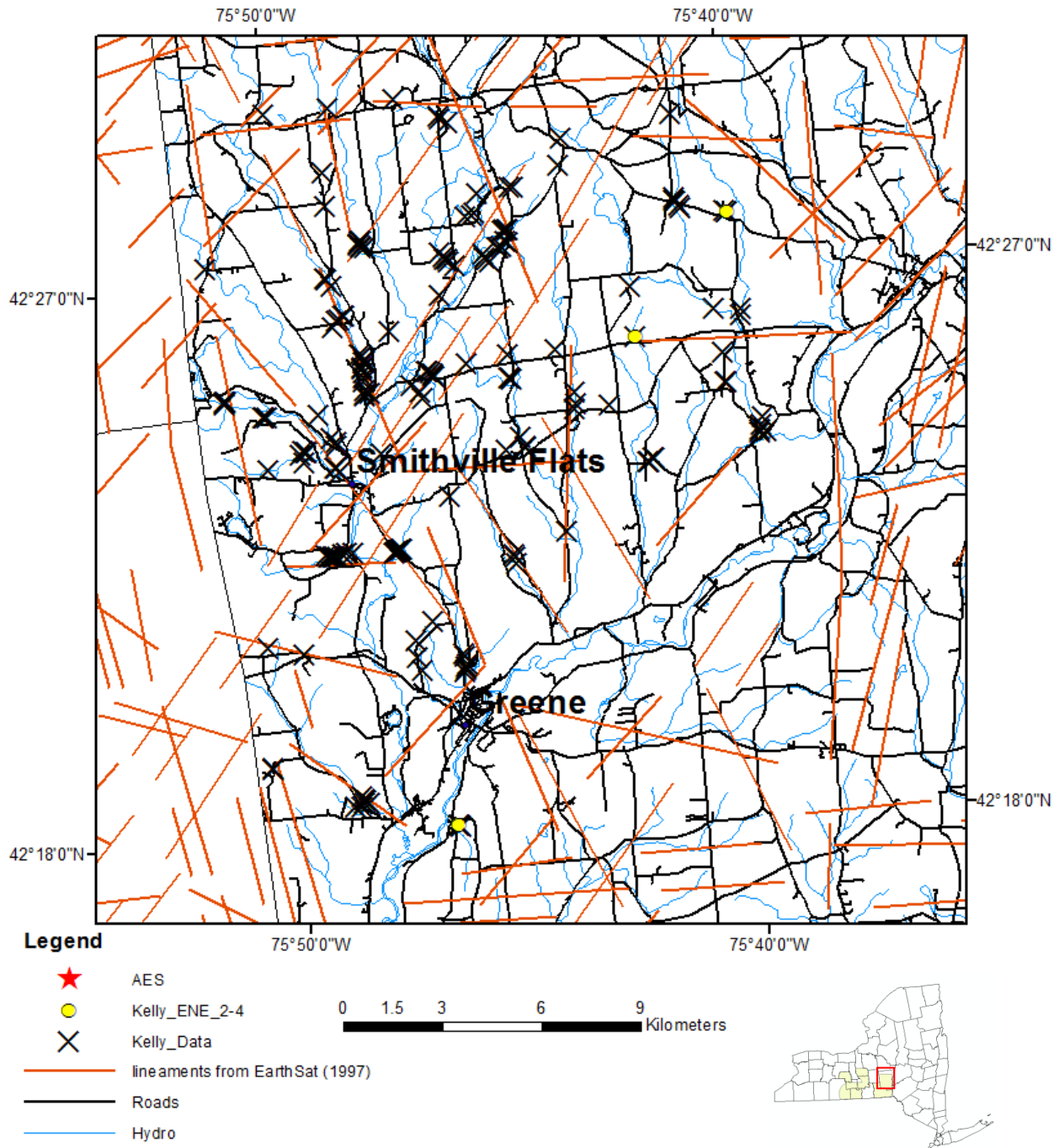


Figure 6.1-155. Southwestern Chenango field sites exhibiting ENE-striking fractures with a frequency of 2 to 4 fractures/m. (McGuire, 2006 and Jacobi, 2007b) Lineaments from EarthSat (1997).



**Remote Sensing Laboratory**  
Dept. of Geology, SUNY at Buffalo



**University at Buffalo**  
The State University of New York

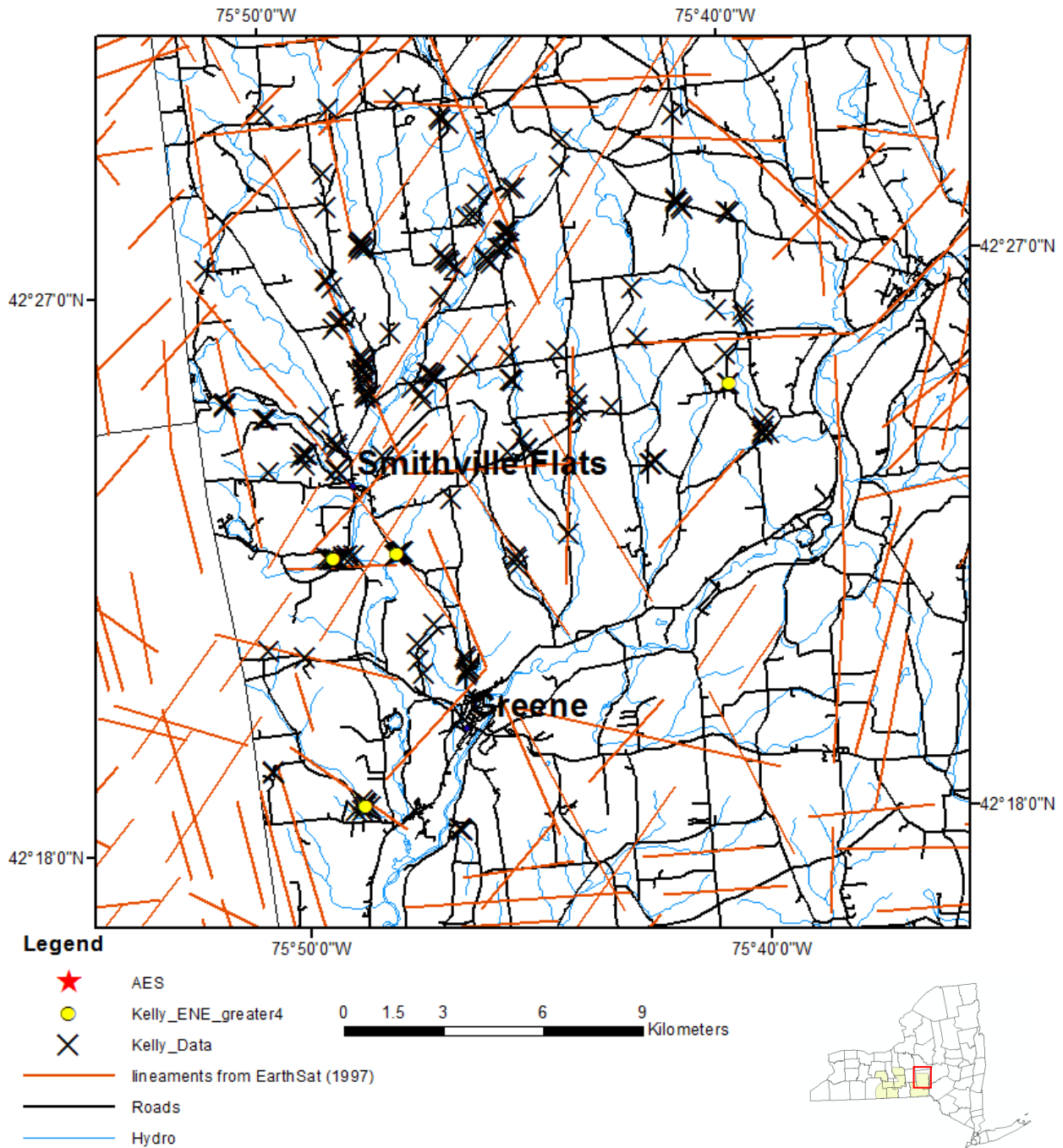


Figure 6.1-156. Southwestern Chenango field sites exhibiting ENE-striking fractures with a frequency of greater than 4 fractures/m. (McGuire, 2006 and Jacobi, 2007b) Lineaments from EarthSat (1997).



**Remote Sensing Laboratory**  
Dept. of Geology, SUNY at Buffalo



**University at Buffalo**  
The State University of New York

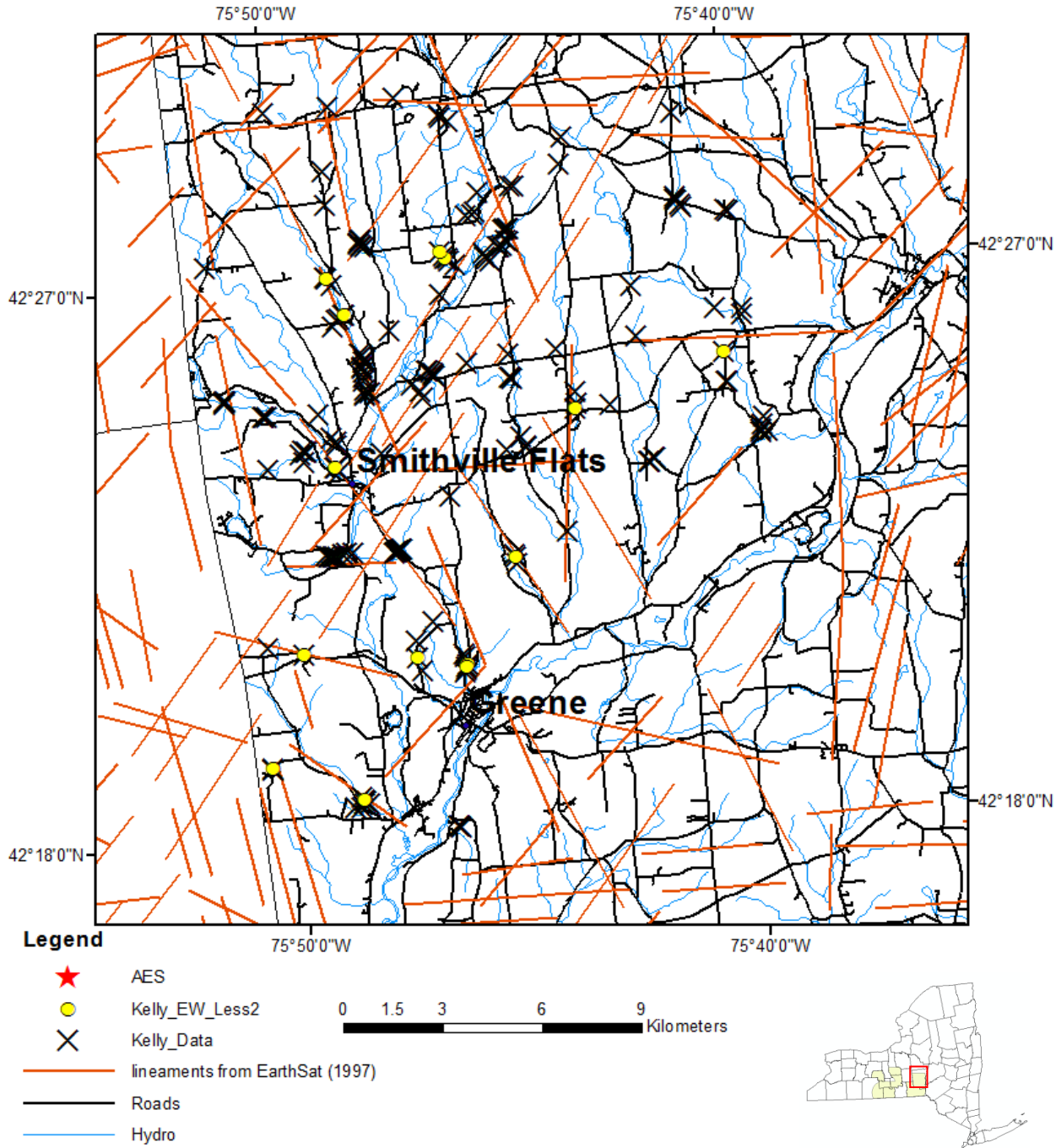


Figure 6.1-157. Southwestern Chenango field sites exhibiting EW-striking fractures with a frequency of less than 2 fractures/m. (McGuire, 2006 and Jacobi, 2007b) Lineaments from EarthSat (1997).



**Remote Sensing Laboratory**  
Dept. of Geology, SUNY at Buffalo



**University at Buffalo**  
The State University of New York

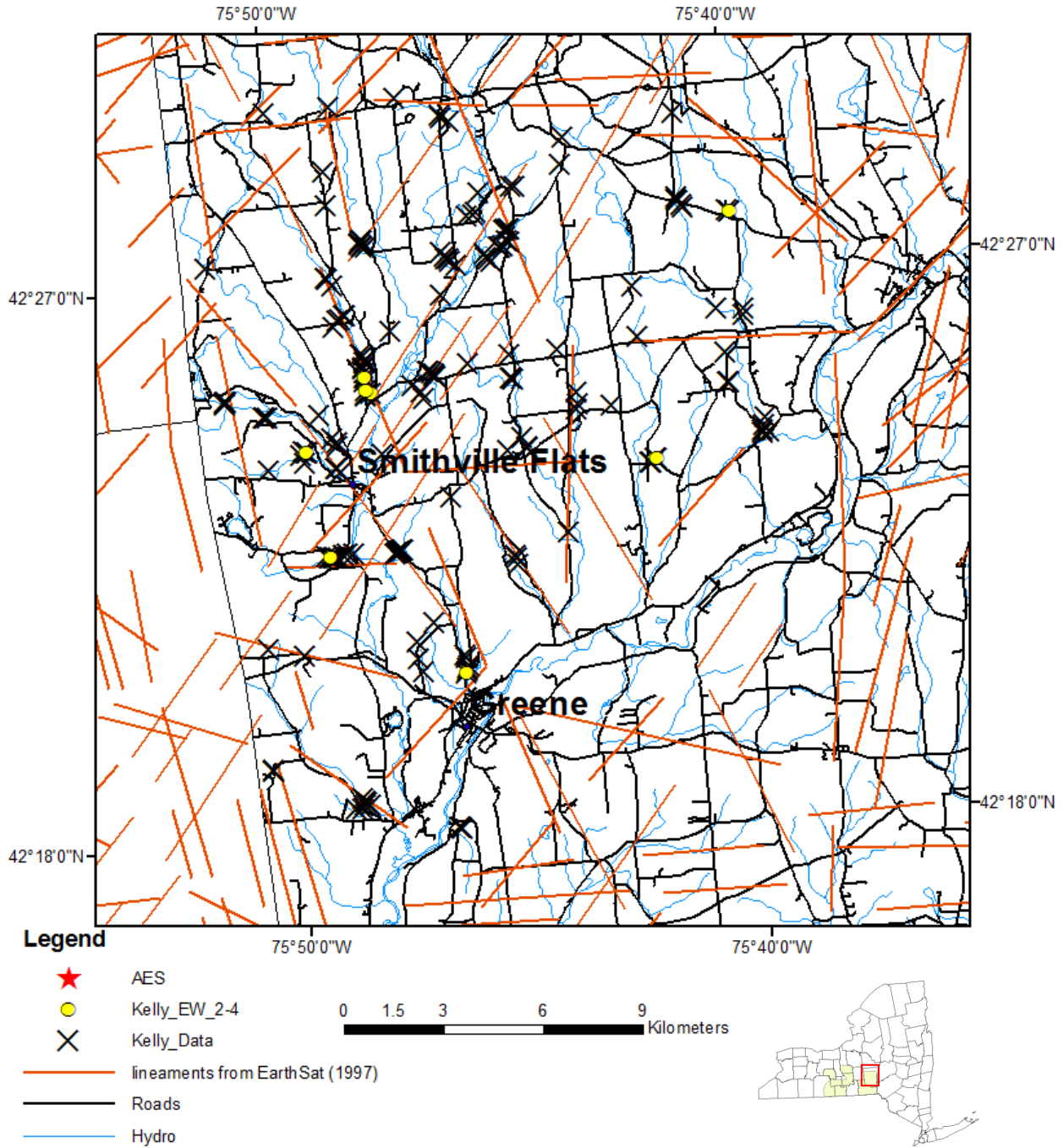


Figure 6.1-158. Southwestern Chenango field sites exhibiting EW-striking fractures with a frequency of 2 to 4 fractures/m. (McGuire, 2006 and Jacobi, 2007b) Lineaments from EarthSat (1997).





**Remote Sensing Laboratory**  
Dept. of Geology, SUNY at Buffalo



**University at Buffalo**  
The State University of New York

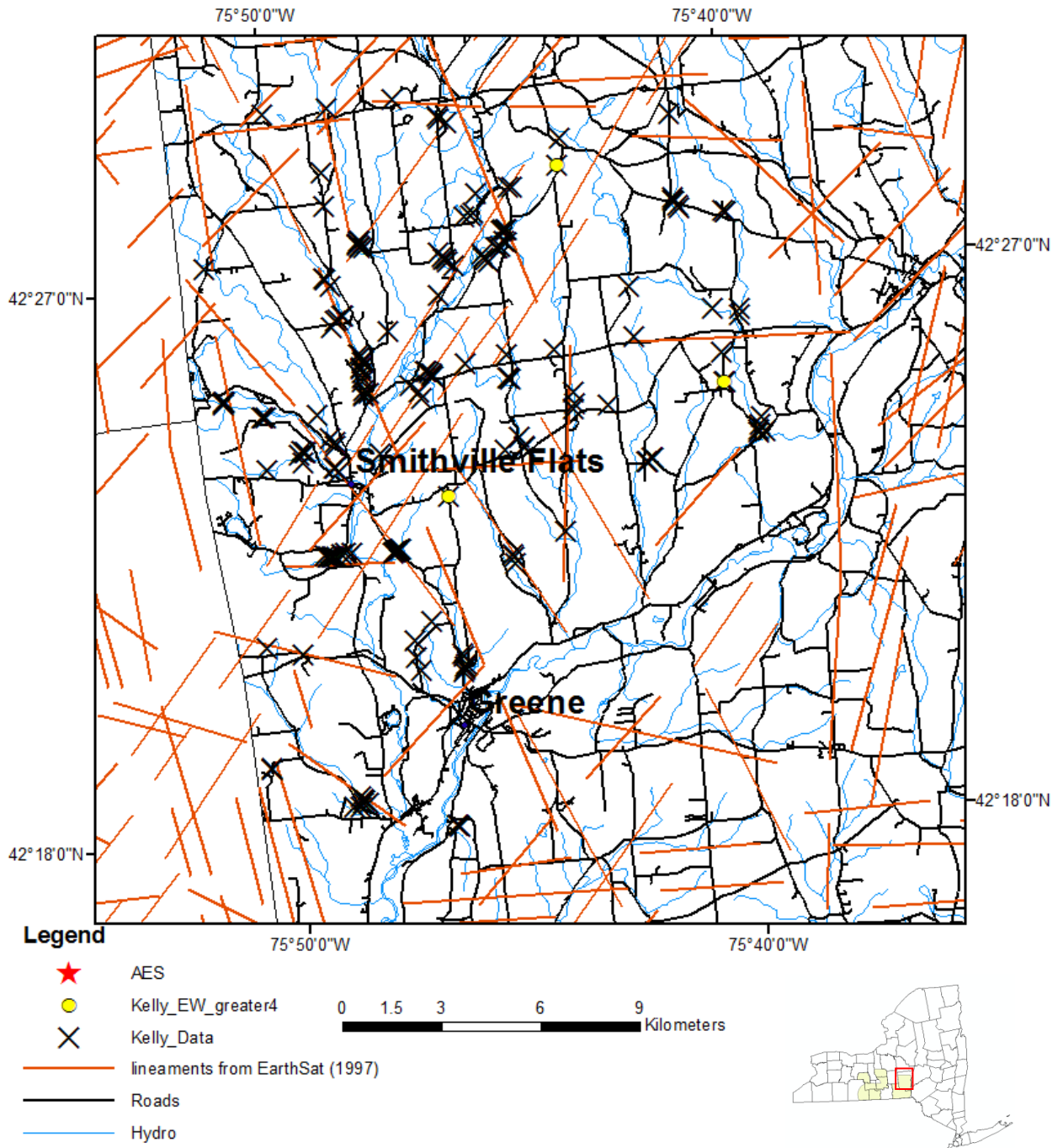


Figure 6.1-159.: Southwestern Chenango field sites exhibiting EW-striking fractures with a frequency of greater than 4 fractures/m. (McGuire, 2006 and Jacobi, 2007b) Lineaments from EarthSat (1997).



**Remote Sensing Laboratory**  
Dept. of Geology, SUNY at Buffalo



**University at Buffalo**  
The State University of New York

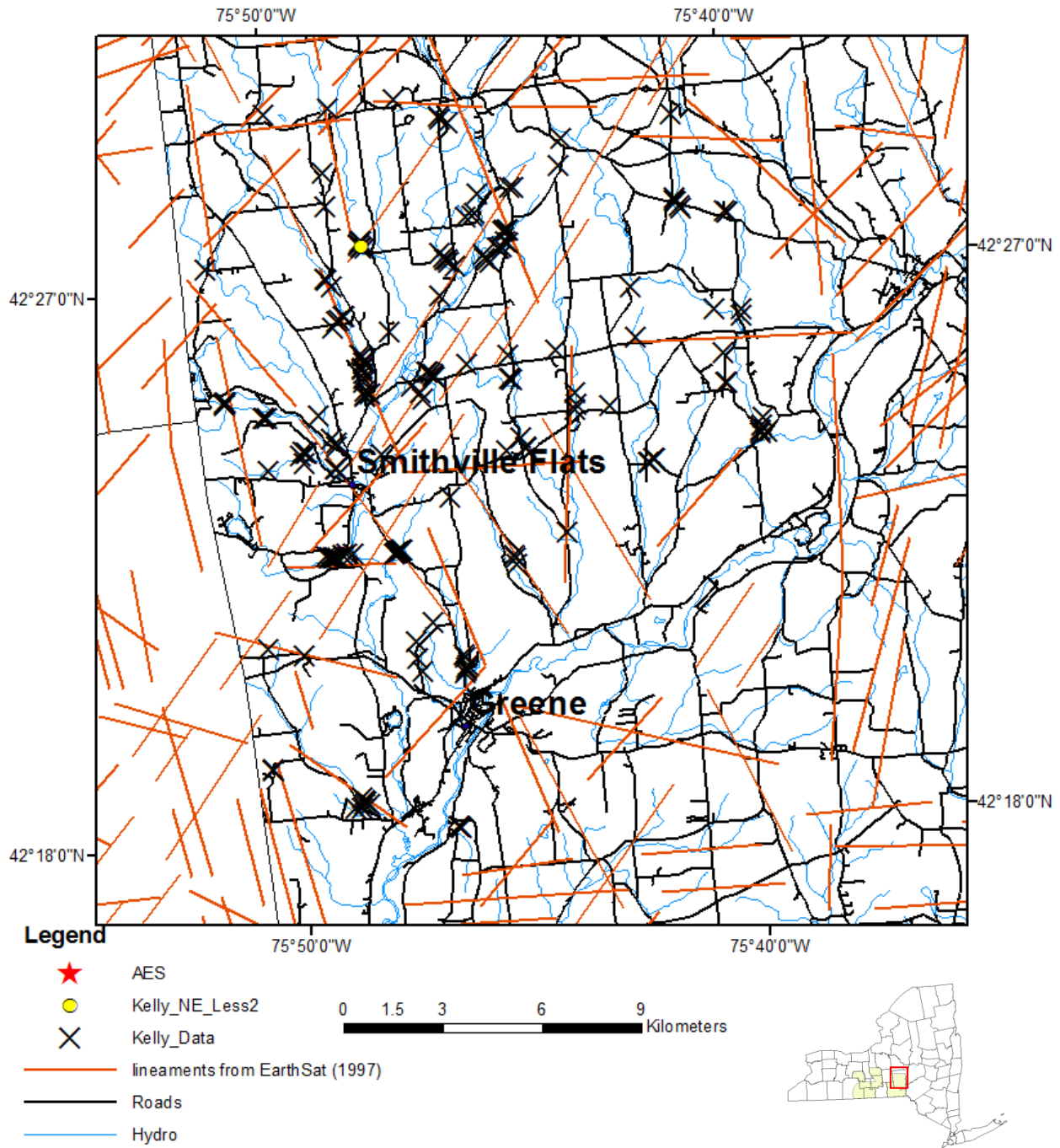


Figure 6.1-160. Southwestern Chenango field sites exhibiting NE-striking fractures with a frequency of less than 2 fractures/m. (McGuire, 2006 and Jacobi, 2007b) Lineaments from EarthSat (1997).



**Remote Sensing Laboratory**  
Dept. of Geology, SUNY at Buffalo



**University at Buffalo**  
The State University of New York

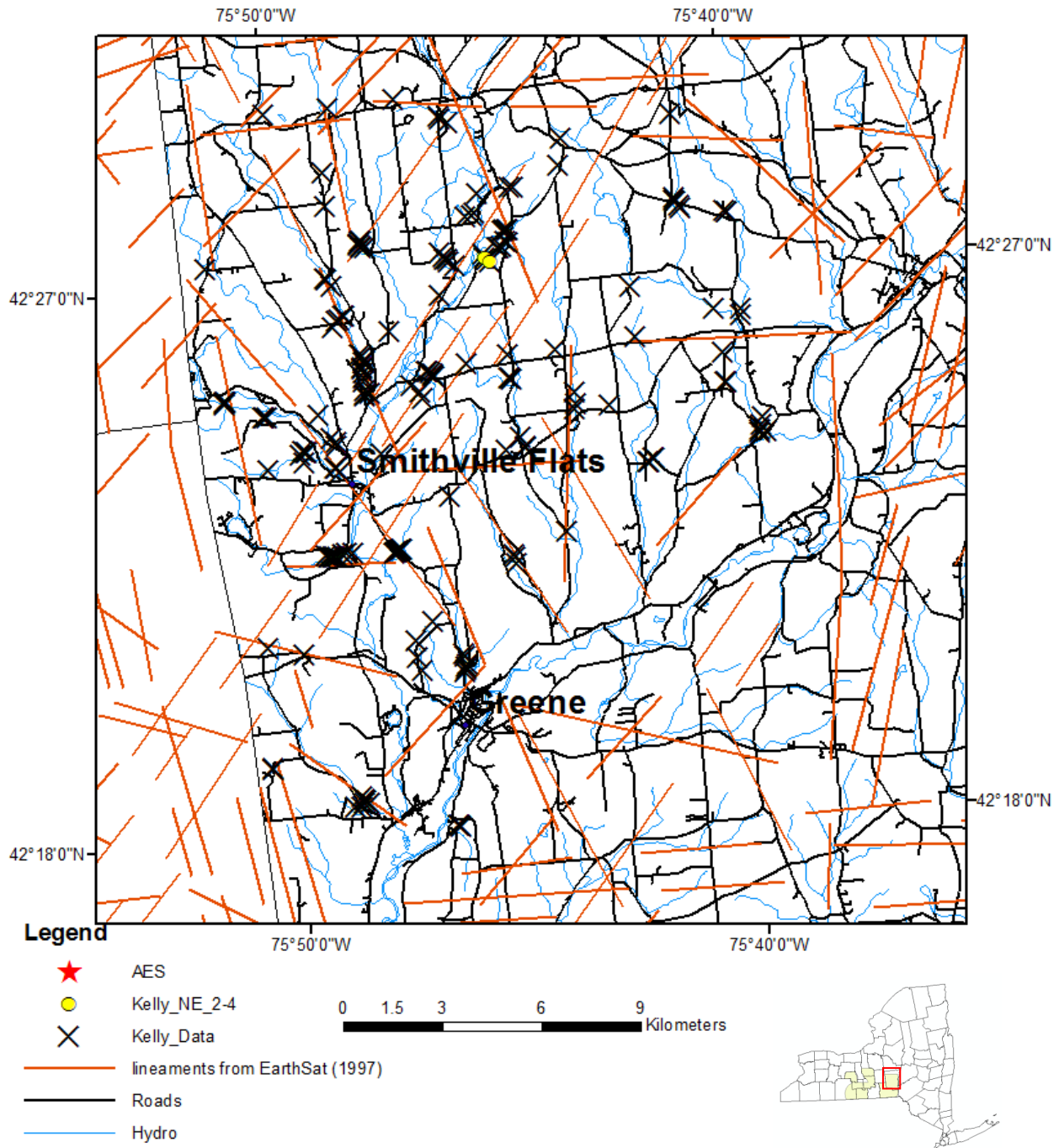


Figure 6.1-161. Southwestern Chenango field sites exhibiting NE-striking fractures with a frequency of 2 to 4 fractures/m. (McGuire, 2006 and Jacobi, 2007b) Lineaments from EarthSat (1997).



**Remote Sensing Laboratory**  
Dept. of Geology, SUNY at Buffalo



**University at Buffalo**  
The State University of New York

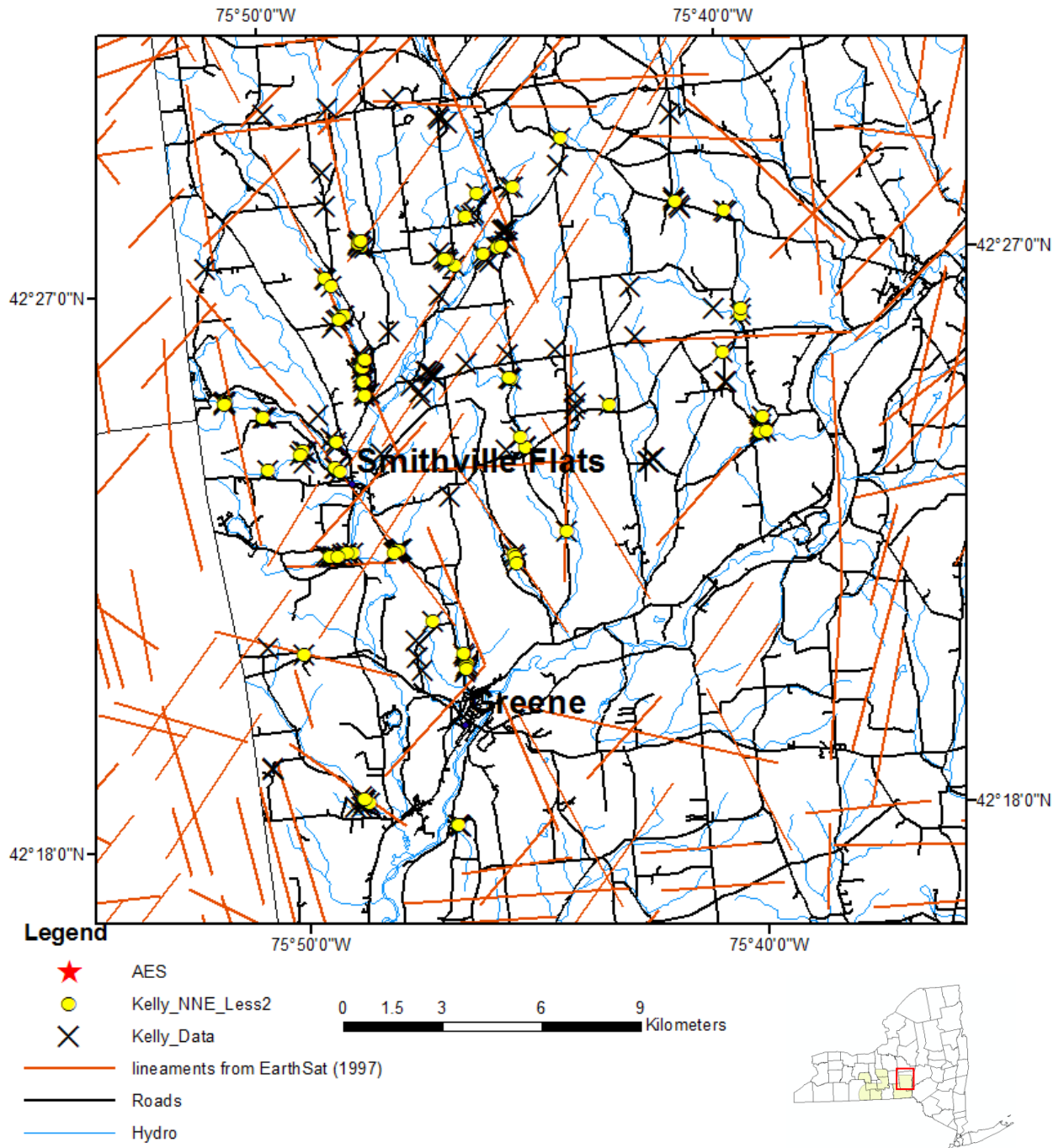


Figure 6.1-162. Southwestern Chenango field sites exhibiting NNE-striking fractures with a frequency of less than 2 fractures/m. (McGuire, 2006 and Jacobi, 2007b) Lineaments from EarthSat (1997).





**Remote Sensing Laboratory**  
Dept. of Geology, SUNY at Buffalo



**University at Buffalo**  
The State University of New York

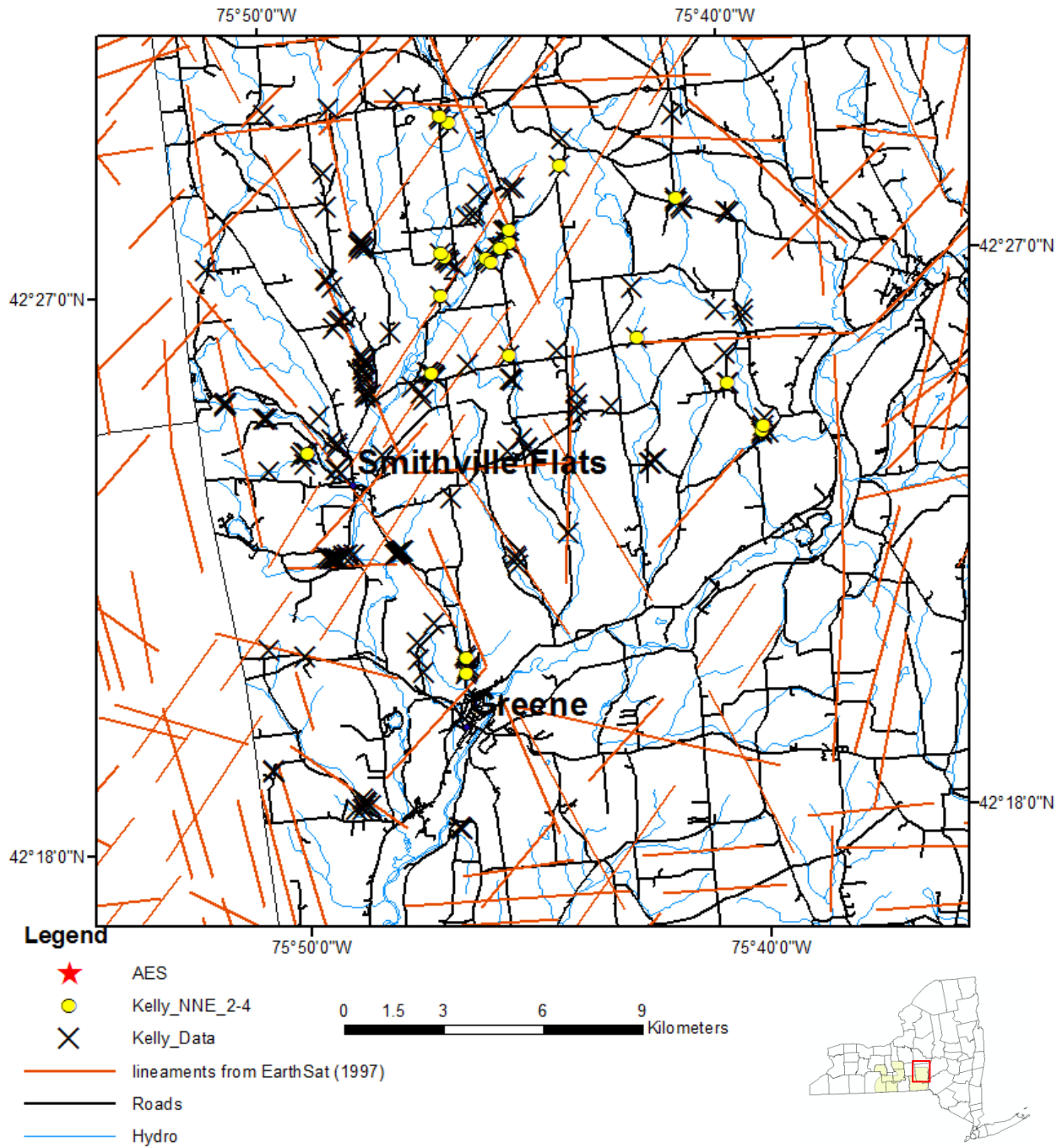


Figure 6.1-163. Southwestern Chenango field sites exhibiting NNE-striking fractures with a frequency of 2 to 4 fractures/m. (McGuire, 2006 and Jacobi, 2007b) Lineaments from EarthSat (1997).



**Remote Sensing Laboratory**  
Dept. of Geology, SUNY at Buffalo



**University at Buffalo**  
The State University of New York

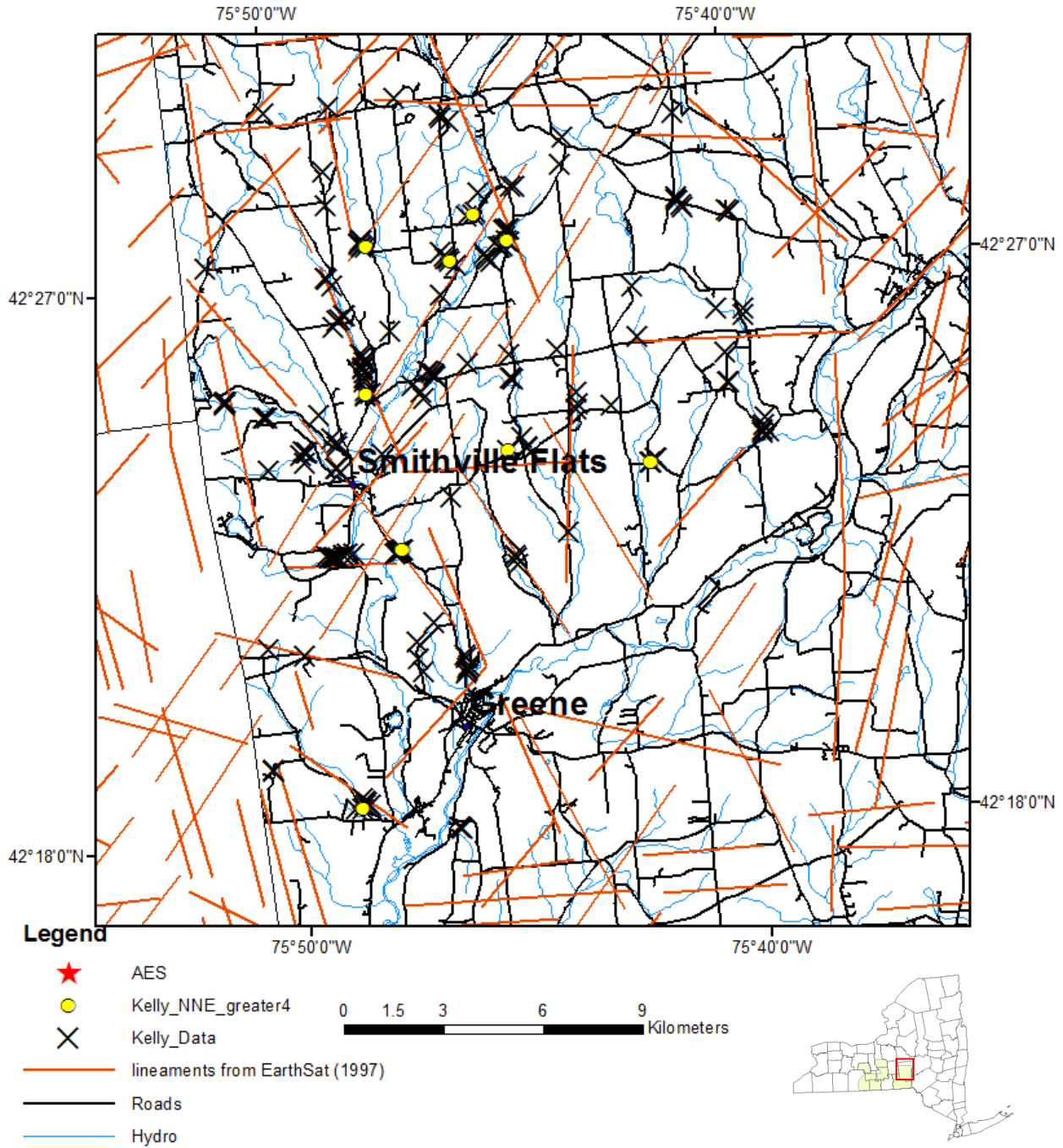


Figure 6.1-164. Southwestern Chenango field sites exhibiting NNE-striking fractures with a frequency of greater than 4 fractures/m. (McGuire, 2006 and Jacobi, 2007b) Lineaments from EarthSat (1997).



**Remote Sensing Laboratory**  
Dept. of Geology, SUNY at Buffalo



**University at Buffalo**  
The State University of New York

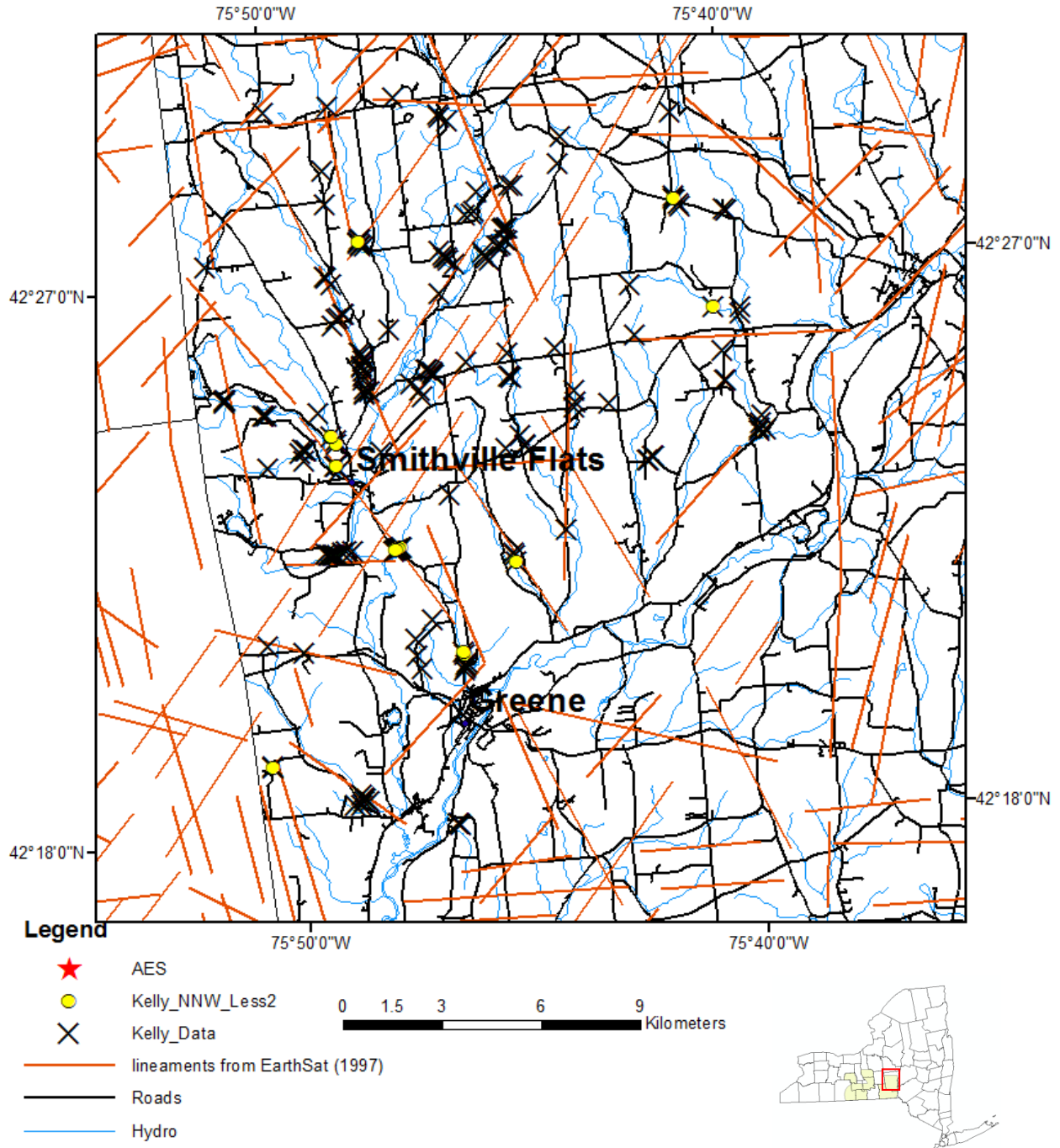


Figure 6.1-165. Southwestern Chenango field sites exhibiting NNW-striking fractures with a frequency of less than 2 fractures/m. (McGuire, 2006 and Jacobi, 2007b) Lineaments from EarthSat (1997).





**Remote Sensing Laboratory**  
Dept. of Geology, SUNY at Buffalo



**University at Buffalo**  
The State University of New York

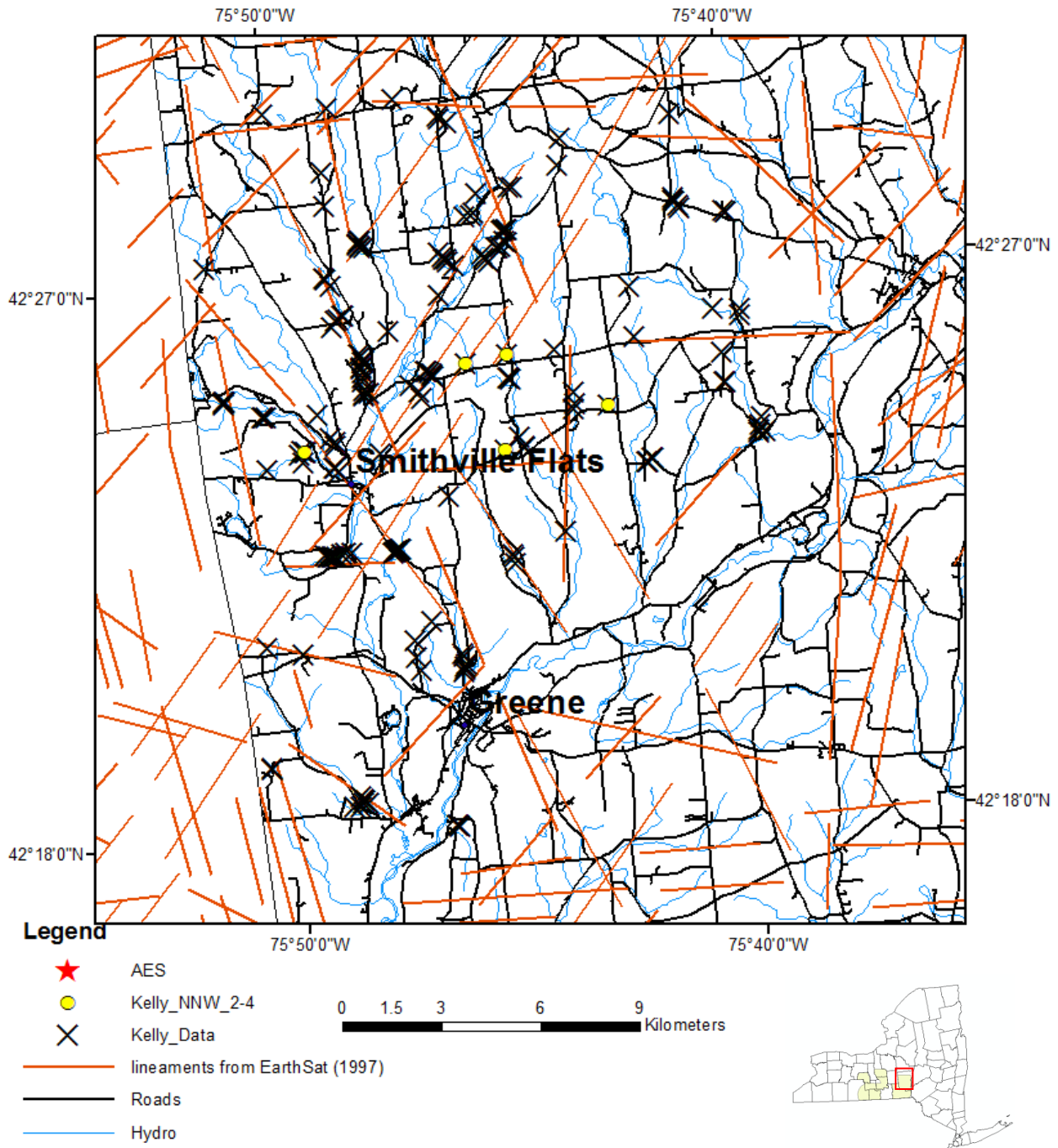


Figure 6.1-166.: Southwestern Chenango field sites exhibiting NNW-striking fractures with a frequency of 2 to 4 fractures/m. (McGuire, 2006 and Jacobi, 2007b) Lineaments from EarthSat (1997).



**Remote Sensing Laboratory**  
Dept. of Geology, SUNY at Buffalo



**University at Buffalo**  
The State University of New York

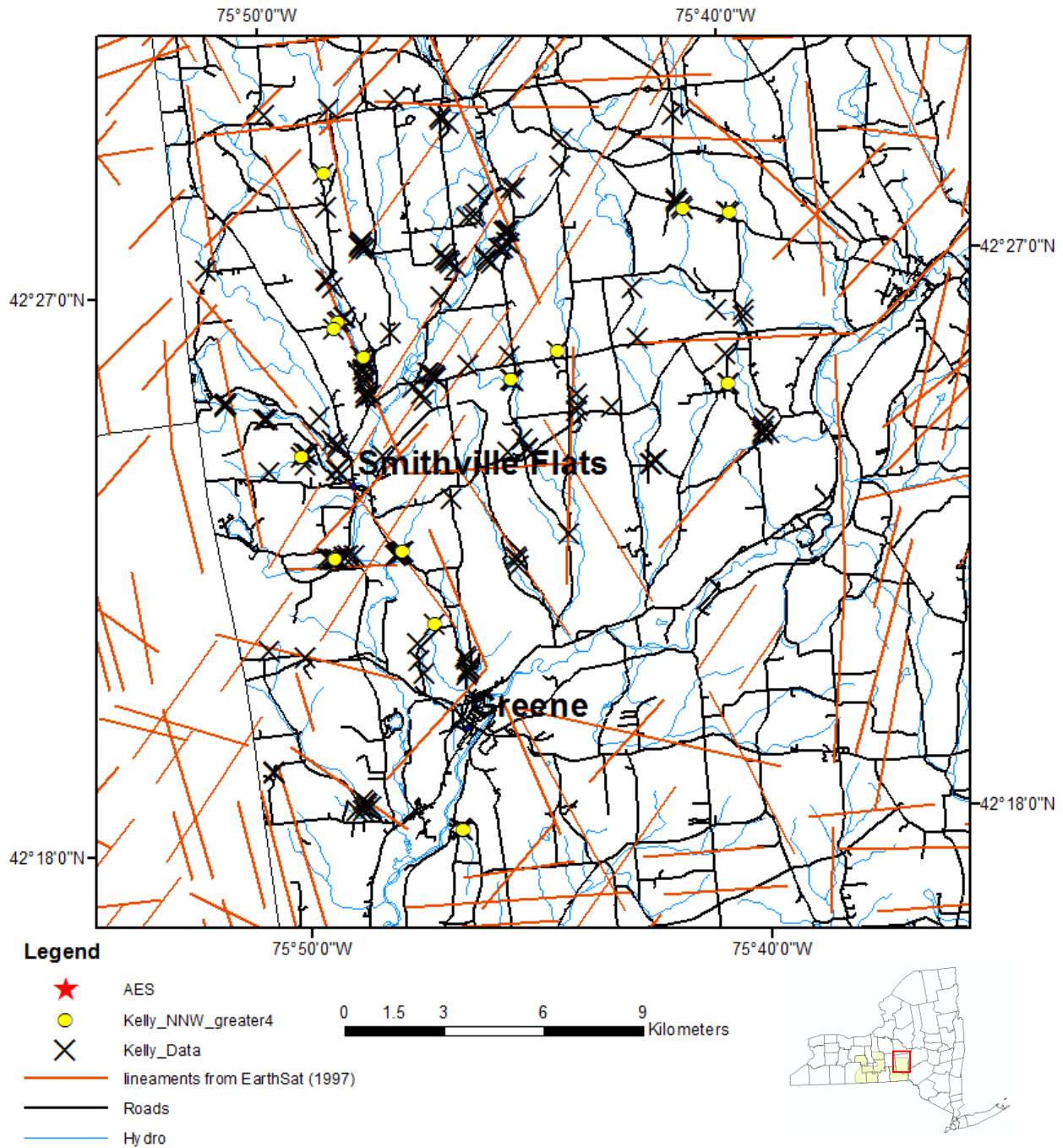


Figure 6.1-167. Southwestern Chenango field sites exhibiting NNW-striking fractures with a frequency of greater than 4 fractures/m. (McGuire, 2006 and Jacobi, 2007b) Lineaments from EarthSat (1997).



**Remote Sensing Laboratory**  
Dept. of Geology, SUNY at Buffalo



**University at Buffalo**  
The State University of New York

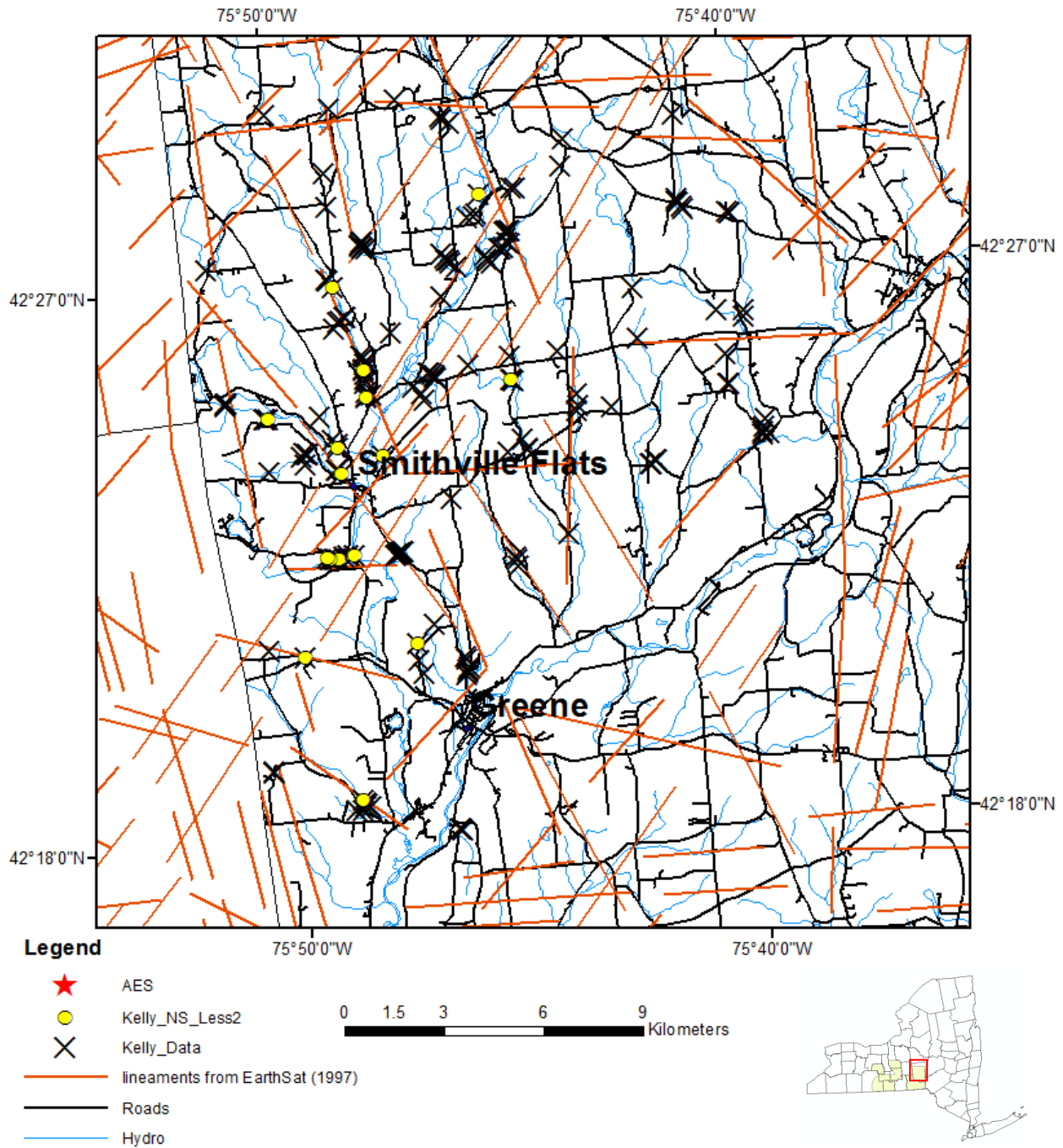


Figure 6.1-168. Southwestern Chenango field sites exhibiting NS-striking fractures with a frequency of less than 2 fractures/m. (McGuire, 2006 and Jacobi, 2007b) Lineaments from EarthSat (1997).



**Remote Sensing Laboratory**  
Dept. of Geology, SUNY at Buffalo



**University at Buffalo**  
The State University of New York

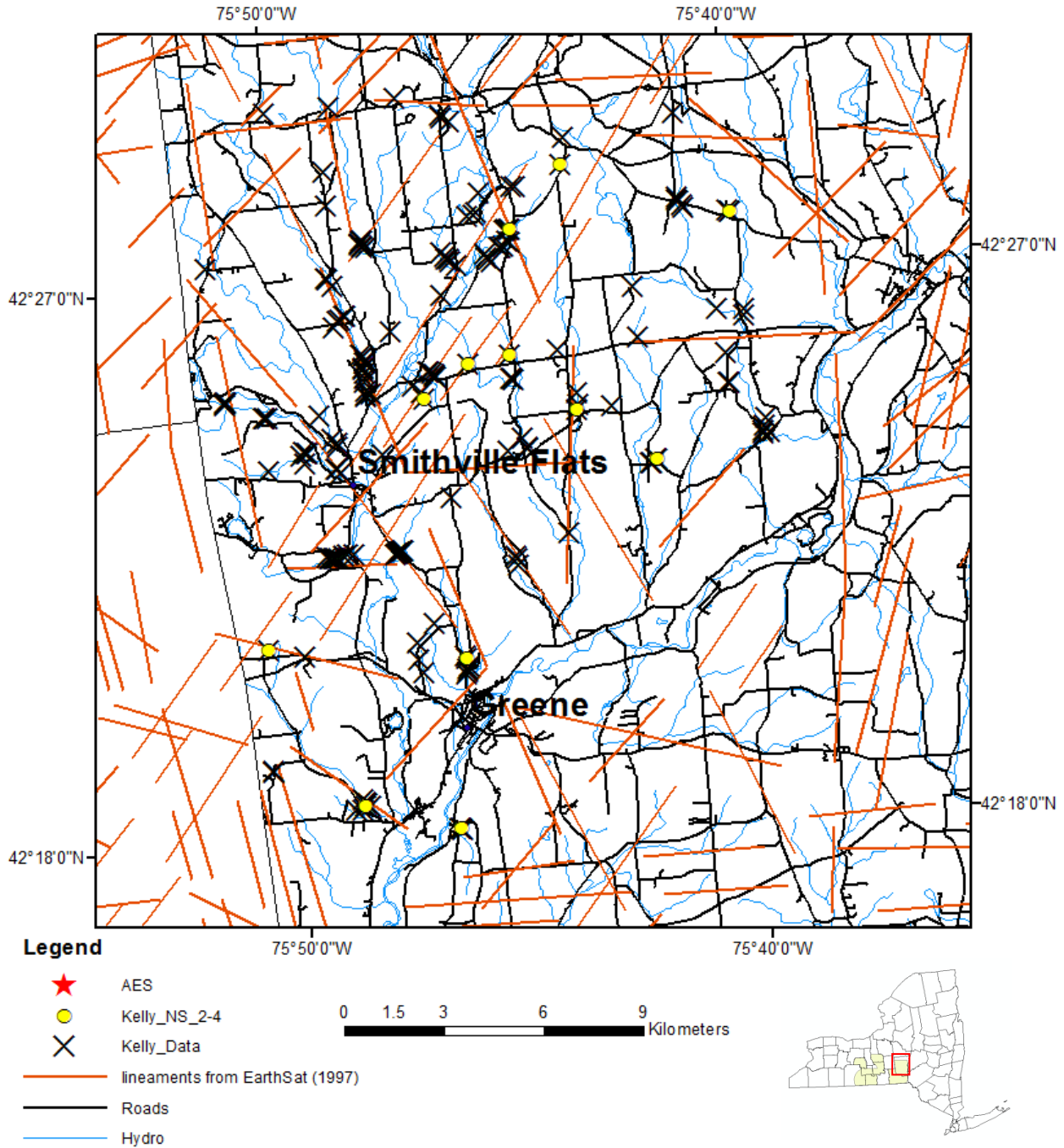


Figure 6.1-169. Southwestern Chenango field sites exhibiting NS-striking fractures with a frequency of 2 to 4 fractures/m. (McGuire, 2006 and Jacobi, 2007b) Lineaments from EarthSat (1997).





**Remote Sensing Laboratory**  
Dept. of Geology, SUNY at Buffalo



**University at Buffalo**  
The State University of New York

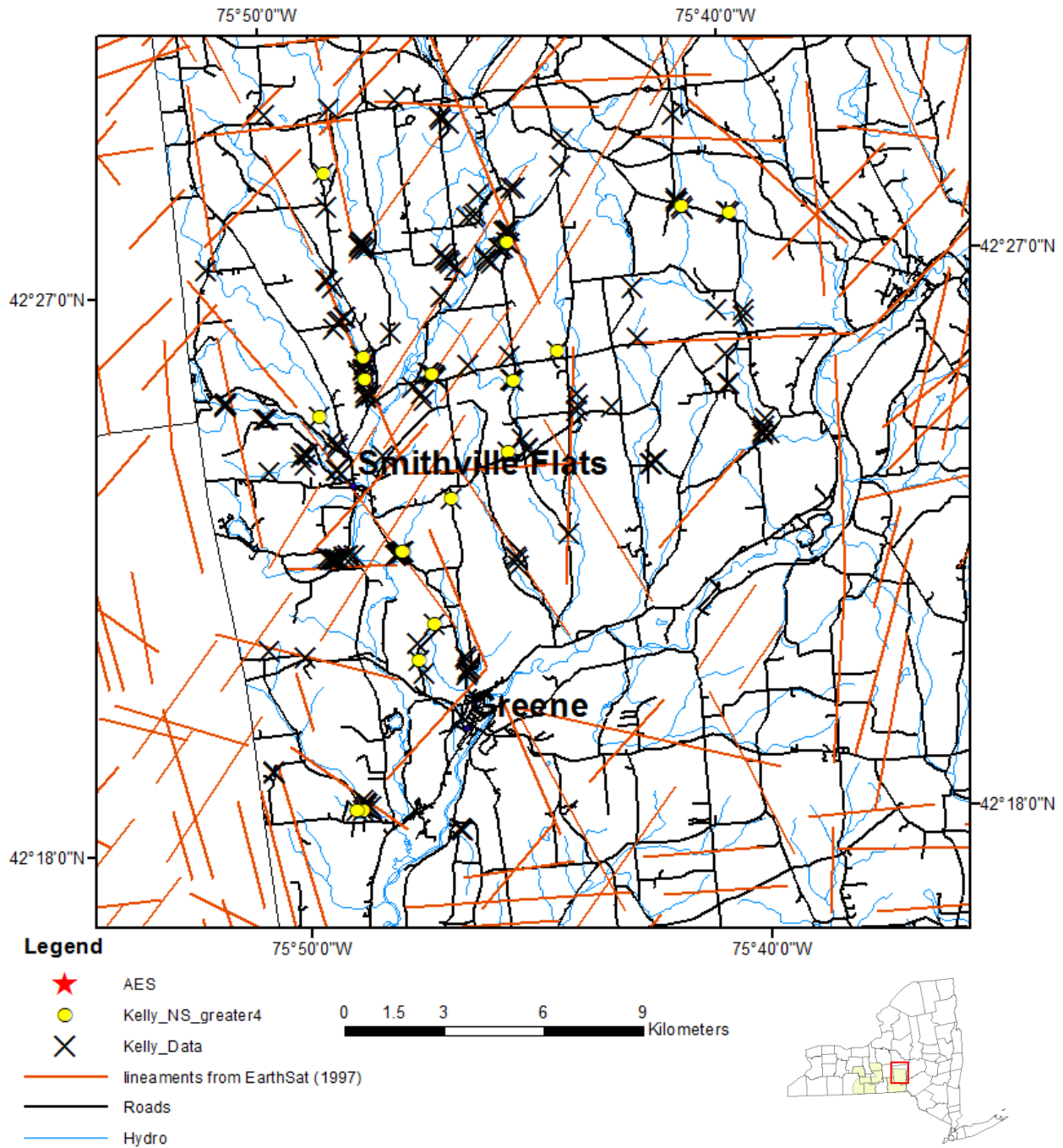


Figure 6.1-170. Southwestern Chenango field sites exhibiting NS-striking fractures with a frequency of greater than 4 fractures/m. (McGuire, 2006 and Jacobi, 2007b) Lineaments from EarthSat (1997).



**Remote Sensing Laboratory**  
Dept. of Geology, SUNY at Buffalo



**University at Buffalo**  
The State University of New York

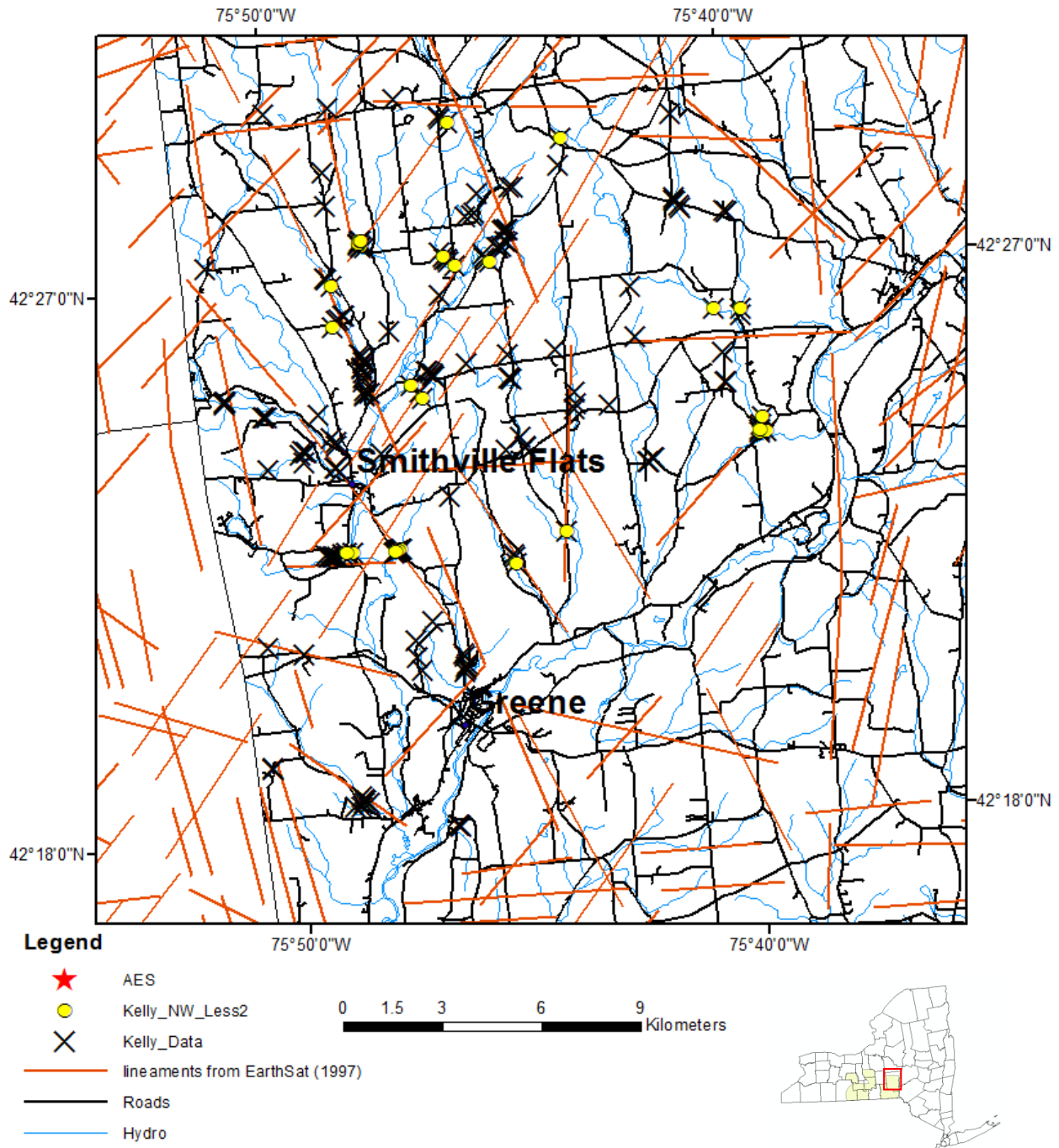


Figure 6.1-171.: Southwestern Chenango field sites exhibiting NW-striking fractures with a frequency of less than 2 fractures/m. (McGuire, 2006 and Jacobi, 2007b) Lineaments from EarthSat (1997).



**Remote Sensing Laboratory**  
Dept. of Geology, SUNY at Buffalo



**University at Buffalo**  
The State University of New York

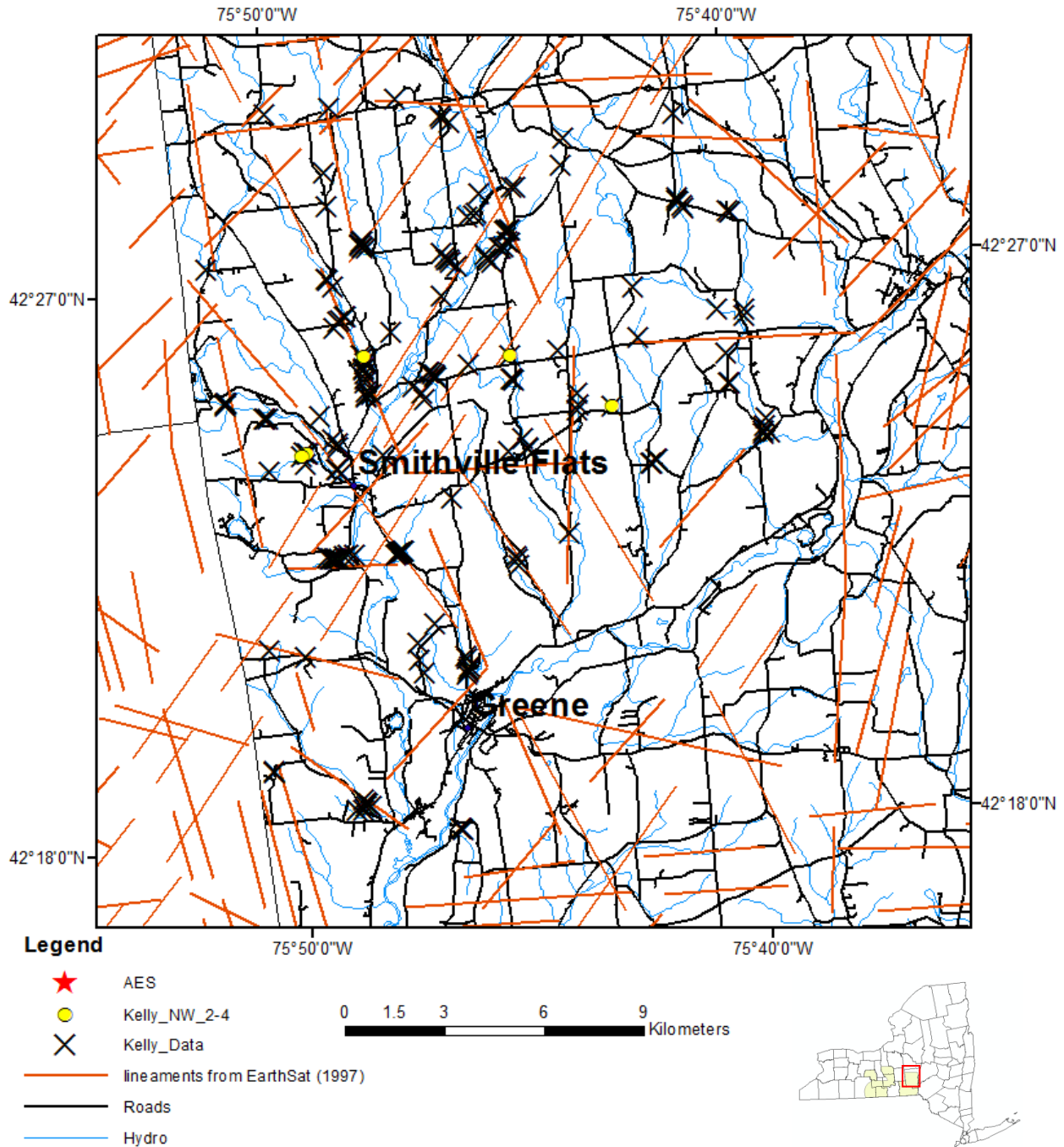


Figure 6.1-172. Southwestern Chenango field sites exhibiting NW-striking fractures with a frequency of 2 to 4 fractures/m. (McGuire, 2006 and Jacobi, 2007b) Lineaments from EarthSat (1997).





**Remote Sensing Laboratory**  
Dept. of Geology, SUNY at Buffalo



**University at Buffalo**  
The State University of New York

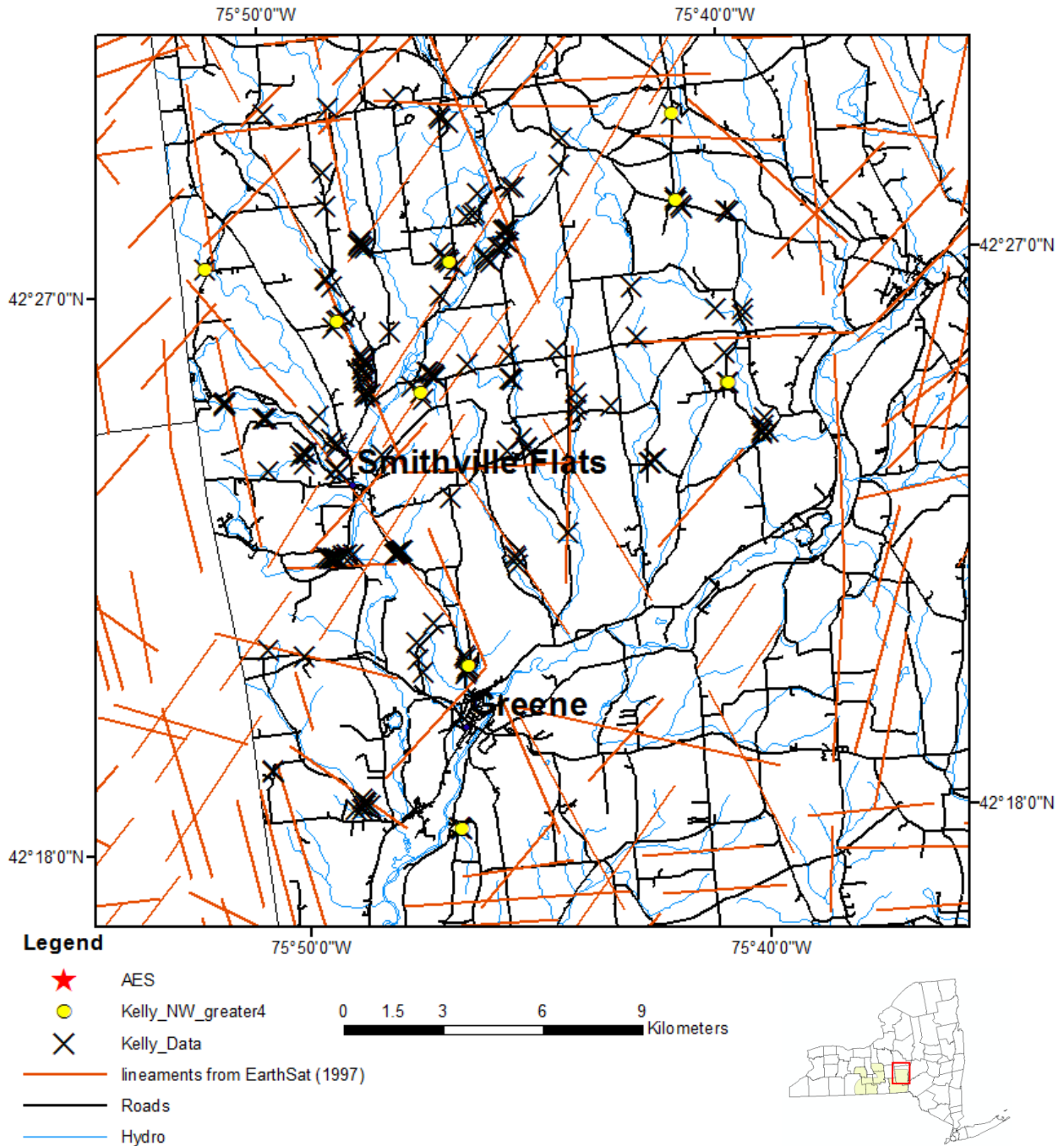


Figure 6.1-173. Southwestern Chenango field sites exhibiting NW-striking fractures with a frequency of greater than 4 fractures/m. (McGuire, 2006 and Jacobi, 2007b) Lineaments from EarthSat (1997).



**Remote Sensing Laboratory**  
Dept. of Geology, SUNY at Buffalo



**University at Buffalo**  
The State University of New York

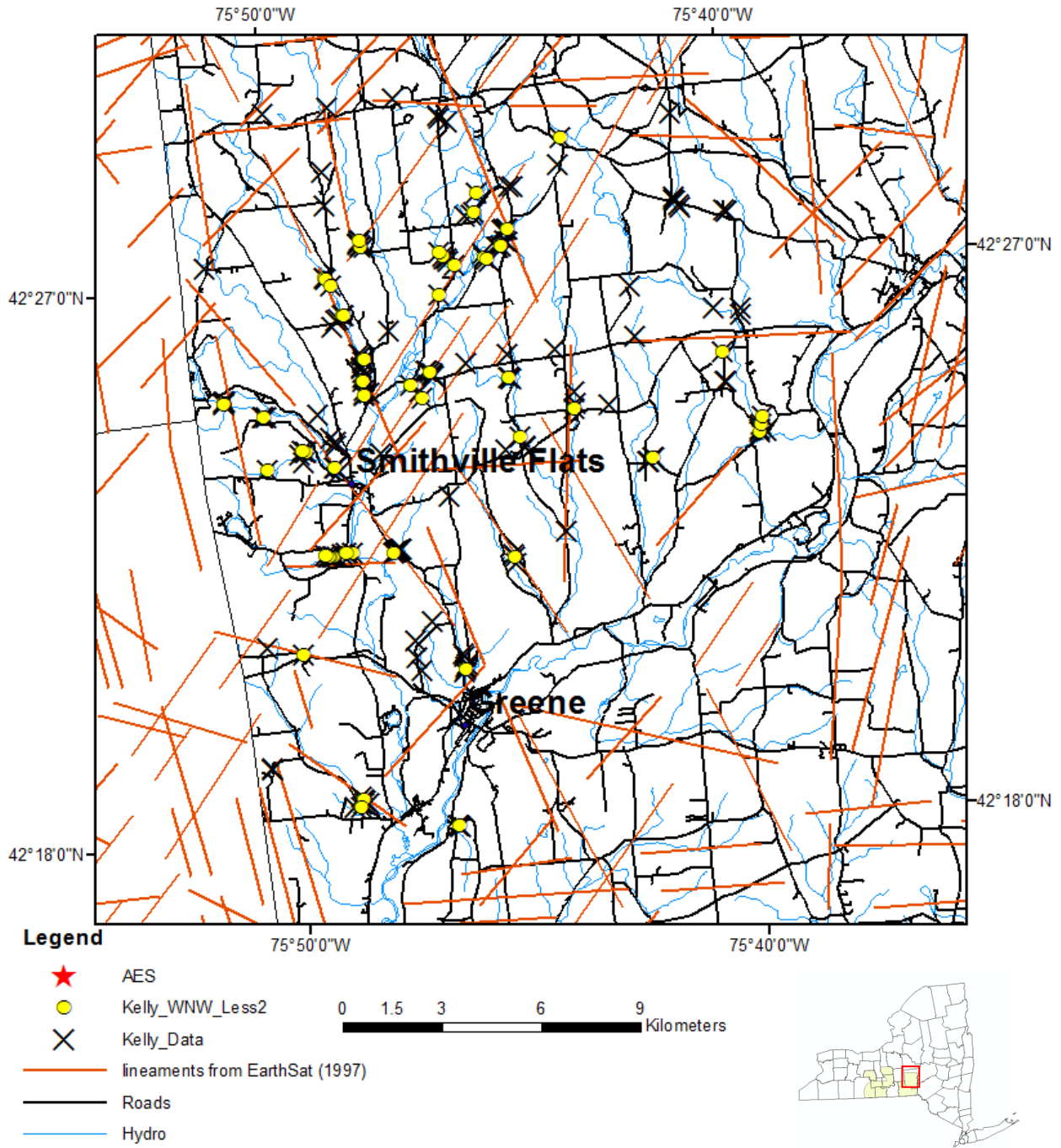


Figure 6.1-174. Southwestern Chenango field sites exhibiting WNW-striking fractures with a frequency of less than 2 fractures/m. (McGuire, 2006 and Jacobi, 2007b) Lineaments from EarthSat (1997).



**Remote Sensing Laboratory**  
 Dept. of Geology, SUNY at Buffalo



**University at Buffalo**  
 The State University of New York

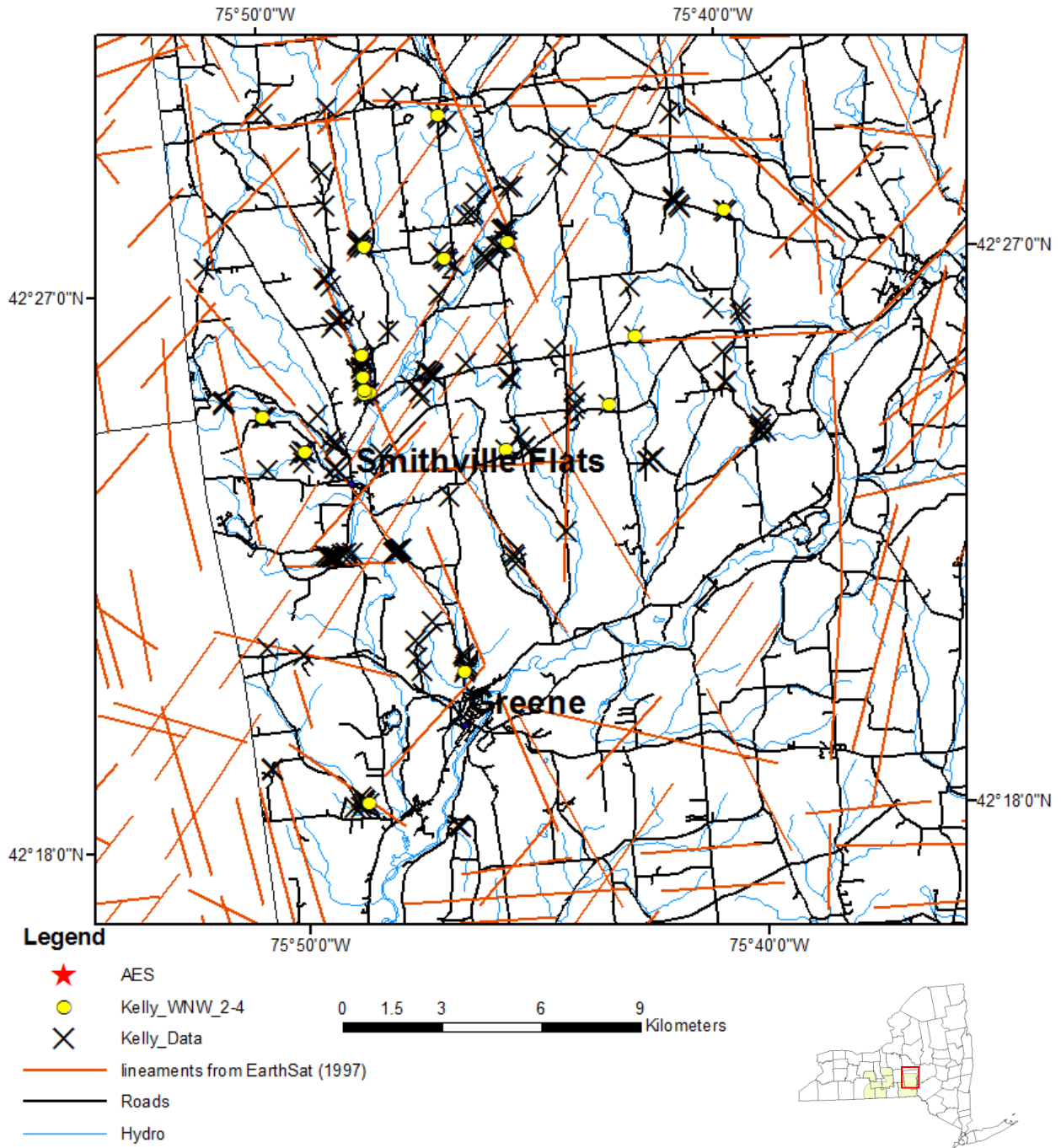


Figure 6.1-175. Southwestern Chenango field sites exhibiting WNW-striking fractures with a frequency of 2 to 4 fractures/m. (McGuire, 2006 and Jacobi, 2007b) Lineaments from EarthSat (1997).



**Remote Sensing Laboratory**  
Dept. of Geology, SUNY at Buffalo



**University at Buffalo**  
The State University of New York

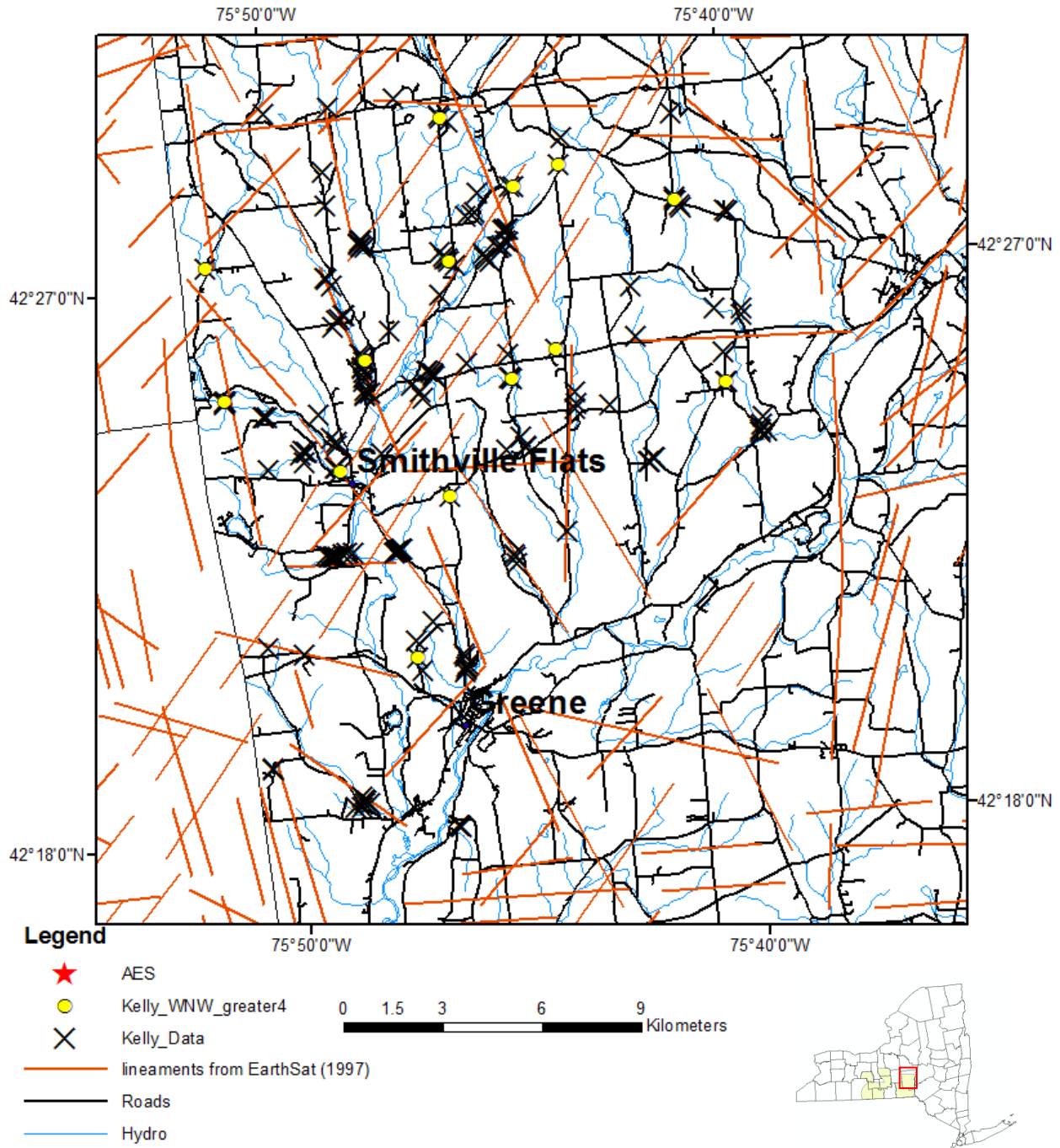


Figure 6.1-176. Southwestern Chenango field sites exhibiting WNW-striking fractures with a frequency of greater than 4 fractures/m. (McGuire, 2006 and Jacobi, 2007b) Lineaments from EarthSat (1997).



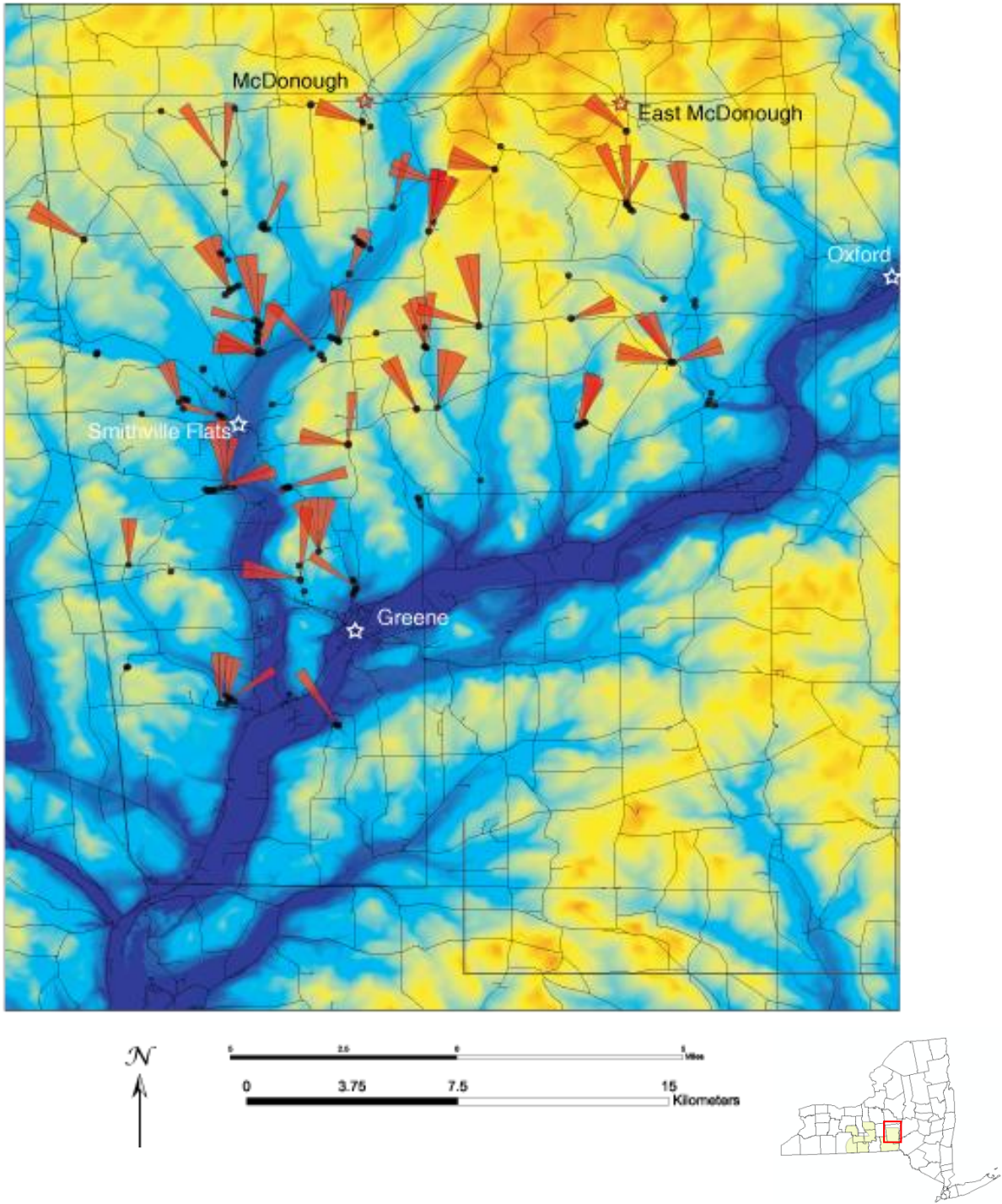


Figure 6.1-177. Southwestern Chenango field sites showing associated rose diagrams of fracture intensification domains on top of a shaded DEM (Jacobi, 2007b).

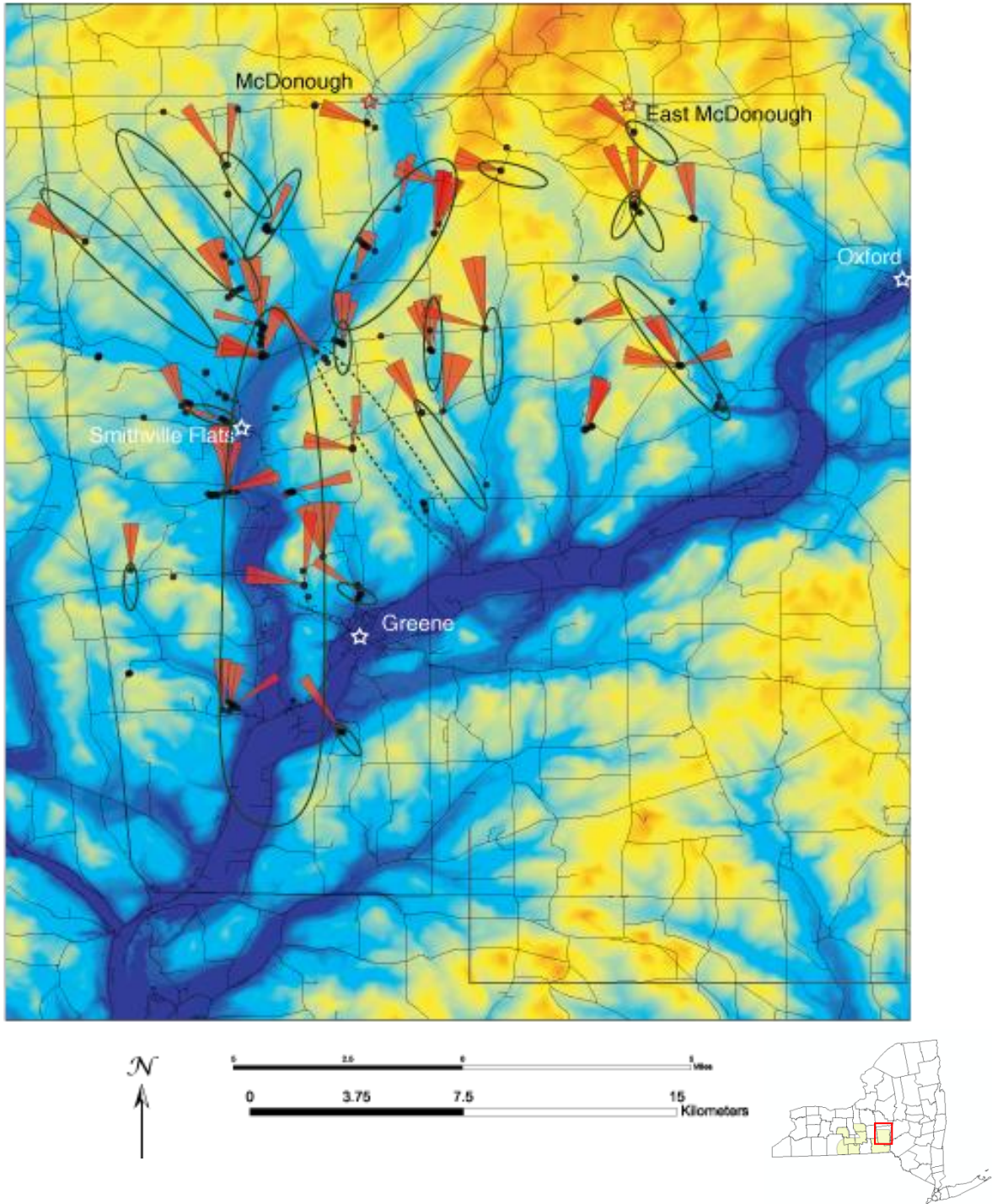


Figure 6.1-178: Southwestern Chenango field sites showing associated rose diagrams of fracture intensification domains on top of a shaded DEM with ellipses highlighting prominent topographic lineaments that are consonant with FID orientations (Jacobi, 2007b).

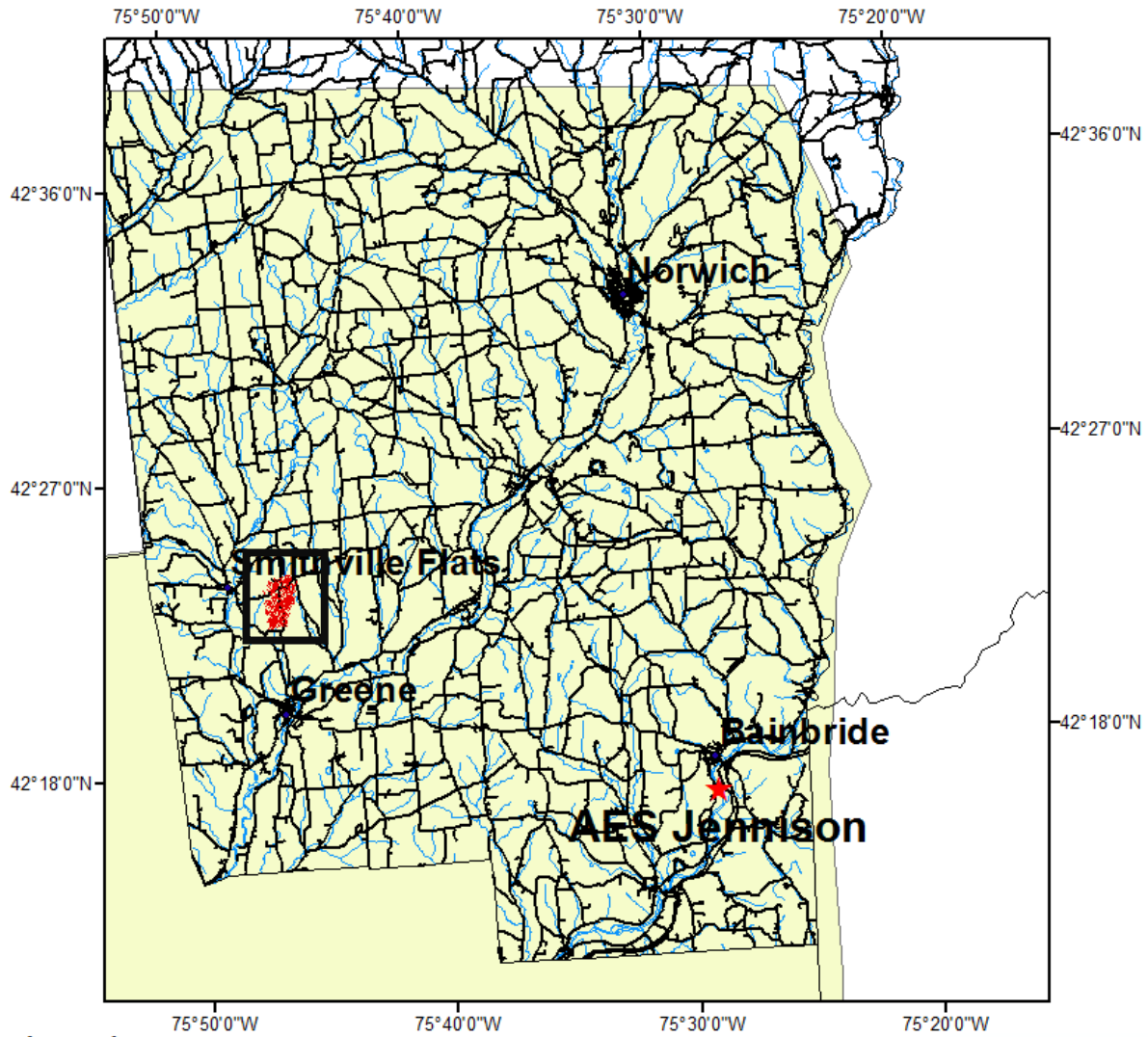







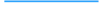

**Remote Sensing Laboratory**  
Dept. of Geology, SUNY at Buffalo



**University at Buffalo**  
The State University of New York



**Legend**

-  AES
-  Fractures
-  Roads
-  Hydro
-  AOI

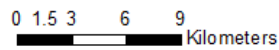


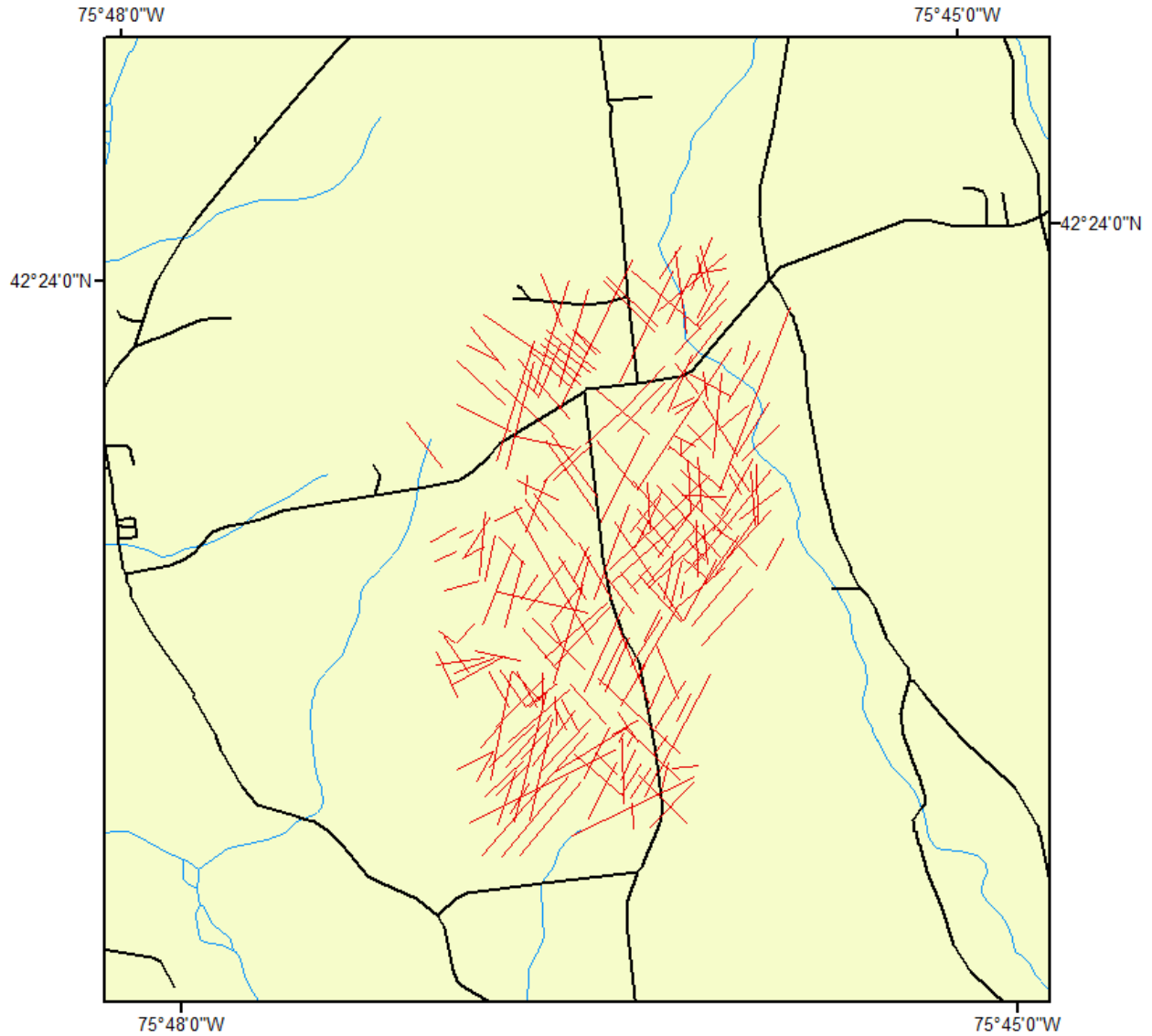
Figure 6.1-179. Index map for Figure 6.1-180. Box with red lines indicates location of lineaments from Pyron et al. (2003) in Figure 6.1-180.








**Remote Sensing Laboratory**  
Dept. of Geology, SUNY at Buffalo



**University at Buffalo**  
The State University of New York



**Legend**

-  AES
-  Fractures
-  Roads
-  Hydro
-  AOI

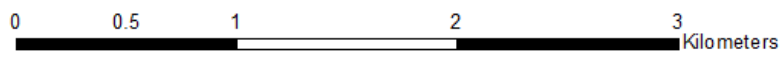


Figure 6.1-180. Lineaments from Pyron et al. (2003) large scale.



Remote Sensing Laboratory  
Dept. of Geology, SUNY at Buffalo



University at Buffalo  
The State University of New York

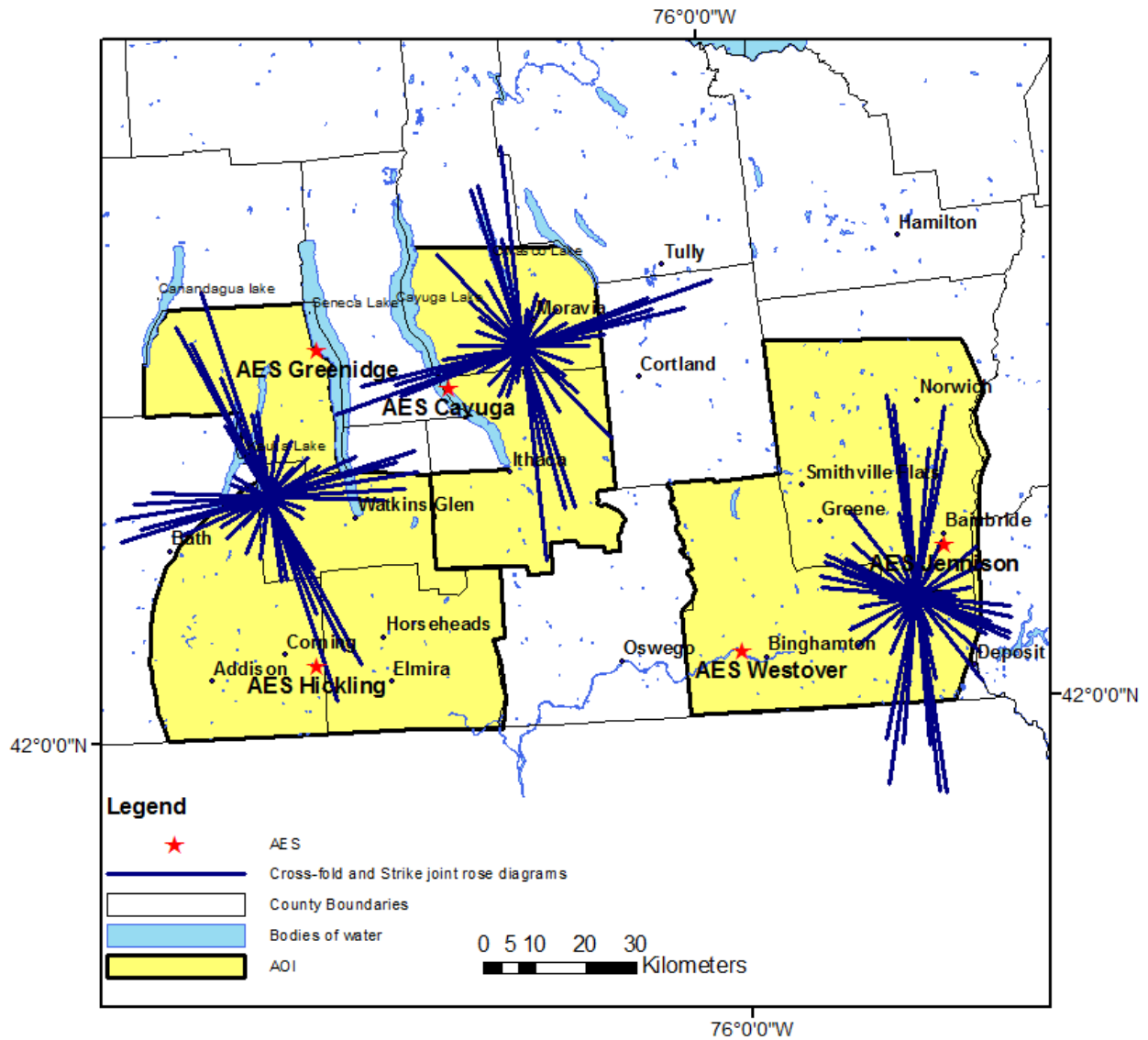
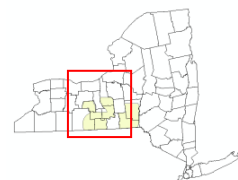


Figure 6.1-181: Joint rose diagrams from Engelder and Oertel (1985)





Remote Sensing Laboratory  
Dept. of Geology, SUNY at Buffalo



University at Buffalo  
The State University of New York

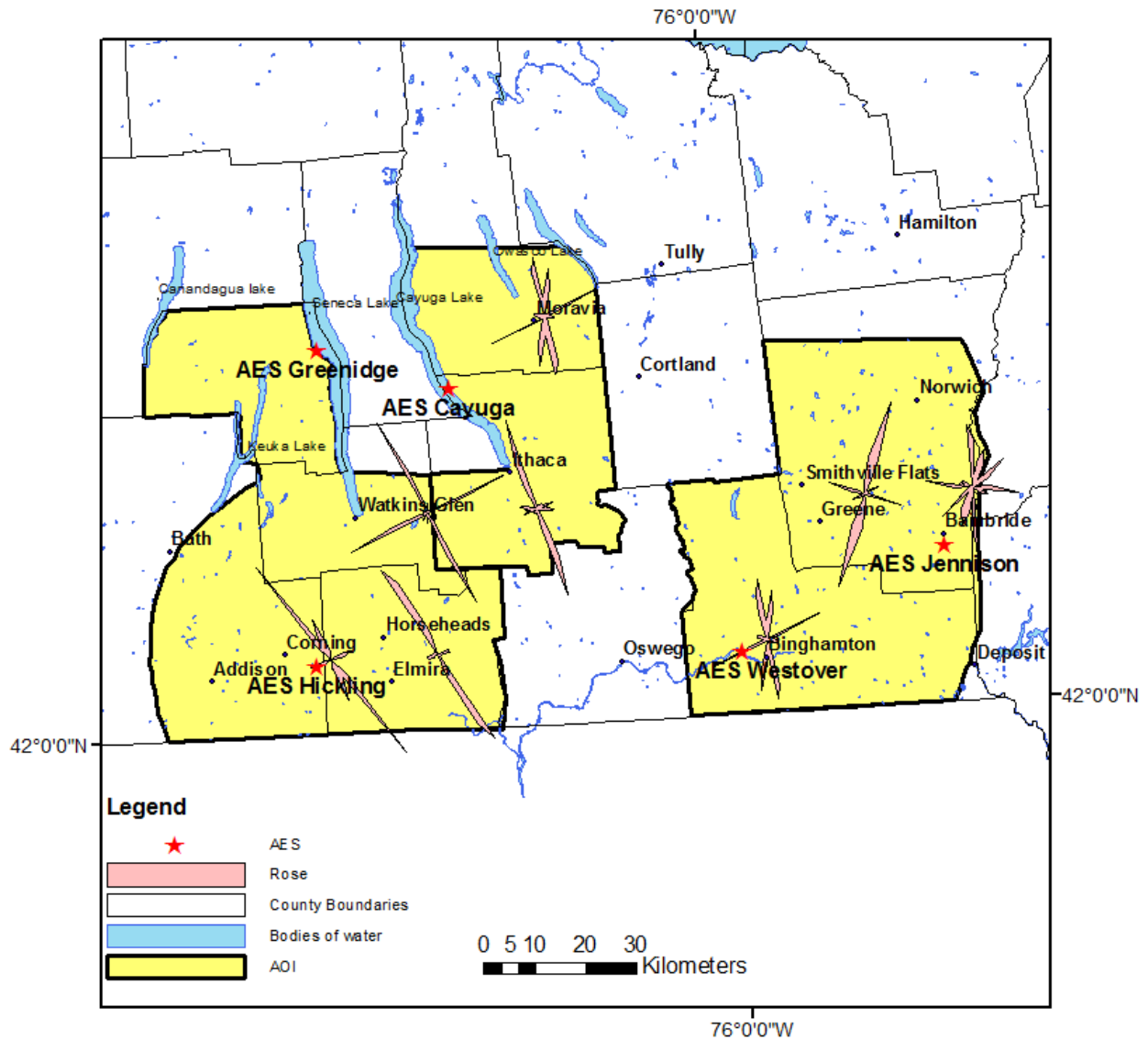


Figure 6.1-182: Rose diagrams of joints from Parker (1942).



Remote Sensing Laboratory  
Dept. of Geology, SUNY at Buffalo



University at Buffalo  
The State University of New York

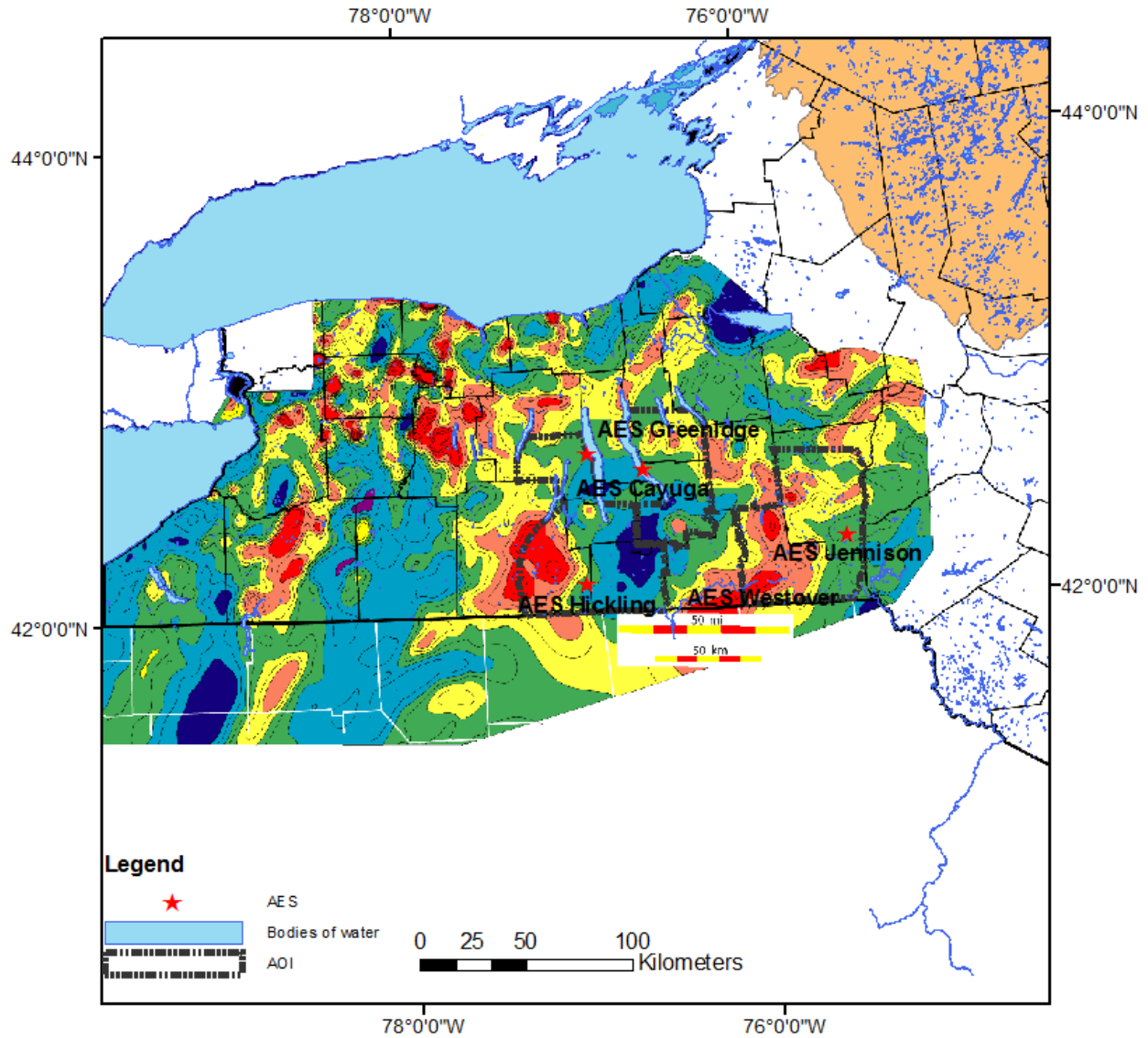


Figure 6.2-1: Smoothed residual aeromagnetics. Contour interval is 50nT. Red indicates relative high and blue relative low. Project area is outlined by the dashed black line. From Jacobi (2002).



Remote Sensing Laboratory  
Dept. of Geology, SUNY at Buffalo



University at Buffalo  
The State University of New York

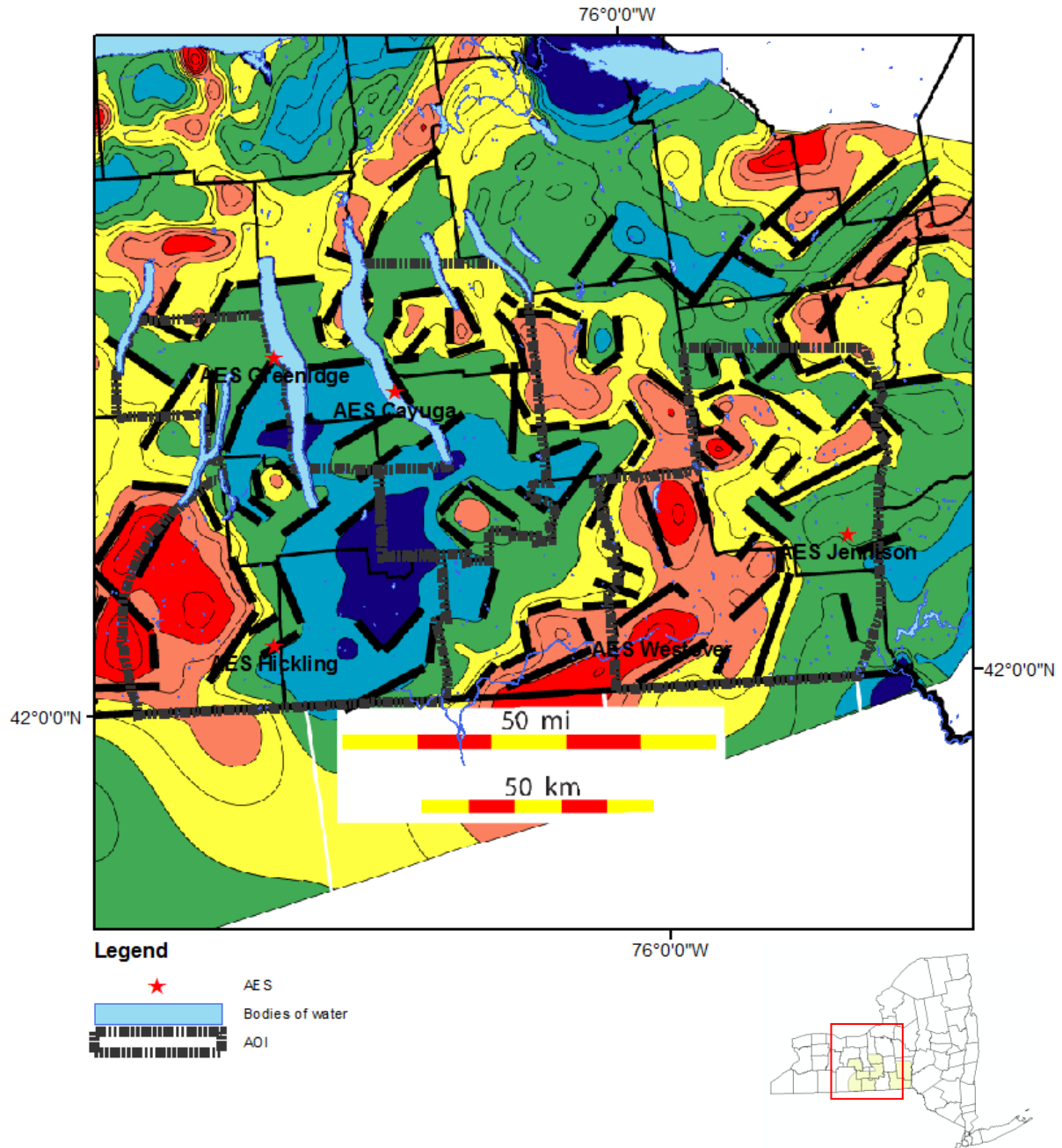


Figure 6.2-2. Smoothed residual aeromagnetics with lineaments (thick black lines) drawn along the trends of significant linear aeromagnetic gradients. Contour interval is 50nT. Red indicated relative high and blue relative low. Project area is outlined by the dashed black line. Aeromagnetics from Jacobi (2002).





Remote Sensing Laboratory  
Dept. of Geology, SUNY at Buffalo



University at Buffalo  
The State University of New York

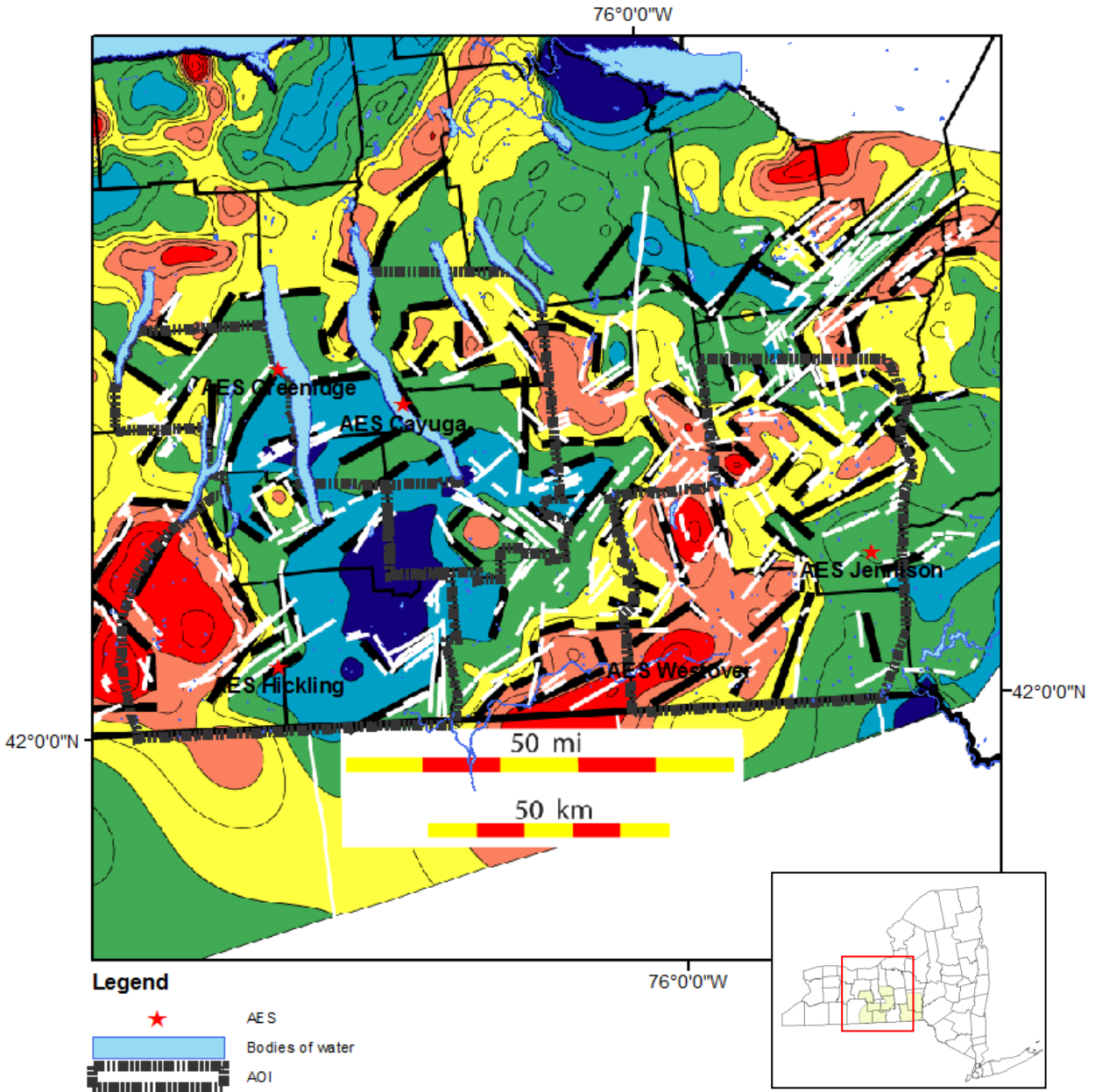


Figure 6.2-3: Smoothed residual aeromagnetics with lineaments. Thick black lines indicate trend of significant linear aeromagnetic gradients and white lines indicate EarthSat (1997) lineaments that are coincident with the aeromagnetic lineaments. Contour interval is 50nT. Red indicated relative high and blue relative low. Project area is outlined by the dashed black line. Aeromagnetics from Jacobi (2002).

TABLE 6.1-1  
Hickling Power Plant  
Lineaments and Faults

| ID NUMBER | ORIENTATION IN DEGREES | DISTANCE FRM FACILITY IN KM | SOURCE        | FIGURE THIS RPT | NOTES       |
|-----------|------------------------|-----------------------------|---------------|-----------------|-------------|
| 1         | 54.5                   | 0.0                         | EarthSat '97  | 3a, 5a          | 1 = 9       |
| 2         | 80.5                   | 1.7                         | EarthSat '97  | 3a, 5a          | 2 = 11 cont |
| 3         | 61.5                   | 2.0                         | EarthSat '97  | 3a, 5a          |             |
| 4         | 326.5                  | 2.2                         | EarthSat '97  | 3a, 5a          |             |
| 5         | 31.5                   | 3.8                         | EarthSat '97  | 3a, 5a          |             |
| 6         | 35.5                   | 4.4                         | EarthSat '97  | 3a, 5a          | 6 = 10      |
| 7         | 70.5                   | 4.4                         | EarthSat '97  | 3a, 5a          |             |
| 7a        | 0.5                    | 4.9                         | EarthSat '97  | 3a, 5a          |             |
| 6a        | 40.5                   | 5.2                         | EarthSat '97  | 3a, 5a          | 6a = 12     |
| 8         | 66.5                   | 5.3                         | EarthSat '97  | 3a, 5a          |             |
| 8c        | 311.5                  | 6.7                         | EarthSat '97  | 3a, 5a          | 8a = 15     |
| 8a        | 45.5                   | 6.9                         | EarthSat '97  | 3a, 5a          |             |
| 8b        | 46.5                   | 7.6                         | EarthSat '97  | 3a, 5a          |             |
| 9         | 54.5                   | 0.8                         | I & M '77     | 4a, 5a          | 9 = 1       |
| 10        | 40.5                   | 4.2                         | I & M '77     | 4a, 5a          | 10 = 6      |
| 11        | 77.5                   | 4.2                         | I & M '77     | 4a, 5a          | 11 cont = 2 |
| 12        | 43.5                   | 5.3                         | I & M '77     | 4a, 5a          | 12 = 6a     |
| 13        | 85.5                   | 5.6                         | I & M '77     | 4a, 5a          |             |
| 14        | 46.5                   | 6.2                         | I & M '77     | 4a, 5a          |             |
| 15        | 45.5                   | 6.9                         | I & M '77     | 4a, 5a          | 15 = 8a     |
| 2         | 50.5                   | 3.9                         | Jacobi flts   | 6a              |             |
| 1         | 69.5                   | 5.5                         | Jacobi flts   | 6a              |             |
| 3         | 70.5                   | 10.3                        | Jacobi flts   | 6a              |             |
| 5         | 338.5                  | 14.8                        | Jacobi flts   | 6a              |             |
| 4         | 344.5                  | 15.4                        | Jacobi flts   | 6a              |             |
| 7         | 68.5                   | 15.6                        | Jacobi flts   | 6a              |             |
| 6         | 341.5                  | 16.6                        | Jacobi flts   | 6a              |             |
| 1         | 74.5                   | 16.3                        | Jac flt zones | 6b              |             |
| 1         | 86.5                   | 3.4                         | Murphy 81     | 6d              |             |
| 2         | 68.5                   | 9.0                         | Murphy 81     | 6d              |             |
| 3         | 66.5                   | 11.1                        | Murphy 81     | 6d              |             |
| 1         | 76.5                   | 8.9                         | Wedel 32      | 7               |             |

EarthSat '97 = EarthSat (1997), I & M '77 = Isachsen and McKendree (1977), Jacobi flts = Jacobi (2002)

Jac flt zones = Jacobi (2002) fault zones, Murphy 81 = Murphy (1981), Wedel 32 = Wedel (1932)

TABLE 6.1-2  
Hickling Power Plant  
Fracture Trends

| SET I (J2) | FIGURE   | SOURCE                  | NOTES |
|------------|----------|-------------------------|-------|
| 329.5      | 8, 9, 13 | Engelder & Geiser, 1980 |       |

| SET II | FIGURE     | SOURCE                  | NOTES                  |
|--------|------------|-------------------------|------------------------|
| 81.5   | 11, 12, 13 | Engelder & Geiser, 1980 |                        |
| 78.5   | 11, 12, 13 | Engelder & Geiser, 1980 |                        |
| 68.5   | 11, 12, 13 | Engelder & Geiser, 1980 |                        |
| 64.5   | 11, 12, 13 | Engelder & Geiser, 1980 |                        |
| 75.5   | 15         | Engelder & Geiser, 1980 | trajectory             |
| 71.5   | 25         | Younes & Engelder, 1999 | about 6.5 km from site |

TABLE 6.1-3  
Greenidge Power Plant  
Lineaments and Faults

| ID NUMBER | ORIENTATION<br>IN DEGREES | DISTANCE<br>FRM FACILITY<br>IN KM | SOURCE           | FIGURE<br>THIS RPT | NOTES             |
|-----------|---------------------------|-----------------------------------|------------------|--------------------|-------------------|
| 1         | 41.5                      | 0.1                               | EarthSat '97     | 3a, 5a             |                   |
| 2         | 322.5                     | 0.0                               | EarthSat '97     | 3a, 5a             |                   |
| 3         | 67.5                      | 3.1                               | EarthSat '97     | 3a, 5a             |                   |
| 4         | 273.5                     | 1.9                               | EarthSat '97     | 3a, 5a             |                   |
| 5         | 273.5                     | 1.0                               | EarthSat '97     | 3a, 5a             |                   |
| 6         | 287                       | 3.2                               | EarthSat '97     | 3a, 5a             |                   |
| 7         | 286.5                     | 1.1                               | EarthSat '97     | 3a, 5a             |                   |
| 8         | 273.5                     | 2.5                               | EarthSat '97     | 3a, 5a             | 8 = IM 1          |
| 9         | 351.5                     | 0.0                               | EarthSat '97     | 3a, 5a             |                   |
| 10        | 71.5                      | 4.0                               | EarthSat '97     | 3a, 5a             |                   |
| 11        | 73.5                      | 3.5                               | EarthSat '97     | 3a, 5a             |                   |
| 12        | 74.5                      | 2.7                               | EarthSat '97     | 3a, 5a             |                   |
| 13        | 67.5                      | 6.2                               | EarthSat '97     | 3a, 5a             |                   |
| 14        | 273.5                     | 6.2                               | EarthSat '97     | 3a, 5a             |                   |
| 15        | 274.5                     | 6.6                               | EarthSat '97     | 3a, 5a             |                   |
| 16        | 67.5                      | 7.1                               | EarthSat '97     | 3a, 5a             |                   |
| 17        | 348.5                     | 6.8                               | EarthSat '97     | 3a, 5a             |                   |
| 18        | 64.5                      | 3.9                               | EarthSat '97     | 3a, 5a             |                   |
| 19        | 66.5                      | 5.0                               | EarthSat '97     | 3a, 5a             |                   |
| 20        | 41.5                      | 6.8                               | EarthSat '97     | 3a, 5a             | 20 a cont. of 21  |
| 21        | 36.5                      | 5.9                               | EarthSat '97     | 3a, 5a             | 21 a cont of 20   |
| 22        | 69.5                      | 5.2                               | EarthSat '97     | 3a, 5a             |                   |
| 23        | 36.5                      | 7.1                               | EarthSat '97     | 3a, 5a             |                   |
| 24        | 36.5                      | 6.5                               | EarthSat '97     | 3a, 5a             |                   |
| 25        | 12.5                      | 7.9                               | EarthSat '97     | 3a, 5a             |                   |
| 26        | 14.5                      | 13.1                              | EarthSat '97     | 3a, 5a             | cont of 26= IM 3  |
| 1         | 273.5                     | 2.5                               | I & M '77        | 4a, 5a             | 1 = ES 8          |
| 2         | 70.5                      | 6.2                               | I & M '77        | 4a, 5a             |                   |
| 3         | 12.5                      | 9.6                               | I & M '77        | 4a, 5a             | 3 = cont of ES 26 |
| 4         | 4.5                       | 3.7                               | I & M '77        | 4a, 5a             |                   |
| 1         | 277.5                     | 2.0                               | Jacobi flts      | 6a                 |                   |
| 2         | 72.5                      | 2.7                               | Jacobi flts      | 6a                 |                   |
| 3         | 351.5                     | 3.0                               | Jacobi flts      | 6a                 | on strike w site  |
| 4         | 76.5                      | 3.6                               | Jacobi flts      | 6a                 |                   |
| 5         | 23.5                      | 6.8                               | Jacobi flts      | 6a                 |                   |
| 6         | 10.5                      | 8.3                               | Jacobi flts      | 6a                 |                   |
| 1         | 73.5                      | 0.6                               | Jac flt zones    | 6b                 |                   |
| 2         | 39.5                      | 5.8                               | Jac flt zones    | 6b                 |                   |
| 1         | 16.5                      | 1.8                               | Jacobi 2007      | 126                |                   |
| 2         | 64.5                      | 3.2                               | Jacobi 2007      | 126                | if extended frm W |
| 1         | 275.5                     | 1.6                               | Bradley et al 41 | 6c                 |                   |
| 2         | 273.5                     | 5.3                               | Bradley et al 41 | 6c                 |                   |
| 1         | 91.5                      | 1.9                               | Murphy 81        | 6d                 |                   |
| 2         | 349.5                     | 3.8                               | Murphy 81        | 6d                 | on strike w site  |
| 3         | 23.5                      | 4.5                               | Murphy 81        | 6d                 |                   |
| 4         | 273.5                     | 5.8                               | Murphy 82        | 6d                 |                   |
| 1         | 89.5                      | 7.8                               | Wedel 32         | 7                  |                   |

EarthSat '97 = EarthSat (1997), I & M '77 = Isachsen and McKendree (1977), Jacobi flts = Jacobi (2002)

Jac flt zones = Jacobi (2002) fault zones, Murphy 81 = Murphy (1981), Wedel 32 = Wedel (1932)

TABLE 6.1-4  
Greenidge Power Plant  
Fracture Trends

| SET I (J2) | FIGURE     | SOURCE   | NOTES                  |
|------------|------------|--|------------------------|
| 317.5      | 8, 9, 13   | Engelder & Geiser, 1980                          | about 6.5 km from site |
| 336.5      | 10         | Faculty and Students of Cornell University, 1959 | about 6.4 km from site |
| 3.5        | 10         | Faculty and Students of Cornell University, 1960 | about 10 km from site  |
| NNW        | 38, 39, 40 | Lugert et al, 2001, Cruz, 2005, Jacobi, 2007     | about 7.6 km from site |
| NS         | 35, 36, 37 | Lugert et al, 2001, Cruz, 2005, Jacobi, 2007     | about 6.2 km from site |

| SET II | FIGURE     | SOURCE                                       | NOTES                   |
|--------|------------|--|-------------------------|
| 80.5   | 11, 12, 13 | Engelder & Geiser, 1980                      | about 7.3 km from site  |
| 82.5   | 11, 12, 13 | Engelder & Geiser, 1980                      | about 12 km from site   |
| 273.5  | 11, 12, 13 | Engelder & Geiser, 1980                      | about 11 km from site   |
| 53.5   | 11, 12, 13 | Engelder & Geiser, 1980                      | about 16 km from site   |
| 71.5   | 15         | Engelder & Geiser, 1980                      | trajectory              |
| 73.5   | 25         | Younes & Engelder, 1999                      | about 15.6 km from site |
| EW     | 47, 48, 49 | Lugert et al, 2001, Cruz, 2005, Jacobi, 2007 | about 7.5 km from site  |

| SET III | FIGURE     | SOURCE                                       | NOTES                  |
|---------|------------|--|------------------------|
| ENE     | 44, 45, 46 | Lugert et al, 2001, Cruz, 2005, Jacobi, 2007 | about 6.5 km from site |

TABLE 6.1-5  
Cayuga Power Plant  
Lineaments and Faults

| ID NUMBER | ORIENTATION<br>in degrees | DISTANCE<br>FRM<br>FACILITY IN<br>KM | SOURCE           | FIGURE THIS<br>RPT | NOTES           |
|-----------|---------------------------|--------------------------------------|------------------|--------------------|-----------------|
| 1         | 69.5                      | 4.3                                  | EarthSat '97     | 3a, 5a, 56-101     |                 |
| 2         | 72.5                      | 3.6                                  | EarthSat '97     | 3a, 5a, 56-101     |                 |
| 3         | 67.5                      | 2.1                                  | EarthSat '97     | 3a, 5a, 56-101     |                 |
| 4         | 66.5                      | 1.4                                  | EarthSat '97     | 3a, 5a, 56-101     |                 |
| 5         | 72.5                      | 3.1                                  | EarthSat '97     | 3a, 5a, 56-101     |                 |
| 6         | 276.5                     | 1.0                                  | EarthSat '97     | 3a, 5a, 56-101     |                 |
| 7         | 359.5                     | 9.0                                  | EarthSat '97     | 3a, 5a, 56-101     | ES 7 = ~ I&M 2  |
| 8         | 361.5                     | 9.7                                  | EarthSat '97     | 3a, 5a, 56-101     |                 |
| 9         | 360.5                     | 10.6                                 | EarthSat '97     | 3a, 5a, 56-101     |                 |
| 10        | 325.5                     | 10.2                                 | EarthSat '97     | 3a, 5a, 56-101     |                 |
| 11        | 320.5                     | 9.5                                  | EarthSat '97     | 3a, 5a, 56-101     |                 |
| 12        | 45.5                      | 10.3                                 | EarthSat '97     | 3a, 5a, 56-101     | ES 12 = ~ I&M 1 |
| 13        | 59.5                      | 10.0                                 | EarthSat '97     | 3a, 5a, 56-101     |                 |
| 14        | 61.5                      | 10.9                                 | EarthSat '97     | 3a, 5a, 56-101     |                 |
| 15        | 57.5                      | 11.6                                 | EarthSat '97     | 3a, 5a, 56-101     |                 |
| 1         | 62.5                      | 6.3                                  | I & M '77        | 4a, 5a             | I&M 1 = ~ ES 12 |
| 2         | 357.5                     | 7.7                                  | I & M '77        | 4a, 5a             | I&M 2 = ~ ES 7  |
| 1         | 92.5                      | 0.9                                  | Jacobi flts      | 6a                 |                 |
| 2         | 71.5                      | 1.0                                  | Jacobi flts      | 6a                 |                 |
| 3         | 353.5                     | 8.2                                  | Jacobi flts      | 6a                 |                 |
| 1         | 67.5                      | 1.1                                  | Jac flt zones    | 6b                 |                 |
| 1         | 326.5                     | 0.9                                  | Jacobi 2007      | 126                |                 |
| 2         | 54.5                      | 2.7                                  | Jacobi 2007      | 126                |                 |
| 3         | 54.5                      | 2.2                                  | Jacobi 2007      | 126                |                 |
| 4         | 54.5                      | 5.2                                  | Jacobi 2007      | 126                |                 |
| 5         | 49.5                      | 11.7                                 | Jacobi 2007      | 126                |                 |
| 1         | NONE                      |                                      | Bradley et al 41 | 6c                 |                 |
| 1         | 359.5                     | 13.3                                 | Murphy 81        | 6d                 |                 |
| 1         | 87.5                      | 5.8                                  | Wedel 32         | 7                  |                 |

EarthSat '97 = EarthSat (1997), I & M '77 = Isachsen and McKendree (1977), Jacobi flts = Jacobi (2002)

Jac flt zones = Jacobi (2002) fault zones, Murphy 81 = Murphy (1981), Wedel 32 = Wedel (1932)



TABLE 6.1-6  
Cayuga Power Plant  
Fracture Trends

| SET I (J2) | FIGURE     | SOURCE   | NOTES                  |
|------------|------------|--|------------------------|
| 356.5      | 8, 9, 13   | Engelder & Geiser, 1980                          | about 5 km from site   |
| 339.5      | 8, 9, 14   | Engelder & Geiser, 1980                          | about 10 km from site  |
| 335.5      | 8, 9, 15   | Engelder & Geiser, 1980                          | about 11 km from site  |
| 336.5      | 10         | Faculty and Students of Cornell University, 1959 | about 1.3 km from site |
| 13.5       | 10         | Faculty and Students of Cornell University, 1960 | about 0 km from site   |
| NNW        | 38, 39, 40 | Lugert et al, 2001, Cruz, 2005, Jacobi, 2007     | about 3 km from site   |
| NS         | 35, 36, 37 | Lugert et al, 2001, Cruz, 2005, Jacobi, 2007     | about 3 km from site   |

| SET II | FIGURE     | SOURCE                                       | NOTES                        |
|--------|------------|--|------------------------------|
| 85.5   | 11, 12, 13 | Engelder & Geiser, 1980                      | about 8 km from site         |
| 69.5   | 11, 12, 13 | Engelder & Geiser, 1980                      | about 4 km from site         |
| 273.5  | 11, 12, 13 | Engelder & Geiser, 1980                      | about 15 km from site        |
| 84.5   | 15         | Engelder & Geiser, 1980                      | trajectory (becomes EW to E) |
| 79.5   | 25         | Younes & Engelder, 1999                      | about 13 km from site        |
| EW/ENE | 47, 48, 49 | Lugert et al, 2001, Cruz, 2005, Jacobi, 2007 | about 3 km from site         |

| SET III | FIGURE     | SOURCE                                       | NOTES                |
|---------|------------|--|----------------------|
| ENE     | 44, 45, 46 | Lugert et al, 2001, Cruz, 2005, Jacobi, 2007 | about 3 km from site |

TABLE 6.1-7  
Westover Power Plant  
Lineaments and Faults

| ID NUMBER | ORIENTATION<br>in degrees | DISTANCE<br>FRM FACILITY<br>IN KM | SOURCE        | FIGURE THIS<br>RPT | NOTES                             |
|-----------|---------------------------|-----------------------------------|---------------|--------------------|-----------------------------------|
| 1         | 309.5                     | 0.0                               | EarthSat '97  | 3a, 5a             |                                   |
| 2         | 315.5                     | 0.5                               | EarthSat '97  | 3a, 5a             |                                   |
| 3         | 43.5                      | 0.6                               | EarthSat '97  | 3a, 5a             |                                   |
| 4         | 42.5                      | 0.9                               | EarthSat '97  | 3a, 5a             |                                   |
| 5         | 32.5                      | 0.7                               | EarthSat '97  | 3a, 5a             |                                   |
| 6         | 39.5                      | 1.0                               | EarthSat '97  | 3a, 5a             |                                   |
| 7         | 40.5                      | 0.9                               | EarthSat '97  | 3a, 5a             |                                   |
| 8         | 47.5                      | 1.2                               | EarthSat '97  | 3a, 5a             |                                   |
| 9         | 44.5                      | 1.3                               | EarthSat '97  | 3a, 5a             |                                   |
| 10        | 40.5                      | 1.4                               | EarthSat '97  | 3a, 5a             |                                   |
| 11        | 36.5                      | 1.6                               | EarthSat '97  | 3a, 5a             |                                   |
| 12        | 286.5                     | 1.8                               | EarthSat '97  | 3a, 5a             |                                   |
| 13        | 319.5                     | 1.0                               | EarthSat '97  | 3a, 5a             |                                   |
| 14        | 304.5                     | 2.4                               | EarthSat '97  | 3a, 5a             |                                   |
| 15        | 279.5                     | 2.4                               | EarthSat '97  | 3a, 5a             |                                   |
| 16        | 333.5                     | 1.9                               | EarthSat '97  | 3a, 5a             | 16 SE cont of 35,<br>ES 16 = IM 5 |
| 17        | 61.5                      | 1.4                               | EarthSat '97  | 3a, 5a             |                                   |
| 18        | 3.5                       | 1.9                               | EarthSat '97  | 3a, 5a             | 18 S cont of 19                   |
| 19        | 359.5                     | 1.1                               | EarthSat '97  | 3a, 5a             | 19 N cont of 18                   |
| 20        | 350.5                     | 1.8                               | EarthSat '97  | 3a, 5a             |                                   |
| 21        | 35.5                      | 1.1                               | EarthSat '97  | 3a, 5a             | ES 21 = IM 5                      |
| 22        | 89.5                      | 1.2                               | EarthSat '97  | 3a, 5a             |                                   |
| 23        | 350.5                     | 1.5                               | EarthSat '97  | 3a, 5a             |                                   |
| 24        | 89.5                      | 2.5                               | EarthSat '97  | 3a, 5a             |                                   |
| 25        | 290.5                     | 2.3                               | EarthSat '97  | 3a, 5a             |                                   |
| 26        | 273.5                     | 3.2                               | EarthSat '97  | 3a, 5a             |                                   |
| 27        | 273.5                     | 2.8                               | EarthSat '97  | 3a, 5a             |                                   |
| 28        | 271.5                     | 2.7                               | EarthSat '97  | 3a, 5a             |                                   |
| 29        | 12.5                      | 2.2                               | EarthSat '97  | 3a, 5a             |                                   |
| 30        | 36.5                      | 2.7                               | EarthSat '97  | 3a, 5a             |                                   |
| 31        | 41.5                      | 2.6                               | EarthSat '97  | 3a, 5a             |                                   |
| 32        | 45.5                      | 2.9                               | EarthSat '97  | 3a, 5a             |                                   |
| 33        | 279.5                     | 2.0                               | EarthSat '97  | 3a, 5a             |                                   |
| 34        | 315.5                     | 1.5                               | EarthSat '97  | 3a, 5a             |                                   |
| 35        | 311.5                     | 2.2                               | EarthSat '97  | 3a, 5a             | 35 NW cont of 16                  |
| 36        | 352.5                     | 2.4                               | EarthSat '97  | 3a, 5a             | ES 36 = IM 7                      |
| 37        | 351.5                     | 2.4                               | EarthSat '97  | 3a, 5a             |                                   |
| 38        | 350.5                     | 1.4                               | EarthSat '97  | 3a, 5a             |                                   |
| 39        | 317.5                     | 2.9                               | EarthSat '97  | 3a, 5a             |                                   |
| 1         | 84.5                      | 0.3                               | I & M '77     | 4a, 5a             | 1 W cont of 2                     |
| 2         | 87.5                      | 0.9                               | I & M '77     | 4a, 5a             | 2 E cont of 1                     |
| 3         | 345.5                     | 0.2                               | I & M '77     | 4a, 5a             |                                   |
| 4         | 352.5                     | 1.0                               | I & M '77     | 4a, 5a             |                                   |
| 5         | 48.5                      | 1.8                               | I & M '77     | 4a, 5a             | IM 5 = ES 21                      |
| 6         | 333.5                     | 1.9                               | I & M '77     | 4a, 5a             | IM 6 = ES 16                      |
| 7         | 350.5                     | 2.2                               | I & M '77     | 4a, 5a             | IM 7 = ES 36                      |
| 8         | 302.5                     | 2.4                               | I & M '77     | 4a, 5a             |                                   |
| 1         | 309.5                     | 0.0                               | Jacobi flts   | 6a                 |                                   |
| 2         | 312.5                     | 10.1                              | Jacobi flts   | 6a                 |                                   |
| 3         | 40.5                      | 4.5                               | Jacobi flts   | 6a                 |                                   |
| 4         | 32.5                      | 6.2                               | Jacobi flts   | 6a                 |                                   |
| 5         | 44.5                      | 9.6                               | Jacobi flts   | 6a                 |                                   |
| 1         | 41.5                      | 0.0                               | Jac flt zones | 6b                 |                                   |
| 2         | 36.5                      | 6.6                               | Jac flt zones | 6b                 |                                   |
| 3         | 87.5                      | 16.0                              | Jac flt zones | 6b                 |                                   |
| 1         | 84.5                      | 1.3                               | Wedel 32      | 7                  |                                   |

EarthSat '97 = EarthSat (1997), I & M '77 = Isachsen and McKendree (1977), Jacobi flts = Jacobi (2002)

Jac flt zones = Jacobi (2002) fault zones, Murphy 81 = Murphy (1981), Wedel 32 = Wedel (1932)

TABLE 6.1-8  
Westover Power Plant  
Fracture Trends

| SET I (J2)<br>(in degrees) | FIGURE   | SOURCE                  | NOTES                |
|----------------------------|----------|-------------------------|----------------------|
| 6                          | 8, 9, 13 | Engelder & Geiser, 1980 | about 6 km from site |
| 350                        | 8, 9, 14 | Engelder & Geiser, 1980 | about 6 km from site |
| 7                          | 8, 9, 14 | Engelder & Geiser, 1980 | about 8 km from site |
| 353                        | 8, 9, 14 | Engelder & Geiser, 1980 | about 8 km from site |
| 5                          | 8, 9, 14 | Engelder & Geiser, 1980 | about 8 km from site |
| 2                          | 23       | Younes & Engelder, 1999 | about 8 km from site |
| 354                        | 23       | Younes & Engelder, 1999 | about 7 km from site |

| SET II | FIGURE     | SOURCE                  | NOTES                                     |
|--------|------------|-------------------------|---|
| 274    | 11, 12, 13 | Engelder & Geiser, 1980 | about 10 km from site                     |
| 283    | 11, 12, 13 | Engelder & Geiser, 1980 | about 15 km from site                     |
| 284    | 11, 12, 13 | Engelder & Geiser, 1980 | about 15 km from site                     |
| 280    | 11, 12, 13 | Engelder & Geiser, 1980 | about 18 km from site                     |
| 288    | 11, 12, 13 | Engelder & Geiser, 1980 | about 21 km from site                     |
| 298    | 15         | Engelder & Geiser, 1980 | trajectory, about 24 km from site         |
| 295    | 15         | Engelder & Geiser, 1981 | trajectory, about 21 km from site         |
| 284    | 15         | Engelder & Geiser, 1981 | trajectory, about 18 km from site         |
| 281    | 16         | Engelder & Geiser, 1982 | trajectory, about 19 km from site         |
| NA     | 25         | Younes & Engelder, 1999 | these nominal Set II are probably set III |
| 289    | 29         | Engelder & Oertel, 1989 | about 33 km from site                     |
| 274    | 29         | Engelder & Oertel, 1989 | about 34 km from site                     |
| 299    | 29         | Engelder & Oertel, 1989 | about 36 km from site                     |
| 279    | 29         | Engelder & Oertel, 1989 | about 39 km from site                     |

| SET III | FIGURE | SOURCE                  | NOTES  |
|---------|--------|-------------------------|--|
| 71      | 25     | Younes & Engelder, 1999 | these nominal Set II are probably set III, about 16 km from site |

TABLE 6.1-9  
Jennison Power Plant  
Lineaments and Faults

| ID NUMBER | ORIENTATION | DISTANCE FROM FACILITY IN KM | SOURCE        | FIGURE THIS RPT | NOTES             |
|-----------|-------------|------------------------------|---------------|-----------------|-------------------|
| 1         | 290.5       | 0.3                          | EarthSat '97  | 3a, 5a          | ES 1 cont of IM 5 |
| 2         | 49.5        | 0.4                          | EarthSat '97  | 3a, 5a          |                   |
| 3         | 76.5        | 0.3                          | EarthSat '97  | 3a, 5a          |                   |
| 4         | 17.5        | 0.2                          | EarthSat '97  | 3a, 5a          |                   |
| 5         | 326.5       | 0.1                          | EarthSat '97  | 3a, 5a          |                   |
| 6         | 350.5       | 1.2                          | EarthSat '97  | 3a, 5a          |                   |
| 7         | 59.5        | 0.9                          | EarthSat '97  | 3a, 5a          |                   |
| 8         | 63.5        | 1.0                          | EarthSat '97  | 3a, 5a          |                   |
| 9         | 55.5        | 0.7                          | EarthSat '97  | 3a, 5a          | N cont(?) of 16   |
| 10        | 57.5        | 1.1                          | EarthSat '97  | 3a, 5a          |                   |
| 11        | 270.5       | 1.5                          | EarthSat '97  | 3a, 5a          | on strike w site  |
| 12        | 86.5        | 2.0                          | EarthSat '97  | 3a, 5a          | on strike w site  |
| 13        | 283.5       | 1.6                          | EarthSat '97  | 3a, 5a          |                   |
| 14        | 280.5       | 1.8                          | EarthSat '97  | 3a, 5a          |                   |
| 15        | 56.5        | 1.5                          | EarthSat '97  | 3a, 5a          | ES 15 = IM 2      |
| 16        | 47.5        | 1.9                          | EarthSat '97  | 3a, 5a          | S cont (?) of 9   |
| 17        | 77.5        | 1.0                          | EarthSat '97  | 3a, 5a          |                   |
| 18        | 67.5        | 1.5                          | EarthSat '97  | 3a, 5a          |                   |
| 19        | 16.5        | 1.3                          | EarthSat '97  | 3a, 5a          |                   |
| 20        | 25.5        | 1.4                          | EarthSat '97  | 3a, 5a          |                   |
| 21        | 25.5        | 1.4                          | EarthSat '97  | 3a, 5a          |                   |
| 22        | 54.5        | 2.2                          | EarthSat '97  | 3a, 5a          | SW cont (?) of 23 |
| 23        | 51.5        | 2.0                          | EarthSat '97  | 3a, 5a          | NE cont (?) of 22 |
| 24        | 56.5        | 2.5                          | EarthSat '97  | 3a, 5a          |                   |
| 25        | 56.5        | 2.6                          | EarthSat '97  | 3a, 5a          |                   |
| 26        | 55.5        | 2.8                          | EarthSat '97  | 3a, 5a          |                   |
| 27        | 339.5       | 2.7                          | EarthSat '97  | 3a, 5a          |                   |
| 28        | 337.5       | 3.1                          | EarthSat '97  | 3a, 5a          |                   |
| 1         | 41.5        | 0.3                          | I & M '77     | 4a, 5a          |                   |
| 2         | 59.5        | 1.8                          | I & M '77     | 4a, 5a          | IM 2 = ES 15      |
| 3         | 75.5        | 1.4                          | I & M '77     | 4a, 5a          |                   |
| 4         | 352.5       | 1.8                          | I & M '77     | 4a, 5a          |                   |
| 5         | 291.5       | 1.4                          | I & M '77     | 4a, 5a          | IM 5 cont of ES 1 |
| 6         | 275.5       | 1.9                          | I & M '77     | 4a, 5a          |                   |
| 7         | 273.5       | 2.6                          | I & M '77     | 4a, 5a          |                   |
| 1         | 61.5        | 5.4                          | Jacobi flts   | 6a              |                   |
| 2         | 51.5        | 5.4                          | Jacobi flts   | 6a              |                   |
| 3         | 88.5        | 0.9                          | Jacobi flts   | 6a              |                   |
| 4         | 16.5        | 0.7                          | Jacobi flts   | 6a              |                   |
| 5         | 53.5        | 11.5                         | Jacobi flts   | 6a              |                   |
| 6         | 11.5        | 11.9                         | Jacobi flts   | 6a              |                   |
| 7         | 339.5       | 12.5                         | Jacobi flts   | 6a              |                   |
| 1         | 61.5        | 0.0                          | Jac flt zones | 6b              |                   |
| 3         | 88.5        | 2.3                          | Jac flt zones | 6b              |                   |

EarthSat '97 = EarthSat (1997), I & M '77 = Isachsen and McKendree (1977), Jacobi flts = Jacobi (2002)

Jac flt zones = Jacobi (2002) fault zones, Murphy 81 = Murphy (1981), Wedel 32 = Wedel (1932)

TABLE 6.1-10  
Jennison Power Plant  
Fracture Trends

| SET I (J2) in degrees                  | FIGURE       | SOURCE                                 | NOTES  |
|--|--------------|--|--|
| 21                                     | 8, 9, 13     | Engelder & Geiser, 1980                | about 29 km from site  |
| 350                                    | 8, 9, 14     | Engelder & Geiser, 1980                | about 29 km from site  |
| 14                                     | 8, 9, 14     | Engelder & Geiser, 1980                | about 23 km from site  |
| 355                                    | 8, 9, 14     | Engelder & Geiser, 1980                | about 23 km from site  |
| 14                                     | 8, 9, 14     | Engelder & Geiser, 1980                | about 23 km from site  |
| 2                                      | 8, 9, 15     | Engelder & Geiser, 1981                | about 23 km from site  |
| 354                                    | 23           | Younes & Engelder, 1999                | about 37 km from site  |
| 19                                     | 23           | Younes & Engelder, 1999                | about 36 km from site  |
| mode = 20-25<br>population = 15-35     | 127, 162-164 | McGuire et al., 2006;<br>Jacobi, 2007b | about 37 km to the center of the mass of sites in B, Figure 127  |
| mode = 25-30<br>population = 5-35      | 127, 137-139 | Terech et al., 2005;<br>Jacobi, 2007b  | about 47 km to the center of the mass of sites in A, Figure 127  |
|  |              |  |  |
| SET II                                 | FIGURE       | SOURCE                                 | NOTES  |
| 288                                    | 11, 12, 13   | Engelder & Geiser, 1980                | about 24 km from site  |
| 297                                    | 11, 12, 13   | Engelder & Geiser, 1980                | about 27 km from site  |
| 274                                    | 11, 12, 13   | Engelder & Geiser, 1980                | about 27 km from site  |
| 294                                    | 11, 12, 13   | Engelder & Geiser, 1980                | about 31 km from site  |
| 303                                    | 15           | Engelder & Geiser, 1980                | trajectory   |
|  | 15           | Engelder & Geiser, 1980                | trajectory   |
|  | 15           | Engelder & Geiser, 1981                | trajectory   |
| NA                                     | 25           | Younes & Engelder, 1999                | these nominal Set II are probably set III                        |
| 283                                    | 29           | Engelder & Oertel, 1989                | about 4 km from site   |
| 274                                    | 29           | Engelder & Oertel, 1989                | about 5 km from site   |
| 274                                    | 29           | Engelder & Oertel, 1989                | about 4 km from site   |
| 278                                    | 29           | Engelder & Oertel, 1989                | about 4 km from site   |
| mode = 285-290<br>population = 280-305 | 127, 174-176 | McGuire et al., 2006;<br>Jacobi, 2007b | about 37 km to the center of the mass of sites in B, Figure 127  |
| mode = 295<br>population = 275-315     | 127, 149-151 | Terech et al., 2005;<br>Jacobi, 2007b  | about 47 km to the center of the mass of sites in A, Figure 127  |
|  |              |  |  |
| SET III                                | FIGURE       | SOURCE                                 | NOTES  |
| 71                                     | 25           | Younes & Engelder, 1999                | these nominal Set II are probably set III, about 27 km from site |